TRANSLATIONAL SIDE OF EMERGING INVASIVE AND NON-INVASIVE STIMULATION THERAPIES

EDITED BY: Jiande Chen, Bruno Bonaz, Leo Cheng and Luming Li
PUBLISHED IN: Frontiers in Neuroscience, Frontiers in Neurology and Frontiers in Physiology

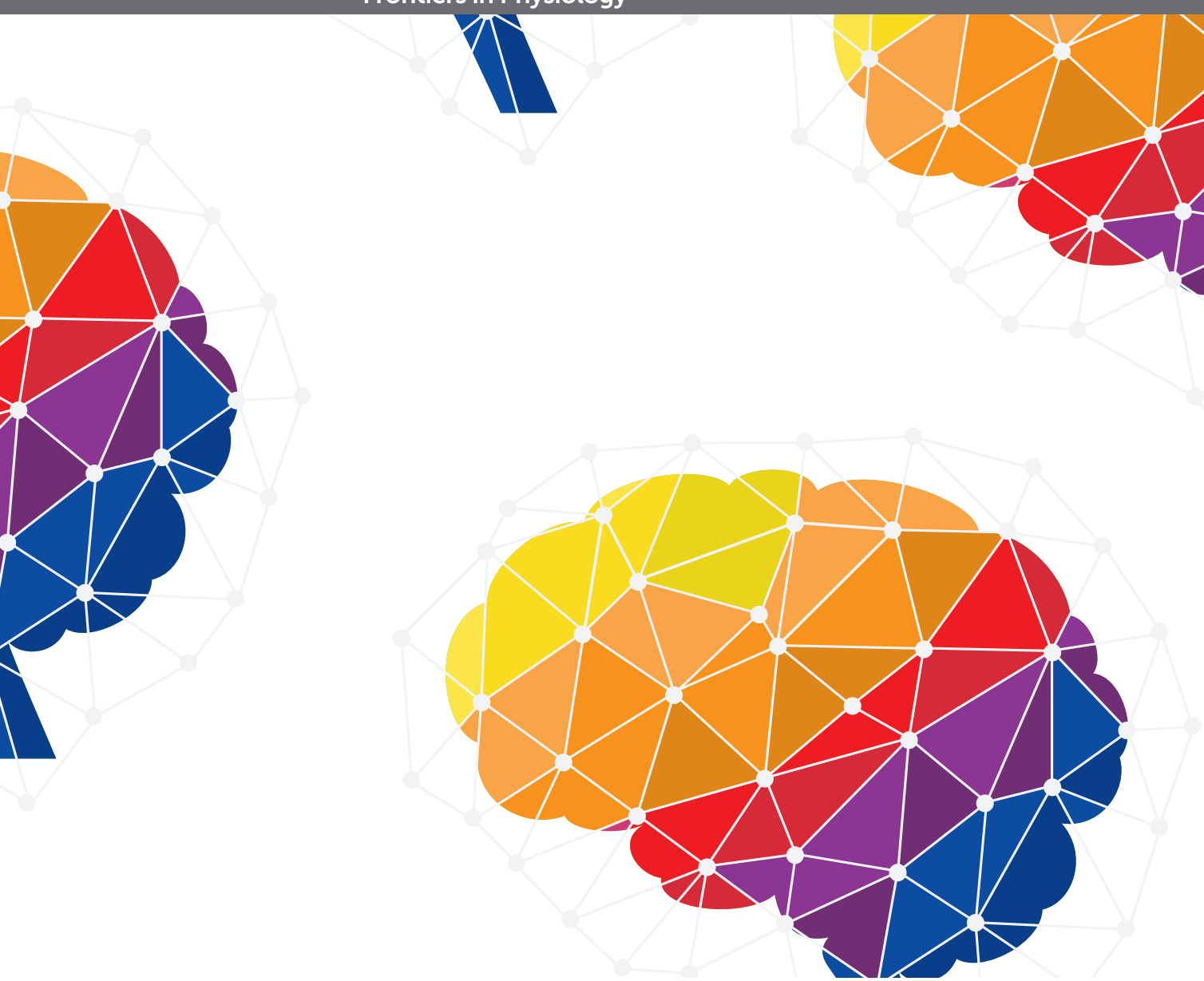

frontiers Research Topics

frontiers

ISSN 1664-8714
ISBN 978-2-88974-535-7
DOI 10.3389/978-2-88974-535-7

About Frontiers

Frontiers is more than just an open-access publisher of scholarly articles: it is a pioneering approach to the world of academia, radically improving the way scholarly research is managed. The grand vision of Frontiers is a world where all people have an equal opportunity to seek, share and generate knowledge. Frontiers provides immediate and permanent online open access to all its publications, but this alone is not enough to realize our grand goals.

Frontiers Journal Series

The Frontiers Journal Series is a multi-tier and interdisciplinary set of open-access, online journals, promising a paradigm shift from the current review, selection and dissemination processes in academic publishing. All Frontiers journals are driven by researchers for researchers; therefore, they constitute a service to the scholarly community. At the same time, the Frontiers Journal Series operates on a revolutionary invention, the tiered publishing system, initially addressing specific communities of scholars, and gradually climbing up to broader public understanding, thus serving the interests of the lay society, too.

Dedication to Quality

Each Frontiers article is a landmark of the highest quality, thanks to genuinely collaborative interactions between authors and review editors, who include some of the world's best academicians. Research must be certified by peers before entering a stream of knowledge that may eventually reach the public - and shape society; therefore, Frontiers only applies the most rigorous and unbiased reviews.
Frontiers revolutionizes research publishing by freely delivering the most outstanding research, evaluated with no bias from both the academic and social point of view. By applying the most advanced information technologies, Frontiers is catapulting scholarly publishing into a new generation.

What are Frontiers Research Topics?

Frontiers Research Topics are very popular trademarks of the Frontiers Journals Series: they are collections of at least ten articles, all centered on a particular subject. With their unique mix of varied contributions from Original Research to Review Articles, Frontiers Research Topics unify the most influential researchers, the latest key findings and historical advances in a hot research area! Find out more on how to host your own Frontiers Research Topic or contribute to one as an author by contacting the Frontiers Editorial Office: frontiersin.org/about/contact

TRANSLATIONAL SIDE OF EMERGING INVASIVE AND NON-INVASIVE STIMULATION THERAPIES

Topic Editors:
Jiande Chen, University of Michigan, United States
Bruno Bonaz, Centre Hospitalier Universitaire de Grenoble, France
Leo Cheng, The University of Auckland, New Zealand
Luming Li, Tsinghua University, China

Citation: Chen, J., Bonaz, B., Cheng, L., Li, L., eds. (2022). Translational Side of Emerging Invasive and Non-Invasive Stimulation Therapies.
Lausanne: Frontiers Media SA. doi: 10.3389/978-2-88974-535-7

Table of Contents

frontiers in Neuroscience

EDITORIAL
published: 23 March 2022
doi: 10.3389/fnins.2022.872551

Editorial: Translational Side of Emerging Invasive and Non-invasive Stimulation Therapies

Leo K. Cheng[1], *Luming Li*[2], *Bruno Bonaz*[3] *and Jiande D. Z. Chen*[4]*

[1] Auckland Bioengineering Institute, University of Auckland, Auckland, New Zealand, [2] National Engineering Laboratory for Neuromodulation, School of Aerospace Engineering, Tsinghua University, Beijing, China, [3] Centre Hospitalier Universitaire Grenoble Alpes, Grenoble, France, [4] Division of Gastroenterology and Hepatology, University of Michigan, Ann Arbor, MI, United States

Keywords: deep brain stimulation (DBS), vagal nerve stimulation (VNS), sacral nerve stimulation (SNS), gastric electrical stimulation, transcutaneous auricular vagus nerve stimulation (taVNS), ultrasound stimulation, electromagnetic field stimulation, sciatic nerve stimulation

Editorial on the Research Topic

Translational Side of Emerging Invasive and Non-invasive Stimulation Therapies

In the past decades, neuroscience research has witnessed dramatic progress in the field of neuromodulation, a stimulation technology that delivers electrical stimuli to modulate nerve activity in targeted areas or organs. It is widely used for the treatment of chronic pain (Coffey, 2001; Ostergard et al., 2014), and also used to modulate the function of target organs such as the heart, gastrointestinal tract or bladder (van Balken et al., 2004; Yin and Chen, 2008; Payne et al., 2019). It is a non-drug-based therapy, generally safe and, in particular, without the side effects of pharmacological treatments.

This Frontiers Research Topic on *Translational Side of Emerging Invasive and Non-invasive Stimulation Therapies* was instigated, in part, due to presentations and discussions at the International Neuromodulation Society's 14th World Congress held in Sydney, Australia, on 25–30 May 2019. The topic editors for this Frontiers Research topic were Professors Jiande Chen, Bruno Bonaz, Leo Cheng, and Luming Li. In total, 93 authors contributed to 14 articles that were published in Frontiers in Neuroscience, Frontiers in Neurology and Frontiers in Physiology.

Functional gastrointestinal disorders are widespread, impart significant economic burden and can greatly reduce quality of life of patients (Everhart and Ruhl, 2009; Sperber et al., 2020). Disorders of the stomach include gastroparesis, functional dyspepsia. Only one device is currently available for delivering gastric electrical stimulation and used for treating nausea and vomiting in patients with gastroparesis (McCallum et al., 2011). However, its efficacy and mechanisms of action remain uncertain (Ducrotte et al., 2020). Cheng et al. review the large variety of electrical stimulation and pacing parameters applied directly to the stomach musculature. Strategies are described to optimize and standardize these stimulation parameters as well as techniques to investigate the mechanisms underlying stimulation techniques. However, it is clear that a number of key challenges remain before such methods are widely used for treating functional gastrointestinal disorders. These include the development of methods to reliably quantify the functional responses to electrical therapies, and the convergence of pacing and stimulation protocols that are able to sustain long-term responses. The integration of mathematical modeling techniques with clinical trials will help to refine and accelerate the development of stimulation protocols and devices. Vagal nerve stimulation is another key target and has been introduced to treat inflammatory bowel diseases such as Crohn's disease and ulcerative colitis (Bonaz et al.). Bonaz et al. review the anti-inflammatory

OPEN ACCESS

Edited and reviewed by:
Joel C. Bornstein,
The University of Melbourne, Australia

***Correspondence:**
Jiande D. Z. Chen
jiandedzchen@gmail.com

Specialty section:
This article was submitted to Autonomic Neuroscience, a section of the journal Frontiers in Neuroscience

Received: *09 February 2022*
Accepted: *21 February 2022*
Published: *23 March 2022*

Citation:
Cheng LK, Li L, Bonaz B and Chen JDZ (2022) Editorial: Translational Side of Emerging Invasive and Non-invasive Stimulation Therapies. Front. Neurosci. 16:872551. doi: 10.3389/fnins.2022.872551

actions of vagal nerve stimulation. Inflammatory bowel disease is a major healthcare concern worldwide, especially in developed countries: it is of a high prevalence, no medications to cure and expensive and difficult to treat. Vagal nerve stimulation has a great potential for treating inflammatory bowel disease mediated via the cholinergic anti-inflammatory pathway. In the review, Bonaz et al. provides neuroanatomical basis of vagal nerve stimulation and discusses how vagal nerve stimulation may improve abnormalities in brain-gut axis. Recently, sacral nerve stimulation was reported to exert similar anti-inflammatory effects in animal models of colitis (Guo et al., 2019) mediated via the spinal afferent and vagal efferent pathways (Tu et al., 2020). The sacral nerve is another branch of the parasympathetic nervous system which innervates the distal colon and rectum as well as other pelvic organs, such as the bladder and genitals. Sacral nerve stimulation is clinically approved for treating overactive bladder, urinary retention and fecal incontinence. In this Research Topic, Jin et al. investigated the use of sacral nerve stimulation for the treatment of visceral hypersensitivity underlying irritable bowel syndrome. In a rodent model of colonic hypersensitivity, sacral nerve stimulation improved visceral pain by inhibiting mast cell overactivation in the colon tissue via the modulation of the autonomic function. Functional anorectal pain is another disorder that is poorly understood. The pathophysiology of this disorder was investigated and a correlation between anal pressure and afferent signaling was determined in a topic article (Zhang et al.).

Deep brain stimulation is one of the most important clinical therapies for several neurological disorders, such as Parkinson's disease, movement disorders, major depression and addiction. Three of the articles in this Frontiers Topic focussed on deep brain stimulation. Sui et al. present a comprehensive review on technical challenges, clinical applications and perspectives and mechanisms of action. Accurate lead localization is an important issue in deep brain stimulation, He and colleagues presented an magnetic resonance-based assessment method to determine the lead localization deviation (He et al.). Appropriate patient screening is critically important in various medical therapies and this is also the case for deep brain stimulation. Wang et al. investigated the predictivity of deep brain stimulation outcome in Parkinson's diseases based on functional connectivity assessed from the rest-state functional magnetic resonance imaging.

A number of commercial devices have received Food and Drug Administration (FDA) approval for the treatment of lower urinary tract dysfunction (van Balken et al., 2004; Siddiqui et al., 2010). Payne et al. developed and applied a new electrode array to record and stimulate the pelvic nerves in conscious rats. They showed that the electrode array could be used for the development of closed-loop neuromodulation devices targeting urological dysfunction. To aid in the development of closed-loop devices, Chen Y. et al. described a method for filtering out electrocardiogram artifacts by sensing-enabled neurostimulator.

Non-invasive electrical stimulation methods are of great interest and provide an attractive option for treating disorders as they do not require surgical implantation of a stimulator or stimulation leads. Chen M. et al. reviewed non-invasive methods for treating cardiac disorders resulting from autonomic imbalance. Various transcutaneous approaches are discussed in this Research Topic, including, transcutaneous auricular vagus nerve stimulation (taVNS), ultrasound stimulation and electromagnetic field stimulation. Andersen et al. presented the use of peripheral electrical stimulation using a circular electrode array on the surface of the forearm with the aim of treating chronic pain (Arendsen et al.) while Machetanz et al. used taVNS to modulate heart function and brain activity.

Of current interest during the current COVID-19 pandemic, Lu et al. presented a technique for remote and wirelessly programming a sacral nerve stimulator for treating chronic pain. Such a method is a critical advance as the pandemic has resulted in major impact on the healthcare system and the ability for patients to travel to their local hospitals.

Diabetes affects 5–10% of general population and is a huge healthcare burden around the world. Type 2 diabetes, a major subtype of diabetes, is closely associated with obesity. Vagal nerve stimulation, a method called VBLOC, has received FDA approval for treating obesity although it has not been widely utilized due to its limited clinical efficacy (Apovian et al., 2017). Gastric electrical stimulation, intestinal electrical stimulation and vagal nerve stimulation have been explored for treating diabetes (Liu et al., 2011; Lebovitz, 2016; Yin et al., 2019; Dong et al., 2021); however, there is a lack of clinical efficacy data. In this Research Topic, Beeve et al. applied sciatic nerve stimulation and reported its neuroskeletal effects in an animal model of type 1 diabetes.

In summary, non-invasive methods may be appropriate for common but relatively mild or moderate disorders, while invasive therapies using an implantable device may be reserved for chronic and severe conditions. In general, the articles in this Frontiers Research Topic have indicated that significant research should be conducted to improve our understanding of the mechanisms underlying these complex disorders. A focus should also be placed on translating methods and findings from animal studies to patients.

AUTHOR CONTRIBUTIONS

LC wrote the first draft. All authors conceived the concept and revised the manuscript. All authors contributed to the article and approved the submitted version.

FUNDING

This work was funded, in part, by the Marsden Fund Council managed by Royal Society Te Apārangi, Ministry of Business Innovation and Employment's Ministry of Business, Innovation and Employment's Catalyst: Strategic fund (for LC), and the National Institutes of Health (NIH) (R01 HD088662 and SPARC OT2OD030538 for LC; and R42DK100212 and 1UG3NS115108 for JC).

ACKNOWLEDGMENTS

We would like to thank all the authors for contributing toward this Frontiers Research Topic.

REFERENCES

Apovian, C. M., Shah, S. N., Wolfe, B. M., Ikramuddin, S., Miller, C. J., Tweden, K. S., et al. (2017). Two-year outcomes of vagal nerve blocking (vBloc) for the treatment of obesity in the recharge trial. *Obes Surg.* 27:169–76. doi: 10.1007/s11695-016-2325-7

Coffey, R. J. (2001). Deep brain stimulation for chronic pain: results of two multicenter trials and a structured review. *Pain Med.* 2, 183–192. doi: 10.1046/j.1526-4637.2001.01029.x

Dong, Y., Yin, J., Zhang, Y., and Chen, J. (2021). Electronic bypass for diabetes: optimization of stimulation parameters and mechanisms of glucagon-like peptide-1. *Neuromodulation* doi: 10.1111/ner.13367. [Epub ahead of print].

Ducrotte, P., Coffin, B., Bonaz, B., Fontaine, S., Bruley Des Varannes, S., Zerbib, F., et al. (2020). Gastric Electrical Stimulation Reduces Refractory Vomiting in a Randomized Crossover Trial. *Gastroenterology* 158, 506.e2–514.e2. doi: 10.1053/j.gastro.2019.10.018

Everhart, J. E., and Ruhl, C. E. (2009). Burden of digestive diseases in the united states part i: overall and upper gastrointestinal diseases. *Gastroenterology* 136, 376–386. doi: 10.1053/j.gastro.2008.12.015

Guo, J., Jin, H., Shi, Z., Yin, J., Pasricha, T., and Chen, J. (2019). Sacral nerve stimulation improves colonic inflammation mediated by autonomic-inflammatory cytokine mechanism in rats. *Neurogastroenterol. Motility* 31, e13676. doi: 10.1111/nmo.13676

Lebovitz, H. E. (2016). Interventional treatment of obesity and diabetes: An interim report on gastric electrical stimulation. *Rev. Endocrine Metab. Dis.* 17, 73–80. doi: 10.1007/s11154-016-9350-7

Liu, J., Xiang, Y., Qiao, X., Dai, Y., and Chen, J. D. (2011). Hypoglycemic effects of intraluminal intestinal electrical stimulation in healthy volunteers. *Obes. Surg.* 21, 224–230. doi: 10.1007/s11695-010-0326-5

McCallum, R. W., Lin, Z., Forster, J., Roeser, K., Hou, Q., and Sarosiek, I. (2011). Gastric electrical stimulation improves outcomes of patients with gastroparesis for up to 10 years. *Clin. Gastroenterol. Hepatol.* 9, 314.e1–319.e1. doi: 10.16/j.cgh.2010.12.013

Ostergard, T., Munyon, C., and Miller, J. P. (2014). Motor cortex stimulation for chronic pain. *Neurosurg. Clin. N. Am.* 25, 693–698. doi: 10.1016/j.nec.2014.06.004

Payne, S. C., Furness, J. B., and Stebbing, M. J. (2019). Bioelectric neuromodulation for gastrointestinal disorders: effectiveness and mechanisms. *Nat. Rev. Gastroenterol. Hepatol.* 16, 89–105. doi: 10.1038/s41575-018-0078-6

Siddiqui, N. Y., Wu, J. M., and Amundsen, C. L. (2010). Efficacy and adverse events of sacral nerve stimulation for overactive bladder: a systematic review. *Neurourol. Urodyn.* 29(Suppl. 1), S18–S23. doi: 10.1002/nau.20786

Sperber, A. D., Bangdiwala, S. I., Drossman, D. A., Ghoshal, U. C., Simren, M., Tack, J., et al. (2020). Worldwide prevalence and burden of functional gastrointestinal disorders, results of rome foundation global study. *Gastroenterology*. 160, 99.e3.−114.e3. doi: 10.1053/j.gastro.2020.04.014

Tu, L., Gharibani, P., Zhang, N., Yin, J., and Chen, J. D. (2020). Anti-inflammatory effects of sacral nerve stimulation: a novel spinal afferent and vagal efferent pathway. *Am. J. Physiol. Gastrointest. Liver Physiol.* 318, G624–G634. doi: 10.1152/ajpgi.00330.2019

van Balken, M. R., Vergunst, H., and Bemelmans, B. L. H. (2004). The use of electrical devices for the treatment of bladder dysfunction: a review of methods. *J. Urol.* 172, 846–851. doi: 10.1097/01.ju.0000134418.21959.98

Yin, J., and Chen, J. D. Z. (2008). Implantable gastric electrical stimulation: ready for prime time? *Gastroenterology* 134, 665–667. doi: 10.1053/j.gastro.2008.01.068

Yin, J., Ji, F., Gharibani, P., and Chen, J. D. (2019). Vagal nerve stimulation for glycemic control in a rodent model of Type 2 diabetes. *Obes. Surg.* 29, 2869–2877. doi: 10.1007/s11695-019-03901-9

Conflict of Interest: The authors declare that the research was conducted in the absence of any commercial or financial relationships that could be construed as a potential conflict of interest.

frontiers in Neurology

ORIGINAL RESEARCH
published: 09 October 2020
doi: 10.3389/fneur.2020.577025

Impaired Anorectal Afferents Is a Potential Pathophysiological Factor Associated to Functional Anorectal Pain

Qi Zhang[1†], Yanni Liu[2†], Qiong Zhang[3], Yuqing Zhang[1], Sangsang Wu[1], Bin Jiang[4] and Min Ni[4]*

[1] Graduate School, Nanjing University of Chinese Medicine, Nanjing, China, [2] Baoji City Hospital of Traditional Chinese Medicine, Baoji, China, [3] Shuyang County Hospital of Traditional Chinese Medicine, Suqian, China, [4] National Centre of Colorectal Disease, Nanjing Hospital of Chinese Medicine, Nanjing, China

OPEN ACCESS

Edited by:
Jiande Chen,
University of Michigan, United States

Reviewed by:
Heiying Jin,
Second Affiliated Hospital of Nanjing University of Chinese Medicine, China
Allan Goldstein,
Massachusetts General Hospital and Harvard Medical School, United States
Gengqing Song,
Case Western Reserve University, United States

***Correspondence:**
Min Ni
minninj@gmail.com

[†] These authors have contributed equally to this work

Specialty section:
This article was submitted to Autonomic Neuroscience, a section of the journal Frontiers in Neurology

Received: 28 June 2020
Accepted: 10 September 2020
Published: 09 October 2020

Citation:
Zhang Q, Liu Y, Zhang Q, Zhang Y, Wu S, Jiang B and Ni M (2020) Impaired Anorectal Afferents Is a Potential Pathophysiological Factor Associated to Functional Anorectal Pain. Front. Neurol. 11:577025. doi: 10.3389/fneur.2020.577025

Background/Aims: Functional anorectal pain (FARP) is a functional gastrointestinal disease, which belongs to chronic pelvic floor pain. The mechanisms of its development are not fully understood. We designed this experiment to evaluate the characteristics of rectal sensory evoked potential (RSEP) and anorectal manometry (ARM) in this population, so as to explore the pathophysiology of FARP.

Methods: The rectal sensory evoked potentials (RSEP) and anorectal manometry (ARM) were performed in 23 patients with FARP and 23 healthy controls. The correlation between the two measurements was investigated.

Results: The results of RSEP showed that (1) the median latency to the first positive peak was 69.2 ± 15.9 ms in patients, compared with 46.5 ± 5.8 ms in controls ($P = 0.000$). (2) The amplitude of evoked potential peaks in the FARP patients was significantly lower than the healthy controls (P1/N1: $P = 0.049$; N1/P2: $P = 0.010$). (3) Compared with the controls, the patients showed a lower maximum voluntary squeeze pressure ($P = 0.009$), lower rectum ($P = 0.007$), and anal sphincter pressures ($P = 0.000$) during strain; and increased maximum tolerance threshold to rectal distention ($P = 0.000$). (4) The resting pressure of the anal sphincter was correlated with the peak amplitude of the RSEP (P1/N1: $r = 0.537$, $P = 0.039$; N1/P2: $r = 0.520$, $P = 0.047$). Considering the different pathophysiological mechanisms of levator ani syndrome and proctalgia fugax, we analyzed data on unspecified functional anorectal pain and obtained similar results.

Conclusions: The RSEP can be used to evaluate the state of afferent pathways in FARP patients; The longer latency and lower peak amplitude of RSEP indicate the functional defects of the anorectal afferent pathway. It can provide an objective evidence for the neuropathy of FARP. In addition, the pathophysiology of FARP is also associated with pelvic floor muscle motor and coordination dysfunction. The correlation between the peak amplitude of the RSEP and the resting pressure of the anal sphincter suggests that there seems to be a correlation between anal pressure and the afferent signaling pathway in patients with FARP.

Keywords: functional anorectal pain, evoked potential, afferent pathway, pathophysiology, anorectal manometry

INTRODUCTION

Functional anorectal pain (FARP) is a disabling disease and can be caused by a variety of factors. Rome IV divides FARP into three subtypes: proctalgia fugax, levator ani syndrome, and unspecified functional anorectal pain (1–3). Levator ani syndrome and unspecified functional anorectal pain are distinguished by whether there is pain when pulling the levator ani muscle backward (4). A previous survey of householders in the United States found that the prevalences of the anorectal pain, levator ani syndrome, and proctalgia fugax were 11.6, 6.6, and 8%, respectively (5), and most of them were women. The patients are often accompanied with mental and emotional disorders that seriously affect the quality of life and mental health of patients.

The pathophysiology of FARP is still unclear. At present, it is generally believed that the over contraction and high tension of pelvic floor muscle are one of the important mechanisms. Levator ani syndrome is considered to be closely related to pelvic floor spasm and can usually be relieved by the biofeedback therapy (6, 7). Rao SS et al. reported that paroxysmal anal hyperkinesis was an outstanding characteristic feature of proctalgia fugax (8). However, in our clinical practice, we have observed that functional anorectal pain is also present in patients with hypotensive pelvic floor muscle, and this group of patients usually have sensation of downward bloating in their anus, and most of them are women.

Abnormal regulation of the nervous system may also lead to FARP. The function of gastrointestinal tract is controlled by the central nervous system, autonomic nervous system, and enteric nervous system. There is a biphasic regulatory pathway between the digestive tract and the central nervous system (9); the brain-gut dysfunction has been proven to be closely related to gastrointestinal disorders (3, 10, 11). The visceral sensory function is one of the important contents in the brain-gut axis research, and heightened visceral perception or visceral hypersensitivity has long been considered as a potential pathogenesis of functional bowel disease (12, 13), especially IBS (14, 15). The mechanism of visceral hypersensitivity has not been fully elucidated. It may be result from the sensitization of nerve afferent pathways originating from the gastrointestinal tract (16). At present, there is a lack of reports in the literature on the sensory abnormality in patients with functional anorectal pain.

Neurophysiological tests can provide useful information regarding the integrity of neuronal innervation and neuromuscular function of the gut. During the last few years, some techniques have provide information regarding gut-brain communication such as Positron Emission Tomography (PET) or functional magnetic resonance imaging (fMRI). Recently, RSEP has been introduced as a new technique that can provide an quantifiable method to evaluate the connections between the afferent tracts, spinal cord, and the cerebral cortex (9). In this study, our aim was to prospectively evaluate and compare RSEP following rectal electrical stimulation and ARM in FARP patients, and healthy controls. So as to evaluate the anorectal sensory and motor functions and neural afferent pathways in FARP patients, and explore possible mechanisms of FARP.

MATERIALS AND METHODS

Subjects

This study was reviewed and approved by the Ethics Committee of Nanjing Hospital of Chinese Medicine (KY2018004). The participants provided their written informed consent to participate in this study. Twenty three patients with FARP were recruited from patients seen in the Anorectal Clinic of Nanjing Hospital of Chinese Medicine. All patients met the Rome IV criteria for functional anal pain. Patients with a history of anorectal surgery, secondary anorectal pain with clear etiology, serious gastrointestinal diseases or oral drugs affecting gastrointestinal functions, serious neurological diseases, spinal injury, or surgery were excluded, as were pregnant women.

In order to exclude the influence of age and gender, the control group consisted of 23 healthy people whose sex and age matched with the patients. These healthy people did not have FARP and diseases listed below: gastrointestinal diseases, severe perianal diseases, or severe cardiovascular. Individuals with any cerebrovascular, urological, gynecological, orthopedic, or malignant tumors were also excluded.

Rectal Sensory Evoked Potentials After Electrical Stimulation

For rectal stimulation, a St. Mark's stimulation electrode was fixed at the tip on the index finger while the other electrode was located at the root of the index finger, and the electrodes were connected to an electrical stimulator (Oxford Instruments, Oxford, Britain). For recording of evoked potential, an active electrode was placed on the subject's central scalp (Cz); a reference electrode was placed on the forehead (Fz); and a grounding electrode was placed on the ankle. This was in accordance with the International Electroencephalogram Society standard (17). The test was conducted in a dark room, unnecessary electrical equipment were turned off to avoid electromagnetic interferences. Subjects were requested to lie relaxed with their eyes closed. The examiner put the index finger into the rectum of the patient with the stimulation electrode located at 9 o'clock of the lithotomy position and 5 cm from the anal margin. The sensory threshold was defined as the minimum stimulation intensity of the patient's perception, and the tolerance threshold was defined as the maximum tolerable intensity. The final stimulus intensity was set at 75% of the mean tolerance threshold. The evaluation was repeated three times to ensure consistency. The electric stimuli were composed of 100 pulses with a pulse width of 0.2 ms, frequency of 1 Hz. The impedance between the electrodes was maintained below 5 kΩ. The RSEP data were obtained using the Oxford myoelectricity-evoked potential apparatus (Oxford Instruments, Oxford, Britain). The sensitivity of the amplifier was 100 μv/div and the recording bandwidth was set to 1∼500 Hz.

After electrical stimulation, three typical main waveforms could be recorded (18), which are labeled P1, N1, and P2, respectively (**Figure 1A**). Positive waves with downward amplitude were represented by P, and negative waves with upward amplitude were represented by N. The time from the start of the stimulus to the appearance of the peak was called

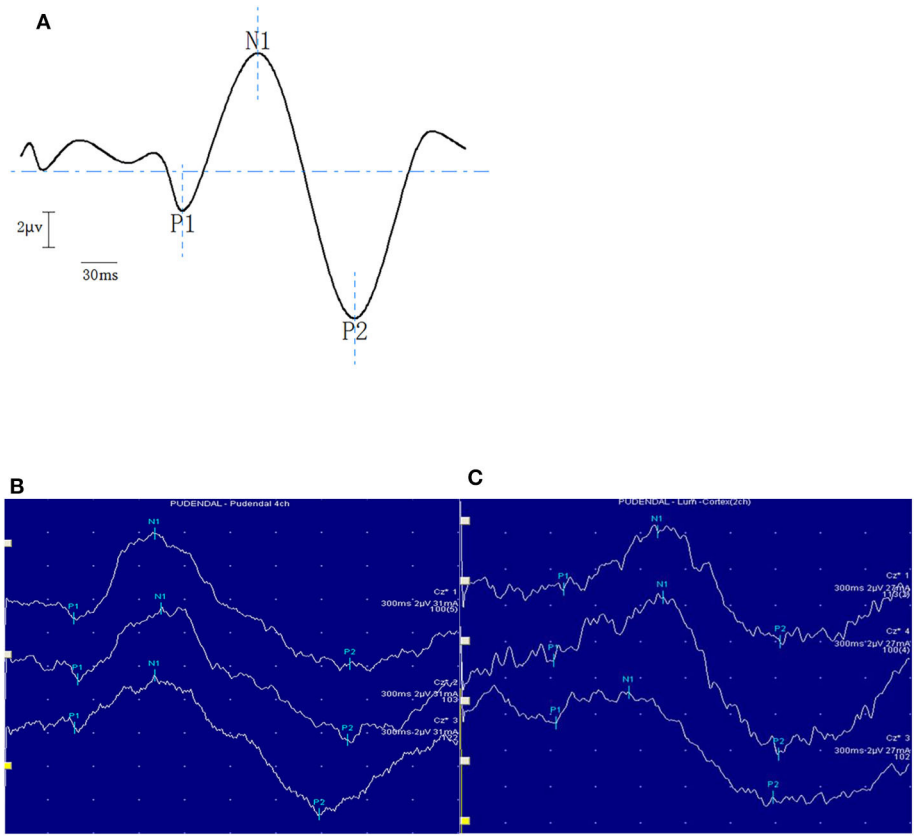

FIGURE 1 | The panel above is the schematic diagram of typical waveforms of RSEP **(A)**. The bottom panel shows typical examples of RSEP responses in a healthy subject **(B)** and in a patient with FARP **(C)**.

the latency. The voltage difference between two consecutive peaks was referred as the amplitude, represented by P1/N1 and N1/P2.

Anorectal Manometric Testing

Anorectal manometry (ARM) was performed via an 8-channel radially distributed water perfusion catheter with a latex balloon attached at the tip of the catheter (Medtronic Synectics, Sweden). Before anorectal manometry, all participants were required to empty their stools to ensure that the rectum was empty. The patient lay on the left side and remained relaxed; the examination was performed by a well-trained doctor. Following measurements were made: rectal motility functions (anal resting pressure, maximum voluntary squeeze pressure, anal sphincter pressure during straining, and rectal pressure during straining) and rectal sensory functions (first sensation, urge to defecate, and maximum tolerance volume of rectal balloon distention). Other measurements included the length of functional anal canal, rectum anal inhibitory reflex (RAIR), contractile reflex of the anorectum during coughing (cough reflex) and defecation reflex. The procedures and measurements followed the standards of previous studies (19, 20).

Statistical Analyses

SPSS 20.0 version was used for statistical analyses. The data are expressed as mean ± standard deviation with 95% confidence interval. Counting data is expressed by frequencies and percentages, Fisher's exact tests is used for comparison between groups. The Mann Whitney *U*-test was used to compare the latency and amplitude of RSEP waves, and parameters of anorectal manometry between the FARP patients and healthy controls. The correlations between the parameters of RSEP and the parameters of anorectal manometry were analyzed by Pearson or Spearman correlation analysis.

RESULTS

Demographics

All 23 patients with FARP were enrolled in the study. There was 21/23 patients with unspecified functional anorectal pain (Unspecified-FARP), and 1/23 patient with proctalgia fugax (PF),1/23 patient with levator ani syndrome(LAS) The average age of the patients was 52.48 (±12.98) years old and gender distribution of the two groups was 18/5 (F/M). There was no significant difference in height, weight or BMI between the patients and healthy controls (**Table 1**). The female patients with

FARP were divided into five groups according to their ages: group I (20–29 years old), group II (30–39 years old), group III (40–49 years old), group IV (50–59 years old), and group V (60 years old and above) (**Figure 2**). Most of the female FARP patients were over 40 years old, mainly distributed in the age group of 50–59 years old. Among 21 patients with unspecified functional anorectal pain, 2 female FARP patients had a history of multiple vaginal deliveries.

Rectal Sensory Evoked Potential

A reproducible RSEP pattern was recorded in all subjects after rectal stimulation. Typical examples of the morphology of RSEP response are shown in **Figures 1B,C**. The latencies and amplitudes of each component of the RSEP of control group are shown in **Table 2**, and there were no differences among RSEP components between men and women subjects.

The latency of P1 was significantly longer in the FARP patients than the healthy controls (69.20 ± 15.91 vs. 46.50 ± 5.77, $P < 0.01$). There was no significant difference in N1 and P2 latency between the two groups. The amplitude of each wave in the FARP patients was significantly lower than the healthy controls (P1/N1: 3.66 ± 2.10 vs. 4.67 ± 2.35; N1/P2: 4.25 ± 3.07 vs. 6.57 ± 2.78, $P < 0.01$). In order to further explore the mechanism of unspecified functional anorectal pain, we compared the RSEP examination of unspecified-FARP patients with that of healthy controls (**Table 3**).

Anorectal Manometry

All 15 of the 23 FARP patients performed anorectal manometry. After comparing the components of ARM between the FARP patients and the healthy controls, we found that the maximum voluntary squeeze pressure in the FARP patients was lower than the healthy controls (107.37 ± 32.53 vs. 135.61 ± 19.13, $P < 0.01$). Meanwhile, the FARP patients showed a significantly lower anal sphincter pressure and rectal pressure during straining ($P < 0.01$). There was no significant difference between the two groups in resting anal pressure, sphincter length. In addition, analrectal manometry results in 13 patients with unspecified-FARP were analyzed, and similar results were obtained (**Table 4**). All the data of 15 FARP patients who completed the two examinations are

TABLE 1 | Demographics of FARP patients and healthy controls.

	FARP ($n = 23$)	Controls ($n = 23$)	*p*
Gender (female)	18	18	–
Age	52.48 ± 12.98	49.91 ± 12.07	0.422
Height (m)	1.63 ± 0.08	1.66 ± 0.70	0.205
Weight (kg)	62.09 ± 9.38	61.65 ± 6.83	0.965
BMI (kg/m^2)	23.46 ± 3.18	22.36 ± 1.62	0.287

Values are given as mean (±SD).

TABLE 2 | Latencies and amplitude of each component of the RSEP response following Rectal Stimulation in healthy controls.

	Total ($n = 23$)	Males ($n = 5$)	Female ($n = 18$)	*p*
P1 latency (ms)	46.50 ± 5.77	46.18 ± 2.77	46.59 ± 6.42	0.914
N1 latency (ms)	101.32 ± 17.78	102.74 ± 23.69	100.93 ± 16.62	0.801
P2 latency (ms)	193.70 ± 34.42	203.98 ± 28.02	190.85 ± 36.18	0.446
P1/N1 amplitude (uV)	4.67 ± 2.35	5.44 ± 1.99	4.46 ± 2.45	0.538
N1/P2 amplitude (uV)	6.57 ± 2.78	7.50 ± 2.76	6.31 ± 2.80	0.491

Values are given as mean (±SD).

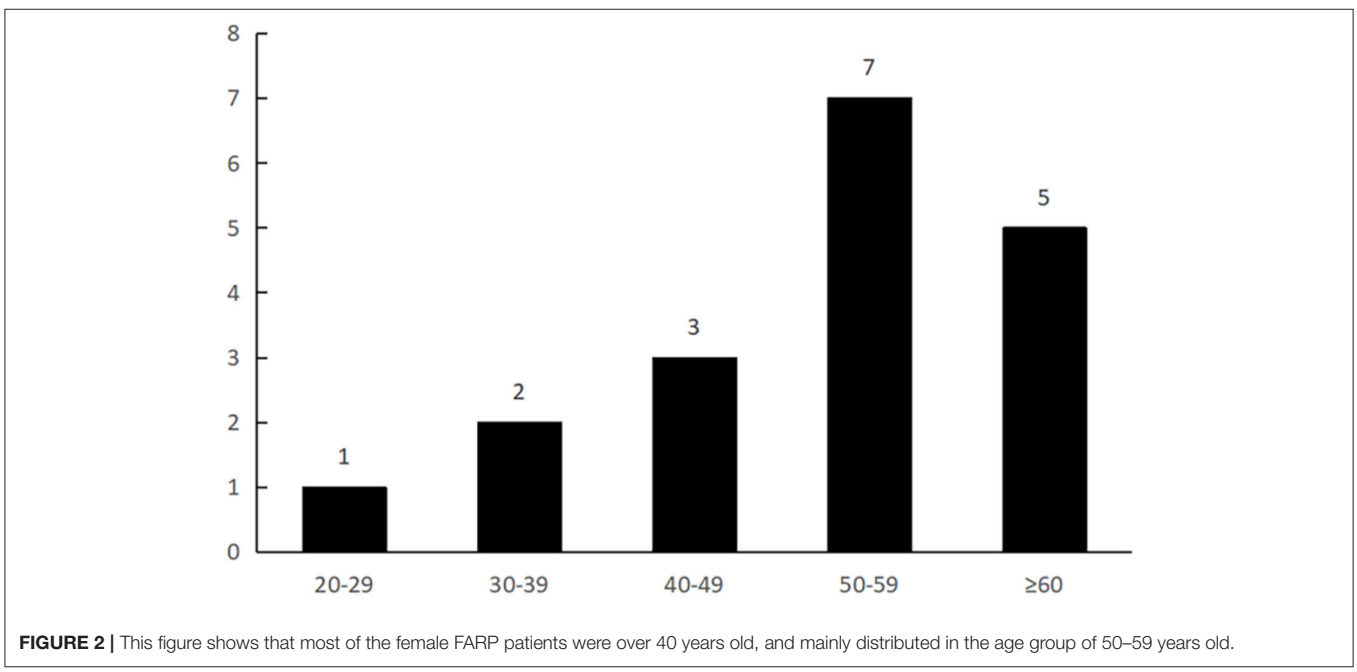

FIGURE 2 | This figure shows that most of the female FARP patients were over 40 years old, and mainly distributed in the age group of 50–59 years old.

TABLE 3 | Latencies and amplitude of each component of the RSEP response following Rectal Stimulation in patients.

	FARP ($n = 23$)	Unspecified-FARP ($n = 21$)	Controls ($n = 23$)	*p*	
				FARP	Unspecified-FARP
P1 latency (ms)	69.20 ± 15.91	68.53 ± 16.13	46.50 ± 5.77	<0.001	<0.001
N1 latency (ms)	112.28 ± 29.35	113.73 ± 30.06	101.32 ± 17.78	0.199	0.155
P2 latency (ms)	168.64 ± 44.57	172.67 ± 44.58	193.70 ± 34.42	0.056	0.133
P1/N1 amplitude (uV)	3.66 ± 2.10	3.47 ± 1.75	4.67 ± 2.35	0.049	0.030
N1/P2 amplitude (uV)	4.25 ± 3.07	4.29 ± 3.08	6.57 ± 2.78	0.010	0.010

Values are given as mean (±SD).

TABLE 4 | Anorectal manometric profiles in patients and healthy controls.

	FARP ($n = 15$)	Unspecified-FARP ($n = 13$)	Controls ($n = 23$)	*p*	
				FARP	Unspecified-FARP
Resting pressure	57.93 ± 16.38	53.54 ± 12.21	59.00 ± 6.52	0.836	0.328
Squeeze pressure	107.37 ± 32.53	103.23 ± 32.56	135.61 ± 19.13	0.009	0.004
Sphincter length	3.23 ± 0.20	3.08 ± 0.28	3.29 ± 0.13	0.145	0.974
Anal sphincter pressureduring straining	30.33 ± 13.67	29.69 ± 14.53	42.13 ± 7.85	0.007	0.012
First sensation	28.67 ± 16.42	29.23 ± 17.54	22.17 ± 7.36	0.442	0.494
Urge	71.33 ± 25.32	71.54 ± 26.09	74.35 ± 16.47	0.497	0.494
Maximum tolerable volume	121.33 ± 48.24	119.23 ± 51.71	185.22 ± 45.61	<0.001	<0.001
Rectal pressure during straining	30.87 ± 17.74	27.15 ± 14.76	55.43 ± 13.67	<0.001	<0.001

Values are given as mean (± SD).

shown in **Table 5**. Among the 15 patients, patients with levator ani syndrome and proctalgia fugax have significantly higher anal resting pressure (93 and 80 mmHg, respectively).

In terms of the rectal sensory function, rectal maximum tolerable volume was reduced in the FARP patients in comparison with the healthy controls (121.33 ± 48.24 vs. 185.22 ± 45.61, $P < 0.01$).There was no significant difference between the two groups in first sensation threshold or the urge to defecate threshold (**Table 4**).

RAIR was present in all patients and all controls. The mean volume of rectal distention needed to initiate RAIR in the healthy controls was 12.63 ± 5.03 mL, while patients needed larger volumes to elicit RAIR (15.33 ± 6.40; $P < 0.05$).

7/15 patients who received ARM showed abnormal defecation reflex, including the patient with levator ani syndrome. However, only one of the healthy controls showed abnormal defecation reflex. There is a significant difference between the two groups ($P < 0.01$). Cough reflex was normal in all subjects.

The Correlation Between RSEP and Anorectal Manometry

The Pearson's correlation analysis showed that resting pressure of the anal sphincter of FARP patients was positively correlated with the amplitude of P1/N1 ($r = 0.537$, $P = 0.039$) (**Figure 3A**)and the amplitude of N1/P2 ($r = 0.520$, $P = 0.047$) (**Figure 3B**). There was no significant correlation between any of RSEP parameters and rectal inhibitory reflex (RAIR) or any of rectal sensory parameters (the first sensation, urge, or maximum tolerance). In addition, we analyzed the relationship between RSEP and ARM parameters in patients with unspecified-FARP and found that there was a significant positive correlation between resting pressure and amplitude of N1/P2 ($r = 0.634$, $P = 0.020$) (**Figure 3C**). There was no significant correlation between the parameters of the two examinations in healthy control group.

DISCUSSION

Chronic anorectal pain is a refractory functional gastrointestinal disease. The Rome Classification provides well-defined diagnostic criteria for functional anorectal pain. However, it is still unclear of the pathophysiology of FARP and a huge challenge to treat FARP, though some advances in the treatment of functional anorectal pain have made recently (21–24). The pathophysiology of functional gastrointestinal diseases is closely related to the neuronal interactions between the brain and gut. RSEP provided objective data regarding the integrity of the afferent pathways. In this study, we found that latency of P1 of RSEP in the FARP patients were significantly longer and the amplitude of each waves were significantly decreased when compared to healthy controls.

ARM is widely used for the detection of abnormalities of sphincter function and rectoanal coordination (25). We found that the anorectal pressure during squeeze or strain, maximum tolerable volume to rectal distension were significantly reduced in 15 FARP patients in this study. After analyzing data of the 15 FARP patients, we found that different subtypes of FARP

TABLE 5 | The data of 15 FARP patients who completed the two examinations.

Diagnosis	Gender	Age	P1 (ms)	N1 (ms)	P2 (ms)	P1/NI (uV)	N1/P2 (uV)	Resting pressure (mmHg)	Squeeze pressure (mmHg)	Sphincter length (cm)	Anal sphincter pressure during straining (mmHg)	Rectal pressure during straining (mmHg)	First sensation (ml)	Urge (ml)	Maximum tolerable volume (ml)	Defecation reflex	RAIR (ml)
Unspecified-FARP	F	33	69.0	110.4	127.2	2.3	1.5	43	80	3	37	18	20	80	130	Abn.	10
	F	76	58.4	84.8	134.0	3.1	3.7	52	88	3.1	12	8	20	70	100	Abn.	10
	F	54	63.6	87.8	182.0	4.3	7.8	66	80	3.1	42	32	20	30	40	Norm.	10
	F	54	55.6	73.0	146.6	2.8	3.2	56	87	3.0	17	12	10	50	130	Abn.	10
	F	53	95.7	167.1	243.9	3.5	5.9	70	104	3.0	47	8	30	80	120	Norm.	20
	F	67	52.8	139.2	189.3	2.4	2.0	52	72	3.1	22	17	20	70	80	Norm.	20
	F	55	80.7	131.1	210.9	4.2	3.2	42	90	3.2	13	20	20	80	130	Abn.	20
	F	48	63.6	83.1	121.2	2.6	5.7	65	147	3.4	43	39	40	80	100	Norm.	30
	M	59	67.8	92.7	136.5	1.3	1.6	53	149	3.3	22	36	20	80	180	Abn.	20
	F	72	104.4	158.4	219.0	3.8	2.0	38	104	3.3	12	36	20	50	80	Norm.	20
	M	58	34.4	58.4	76.2	2.0	1.7	66	156	3.7	35	51	30	50	120	Norm.	10
	F	43	60.3	112.2	170.4	2.4	2.8	62	131	3.3	55	50	70	140	250	Norm.	10
	F	62	75.3	110.4	132.9	1.1	1.4	31	53	3.1	29	26	60	70	90	Norm.	10
LAS	M	55	65.0	83.4	131.0	9.3	6.8	93	148	3.4	30	40	20	50	130	Abn.	20
PF	F	52	87.6	110.7	121.8	2.0	0.96	80	121	3.4	39	70	30	90	140	Abn.	10

LAS, levator ani syndrome; PF, proctalgia fugax; F, female; M, male; Norm., normal; Abn., abnormal.

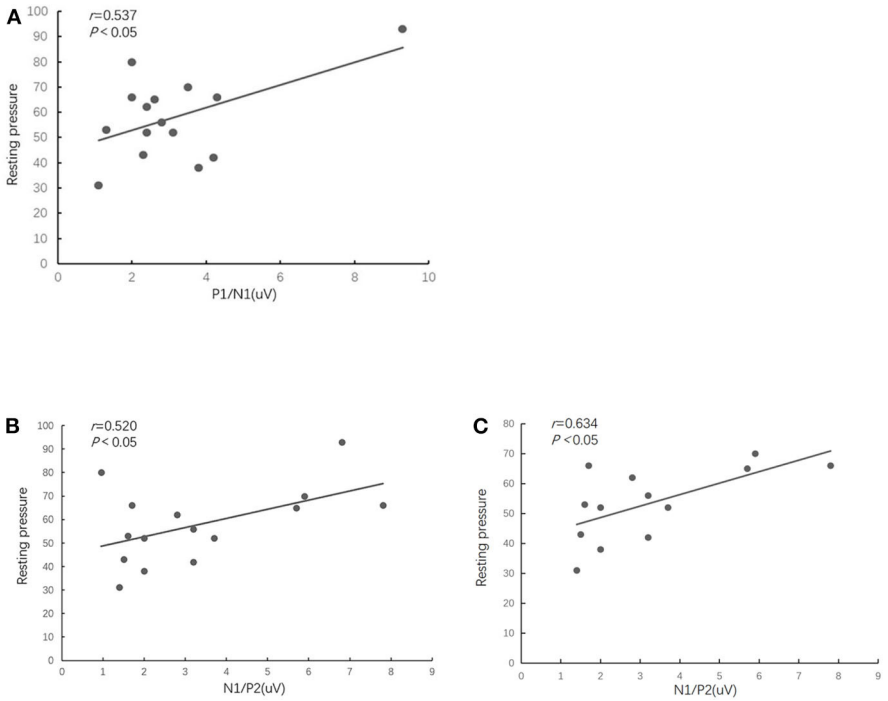

FIGURE 3 | The scatterplot shows that the FARP patients' resting pressure of the anal sphincter was positively correlated with the amplitude of P1/N1 **(A)** and the amplitude of N1/P2 of RSEP **(B)**. There was a significant positive correlation between resting pressure and amplitude of N1/P2 in patients with unspecified-FARP **(C)**.

had different resting pressure characteristics, For example, 2/13 unspecified-FARP showed lower resting pressure while other unspecified-FARP FARP patients haven't change. But the PF and LAS patients showed higher anal resting pressure and abnormal anal relaxation reflex, which was consistent with the previous studies (8, 26), and pain in these patients might be related to the excessive activity of anal sphincter. These patients reported a sensation of downward bloating in their anus and most of them were middle-aged or older women. One possible mechanism might be attributed to pelvic floor muscle dysfunction. This might be closely related to vaginal delivery, age, and chronic constipation. Egorov et al. (27) reported that the pelvic muscle function decreased with age, and tissue elasticity decreased with multiple vaginal deliveries. In our study, 2 female FARP patients had a history of multiple vaginal deliveries. This might also be related to laceration of levator ani caused by natural labor in some women (28). Compared with the healthy controls, patients with FARP have a higher rate of abnormal defecation reflex, which seems to suggest that anorectal discordance may be one of the mechanisms leading to FARP.

Somatosensory EPs (SEPs) has advantages over other brain imaging techniques given its relative portability, inexpensiveness, availability. It can be used to evaluate the somatosensory pathway at the peripheral, spinal, cortical, and subcortical level (16). By stimulating the rectum and recording the potential changes of neurons in the cerebral cortex one can investigate the nerve transfer function from the rectum to the pelvic floor nerve and then to the spinal cord and the cerebral cortex. RSEP has been carried out in healthy people (29) and the fluctuation range of the data in the healthy control group in our study was basically the same as the above study. The RSEP has been widely used to evaluate the visceral sensitivity mechanism in IBS. Chan et al. found that compared to healthy subjects, irritable bowel syndrome patients demonstrated higher prevalence of cerebral evoked potential early peaks postprandially, and uniformly shorter cerebral evoked potential latencies both before and after feeding (30). Conversely, the prolongation of SEP latency has been reported in fecal incontinence and constipation (31, 32). This is thought to be related to receptor dysfunction, reduced activation of afferent nerves, or slowed peripheral nerve conduction (28). In our study, the FARP patients showed a longer latency of P1 in the RSEP. This finding once again demonstrated the impairment of the afferent pathway in FARP. The mechanism might be similar to fecal incontinence and constipation.

Conscious perception implies sensory connectivity between the rectum and the brain (33). Sensory threshold to rectal distention is also an important indicator of the rectal-brain afferent pathway. Törnblomd et al. compared the rectal sensory thresholds between IBS patients and healthy people, and found that the sensory thresholds in IBS patients were decreased (34). The increase of rectal threshold is a manifestation of rectal hyposensitivity, which is closely related to the disorder of the hindgut function, and usually manifested as fecal incontinence and constipation (35). The rectal sensory function has not been investigated in FARP. In our study, the FARP patients showed lower maximum tolerance threshold. Although the sensory

threshold level in the ARM test can reflect the state of rectal sensory function to a certain extent, it has higher requirements on the cooperation degree and cognition of the test, and there may be some subjective deviations as well. In contrast, the RSEP is a more sensitive detection method that responds to the sensory pathways. The correlation between the resting pressure of the anal sphincter and the amplitude of the RSEP implied that there may be a relationship between anal sphincter pressure and neuropathy. Which still remains to be further studied.

The RAIR is a phenomenon in which the anal internal sphincter is temporarily relaxed due to the transient distension of the rectum. It plays an important role in bowel control and defecation (36). Studies have shown that the presence of RAIR is unrelated to the integrity of spinal cord and brain nerve centers, but requires a complete intramural pathway (37). Beuret-blanquart et al. have shown that the RAIR reflex appears to be controlled by autonomic neural pathways, especially the parasympathetic nervous system (38, 39). In our study, RAIR was present in 15 FARP patients after ARM, although FARP patients need larger volumes to elicit RAIR, which may indicate the integrity of intramural pathway in these patients. The difference in eliciting volume may be related to rectal compliance and sensory function abnormalities.

The limitations of our study include the small sample size and a comparative study among different subtypes could not be performed. Also, in this study, we didn't evaluat efferent pathways in FARP patients, and also deserves further study.

In conclusion, rectal sensory evoked potential is safe and well-tolerated and appears to be a useful technique for the detection of neuropathy, the test can provide an objective evidence for neuropathy and a new dimension toward our understanding of the mechanisms of FARP.

DATA AVAILABILITY STATEMENT

The raw data supporting the conclusions of this article will be made available by the authors, without undue reservation.

ETHICS STATEMENT

The studies involving human participants were reviewed and approved by Ethics Committee of Nanjing Hospital of Chinese Medicine. The patients/participants provided their written informed consent to participate in this study.

AUTHOR CONTRIBUTIONS

MN and BJ conceived and designed research. QiZ and YL conducted research and wrote the initial paper. QioZ, YZ, and SW collected date. MN revised the paper and had primary responsibility for final content. All authors read and approved the final manuscript.

FUNDING

The work described in this paper was supported by grants from Jiangsu Provincial Key Research and Development Program funded under the Science and Technology Department of Jiangsu Province (No. BE2018612) and Jiangsu Health Department Youth Talent Support Program funded under the Department of Health of Jiangsu Province (No. SQWR-201701).

REFERENCES

1. Rao SS, Bharucha AE, Chiarioni G, Felt-Bersma R, Knowles C, Malcolm A, et al. Functional anorectal disorders. *Gastroenterology*. (2016) 150:1430–42. doi: 10.1053/j.gastro.2016.02.009
2. Simren M, Palsson OS, Whitehead WE. Update on rome IV criteria for colorectal disorders: implications for clinical practice. *Curr Gastroenterol Rep*. (2017) 19:15. doi: 10.1007/s11894-017-0554-0
3. Drossman DA, Hasler WL. Rome IV—functional GI disorders: disorders of gut-brain interaction. *Gastroenterology*. (2016) 150:1257–61. doi: 10.1053/j.gastro.2016.03.035
4. Bharucha AE, Lee TH. Anorectal and pelvic pain. *Mayo Clin Proc*. (2016) 91:1471–86. doi: 10.1016/j.mayocp.2016.08.011
5. Drossman DA, Li Z, Andruzzi E, Temple RD, Talley NJ, Thompson WG, et al. U.S. householder survey of functional gastrointestinal disorders. Prevalence, sociodemography, and health impact. *Dig Dis Sci*. (1993) 38:1569–80. doi: 10.1007/BF01303162
6. Chiarioni G, Nardo A, Vantini I, Romito A, Whitehead WE. Biofeedback is superior to electrogalvanic stimulation and massage for treatment of levator ani syndrome. *Gastroenterology*. (2010) 138:1321–9. doi: 10.1053/j.gastro.2009.12.040
7. Grimaud J-C, Bouvier M, Naudy B, Guien C, Salducci J. Manometric and radiologic investigations and biofeedback treatment of chronic idiopathic anal pain. *Dis Colon Rectum*. (1991) 34:690–5. doi: 10.1007/BF02050352
8. Lascano AM, Lalive PH, Hardmeier M, Fuhr P, Seeck M. Clinical evoked potentials in neurology: a review of techniques and indications. *Neurol Neurosurg Psychiatry*. (2017) V88N8:688–96. doi: 10.1136/jnnp-2016-314791
9. Remes-Troche JM, Tantiphlachiva K, Attaluri A, Valestin J, Yamada T, Hamdy S, et al. A bi-directional assessment of the human brain-anorectal axis. *Neurogastroenterol Motil*. (2011) 23:240–8. doi: 10.1111/j.1365-2982.2010.01619.x
10. Greenwood-Van Meerveld B, Johnson AC, Grundy D. Gastrointestinal physiology and function. *Handb Exp Pharmacol*. (2017) 239:1–16. doi: 10.1007/164_2016_118
11. Mertz, HR. Overview of functional gastrointestinal disorders: dysfunction of the brain-gut axis. *Gastroenterol Clin North Am*. (2003) 32:463–76. doi: 10.1016/s0889-8553(03)00019-0
12. Mayer EA, Gebhart FG. Basic and clinical aspects of visceral hyperalgesia. *Gastroenterology*. (1994) 107:271–93. doi: 10.1016/0016-5085(94)90086-8
13. Camilleri M. Testing the sensitivity hypothesis in practice: tools and methods, assumptions and pitfalls. *Gut*. (2002) 51(Suppl. 1):i34–40. doi: 10.1136/gut.51.suppl_1.i34
14. Barbara G, Cremon C, De Giorgio R, Dothel G, Zecchi L, Bellacosa L, et al. Mechanisms underlying visceral hypersensitivity in irritable bowel syndrome. *Curr Gastroenterol Rep*. (2011) 13:308–15. doi: 10.1007/s11894-011-0195-7
15. Delvaux M. Role of visceral sensitivity in the pathophysiology of irritable bowel syndrome. *Gut*. (2002) 51(Suppl. 1):i67–71. doi: 10.1136/gut.51.suppl_1.i67
16. Mertz H. Review article: visceral hypersensitivity. *Aliment Pharmacol Ther*. (2003) 17:623–33. doi: 10.1046/j.1365-2036.2003.01447.x
17. Ridding MC, Ziemann U. Determinants of the induction of cortical plasticity by non-invasive brain stimulation in healthy subjects. *J Physiol*. (2010) 588:2291–304. doi: 10.1113/jphysiol.2010.190314

18. Hobday DI, Hobson AR, Sarkar S, Furlong PL, Thompson DG, Aziz Q. Cortical processing of human gut sensation: an evoked potential study. *Am J Physiol Gastrointest Liver Physiol*. (2002) 283:G335–9. doi: 10.1152/ajpgi.00230.2001
19. Otto SD, Clewing JM, Gröne J, Buhr HJ, Kroesen AJ. Repeatability of anorectal manometry in healthy volunteers and patients. *J Surg Res*. (2013) 185:e85–92. doi: 10.1016/j.jss.2013.06.008
20. Chaliha C, Sultan AH, Emmanuel AV. Normal ranges for anorectal manometry and sensation in women of reproductive age. *Colorectal Dis*. (2007) 9:839–44. doi: 10.1111/j.1463-1318.2007.01212.x
21. Ooijevaar RE, Felt-Bersma RJF, Han-Geurts IJ, van Reijn D, Vollebregt PF, Molenaar CBH. Botox treatment in patients with chronic functional anorectal pain: experiences of a tertiary referral proctology clinic. *Tech Coloproctol*. (2019) 23:239–44. doi: 10.1007/s10151-019-01945-8
22. Rongqing G, Yafei W, Zhimin W, Feng L, Yuantao L, Xinhua C, et al. Treatment outcome of acute sacral nerve stimulation in functional anorectal pain. *Pain Pract*. (2019) 19:390–6. doi: 10.1111/papr.12751
23. Takano S, Arakawa H. Bilateral posterior tibial nerve stimulation for functional anorectal pain–short term outcome. *Int J Colorectal Dis*. (2016) 31:1053–4. doi: 10.1007/s00384-015-2380-x
24. Bharucha AE, Trabuco E. Functional and chronic anorectal and pelvic disorders. *Gastroenterol Clin North Am*. (2008) 37:685–96. doi: 10.1016/j.gtc.2008.06.002
25. Carrington EV, Scott SM, Bharucha A, Mion F, Remes-Troche JM, Malcolm A, et al. Expert consensus document: advances in the evaluation of anorectal function. *Nat Rev Gastroenterol Hepatol*. (2018) 15:309–23. doi: 10.1038/nrgastro.2018.27
26. Eckardt VF, Dodt O, Kanzler G, Bernhard G. Anorectal function and morphology in patients with sporadic proctalgia fugax. *Dis Colon Rectum*. (1996) 39:755–62. doi: 10.1007/bf02054440
27. Egorov V, Lucente V, van Raalte H, Sarvazyan, N. Biomechanical mapping of the female pelvic floor: changes with age, parity and weight. *Pelviperineology*. (2019) 38:3–11.
28. van Delft K, Sultan AH, Thakar R, Schwertner-Tiepelmann N, Kluivers K. The relationship between postpartum levator ani muscle avulsion and signs and symptoms of pelvic floor dysfunction. *BJOG*. (2014) 121:1164–72. doi: 10.1111/1471-0528.12666
29. Harris ML, Hobson AR, Hamdy S, Thompson DG, Akkermans LM, Aziz Q. Neurophysiological evaluation of healthy human anorectal sensation. *Am J Physiol Gastrointest Liver Physiol*. (2006) 291:G950–8. doi: 10.1152/ajpgi.00010.2006
30. Chan YK, Herkes GK, Badcock C, Evans PR, Bennett E, Kellow JE. Alterations in cerebral potentials evoked by rectal distension in irritable bowel syndrome. *Am J Gastroenterol*. (2001) 96:2413–7. doi: 10.1111/j.1572-0241.2001.04088.x
31. Burgell RE, Lelic D, Carrington EV, Lunniss PJ, Olesen SS, Surguy S, et al. Assessment of rectal afferent neuronal function and brain activity in patients with constipation and rectal hyposensitivity. *Neurogastroenterol Motil*. (2013) 25:260–7. doi: 10.1111/nmo.12047
32. Giani I, Novelli E, Martina S, Clerico G, Luc AR, Trompetto M, et al. The effect of sacral nerve modulation on cerebral evoked potential latency in fecal incontinence and constipation. *Ann Surg*. (2011) 254:90–6. doi: 10.1097/SLA.0b013e3182196ff4
33. Knowles CH. Human studies of anorectal sensory function. *Ir J Med Sci*. (2018) 187:1143–47. doi: 10.1007/s11845-018-1847-5
34. Törnblom H, Van Oudenhove L, Tack J, Simrén M. Interaction between preprandial and postprandial rectal sensory and motor abnormalities in IBS. *Gut*. (2014) 63:1441–9. doi: 10.1136/gutjnl-2013-305853
35. Burgell RE, Scott SM. Rectal hyposensitivity. *J Neurogastroenterol Motil*. (2012) 18:373–84. doi: 10.5056/jnm.2012.18.4.373
36. Sangwan YP, Solla JA. Internal anal sphincter: advances and insights. *Dis Colon Rectum*. (1998) 41:1297–311. doi: 10.1007/bf02258232
37. Meunier P, Mollard P. Control of the internal anal sphincter (manometric study with human subjects). *Pflugers Arch*. (1977) 370:233–9. doi: 10.1007/bf00585532
38. Carlstedt A, Nordgren S, Fasth S, Appelgren L, Hultén L. Sympathetic nervous influence on the internal anal sphincter and rectum in man. *Int J Colorectal Dis*. (1988) 3:90–95. doi: 10.1007/bf01645312
39. Beuret-Blanquart F, Weber J, Gouverneur JP, Demangeon S, Denis P. Colonic transit time and anorectal manometric anomalies in 19 patients with complete transection of the spinal cord. *J Auton Nerv Syst*. (1990) 30:199–207. doi: 10.1016/0165-1838(90)90251-d

Conflict of Interest: The authors declare that the research was conducted in the absence of any commercial or financial relationships that could be construed as a potential conflict of interest.

frontiers in Neuroscience

BRIEF RESEARCH REPORT
published: 08 December 2020
doi: 10.3389/fnins.2020.594696

Management of Intractable Pain in Patients With Implanted Spinal Cord Stimulation Devices During the COVID-19 Pandemic Using a Remote and Wireless Programming System

Yang Lu[1,2†], Duo Xie[2†], Xiaolei Zhang[1], Sheng Dong[1], Huifang Zhang[1], Beibei Yu[1], Guihuai Wang[1], James Jin Wang[1]* and Luming Li[2,3,4,5]**

[1] Department of Neurosurgery, Beijing Tsinghua Changgung Hospital, School of Clinical Medicine, Tsinghua University, Beijing, China, [2] National Engineering Laboratory for Neuromodulation, School of Aerospace Engineering, Tsinghua University, Beijing, China, [3] Precision Medicine and Healthcare Research Center, Tsinghua-Berkeley Shenzhen Institute, Tsinghua University, Shenzhen, China, [4] IDG/McGovern Institute for Brain Research at Tsinghua University, Beijing, China, [5] Institute of Epilepsy, Beijing Institute for Brain Disorders, Beijing, China

As COVID-19 rampages throughout the world and has a major impact on the healthcare system, non-emergency medical procedures have nearly come to a halt due to appropriate resource reallocation. However, pain never stops, particularly for patients with chronic intractable pain and implanted spinal cord stimulation (SCS) devices. The isolation required to fight this pandemic makes it impossible for such patients to adjust the parameters or configuration of the device on site. Although telemedicine has shown a great effect in many healthcare scenarios, there have been fewer applications of such technology focusing on the interaction with implanted devices. Here, we introduce the first remote and wireless programming system that enables healthcare providers to perform video-based real-time programming and palliative medicine for pain patients with a SCS implant. During the COVID-19 pandemic from January 23, 2020, the date of lockdown of Wuhan, to April 30, 2020, 34 sessions of remote programming were conducted with 16 patients. Thirteen of the 16 patients required programming for parameter optimization. Improvement was achieved with programming adjustment in 12 of 13 (92.3%) cases. Eleven of the 16 (68.8%) patients reported that the system was user-friendly and met their needs. Five patients complained of an unstable connection resulting from the low network speed initially, and three of these patients solved this problem. In summary, we demonstrated that a remote wireless programming system can deliver safe and effective programming operations of implantable SCS device, thereby providing palliative care of value to the most vulnerable chronic pain patients during a pandemic.

Clinical Trial Registration: www.clinicaltrials.gov, identifier NCT 03858790.

Keywords: chronic intractable pain, spinal cord stimulation, remote programming, telemedicine, COVID-19

OPEN ACCESS

Edited by:
Winfried Mayr,
Medical University of Vienna, Austria

Reviewed by:
Fabricio Lima Brasil,
Santos Dumont Institute (ISD), Brazil
Danilo Pani,
University of Cagliari, Italy

***Correspondence:**
Guihuai Wang
guihuai_wang@163.com
James Jin Wang
wja01068@btch.edu.cn
Luming Li
lilm@mail.tsinghua.edu.cn

† These authors have contributed equally to this work

Specialty section:
This article was submitted to Neuroprosthetics, a section of the journal Frontiers in Neuroscience

Received: *10 September 2020*
Accepted: *16 November 2020*
Published: *08 December 2020*

Citation:
Lu Y, Xie D, Zhang X, Dong S, Zhang H, Yu B, Wang G, Wang JJ and Li L (2020) Management of Intractable Pain in Patients With Implanted Spinal Cord Stimulation Devices During the COVID-19 Pandemic Using a Remote and Wireless Programming System. Front. Neurosci. 14:594696. doi: 10.3389/fnins.2020.594696

INTRODUCTION

The world has changed rapidly due to the disastrous Coronavirus Disease 2019 (COVID-19) pandemic. By the end of July 2020, there were over 19 million confirmed cases of infection and 712,000 deaths due to COVID-19 worldwide. Many countries have issued strict isolation measures or have at least advocated "social distancing" in people's daily lives. Governments and medical providers have had to reallocate labor and material resources to deal with this abrupt emergency. Thus, elective operations/therapies and non-emergency medical procedures have nearly all come to a halt in most medical centers. Patients are also avoiding visiting medical facilities that may be considered a potential source of infection (Keesara et al., 2020). Consequently, some medical needs could be delayed and not met. For patients with demands that cannot be delayed and are impossible to fulfill with the medical resources on site because of isolation protocols or resource limitations, telemedicine has offered an alternative solution (Keesara et al., 2020).

Telemedicine has gradually been adopted by patients over the last decade (Adamse et al., 2018). During the current COVID-19 pandemic, the demand for treatment at a distance from healthcare providers surged essentially overnight (Calton et al., 2020; Humphreys et al., 2020). These changed conditions have boosted reform of the healthcare system. In response, the Chinese government launched a series of policies to support the development of telemedicine and "cloud hospitals." In March 2020, the United States government announced that telemedicine services would be reimbursed by the Medicare and Drug Enforcement Administration, who allowed the prescription of controlled medicine via telemedicine (ATA, 2020).

In most pain management settings, telemedicine has been used in the form of video consultation, which mainly focuses on complaints that can be orally solved, such as palliative care and self-management skills. Some reviews have identified small to moderate reductions in pain, disability, and psychological symptoms in intervention groups applying telemedicine when compared with the control (including standard pain care or waitlist control) (Buhrman et al., 2016; Mariano et al., 2019). However, no therapeutic difference was found when compared to the active control (such as on-site therapies) (Mariano et al., 2019). Remotely delivered physical exercise interventions have also been proposed to reduce pain in patients as a substitute for the usual care (Adamse et al., 2018). However, for addressing more specific demands in a complex situation such as for a patient with chronic intractable pain who has a spinal cord stimulation (SCS) implant, video-based consultation alone is not sufficient. These patients usually require several programming sessions (mostly over 3 months) to achieve a stable therapeutic effect after implantation. When people with chronic pain are deprived of appropriate assessment and treatment, their condition can worsen significantly. Lead migration, scar-related impedance change, and habituation to the therapy require further programming and regular adjustments (North et al., 2005; Kumar et al., 2008). Considering that patients with chronic pain usually suffer from depression and anxiety, further negative emotions brought on by COVID-19 could exacerbate the pain (Eccleston et al., 2020). These unmet demands require multi-dimensional interactions and teleprogramming of the stimulator by distance.

Here, we introduce the first time remote and wireless programming system for a SCS implant, which enables chronic pain patients to receive timely adjustment of parameters and configurations with only a smartphone and access to a 4G/5G/WiFi network at home.

MATERIALS AND METHODS

Participants

The patients in this study were recruited for a multi-center clinical trial (Lu et al., 2020). Patients with chronic intractable pain were recruited at our center from January 2019 to December 2019. Patients were screened from electronic medical records and then approached to complete the verification of the inclusion/exclusion criteria and provided consent. The inclusion criteria were the following: (1) chronic intractable pain that has lasted for at least 3 months and is refractory to the conservative therapies, including oral medications, nerve block, epidural corticosteroids, physical and psychological rehabilitation therapy, and chiropractic care; (2) aged over 18; (3) good compliance and ability to complete post-operative follow-up; and (4) understanding of the method and willingness to sign the informed consent. The exclusion criteria were the following: (1) pregnancy, breast feeding, plan to be pregnant or unwilling to use contraceptive methods; (2) bleeding complications or coagulation disorders; (3) severe mental or cognitive disorders, leading to inability to cooperate during surgery and post-operative programming; (4) life expectancy of less than one-year; (5) need for therapy or examination that could not be provided with an implanted pulse generator (IPG), such as magnetic resonance imaging and thermo-therapy; and (6) other inappropriate situations that were determined by the investigators.

All patients were implanted with IPG successfully, including 10 males and six females, with an average age of 60.1 ± 9.9 years (range 39–74 years old). None of the patients had a device infection except for one patient who complained of red skin at the IPG incision site but had no fever or pain. Two female patients had mild discomfort at the IPG site, but no further surgical treatment was required. There were three cases of spinal cord injury, two cases of peripheral nerve injury, two cases of brachial plexus avulsion, two cases of failed back surgery syndrome, and one case each of complex regional pain syndrome, neuropathic pain, amputated limb pain, phantom limb pain, failed cervical surgery syndrome, syringomyelia, and lower limb ischemic pain in this study.

Intervention

In accordance with standard clinical practice (Kapural et al., 2015), patients first underwent a screening phase of SCS (with a percutaneous lead or paddle lead) lasting up to 10–14 days with an external stimulator to determine the short-term response. Patients that experienced 50% or greater pain reduction based on the visual analog scale from baseline were then eligible to proceed to permanent implantation.

Stimulation parameters were adjusted to optimally overlap paresthesia with the region of the pain area when the patients left the hospital (mean ± SD of the minimum and maximum programmed parameters: frequency, 70.2 ± 30.0 Hz; amplitude, 4.6 ± 2.8 mA; and pulse width, 310 ± 148 μs). Subsequently, intraoperative paresthesia testing and associated device programming were performed in the hospital, as needed based on patient feedback in standard clinic visits. Oral analgesics were stabilized from 28 days before enrollment until activation of the implanted SCS system, in addition to perioperative analgesics. Adjustments were then allowed under the guidance of the attending physician as medically necessary.

Introduction of the Remote Programming System

Based on our previously developed telemedicine system (Chen et al., 2014, 2015c), the SCS remote programming system, called the PINS remote programming system, was developed in 2019. The PINS remote programming system can provide multi-dimensional interaction between healthcare providers and chronic pain patients through a computer with PINS remote programming software installed on the physician side, a smartphone with the PINS remote programming application and patient's external programmer on the IPG patient side, and a 4G/5G/WiFi network with an upload speed of no less than 1 MB.

Before the connection, the smartphone and the external programmer-activated IPG were paired. Then, according to the patients' requests or previously stated reservation, the healthcare provider logged into the programming system and established the connection with the patient's smartphone after activation of the IPG with patient's external programmer. The smartphone could receive bidirectional, high-definition, and real-time video signals and programming instructions using the public network. The connections between the smartphone and IPG are generated via Bluetooth. Finally, the IPG could work with the physician's instructions (**Figure 1A**).

To introduce briefly, the remote programming system consists of three modules: the patient management module, teleprogram module, and video communication module. More details can be found in our patents (Chen et al., 2015a,b,d).

The patient management module was designed to build a stable connection between patients and physicians. A list of the patients and their status is shown on the webpage of the patient management module. The physician could only have access to his or her own patients. Once a patient logs into the system. They send their connection request to the physician. The physician could then choose to accept the request and establish a logical connection with the patient. At the same time, the management module would restrict the physician's permission to connect with other patients.

The teleprogram module was designed to provide a platform for SCS remote programming. After a patient is connected to the physician, the patient listens to programming instructions from the server station, which were sent by the physician from the teleprogram module. A telemetry command will then be sent before the programming begins to ensure that all of the hardware or information links are in place. The physician's computer client could store the patient's medical records, electrode images, and previous programming records (**Figure 1B**). Healthcare providers can easily implement the adjustments of stimulation parameters (including contact mapping, selection of frequency, amplitude, pulse width, etc.), battery status check, electrode impedance check, and device troubleshooting on the teleprogram module. The programming records of every session will be stored in the physician's client, uploaded to the database, and sent back to patients.

A video-recording function was developed based on the Web Real-Time Communication (WebRTC) technology. An open-source project of the STUN protocol was built to support the main signaling service, including taking advantage of the TURN protocol to penetrate firewalls if direct P2P connectivity cannot be established.

Furthermore, the patient's client was designed as a smartphone terminal aimed at assisting patients in interaction with physicians, symptom management, and setting new adjustment parameters. With this client, patient could choose a physician and make a reservation for the remote programming service at home. Medical history, daily outcome reports, and uploaded imaging examinations of the patients are helpful in the management of symptoms and communication with physicians. As for the patients, the only potential restriction is an unstable network. The smartphone app will initially test the network and pair the programmer, and it then alerts the patients if an unstable connection occurs or pairing fails.

Technological Considerations

The top two concerns of the remote programming are safety and confidentiality. Several appropriate data transmission protection technologies were adopted to ensure the security and confidentiality of communication, such as Hypertext Transfer Protocol Secure (HTTPS) between server and clients, bidirectional identity authentication technology based on digital certificate and short-distance wireless transmission with Bluetooth data transmission technology. The telemedicine system integrates multi-level data isolation and validation procedures without losing real-time performance. Transmission of programming instructions is encrypted between the mutual identity authenticated servers and clients. Also, safety protection mechanisms include functions of automatic instruction back-up, offline parameter recovery, and emergency stimulator shutdown. All of them are available and can be controlled by either programmer or patient. Furthermore, the notes from each encounter can be uploaded to a cloud-based database and can be accessed by any practitioner from any specialty at any time.

However, accidental disconnection resulted from unstable network, or inappropriate amplitude selection may cause severe adverse event. Unlike face-to-face interaction in hospital in which physicians could solve the problem immediately, we suggest at least one caregiver could keep accompany with the patient during the programming process. All patients and at least one caregiver should be made familiar with the remote programming and be able to cooperate with investigators to complete the whole procedure before leaving the hospital. Also, an incremental increase of the amplitude is recommended. In case any discomfort of patient or disconnection happens, the caregiver

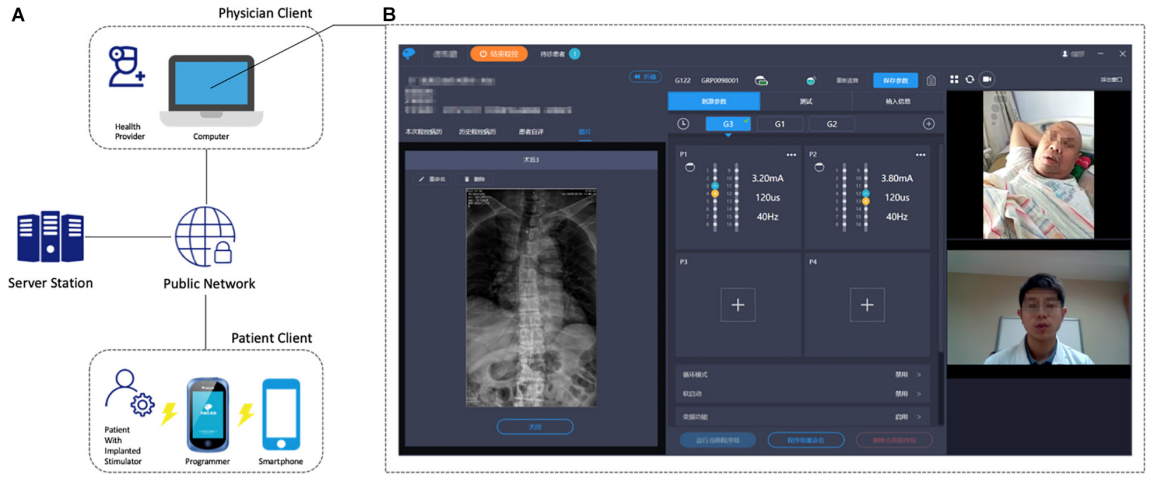

FIGURE 1 | (A) General architecture of the remote programming system. **(B)** Physician client illustration with the real-time video consultation (right), parameter and configuration adjustment (middle), and the patient's medical record (left). The patient sent a WebRTC request to the signaling server, which is subsequently relayed to the physician client. If an online physician replies to the WebRTC request, a P2P connection will be established, and video stream is facilitated between the two clients.

could restore the pre-programming settings with "one key recovery" or even shutdown the stimulator as quickly as possible.

RESULTS

The system was launched in 2019, and over 20 patients received this remote-programming-equipped G122R SCS (PINS Medical, Beijing) implantation at our center. From January 23, 2020, the date of lockdown of Wuhan, China, to April 30, 2020, 34 sessions for 16 patients with remote programming were implemented (**Table 1**). All of the programming practices were performed by a single doctor (Yang Lu) at his home or from our hospital in Beijing. The 16 patients underwent a total of 34 remote programming sessions, with an average adjustment frequency of 2.1 times/patient; the average program control time/adjustment was 43.1 ± 15 min (13–90 min) according to the records of the database.

Our cohort has different types of SCS indications. In contrast to the most common indication for SCS in United States is failed back surgery syndrome (FBSS), spinal-cord-injury-related pain is the most common indication in China. This suggests that patients that undergone more remote programming episodes likely underwent an SCS operation more recently. However, one patient with complex regional pain syndrome completed the remote programming five times owing to the poor quality of the internet connection and device failure (abnormal contact impedance).

Given the thorough penetration of smartphones in China, most of the patients could complete the service on their own or with the assistance of caregivers. Even for the four patients over the age of 70 years who do not use smartphones often, caregivers could help them to proceed with the entire remote programming session.

Thirteen of the 16 patients required programming for parameter optimization. This improvement was achieved with programming adjustment in 12 of 13 cases. Two of the 16 patients sought help because of intolerance to the induced paresthesia with a high amplitude. This is a typical dilemma for the patients using traditional low-frequency stimulation, which requires achieving a balance between the therapeutic effect and paresthesia. The last of the 16 patients experienced reddening of the skin near the incision site but no pain or fever. Since there were no clinical signs of infection, a subsequent follow-up was suggested for monitoring.

Eleven of the 16 patients reported that the system was user-friendly and met their needs. Five patients complained of an unstable connection resulting from a low network speed, three of whom solved this problem by changing the hotspot or using a 4G network. The other two patients could not solve this problem owing to limited resources. However, these two patients were able to complete the parameter adjustment with our adamant efforts and many reconnection attempts (over 2 h per patient). No adverse events occurred in the 34 programming sessions.

DISCUSSION

With regard to neuromodulation therapies, such as SCS, deep brain stimulation (DBS), vagal nerve stimulation, and sacral nerve neuromodulation, implantation of the device is only the first step, and post-operative programming is important for achieving long-term curative effect. Previous studies have proposed that remote programming technology could provide a safe, reliable, and efficient programming service for patients with reduced time and financial cost (Zhang et al., 2019, 2020b). This study represents the first introduction of remote programming technology for patients with chronic pain implanted with an SCS device.

Similar to DBS, patients implanted with an SCS device could receive programming in a face-to-face fashion or adjust the parameters by themselves at home within a limited range preset by the physicians. Self-adjustment has

proved to be feasible and practical, and it significantly reduces the consultation time (Bally et al., 2019). However, this self-adjustment also needs to be performed under the supervision of the treating physicians, and patients cannot deal with a specific contact change or hardware malfunction by themselves. This had led to a huge demand for a remote programming system for these neuromodulation therapies, especially under extreme conditions such as the current COVID-19 pandemic.

For the patients with unsatisfactory post-operative outcomes with traditional parameters or configurations, many novel technologies have been developed in the field of neuromodulation therapies over the last few years, including current-based programming, interleaved programming, fractionated current, variable frequency stimulation, and directional current-steering technologies in DBS (Jia et al., 2017; Wagle Shukla et al., 2017) as well as 10-kHz high-frequency stimulation (Kapural et al., 2015), burst stimulation

TABLE 1 | Characteristics of the 16 patients who received remote programming during the COVID-19 pandemic.

No.	Gender	Age	Diagnosis	Operation date	Programming times	Reason	Outcome	Patient's rating for the remote programming
1	M	62	Periphery nerve injury	2019/11/5	3	Therapeutic effect decrease	Parameters adjustment (little improvement)	User-friendly
2	M	62	CRPS	2019/7/11	5	Therapeutic effect decrease (abnormal impedance of contacts)	Parameters and configuration adjustment (considerate improvement)	Connection unstable (resolved with changed network)
3	F	54	FBSS	2019/12/25	2	Therapeutic effect decrease	Parameters and configuration adjustment (considerate improvement)	User-friendly
4	F	55	Neuropathic pain	2019/12/24	2	Therapeutic effect decrease	Parameters and configuration adjustment (considerate improvement)	User-friendly
5	M	56	Amputated limb pain	2019/12/31	3	Therapeutic effect unstable	Change to sub-threshold stimulation (considerate improvement)	User-friendly
6	M	74	FBSS	2019/8/13	2	Intolerance to the traditional stimulation pattern	Oral comforting with lower amplitude	Connection unstable
7	M	55	Brachial plexus avulsion	2019/5/23	1	Therapeutic effect decrease	Parameters adjustment (no improvement)	Connection unstable (resolved with changed network)
8	M	55	Phantom limb pain	2020/1/3	3	Therapeutic effect decrease	Parameters and configuration adjustment (considerate improvement)	Connection unstable (resolved with changed network)
9	F	70	Spinal cord injury	2019/7/17	3	Therapeutic effect unstable	Parameters and configuration adjustment (some improvement)	User-friendly
10	M	74	Spinal cord injury	2019/7/4	1	Therapeutic effect decrease	Parameters adjustment (little improvement)	Connection unstable
11	F	73	FCSS	2019/10/28	2	Therapeutic effect unstable	Parameters and configuration adjustment (some improvement)	User-friendly
12	F	39	Spinal cord injury	2019/8/13	1	Red incision, without fever or pain	Continuous follow-up	User-friendly
13	M	68	Syringomyelia	2019/7/29	2	Therapeutic effect decrease	Parameters and configuration adjustment (some improvement)	User-friendly
14	M	48	Lower limb ischemic pain	2019/8/6	1	Therapeutic effect decrease	Parameters and configuration adjustment (some improvement)	User-friendly y
15	F	57	Brachial plexus avulsion	2019/7/17	1	Intolerance to the traditional stimulation pattern	Parameters adjustment (little improvement)	User-friendly
16	M	59	Periphery nerve injury	2019/12/9	2	Therapeutic effect decrease	Parameters adjustment (little improvement)	User-friendly

CRPS, complex regional pain syndrome; FBSS, failed back surgery syndrome; FCSS, failed cervical surgery syndrome.

(Ahmed et al., 2018), and high-density stimulation in SCS (De Jaeger et al., 2017). These new paradigms require a deep understanding of the underlying therapies. Some stimulation patterns require several hours to several days to achieve a real and optimal response. There is no doubt that a physician's operation and follow-up are inevitable additions to these patterns. Remote programming enables physicians to switch between different stimulation patterns and observe the therapeutic effect efficiently and conveniently.

Several retrospective studies have explored the effect of the DBS remote programming (Zhang et al., 2020a,b), which showed that over 80% of the patients were satisfied with the remote programming. Evaluation of the patients' symptoms is always a challenge for DBS remote programming. Bradykinesia, tremor, and dyskinesia are easy to follow over video, whereas rigidity is more of a challenge to monitor remotely. In addition, it usually takes longer for the therapeutic effects of DBS to be evident for symptoms such as dyskinesia and tremors. By contrast, patients with pain could receive a real-time response to the stimulation in most cases. In this regard, symptom evaluation is much easier for the SCS remote programming relative to DBS.

Furthemore, pain treatment is not only about pain suppression itself, which has been particularly evident during the COVID-19 pandemic (Cohen et al., 2020) and has also emerged in this study. Within the 34 programming sessions, many patients expressed their anxiety and stress about their situation, especially those who were receiving inadequate care owing to greater isolation due to the lockdown. Anxiety and hopelessness are exacerbated by social isolation, and these negative moods aggravate the pain in a vicious cyclical manner. Thus, it is important to deliver palliative care for these patients in a timely manner. Healthcare providers need to be aware that many of the behavioral components of remote programming are not only potentially helpful for managing pain but also for emotional distress related to the COVID-19 pandemic. A retrospective study on DBS remote programming also found that some patients were satisfied with the programming sessions with no adjustment of the parameters required during the COVID-19 pandemic. This could be due to their expectations and the quality of the psychological support they received during the programming sessions (Zhang et al., 2020a). Empowered by the real-time video-based remote programming system, the demand for management of emotional distress could be met. We believe that reassuring SCS patients that they will be supported and their problems will be addressed during this pandemic at home is as important as the remote programming process.

Remote programming is cost-effective and convenient for patients with SCS and their families. However, before the interaction with healthcare providers can be efficiently established, several preparations need to be in place; these may include measures that ensure patients or their families know to use a smartphone and to keep updating the programming application using a stable network environment. As patients and at least one caregiver are requested to be familiar with the remote programming system, we expect to continue to face obstacles such as communication failure, poor network speed, and difficulty in following the orders when using the smartphone on their first attempt. In addition, a remote programming session is usually more laborious and time-consuming than face-to-face programming. For healthcare providers, patience and practice will help to ensure effective and efficient implementation of remote programming. For technology companies, improving the quality and efficiency is always a goal. We believe that with the continued development of technology, the system could become more intelligent, efficient, and effective at low cost.

If an increasing number of patients access to the remote programming service, the workflow should be designed to minimize the healthcare provider's burden. The teleprogramming team should be organized, including physicians, nurses, and technicians. Team cooperation could schedule visits, remotely train patients and families, resolve technological problems, and optimize the workflow. We suggest that before the start of formal remote programming, team members should recheck the schedule, smooth the network, and ensure patient and family computer literacy.

At the beginning of 2020, the whole world witnessed this unprecedented pandemic; everyone is a fighter against the invisible enemy, and we must all practice "social distancing." During this invisible war, patients with chronic intractable pain with an implanted SCS implant suffer from exacerbated pain helplessly and cannot receive individualized programming on site under these circumstances of isolation. We have demonstrated that the PINS remote wireless programming system allows for connection between patients and healthcare providers within this context, delivers safe and effective remote programming services, and provides palliative care value to the most vulnerable population of chronic pain patients.

With clinical implementation and feedback, we concluded that this remote wireless programming system is an effective and safe method for delivering parameter adjustment, thus improving the quality of life of chronic pain patients.

DATA AVAILABILITY STATEMENT

The raw data supporting the conclusions of this article will be made available by the authors, without undue reservation.

ETHICS STATEMENT

The studies involving human participants were reviewed and approved by Ethics committee of Beijing Tsinghua Changgung Hospital. The patients/participants provided their written informed consent to participate in this study. Written informed consent was obtained from the individual(s) for the publication of any potentially identifiable images or data included in this article.

AUTHOR CONTRIBUTIONS

GW and LL contributed to the conception, the study design, the acquisition, the analysis, the interpretation of data, and the preparation of the manuscript. JW contributed to the study design and the editing of the manuscript. YL contributed to

the acquisition of data, manuscript writing, and the editing of the manuscript. DX contributed to the study design, the interpretation of data, and editing of the manuscript. SD and XZ contributed to the study design, the analysis, and the interpretation of data. BY and HZ contributed to the interpretation of data and the editing of the manuscript. All authors contributed to the article and approved the submitted version.

FUNDING

This study was supported by the National Key Research and Development Program of China (2016YFC0105502), National Natural Science Foundation of China (81527901), Shenzhen International Cooperative Research Project (GJHZ20180930110402104), and Beijing Science and Technology Project (Z171100001017109).

REFERENCES

ATA, (2020). *Policy Update, 3.17.20. 2020*. Available at: https://info.americantelemed.org/covid-19-cms-hhs-dea-updates-3-17-20 (accessed March 22, 2020).

Adamse, C., Dekker-Van Weering, M. G., van Etten-Jamaludin, F. S., and Stuiver, M. M. (2018). The effectiveness of exercise-based telemedicine on pain, physical activity and quality of life in the treatment of chronic pain: a systematic review. *J. Telemed. Telecare* 24, 511–526. doi: 10.1177/1357633X17716576

Ahmed, S., Yearwood, T., De Ridder, D., and Vanneste, S. (2018). Burst and high frequency stimulation: underlying mechanism of action. *Expert. Rev. Med. Devices* 15, 61–70. doi: 10.1080/17434440.2018.1418662

Bally, J. F., Rohani, M., Ruiz-Lopez, M., Paramanandam, V., Munhoz, R. P., Hodaie, M., et al. (2019). Patient-adjusted deep-brain stimulation programming is time saving in dystonia patients. *J. Neurol.* 266, 2423–2429. doi: 10.1007/s00415-019-09423-9429

Buhrman, M., Gordh, T., and Andersson, G. (2016). Internet interventions for chronic pain including headache: a systematic review. *Int. Interv.* 4, 17–34. doi: 10.1016/j.invent.2015.12.001

Calton, B., Abedini, N., and Fratkin, M. (2020). Telemedicine in the time of coronavirus. *J. Pain Symptom Manag.* 60, e12–e14. doi: 10.1016/j.jpainsymman.2020.03.019

Chen, Y., Chen, H., Ma, B., Hao, H., Li, L., and Beijing Pins Medical. (2015a). *A Working Method of Remote Monitoring System for Implanted Medical Equipment. China patent application. CN201510115286.2*.

Chen, Y., Chen, H., Ma, B., Lu, C., Hao, H., Li, L., et al. (2015b). *Patient Client of Remote Monitoring System for Implanted Medical Equipment. China patent application CN201510114369.X*.

Chen, Y., Hao, H., Chen, H., and Li, L. (2015c). The study on a telemedicine interaction mode for deep brain stimulation postoperative follow-up. *Conf. Proc. IEEE Eng. Med. Biol. Soc.* 2015, 186–189. doi: 10.1109/EMBC.2015.7318331

Chen, Y., Hao, H., Chen, H., Tian, Y., and Li, L. (2014). The study on a real-time remote monitoring system for Parkinson's disease patients with deep brain stimulators. *Conf. Proc. IEEE Eng. Med. Biol. Soc.* 2014, 1358–1361. doi: 10.1109/EMBC.2014.6943851

Chen, Y., Hao, H., Li, L., Chen, H., Lu, C., Ma, B., et al. (2015d). *A Remote Monitoring System for Implanted Medical Equipment. China patent application CN201510114358.1*.

Cohen, S. P., Baber, Z. B., Buvanendran, A., McLean, L., Chen, Y., Hooten, W. M., et al. (2020). Pain management best practices from multispecialty organizations during the COVID-19 pandemic and public health crises. *Pain Med.* 21, 1331–1346. doi: 10.1093/pm/pnaa127

De Jaeger, M., van Hooff, R. J., Goudman, L., Valenzuela Espinoza, A., Brouns, R., Puylaert, M., et al. (2017). High-density in spinal cord stimulation: virtual expert registry (DISCOVER): study protocol for a prospective observational trial. *Anesth. Pain Med.* 7:e13640. doi: 10.5812/aapm.13640

Eccleston, C., Blyth, F. M., Dear, B. F., Fisher, E. A., Keefe, F. J., Lynch, M. E., et al. (2020). Managing patients with chronic pain during the COVID-19 outbreak: considerations for the rapid introduction of remotely supported (eHealth) pain management services. *Pain* 161, 889–893. doi: 10.1097/j.pain.0000000000001885

Humphreys, J., Schoenherr, L., Elia, G., Saks, N. T., Brown, C., Barbour, S., et al. (2020). Rapid implementation of inpatient telepalliative medicine consultations during COVID-19 Pandemic. *J. Pain Symptom Manag.* 60, e54–e59. doi: 10.1016/j.jpainsymman.2020.04.001

Jia, F., Hu, W., Zhang, J., Wagle Shukla, A., Almeida, L., Meng, F. G., et al. (2017). Variable frequency stimulation of subthalamic nucleus in Parkinson's disease: rationale and hypothesis. *Park. Relat. Disord.* 39, 27–30. doi: 10.1016/j.parkreldis.2017.03.015

Kapural, L., Yu, C., Doust, M. W., Gliner, B. E., Vallejo, R., Sitzman, B. T., et al. (2015). Novel 10-kHz high-frequency therapy (HF10 Therapy) is superior to traditional low-frequency spinal cord stimulation for the treatment of chronic back and leg pain: the senza-rct randomized controlled trial. *Anesthesiology* 123, 851–860. doi: 10.1097/ALN.0000000000000774

Keesara, S., Jonas, A., and Schulman, K. (2020). Covid-19 and health care's digital revolution. *N. Engl. J. Med.* 382:e82. doi: 10.1056/NEJMp2005835

Kumar, K., Taylor, R. S., Jacques, L., Eldabe, S., Meglio, M., Molet, J., et al. (2008). The effects of spinal cord stimulation in neuropathic pain are sustained: a 24-month follow-up of the prospective randomized controlled multicenter trial of the effectiveness of spinal cord stimulation. *Neurosurgery* 63, 762–770. doi: 10.1227/01.NEU.0000325731.46702.D9

Lu, Y., Mao, P., Wang, G., Tao, W., Xiong, D., Ma, K., et al. (2020). Spinal cord stimulation for chronic intractable trunk or limb pain: study protocol for a Chinese multicenter randomized withdrawal trial (CITRIP study). *Trials* 21:834. doi: 10.1186/s13063-020-04768-4763

Mariano, T. Y., Wan, L., Edwards, R. R., and Jamison, R. N. (2019). Online teletherapy for chronic pain: a systematic review. *J. Telemed. Telecare* 5, 1357633X19871746. doi: 10.1177/1357633X19871746

North, R. B., Kidd, D. H., Farrokhi, F., and Piantadosi, S. A. (2005). Spinal cord stimulation versus repeated lumbosacral spine surgery for chronic pain: a randomized, controlled trial. *Neurosurgery* 56, 98–106.

Wagle Shukla, A., Zeilman, P., Fernandez, H., Bajwa, J. A., and Mehanna, R. (2017). DBS programming: an evolving approach for patients with Parkinson's disease. *Parkinsons Dis.* 2017:8492619. doi: 10.1155/2017/8492619

Zhang, C., Zhu, K., Lin, Z., Huang, P., Pan, Y., Sun, B., et al. (2020a). Utility of deep brain stimulation telemedicine for patients with movement disorders during the COVID-19 outbreak in China. *Neuromodulation* doi: 10.1111/ner.13274

Zhang, J., Hu, W., Chen, H., Meng, F., Li, L., and Okun, M. S. (2020b). Implementation of a novel bluetooth technology for remote deep brain stimulation programming: the pre- and post-covid-19 beijing experience. *Mov. Disord.* 35, 909–910. doi: 10.1002/mds.28098

Zhang, P., Zhang, Y. G., Liao, L. M., Shen, J. W., Yang, Y. B., Zhang, J. Z., et al. (2019). Application of internet+-based Tsinghua PINS remote tech to improve sacral neuromodulation programming procedure. *Int. Urol. Nephrol.* 51, 627–632. doi: 10.1007/s11255-019-02115-2113

Conflict of Interest: JW and GW have received research support from Beijing PINS Medical Co., (donated SCS devices for pain). LL reports personal fees from Beijing Pins Medical Co., outside the submitted work.

The remaining authors declare that the research was conducted in the absence of any commercial or financial relationships that could be construed as a potential conflict of interest.

frontiers in Physiology

SYSTEMATIC REVIEW
published: 15 December 2020
doi: 10.3389/fphys.2020.550578

Non-invasive Autonomic Neuromodulation Is Opening New Landscapes for Cardiovascular Diseases

Mingxian Chen[1†], *Songyun Wang*[2†], *Xuping Li*[1], *Lilei Yu*[2], *Hui Yang*[1], *Qiming Liu*[1], *Jianjun Tang*[1*] and *Shenghua Zhou*[1*]

[1] Department of Cardiology, The Second Xiangya Hospital of Central South University, Changsha, China, [2] Department of Cardiology, Renmin Hospital, Wuhan University, Wuhan, China

Autonomic imbalance plays a crucial role in the genesis and maintenance of cardiac disorders. Approaches to maintain sympatho-vagal balance in heart diseases have gained great interest in recent years. Emerging therapies However, certain types of emerging therapies including direct electrical stimulation and nerve denervation require invasive implantation of a generator and a bipolar electrode subcutaneously or result in autonomic nervous system (ANS) damage, inevitably increasing the risk of complications. More recently, non-invasive neuromodulation approaches have received great interest in ANS modulation. Non-invasive approaches have opened new fields in the treatment of cardiovascular diseases. Herein, we will review the protective roles of non-invasive neuromodulation techniques in heart diseases, including transcutaneous auricular vagus nerve stimulation, electromagnetic field stimulation, ultrasound stimulation, autonomic modulation in optogenetics, and light-emitting diode and transcutaneous cervical vagus nerve stimulation (gammaCore).

Keywords: heart, cardiovascular disease, autonomic nervous system, neuromadulation, non-invasive

OPEN ACCESS

Edited by:
Luming Li,
Tsinghua University, China

Reviewed by:
Bruno Bonaz,
Centre Hospitalier Universitaire de Grenoble, France
Moacir Fernandes Godoy,
Faculty of Medicine of São José do Rio Preto, Brazil

***Correspondence:**
Jianjun Tang
tom200210@csu.edu.cn
Shenghua Zhou
zhoushenghua@csu.edu.cn

†These authors have contributed equally to this work

Specialty section:
This article was submitted to Autonomic Neuroscience, a section of the journal Frontiers in Physiology

Received: *09 April 2020*
Accepted: *27 October 2020*
Published: *15 December 2020*

Citation:
Chen M, Wang S, Li X, Yu L, Yang H, Liu Q, Tang J and Zhou S (2020) Non-invasive Autonomic Neuromodulation Is Opening New Landscapes for Cardiovascular Diseases. Front. Physiol. 11:550578. doi: 10.3389/fphys.2020.550578

INTRODUCTION

Cardiovascular diseases are the leading cause of death with high morbidity and mortality (Roth et al., 2017). Autonomic nervous system (ANS) imbalance is associated with disease progression and negative clinical outcomes (Shen and Zipes, 2014; Lai et al., 2019). It usually participates in the genesis and maintenance of various cardiovascular diseases, including heart failure, arrhythmias, acute myocardial infarction, and hypertension. However, cardiac disorders can in turn further aggravate the imbalance of the ANS, resulting in a vicious cycle between autonomic imbalance and cardiovascular diseases (Chen et al., 2019). Therefore, the ANS has been regarded as an important target to break this vicious cycle (Chen et al., 2015a,b). Due to the limited effectiveness of pharmacologic agents on ANS regulation, device-based neuromodulation has led to interest in applications for cardiovascular disorders. Additionally, cardiac neuromodulation has been successfully performed to modulate the cardiac ANS in the treatment of these disorders by extensive research (Sohinki and Stavrakis, 2019; Waldron et al., 2019).

Approaches via electrical devices or nerve denervation are mainly designed to modulate ANS activity and have become an emerging therapeutic strategy for the treatment of cardiovascular diseases (Cook et al., 2014). According to anatomical placement or nerve denervation,

neurostimulation therapies can be divided into invasive and non-invasive approaches. Invasive or minimally invasive therapeutic approaches include cervical vagal stimulation (Chen et al., 2016), baroreceptor activation therapy (Sheng et al., 2016), spinal cord stimulation (Lopshire and Zipes, 2014), ganglionated plexi ablation (Zipes, 2017), ganglionated plexi stimulation (Wang S. et al., 2015), renal sympathetic nerve denervation (Yu et al., 2017a,b), and left cardiac sympathetic nerve denervation (Cha et al., 2019). However, these approaches sometimes unavoidably increase the potential risk of hardware-related complications and serious adverse events, including permanent neurological damage. Importantly, electrodes surrounding the nerve trunk sometimes produce scar tissue (fibrosis), which can potentially increase the stimulation threshold. These complications may contribute to the translation failure of some types of device-related stimulation (Olshansky, 2016; Sahyouni et al., 2017).

Recently, non-invasive neuromodulation approaches have received great interest in ANS modulation for the treatment of cardiovascular diseases. The "non-invasive" techniques in this review refer to interventions that do not use electrodes around the nerve trunk or cause damage to nerve fibers. Importantly, the advantages of non-invasive approaches, such as low cost, portability, and ease of use, have promoted rapid evolution in recent decades (Schluter et al., 2018). Furthermore, non-invasive approaches are an attractive option for clinicians as novel therapies and are highly recommended for the treatment of cardiovascular diseases. Non-invasive neuromodulation has gradually and widely been applied in experimental evidence and clinical trials of heart diseases. In this review, we discuss the protective impact of non-invasive neuromodulation on the treatment of cardiovascular diseases.

CARDIAC AUTONOMIC NERVOUS SYSTEM AND INVASIVE NEUROMODULATION

The cardiac autonomic nervous system (CANS) consists of an extrinsic autonomic cardiac nervous system (EACNS) and an intrinsic autonomic cardiac nervous system (ICANS). The EACNS comprises fibers that mediate connections between the heart and the nervous system, whereas the ICANS consists of primarily autonomic nerve fibers once they enter the pericardial sac (**Figure 1**) (Zipes, 2008; Wickramasinghe and Patel, 2013; Chen et al., 2014).

The ECANS is made up of sympathetic and parasympathetic fibers. The sympathetic fibers are mainly derived from cervical ganglia, stellate ganglia, and thoracic ganglia along with the spinal cord; these fibers form the superior, middle, and inferior cardiac nerves and terminate on the surface of the heart (Witt et al., 2017). Renal sympathetic nerves (RSNs), which include efferent and afferent fibers, are adjacent to the wall of the renal artery and crucial for the production of catecholamines contributing to hypertension. Studies have shown an association between the left stellate ganglion (LSG) and RSNs. Afferent RSNs can affect the nerve activity of the LSG by modulating central sympathetic outflow. The nucleus ambiguous of the medulla oblongata delivers parasympathetic fibers predominantly into the vagal nerve (Ripplinger et al., 2016). The terminals of the vagal nerve relay to the fat pad of the heart and form the ganglion plexus (GP), mainly called the ICANS. GPs are divided into atrial and ventricular GPs located on the surface of the heart. GPs are the integration centers that modulate the intricate autonomic interactions between the ECANS and ICANS (Chen et al., 2014; Brack, 2015).

Afferent fibers are divided into vagal and sympathetic afferents (Burger and Verkuil, 2018). Cardiovascular receptors, including chemoreceptors and baroreceptors, transmit signals from cardiac activity or tissue injury to afferent cardiac nerves. Cardiac afferent fibers deliver signals to the nucleus tractus solitaries (NTS) and dorsomedial spinal trigeminal tract (Zoccal et al., 2014). After NTS receiving information, it projects to caudal ventrolateral medulla (CVM) and rostral ventrolateral medulla (RVM) to coordinate the activity of sympathetic nervous system, and then it finally leads to decrease sympathetic tone outflow. At the same time, NTS also projects information to the dorsal motor nucleus (DMN) of the vagus and contributes to vagal nerve activity enhancement (Ricardo and Koh, 1978). Currently, emerging therapies, including vagus nerve stimulation, baroreflex activation therapy, spinal cord stimulation, renal nerve denervation, left stellate ganglion ablation, GP ablation, and GP stimulation, have been widely applied in cardiovascular diseases (Clancy et al., 2014; Zubcevic et al., 2019).

THE POTENTIAL RISKS OF INVASIVE NEUROMODULATION

Device-related neuromodulation consists of a generator and electrodes. Implantation of the generator and electrodes requires surgery, especially for children; this approach requires a general anesthetic and at least an overnight stay in the hospital. For instance, the electrodes of some device-based stimulation are designed to surround the nerve trunk to deliver electrical information. A fibrotic scar around the interface induced by the inflammatory response can increase impedance. This leads to the inefficient transduction of electrical signals (Eldabe et al., 2016; Lotti et al., 2017).

The application of invasive neuromodulation is also limited by a variety of potential complications. Complications can be divided into device-related and biologic aspects (Doruk Camsari et al., 2018). Device-related complications include lead fracture or migration, intermittent stimulation, over- or under-stimulation, loose connections, hardware malfunction, battery replacement, and communication failure with the generator (Levy, 2013). Biologic complications consist of epidural hemorrhage, infection, voice disturbances, cough, headache, paralysis, cerebrospinal fluid leakage, pain over the implant site, allergic reactions, skin breakdown, surgical costs, and the need for post-operative monitoring (Levy et al., 2011; Shamji et al., 2015; Petraglia et al., 2016).

Non-invasive neuromodulation is a relatively new and promising method with potential advantages as an alternative

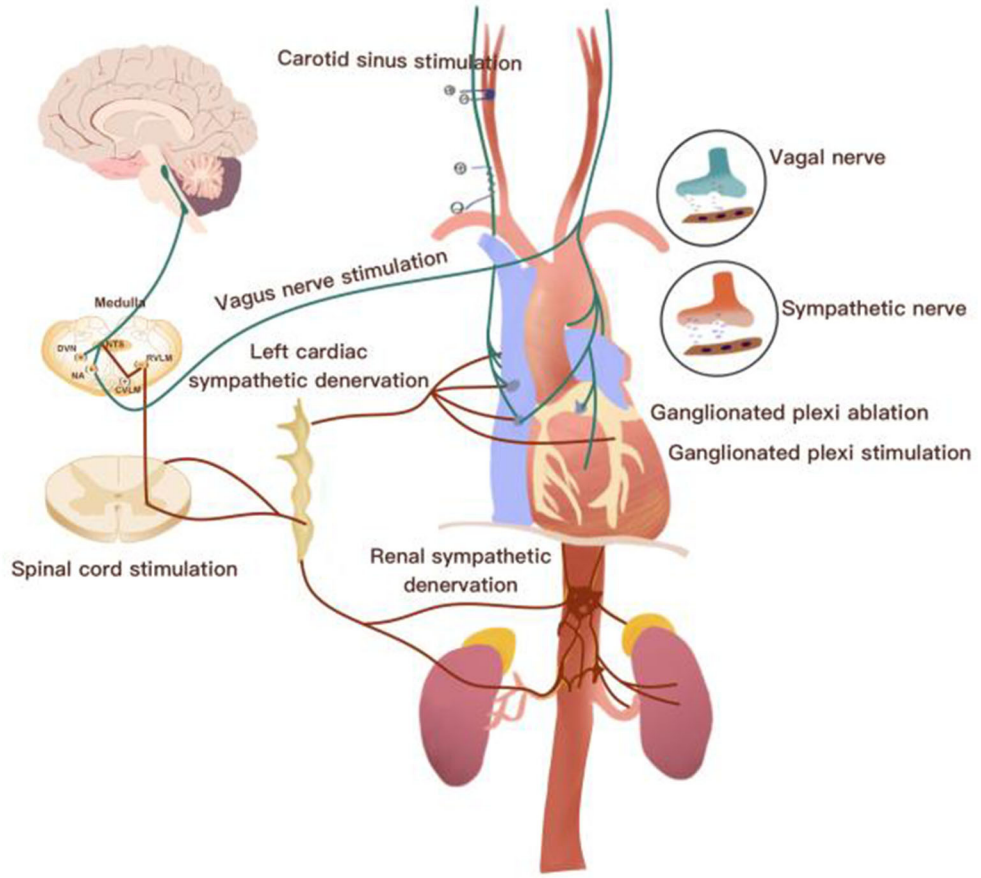

FIGURE 1 | Overview of the neurocardiac axis and invasive neuromodulatory approaches. CVLM, caudal ventrolateral medulla; DVN, dorsal vagal nucleus; IML, intermediolateral cell column; NTS, nucleus of the solitary tract; RVLM, rostroventrolateral medulla.

to invasive neuromodulation. Non-invasive neuromodulation is easier and less invasive than traditional neuromodulation, thus reducing the risk of complications (Eldabe et al., 2016; Cotero et al., 2019).

NON-INVASIVE NEUROMODULATION AND CARDIOVASCULAR DISEASES

Electrical device stimulation and sympathetic nerve denervation have progressively been a focus of non-pharmaceutical approaches for the treatment of cardiovascular diseases (Lohmeier and Hall, 2019). Recently, current non-invasive neuromodulation techniques have gained particular interest in cardiovascular disorders. They not only provide deep insight into autonomic circuit physiology but also can be applied for therapeutic purposes (**Table 1** and **Figure 2**).

Transcutaneous Auricular Vagus Nerve Stimulation and Cardiovascular Diseases

The auricular branch of the vagus nerve (ABVN), a powerful nerve entering the brain, is the only afferent peripheral branch of the vagus nerve that is located in the skin. The ABVN delivers information to the central ANS. After integration, it finally causes an increase in vagal nerve activity and a reduction in sympathetic tone. Transcutaneous auricular vagus nerve stimulation (ta-VNS) is a non-invasive method applied to electrically regulate vagal tone and brain activity by the vagal afferent pathway (Kaniusas et al., 2019a,b). Clancy et al. (2014) demonstrated that ta-VNS could increase parasympathetic predominance assessed by heart rate viability and could reduce sympathetic nerve activity detected by microneurography. Decades ago, ta-VNS was first applied for cognitive, emotional, and neurological modulation, with a similar effect as invasive cervical vagus nerve stimulation. In recent years, because of the novel and non-invasive technology, ta-VNS has been applied in both research and therapy as a medical treatment tool for cardiovascular diseases (Shiozawa et al., 2014; Redgrave et al., 2018).

Recently, as a type of non-invasive neuromodulation, ta-VNS has been gradually and widely applied to treat cardiac diseases, including atrial fibrillation (AF), acute and chronic ischemia diseases, and heart failure induced by autonomic imbalance. Previous studies have shown that high-intensity vagus nerve stimulation induces HF, but low-level vagus nerve stimulation

TABLE 1 | Studies of non-invasive autonomic neuromodulations in the treatment of cardiovascular diseases.

Modulation	References	Species	Parts	Parameters	Models	Results
Tragus nerve stimulation	Yu et al. (2013)	Canine	Ear	The voltage of 80% below the threshold	Atrial fibrillation	Inhibit AF and electrophysiological changes
	Chen et al. (2015c)	Canine	Right Ear	The voltage of 80% below the threshold	Atrial fibrillation	Inhibit AF by the expression of connexs
	Chen et al. (2015d)	Canine	Left-sided tragus	The voltage of 80% below the threshold	Atrial fibrillation	Inhibit AF by conexin expression
	Wang et al. (2014)	Canine	Left-sided tragus	The voltage of 80% below the threshold	Chronic myocardial infarction	Ameliorate ventricular remodeling and function
	Wang S. et al. (2015)	Canine	Left-sided tragus	The voltage of 80% below the threshold	Chronic myocardial infarction	Improve ventricular remodeling by the expression of collagen, TGF-β, MMP-9
	Yu et al. (2016)	Canines	Left-sided ear	The voltage of 80% below the threshold	Chronic myocardial infarction	Inhibit LSG activity and remodeling
	Zhou et al. (2016)	Canine	Right tragus	The voltage of 80% below the threshold	Ligh-frequency stimulation of RSG	Suppress RSG activity and sympathetically induced sinus node acceleration
	Zhou et al. (2019)	Rats	Tragus	(20 Hz, 2 mA, 0.2 ms) was implemented for 30 min daily for 4 weeks	Heart failure with preserved ejection fraction	Ameliorate diastolic dysfunction, and attenuate cardiac inflammation and fibrosis
	Nasi-Er et al. (2019)	Dogs	Bilateral Ears	50% of the threshold voltage	Acute myocardial infarction	Attenuate electrophysiological changes and ventricular structural remodeling, inhibit VAs
	Stavrakis et al. (2015)	Patients	Ear			
	Yu et al. (2017c)	Patients	Ear	50% lower than the electric current that slowed the sinus rate	Ischemia reperfusion injury	Reduce VAs Attenuate cardiac function
Magnetic field stimulation	Wang et al. (2016)	Canine	Left stellate ganglion	1 HZ; stimulation time 8 s; interstimulus interval, 5 s	Acute myocardial infarction	Inhibit LSG activity and VAs
	Nishikawa et al. (2017)	Patients	Right cervical vagus nerve	Frequency 5 or 20 Hz, pulse to 250 us	Healthy	No side effects without bradycardia and arterial pressure changes
Ultrasonic stimulation	Wang et al. (2019a)	Dogs	LSG	Frequency 1 MHz, Pulse repetition frequency 1 KHz, Duty cycle 8 s, Duty cycle % 50%	Acute myocardial infarction	Suppress LSG activity and VAs
Optogenetic stimulation	Yu et al. (2017d)	Canine	LSG	Light-emitting diode illumination (565 nm)	Myocardial infarction	Inhibit LSG activety and VAs
Light-emitting diode	Wang et al. (2019b)	Rats	Brain	Peak wavelength, 610 nm; power intensity, 1.7 mW/cm^2; energy density, 2.0 J/cm^2	Acute myocardial infarction	Inhibit LSG activity and VAs. Reduce inflammation
	Wang et al. (2019c)	Rats	Brain	Peak wavelength, 610 nm; power intensity, 1.7 mW/cm^2; energy density, 2.0 J/cm^2	Acute myocardial ischemia reperfusion injury	Inhibit LSG activity and VAs. Reduce inflammation

LSG, left stellate ganglion; MMP, matrix metalloproteinase; RSG, right stellate ganglion; TGF, transforming growth factor; VAs, ventricular arrhythmias.

(LL-VNS) has been proven to suppress AF (Zhang et al., 2009; Sheng et al., 2011; Shen et al., 2013). Low-level ta-VNS (LL-ta-VNS) has the same effect as LL-VNS. Yu et al. (2013) first reported that LL-ta-VNS could reverse RAP-induced atrial remodeling and inhibit AF inducibility in canine models. This indicates that LL-ta-VNS is a potential non-invasive approach for AF treatment. We further found that LL-ta-VNS inhibited AF by modulating the expression of atrial connexin40 and connexin43 (Chen et al., 2015c,d). Later, Stavrakis et al. (2015, 2017) showed that LL-ta-VNS suppressed AF and decreased inflammatory cytokines in patients with paroxysmal AF in a clinical study. Later, they continued to conduct a TREAT AF trial to prove the long-term effect of LL-ta-VNS.

Beyond its atrial protective effects, LL-ta-VNS has also been applied to research left ventricular remodeling and arrhythmias. Wang et al. (2014) and Wang Z. et al. (2015) showed that chronic intermittent LL-ta-VNS could attenuate left ventricular remodeling in conscious dogs with healed myocardial infarction. It demonstrated ventricular protection against ta-VNS. Chronic LL-ta-VNS could reduce the inducibility of ventricular arrhythmia, LSG neural activity, and sympathetic neural remodeling in a post-infarction canine model. Downregulation

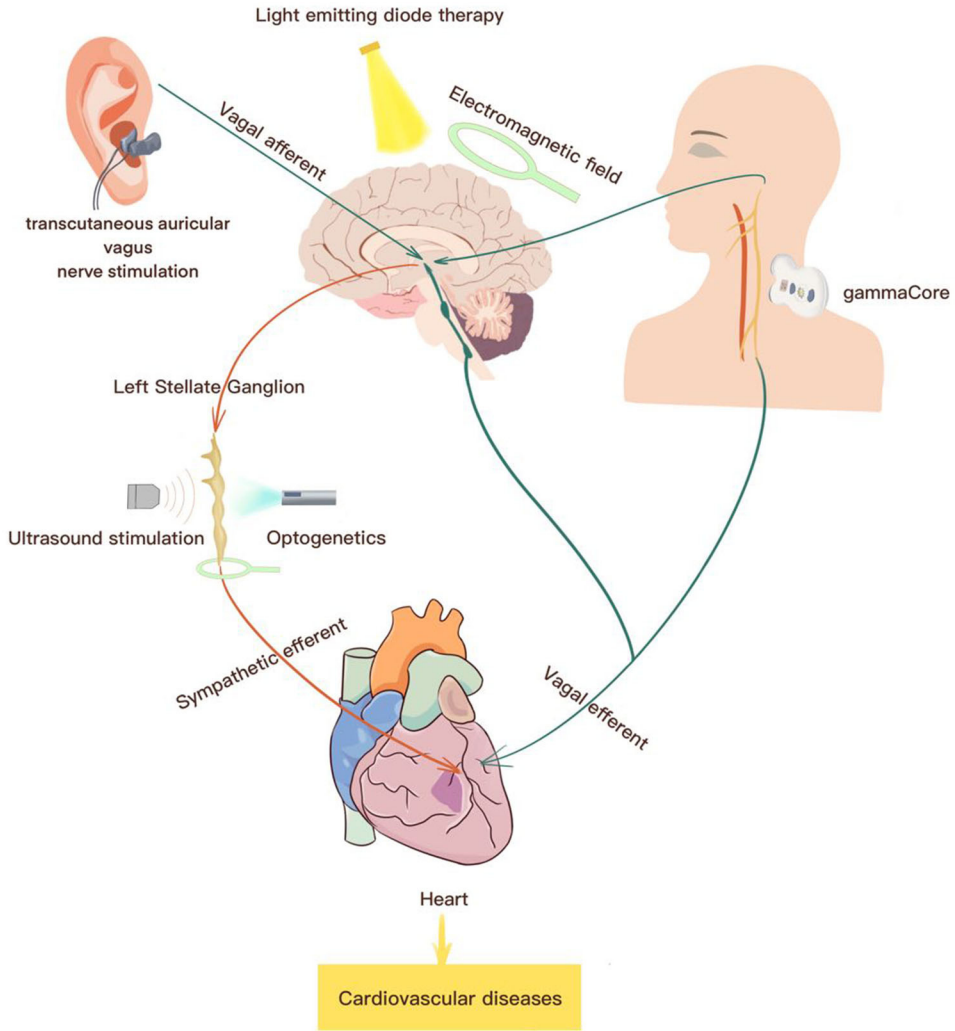

FIGURE 2 | Summary of potential non-invasive neuromodulations for the treatment of cardiovascular diseases. Current therapeutic strategies for the treatment of cardiovascular diseases include transcutaneous auricular vagus nerve stimulation, electromagnetic field stimulation, ultrasound stimulation, optogenetics for stimulation, transcutaneous cervical nerve stimulation.

of nerve growth factor protein and upregulation of SK2 protein in the LSG contributed to the salutary effects of LL-ta-VNS (Yu et al., 2016). Nasi-Er et al. also demonstrated that TS reduced the occurrence of spontaneous ventricular arrhythmias in conscious dogs with MI. The potential mechanisms of anti-ventricular arrhythmias may increase ventricular electrical stability and alleviate ventricular interstitial fibrosis (Nasi-Er et al., 2019). In a recent patient study, Yu et al. (2017c) found that LL-ta-VNS reduced the incidence of reperfusion-related ventricular arrhythmias during the first 24 h after acute myocardial infarction and improved left ventricular function 5–7 days after reperfusion along with reduced venous cytokine levels.

Sympathetic activity can regulate sinus node acceleration. Zhou et al. (2016) performed a study and showed that right-sided ta-VNS could inhibit sinus node acceleration induced by sympathetic nerves. Its potential mechanism may suppress right-sided stellate ganglion activity by modulating SK2, c-fos, and nerve growth factor protein expression. Currently, there is limited evidence to prove that drugs can improve the outcomes of heart failure with preserved ejection fraction. Interestingly, Po et al. also demonstrated that LL-ta-VNS could effectively treat heart failure with preserved ejection fraction in a rat model. It attenuated cardiac remodeling by inhibiting left ventricular fibrosis and inflammatory cell infiltration (Zhou et al., 2019). However, further trials are needed to study and support the observed beneficial effects in clinical settings.

However, because of the absence of standards regarding stimulation protocols, the parameters of ta-VNS have not been used consistently in research (Borges et al., 2019). Several studies have not shown positive effects of ta-VNS on vagal-related heart rate viability. The heterogeneous results may be due to the use of different stimulation parameters, differing in electrode placement

areas on the ear, pulse width, frequency, and on–off cycle (Burger et al., 2016, 2017, 2019; De Couck et al., 2017).

Electromagnetic Fields in the CANS and Cardiovascular Diseases

Electromagnetic waves are waves caused by vibrations between an electric field and a magnetic field. Electromagnetic waves transfer energy to tissues, resulting in functional changes or structural damage. Electromagnetic fields (EMFs) were first explored for use in diagnosing human diseases. In recent years, because of their non-invasive and safe advantages, EMFs have been developed and applied to treat a wide range of diseases, such as nervous system disorders, cardiovascular diseases, diabetes, spinal cord injuries, ulcers, and asthma (Schestatsky et al., 2013; Cabrerizo et al., 2014; Vernieri et al., 2014; Chervyakov et al., 2015).

Interestingly, EMF exposure can affect the structure and modulate the function of the ANS. EMFs can significantly change the physiological properties of the CANS neural network by the results of some ionic flux changes. A study showed that EMF exposure could increase sympathetic vasoconstrictor activity (Braune et al., 2002). Different parameters (frequencies and amplitudes) of stimulation contribute to different results. Recently, Wang et al. (2016) showed that EMF stimulation located on the surface of the left stellate ganglion could effectively reduce sympathetic activity and the incidence of ventricular arrhythmias in myocardial infarction canine models. EMF stimulation was applied with low frequency (1 Hz, intensity at ∼90% of the motor threshold; 8 s on, 10 s off). EMF stimulation of the left stellate ganglion is a novel therapeutic strategy for treating ventricular arrhythmias associated with autonomic imbalance. Among EMFs for the vagus nerve, Nishikawa et al. (2017) found that EMFs could induce transient heart rate reduction in some healthy individuals but failed to induce sustained bradycardia and arterial pressure changes. This indicates that the magnetic focus and optimized stimulation need further improvement for beneficial effects in acute myocardial infarction. Scherlag et al. used a low-frequency electromagnetic field (LL-EMF) to expose the chest for 35 min in canine AF models and found that LL-EMF could successfully inhibit AF for 3–4 h (Yu et al., 2015). As is well-known, pericardial fat pads, including ganglion plexi, exist in high numbers on the surface of the heart. Whether LL-EMFs suppress AF by affecting the ganglion plexus remains unknown. There is still a need for further studies to prove this influence.

EMFs have the advantages of simplicity, low operating costs, and unproven harmful effects. EMFs show promising potential in the treatment of cardiovascular diseases by autonomic neuromodulation.

Ultrasound Stimulation of the CANS and Cardiovascular Diseases

In the 1950s, ultrasound was applied to visualize tissue structure for diagnostic applications (Edler and Lindstrom, 2004). Ultrasound was also used for therapeutic indications as an ablative approach for the treatment of Parkinson's disease in earlier decades (Leinenga et al., 2016). Therapeutic ultrasound stimulation technologies are currently approved by the United States Food and Drug Administration (FDA) and used for the treatment of multiple diseases. Ultrasound stimulation parameters (frequency, amplitude, pulse duration) can be optimized for therapeutic or diagnostic applications (Downs et al., 2018). Ultrasound waves are transmitted into tissues. A portion of the waves are converted into thermal energy. Ultrasound waves affect tissues via thermal and non-thermal mechanisms. The functional changes in tissues are decided by the frequency and intensity of the ultrasound waves (dosage) and the types of tissues that are exposed to ultrasound. Ultrasound stimulation of the neural system as acoustic neuromodulation has received great interest due to its non-invasive advantage (Kim et al., 2014).

Ultrasound neuromodulation can stimulate or inhibit neural structures, which can be classified as central nervous system or peripheral nervous system influences. Transcranial ultrasound stimulation can target special brain regions and modulate specific neuronal pathways or nuclei. It has been widely researched in basic neuroscience and has been recommended as a potential therapy for neurological diseases (Bystritsky et al., 2011). In terms of the focus on the peripheral nervous system, Wasilczuk et al. (2019) observed that low-intensity focused ultrasound stimulation of the vagus nerve exerted anti-inflammatory effects and significantly reduced tumor factor necrosis-α levels. Recently, ultrasound-induced neuromodulation has gained interest due to its potential to non-invasively modulate ANS activity for the treatment of cardiovascular diseases. Wang et al. (2019a) showed that low-intensity ultrasound stimulation reduced ventricular arrhythmias by modulating sympathetic neural activity in a myocardial infarction canine model.

Optogenetics in Autonomic Neuromodulation for Cardiovascular Diseases

In 2006, Deisseroth et al. first referred to the word "optogenetics" (Deisseroth et al., 2006). Optogenetics offers a technique to control and monitor the activity of excitable cells by light. This method genetically affects the expression of light-sensitive ion channels, known as opsins, to achieve precise control of targeted cell activity (Deisseroth, 2011). Recently, optogenetics has been widely developed and used in the field of neuroscience and cardiac tissues to control the activity of specific neuron and myocardial populations. It has been applied for the treatment of neurological disorders in experiments (Boyden, 2015). Optogenetics also contributes to further explaining the mechanisms of the initiation, perpetuation, and termination of arrhythmias in cardiac areas (Nussinovitch and Gepstein, 2015; Vogt et al., 2015; Hulsmans et al., 2017).

More recently, optogenetics has enabled the spatially and temporally specific stimulation of cardiac autonomic neurons using light. Photostimulation of neurons expressing the light-gated cation channel channelrhodopsin modulates cardiac autonomic nerve activity and then evaluates the potential cardiovascular changes (Wengrowski et al., 2015; Yamamoto et al., 2015; Gepstein and Gruber, 2017).

Optogenetics selectively stimulates the cardiac ANS by the release of acetylcholine or norepinephrine (Abbott et al., 2013). Yu et al. (2017d) first applied optogenetics to regulate the activity of the left stellate ganglion to prevent ventricular arrhythmias induced by acute myocardial infarction in canine models. Virus was transfected into left stellate ganglion neurons to induce the expression of ArchT proteins. Proper illumination (565 nm) activated ArchT and caused hyperpolarizing currents in the neurons. Optogenetics reversibly suppressed the cardiac sympathetic tone and then exerted a protective role against ventricular arrhythmias associated with autonomic nerve dysfunction.

Light-Emitting Diode Therapy in the Modulation of the CANS for Cardiovascular Diseases

In the late 1960s, light-emitting diode (LED) therapy was first discovered (Li et al., 2013). LED therapy has been recently introduced into medicine and widely applied in dermatology. LED photomodulation is a non-thermal technology used to modulate cellular activity with light, and photons are absorbed by mitochondrial chromophores in cells. It has been reported that low-intensity LED phototherapy has various protective effects, including inhibiting the inflammatory response and increasing collagen synthesis. Because of the non-invasive therapy with side effects reported in the published literature, LED therapy has gradually been applied in cardiovascular diseases (Gold, 2011; Avci et al., 2014; Capalonga et al., 2016; Sorbellini et al., 2018).

Recently, Wang et al. (2019b) reported that LED therapy reduced post-infarction ventricular arrhythmias by modulating the neuroimmune network. In this study, LED therapy significantly suppressed the activity of the left stellate ganglion and reduced the levels of pro-inflammatory cytokines through the inhibition of microglial activation in the hypothalamic paraventricular nucleus. LED therapy might reduce myocardial ischemia/reperfusion-induced ventricular arrhythmias by attenuating microglial and sympathetic over-activation. They also proved that LED therapy has the same indirect effects of sympathetic activity in a rat model of acute myocardial ischemia/reperfusion injury (Wang et al., 2019c). This indicates that LED affects the ANS through the inhibition of inflammation rather than through direct effects. Currently, there is no evidence to prove that LED can directly activate ANS.

gammaCore (Non-invasive Cervical Vagus Nerve Stimulation) and Cardiovascular Diseases

gammaCore, a non-invasive cervical vagus nerve stimulator, is already an FDA-approved device for the treatment of primary headache disorders. It is used by sending mild electrical stimulation through the skin to activate the vagus nerve from outside the body. It is programmed for stimulation in cycles for 2 min, and one treatment consists of three cycles (Akdemir and Benditt, 2016; Mwamburi et al., 2017).

This kind of non-invasive neuromodulation has been used to treat cluster headaches (Simon and Blake, 2017). Current clinical evidence shows that gammaCore can reduce the frequency and intensity of cluster headache attacks in some patients (Tassorelli et al., 2018). It can also reduce the need for medication. This is likely to lead to significant quality of life benefits for people living with this condition.

gammaCore™ is a simple-to-use, handheld medical device that enables patients to self-administer discrete doses of non-invasive vagus nerve stimulation (nVNS) therapy. Cost analysis suggests that using gammaCore may lead to cost savings (Mwamburi et al., 2018). However, there is no evidence for the treatment of cardiovascular diseases by gammaCore™. The effect of gammaCore™ on the treatment of cardiovascular diseases needs further study in both experimental and clinical areas. It is an emerging and potential type of neuromodulation for the treatment of cardiovascular diseases.

POTENTIAL OPPORTUNITIES AND CHALLENGES

Non-invasive neuromodulation provides opportunities for better understanding ANS circuits and neurophysiological responses (Boes et al., 2018). It also provides a potential therapeutic target for the treatment of cardiovascular diseases. These kinds of neuromodulation are usually low-cost, portable, and easy to use. Due to the novel and non-invasive approach, it is an attractive therapy for clinical doctors. Patients with non-invasive neuromodulations maybe have a better compliance. Clinical doctor can wirelessly re-set up parameters when patients with chronic pain or movement disorder at home. Non-invasive neuromodulation of the ANS has opened new frontiers for the application of cardiovascular disorders.

However, the road of non-invasive neuromodulations translation in cardiovascular diseases, the same as invasive neuromodulations, is also not flat. There is still a long way to go to translate clinical application to treatment of cardiovascular diseases. For example, divergent results also exist. A dose-response curve is estimated to determine the proper dosage and achieve the most probable benefit in pharmacological trials (Mann and Deswal, 2003). It should also be recommended for invasive and non-invasive neuromodulation (Zannad et al., 2015; Byku and Mann, 2016; DiCarlo et al., 2018). The efficacy of non-invasive neuromodulation might be variable. Multiple reasons might be responsible for the divergent results, including individual differences, protocol parameters (current intensity, frequency, duty cycle), and failure to engage the appropriate neurobiological target. To optimize efficacy and preserve safety, further basic research and clinical studies need to be performed to assess the long-term effects of non-invasive neuromodulation.

CONCLUSIONS

Autonomic dysfunction plays an important role in the process of cardiovascular disorders. Neuromodulation has been proven to be an emerging non-pharmacological approach for the treatment of cardiovascular diseases in basic research and clinical studies. Based on anatomy and nerve denervation, neurostimulation approaches are divided into invasive and non-invasive approaches. Invasive neuromodulation approaches

are usually hampered by the potential risks of complications, side effects, increases in electrical impedance, and even perpetual nerve damage. Recently, non-invasive neuromodulation approaches have received great interest in the treatment of cardiovascular diseases. However, due to the limited evidence, further experimental studies and clinical trials are still needed.

DATA AVAILABILITY STATEMENT

The raw data supporting the conclusions of this article will be made available by the authors, without undue reservation.

AUTHOR CONTRIBUTIONS

MC, XL, and SW participated in the study design and drafted the manuscript. SZ and MC were responsible for writing the manuscript. LY, QL, and JT participated in the overall editing and approval of the paper. All authors contributed to the article and approved the submitted version.

FUNDING

Financial support was obtained from the National Natural Science Foundation of China Nos. 81270257 and 81800302 and Provincial Natural Science Foundation of Hunan No. 2019JJ50871.

ACKNOWLEDGMENTS

The authors would like to thank Minjia Xiao and Jiaying Liao for modification.

REFERENCES

Abbott, S. B., DePuy, S. D., Nguyen, T., Coates, M. B., Stornetta, R. L., and Guyenet, P. G. (2013). Selective optogenetic activation of rostral ventrolateral medullary catecholaminergic neurons produces cardiorespiratory stimulation in conscious mice. *J. Neurosci.* 33, 3164–3177. doi: 10.1523/JNEUROSCI.1046-12.2013

Akdemir, B., and Benditt, D. G. (2016). Vagus nerve stimulation: An evolving adjunctive treatment for cardiac disease. *Anatol. J. Cardiol.* 16, 804–810. doi: 10.14744/AnatolJCardiol.2016.7129

Avci, P., Gupta, G. K., Clark, J., Wikonkal, N., and Hamblin, M. R. (2014). Low-level laser (light) therapy (LLLT) for treatment of hair loss. *Lasers Surg. Med.* 46, 144–151. doi: 10.1002/lsm.22170

Boes, A. D., Kelly, M. S., Trapp, N. T., Stern, A. P., Press, D. Z., and Pascual-Leone, A. (2018). Noninvasive brain stimulation: challenges and opportunities for a new clinical specialty. *J. Neuropsychiatry Clin. Neurosci.* 30, 173–179. doi: 10.1176/appi.neuropsych.17110262

Borges, U., Laborde, S., and Raab, M. (2019). Influence of transcutaneous vagus nerve stimulation on cardiac vagal activity: not different from sham stimulation and no effect of stimulation intensity. *PLoS ONE* 14:e0223848. doi: 10.1371/journal.pone.0223848

Boyden, E. S. (2015). Optogenetics and the future of neuroscience. *Nat. Neurosci.* 18, 1200–1201. doi: 10.1038/nn.4094

Brack, K. E. (2015). The heart's 'little brain' controlling cardiac function in the rabbit. *Exp. Physiol.* 100, 348–353. doi: 10.1113/expphysiol.2014.080168

Braune, S., Riedel, A., Schulte-Monting, J., and Raczek, J. (2002). Influence of a radiofrequency electromagnetic field on cardiovascular and hormonal parameters of the autonomic nervous system in healthy individuals. *Radiat. Res.* 158, 352–356. doi: 10.1667/0033-7587(2002)158[0352:IOAREF]2.0.CO;2

Burger, A. M., Van der Does, W., Thayer, J. F., Brosschot, J. F., and Verkuil, B. (2019). Transcutaneous vagus nerve stimulation reduces spontaneous but not induced negative thought intrusions in high worriers. *Biol. Psychol.* 142, 80–89. doi: 10.1016/j.biopsycho.2019.01.014

Burger, A. M., and Verkuil, B. (2018). Transcutaneous nerve stimulation via the tragus: are we really stimulating the vagus nerve? *Brain Stimul.* 11, 945–946. doi: 10.1016/j.brs.2018.03.018

Burger, A. M., Verkuil, B., Fenlon, H., Thijs, L., Cools, L., Miller, H. C., et al. (2017). Mixed evidence for the potential of non-invasive transcutaneous vagal nerve stimulation to improve the extinction and retention of fear. *Behav. Res. Ther.* 97, 64–74. doi: 10.1016/j.brat.2017.07.005

Burger, A. M., Verkuil, B., Van Diest, I., Van der Does, W., Thayer, J. F., and Brosschot, J. F. (2016). The effects of transcutaneous vagus nerve stimulation on conditioned fear extinction in humans. *Neurobiol. Learn. Mem.* 132, 49–56. doi: 10.1016/j.nlm.2016.05.007

Byku, M., and Mann, D. L. (2016). Neuromodulation of the failing heart: lost in translation? *JACC Basic Transl. Sci.* 1, 95–106. doi: 10.1016/j.jacbts.2016.03.004

Bystritsky, A., Korb, A. S., Douglas, P. K., Cohen, M. S., Melega, W. P., Mulgaonkar, A. P., et al. (2011). A review of low-intensity focused ultrasound pulsation. *Brain Stimul.* 4, 125–136. doi: 10.1016/j.brs.2011.03.007

Cabrerizo, M., Cabrera, A., Perez, J. O., de la Rua, J., Rojas, N., Zhou, Q., et al. (2014). Induced effects of transcranial magnetic stimulation on the autonomic nervous system and the cardiac rhythm. *ScientificWorldJournal* 2014:349718. doi: 10.1155/2014/349718

Capalonga, L., Karsten, M., Hentschke, V. S., Rossato, D. D., Dornelles, M. P., Sonza, A., et al. (2016). Light-emitting diode therapy (LEDT) improves functional capacity in rats with heart failure. *Lasers Med. Sci.* 31, 937–944. doi: 10.1007/s10103-016-1922-y

Cha, Y. M., Li, X., Yang, M., Han, J., Wu, G., Kapa, S. C., et al. (2019). Stellate ganglion block and cardiac sympathetic denervation in patients with inappropriate sinus tachycardia. *J. Cardiovasc. Electrophysiol.* 30, 2920–2928. doi: 10.1111/jce.14233

Chen, M., Li, X., Yang, H., Tang, J., and Zhou, S. (2019). Hype or hope: vagus nerve stimulation against acute myocardial ischemia-reperfusion injury. *Trends Cardiovasc. Med.* doi: 10.1016/j.tcm.2019.10.011

Chen, M., Yu, L., Liu, Q., Wang, Z., Wang, S., Jiang, H., et al. (2015c). Low level tragus nerve stimulation is a non-invasive approach for anti-atrial fibrillation via preventing the loss of connexins. *Int. J. Cardiol.* 179, 144–145. doi: 10.1016/j.ijcard.2014.10.114

Chen, M., Yu, L., Liu, Q., Wang, Z., Wang, S., Zhou, L., et al. (2015a). Noninvasive vagus nerve stimulation: a novel promising modulator for cardiac autonomic nerve system dysfunction. *Int. J. Cardiol.* 187, 338–339. doi: 10.1016/j.ijcard.2015.03.317

Chen, M., Yu, L., Zhou, X., Liu, Q., Jiang, H., and Zhou, S. (2015b). Low-level vagus nerve stimulation: an important therapeutic option for atrial fibrillation treatment via modulating cardiac autonomic tone. *Int. J. Cardiol.* 199, 437–438. doi: 10.1016/j.ijcard.2015.07.083

Chen, M., Zhou, X., Liu, Q., Sheng, X., Yu, L., Wang, Z., et al. (2015d). Left-sided noninvasive vagus nerve stimulation suppresses atrial fibrillation by upregulating atrial gap junctions in canines. *J. Cardiovasc. Pharmacol.* 66, 593–599. doi: 10.1097/FJC.0000000000000309

Chen, M., Zhou, X., Yu, L., Liu, Q., Sheng, X., Wang, Z., et al. (2016). Low-level vagus nerve stimulation attenuates myocardial ischemic reperfusion injury by antioxidative stress and antiapoptosis reactions in canines. *J. Cardiovasc. Electrophysiol.* 27, 224–231. doi: 10.1111/jce.12850

Chen, P. S., Chen, L. S., Fishbein, M. C., Lin, S. F., and Nattel, S. (2014). Role of the autonomic nervous system in atrial fibrillation: pathophysiology and therapy. *Circ. Res.* 114, 1500–1515. doi: 10.1161/CIRCRESAHA.114.303772

Chervyakov, A. V., Chernyavsky, A. Y., Sinitsyn, D. O., and Piradov, M. A. (2015). Possible mechanisms underlying the therapeutic effects of transcranial magnetic stimulation. *Front. Hum. Neurosci.* 9:303. doi: 10.3389/fnhum.2015.00303

Clancy, J. A., Mary, D. A., Witte, K. K., Greenwood, J. P., Deuchars, S. A., and Deuchars, J. (2014). Non-invasive vagus nerve stimulation in healthy humans reduces sympathetic nerve activity. *Brain Stimul.* 7, 871–877. doi: 10.1016/j.brs.2014.07.031

Cook, I. A., Espinoza, R., and Leuchter, A. F. (2014). Neuromodulation for depression: invasive and noninvasive (deep brain stimulation, transcranial magnetic stimulation, trigeminal nerve stimulation). *Neurosurg. Clin. North Am.* 25, 103–116. doi: 10.1016/j.nec.2013.10.002

Cotero, V., Fan, Y., Tsaava, T., Kressel, A. M., Hancu, I., Fitzgerald, P., et al. (2019). Noninvasive sub-organ ultrasound stimulation for targeted neuromodulation. *Nat. Commun.* 10:952. doi: 10.1038/s41467-019-08750-9

De Couck, M., Cserjesi, R., Caers, R., Zijlstra, W. P., Widjaja, D., Wolf, N., et al. (2017). Effects of short and prolonged transcutaneous vagus nerve stimulation on heart rate variability in healthy subjects. *Auton. Neurosci.* 203, 88–96. doi: 10.1016/j.autneu.2016.11.003

Deisseroth, K. (2011). Optogenetics. *Nat. Methods* 8, 26–29. doi: 10.1038/nmeth.f.324

Deisseroth, K., Feng, G., Majewska, A. K., Miesenbock, G., Ting, A., and Schnitzer, M. J. (2006). Next-generation optical technologies for illuminating genetically targeted brain circuits. *J. Neurosci.* 26, 10380–10386. doi: 10.1523/JNEUROSCI.3863-06.2006

DiCarlo, L. A., Libbus, I., Kumar, H. U., Mittal, S., Premchand, R. K., Amurthur, B., et al. (2018). Autonomic regulation therapy to enhance myocardial function in heart failure patients: the ANTHEM-HFpEF study. *ESC Heart Fail.* 5, 95–100. doi: 10.1002/ehf2.12241

Doruk Camsari, D., Kirkovski, M., and Croarkin, P. E. (2018). Therapeutic applications of invasive neuromodulation in children and adolescents. *Psychiatr. Clin. North Am.* 41, 479–483. doi: 10.1016/j.psc.2018.04.008

Downs, M. E., Lee, S. A., Yang, G., Kim, S., Wang, Q., and Konofagou, E. E. (2018). Non-invasive peripheral nerve stimulation via focused ultrasound *in vivo*. *Phys. Med. Biol.* 63:035011. doi: 10.1088/1361-6560/aa9fc2

Edler, I., and Lindstrom, K. (2004). The history of echocardiography. *Ultrasound Med. Biol.* 30, 1565–1644. doi: 10.1016/S0301-5629(99)00056-3

Eldabe, S., Buchser, E., and Duarte, R. V. (2016). Complications of spinal cord stimulation and peripheral nerve stimulation techniques: a review of the literature. *Pain Med.* 17, 325–336. doi: 10.1093/pm/pnv025

Gepstein, L., and Gruber, A. (2017). Optogenetic neuromodulation of the heart. *J. Am. Coll. Cardiol.* 70, 2791–2794. doi: 10.1016/j.jacc.2017.10.003

Gold, M. H. (2011). Light-emitting diode. *Curr. Probl. Dermatol.* 42, 173–180. doi: 10.1159/000328326

Hulsmans, M., Clauss, S., Xiao, L., Aguirre, A. D., King, K. R., Hanley, A., et al. (2017). Macrophages facilitate electrical conduction in the heart. *Cell.* 169, 510–522 e20. doi: 10.1016/j.cell.2017.03.050

Kaniusas, E., Kampusch, S., Tittgemeyer, M., Panetsos, F., Gines, R. F., Papa, M., et al. (2019a). Current directions in the auricular vagus nerve stimulation II–an engineering perspective. *Front. Neurosci.* 13:772. doi: 10.3389/fnins.2019.00772

Kaniusas, E., Kampusch, S., Tittgemeyer, M., Panetsos, F., Gines, R. F., Papa, M., et al. (2019b). Current directions in the auricular vagus nerve stimulation I–a physiological perspective. *Front. Neurosci.* 13:854. doi: 10.3389/fnins.2019.00854

Kim, H., Chiu, A., Lee, S. D., Fischer, K., and Yoo, S. S. (2014). Focused ultrasound-mediated non-invasive brain stimulation: examination of sonication parameters. *Brain Stimul.* 7, 748–756. doi: 10.1016/j.brs.2014.06.011

Lai, Y., Yu, L., and Jiang, H. (2019). Autonomic neuromodulation for preventing and treating ventricular arrhythmias. *Front. Physiol.* 10:200. doi: 10.3389/fphys.2019.00200

Leinenga, G., Langton, C., Nisbet, R., and Gotz, J. (2016). Ultrasound treatment of neurological diseases–current and emerging applications. *Nat. Rev. Neurol.* 12, 161–174. doi: 10.1038/nrneurol.2016.13

Levy, R., Henderson, J., Slavin, K., Simpson, B. A., Barolat, G., Shipley, J., et al. (2011). Incidence and avoidance of neurologic complications with paddle type spinal cord stimulation leads. *Neuromodulation* 14, 412–422; discussion 22. doi: 10.1111/j.1525-1403.2011.00395.x

Levy, R. M. (2013). Device complication and failure management in neuromodulation. *Neuromodulation* 16, 495–502. doi: 10.1111/ner.12148

Li, N., Oida, S., Tulevski, G. S., Han, S. J., Hannon, J. B., Sadana, D. K., et al. (2013). Efficient and bright organic light-emitting diodes on single-layer graphene electrodes. *Nat. Commun.* 4:2294. doi: 10.1038/ncomms3294

Lohmeier, T. E., and Hall, J. E. (2019). Device-based neuromodulation for resistant hypertension therapy. *Circ. Res.* 124, 1071–1093. doi: 10.1161/CIRCRESAHA.118.313221

Lopshire, J. C., and Zipes, D. P. (2014). Spinal cord stimulation for heart failure: preclinical studies to determine optimal stimulation parameters for clinical efficacy. *J. Cardiovasc. Transl. Res.* 7, 321–329. doi: 10.1007/s12265-014-9547-7

Lotti, F., Ranieri, F., Vadala, G., Zollo, L., and Di Pino, G. (2017). Invasive intraneural interfaces: foreign body reaction issues. *Front. Neurosci.* 11:497. doi: 10.3389/fnins.2017.00497

Mann, D. L., and Deswal, A. (2003). Angiotensin-receptor blockade in acute myocardial infarction–a matter of dose. *N. Engl. J. Med.* 349, 1963–1965. doi: 10.1056/NEJMe038163

Mwamburi, M., Liebler, E. J., and Tenaglia, A. T. (2017). Review of non-invasive vagus nerve stimulation (gammaCore): efficacy, safety, potential impact on comorbidities, and economic burden for episodic and chronic cluster headache. *Am. J. Manag. Care* 23, S317–S325.

Mwamburi, M., Tenaglia, A. T., Leibler, E. J., and Staats, P. S. (2018). Cost-effectiveness of noninvasive vagus nerve stimulation for acute treatment of episodic migraine and role in treatment sequence strategies. *Am. J. Manag. Care* 24, S527–S533.

Nasi-Er, B. G., Wenhui, Z., HuaXin, S., Xianhui, Z., Yaodong, L., Yanmei, L., et al. (2019). Vagus nerve stimulation reduces ventricular arrhythmias and increases ventricular electrical stability. *Pacing Clin. Electrophysiol.* 42, 247–256. doi: 10.1111/pace.13585

Nishikawa, T., Saku, K., Todaka, K., Kuwabara, Y., Arai, S., Kishi, T., et al. (2017). The challenge of magnetic vagal nerve stimulation for myocardial infarction - preliminary clinical trial. *Conf. Proc. IEEE Eng. Med. Biol. Soc.* 2017, 4321–4324. doi: 10.1109/EMBC.2017.8037812

Nussinovitch, U., and Gepstein, L. (2015). Optogenetics for *in vivo* cardiac pacing and resynchronization therapies. *Nat. Biotechnol.* 33, 750–754. doi: 10.1038/nbt.3268

Olshansky, B. (2016). Vagus nerve modulation of inflammation: cardiovascular implications. *Trends Cardiovasc. Med.* 26, 1–11. doi: 10.1016/j.tcm.2015.03.016

Petraglia, F. W. III, Farber, S. H., Gramer, R., Verla, T., Wang, F., Thomas, S., et al. (2016). The incidence of spinal cord injury in implantation of percutaneous and paddle electrodes for spinal cord stimulation. *Neuromodulation* 19, 85–90. doi: 10.1111/ner.12370

Redgrave, J., Day, D., Leung, H., Laud, P. J., Ali, A., Lindert, R., et al. (2018). Safety and tolerability of transcutaneous vagus nerve stimulation in humans; a systematic review. *Brain Stimul.* 11, 1225–1238. doi: 10.1016/j.brs.2018.08.010

Ricardo, J. A., and Koh, E. T. (1978). Anatomical evidence of direct projections from the nucleus of the solitary tract to the hypothalamus, amygdala, and other forebrain structures in the rat. *Brain Res.* 153, 1–26. doi: 10.1016/0006-8993(78)91125-3

Ripplinger, C. M., Noujaim, S. F., and Linz, D. (2016). The nervous heart. *Prog. Biophys. Mol. Biol.* 120, 199–209. doi: 10.1016/j.pbiomolbio.2015.12.015

Roth, G. A., Johnson, C., Abajobir, A., Abd-Allah, F., Abera, S. F., Abyu, G., et al. (2017). Global, regional, and national burden of cardiovascular diseases for 10 causes, 1990 to 2015. *J. Am. Coll. Cardiol.* 70, 1–25. doi: 10.1016/j.jacc.2017.04.052

Sahyouni, R., Chang, D. T., Moshtaghi, O., Mahmoodi, A., Djalilian, H. R., and Lin, H. W. (2017). Functional and histological effects of chronic neural electrode implantation. *Laryngosc. Investig. Otolaryngol.* 2, 80–93. doi: 10.1002/lio2.66

Schestatsky, P., Simis, M., Freeman, R., Pascual-Leone, A., and Fregni, F. (2013). Non-invasive brain stimulation and the autonomic nervous system. *Clin. Neurophysiol.* 124, 1716–1728. doi: 10.1016/j.clinph.2013.03.020

Schluter, R. S., Daams, J. G., van Holst, R. J., and Goudriaan, A. E. (2018). Effects of non-invasive neuromodulation on executive and other cognitive functions in addictive disorders: a systematic review. *Front Neurosci.* 12:642. doi: 10.3389/fnins.2018.00642

Shamji, M. F., Westwick, H. J., and Heary, R. F. (2015). Complications related to the use of spinal cord stimulation for managing persistent postoperative

neuropathic pain after lumbar spinal surgery. *Neurosurg. Focus* 39:E15. doi: 10.3171/2015.7.FOCUS15260

Shen, M. J., and Zipes, D. P. (2014). Role of the autonomic nervous system in modulating cardiac arrhythmias. *Circ. Res.* 114, 1004–1021. doi: 10.1161/CIRCRESAHA.113.302549

Shen, X., Scherlag, B. J., He, B., Sun, J., Mei, G., and Po, S. S. (2013). The role of the atrial neural network in atrial fibrillation: the metastatic progression hypothesis. *J. Atr. Fibrillation* 6:882. doi: 10.4022/jafib.882

Sheng, X., Chen, M., Huang, B., Liu, J., Zhou, L., Bao, M., et al. (2016). Cardioprotective effects of low-level carotid baroreceptor stimulation against myocardial ischemia-reperfusion injury in canine model. *J. Interv. Card Electrophysiol.* 45, 131–140. doi: 10.1007/s10840-015-0094-1

Sheng, X., Scherlag, B. J., Yu, L., Li, S., Ali, R., Zhang, Y., et al. (2011). Prevention and reversal of atrial fibrillation inducibility and autonomic remodeling by low-level vagosympathetic nerve stimulation. *J. Am. Coll. Cardiol.* 57, 563–571. doi: 10.1016/j.jacc.2010.09.034

Shiozawa, P., Silva, M. E., Carvalho, T. C., Cordeiro, Q., Brunoni, A. R., and Fregni, F. (2014). Transcutaneous vagus and trigeminal nerve stimulation for neuropsychiatric disorders: a systematic review. *Arq. Neuropsiquiatr.* 72, 542–547. doi: 10.1590/0004-282X20140061

Simon, B., and Blake, J. (2017). Mechanism of action of non-invasive cervical vagus nerve stimulation for the treatment of primary headaches. *Am. J. Manag. Care* 23, S312–S316.

Sohinki, D., and Stavrakis, S. (2019). New approaches for treating atrial fibrillation: focus on autonomic modulation. *Trends Cardiovasc. Med.* 30, 433–439. doi: 10.1016/j.tcm.2019.10.009

Sorbellini, E., Rucco, M., and Rinaldi, F. (2018). Photodynamic and photobiological effects of light-emitting diode (LED) therapy in dermatological disease: an update. *Lasers Med. Sci.* 33, 1431–1439. doi: 10.1007/s10103-018-2584-8

Stavrakis, S., Humphrey, M. B., Scherlag, B., Iftikhar, O., Parwani, P., Abbas, M., et al. (2017). Low-level vagus nerve stimulation suppresses post-operative atrial fibrillation and inflammation: a randomized study. *JACC Clin. Electrophysiol.* 3, 929–938. doi: 10.1016/j.jacep.2017.02.019

Stavrakis, S., Humphrey, M. B., Scherlag, B. J., Hu, Y., Jackman, W. M., Nakagawa, H., et al. (2015). Low-level transcutaneous electrical vagus nerve stimulation suppresses atrial fibrillation. *J. Am. Coll. Cardiol.* 65, 867–875. doi: 10.1016/j.jacc.2014.12.026

Tassorelli, C., Grazzi, L., de Tommaso, M., Pierangeli, G., Martelletti, P., Rainero, I., et al. (2018). Noninvasive vagus nerve stimulation as acute therapy for migraine: the randomized PRESTO study. *Neurology* 91, e364–e373. doi: 10.1212/WNL.0000000000005857

Vernieri, F., Altamura, C., Palazzo, P., Altavilla, R., Fabrizio, E., Fini, R., et al. (2014). 1-Hz repetitive transcranial magnetic stimulation increases cerebral vasomotor reactivity: a possible autonomic nervous system modulation. *Brain Stimul.* 7, 281–286. doi: 10.1016/j.brs.2013.12.014

Vogt, C. C., Bruegmann, T., Malan, D., Ottersbach, A., Roell, W., Fleischmann, B. K., et al. (2015). Systemic gene transfer enables optogenetic pacing of mouse hearts. *Cardiovasc. Res.* 106, 338–343. doi: 10.1093/cvr/cvv004

Waldron, N. H., Fudim, M., Mathew, J. P., and Piccini, J. P. (2019). Neuromodulation for the treatment of heart rhythm disorders. *JACC Basic Transl. Sci.* 4, 546–562. doi: 10.1016/j.jacbts.2019.02.009

Wang, S., Li, B., Li, X., Wu, L., and Jiang H (2019a). Low intensity ultrasound stimulation might reduce ventricular arrhythmias by modulation sympathetic neural activity in myocardial infarction canine model. *J. Am. Coll. Cardiol.* 73:1. doi: 10.1016/S0735-1097(19)31139-8

Wang, S., Li, H., Yu, L., Chen, M., Wang, Z., Huang, B., et al. (2015). Anti-arrhythmic effects of atrial ganglionated plexi stimulation is accompanied by preservation of connexin43 protein in ischemia-reperfusion canine model. *Int. J. Clin. Exp. Med.* 8, 22098–22107.

Wang, S., Wu, L., Li, X., Li, B., Zhai, Y., Zhao, D., et al. (2019c). Light-emitting diode therapy protects against ventricular arrhythmias by neuro-immune modulation in myocardial ischemia and reperfusion rat model. *J. Neuroinflammation* 16:139. doi: 10.1186/s12974-019-1513-5

Wang, S., Wu, L., Zhai, Y., Li, X., Li, B., Zhao, D., et al. (2019b). Noninvasive light emitting diode therapy: a novel approach for postinfarction ventricular arrhythmias and neuroimmune modulation. *J. Cardiovasc. Electrophysiol.* 30, 1138–1147. doi: 10.1111/jce.13974

Wang, S., Zhou, X., Huang, B., Wang, Z., Zhou, L., Wang, M., et al. (2016). Noninvasive low-frequency electromagnetic stimulation of the left stellate ganglion reduces myocardial infarction-induced ventricular arrhythmia. *Sci. Rep.* 6:30783. doi: 10.1038/srep30783

Wang, Z., Yu, L., Huang, B., Wang, S., Liao, K., Saren, G., et al. (2015). Low-level transcutaneous electrical stimulation of the auricular branch of vagus nerve ameliorates left ventricular remodeling and dysfunction by downregulation of matrix metalloproteinase 9 and transforming growth factor beta1. *J. Cardiovasc. Pharmacol.* 65, 342–348. doi: 10.1097/FJC.0000000000000201

Wang, Z., Yu, L., Wang, S., Huang, B., Liao, K., Saren, G., et al. (2014). Chronic intermittent low-level transcutaneous electrical stimulation of auricular branch of vagus nerve improves left ventricular remodeling in conscious dogs with healed myocardial infarction. *Circ. Heart Fail.* 7, 1014–1021. doi: 10.1161/CIRCHEARTFAILURE.114.001564

Wasilczuk, K. M., Bayer, K. C., Somann, J. P., Albors, G. O., Sturgis, J., Lyle, L. T., et al. (2019). Modulating the inflammatory reflex in rats using low-intensity focused ultrasound stimulation of the vagus nerve. *Ultrasound Med. Biol.* 45, 481–489. doi: 10.1016/j.ultrasmedbio.2018.09.005

Wengrowski, A. M., Wang, X., Tapa, S., Posnack, N. G., Mendelowitz, D., and Kay, M. W. (2015). Optogenetic release of norepinephrine from cardiac sympathetic neurons alters mechanical and electrical function. *Cardiovasc. Res.* 105, 143–150. doi: 10.1093/cvr/cvu258

Wickramasinghe, S. R., and Patel, V. V. (2013). Local innervation and atrial fibrillation. *Circulation* 128, 1566–1575. doi: 10.1161/CIRCULATIONAHA.113.001596

Witt, C. M., Bolona, L., Kinney, M. O., Moir, C., Ackerman, M. J., Kapa, S., et al. (2017). Denervation of the extrinsic cardiac sympathetic nervous system as a treatment modality for arrhythmia. *Europace* 19, 1075–1083. doi: 10.1093/europace/eux011

Yamamoto, K., Lalley, P., and Mifflin, S. (2015). Acute intermittent optogenetic stimulation of nucleus tractus solitarius neurons induces sympathetic long-term facilitation. *Am. J. Physiol. Regul. Integr. Comp. Physiol.* 308, R266–R275. doi: 10.1152/ajpregu.00381.2014

Yu, L., Dyer, J. W., Scherlag, B. J., Stavrakis, S., Sha, Y., Sheng, X., et al. (2015). The use of low-level electromagnetic fields to suppress atrial fibrillation. *Heart Rhythm* 12, 809–817. doi: 10.1016/j.hrthm.2014.12.022

Yu, L., Huang, B., Po, S. S., Tan, T., Wang, M., Zhou, L., et al. (2017c). Low-level tragus stimulation for the treatment of ischemia and reperfusion injury in patients with ST-segment elevation myocardial infarction: a proof-of-concept study. *JACC Cardiovasc. Interv.* 10, 1511–1520. doi: 10.1016/j.jcin.2017.04.036

Yu, L., Huang, B., Wang, Z., Wang, S., Wang, M., Li, X., et al. (2017b). Impacts of renal sympathetic activation on atrial fibrillation: the potential role of the autonomic cross talk between kidney and heart. *J. Am. Heart Assoc.* 6:e004716. doi: 10.1161/JAHA.116.004716

Yu, L., Huang, B., Zhou, X., Wang, S., Wang, Z., Wang, M., et al. (2017a). Renal sympathetic stimulation and ablation affect ventricular arrhythmia by modulating autonomic activity in a cesium-induced long QT canine model. *Heart Rhythm* 14, 912–919. doi: 10.1016/j.hrthm.2017.02.010

Yu, L., Scherlag, B. J., Li, S., Fan, Y., Dyer, J., Male, S., et al. (2013). Low-level transcutaneous electrical stimulation of the auricular branch of the vagus nerve: a noninvasive approach to treat the initial phase of atrial fibrillation. *Heart Rhythm* 10, 428–435. doi: 10.1016/j.hrthm.2012.11.019

Yu, L., Wang, S., Zhou, X., Wang, Z., Huang, B., Liao, K., et al. (2016). Chronic intermittent low-level stimulation of tragus reduces cardiac autonomic remodeling and ventricular arrhythmia inducibility in a post-infarction canine model. *JACC Clin. Electrophysiol.* 2, 330–339. doi: 10.1016/j.jacep.2015.11.006

Yu, L., Zhou, L., Cao, G., Po, S. S., Huang, B., Zhou, X., et al. (2017d). Optogenetic modulation of cardiac sympathetic nerve activity to prevent ventricular arrhythmias. *J. Am. Coll. Cardiol.* 70, 2778–2790. doi: 10.1016/j.jacc.2017.09.1107

Zannad, F., De Ferrari, G. M., Tuinenburg, A. E., Wright, D., Brugada, J., Butter, C., et al. (2015). Chronic vagal stimulation for the treatment of low ejection fraction heart failure: results of the NEural Cardiac TherApy foR Heart Failure (NECTAR-HF) randomized controlled trial. *Eur. Heart J.* 36, 425–433. doi: 10.1093/eurheartj/ehu345

Zhang, Y., Ilsar, I., Sabbah, H. N., Ben David, T., and Mazgalev, T. N. (2009). Relationship between right cervical vagus nerve stimulation

and atrial fibrillation inducibility: therapeutic intensities do not increase arrhythmogenesis. *Heart Rhythm* 6, 244–250. doi: 10.1016/j.hrthm.2008.10.043

Zhou, L., Filiberti, A., Humphrey, M. B., Fleming, C. D., Scherlag, B. J., Po, S. S., et al. (2019). Low-level transcutaneous vagus nerve stimulation attenuates cardiac remodelling in a rat model of heart failure with preserved ejection fraction. *Exp. Physiol.* 104, 28–38. doi: 10.1113/EP087351

Zhou, X., Zhou, L., Wang, S., Yu, L., Wang, Z., Huang, B., et al. (2016). The use of noninvasive vagal nerve stimulation to inhibit sympathetically induced sinus node acceleration: a potential therapeutic approach for inappropriate sinus tachycardia. *J. Cardiovasc. Electrophysiol.* 27, 217–223. doi: 10.1111/jce.12859

Zipes, D. P. (2008). Heart-brain interactions in cardiac arrhythmias: role of the autonomic nervous system. *Clev. Clin. J. Med.* 75, S94–S96. doi: 10.3949/ccjm.75.Suppl_2.S94

Zipes, D. P. (2017). Ablation of atrial gangionated plexi to treat symptomatic sinus bradycardia. *JACC Clin. Electrophysiol.* 3, 960–961. doi: 10.1016/j.jacep.2017.02.010

Zoccal, D. B., Furuya, W. I., Bassi, M., Colombari, D. S., and Colombari, E. (2014). The nucleus of the solitary tract and the coordination of respiratory and sympathetic activities. *Front. Physiol.* 5:238. doi: 10.3389/fphys.2014.00238

Zubcevic, J., Richards, E. M., Yang, T., Kim, S., Sumners, C., Pepine, C. J., et al. (2019). Impaired autonomic nervous system-microbiome circuit in hypertension. *Circ. Res.* 125, 104–116. doi: 10.1161/CIRCRESAHA.119.313965

Conflict of Interest: The authors declare that the research was conducted in the absence of any commercial or financial relationships that could be construed as a potential conflict of interest.

frontiers in Neuroscience

ORIGINAL RESEARCH
published: 17 December 2020
doi: 10.3389/fnins.2020.619275

Recording of Electrically Evoked Neural Activity and Bladder Pressure Responses in Awake Rats Chronically Implanted With a Pelvic Nerve Array

*Sophie C. Payne[1,2], Nicole M. Wiedmann[3], Calvin D. Eiber[3], Agnes W. Wong[3], Philipp Senn[1,2], Peregrine B. Osborne[3], Janet R. Keast[3] and James B. Fallon[1,2,4]**

[1] Bionics Institute, Fitzroy, VIC, Australia, [2] Medical Bionics Department, University of Melbourne, Melbourne, VIC, Australia, [3] Department of Anatomy and Neuroscience, University of Melbourne, Melbourne, VIC, Australia, [4] Department of Otolaryngology, University of Melbourne, Melbourne, VIC, Australia

OPEN ACCESS

Edited by:
Jiande Chen, University of Michigan, United States

Reviewed by:
Changfeng Tai, University of Pittsburgh, United States
Sanghoon Lee, Daegu Gyeongbuk Institute of Science and Technology (DGIST), South Korea

***Correspondence:**
James B. Fallon
jfallon@bionicsinstitute.org

Specialty section:
This article was submitted to Autonomic Neuroscience, a section of the journal Frontiers in Neuroscience

Received: *19 October 2020*
Accepted: *25 November 2020*
Published: *17 December 2020*

Citation:
Payne SC, Wiedmann NM, Eiber CD, Wong AW, Senn P, Osborne PB, Keast JR and Fallon JB (2020) Recording of Electrically Evoked Neural Activity and Bladder Pressure Responses in Awake Rats Chronically Implanted With a Pelvic Nerve Array. Front. Neurosci. 14:619275. doi: 10.3389/fnins.2020.619275

Bioelectronic medical devices are well established and widely used in the treatment of urological dysfunction. Approved targets include the sacral S3 spinal root and posterior tibial nerve, but an alternate target is the group of pelvic splanchnic nerves, as these contain sacral visceral sensory and autonomic motor pathways that coordinate storage and voiding functions of the bladder. Here, we developed a device suitable for long-term use in an awake rat model to study electrical neuromodulation of the pelvic nerve (homolog of the human pelvic splanchnic nerves). In male Sprague-Dawley rats, custom planar four-electrode arrays were implanted over the distal end of the pelvic nerve, close to the major pelvic ganglion. Electrically evoked compound action potentials (ECAPs) were reliably detected under anesthesia and in chronically implanted, awake rats up to 8 weeks post-surgery. ECAP waveforms showed three peaks, with latencies that suggested electrical stimulation activated several subpopulations of myelinated A-fiber and unmyelinated C-fiber axons. Chronic implantation of the array did not impact on voiding evoked in awake rats by continuous cystometry, where void parameters were comparable to those published in naïve rats. Electrical stimulation with chronically implanted arrays also induced two classes of bladder pressure responses detected by continuous flow cystometry in awake rats: voiding contractions and non-voiding contractions. No evidence of tissue pathology produced by chronically implanted arrays was detected by immunohistochemical visualization of markers for neuronal injury or noxious spinal cord activation. These results demonstrate a rat pelvic nerve electrode array that can be used for preclinical development of closed loop neuromodulation devices targeting the pelvic nerve as a therapy for neuro-urological dysfunction.

Keywords: micturition, continence, splanchnic nerve, neuromodulation, pelvic ganglion

INTRODUCTION

Electrical neuromodulation (neurostimulation) is an effective therapeutic technology for treating lower urinary tract (LUT) dysfunction in some patients. The United States Food and Drug Administration (FDA) has approved two targets—the sacral S3 spinal root and posterior tibial nerve (de Groat and Tai, 2018)—which are now well established, with commercial devices widely used to deliver safe, effective therapy. However, neither is effective across the full range of urological indications, including many neuro-urological conditions caused by dysfunction in the neural circuit that controls normal storage and voiding (micturition) and other urological functions.

Preclinical studies in animal models suggest that the pelvic nerve (rodent homolog of human pelvic splanchnic nerves) is a potential neuromodulation target for neuro-urological and other pelvic functional disorders (Crook and Lovick, 2017; Langdale et al., 2017; Crook et al., 2018; Langdale et al., 2020). For example, in cats and rodents, these paired nerves contain the majority of external sacral sensory and autonomic motor projections needed for bladder sensation and contraction. More specifically, they contain all LUT visceral sensory axons projecting from sacral dorsal root ganglia to the bladder and urethra, and all sacral spinal preganglionic axons that innervate postganglionic neurons in pelvic ganglia (inferior hypogastric plexus in human). Pelvic ganglia provide the parasympathetic motor innervation of the bladder and urethra smooth muscle. The predominance of visceral LUT afferents and autonomic efferents differentiates this pelvic nerve pathway as a neuromodulation target from existing devices (i.e., sacral, tibial, and pudendal nerve stimulation; transcutaneous stimulation of pudendal nerve or foot; Goldman et al., 2008; Yoo et al., 2009; Peters et al., 2010; Opisso et al., 2013; Ammi et al., 2014; Chen et al., 2014), which instead generally target somatic nerves and their central circuits. On this basis, electrical neuromodulation of pelvic nerves can be compared to vagal neuromodulation used to primarily target autonomic preganglionic efferent and visceral afferent axons.

Targeting pelvic nerve neuromodulation to urological dysfunction will require overcoming some known challenges. First, it needs to be determined if electrical pelvic nerve stimulation can be used to produce predictable therapeutic outcomes. Animal models allow the urodynamic effects of electrical pelvic nerve stimulation to be measured by constant flow cystometry. This assay is based on a method of functional clinical assessment and uses a catheter to fill the bladder and record physiological LUT activity by measuring changes in the intra-vesical pressure. The resulting cystometrogram is used to track micturition cycles comprising repeated episodes of bladder filling followed by the coordinated contraction of the bladder and opening of the urethral rhabdosphincter that expels urine (Andersson et al., 2011). This activity is produced by a peripheral LUT sensorimotor system controlled by a neural control circuit in spinal cord and brain. Previous work in anesthetized animal models has established that pelvic neuromodulation can both facilitate (Andersson et al., 1990; Dalmose et al., 2002; Peh et al., 2018) or inhibit LUT activity (Crook and Lovick, 2017). However, further characterization of the stimulus-response relationship is clearly needed and strategies to limit off-target effects on other pelvic organs that receive input from the pelvic nerve (e.g., lower bowel and sex organs). For clinical translation, it will also be necessary to optimize devices used for pelvic neuromodulation by adapting designs used for large somatic nerves or visceral nerves such as the proximal branches of the vagus (Fallon and Carter, 2016; Horn et al., 2019; Naufel et al., 2020). Another strategy is to design devices that can self-calibrate by using evoked compound action potentials (ECAPs) to adjust electrical stimulus parameters (Bouton and Czura, 2018; Parker, 2018; Parker et al., 2018).

In this study, we demonstrate that a custom four-electrode planar array can be surgically implanted over the distal end of the pelvic nerve and used to produce urodynamic effects by electrical neuromodulation in awake male rats. The array design most commonly used in the clinic has electrodes placed outside the epineurium in a spiral, split-cylinder or folding cuff that surrounds a length of nerve (Guiraud et al., 2016; Larson and Meng, 2020). Cuff electrode designs limit damage associated with invasive inter- and intra-fascicular designs (Naufel et al., 2020) and provide an electrically insulating enclosure which increases the electrical coupling between the nerves and the stimulating electrodes, reducing thresholds. However, cuff electrodes retain the risk of damaging small nerves by constriction, edge abrasion or evoking a foreign body response that affects the physiological properties of nerve firing (Gonzalez-Gonzalez et al., 2018; Lee et al., 2019; Larson and Meng, 2020). We have used a custom planar array that can be positioned adjacent to the pelvic nerve but is anchored to the surrounding tissue. The design using four electrodes also allowed a recording pair to be used for detecting ECAPs generated by stimulation from the alternate electrode pair. The effects of pelvic nerve implantation and stimulation on voiding were assessed using continuous flow cystometry in awake male rats for periods of up to 8 weeks. At the completion of these longer-term chronic studies, immunohistochemical studies on ganglia and spinal tissues were used to assess whether surgical attachment of the array directly injured neural projections through the pelvic nerve. Patterns of immediate early gene (c-Fos) expression in the lumbosacral cord to identify potential activation of nociceptive circuits were also examined.

MATERIALS AND METHODS

Animals

All animal procedures were approved by the Animal Ethics Committees of St. Vincent's Hospital (Melbourne), the Bionics Institute or University of Melbourne, and complied with the Australian Code for the Care and Use of Animals for Scientific Purposes (National Health and Medical Research Council of Australia). A total of 24 male Sprague-Dawley rats (8–9 weeks, Biomedical Sciences Animal Facility, University of Melbourne; or Animal Resource Centre, Western Australia) were used for experiments. Implanted rats were housed individually with

environmental enrichment under a 12 h light/dark cycle with *ad libitum* access to standard chow and water.

Design of a Custom Planar Four-Electrode Array

The pelvic nerve electrode array (**Figure 1A**) consisted of four platinum (99.95%) electrodes embedded in a medical grade silicone elastomer cuff. Individually insulated 50 μm diameter platinum/iridium (90/10) wires were welded to each electrode and formed a helical cable which traversed to a percutaneous connector. Each platinum electrode had an exposed recessed surface area of 0.36 mm^2 (1.8 mm × 0.2 mm). The distance between adjacent electrodes (E1– E2, or E3–E4, center to center) was 0.75 mm, while the distance between electrode pairs (E1–E2 to E3–E4, center to center) was 2.85 mm (**Figure 1B**). A Dacron

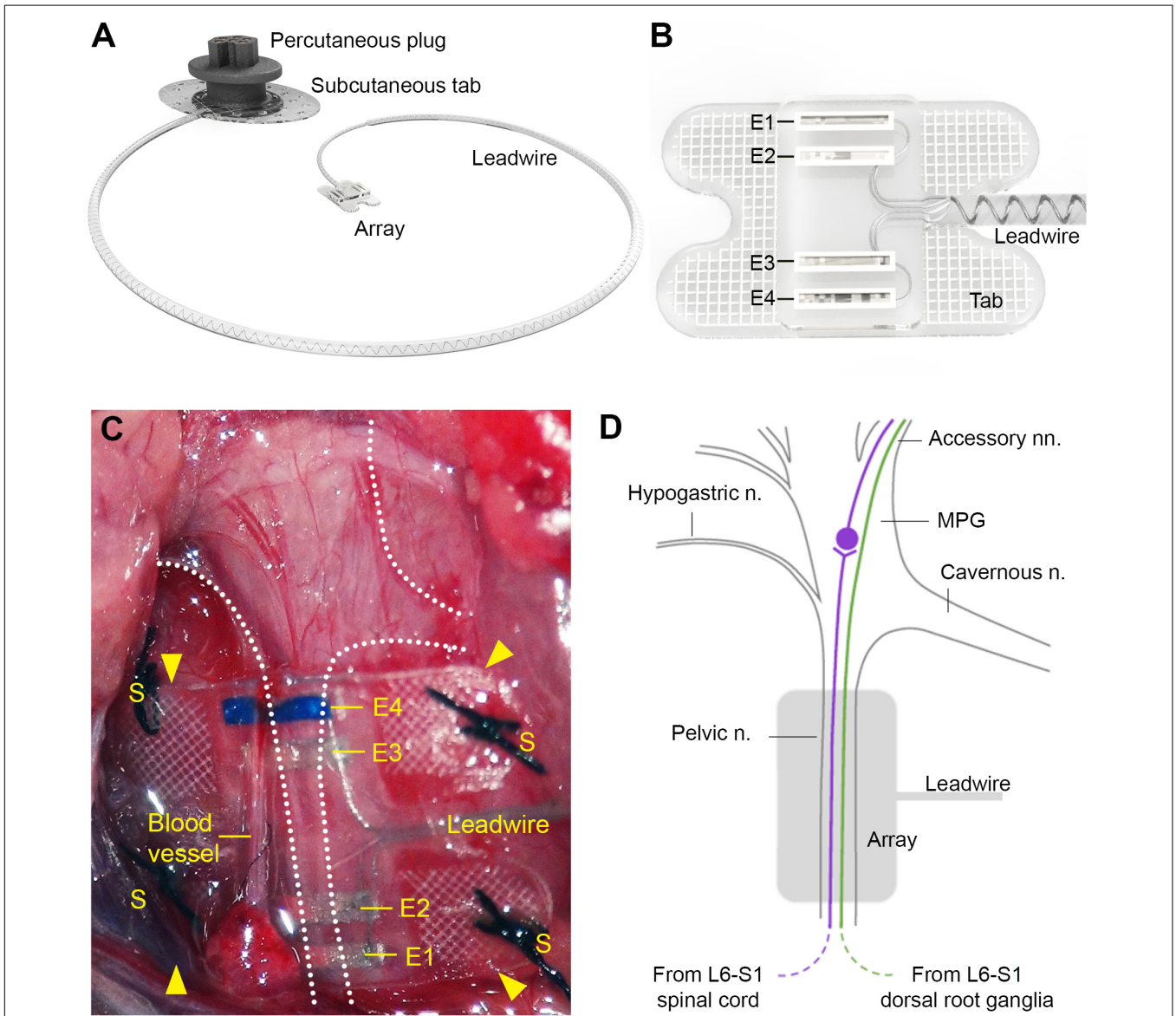

FIGURE 1 | Design of the pelvic nerve electrode array. **(A)** Rendered drawing shows the pelvic nerve array, cable, and percutaneous plug. **(B)** The pelvic nerve array had two platinum electrode pairs (E1–E2, E3–E4) that could be used to stimulate or record evoked neural responses. The array was anchored by suturing the silicon-embedded Dacron tab to connective tissue overlying the prostate gland. **(C)** An *in vivo* image of the implanted pelvic nerve array overlying the right pelvic nerve. Sutures are indicated by "S" and electrodes are indicated by "E1" (closest to the bladder) to "E4" (closest to the spinal cord). **(D)** Schematic diagram indicates the anatomy of the right major pelvic ganglion and its associated nerves, with the location of the electrode array indicated (gray). The pelvic nerve contains parasympathetic preganglionic (motor) axons originating from the intermediolateral column of the L6-S1 cord and sensory axons from the L6-S1 dorsal root ganglia. Preganglionic axons synapse on ganglion neurons that then project to the bladder via the accessory nerves. Sensory axons project to the bladder and colon via the same nerves. Ganglion neurons innervating other pelvic organs are not shown, but include neurons projecting to erectile tissue via the cavernous nerve. Sympathetic ganglion neurons are innervated by spinal preganglionic axons entering the ganglion via the hypogastric nerve (not visible here).

embedded silicone tab surrounded the electrode (**Figure 1B**) to allow anchoring of the array (using sutures) to connective tissue on the surface of the prostate.

Surgery

Rats were surgically implanted with a pelvic nerve array and a bladder catheter for use in awake ECAP or urodynamic recordings. All surgical procedures were performed under isoflurane anesthesia (3% for induction and 1.8–2% for maintenance, in 1.5–2 l/min oxygen) and aseptic conditions. Analgesia was provided using buprenorphine (Temgesic, 0.5 mg/kg, s.c.) administered prior to surgery and ∼10 h post-surgery.

Pelvic Nerve Array

This protocol is described in detail in Fallon et al. (2020). To implant the device, the electrode array attached to the lead wire was first subcutaneously tunneled through a skin incision along the dorsal-lumbar aspect of the spine to exit through a ventral midline abdominal incision. This ventral abdominal incision was used to access the abdominal cavity to gently retract the prostate and reveal the right pelvic ganglia and connecting nerves (**Figures 1C,D**). The pelvic nerve was then identified and carefully cleared of surrounding fat and connective tissue to allow good contact of the electrode and onto the nerve. Care was taken to identify rectal nerves and to avoid damage to them and blood vessels during clearing of connective tissue and implantation of the array. The array was then positioned against the pelvic nerve close to the pelvic ganglion, so that it was aligned with the nerve running perpendicular across all four electrodes. The four tabs were used to suture (7'0 silk, Ethicon, Somerville, NJ, United States) the array to connective tissue superficial to the prostate. The abdominal cavity was then closed around the lead wire and the muscle and skin sutured closed, after which the rat was rotated to expose the dorsal-lumbar aspect of the spine to allow the percutaneous pedestal to be sutured and skin closed around the plug.

Bladder Catheter Implantation

This protocol is described in detail in Keast et al. (2020a). After exposing the bladder via a ventral midline abdominal incision, the dome was punctured with an 18G needle to allow insertion of polyethylene catheter (PE-10: od: 0.61 mm × id: 0.28 mm; SteriHealth, VIC, Australia) with a flared end (made by heating the tubing). This was secured with a purse-string suture [sterile monofilament suture II PDS (polydioxanone); Ethicon]. The length of the catheter was then passed through a subcutaneous tunnel and externalized by anchoring to the interscapular skin. The free end of the catheter was sealed to prevent leakage. The abdominal wound was closed using suture, and the skin closed using surgical skin staples (Fine Science Tools, Foster City, CA, United States). In the postsurgical period prior to testing, the catheter was infused with Gentamicin (0.2 ml, 40 mg/ml) for 3 days and then daily with 0.9% saline (0.5 ml) (Keast et al., 2020a).

Recording and Analysis

Electrically Evoked Compound Action Potentials and Impedance Testing

A total of five rats (Animal Resource Centre, Western Australia) were used for end-of-life ECAP recordings under urethane anesthesia (1.2 g/kg subcutaneous, Merck (Sigma-Aldrich, St Louis, MO, United States). All rats were placed on a heated pad and kept hydrated (1 ml sterile physiological saline/100 g) for the duration of the recording, after which all rats were euthanized (300 mg/kg intramuscular Lethobarb; Virbac, Wetherill Park, NSW Australia). In a separate cohort, in-life ECAP recordings were also made in three awake rats chronically implanted with a pelvic nerve electrode array. As described in Fallon and Payne (2020), ECAPs were recorded by stimulating with electrode pair E1–E2 (bipolar stimulation, 100 μs pulse width with 50 μs interphase gap; 10 Hz) and recording with electrode pair E3–E4 (bipolar recording). Two sets of ECAPs (averaged from a total of 50 responses each) were made at currents from 0 to 2 mA in 0.1 mA steps. Recordings were sampled at a rate of 100 kHz and filtered (high pass: 300 Hz; low pass: 5000 Hz; voltage gain 10^2). The ECAP threshold was defined as the minimum stimulus intensity producing a response amplitude of at least 0.05 μV in both recordings.

During the chronic implantation period, the functionality of electrodes was routinely tested by measuring the common ground impedance of electrodes (Fallon et al., 2009). Biphasic current pulses (25 μs per phase and current of 931 μA) were passed between the electrode of interest and all other implanted electrodes, and the peak voltage at the end of the first phase (V_{total}) measured. The V_{total} value was then used to calculate total impedance (Z_{total}) using Ohm's law (Z = voltage/current).

Colonic Pressure Responses During Pelvic Nerve Stimulation

In three urethane anesthetized rats, a balloon-catheter was used to monitor pressure in the colon during pelvic nerve stimulation. The latex balloon and the end of the catheter was inserted 8 cm into the distal colon via the rectum and secured to the tail using tape. Sterile saline was infused via the catheter to inflate the colonic balloon to pressures of about 30–35 mm Hg. Colonic pressure changes (MLT0670, ADInstruments, NSW, Australia) were recorded (Cerebrus, Blackrock, Preston, VIC, Australia) in response to pelvic nerve electrical stimulation delivered at 10 Hz, 100 μs pulse width and current of 1 mA. This stimulation level was confirmed to be supra-threshold for all evoked neural populations by recording ECAPs.

Bladder Pressure Responses During Cystometry and Pelvic Nerve Stimulation

In our initial studies performed to establish the surgical procedures (n = 12), many of the bladder pressure recordings were challenged by several technical issues, such as grooming and exploratory behaviors of the rat and unstable baseline pressures. For detailed quantitative analyses of voiding parameters, we therefore established a habituation protocol similar to that described in Keast et al. (2020a), i.e., prior to cystometry testing, the animals (n = 12) were habituated to the testing

environment for 3 consecutive days for 30 min per session. The habituation procedure was also important to reduce effects of these non-voiding related behaviors on c-Fos expression (see below) during the testing period. These habituations and experimental cystometry sessions were confined to the morning to minimize effects of diurnal variation. In these sessions, each rat was placed unrestrained in a clear Perspex box (20.5 × 20.5 × 14 cm) with a mesh floor, elevated on a 45 cm high frame. This allowed free flow of urine during voiding. During habituation periods, the percutaneous plug and catheter were connected, but no stimulation or saline infusion was delivered.

Between 7 and 18 days following the implantation surgery, cystometry and stimulation testing was conducted over a 2-h period. Saline was infused at a rate of 100 μl per minute (HA33, Harvard Apparatus, Holliston, MA, United States) and pressure changes during cystometry testing were transduced (MLT0670, ADInstruments), amplified (PowerLab 4/26, ADInstruments), sampled at 1 kHz (PowerLab, AD Instruments) and viewed using Labchart (AD Instruments). After establishing a stable baseline pressure and inter-void interval (Andersson et al., 2011) the pelvic nerve was stimulated using a custom made external stimulator (Fallon et al., 2018) to deliver 10 s of biphasic current pulses (100 μs pulse width, rate of 10–25 Hz, current levels 0.5–1.5 mA) at selected stages of the micturition cycle. For a subset of experiments, following the cystometry and stimulation testing, each rat was returned to its home cage for 2 h to maximize activity-dependent translation of c-Fos protein (Yap and Greenberg, 2018). Animals were then anesthetized (ketamine: 100 mg/kg and xylazine: 10 mg/kg, intra-peritoneal) and perfused intracardially with fixative, prior to tissue removal for histological study (see below).

Cystometry data were analyzed using customized MATLAB software (R2019b, MathWorks, MA, United States). Voiding contractions induced by continuous flow cystometry were recorded for three cycles prior to the delivery of stimulation and analyzed to determine standard urodynamic parameters (Andersson et al., 2011; Fraser et al., 2020; **Table 1**). To facilitate comparison with other studies absolute bladder pressures were converted to relative pressures (**Table 1**) by subtracting the minimum pressure after voiding contractions. High-frequency pressure oscillations (HFPOs), which in rodents are caused by activity of the urethral rhabdosphincter which permits the flow of urine (Andersson et al., 2011; Fraser et al., 2020), detected during voiding contractions were also analyzed to estimate the center frequency of oscillation.

Bladder pressure responses to stimulation were classified as voiding or non-voiding contractions based on the visible excretion of urine. This was typically accompanied by a period of high frequency bladder pressure oscillation.

Immunohistochemical Analysis of Nerve Injury Markers

Pelvic ganglia and dorsal root ganglia (L6 and S1), ipsilateral and contralateral to the implant were removed from two rats, 50 days post-implantation and immunostained for neural injury markers. Specifically, these animals were anesthetized (ketamine: 100 mg/kg and xylazine: 10 mg/kg, intra-peritoneal) and perfused intracardially with saline (0.9% sodium chloride, 1% sodium nitrite, and 5000 IU/ml heparin) then fixative (4% paraformaldehyde in 0.1 M phosphate buffer, pH 7.4). The detailed perfusion method has been published (Keast and Osborne, 2019). The dissected ganglia were then post-fixed overnight in the same fixative. Following three 15-min washes (0.1 M phosphate-buffered saline; PBS, pH 7.2), the ganglia were cryoprotected (0.1 M PBS containing 30% sucrose), embedded in an inert mounting medium (OCT; Tissue-Tek, Sakura, Torrance, CA, United States) then sectioned on a cryostat. Serial frozen sections (14 μm) aligned with the major axis of each ganglion were collected onto gelatin-subbed slides. These were washed in PBS and incubated in PBS containing 10% non-immune horse serum and 0.1% Triton X-100. Sections were then incubated for 18–24 h at room temperature with an antibody against: ATF-3 (host rabbit; 1:500, Santa Cruz Biotechnology; sc-188, batch J2209; RRID:AB_2258513); calcitonin gene-related peptide (CGRP) (host goat, 1:2000; AbD Serotec, now Bio-Rad, Gladesville, NSW, Australia; 1720-9007, batch 1705; RRID:AB 2290729; or synaptophysin (host mouse, 1:200; Dako, now Agilent Technologies, Mulgrave, VIC, Australia; M0776, batch 13; RRID:AB_2199013). After washes in PBS, sections were then incubated for 2 h at room temperature with fluorescent secondary antibodies (Jackson Immunoresearch, West Grove, PA, United States): anti-mouse AF488 (1:2000,

TABLE 1 | Urodynamic parameters of unstimulated voiding during continuous cystometry in awake male rats after implanting pelvic nerve arrays.

Parameter (units)[a]	Mean (95% CI) n = 9 rats[b]	Wiedmann et al., 2020 Mean (95% CI) n = 6 rats[b]
Minimum pressure (mmHg)	10.3 (7.4–13.2)	–
Relative threshold pressure (mmHg)	6.6 (4.7–8.4)	4.5 (1.8–7.3)
Relative peak (closing) pressure (mmHg)	51.2 (39.5–63.0)	44. 6 (15.3–74)
Contraction duration (s)	28.9 (17.1–37.5)	37.2 (25.1–49.3)
Inter-void interval (min)	7.6 (5.9–9.4)	8 (5.3–10.6)
HFPO[c] frequency (Hz)	10.7 (8.3–13.0)	–

[a] *Andersson et al., 2011; Fraser et al., 2020.*
[b] *Cystometry in awake male Sprague-Dawley rats.*
[c] *HFPO, high frequency pressure oscillation due to rhabdosphincter activity.*

715-545-150, RRID:AB_2340846); anti-goat AF594 (1:500, 705-855-147, RRID:AB 2340433); anti-rabbit AF488 (1:1000, 711-545-152, RRID:AB 2313584). Sections were then washed in PBS, mounted onto glass slides, cover-slipped with carbonate-buffered glycerol (pH 8.6) and viewed using a Zeiss AxioImager M2 (Zeiss, Oberkochan, Germany). Sections were assessed qualitatively to determine the features of structures labeled for each of the neural markers. Representative regions of ganglion were imaged to document the primary outcomes.

Neuronal c-Fos Activity Mapping in Spinal Cord

Neuronal activity mapping was used to detect electrically evoked noxious neuronal activation in lumbosacral spinal cord. After completing the final test session of electrical pelvic nerve stimulation (100 μs pulse width, rate of 10–25 Hz, current levels 0.5–1.5 mA) and cystometry recording on post-surgery day 10, three animals were returned to their home cage for 2 h before being anesthetized and fixed (see above). As described in Keast et al. (2020b), the spinal cord was removed and segments L5-S2 post-fixed for 1 h in the same fixative. Following three 1 h washes (0.1 M phosphate-buffered saline; PBS, pH 7.2), the tissue was cryoprotected (0.1 M PBS containing 30% sucrose), embedded in an inert mounting medium (OCT; Tissue-Tek, Sakura, Torrance, CA, United States) then sectioned on a cryostat. Sections (40 μm) were cut in the transverse plane and collected as four 1:4 series (160 μm between sections), such that five sections per spinal segment were to be investigated for c-Fos expression (see below). Specifically, free-floating sections were washed in 0.1 M PBS (pH 7.2) before being incubated for 2 h in 0.1 M PBS containing 10% non-immune horse serum (NHS; Sigma-Aldrich) and 0.5% Triton X-100. Sections were then incubated for 48–72 h at room temperature with an antibody against c-Fos [1:100; Santa Cruz Biotechnology, Inc., Santa Cruz, CA, United States; (E-8) sc-166940; batch D2318; RSID: AB_10609634]. The c-Fos antibody was diluted in PBS containing 0.1% sodium azide, 2% NHS, and 0.5% Triton X-100. After washes in PBS, sections were then incubated for 4 h at room temperature with Cy3-labeled donkey anti-mouse (Jackson Immunoresearch, West Grove, PA, United States; 715-165-150; batch 89001; RSID: AB_2340813; 1:2000). Sections were then washed in PBS, mounted onto glass slides, and cover-slipped with carbonate-buffered glycerol (pH 8.6).

For each spinal cord segment (L5-S2), the five spinal cord sections were anatomically ordered from rostral to caudal. Entire transverse sections were imaged (tile scanned at 12 Bit, pixel scaling 0.645 μm × 0.645 μm) using an AxioImager M2 microscope and AxioCam monochrome digital camera controlled by Zen software (Zeiss, Oberkochan, Germany). In each section from each of the segments, positive neurons were counted across spinal cord regions, defined by the boundaries described previously (Watson et al., 2009; **Figure 5A**). For segments L6 and S1, the sacral preganglionic nucleus (SPN) was defined as previously outlined in our earlier study (Forrest et al., 2015). Neurons were counted using ImageJ FIJI Cell Counter plugin, where a marker (denoting the xy coordinate) was designated for each positive cell.

Statistics

Data reporting on latency and threshold of electrically evoked responses are presented as median ± interquartile range (IQR). Differences between electrically evoked neural thresholds data were not normally distributed, and were therefore statistically evaluated using a (repeated measures) non-parametric Friedman test and Dunn's *post hoc* test. c-Fos Neuron counts in the spinal cord were analyzed using R Project for Statistical Computing (Version 3.5.2; RRID:SCR_001905) and RStudio (Version 1.1.4; RRID:SCR_000432). Two-sample comparisons were made using exact Welsh two sample *t*-tests to estimate means, 95% CIs and *P*-values. Corrections for multiple testing were made using the Hommel step-up modification of the Bonferroni procedure (Blakesley et al., 2009).

Figure Preparation

Monochrome images were digitally colorized and the contrast and brightness adjusted to best represent the immunostaining as viewed directly with the microscope. Figures were prepared using Adobe Creative Suite (Adobe Systems, San Jose, CA United States).

RESULTS

Electrically Evoked Compound Action Potentials

To determine if the pelvic nerve array could stimulate and record ECAPs, devices were unilaterally implanted in five urethane-anesthetized rats. In all cases, ECAPs with complex waveforms could be recorded from the non-stimulating electrode pair during graded electrical stimulation; these ECAPS could be separated from the stimulation artifact (**Figures 2A,B**). At supra-threshold stimulation levels these waveforms showed positive peaks centered at: P1, 1.80 ms (range 1.65–2.90 ms, $n = 5$); P2, 3.48 ms (2.51–4.16 ms); and P3, 3.77 ms (3.25–5.67 ms). Approximate conduction velocities for these populations are 1.60 m/s (P1, 0.98–1.72 m/s), 0.82 m/s (P2, 0.35–1.13 m/s) and 0.78 m/s (P3, 0.50–0.88 m/s). The mean stimulation threshold of these peaks increased in the order of the first (P1: 377 μA, 267–783 μA), second (P2: 648 μA, 595–648 μA) and third (P3: 930 μA, 550–1225 μA) responding populations (main effect: non-parametric Friedman's within-subject ANOVA: $P = 0.039$, $n = 5$) (**Figure 2C**). However, in one rat the threshold of P2 was higher than P1 (**Figures 2B,C**).

The ability of the pelvic nerve array to stimulate and record evoked neural potentials was evaluated in chronically implanted rats ($n = 4$) following surgery and prior to cystometry testing. Three neural populations, distinguished by their distinct latencies, were consistently recruited in all animals at 0 and 1 week following implantation. The first responding fiber population (P1) had a mean latency of 2.27 ms (range: 1.93–2.65 ms), second responding fibers (P2) had a mean latency

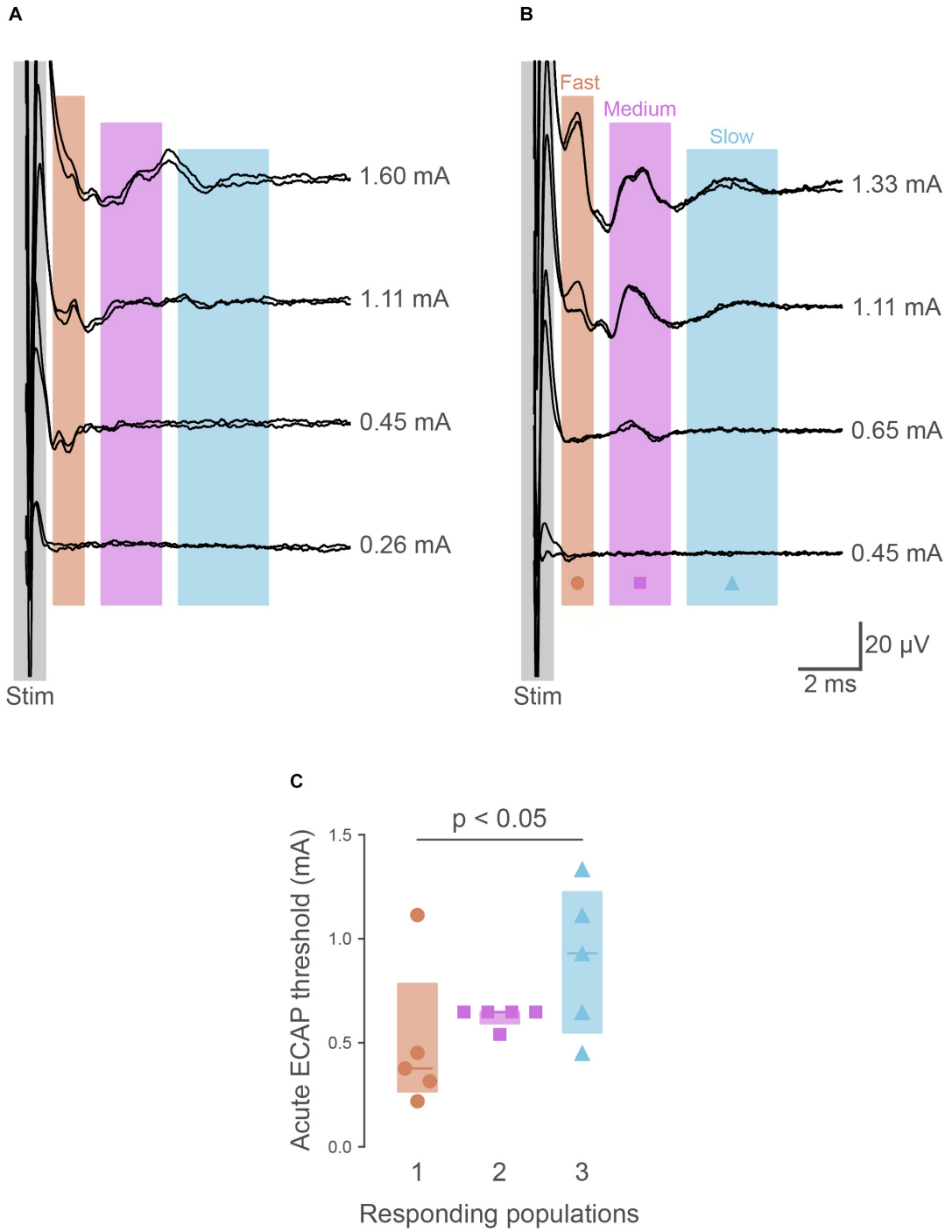

FIGURE 2 | Recordings of electrically evoked neural responses. **(A)** Typically (n = 4 of 5), the first responding neural populations had lower thresholds than later responding populations. **(B)** In one animal, the first responding neural fiber population had a higher threshold than the second. **(C)** Quantification of neural thresholds shows the third responding neural population had significantly higher thresholds (P = 0.034) than the first responding. The graph shows data from individual rats, median ± interquartile range.

of 3.92 ms (range: 3.19–4.44 ms), and the third (P3) had a mean latency of 5.62 ms (range: 4.57–6.72 ms). Approximate conduction velocities for these populations are 1.26 m/s (P1, 1.08–1.48 m/s), 0.73 m/s (P2, 0.64–0.89 m/s) and 0.51 m/s (P3, 0.42–0.62 m/s). Neural thresholds of first (P1, week 0: 391 ± 138 µA, week 1: 643 ± 300 µA), second (P2, week 0: 677 ± 149 µA, week 1: 1051 ± 275 µA) and third (P3, week 0: 713 ± 119 µA, week 1: 1263 ± 333 µA) responding fiber

populations significantly increased at 1 week (Friedman test, $P = 0.039$, $n = 4$, **Figure 2C**).

Electrode impedances were used to monitor the electrical stability and functionality of each electrode in an array following implantation and surgical recovery. The mean electrode impedance prior to implantation) was 4.19 ± 0.17 kΩ (range 3.16–5.03, $n = 38$ electrodes, 10 arrays). On post-surgical day 1, this increased to 7.25 ± 0.79 kΩ (range: 4.54–15.18 kΩ), and further increased after 2 weeks implantation to 12.04 ± 1.15 kΩ (range: 6.24–18.3 kΩ, 38 electrodes in 10 arrays) and 8 weeks implantation to 13.1 ± 2.06 kΩ (8.0–20.2 kΩ, $n = 8$ electrodes, 2 arrays). No short circuits occurred during the implantation period, and only 2 out of 40 electrodes became open circuit (both within 2 weeks of implantation). In experiments where an electrode became open, stimulation of the pelvic nerve could still be delivered through the remaining electrodes in the array.

Colonic Pressure Changes and Non-urological Effects of Pelvic Nerve Array Stimulation

Effects of electrical pelvic nerve stimulation were determined on colorectal motility in anesthetized rats. Only 1 of 3 animals responded, showing a small increase in colonic pressure of 2.6 ± 0.1 mm Hg (mean ± SEM, 13 within-subject replicate responses) time locked to pelvic nerve stimulation. No evidence of penile erection was detected by visual monitoring during these trials. Stimulation was confirmed to be suprathreshold by recording ECAPs from all three neural populations (P1–P3).

Urodynamic Effects of Pelvic Nerve Array Implantation and Stimulation in Awake Rats

To study urodynamic effects of the implantation of the pelvic nerve electrode array and stimulation, bladder pressure was measured by continuous-flow cystometry in awake rats (**Figures 3A,B**). Most recordings were made between 7 and 18 days after surgery, but in two rats recordings were made 8 weeks after surgery (**Figure 3E**). No obvious adverse behavioral responses to implantation or electrical pelvic nerve stimulation were detected by visual observation of the animals, and stimulation did not cause expulsion of fecal pellets ($n = 10$ animals) or penile erection ($n = 6$). On the day of euthanasia, there were no observed signs of irritation, swelling, infection or adverse reactions to the percutaneous pedestal, lead wire, and electrode array.

The effects of implantation of the pelvic nerve electrode array on filling evoked voiding contractions ($n = 9$) are summarized in **Table 1** and **Figure 3C**. These urodynamic parameters were comparable to published values (Zhao et al., 2010; Andersson et al., 2011; Fraser et al., 2020; Wiedmann et al., 2020). Our priority in assessing the effects of stimulation of the pelvic nerve was to determine the ability of stimulation to evoke a voiding contraction. Therefore, we targeted the majority of our stimulation to occur during a period where the bladder was at least partly filled (estimated as 50–80% based on the time elapsed since the previous filling-evoked void) to ensure the bladder contained sufficient urine for a visible voiding response. Electrical pelvic nerve stimulation was assessed in eight rats in which experimental cystometry sessions were performed following habituation. When delivered during this partly filled state, electrical stimulation of the pelvic nerve was immediately followed by post-stimulation voiding (urine release) in seven of eight rats and was repeated in 3–6 cycles in six of these rats (**Figures 3A,B,D**). Each void was accompanied by a rapid, transient rise in bladder pressure and high frequency oscillations during this period of elevated pressure that we interpret as indicative of urethral sphincter function characteristic of rodents (**Figure 3B2**). Given we targeted a partial fill of 50–80%, we consider it unlikely that on each of these occasions we inadvertently chose the precise time for pelvic nerve stimulation that the animal would have normally voided. In support of these being stimulus evoked voiding contractions, in two rats stimulus evoked voiding was even more clearly demonstrated by the pelvic nerve induced void occurring very early in the normal void cycle (**Figures 3A,B1**).

Electrical stimulation of the pelvic nerve also produced non-voiding bladder pressure responses (not accompanied by release of urine) in six of eight rats (**Figure 3D**). These non-voiding responses could occur independently, or within the same cystometry session as post-stimulation voiding contractions. In the latter case, it was common to observe stimulus evoked voiding contractions early in the experimental session, but as the session progressed, voiding responses became less frequent and non-voiding pressure changes become more common.

The long-term effects of implantation of the pelvic nerve electrode array and stimulation on bladder pressure was also tested in two animals that had arrays implanted for 8 weeks. In both cases, stimulation produced both voiding (indicated in as "eV" in **Figure 3E**) and non-voiding responses (indicated in as "eNVC" in **Figure 3E**) during cystometry (**Figure 3E**). The urodynamic parameters of filling evoked voids and stimulation evoked voids where similar to those in rats implanted for the shorter duration.

Post-mortem Analysis of Pathology After Chronic Implantation of Pelvic Nerve Array

On the day of euthanasia, a macroscopic examination of the status of the tissue surrounding the percutaneous connector, cable and pelvic nerve electrode array was conducted. In all of the experimental implanted animals, including the two rats in the 8 weeks recovery group, fibrous tissue surrounding the percutaneous connector and the subcutaneous cable was free from infection and no signs of irritation or inflammation were observed. We also performed a more detailed investigation in the two animals that were implanted for the longest duration (8 weeks). Here, the bladder catheter appeared firmly implanted into the dome of the bladder, and the catheter-bladder entry point had healed well and had no structural or intravesicular irregularities or disruptions. The prostate, seminal vesicles and vas deferens were free from adhesions, infection, inflammation

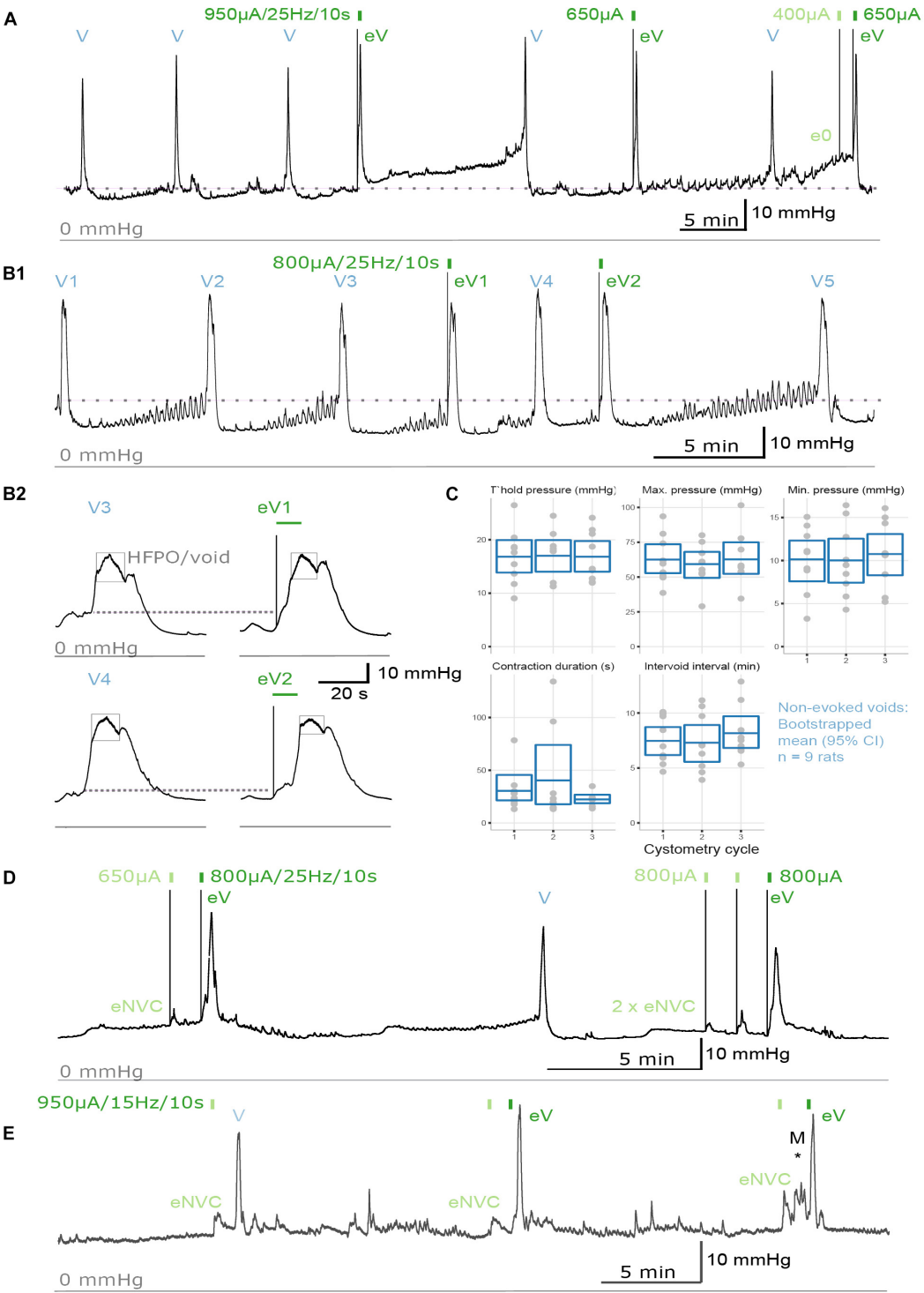

FIGURE 3 | Urodynamic effects of pelvic nerve array implantation and stimulation in awake rats. **(A,B)** Cystometrogram from an awake male rat recorded before and after pelvic nerve stimulation (indicated by rectangles) at 10 days following implantation. **(A,B1)** Implantation of the pelvic nerve array did not affect cystometry-induced voiding (V). Electrical stimulation of the pelvic nerve sometimes evoked urine-producing voids (eV), and rarely caused a null response (e0). **(B2)** Evoked voids were accompanied by characteristic rapid, transient rise in bladder pressure and high frequency oscillations during the period of elevated pressure (eV1, eV2). **(C)** Plots of urodynamic parameters versus cystometry cycle measured in nine awake male rats from contractions recorded prior to any electrical pelvic nerve stimulation. Plotted are data for each subject with boxes showing the mean and 95% CI. **(D)** Electrical stimulation of the pelvic nerve also produced an evoked-non-voiding contraction (eNVC) which resulted in an increase in bladder pressure that was not accompanied with the release of urine. **(E)** At 8 weeks following implantation, stimulation evoked voiding (eV) and non-voiding responses (eNVC) during cystometry. Pressure changes due to animal movement is indicated as "M*."

and vascular disruptions. The implanted lobe of the prostate appeared normal and was comparable to the non-implanted, contralateral prostate lobe. A thin fibrous tissue encapsulation had formed around the array further stabilizing the device. The tissue encapsulation was restricted to the vicinity of the pelvic nerve array and did not spread from this area to affect adjacent tissues. Suturing of the electrode array to the soft tissue overlying the prostate had not caused any macroscopic damage to the prostate, pelvic nerve or blood vessels. Furthermore, no irritation, hemorrhaging or hematomas were observed within adjacent tissue.

Immunohistochemical Analysis of Neural Injury Markers in Ganglia

Immunohistochemical visualization of neural markers was performed in ganglia dissected from two rats, 50 days after implantation surgery. Several approaches were chosen to determine if this chronic implantation led to significant neural damage. The pelvic nerve contains the major source of LUT afferent axons, which project from sensory neurons in the lumbosacral (L6 and S1) DRG (Nadelhaft and Booth, 1984). To determine if these axons were damaged by the implanted device we performed immunohistochemistry on these ganglia to detect neuronal expression of the neural injury marker ATF-3 [activating transcription factor-3 (Tsujino et al., 2000; Payne et al., 2015)]. ATF3-positive neuronal nuclei were absent or rare in sections taken from ganglia either ipsi- or contralateral to the implant (**Figure 4A**). As a positive control, we stained sections from archived DRG in which sacral bladder afferents had been injured by surgical transection of the accessory nerves (mixed sensory-autonomic tracts projecting to the bladder) (Payne et al., 2015). As expected, numerous ATF3-positive neuronal nuclei could be observed in these ganglia (**Figure 4B**).

The MPG contains most of the autonomic ganglion neurons that project to the pelvic organs, including innervation of the LUT. We considered that the close proximity of the implanted pelvic nerve array to the MPG could potentially injure MPG neurons, either during the surgical implantation procedure or the postsurgical experimental period. However, very few or no ATF3-positive neuronal nuclei (**Figure 4C**) were seen in sections from MPG ipsi- or contralateral to the array, whereas numerous ATF3-positive nuclei were present in sections of archived MPG from a prior study on accessory nerve injury, used as the positive control (Payne et al., 2015; **Figure 4D**).

As an alternative approach to assess the impact of the implantation surgery, we examined within the MPG several classes of axons that are known to project in the pelvic nerve

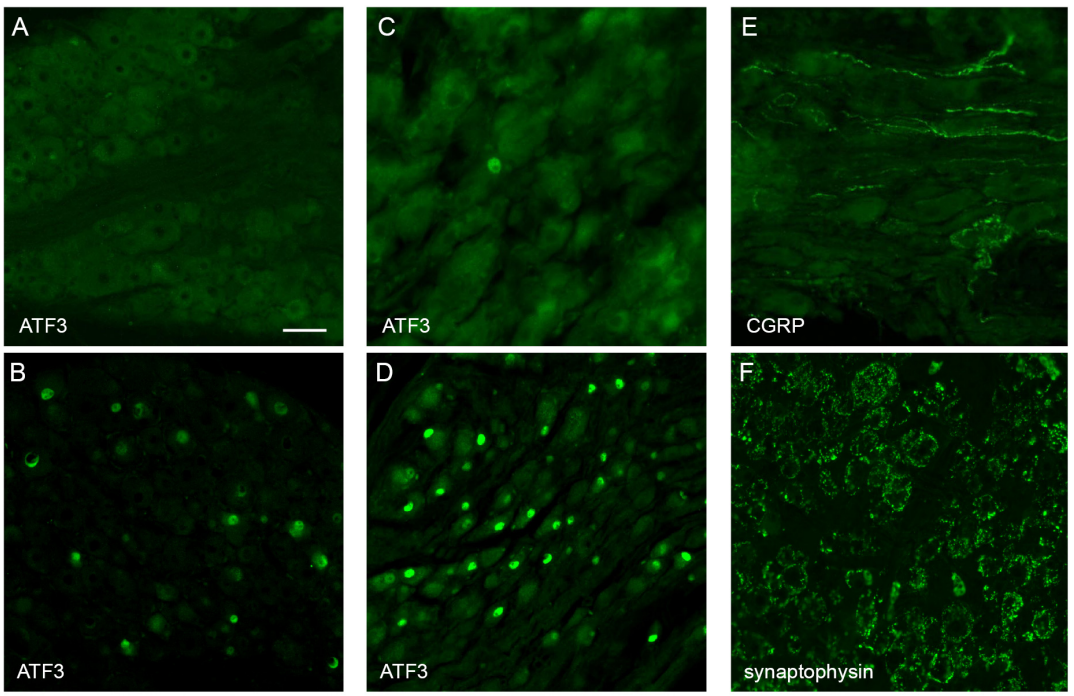

FIGURE 4 | Histological assessment of L6 dorsal root ganglia (DRG) and major pelvic ganglia (MPG) from male rats. Panels **(A,C,E,F)** show ganglia ipsilateral to the array surgery. **(B,D)** are archived ganglia from an earlier axotomy study (Payne et al., 2015), sectioned and immunolabelled as a technical control for the current study; in this earlier study the accessory nerves (mixed sensory-autonomic nerves projecting from the MPG to the bladder) were transected and tissues dissected one week later. **(A)** A DRG ipsilateral to the array surgery shows no ATF3-positive nuclei. **(B)** A DRG from the prior accessory nerve axotomy study shows numerous ATF3-positive neuronal nuclei. **(C)** MPG ipsilateral to the array surgery shows a single ATF3-positive nucleus amongst many neurons with ATF3-negative nuclei. **(D)** The MPG from the prior axotomy study shows numerous ATF3-positive neuronal nuclei. **(E)** In the MPG ipsilateral to array surgery, peptidergic sensory axons traverse the ganglion tissue. **(F)** The MPG ipsilateral to the array surgery shows numerous synaptic boutons immunolabelled for synaptophysin, surrounding each of the MPG neurons. Calibration bar in A represents (μm): A (50 μm), B (50 μm), C (30 μm), D (60 μm), E (30 μm), F (50 μm).

and then traverse or terminate in the MPG. First, using a marker of the peptidergic class of sensory axons, CGRP, many axons were observed to traverse both ipsi- and contralateral MPG (**Figure 4E**). The other major class of axons projecting in the pelvic nerve originates from sacral preganglionic neurons. These parasympathetic pre-motor neurons are essential for the voiding reflex; their axons innervate cholinergic pelvic ganglion neurons, which in turn cause contraction of the bladder muscle (detrusor). Injury to sacral preganglionic axons was examined by assessing the presence of synaptic boutons associated with pelvic ganglion neurons. If preganglionic axons traveling in the pelvic nerve were damaged, these would be lost from the majority of MPG neurons (the other neurons are innervated by lumbar spinal axons traveling in the hypogastric nerve). We found that following 50 days implantation of the device, synaptic boutons innervated the entire population of MPG neurons, ipsilateral and contralateral to the surgery (**Figure 4F**). Taken together, these observations suggest that implantation surgery did not cause significant damage to preganglionic or sensory axons projecting in the pelvic nerve, or the nearby MPG neurons.

Immunohistochemical Analysis of Noxious Neuronal Activity in Spinal Cord

Neuronal activity (c-Fos) mapping in sacral spinal cord was used to detect noxious activation caused by the implanted arrays. Changes in c-Fos expression was assessed (n = 3) on day 10 of implantation, following 60 min of cystometry and pelvic nerve stimulation testing. In spinal segments L5-S1, neurons with c-Fos^{+} nuclei were most densely distributed in dorsal horn, the sacral dorsal commissural nucleus (SDCom) and the SPN of segments L6 and S1 (**Figures 5A–C**), consistent with our recent activity mapping study of cystometry in awake male rats (Wiedmann et al., 2020). No difference was detected in the pattern of c-Fos between the two sides of the spinal cord (**Figure 5D**). No activation of lamina I neurons was detected in either the stimulated side (array implanted on the pelvic nerve) or the contralateral side (**Figure 5C**).

DISCUSSION

Stimulation of the pelvic splanchnic nerves may provide therapeutic benefits for a range of LUT conditions. Here we developed an electrode array that interfaced with the rodent homolog of these nerves, the pelvic nerve, without surgical manipulation of the epineurium. For periods of up to 8 weeks following implantation period, our pelvic nerve electrode array recorded electrically evoked neural activity, caused minimal off-target effects to stimulation and induced voiding and non-voiding contractions of the urinary bladder. Furthermore, during long-term implantation our array remained functional and was well tolerated, with no immunohistochemical signs of damage to sacral sensory pathways projecting in the pelvic nerve or adjacent neural tissue of the major pelvic ganglion. Taken together, these findings support that our custom developed pelvic nerve array is an effective and safe design for long-term implantation and stimulation of small autonomic nerves.

The sharp edges and stiffness of cuff electrode designs often evoke a foreign body response and fibrosis, affecting the physiological properties of nerve firing and the stimulation threshold of the electrodes (Loeb and Peck, 1996; Vince et al., 2005; Wodlinger and Durand, 2011; Restaino et al., 2014). Many small visceral nerves, such as the pelvic nerve, have a prevalence of unmyelinated axons and thinner epineurium, increasing their susceptibility to damage (Grill et al., 2009; McCallum et al., 2017; Gonzalez-Gonzalez et al., 2018). Therefore soft, thin, highly flexible cuff arrays made of thiol-ene/acrylate shaped memory polymer have been used for recording spontaneous neural activity in anesthetized rats during cystometry-induced voiding (Gonzalez-Gonzalez et al., 2018). To overcome the challenges posed by interfacing to small, visceral nerves, we developed a silicone based, extraneural electrode array that was placed on top of the pelvic nerve. This approach did not require surgical manipulation of the nerve, nor did the array physically restrict the nerve. The design also allowed for a "one size fits all" approach and could potentially be utilized for the implantation onto other small nerves. Finally, during the 2- and 8-week implantation periods, only 2 out of 40 individual electrodes failed, both due to a break causing an open circuit, suggesting that our electrode design was robust and suitable for chronic use.

Long-term implantation of the pelvic nerve array was well tolerated by the surrounding pelvic organs and implanted neural tissue. No infections or adverse impact to implanted neural or prostate tissue were seen and the foreign body tissue response formed around the array appeared benign and aided in stabilizing the implant, similar to that described previously (Payne et al., 2018). Neural tissue damage induced by the implanted array was minimal, as evidenced by the robust natural and stimulation-induced voiding responses induced by cystometry testing. This was consistent with our immunohistochemical assessment of neural markers, selected to reveal damage to axons projecting in the pelvic nerve. Sensory neurons in sacral dorsal root ganglia detect bladder distension and project to the bladder via the pelvic nerve and the major pelvic ganglion. Ipsilateral to the implanted array, sacral dorsal root ganglion neurons showed negligible expression of the injury marker ATF3, and their CGRP-positive axons were retained in the major pelvic ganglia. The integrity of the bladder motor pathway was also indicated by the retention of synaptic boutons associated with pelvic ganglion neurons. In this ganglion, neurons expressing ATF3 were rare, indicating they were undamaged by the implantation surgery. Together, these observations support our functional assessment that the sensory and motor components of the pelvic nerve remain healthy after implantation of the array, however it is possible that quantitation of axons within these peripheral tissues or the LUT itself would reveal more subtle effects of surgery.

In this study, the spacing between bipolar electrode pairs was a unique design feature that allowed for the recording of three neural populations, distinguished by the latencies of their response. Generally (n = 4 of 5 rats), the fastest responding neural population had lower neural thresholds than the slowest responding population, consistent with the size recruitment principle. However, in one animal

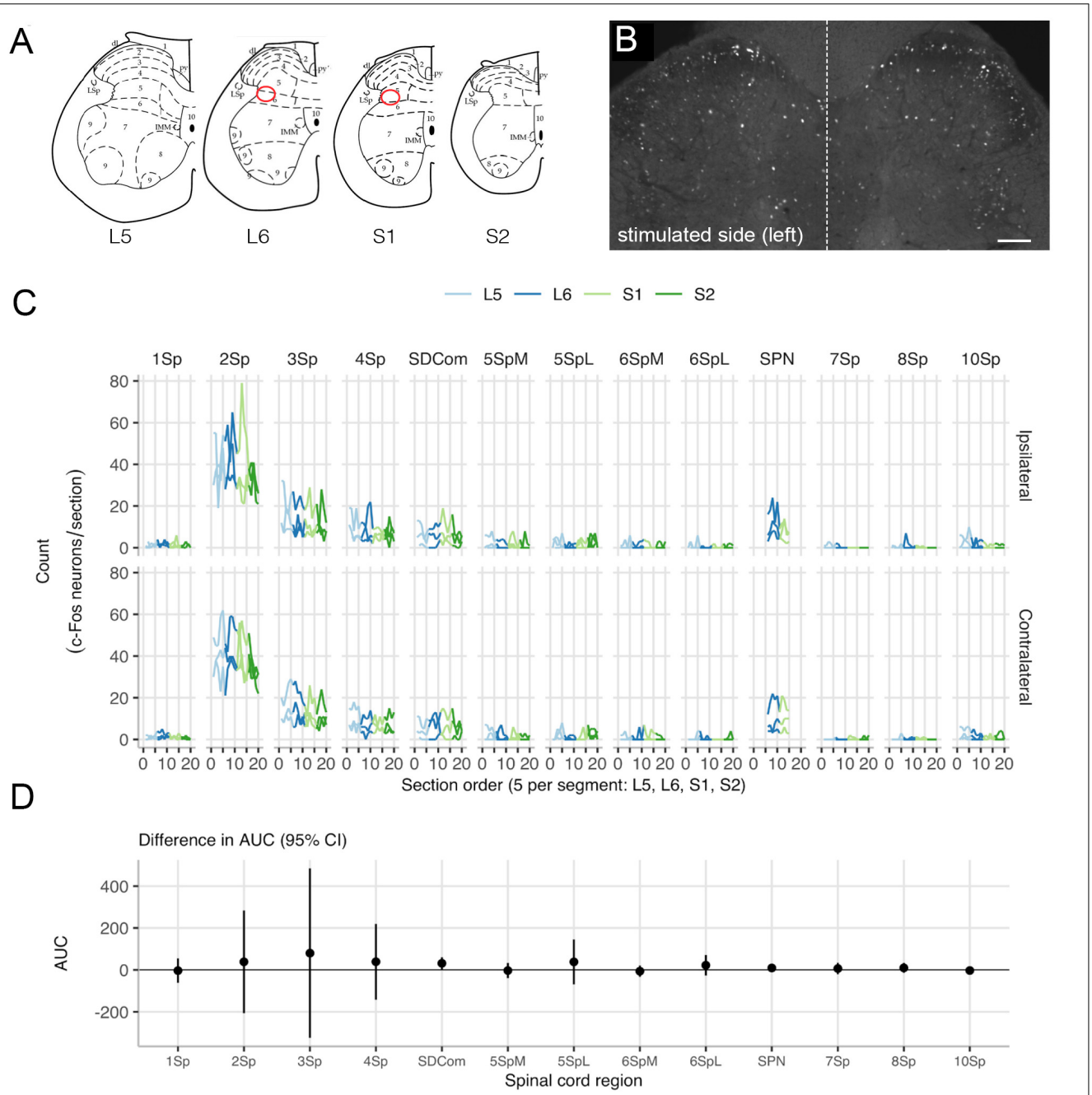

FIGURE 5 | Mapping c-Fos expression in the lumbosacral cord after pelvic nerve stimulation and implantation of an electrode array. **(A)** Expression of c-Fos in neuronal nuclei was mapped in relation to specific spinal regions (Watson et al., 2009). Preganglionic neurons that project in the pelvic nerve are aggregated in the sacral parasympathetic nucleus (SPN), indicated by the red oval. **(B)** An example of c-Fos immunoreactivity showing both sides of an L6 spinal cord section, from a rat where the left pelvic nerve was implanted with an electrode array. This animal underwent regular filling cystometry in addition to activation of the pelvic nerve via the array. **(C)** Spatial analysis of c-Fos-immunoreactive neuron counts in lumbosacral cord shows there were no differences between the left side that received an implant and stimulation, and the right (i.e., control) side. **(D)** Data from each rat is plotted separately (thin lines) as well as the mean for each side (thick line). The region of interest (ROI) neuronal counts by subject show rostrocaudal distribution across spinal cord segments L5 to S2. ROIs: lamina I (1Sp), lamina II (2Sp), lamina III (3Sp), lamina IV (4Sp), sacral dorsal commissural nucleus (SDCom), lamina V (5Sp), lamina VI (6Sp), sacral preganglionic nucleus (SPN), lamina VII (7Sp), lamina VIII (8Sp), and lamina X (10Sp). Scale bar in B represents 100 μm.

the first responding neural population showed higher thresholds than the second responding population. This deviation from the size recruitment principle was likely due to the *in vivo* environment, with the electrode-neural distance having a large impact on fiber recruitment. The exact conduction velocity of the neural responses cannot

be determined as the precise location of activation is not known, however the conduction velocities of these three neural populations were consistent with that of subpopulations of myelinated A-fiber (1.6–21 m/s) and unmyelinated C-fibers (0.5–1.6 m/s) identified previously in the pelvic nerve (Shea et al., 2000).

Off-target effects can potentially limit therapeutic stimulation delivery, thereby compromising or limiting the effectiveness of stimulation treatment (Waltz, 2016; Payne et al., 2019). Our pelvic nerve electrode array could potentially impact activity of several pelvic organs, as sensory and motor pathways in this nerve innervate the LUT, lower bowel and reproductive organs (Keast, 2006). Our initial study to investigate efficacy of pelvic nerve stimulation on LUT function did not investigate other potential outcomes of stimulation but did observe acute increases in colonic pressure in the minority (n = 1 of 3) of rats, but no penile erection. Without more targeted physiological assays, we cannot discount an impact of pelvic nerve stimulation on non-LUT targets or the vasculature. It may also be possible to target pelvic nerve stimulation to particular neural populations, as afferents innervating the LUT have recently been identified as spatially segregated from rectal afferents (Bertrand et al., 2020). Another potential outcome of pelvic nerve stimulation is activation of nociceptive sensory axons projecting to the bladder. We did not identify behaviors indicating pain during electrode activation, and our studies of c-Fos expression did not detect upregulation in lamina 1 of the spinal cord dorsal horn following pelvic nerve stimulation and cystometry testing in awake rats, either ipsi- or contralateral to the implanted array. This pattern of c-Fos upregulation is characteristic of responses to noxious stimuli in the bladder (Birder and de Groat, 1992, 1993; Lanteri-Minet et al., 1995; Kakizaki et al., 1996; Vizzard, 2000). Our observation of c-Fos expression in other regions of the spinal cord demonstrated non-nociceptive pathways typically activated by cystometry, as reported previously (Birder and de Groat, 1992, 1993; Wiedmann et al., 2020).

A major aim of our study was to assess the efficacy of the pelvic nerve array to induce voiding in the awake, unrestrained rat, including in a chronic, post-surgical setting. Two types of LUT activity were observed: voiding and non-voiding contractions. To our knowledge, this is the first study that has demonstrated pelvic nerve stimulation induced voiding in awake, unrestrained rats. Therefore, we felt it critical to use visual confirmation of stimulus induced voiding. This resulted in the requirement of delivering stimulation to a partially full bladder, to ensure the bladder contained sufficient urine for a visible voiding response. We targeted 50–80% full, based on the time elapsed since the previous void, but precise estimates of "typical" voiding cycle duration were difficult to achieve because many rats showed voiding cycles of variable duration. We also considered choosing stimulation times based on bladder pressure rather than duration since last void, but this also had some limitations in animals where there were movement artifacts (rat moving around the cage) or small, unrelated fluctuations in baseline bladder pressure. The variable duration of voiding cycles also makes it possible that some of our stimuli were delivered when the animal would have voided normally, however we consider it unlikely that in the 27 trials in eight rats where we observed a void within 30 s of our stimulation this was always the case. Furthermore, **Figures 3A,B1** clearly demonstrate stimulus induced voiding very early in the normal void cycle. In rats where pelvic nerve stimulation was never associated with a void, the most parsimonious explanation is poor surgical placement of the stimulating array. As ECAP recordings were not performed in all animals, we cannot confirm neural activation in these animals. We have not yet conducted studies to determine the mechanism by which the stimulation initiated voiding or non-voiding contractions. To initiate voiding, it is likely that A-δ sensory pathways were activated, initiating the synchronized coordination of autonomic and somatic motor pathways to contract the bladder while relaxing the urethra and urethral rhabdosphincter (de Groat and Yoshimura, 2009). In some experiments, we also identified stimulation parameters that evoked non-voiding contractions. Pelvic nerve-evoked non-voiding contractions of the detrusor muscle have also been reported in anesthetized rats (Crook and Lovick, 2017; Peh et al., 2018), dogs (Andersson et al., 1990) and pigs (Dalmose et al., 2002) and ascribed to activation of sacral parasympathetic pathways based on nerve crush experiments (Dalmose et al., 2002).

Pelvic nerve stimulation induced voiding was achieved up to 8 weeks post-implantation, our chosen experimental endpoint; however, the continued health of the animals at this time indicates that longer periods of implantation are feasible. Therefore, in summary, the present study demonstrates the efficacy and safety of a novel electrode array designed for long-term stimulation of a small visceral nerve and supports the translation of pelvic nerve stimulation as a potential treatment for a range of LUT dysfunctions.

DATA AVAILABILITY STATEMENT

The raw data supporting the conclusions of this article will be made available by the authors, without undue reservation.

ETHICS STATEMENT

The animal study was reviewed and approved by the Animal Ethics Committees of St. Vincent's Hospital (Melbourne) Animal Ethics Committees of the University of Melbourne.

AUTHOR CONTRIBUTIONS

All authors made substantial, direct, and intellectual contributions to the study and manuscript. SP conceived and designed the experiments, analyzed and interpreted data, and drafted the manuscript. NW, AW, and PS designed and executed experiments. CE analyzed data and prepared **Figures 2**, **3**. PO, JK, and JF conceived and designed research, interpreted data,

and revised the manuscript. All authors approved the final version of the manuscript.

FUNDING

Research reported in this publication received funding from GSK Bioelectronics Innovation Challenge (JF and JK). This funder was not involved in the study design, collection, analysis, interpretation of data, the writing of this article, or the decision to submit it for publication. The study also received funding from the National Institutes of Health, Office of the Director, Stimulating Peripheral Activity to Relieve Conditions (SPARC) Program, Award Number OT2OD023872 (JK, PO, and JF). The content is solely the responsibility of the authors and does not necessarily represent the official views of the National Institutes of Health.

ACKNOWLEDGMENTS

We would like to acknowledge Kiyotada Naito for surgical assistance, Alex Thompson for technical assistance with electrical equipment, Ross Thomas for the manufacture and refinement of the array design, and Edmond Capelea for early electrode design concepts, Amy Morley and Victoria Barrett for laboratory assistance, and Erin Smyth for electrophysiological support. We would also like to acknowledge Professors John B. Furness and Robert K. Shepherd for initial intellectual input on some of the research concepts and design.

REFERENCES

Ammi, M., Chautard, D., Brassart, E., Culty, T., Azzouzi, A. R., and Bigot, P. (2014). Transcutaneous posterior tibial nerve stimulation: evaluation of a therapeutic option in the management of anticholinergic refractory overactive bladder. *Int. Urogynecol. J.* 25, 1065–1069. doi: 10.1007/s00192-014-2359-0

Andersson, K. E., Soler, R., and Fullhase, C. (2011). Rodent models for urodynamic investigation. *Neurourol. Urodyn.* 30, 636–646. doi: 10.1002/nau.21108

Andersson, P. O., Sjogren, C., Uvnas, B., and Uvnas-Moberg, K. (1990). Urinary bladder and urethral responses to pelvic and hypogastric nerve stimulation and their relation to vasoactive intestinal polypeptide in the anaesthetized dog. *Acta Physiol. Scand.* 138, 409–416. doi: 10.1111/j.1748-1716.1990.tb08864.x

Bertrand, M. M., Korajkic, N., Osborne, P. B., and Keast, J. R. (2020). Functional segregation within the pelvic nerve of male rats: a meso- and microscopic analysis. *J. Anat.* 237, 757–773. doi: 10.1111/joa.13221

Birder, L. A., and de Groat, W. C. (1992). Increased c-fos expression in spinal neurons after irritation of the lower urinary tract in the rat. *J. Neurosci.* 12, 4878–4889. doi: 10.1523/JNEUROSCI.12-12-04878.1992

Birder, L. A., and de Groat, W. C. (1993). Induction of c-fos expression in spinal neurons by nociceptive and nonnociceptive stimulation of LUT. *Am. J. Physiol.* 265(2 Pt 2), R326–R333. doi: 10.1152/ajpregu.1993.265.2.R326

Blakesley, R. E., Mazumdar, S., Dew, M. A., Houck, P. R., Tang, G., Reynolds, C. F. III, et al. (2009). Comparisons of methods for multiple hypothesis testing in neuropsychological research. *Neuropsychology* 23, 255–264. doi: 10.1037/a0012850

Bouton, C. E., and Czura, C. J. (2018). "Chapter 131 – Sensing and decoding neural signals for closed-loop neuromodulation and advanced diagnostics in chronic disease and injury," in *Neuromodulation*, 2nd Edn, eds E. S. Krames, P. H. Peckham, and A. R. Rezai (Cambridge, MA: Academic Press), 1541–1549. doi: 10.1016/b978-0-12-805353-9.00131-5

Chen, M. L., Chermansky, C. J., Shen, B., Roppolo, J. R., de Groat, W. C., and Tai, C. (2014). Electrical stimulation of somatic afferent nerves in the foot increases bladder capacity in healthy human subjects. *J. Urol.* 191, 1009–1013. doi: 10.1016/j.juro.2013.10.024

Crook, J. J., Brouillard, C. B. J., Irazoqui, P. P., and Lovick, T. A. (2018). Chronic implantation of cuff electrodes on the pelvic nerve in rats is well tolerated and does not compromise afferent or efferent fibre functionality. *J. Neural. Eng.* 15:024001. doi: 10.1088/1741-2552/aaa569

Crook, J. J., and Lovick, T. A. (2017). High frequency stimulation of the pelvic nerve inhibits urinary voiding in anesthetized rats. *Front. Physiol.* 8:623. doi: 10.3389/fphys.2017.00623

Dalmose, A. L., Rijkhoff, N. J., Andersen, I. S., Stefania, D., Jorgensen, T. M., and Djurhuus, J. C. (2002). Bladder and urethral responses to pelvic nerve stimulation in the pig. *Scand. J. Urol. Nephrol. Suppl.* 36, 34–45. doi: 10.1080/003655902320765944

de Groat, W. C., and Tai, C. (2018). "Chapter 19 – Mechanisms of action of sacral nerve and peripheral nerve stimulation for disorders of the bladder and bowel," in *Neuromodulation*, 2nd Edn, eds E. S. Krames, P. H. Peckham, and A. R. Rezai (Cambridge, MA: Academic Press), 221–236. doi: 10.1016/b978-0-12-805353-9.00019-x

de Groat, W. C., and Yoshimura, N. (2009). Afferent nerve regulation of bladder function in health and disease. *Handb. Exp. Pharmacol.* 194, 91–138. doi: 10.1007/978-3-540-79090-7_4

Fallon, J. B., and Carter, P. M. (2016). "Principles of recording from and electrical stimulation of neural tissue," in *Neurobionics: The Biomedical Engineering of Neural Protheses*, 1st Edn, ed. R. K. Shepherd (New Jersey, NJ: John Wiley & Sons, Inc.).

Fallon, J. B., Irvine, D. R., and Shepherd, R. K. (2009). Cochlear implant use following neonatal deafness influences the cochleotopic organization of the primary auditory cortex in cats. *J. Comp. Neurol.* 512, 101–114. doi: 10.1002/cne.21886

Fallon, J. B., and Payne, S. C. (2020). *Electrophysiological Recording of Electrically-Evoked Compound Action Potentials*. protocols.io. doi: 10.17504/protocols.io.bfwyjpfw

Fallon, J. B., Payne, S. C., Keast, J. R., and Osborne, P. B. (2020). *Implantation of A Pelvic Nerve Array in Rats*. protocols.io. doi: 10.17504/protocols.io.bjvxkn7n

Fallon, J. B., Senn, P., and Thompson, A. C. (2018). "A highly configurable neurostimulator for chronic pre-clinical stimulation studies," in *Proceedings of the Neural Interfaces Conferences*, Minneapolis, MN.

Forrest, S. L., Payne, S. C., Keast, J. R., and Osborne, P. B. (2015). Peripheral injury of pelvic visceral sensory nerves alters GFRalpha (GDNF family receptor alpha) localization in sensory and autonomic pathways of the sacral spinal cord. *Front. Neuroanat.* 9:43. doi: 10.3389/fnana.2015.00043

Fraser, M. O., Smith, P. P., Sullivan, M. P., Bjorling, D. E., Campeau, L., Andersson, K. E., et al. (2020). Best practices for cystometric evaluation of lower urinary tract function in muriform rodents. *Neurourol. Urodyn.* 39, 1868–1884. doi: 10.1002/nau.24415

Goldman, H. B., Amundsen, C. L., Mangel, J., Grill, J., Bennett, M., Gustafson, K. J., et al. (2008). Dorsal genital nerve stimulation for the treatment of overactive bladder symptoms. *Neurourol. Urodyn.* 27, 499–503. doi: 10.1002/nau.20544

Gonzalez-Gonzalez, M. A., Kanneganti, A., Joshi-Imre, A., Hernandez-Reynoso, A. G., Bendale, G., Modi, R., et al. (2018). Thin film multi-electrode softening cuffs for selective neuromodulation. *Sci. Rep.* 8:16390. doi: 10.1038/s41598-018-34566-6

Grill, W. M., Norman, S. E., and Bellamkonda, R. V. (2009). Implanted neural interfaces: biochallenges and engineered solutions. *Annu. Rev. Biomed. Eng.* 11, 1–24. doi: 10.1146/annurev-bioeng-061008-124927

Guiraud, D., Andreu, D., Bonnet, S., Carrault, G., Couderc, P., Hagege, A., et al. (2016). Vagus nerve stimulation: state of the art of stimulation and recording strategies to address autonomic function neuromodulation. *J. Neural. Eng.* 13:041002. doi: 10.1088/1741-2560/13/4/041002

Horn, C. C., Ardell, J. L., and Fisher, L. E. (2019). Electroceutical targeting of the autonomic nervous system. *Physiology (Bethesda)* 34, 150–162. doi: 10.1152/physiol.00030.2018

Kakizaki, H., Yoshiyama, M., and de Groat, W. C. (1996). Role of NMDA and AMPA glutamatergic transmission in spinal c-fos expression after urinary tract

irritation. *Am. J. Physiol.* 270(5 Pt 2), R990–R996. doi: 10.1152/ajpregu.1996.270.5.R990

Keast, J. R. (2006). Plasticity of pelvic autonomic ganglia and urogenital innervation. *Int. Rev. Cytol.* 248, 141–208. doi: 10.1016/S0074-7696(06)48003-7

Keast, J. R., and Osborne, P. B. (2019). *Intracardiac Perfusion with Fixative for Anatomical Studies*. protocols.io. doi: 10.17504/protocols.io.w3ffgjn

Keast, J. R., Osborne, P. B., and Wiedmann, N. (2020a). *Cystometry in Awake Rats*. protocols.io. doi: 10.17504/protocols.io.bakjicun

Keast, J. R., Osborne, P. B., and Wiedmann, N. (2020b). *Immunohistochemical Labelling of Spinal Cord Neurons Involved in Bladder Activity*. protocols.io. doi: 10.17504/protocols.io.bakkicuw

Langdale, C. L., Hokanson, J. A., Milliken, P. H., Sridhar, A., and Grill, W. M. (2020). Stimulation of the pelvic nerve increases bladder capacity in the PGE2 cat model of overactive bladder. *Am. J. Physiol. Renal Physiol.* 318, F1357–F1368. doi: 10.1152/ajprenal.00068.2020

Langdale, C. L., Hokanson, J. A., Sridhar, A., and Grill, W. M. (2017). Stimulation of the pelvic nerve increases bladder capacity in the prostaglandin E2 rat model of overactive bladder. *Am. J. Physiol. Renal Physiol.* 313, F657–F665. doi: 10.1152/ajprenal.00116.2017

Lanteri-Minet, M., Bon, K., de Pommery, J., Michiels, J. F., and Menetrey, D. (1995). Cyclophosphamide cystitis as a model of visceral pain in rats: model elaboration and spinal structures involved as revealed by the expression of c-Fos and Krox-24 proteins. *Exp. Brain Res.* 105, 220–232. doi: 10.1007/bf00240958

Larson, C. E., and Meng, E. (2020). A review for the peripheral nerve interface designer. *J. Neurosci. Methods* 332:108523. doi: 10.1016/j.jneumeth.2019.108523

Lee, S., Wang, H., Xian Peh, W. Y., He, T., Yen, S.-C., Thakor, N. V., et al. (2019). Mechano-neuromodulation of autonomic pelvic nerve for underactive bladder: a triboelectric neurostimulator integrated with flexible neural clip interface. *Nano Energy* 60, 449–456. doi: 10.1016/j.nanoen.2019.03.082

Loeb, G. E., and Peck, R. A. (1996). Cuff electrodes for chronic stimulation and recording of peripheral nerve activity. *J. Neurosci. Methods* 64, 95–103. doi: 10.1016/0165-0270(95)00123-9

McCallum, G. A., Sui, X., Qiu, C., Marmerstein, J., Zheng, Y., Eggers, T. E., et al. (2017). Chronic interfacing with the autonomic nervous system using carbon nanotube (CNT) yarn electrodes. *Sci. Rep.* 7:11723. doi: 10.1038/s41598-017-10639-w

Nadelhaft, I., and Booth, A. (1984). The location and morphology of preganglionic neurons and the distribution of visceral afferents from the rat pelvic nerve: a horseradish peroxidase study. *J. Comp. Neurol.* 226, 238–245. doi: 10.1002/cne.902260207

Naufel, S., Knaack, G. L., Miranda, R., Best, T. K., Fitzpatrick, K., Emondi, A. A., et al. (2020). DARPA investment in peripheral nerve interfaces for prosthetics, prescriptions, and plasticity. *J. Neurosci. Methods* 332:108539. doi: 10.1016/j.jneumeth.2019.108539

Opisso, E., Borau, A., and Rijkhoff, N. J. (2013). Subject-controlled stimulation of dorsal genital nerve to treat neurogenic detrusor overactivity at home. *Neurourol. Urodyn.* 32, 1004–1009. doi: 10.1002/nau.22359

Parker, J. L. (2018). "Chapter 32 – Implanted sensors in neuromodulation via electrical stimulation," in *Neuromodulation*, 2nd Edn, eds E. S. Krames, P. H. Peckham, and A. R. Rezai (Cambridge, MA: Academic Press), 451–463. doi: 10.1016/b978-0-12-805353-9.00032-2

Parker, J. L., Shariati, N. H., and Karantonis, D. M. (2018). Electrically evoked compound action potential recording in peripheral nerves. *Bioelectron. Med.* 1, 71–83. doi: 10.2217/bem-2017-0005

Payne, S. C., Belleville, P. J., and Keast, J. R. (2015). Regeneration of sensory but not motor axons following visceral nerve injury. *Exp. Neurol.* 266, 127–142. doi: 10.1016/j.expneurol.2015.02.026

Payne, S. C., Burns, O., Stebbing, M., Thomas, R., de Silva, A., Sedo, A., et al. (2018). Vagus nerve stimulation to treat inflammatory bowel disease: a chronic, preclinical safety study in sheep. *Bioelectron. Med.* 1, 235–250. doi: 10.2217/bem-2018-0011

Payne, S. C., Furness, J. B., and Stebbing, M. J. (2019). Bioelectric neuromodulation for gastrointestinal disorders: effectiveness and mechanisms. *Nat. Rev. Gastroenterol. Hepatol.* 16, 89–105. doi: 10.1038/s41575-018-0078-6

Peh, W. Y. X., Mogan, R., Thow, X. Y., Chua, S. M., Rusly, A., Thakor, N. V., et al. (2018). Novel neurostimulation of autonomic pelvic nerves overcomes bladder-sphincter dyssynergia. *Front. Neurosci.* 12:186. doi: 10.3389/fnins.2018.00186

Peters, K. M., Killinger, K. A., Boguslawski, B. M., and Boura, J. A. (2010). Chronic pudendal neuromodulation: expanding available treatment options for refractory urologic symptoms. *Neurourol. Urodyn.* 29, 1267–1271.

Restaino, S. M., Abliz, E., Wachrathit, K., Krauthamer, V., and Shah, S. B. (2014). Biomechanical and functional variation in rat sciatic nerve following cuff electrode implantation. *J. Neuroeng. Rehabil.* 11:73. doi: 10.1186/1743-0003-11-73

Shea, V. K., Cai, R., Crepps, B., Mason, J. L., and Perl, E. R. (2000). Sensory fibers of the pelvic nerve innervating the rat's urinary bladder. *J. Neurophysiol.* 84, 1924–1933. doi: 10.1152/jn.2000.84.4.1924

Tsujino, H., Kondo, E., Fukuoka, T., Dai, Y., Tokunaga, A., Miki, K., et al. (2000). Activating transcription factor 3 (ATF3) induction by axotomy in sensory and motoneurons: a novel neuronal marker of nerve injury. *Mol. Cell. Neurosci.* 15, 170–182. doi: 10.1006/mcne.1999.0814

Vince, V., Brelen, M. E., Delbeke, J., and Colin, I. M. (2005). Anti-TNF-alpha reduces the inflammatory reaction associated with cuff electrode implantation around the sciatic nerve. *J. Neuroimmunol.* 165, 121–128. doi: 10.1016/j.jneuroim.2005.04.019

Vizzard, M. A. (2000). Alterations in spinal cord Fos protein expression induced by bladder stimulation following cystitis. *Am. J. Physiol. Regul. Integr. Comp. Physiol.* 278, R1027–R1039. doi: 10.1152/ajpregu.2000.278.4.R1027

Waltz, E. (2016). A spark at the periphery. *Nat. Biotechnol.* 34, 904–908. doi: 10.1038/nbt.3667

Watson, C., Paxinos, G., Kayalioglu, G., and Heise, C. (2009). *The Spinal Cord: A Christopher and Dana Reeve Foundation Text and Atlas*. Amsterdam: Academic Press.

Wiedmann, N. M., Wong, A. W., Keast, J. R., and Osborne, P. B. (2020). Sex differences in c-Fos and EGR-1/Zif268 activity maps of rat sacral spinal cord following cystometry-induced micturition. *J. Comp. Neurol.* 1–16. doi: 10.1002/cne.24949

Wodlinger, B., and Durand, D. M. (2011). "Recovery of neural activity from nerve cuff electrodes," in *Proceedings of the 2011 Annual International Conference of the IEEE Engineering in Medicine and Biology Society, Boston, MA*, (Piscataway, NJ: IEEE), 4653–4656.

Yap, E. L., and Greenberg, M. E. (2018). Activity-regulated transcription: bridging the gap between neural activity and behavior. *Neuron* 100, 330–348. doi: 10.1016/j.neuron.2018.10.013

Yoo, P. B., Horvath, E. E., Amundsen, C. L., Webster, G. D., and Grill, W. M. (2009). Intraurethral activation of excitatory bladder reflexes in persons with spinal cord injury. *Conf. Proc. IEEE Eng. Med. Biol. Soc.* 2009, 6781–6784. doi: 10.1109/IEMBS.2009.5333982

Zhao, W., Aboushwareb, T., Turner, C., Mathis, C., Bennett, C., Sonntag, W. E., et al. (2010). Impaired bladder function in aging male rats. *J. Urol.* 184, 378–385. doi: 10.1016/j.juro.2010.03.004

Conflict of Interest: Research reported in this publication received funding from GSK Bioelectronics Innovation Challenge (JF and JK). This funder was not involved in the study design, collection, analysis, interpretation of data, the writing of this article or the decision to submit it for publication.

The remaining authors declare that the research was conducted in the absence of any commercial or financial relationships that could be construed as a potential conflict of interest.

frontiers in Neurology

REVIEW
published: 28 January 2021
doi: 10.3389/fneur.2020.597451

Deep Brain Stimulation Initiative: Toward Innovative Technology, New Disease Indications, and Approaches to Current and Future Clinical Challenges in Neuromodulation Therapy

Yanan Sui[1†], Ye Tian[1†], Wai Kin Daniel Ko[1†], Zhiyan Wang[1], Fumin Jia[1], Andreas Horn[2], Dirk De Ridder[3], Ki Sueng Choi[4,5,6], Ausaf A. Bari[7], Shouyan Wang[8], Clement Hamani[9], Kenneth B. Baker[10,11], Andre G. Machado[10,11], Tipu Z. Aziz[12], Erich Talamoni Fonoff[13,14], Andrea A. Kühn[2], Hagai Bergman[15,16], Terence Sanger[17], Hesheng Liu[18], Suzanne N. Haber[19,20*] and Luming Li[1*]*

[1] National Engineering Laboratory for Neuromodulation, Tsinghua University, Beijing, China, [2] Charité, Department of Neurology, Movement Disorders and Neuromodulation Unit, University Medicine Berlin, Berlin, Germany, [3] Section of Neurosurgery, Department of Surgical Sciences, Dunedin School of Medicine, University of Otago, Dunedin, New Zealand, [4] Department of Psychiatry and Behavioural Science, Emory University, Atlanta, GA, United States, [5] Department of Radiology, Mount Sinai School of Medicine, New York, NY, United States, [6] Department of Neurosurgery, Mount Sinai School of Medicine, New York, NY, United States, [7] Department of Neurosurgery, University of California, Los Angeles, Los Angeles, CA, United States, [8] Institute of Science and Technology for Brain-Inspired Intelligence, Fudan University, Shanghai, China, [9] Harquail Centre for Neuromodulation, Sunnybrook Research Institute, Toronto, ON, Canada, [10] Department of Neurosciences, Lerner Research Institute, Cleveland Clinic, Cleveland, OH, United States, [11] Neurological Institute, Cleveland Clinic, Cleveland, OH, United States, [12] Department of Neurosurgery, John Radcliffe Hospital, Nuffield Department of Surgical Sciences, University of Oxford, Oxford, United Kingdom, [13] Department of Neurology, University of São Paulo Medical School, São Paulo, Brazil, [14] Hospital Sírio-Libanês and Hospital Albert Einstein, São Paulo, Brazil, [15] Department of Medical Neurobiology (Physiology), Institute of Medical Research–Israel-Canada (IMRIC), Faculty of Medicine, Jerusalem, Israel, [16] The Edmond and Lily Safra Center for Brain Research (ELSC), The Hebrew University and Department of Neurosurgery, Hadassah Medical Center, Hebrew University, Jerusalem, Israel, [17] University of Southern California, Children's Hospital Los Angeles, Los Angeles, CA, United States, [18] Department of Neuroscience, College of Medicine, Medical University of South Carolina, Charleston, SC, United States, [19] Department of Pharmacology and Physiology, University of Rochester School of Medicine & Dentistry, Rochester, NY, United States, [20] McLean Hospital and Harvard Medical School, Belmont, MA, United States

Deep brain stimulation (DBS) is one of the most important clinical therapies for neurological disorders. DBS also has great potential to become a great tool for clinical neuroscience research. Recently, the National Engineering Laboratory for Neuromodulation at Tsinghua University held an international Deep Brain Stimulation Initiative workshop to discuss the cutting-edge technological achievements and clinical applications of DBS. We specifically addressed new clinical approaches and challenges in DBS for movement disorders (Parkinson's disease and dystonia), clinical application toward neurorehabilitation for stroke, and the progress and challenges toward DBS for neuropsychiatric disorders. This review highlighted key developments in (1) neuroimaging, with advancements in 3-Tesla magnetic resonance imaging DBS compatibility for exploration of brain network mechanisms; (2) novel DBS recording capabilities for uncovering disease pathophysiology; and (3) overcoming

OPEN ACCESS

Edited by:
Vitor Engracia Valenti, São Paulo State University, Brazil

Reviewed by:
Stephen Tisch, St Vincent's Hospital Sydney, Australia
Ron Alterman, Beth Israel Deaconess Medical Center and Harvard Medical School, United States
Laura Cif, University Hospital Montpellier, Montpellier, France
Luigi M. Romito, Fondazione IRCCS Istituto Neurologio Carlo Besta, Italy

***Correspondence:**
Hesheng Liu
liuhe@musc.edu
Suzanne N. Haber
Suzanne_Haber@urmc.rochester.edu
Luming Li
lilm@tsinghua.edu.cn

[†]These authors have contributed equally to this work

Specialty section:
This article was submitted to Autonomic Neuroscience, a section of the journal Frontiers in Neurology

Received: *21 August 2020*
Accepted: *23 November 2020*
Published: *28 January 2021*

Citation:
Sui Y, Tian Y, Ko WKD, Wang Z, Jia F, Horn A, De Ridder D, Choi KS, Bari AA, Wang S, Hamani C, Baker KB, Machado AG, Aziz TZ, Fonoff ET, Kühn AA, Bergman H, Sanger T, Liu H, Haber SN and Li L (2021) Deep Brain Stimulation Initiative: Toward Innovative Technology, New Disease Indications, and Approaches to Current and Future Clinical Challenges in Neuromodulation Therapy. Front. Neurol. 11:597451. doi: 10.3389/fneur.2020.597451

global healthcare burdens with online-based DBS programming technology for connecting patient communities. The successful event marks a milestone for global collaborative opportunities in clinical development of neuromodulation to treat major neurological disorders.

Keywords: neuromoxdulation, depression, deep brain stimulation, MRI compatibility, gait disability

INTRODUCTION

The National Engineering Laboratory for Neuromodulation (NELN) at Tsinghua University organized its first deep brain stimulation (DBS) initiative meeting in Beijing on October 11–12, 2018. Leading experts in neuromodulation, specifically in the field of DBS, were in attendance for discussions on the latest research in neuromodulation technologies and applications, clinical indications, as well as current and foreseeable challenges in DBS therapy. Participants from multidisciplinary backgrounds that included neural engineers, neurosurgeons, neurologists, neuroscientists, and industry professionals engaged in round-table discussions following the thematic sessions and presentations. With expert updates and reports on the latest clinical approaches, there were open discussions on the opportunities in neuromodulation with recent technological advancements. This included an exchange of ideas on the connectome approach to DBS, novel developments of 3-Tesla magnetic resonance imaging (3T MRI)-compatible DBS devices and the use of neuroimaging to understand the neurocircuitry of effective DBS, including demonstrations of the latest DBS neural recording technology in real patients. This meeting came to provide reports of recent DBS application for unmet clinical needs, such as gait disability in Parkinson's disease (PD) and stroke rehabilitation, and the challenges in the current transition of DBS therapy toward neuropsychiatric disorders, including depression and memory disorders.

Abbreviations: 2-DG, 2-deoxyglucose; 3T MRI, 3-Tesla magnetic resonance imaging; AD, Alzheimer's disease; AI, artificial intelligence; ALIC, anterior limb of the internal capsule; ANT, anterior nucleus of thalamus; APA, anticipatory postural adjustment; APP, amyloid precursor protein; ChAT5, choline-acetyltransferase 5; dACC, dorsal anterior cingulate cortex; DBS, deep brain stimulation; dMRI, diffusion magnetic resonance imaging; DN, dentate nucleus; EC, entorhinal cortex; FOG, freezing of gait; GPi, globus pallidus internal segment; HMMs, hidden Markov models; IEC, International Electrotechnical Commission; IPG, implantable pulse generator; LFPs, local field potentials; MDD, major depressive disorder; MERs, microelectrode recordings; MFB, medial forebrain bundle; MPTP, methyl-phenyl-tetrahydropyridine; MSA, multiple system atrophy; NELN, National Engineering Laboratory for Neuromodulation; NHP, nonhuman primate; NMU, neuromodulation monitoring unit; OCD, obsessive–compulsive disorder; OFC, orbitofrontal cortex; PD, Parkinson's disease; PET, positron emission tomography; PIGDs, postural instability and gait disorders; PPN, pedunculopontine nucleus; PSP, progressive supranuclear palsy; RF, radiofrequency; RMS, root mean square; SAR, specific absorption rate; SCC, subgenual cingulate cortex; SCGwm, subgenual cingulate gyrus white matter; SCS, spinal cord stimulation; sl-MFB, superolateral branch of the medial forebrain bundle; STN, subthalamic nucleus; TMS, transcranial magnetic stimulation; TUG, Timed Up and Go; VC/VS, ventral capsule/ventral striatum; VIM, ventral intermediate; vmPFC, ventromedial prefrontal cortex; VFS, variable frequency stimulation; VTA, volume of tissue activated.

With the current rapid and widespread rise of neuromodulation therapies in China and across the globe, NELN's first DBS initiative meeting set out to stimulate collaborations between leaders in clinical, engineering, and basic science research for the rapid translation of therapies using state-of-the-art technologies. Marking a unique milestone in fostering international collaborations in DBS research, we report here a summary of the meeting that covers topic overviews, presentations, and follow-up discussions aiding to uncover expert perspectives and support advancements in the field of neuromodulation as we progress into the future.

SOME RECENT DEEP BRAIN STIMULATION TECHNOLOGY ADVANCEMENTS

MRI Compatibility

Among patients with an active implantable medical device, it is estimated that ∼50–75% will require an MRI scan during the time course of treatment (1). In 2016, it was reported that 66–75% of DBS patients treated for movement disorders required an MRI scan within 10 years of device implantation (2). However, clear dangers exist for DBS patients under MRI, specifically the potential for permanent neurological damage due to radiofrequency (RF) lesioning caused by heating of DBS electrodes (3). Indeed, the main risk in MRI comes from wires enclosed in DBS extensions and leads, which can receive RF energy from the MRI magnetic field, inducing current discharge through contacts that align at the tip of the lead. This can cause thermal damage to the surrounding brain tissue. Therefore, inhibiting MRI RF-induced heat remains key for addressing the safety of patients implanted with DBS devices under MRI.

While some DBS device manufacturers claim safety under 1.5T MRI, DBS devices available to patients across global markets are still considered to be unsafe under 3T MRI, limiting patients from imaging and diagnostic benefits. Currently, patients can only use head/body coils for scanning under 1.5T, with the head specific absorption rate (SAR) value being <0.1 W/kg or the B1RMS value remaining below 2.0 uT (4). This is far lower than the upper limit of 2.0 W/kg of patients without medical devices for MRI (5), as set by the International Electrotechnical Commission (IEC) standard.

With the limitations of low-quality imaging using 1.5T MRI, clinical research in DBS patients would greatly benefit from advances in MRI compatibility. Following laboratory evaluations and preclinical testing, a study conducted by the NELN was reported for testing the safety and efficacy of high-field 3T MRI-compatible DBS system in PD patients. The clinical trial

was initiated in November 2016, and the final follow-up was completed in June 2018. A total of 24 PD patients were screened, and 14 subjects were eligible for the study. Follow-ups were successfully completed at 1, 3, 6, and 12 months, with an average time of 4.12 h taken per patient for anatomical and brain function 3T MRI scan. No adverse events were found that related to MRI (6) (**Figure 1**).

Recording Neural Signals in Deep Brain Stimulation

Electrophysiological recordings of oscillatory neural networks remain an important tool for advancing brain research. In PD, β-band oscillations detected from the basal ganglia correspond to the degree of motor symptoms, such as rigidity and L-3,4-dihydroxyphenylalanine (L-DOPA)-induced dyskinesia, representing a pathophysiological marker of movement disorders that are beyond parkinsonism alone (7–10). Previous clinical studies have recorded neural activity intraoperatively during DBS surgery, with local field potentials (LFPs) being captured from external cables connected to DBS leads. With limited data recording and subsequent processing being completed after DBS implantation, along with potential complications from microlesion effect and edema along lead trajectories, studies of disease pathophysiology have been limited with such methods. Current implantable LFP-recording DBS systems are available but generally have a non-rechargeable battery lasting 3–5 years. Notably, these devices have high power consumption that results from LFP acquisition and readouts, limiting the time of use and requires earlier replacement of the implantable pulse generator (IPG), a factor that is not favored by patients. The need for extending the longevity of the DBS recording device remains at the forefront of neural engineering research. This would allow for efficient long-term LFP recordings, for example, to assess the changes of β-band oscillations in response to motor symptoms over time. Hopefully, more research on θ-band relating to tremor and prokinetic γ-band can help us develop robust algorithms for closed-loop control.

While the implantable DBS device PC+S produced by Medtronic has been used in previous research, its storage capacity in the IPG has limitations for long-term continuous recordings that often require massive LFP data storage. To resolve such issues, streaming of data to an external storage provides a solution for unlimited data collection and simultaneous assessment of physiological signals, such as movement behaviors, in a freely moving environment that allows for sophisticated clinical experimentation. The latest DBS devices for LFP recordings would be expected to include (1) large-capacity battery or wireless charging technology that fulfills long-term implantation acceptable to patients receiving treatment, (2) continuous high-precision data acquisition capability, (3) real-time external transmission that is wireless and therefore can be applied in freely moving conditions, and (4) multiple differential signal acquisition channels that can function simultaneously with DBS-ON, with sampling rates exceeding 500 Hz.

Here, the NELN demonstrated and reported PD patients implanted with DBS device G102RS from PINS Medical Ltd., a device engineered with rechargeable LFP-sensing and data streaming capacity. The first clinical trial has been completed in PD patients ($n = 13$) with a successful post-surgery follow-up through 12 months. Preliminary data have been used to characterize components of β-band oscillations during sleep states (11). Furthermore, it is reported that the response of β-band oscillations to high-frequency DBS is changed over time, which is a likely result from changes in neural network plasticity.

Remote Online Deep Brain Stimulation Programming

Following implantation of a DBS device, postoperative DBS programming conducted by specialists is a vital part of achieving optimal clinical efficacy in patients (12). However, practical burdens in the clinical setting exist such as limited specialists available, time constraints, patient travel to specialist centers, and additional care costs (13). In recent years, the NELN has developed a remote online DBS programming system that operates with hardware-level protection for remote communication security (14). This has been specifically aimed at alleviating common healthcare burdens in the field of DBS worldwide. To date, the number of patients who have successfully used the remote DBS program control in China has exceeded 3,000 and has also been implemented between different countries, such as the UK, Spain, and Singapore, for patient management.

The development of the remote programming technology has notably reduced the burden of patient visits. In a recent survey with approximately 200 patients, costs and time-spent related to follow-up have both been reduced by >90%. Remote programming allows for clinical evaluations to be conducted through video and audio streams with Unified Parkinson's Disease Rating Scale (UPDRS)-III scoring and physical examination. As we look to the future, there is a natural evolution toward machine learning algorithm applications for automatic movement evaluation and objective output readings. Such applications allow for significantly increasing the amount of data collected on disease progression and enriching data pools for diagnoses and potential use toward future closed-loop systems.

Variable Frequency Stimulation

High-frequency stimulation of the subthalamic nucleus (STN) through DBS in PD patients is a well-established application for alleviating parkinsonism. However, the application of high-frequency stimulation fails to alleviate axial disabilities in PD patients, which may occur due to disease progression, surgical injury, and side effects of electrical stimulation (15). Previous reports of low-frequency stimulation in PD have demonstrated the alleviation of axial disability but may compromise improvements in parkinsonism (16, 17). A recent pilot study completed has shown the promising effects of variable frequency stimulation (VFS), which applies alternating high- and low-frequency stimulations for freezing of gait (FOG) in PD patients (18). The long-term stability of VFS application is now being evaluated in a large clinical trial. In addition, video data collected

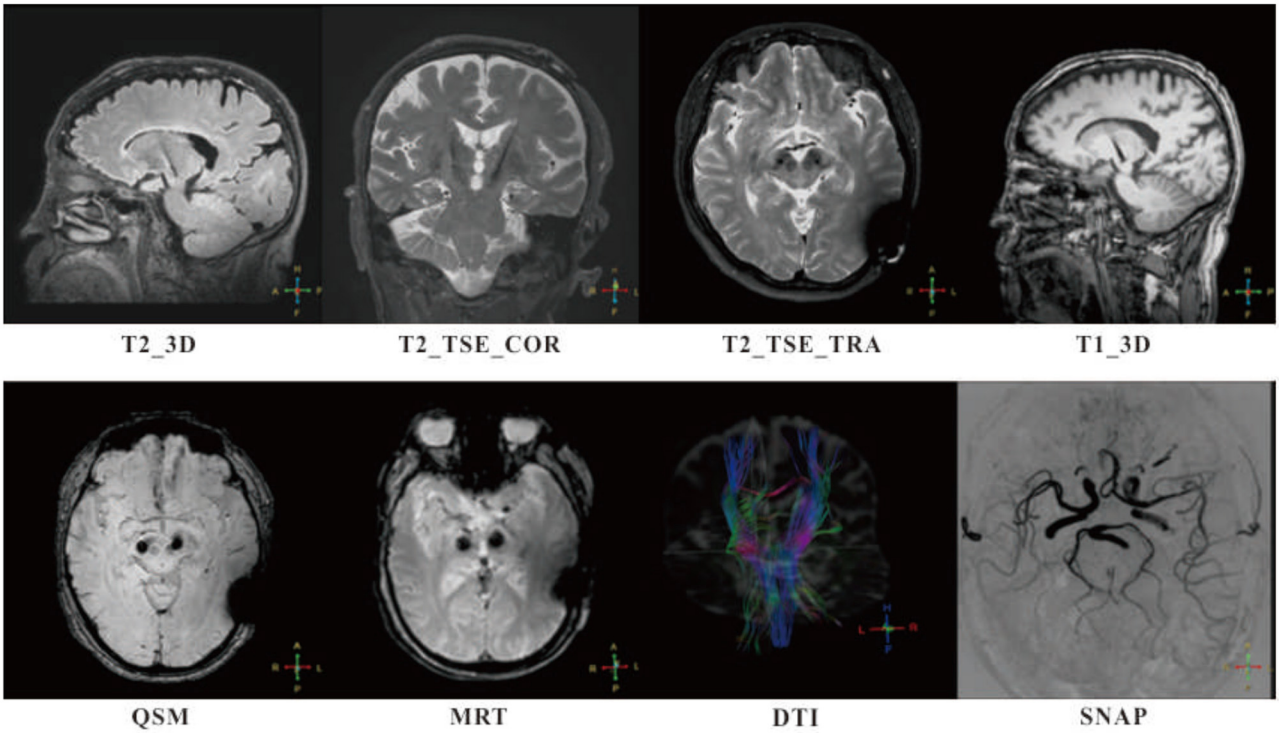

FIGURE 1 | Follow-ups of patients with MR-compatible deep brain stimulation (DBS) implanted were successfully completed at 1, 3, 6, and 12 months, with intensive 3T MR scan. High in-plan resolution T2-weighted fast spin echo sequences (T2_TSE_COR and T2_TSE_TRA) and high specific absorption rate (SAR) isotropic sequences (T1_3D, T2_3D, and QSM) were adopted for anatomy analysis. Simultaneous non-contrast angiographies (SNAP) and diffusion tensor imaging (DTI) were taken for monitoring potential lesion on blood vessels and edema occurrence. A special sequence, magnetic resonance thermometry (MRT) used for tissue temperature online assessment. No adverse events were found that related to MRI.

from previous trials have been assessed with automatic classification and scoring based on machine learning methods to evaluate typical Timed Up and Go (TUG) tasks. This is now being utilized for objective classifications of FOG under separate analyses.

Perspective of Artificial Intelligence for Deep Brain Stimulation

Artificial intelligence (AI) has great potential in medicine. Being broadly defined as the development of intelligent machines, the field of AI focuses on capabilities, such as understanding human languages and natural scenes, and development methods, such as machine learning (19–21). Machine learning entails building knowledge from patterns in data rather than being specified by human programmers. Much of the recent success in AI has come from the aggregation of massive training data and new computing systems for large-scale learning. New algorithms and systems have accelerated the widespread experimentation for prediction problem as supervised learning. In real-world situations, there is the desire to take strategies based on predictions. A next target for learning systems is data-driven decision-making.

Recent achievements in AI (including machine learning, computer vision, natural language processing) have the potential to improve our understanding of neurological disorders and corresponding treatments. In specific relation to DBS, there can be difficulty and time expenditure in finding optimal parameters for each patient. AI may help shape effective treatment for some of the most prevalent neurological disorders, such as PD, based on previous data (**Figure 2**). Future developments toward robust online learning techniques that explore large decision spaces and adapt to feedback in real time are essential to online learning problems. The application of AI techniques may allow us to uncover the mechanisms of DBS and the understanding of how DBS influences brain networks (11). It is noteworthy that recent advances in MRI-compatible DBS devices are allowing for acquisition of neuroimages during stimulation. It can be envisioned that a combination of advanced imaging techniques and AI techniques can facilitate the identification of DBS surgical targets in individual patients. Indeed, personalized implantation and automatic stimulation strategies can be aimed to maximize safety and efficacy of optimal treatment benefits and improve patient care.

Overall, advances in machine learning and robotics have the potential to improve health care delivery, from scheduling

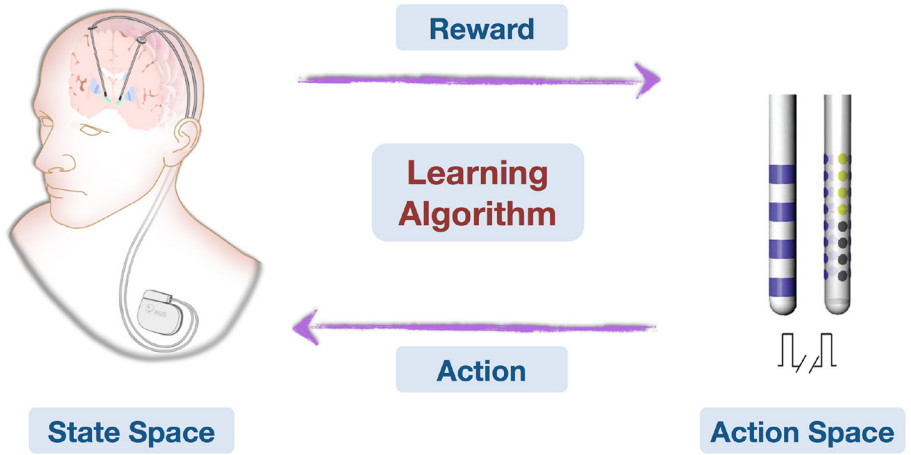

FIGURE 2 | This is an illustration on how deep brain stimulation parameters can be learned and optimized online with feedback. Patient conditions are represented in the State Space. Action Space contains all possible stimulating patterns. The Learning Algorithm learns from domain knowledge and history data, then observes treatment effects (Reward) and optimizes stimulating pattern (Action) online.

treatment plans to guiding surgical procedures, that are beyond current clinical capabilities. While these technologies shed light on the way toward better treatment, they also pose new challenges in terms of scale, complexity, safety, robustness, and efficacy.

INNOVATIONS THAT AIM AT UNCOVERING DEEP BRAIN STIMULATION MECHANISMS OF ACTION

Toward Connectomic Deep Brain Stimulation

It was long thought that DBS exerts its function by local modulation of the target region itself, and a large number of studies have focused on such *local* effects by delineating optimal "sweet spots" for effective DBS. However, accumulating evidence suggests that DBS modulates fiber tracts or distributed brain networks and that such effects may be equally important for optimal treatment outcome (22–27). This has given way to a paradigm shift in the field of DBS, away from localized targeting and toward modulation of whole-brain networks by invasive neuromodulation.

In a parallel development, in the field of neuroimaging, the concept of the *connectome*, a formal mathematical description of brain regions and their interconnections was introduced in 2005 (28). Given the strong impact of the *connectomics* concept on the neuroimaging field, it is somewhat surprising that, so far, only a handful of studies have applied it to DBS (22, 29–31). One reason for this may be that patient-specific connectivity data [resting-state functional MRI (rs-fMRI) or diffusion MRI (dMRI)] are usually not acquired within clinical routine and are hard, if not impossible, to acquire postoperatively.

To overcome this limitation, Horn et al. (23, 32–34) established a method that combines normative connectomes, i.e., average brain connectomes that are estimated on large cohorts of subjects, with DBS electrode reconstructions from a single patient. This concept has been successfully applied to other areas of clinical neuroimaging, for instance, to map stroke symptoms to brain regions (26, 28, 35) or to explain varying results of transcranial magnetic stimulation (TMS) treatment (36). A recent publication has demonstrated the feasibility of this concept for DBS (23). Here, the authors estimated the structural and functional connectivity profile of effective ventral intermediate (VIM) nucleus DBS by transforming an optimal literature-based DBS coordinate to standard stereotactic [Montreal Neurosciences Institute (MNI)] space and combining it with normative connectomes. A second study demonstrated that clinical DBS improvement can be predicted based on the connectivity profiles of electrodes alone (25) (**Figure 3**). Specifically, the structural and functional "connectivity fingerprints" of DBS electrodes in 95 PD patients operated on at two centers were highly predictive of their clinical motor improvement. In fact, the optimal connectivity profile of effective STN-DBS could be informed exclusively on data from the first DBS center and then used to accurately predict outcome in patients from the second center. The study demonstrated that brain connectivity may play a crucial role in the DBS mechanism of action and that it may be used to predict treatment outcome across cohorts and centers. Recently, the concept was transferred to essential tremor (37) and obsessive–compulsive disorder (OCD) (38). After further validation, resulting "effective treatment networks" of these and similar studies could in the future be used to guide both DBS programming and surgery. Moreover, networks could potentially be used to guide non-invasive brain stimulation since they define cortical areas that may play a role in disease-specific and therapeutic circuitries.

Studying Effects of Deep Brain Stimulation in Individual Patients

DBS is a well-established functional neurosurgical technique that has recently observed rapid development as a potential

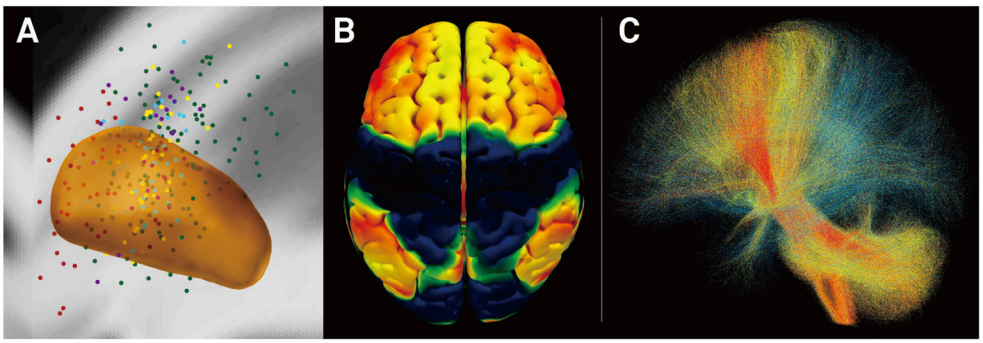

FIGURE 3 | Connectivity predicts deep brain stimulation (DBS) outcome in Parkinson's disease (25). **(A)** Active stimulation coordinates from five cohorts out of two DBS centers mapped to subcortical anatomy [subthalamic nucleus (STN) shown in orange]. **(B)** Cortical connectivity map predictive of clinical outcome analyzed using normative-connectome based on resting-state functional MRI (rs-fMRI). Hot colors show areas that are associated with good clinical outcome if the electrode is strongly connected to them. In contrast, functional anticorrelation to areas in cold colors is associated with beneficial outcome. **(C)** Fiber tracts associated with good (red), intermediate (yellow), or poor (blue) clinical outcome. Connectivity profiles shown in **(B,C)** are able to predict motor improvement in out-of-sample data (across DBS cohorts and centers; R in the range of 0.5; ∼20% variance explained).

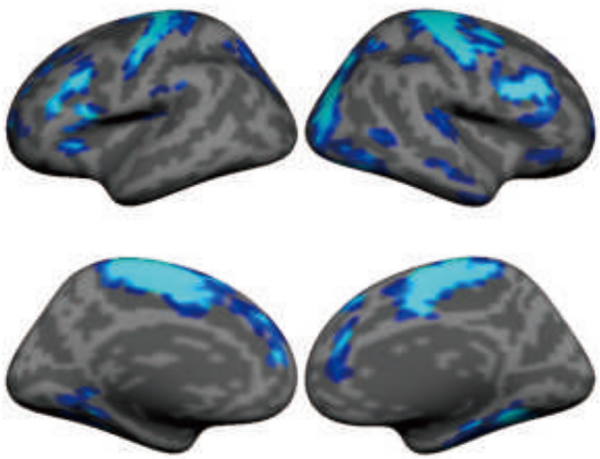

FIGURE 4 | Subthalamic nucleus stimulation suppresses functional activity in large-scale brain networks, including sensorimotor and association regions in the frontal lobe. The map shows the functional MRI (fMRI) contrast between "DBS on" condition and "DBS off" condition in 11 patients with Parkinson's disease. Functional data were recorded using 3-Tesla MRI when deep brain stimulation (DBS) was turned on (36-s blocks) and off (24-s blocks) using a block design.

treatment for neuropsychiatric disorders (27, 39). Not only does DBS mimic the effects of neuropharmacological treatment, but it currently offers key advantages with fewer side effects and greater adjustability. Although DBS has achieved great success in treating movement disorders such as PD and dystonia, a broader use of DBS for other neurological disorders is facing two major challenges. The first lies in accurate application in individual patients, as patients with neurological and psychiatric disorders are highly heterogeneous in terms of their symptom expression, disease progression, and more importantly their brain functional network organization. A personalized implantation/stimulation strategy is thus necessary to maximize the treatment benefits and improve patient care. The second challenge is the lack of in-depth understanding of how DBS impacts wider brain networks largely due to the lack of means to study the immediate and long-term stimulation effects on large-scale brain networks *in vivo*. A better appreciation of the mechanism of DBS is crucial in order to extend this important technique from treating movement disorders to a broader spectrum of brain diseases including Alzheimer's disease (AD), stroke, and neuropsychiatric disorders.

Understanding the neurophysiology, connectivity, and neuropathology at the level of individual patients is key to furthering the success of DBS treatment. To date, DBS applications are largely based on the presumption that current models of disease, which are predominantly derived from neuroimaging studies that identify brain abnormalities at a group level (40), can be directly applied to individual patients. However, it is becoming increasingly recognized that interindividual variability exists not only in macroscopic and microscopic brain anatomy (41–43) but also in the organization of functional systems, i.e., the topography and connectivity of functional regions may vary drastically across individuals (44, 45). Compared to unimodal sensory and motor functions, higher-order cognitive functions demonstrate substantial variability across individuals. Recent studies suggest that the high level of interindividual variability in higher-order functions may be a fundamental principle of brain organization and a critical outcome of human brain evolution (44–46). Disease models concerning motor circuits, which have a relatively low degree of interindividual variability, might be directly applied to individual patients to guide DBS treatment. For example, targeting the STN and globus pallidus internal segment (GPi) provides efficient treatment of akinesia, tremor, and rigidity in most PD patients (47). However, even with well-defined targets, not all patients seem to benefit from DBS to the same degree.

The picture becomes more complicated with the application of DBS in psychiatric disorders. For example, a recent report of the application of DBS to the subcallosal cingulate for treatment-resistant depression yielded unsatisfactory results, with DBS failing to demonstrate a superior effect to sham stimulation (40). A subsequent trial has suggested that DBS targeting and parameters need to be optimized for individual patients in order to demonstrate treatment efficacy (48). Specifically, it was found that treatment responders shared a common pattern of white matter connectivity within the subcallosal cingulate region (49). These results suggest that it is necessary to develop patient-specific targets and cortical responsivity measures to identify precise DBS targets. On a systems level, it is crucial to develop non-invasive metrics of brain functional and structural connectivity, at an individual level, to make DBS treatment viable and to improve the cost–benefit ratio for patients. Recent technical advancement in functional connectivity MRI research has made it possible to localize functional networks at the single-subject level (50–52), which could thus be used to guide personalized DBS treatment. For example, the work by Wang et al. (52) has established a technology to parcellate cortical functional networks in individuals, which is highly sensitive to the characteristics of the individual and is able to capture intersubject variability. Functional networks localized using this parcellation technology were also validated by invasive cortical stimulation mapping in surgical patients. Such techniques may be essential for identifying DBS targets in individual patients in the near future.

Understanding the immediate and long-term effects of DBS on large-scale brain networks requires technologies that can read out brain signals *in vivo*. Until recently, due to technical constraints, the local and remote effects of DBS have only been measured with electroencephalography using external leads and formed the basis for the investigation of brain response to DBS (53). Recent technological developments allow for the concurrent recording of LFPs and high-field MRI during DBS (54). The implications of these developments are profound (47). DBS significantly suppressed beta activity (13∼35 Hz), but the suppression effect appeared to gradually attenuate during a 6-month follow-up period after surgery (55). The concurrent recording of LFPs allows for the characterization of pathophysiological neuronal firing patterns, the investigation of the clinical response according to application parameters, and the development and testing of new disease models. This technological advancement has benefited the study of, for example, the abnormal oscillatory activity (13–35 Hz) in PD, the pivotal role of the STN in basal ganglia physiology and pathophysiology, and the use of β-band oscillations as biomarkers to devise closed-loop DBS systems to deliver a more neurophysiologically efficient therapy. Nevertheless, electrophysiological signals recorded from implanted electrodes only reflect neural responses at local structures rather than the effects on large-scale, distributed functional networks. Obtaining a comprehensive picture of DBS effects on the human brain is now possible, thanks to the recent development of DBS devices that are compatible with high-field MRI (54). Taking advantage of these novel devices, we are able to record functional activity across the entire brain during DBS using 3T MRI. The high-quality imaging data can capture the changes in the large-scale brain networks when DBS is turned on and turned off. The data presented by Liu et al. (52) demonstrate immediate, strong suppression of brain activity in the sensorimotor cortex after STN stimulation in PD patients (**Figure 4**). This DBS-fMRI technology allows for examining the validity of potential DBS targets for a variety of brain disorders, eventually leading to a broader use of DBS.

Taken together, DBS has the potential to revolutionize the treatment of neurological and psychiatric disorders and to improve our understanding of human brain function. However, before DBS can be implemented into standard practice for a broad range of disorders, a better understanding of how it affects large-scale brain networks and identification of precise targets in individual patients are necessary. The development of individualized functional imaging techniques and MRI-compatible DBS devices will greatly facilitate research in this important field.

Neurocircuitry Underlying Effective Deep Brain Stimulation for Mental Health Disorders

DBS is a promising therapeutic approach for patients with treatment-resistant mental health disease, including OCD and major depressive disorder (MDD) (56–58). MDD and OCD involve key elements of the cortico-cortical and cortico-basal ganglia networks. These networks include the ventromedial prefrontal cortex (vmPFC), orbitofrontal cortex (OFC), dorsal anterior cingulate cortex (dACC), and the basal ganglia structures, striatum, and STN (59). DBS primarily targets myelinated fibers that carry information from and to the above structures. As such, the most common DBS targets are (1) the subgenual cingulate gyrus white matter (SCGwm), the white matter adjacent to cortical areas 32 and 25; (2) the anterior limb of the internal capsule (ALIC) that carries descending and ascending cortical fibers; and (3) the connections of the STN, including the hyperdirect pathway that carries cortico- STN fibers (56–58).

The work by Haber et al. (59) has used a combination of nonhuman primate (NHP) tracing experiments and NHP and human dMRI to delineate the organization of PFC fiber pathways, which allows insight into which connections are likely to be involved at each DBS electrode site. The work has focused on how cortical fibers are organized within the SCGwm, ALIC, and STN and the fibers and terminal fields likely to be affected by DBS electrodes placed within those regions.

The SCGwm site is primarily used for treatment-resistant depression. The most effective SCGwm contacts (1 and 2) are at the border between the SCG and the inferior rostral gyrus (60). Fibers that pass through this region include multiple connection involving the entire ventral surface of the frontal cortex (**Figure 5A**). Contact 1 is within the inferior rostral gyrus white matter, contact 2 is within the SCG, and contracts 0 and 3 are ventral and dorsal, respectively. Contacts 0–2 will involve (1) all connections from vmPFC areas adjacent to the electrode contacts (both cortical and subcortical projections); (2) uncinate

fasciculus fibers from non-adjacent vmPFC and medial OFC as they travel medially to other ventral PFC areas; (3) a subset of lateral OFC fibers traveling medially to innervate medial PFC areas; (4) axons traveling from the contralateral vmPFC and medial OFC; and (5) a subset of anterior vmPFC and medial OFC en route to the corpus callosum through the uncinate fasciculus. Contact 3 involves primarily fibers in the corpus callosum. In addition, this site captures a subset of fibers traveling from the medial OFC and posterior lateral OFC to the cingulum bundle and superior longitudinal fasciculus (61).

The ALIC site is used for both treatment-resistant MDD and OCD. Fibers from different cortical regions follow predictable trajectories to, and locations within, the ALIC. The relative position of fibers from different cortical areas, within the ALIC, demonstrates the topology, and specifically the ALIC segmentation, based on PFC origin of fibers. Fibers arising from dorsal regions travel within the capsule dorsal to those from ventral cortical areas. Axons derived from medial areas travel within the capsule medial to those from lateral regions (**Figure 5B**). The organization shows how stimulation in different locations throughout the ALIC is likely to impact projections of different cortical areas, including the ventrolateral PFC (vlPFC), dorsolateral PFC (dlPFC), dorsomedial PFC, and dACC. Each contact placed within the ALIC activates a different subset of corticothalamic and brain stem fibers. In particular, an electrode contact targeting the ventralmost part of the ALIC will likely impact primarily fibers from the vmPFC and OFC. More dorsal contacts/lesions will impact lateral OFC, ventrolateral PFC, and dACC fibers. The most dorsal contacts/lesions will impact primarily the dorsomedial and dorsolateral PFC. In addition to consideration of the dorsoventral position of electrodes or lesions, the rostrocaudal position is also important (61, 62).

The effectiveness of DBS for depression at the SCGwm and ALIC sites has not been directly compared with respect to patient selection criteria. Nonetheless, both sites are effective in over 50% of otherwise treatment-resistant patients (63, 64). Stimulation at the SCGwm site captures all cortical and subcortical projections from the area surrounding each contact site. However, it also captures fibers from non-adjacent cortical areas passing through the target, including connections between different vPFC areas, and OFC fibers traveling to corpus callosum, medial forebrain bundle (MFB), cingulum bundle, and superior longitudinal fasciculus. In addition, this target captures the extensive brain stem connections from the SCG. In contrast, ALIC site does not directly involve corticocortical fibers. Rather, each contact in the ALIC site involves a different combination of thalamic and/or brain stem bundles. Of particular importance is that both DBS targets capture subsets of fibers that include both thalamic and brain stem fibers. Thus, an important part of the clinical effectiveness of DBS is likely to require a combination of thalamic and brain stem fibers.

The STN site, commonly used for PD is now experimentally used for OCD. In addition to the STN connections to both pallidal segments, there is an important direct cortico-STN connection that is referred to as the hyperdirect pathway. This pathway is also organized in a specific and general topographic manner. M1 projects to the dorsolateral STN, with area 6 projecting ventromedially to these terminals. Overall, PFC projections are concentrated and anterior to motor control projections. While dorsal PFC projections occupy the medial half of the STN, vmPFC and dACC dense terminal fields are located in the rostral and anterior, medial tip. This area also receives the limbic input from the pallidum, in particular, projections from the ventral pallidum (65). The delineation of limbic and cognitive hyperdirect pathways has been key for developing a DBS site for the treatment of OCD (58). It has also contributed to our understanding of non-motor effects of DBS in PD. Taken together, DBS for motor disorders such as PD targets the lateral STN regions, while the target for OCD targets the medial STN. Effectiveness of DBS for OCD at the ALIC and STN sites is now being compared at several clinical sites.

DEEP BRAIN STIMULATION FOR MAJOR DEPRESSION AND ADDICTION

MDD has been known to exist since the origins of humankind. Hippocrates (460–370 BC) referred to MDD as "melancholy." Being a highly heterogeneous disorder, symptoms of MDD affect a range of behavioral domains including mood, sleep, sexual behavior, and motor functioning. MDD has a 1-year prevalence of 3–5% and lifetime prevalence of 15–20%. It has been reported that MDD is on the uprise (increase of 10% between 2005 and 2010), leading to an incremental economic burden for individuals with MDD. The cost increased by 21.5% (from $173.2 billion to $210.5 billion) (66).

DBS for MDD has demonstrated clinical benefit in three brain regions in open-label trials, including the ventral capsule/ventral striatum (VC/VS), the subgenual cingulate cortex (SCC), and the superolateral branch of the medial forebrain bundle (sl-MFB) (40, 67, 68). Two large, industry-sponsored sham-controlled randomized controlled trials (RCTs) of DBS for depression failed, one targeting BA25 and one targeting the ventral capsula (68). The BA25 trial (BROADEN) was halted when interim analyses showed a low likelihood of meeting primary endpoints. The outcomes of these trials have caused the field to question fundamental aspects of these therapies, including patient selection, trial design, network targeting, funding, and, of course, efficacy itself.

A number of lessons can be gleaned from these trials. (1) The underlying disorder, major depression, is not well-understood. We need better biomarkers to further delineate and stratify various forms of depression. (2) There is a need for identification of better outcome measures analogous to those used in DBS for movement disorders. For example, specific motor variables such as bradykinesia, rigidity, and tremor are utilized to determine the outcome of DBS for PD while psychiatric scales tend to focus on more holistic and subjective disease outcomes. Furthermore, these variables could also be used to identify patients most likely to respond to DBS. Thus, the best PD candidate is not simply the patient with the worst overall disease but one with specific levodopa-responsive symptoms. (3) There is shift, now, from the single-target approach to a network-based model of neuropsychiatry in which target selection is patient and disease

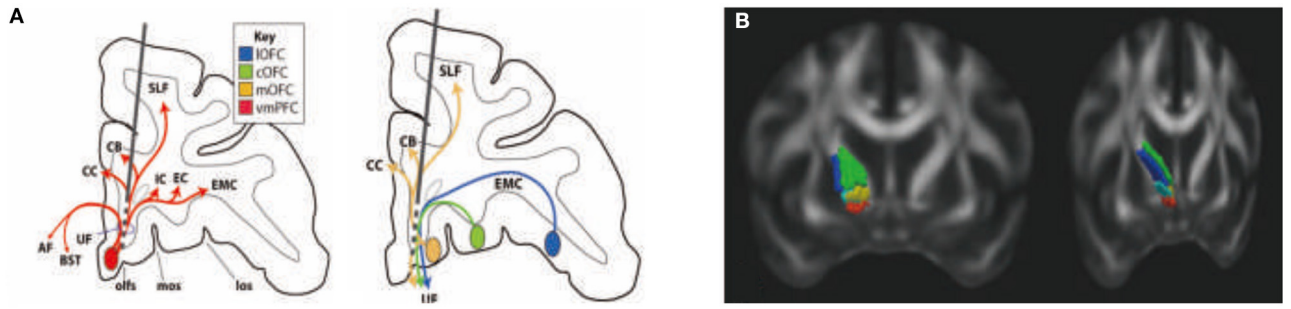

FIGURE 5 | Rules ventral prefrontal cortical axons use to reach their targets: implications for diffusion tensor imaging tractography and deep brain stimulation for psychiatric illness (61). Organization of fibers passing through the subgenual cingulate gyrus white matter (SCGwm) **(A)** and anterior limb of the internal capsule (ALIC) **(B)**. **(A)** Schematic of an electrode passing through the SCGwm, indicating the cortical fibers involved at each contact. AF, amygdala fugal pathway; CB, cingulate bundle; CC, corpus callosum, EC, external capsule; EMC, extreme capsule; IC, internal capsule; los, lateral orbital sulcus; mos, medial orbital sulcus; olfs, olfactory sulcus; SLF, superior longitudinal fasciculus; UF, uncinate fasciculus. **(B)** Organization of fibers in the human ALIC. Red, OFC and vmPFC fibers; yellow, ventrolateral PFC fibers; light blue, dACC fibers; green, dorsolateral PFC fibers; blue, dorsomedial PFC fibers.

specific. (4) We need to leverage structural and functional neuroimaging to better identify these network nodes. (5) We need to change our attitudes with regard to trial designs to support more flexible designs and to aggregate data across trials. (6) Finally, ongoing advancements in DBS hardware and software (such as directional electrodes and closed-loop devices) will result in increasing the therapeutic index and efficacy of DBS for psychiatric disorders. Thus, the field of psychiatric neurosurgery finds itself at a crossroads. Despite the setbacks of these so-called "failed" trials, the clinical and financial burden of psychiatric diseases continues to grow, as does the theoretical rationale for DBS therapy, with increased commitment from various national and international agencies.

In addition to major depression, substance addiction is one of the most prevalent and costly health problems globally. Standard medical therapy is often not curative, and relapse is common. Research over the past several decades on the neural underpinnings of addiction has implicated a network of structures within the brain shown to be altered in patients with substance abuse. While invasive neuromodulation such as DBS and VNS have proven to be effective in treating depression, OCD, and epilepsy, there is increasing interest and data with regard to their potential application in the treatment of severe, intractable substance abuse and addiction. Several neuromodulatory techniques and brain targets are currently under investigation in patients with various substance abuse disorders (69).

The current work by Bari et al. (70, 71) is aimed to apply the lessons learned from DBS for depression toward the application of DBS and other forms of invasive neuromodulation toward addiction. Thus, using probabilistic tractography, Bari et al. have identified specific limbic structures associated with nicotine addiction and impulsivity (currently under review with human brain mapping). In addition, brain mapping data from patients undergoing DBS for post-traumatic stress disorder (PTSD) combined with a normative connectomic approach has supported the role of the amygdala in regulating reward-related emotions. These efforts provide the background on which to design more informed trials of invasive neurmodulation for nicotine and other forms of addiction.

Toward Deep Brain Stimulation Targets and Stimulation Designs for Depression

The neural correlates of MDD have only been partially unraveled and involve both activity and connectivity changes. Based on neuroimaging, a neural circuit taxonomy for depression and anxiety has been developed (72). This suggests that rumination is the consequence of hyperconnectivity within the default mode network, inattention due to hypoconnectivity within the frontoparietal attentional networks, anhedonia and context insensitivity to a dysfunctional positive affect network, and anxious avoidance to hypoconnectivity within the salience network and hyperconnectivity between salience and default mode network (72).

Before medications were discovered that could treat MDD, psychosurgical techniques were developed to address this complex pathology. Whereas, the initial approach was to perform a large frontal lobotomy, the development of stereotactic approaches in 1947 permitted smaller and better targeted lesions resulting in four kinds of psychosurgery: (1) cingulotomy, (2) anterior capsulotomy, (3) subcaudate tractotomy, and (4) limbic leucotomy (combination of 1+3). Even though psychosurgery came under public attack and was nearly forbidden, a dilemma arises with recent disinterest and disengagement of the big pharma in developing novel medications for brain disorders.

Based on modern structural imaging with tractography, it is now clear that these four targeted regions functionally converge at the pgACC, extending into the OFC, and are connected *via* the forceps minor and the anterior thalamic radiations to subgenual cingulate regions. Anatomically, this convergence may derive from the superolateral branch of the MFB, a structure that connects these frontal areas to the origin of the mesolimbic dopaminergic "reward" system in the midbrain ventral tegmental area, which is a possible final common pathway.

From the initial work by Mayberg et al. (49) the subgenual anterior cingulate has been selected as a target for depression,

yet others have targeted the MFB. However, there seems to be a problem. Open-label studies for MDD are all positive including a meta-review of meta-analyses. Yet two controlled trials for MDD were both negative, one targeting BA25 and one targeting ventral capsule/striatum. This is in keeping with a larger problem that today, no target—whatever the disease—can meet the criteria for clinical efficacy as recently defined by an international committee for neurosurgery for psychiatric disorders. How can we overcome this problem? Should the neuromodulation community look for new targets, use novel stimulation designs, or a combination of the two?

Based on historical data from destructive psychosurgery, as well as modern functional and structural imaging, new targets for neuromodulation can be proposed: the dACC has been a target for the treatment of MDD with lesioning, TMS, and implants. Similarly, functional imaging suggests that also the left amygdala, right parahippocampal area, pgACC, caudate nucleus, insula, as well as the DLPFC and VLPFC could be potential targets for neuromodulation for MDD.

Another critical question is what is the ideal pattern of stimulation? DBS for movement disorders applies fairly standardized stimulation parameters, consisting of a frequency of 130 Hz, pulse widths <300 μs and variable amplitudes. Recently, burst stimulation has been developed, and this stimulation design applies the natural frequency of the targeted area, e.g., 6 Hz at the ACC, 20 Hz at the DLPFC, 4–8 Hz at the somatosensory and auditory cortex. Thus, effective outcomes can only be expected if both the target and stimulation design match. Interestingly, novel stimulation designs such as noise stimulation can be developed to prevent the brain of habituating to the stimulation. Noise can come in various forms, also called colors, from white to pink to brown and black, with an increasing steeper slope, following a $1/f^{\beta}$ with $\beta = 0, 1, 2, 3$ for white, pink, brown, and black, respectively. Considering that connectivity is both hypo- and hyper-, a combination of burst and noise may be essential to normalize dysconnectivity in MDD, with burst stimulation potentially increasing connectivity and noise stimulation desynchronizing activity, i.e., decreasing connectivity.

Yet still another form of neurostimulation can be developed, called reconditioning stimulation. The concept is that electrical stimulation is paired to external stimuli, as first proposed in a seminal paper in tinnitus. This concept can be adjusted to treating depression and has as advantage that the paired stimulation exerts a learning effect on the brain, instead of only suppressing hyperactivity or blocking hyperconnectivity, which is the mainstay of current neurostimulation approaches. The adaptation would be to pair external hedonic stimuli to rewarding stimuli delivered at different parts of the reward circuitry.

In summary, novel targets combined with novel stimulation designs pave the way for improved treatments for MDD and entirely novel approaches, such as reconditioning stimulation, might be yet another approach to treat this most debilitating of brain disorders.

Pathway-Specific Targeting for Subcallosal Cingulate Deep Brain Stimulation

DBS of the subcallosal cingulate white matter (SCC DBS) is an emerging strategy for treatment-resistant depression (56). Clinical trials show response rates at 6 months across studies range from 41 to 66% with sustained and increased response over time (40, 73). A challenge to effectively disseminate this nascent treatment remains in the fact that there is an absence of biomarkers to guide lead placement or to titrate stimulation parameters during follow-up care. Unlike PD, where intraoperative electrophysiology is routinely employed to define the anatomical–functional placement of the lead and titrate stimulus parameters to moderate symptoms in real time, such mechanistically guided biomarkers for depression are lacking. Furthermore, the SCC target is in the white matter, without demarcated anatomical boundaries. As such, individualized mapping of the target and its precise cortical connections is a critical first step to standardize the procedure.

Targeting the SCC white matter was based on converging imaging data demonstrating changes in SCC activity with antidepressant response to a variety of standard treatments (74, 75). Selection of this target was further supported by an extensive literature demonstrating monosynaptic connections between the subcallosal cingulate and specific frontal, limbic, subcortical, and brain stem sites involved in mood regulation, depression, and the antidepressant response (76, 77). Specific placement of the DBS electrodes was therefore determined by local anatomy. Approximate coordinates were derived from PET imaging studies localizing the subcallosal cingulate region (Brodmann area 25) and adjacent white matter and were then combined with anatomical landmarks identified in standard neurosurgical atlases. Tractography-guided connectomic approach to SCC electrode implantation has been found to improve the precision of surgical targeting following an initial feasibility study (49, 78).

In the latest developments by Choi et al. (79) refinement of surgical targeting has been aided by using tractography guidance. White matter pathways have now been mapped in responders and non-responders in the first study cohort to define the necessary and sufficient pathways that must be stimulated to achieve a full antidepressant effect (78). These maps utilize individualized models of the volume of tissue activated (VTA) derived from each patient's diffusion tractography scan (80). Successful prospective targeting in the most recent cases of 11 patients has resulted in successful mapping of responders group. These latest results confirm that prospective targeting of four key white matter bundles (cingulum, uncinate fasciculus, forceps minor, and frontal-striatal; **Figure 6**) can be performed reliably in individual patients, and use of this method improves long-term outcomes.

Perspectives of Deep Brain Stimulation for Memory Disorders

Memory deficits are a characteristic feature of numerous neuropsychiatric disorders, including various forms of dementias. To date, no effective treatment exists for memory deficits in dementia. Commonly used medications

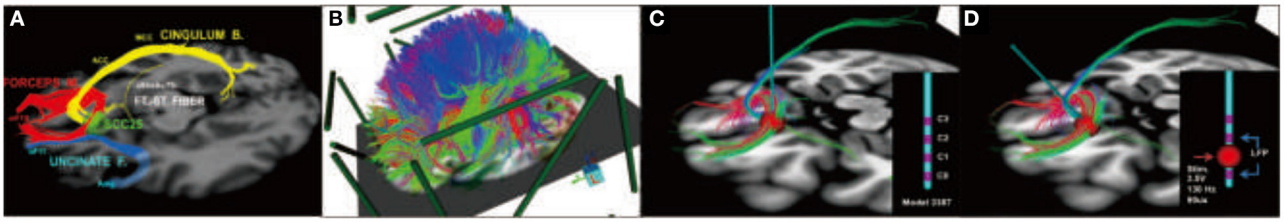

FIGURE 6 | Prospective targeting of these four white matter bundles can be performed reliably in individual patients, and use of this method improves long-term outcomes. **(A)** Four-bundle white matter "blueprint": cingulum (yellow), uncinate fasciculus (blue), forceps minor (red), frontal-striatal (white). **(B)** Whole-brain tractography loaded in patient-specific stereotactic frame space using StimVision. **(C)** Visualizing tracts passing through the volume of tissue activated (VTA) to define optimal target location that best visually matched the "blueprint." **(D)** Finalization of lead trajectory with the neurosurgeon to avoid cerebral vasculature and choosing the point of entry.

are acetylcholinesterase inhibitors, but the overall response is not very satisfactory (81). Neuromodulation strategies, including DBS, have been recently proposed for the treatment of these conditions.

The use of electrical stimulation for the study of memory problems is not new. In animal models, stimulation of various brain regions has been conducted in attempts to investigate physiological aspects in several learning and memory paradigms (82, 83). Early reports administering high current intensities to limbic structures in rodents undergoing memory tests reported stimulation-induced memory deterioration (82, 84). In contrast, stimulation regimens suited to induce plasticity (85, 86) were found to improve memory.

In humans, memory improvement has been reported in patients with epilepsy receiving entorhinal cortex (EC) (87) or anterior nucleus of thalamus (ANT) DBS (88). However, impairment has also been described particularly when stimulation was delivered acutely at relatively high currents (89). A patient with morbid obesity treated with DBS in the hypothalamic/forniceal region presented dejà vu sensations (90). In this same patient, stimulation was found to modulate the activity of the mesial temporal lobe and improve hippocampal memory function, as measured with neuropsychological testing (90).

A few years ago, a phase 1 clinical trial was conducted to test the safety of fornix DBS in six patients with AD (91). In addition to promising clinical findings, DBS was shown to modulate the activity of mesial temporal lobe structures and increase brain metabolism in temporal and parietal regions, as revealed by positron emission tomography (PET) scan (91). Following that study, a phase II trial of fornix DBS in mild AD (ADVANCE) was conducted (92). Forty-two patients were recruited in centers across the United States and Canada. It consisted of a 12-month double-blinded randomized controlled study comparing active and sham stimulation. When all patients were considered, no significant differences were observed in the Alzheimer's Disease Assessment Scale–Cognitive (ADASCog) 13 scores between groups (92). Interestingly, however, patients older than 65 receiving DBS seemed to have had a slower disease progression (though no significant differences were detected compared to sham-treated individuals of the same age group) (92). Another DBS target proposed for the treatment of AD is the nucleus basalis of Meynert, with preliminary studies showing promising results in different clinical types (93).

To explain potential mechanisms of stimulation, preclinical work has been conducted. In one of these studies, Gratwicke et al. (94, 95) stimulated the EC of AD transgenic animals. The authors found significant improvements in animals receiving DBS compared to sham treatment in the Morris water maze and novel object recognition tests. Remarkably, DBS reduced the number of Aβ plaques, as well as tau, phosphorylated tau, and amyloid precursor protein (APP) in the hippocampus of transgenic animals (94).

Taken together, the effects of stimulation on memory seem to vary as a function of the current intensity, target, and duration of treatment. Promising results have been reported in degenerative disorders, including AD. In animal models, DBS has been shown not only to improve memory function but also to have neuroprotective effects. Recent clinical trials in AD patients have shown promising enough results to warrant large-scale studies.

LATEST APPROACHES IN DEEP BRAIN STIMULATION FOR MOVEMENT DISORDERS

From Primate to Man: Pedunculopontine Nucleus Stimulation as a Therapy for Patients With Parkinsonian Disorders

FOG and falls are two of the most disabling symptoms of PD affecting upward of 10% of such patients (96). The introduction of L-DOPA in 1975 was so miraculous in reversing the cardinal signs of PD that it led to an initial discontinuation of functional neurosurgery, as it was felt that a single drug could be found to have similar beneficial effects with less potential side effects in movement disorders (97). However, it became apparent that with time, after 5 years, upward of 60% of patients would develop crippling medication-induced side effects such as dyskinesias. To move forward, a better understanding of the disease was needed. The problem was that, at that time, there was no animal model to better understand the disease pathology.

Serendipity came into play with the report in 1983 by Langston and Ballard (98) and Langston et al. (99) of a young

man admitted in a presumed catatonic state unresponsive to psychiatric therapies. However, when given L-DOPA, his symptoms were reversed. Subsequently, a series of these patients were reported to have been rendered parkinsonian by self-administration of a pethidine analog, methyl-phenyl-tetrahydropyridine (MPTP). After one patient overdosed on cocaine and died, the autopsy conducted showed the changes in the brain similar to those seen in PD, particularly loss of nigral dopaminergic neurons. In 1983, Burns et al. (100) administered MPTP to NHPs and produced an experimental model of PD, mimicking bradykinesia, forward flexed posture, and rigidity. These animals were also highly responsive to L-DOPA therapy.

Subsequent studies using the MPTP-lesioned NHP model of PD with electrophysiology and 2-deoxyglucose (2-DG) studies (101) led to a key pathophyisiological understanding of PD, in which loss of nigral dopamine leads to disinhibition of the STN, causing an excessive inhibitory drive from the medial pallidum to ascending and descending pathways to the thalamus and upper brain stem. Two pioneering studies confirmed that lesioning the STN, using either neurotoxin (102) or surgical radiofrequency electrodes (103), reversed experimental parkinsonism. Lesioning the STN was not considered an option for fear of inducing hemiballism; therefore, it was the finding that high-frequency stimulation of the STN in the NHP model that made it clinically applicable. Very soon after, STN HFS became to be the most accepted treatment for advanced PD.

With time, it became apparent that even with medication and STN-DBS, PD patients were not resistant to FOG and falls. Certain lines of evidence suggest that the upper brain stem might be relevant to understanding this. For example, in decerebrate rats, cats, and dogs, electrical or chemical stimulation in the mesencephalic motor region induces walking. The particular brain region, the pedunculopontine nucleus (PPN), was shown to degenerate in PD and other akinetic disorders such as multiple system atrophy (MSA) and progressive supranuclear palsy (PSP). In addition, 2-DG studies have indicated that MPTP-lesioned NHPs have excessive inhibition of the PPN.

A lesion or high-frequency stimulation of the PPN in healthy NHPs induces akinesia (104). Once rendered parkinsonian with MPTP administration, microinjections of bicuculline [gamma aminobutyric acid (GABA) antagonist] directly into the PPN reverses akinesia and imbalance, as does low-frequency PPN stimulation (105). The finding that PPN stimulation alleviated movement abnormalities in the MPTP-lesioned NHP was translated rapidly to treat PD patients by clinical groups in the UK (Bristol) and Italy (Rome), with low-frequency stimulation (around 20–30 Hz) being employed (106, 107). These early clinical studies noted an effect of PPN stimulation that mimicked those found in the NHPs, which was an improvement in akinesia, in addition to gait and posture. This was later followed by a clinical study of six PD patients with dual STN and PPN stimulation (108). Results suggested modest improvements in akinesia and more marked beneficial effects in FOG and postural instability, with the suggestion of STN and PPN DBS being complementary. However, a major issue arose regarding the target that appeared to lie in the neighboring peri-peduncular nucleus. This has since prompted a debate on the exact location of the PPN, and this remains a controversial issue (109–112).

Two further clinical series have reported PPN stimulation in two differing scenarios (1) dual bilateral STN and PPN stimulation and (2) single-target unilateral PPN stimulation (113, 114). These studies have reported very modest therapeutic effects of PPN stimulation, largely limited to FOG and postural instability. One study found very limited effects even on FOG and questioned the clinical utility of this treatment (113). However, several aspects in the clinical application of PPN stimulation in these studies could have affected therapeutic efficacy. Indeed, some patients were selected for PPN stimulation with severe motor fluctuations requiring STN stimulation and variable degrees of gait disturbance (108, 113). For example, PD patients were selected for PPN stimulation to treat FOG that developed during STN stimulation. Other patients had been selected for PPN stimulation who had not experienced FOG that persisted "on medication" or having recurrent falls (113, 114). It remains possible that co-stimulation of the STN could influence the efficacy of PPN stimulation due to the substantial reciprocal connections between the two targets (115). In this regard, it should be noted that high-frequency stimulation required for STN stimulation (i.e., 130 Hz) appears to worsen gait when delivered to the PPN. It has been found that the PPN was targeted above the pontomesencephalic junction with choline-acetyltransferase 5 (ChAT5) staining studies in humans, suggesting that lead placement could have missed the caudal extent of the nucleus, which is most degenerate in PD (116–118). Moreover, a clinical study by Thevathasan et al. (119) demonstrated that bilateral PPN stimulation provides a greater therapeutic effect over unilateral stimulation.

It is apparent that there are some questions remaining regarding the effect of PPN stimulation in parkinsonian FOG and falls, i.e., the exact target and the best patient candidates are still debated. It is noteworthy that the outcomes measured with UPDRS may lack sensitivity for gait and posture. Indeed, the precise effects of PPN stimulation on motor function in PD including gait are not established (120). However, in recent years, it has been reported in a meta-analysis of several well-documented PPN stimulation studies that patients ON or OFF medication are better with PPN stimulation (121).

Novel Neuromodulation Applications for Gait Disorders in Parkinson's Disease

Postural instability and gait disorders (PIGDs) are debilitating phenomena that frequently impair locomotion and can significantly affect quality of life in PD patients (122). Prevalence of PIGD tends to follow the severity of disease; it is the most common cause of falls, which are associated with an increase in morbidity and mortality in PD (122). Besides the effects of STN and GPi DBS on PIGD responsive to levodopa, PPN DBS was the first neuromodulatory technique directly applied for the treatment of PIGD, with success recorded in many reports (123). In addition, there have been some reports on dual stimulation STN/SNr and VFS of STN as possible neuromodulatory methods for PIGD (124, 125).

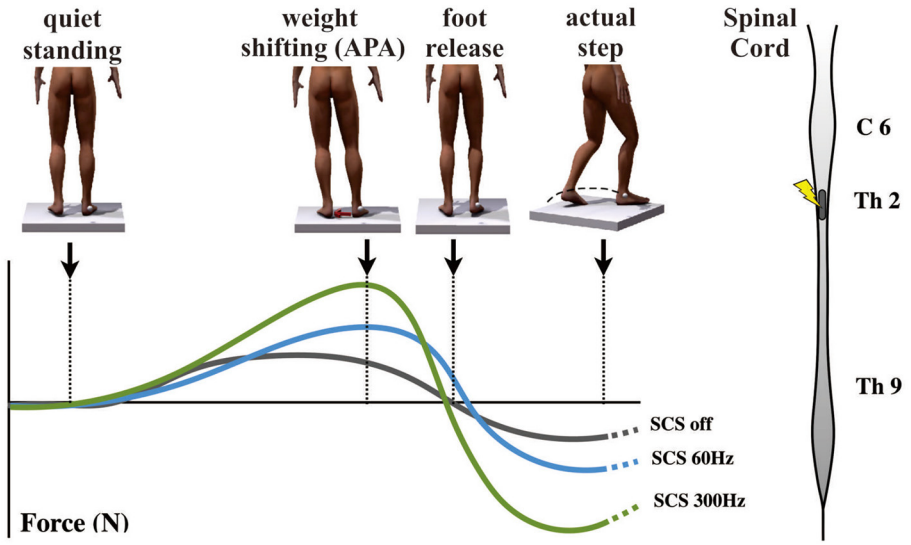

FIGURE 7 | Effects of spinal cord stimulation on postural control in Parkinson's disease patients with freezing of gait (132). On the top left, the figures show the representation of the step initiation task from quiet standing to the actual step, showing the marker on the right malleolus to detect the moment that the foot clears the floor. The graph below shows body weight shifting toward the supporting leg [anticipatory postural adjustment (APA)] during the three different conditions [gray curve, spinal cord stimulation (SCS) OFF; blue curve, 60 Hz-CS; green curve, 300 Hz-SCS]. On the right is a representation of the spinal cord showing the site of stimulation (T2) used in the same report.

Since the first experimental report from Fuentes et al. (126) showing that spinal cord stimulation (SCS) could enhance locomotion in murine PD models, and more recently in NHPs (127), SCS has been considered as a possible treatment for FOG in PD. Increasing evidence suggests that SCS improves treatment-resistant PIGD in PD patients (128). Recently, Pinto de Souza et al. (129) have reported positive effects of high-frequency SCS (300 Hz) on gait, improving the performance in various gait tests, which were reproduced during double-blinded assessments. It was also seen that continuous SCS chronically reduced FOG episodes, improved UPDRS-III motor scale scores, and self-reported quality of life (129). These results are in line with previous clinical observations and findings recorded in parkinsonian animal models (126, 127). More recently, Samotus et al. (130) also showed positive effects of SCS for gait dysfunction in PD patients. In comparison to early reports, the selection of PD patients with locomotor problems were more precise (130), in which motor symptoms, gait performance, and FOG were closely followed with adequate evaluations.

Despite that positive results have been reported, the mechanisms by which SCS may improve FOG are still elusive. Considering that the exact mechanism of FOG itself is also not completely understood, the study of SCS might converge with the study of FOG. Normal gait requires an exact coordination of postural adjustment in advance of each step forward, namely, anticipatory postural adjustment (APA). During imminent FOG episodes, the intention to walk is uncoupled from the triggering of APA, with consequent failure of the forward movement. This often results in knee trembling and failure to initiate gait. In PD, FOG episodes are associated with deficient APA. Physiological evidence, functional imaging, and clinicopathologic studies suggest that FOG is mainly associated with disorders of frontal cortical regions [e.g., supplementary motor area (SMA)] that

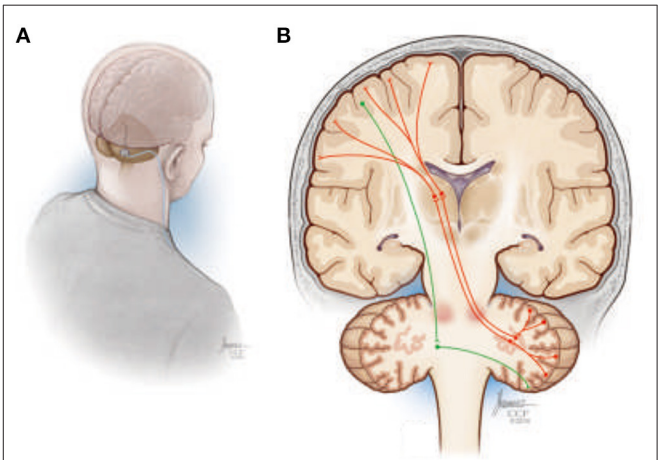

FIGURE 8 | (A) Illustration depicting a suboccipital approach to delivering deep brain stimulation therapy to the cerebellar dentate nucleus. **(B)** Simplified overview of the human dentatothalamocortical (DTC) and corticopontocerebellar (CPC) pathways. The DTC (red) projects through the ipsilateral superior cerebellar peduncle, decussating at the level of the pons, to terminate in contralateral thalamus, where its activity influences widespread thalamocortical interactions. The CPC is shown in green descending from the cortex, decussating in the ipsilateral pons, and terminating in the contralateral cerebellar hemisphere.

comprise a known brain circuitry dedicated to APA control (131). In NHPs, SCS increases neuronal firing of the primary motor cortex and decreases pathological cortico-striatal synchronous low-frequency waves showing that SCS does influence the oscillatory activity in multiple structures of brain motor circuits (127). In fact, SCS may disrupt the aberrant inhibition from the GPi to the thalamus and SMA. As part of the circuit that controls APA, the SMA has corticofugal projections to the PPN, a region particularly involved in gait initiation (as described above). Since the activity of SMA, globus pallidus, and PPN is abnormal in PD patients with FOG, SCS could potentially modulate this circuit and improve APA and gait initiation.

Recent work by de Lima-Pardini et al. (132) has recently reported that SCS at 300 Hz effectively reduces the time of FOG with simultaneous correction of altered APA, which is reported in PD patients with FOG (**Figure 7**). These results corroborated with initial clinical data demonstrating significant progress toward revealing mechanisms by which SCS may improve FOG. It is possible that by stimulating ascending spinal pathways, SCS may correct pathological oscillatory activity in the circuits that mediate FOG, subsequently inhibiting episodes of FOG in PD patients. Conversely, SCS has failed to improve reactive posture control. It is possible that SCS may have different effects on the two mechanisms of postural control that are known to be reactive and anticipatory. While APA mechanisms are thought to be dependent on thalamo-cortical-striatal loops highly influenced by attentional and environmental changes, reactive posture control to external and unpredictable triggers relies on neuronal circuitries involving the brain stem and spinal cord with less influence from the cortex.

Despite various reports on the positive effects of SCS on FOG, there is still skepticism regarding this treatment since some PD symptoms can improve remarkably with placebo or during startle responses upon threats. In order to differentiate the effect of SCS from placebo, Pinto de Souza et al. (129) performed a double-blind study comparing the effects of stimulation at 300 and 60 Hz, once both frequencies elicited indistinguishable paresthesia. It was found that only the stimulation at 300 Hz improved gait performance and reduced episodes of FOG, while the effects of the lower frequency were similar to no stimulation.

In summary, there is increasing evidence for SCS-induced improvements in gait disturbances for PD, especially FOG. However, evidence from comparative studies with larger patient populations and data from prospective placebo-controlled trials is still lacking. The exact mechanisms and circuits mediating the expression of FOG are still uncertain. In addition, the optimal level for spinal stimulation, specific structures (segmental short circuits or ascending tracts) for effects of SCS, the most effective electrode geometry and specific parameters of stimulation remain undefined (133). Besides its potential therapeutic use, the development of SCS for the treatment of PD symptoms may also contribute to a better understanding of locomotor behaviors and complex pathophysiology of neurological disturbances, specifically FOG (134).

Deep Brain Stimulation to Enhance Chronic Post-stroke Rehabilitation

Ischemic stroke is a major cause of long-term disability in the industrialized world, with chronic debilitating motor impairments significantly impacting quality of life for more than one third of stroke survivors. Current standard-of-care treatment for those left with motor sequelae is largely limited to subacute physical therapy. However, long-term disabling deficits for most patients persist despite best efforts. As a result, there is substantial interest in identifying new ways to enhance post-stroke recovery and rehabilitation, including invasive and non-invasive neurostimulation-based approaches. Progress has been limited to date, however, with most clinical studies yielding limited or variable efficacy in improving motor function using current approaches.

Machado and Baker (135) have previously proposed that chronic stimulation of cerebellar dentate nucleus (DN; **Figure 8A**) should, through activation of the net excitatory glutamatergic dentatothalamocortical pathway, upregulate thalamocortical activity and cerebral cortical excitability across prefrontal, frontal, and parietal cortical regions (**Figure 8B**), establishing a basal environment more compatible with functional neuroplastic reorganization. The work over the past decade, using preclinical models of middle cerebral artery ischemia, that stimulation of the lateral cerebellar nucleus (the rodent homolog of the human DN) does indeed facilitate motor recovery when paired with rehabilitation, with the magnitude of the effect sensitive to stimulation frequency (136, 137). Moreover, the electrophysiological and histological data implicate frequency-specific changes in cortical excitability and enhanced functional reorganization of surviving perilesional cortex as potential therapeutic mechanisms, with improvements in motor function accompanied by increased expression of markers of synaptic plasticity, synaptogenesis, and neurogenesis in the perilesional cortex (138, 139).

Based upon the preclinical work, a first-in-human trial (NCT02835443) to translate DN-DBS as a treatment for upper extremity hemiparesis in chronic post-stroke patients commenced in 2016. With additional support from the National Institutes of Health Brain Initiative, the trial will extend beyond establishing the safety, feasibility, and efficacy of the approach to directly examine the acute and chronic effects of DN-DBS on cerebral cortical excitability and motor representation using TMS-based techniques as well as the topography of motor-related LFP activity in the DN region. All these data are further being incorporated into MRI-based patient-specific anatomical models of the deep cerebellar region to facilitate next-generation lead design and targeting techniques, while using the LFP data to develop physiological classifiers to inform future treatment paradigms, including possible closed-loop approaches. Finally, ongoing preclinical studies are focusing on therapy refinement and optimization, including a potential role for a more physiologic-based, closed-loop stimulation system that more directly stimulates delivery with motor activity.

Current Clinical Deep Brain Stimulation Approaches for Dystonia

DBS of the GPi is an effective treatment for medical refractory dystonia and reduces not only motor impairment but also other disabilities (140–144). Within the last two decades, DBS has progressively evolved into a widely available therapeutic strategy for generalized and segmental dystonia. More recently, it was also successfully applied in patients with cervical dystonia or cases that were resistant to botulinum toxin treatment (145). Long-term effects and side effects of this potentially lifelong therapy are of special interest. More recent retrospective reports of DBS for dystonia includes follow-up periods of 5–7 years (146–149) with sometimes even longer observation periods in individual cases, i.e., 6–10 years (148) and overall good clinical outcome of 50–80% mean improvement of dystonia. However, individual factors that remain reliable for predicting DBS outcome in dystonia are still difficult to define. Several factors such as gene mutation status, age at surgery, disease duration, presence of musculoskeletal deformities, predominance of phasic vs. tonic movements, the size of the globus pallidus, and optimal stimulation parameters are widely discussed to have a possible influence on stimulation effects (148–152). Brüggemann et al. (150) now report that patients genetically confirmed with DYT1 and DYT6 dystonia have significant and enduring effects of pallidal stimulation. Furthermore, Isaias et al. (149) and Lumsden et al. (151) report cases with disease duration being an important factor, e.g., with respect to developing fixed musculoskeletal deformities, also highlighting the importance to differentiate between isolated dystonia and patients with combined/complex dystonia because the latter shows a significantly reduced benefit of pallidal DBS.

While the clinical benefit of DBS in cervical and other focal dystonias is well-documented, the underlying therapeutic mechanism remains to be elucidated. Converging evidence points to a modulation of aberrant neural population activity in the basal ganglia through high-frequency stimulation (9, 153, 154). In recent years, DBS has enabled the unique opportunity to record oscillatory activity as LFPs directly from the basal ganglia during surgery and in a postoperative interval, with the DBS electrodes externalized. Here, oscillatory patterns of pallidal LFPs were found to differ in a disease-specific manner (155, 156). The best characterized pathological oscillatory phenomenon has been described in patients with PD, where STN β oscillatory activity (13–30 Hz) at rest is suppressed by dopaminergic medication and is directly correlated with patient symptom severity (9). In dystonia, low-frequency activity in the θ-α range (4–12 Hz; subsequently referred to as θ, as most peaks in dystonia are in the 4–10-Hz range) is predominant in the GPi and correlates with symptom severity (157). Indeed, θ activity in dystonia patients with phasic movements has been shown to be suppressed by high-frequency DBS (154). Thus, pallidal θ activity has been proposed as a potential pathophysiological hallmark of dystonia. It can be envisioned that adaptive closed-loop DBS using pallidal θ activity as a biomarker could be efficiently used for controlling dystonic motor symptoms in patients.

Automatic Classification of Pallidal Borders During Awake and Asleep Deep Brain Stimulation Procedures for Dystonia

DBS of the GPi in patients with dystonia can reduce motor symptoms and improve their quality of life (158–160). With the current limits of today's brain imaging techniques in resolution, distortion, and possible brain shift (161), together with the broad distribution of DBS centers (>1,000 worldwide with many non-academic centers), the outcome of many DBS procedures might be less optimal because of mis-localization of the DBS leads (13, 162). To enable better localization of the DBS target, pallidal borders can be visibly and audibly detected by electrophysiological microelectrode recordings (MERs) during DBS procedures. Even given ideal conditions, the detection of the striato-pallidal borders is never an easy task even for an expert electrophysiologist.

Previously, it has reported a real-time automated procedure (163, 164) for the detection of the borders and subdomains of the STN using hidden Markov models (HMMs) in PD patients (165). Venkatraghavan et al. also reported an algorithm for detection of the striato-pallidal borders, with a dataset including 116 GPi trajectories from 42 patients consisting of 11,774 MERs in five classes of disease (awake PD patients, awake and lightly anesthetized genetic and non-genetic dystonia patients (166), with the current work now under review for publication; *Journal of Neuro-engineering*). Using the L_1-distance measure in root mean square (RMS) and power spectral densities of the MER, Bergman et al. has found that awake and light anesthesia (with sevoflurane and N_2O, minimum alveolar concentration (MAC) = 0.3–0.6) dystonia classes with and without anesthesia can be merged. Therefore, depth (MAC) of anesthesia was reduced 10–15 min before the beginning of the MER and restored deep surgical anesthesia after the end of the MER exploration in each hemisphere. It was found that significant differences exist between the RMS and spectral features of the striato-pallidal trajectory. Bergman et al. reported training on the HMM on trajectories with striato-pallidal labels as inputs in three different disease classes (PD, genetic and non-genetic dystonia) using the decision of an expert electrophysiologist as gold standard labels. Then, the performance of the HMM algorithm was tested with a leave-one-out cross-validation. The HMM was found to achieve performance on par with an expert electrophysiologist across the striatum-GPe, GPe-GPi, and GPi-exit transitions in the three disease classes (167).

In conclusion, as for STN DBS, GPi automated navigation systems can potentially shorten the length of electrophysiological mapping to <15 min per hemisphere, while implanting the DBS lead within the optimal location. A reduced procedure time and improved targeting would be expected to lead to better clinical outcomes in GPi DBS therapy for dystonia.

Long-Term Awake Multi-Electrode Monitoring in Children With Acquired Combined Dystonia

Acquired combined dystonia remains a difficult disorder to treat partly because of the variability of causes and symptoms. Dystonia has multiple potential anatomic origins, including basal ganglia, cerebellum, thalamus, and prefrontal cortex. Despite these origins, the specific postures generated are often remarkably similar, and a review of 3 years of clinic videos shows that almost all children have at least one of seven stereotypical postures, no matter what their underlying etiology (168). This has led to the conjecture that these postures are due to similar somatotopy within the motor cortex, so that any brain region capable of stimulating contiguous regions of motor cortex will cause a similar posture. This finding is reminiscent of the very limited sets of postures seen with long-train electrical stimulation of the motor cortex (169). If unfocused stimulation of motor cortex is the final common pathway, then dystonia is a very non-specific symptom, and successful treatment using DBS will require uncovering the anatomic origin of the disorder in each child.

In order to do this, Sanger et al. (170) have developed a new procedure that includes test stimulation and recording from multiple externalized electrodes while children are admitted to a neuromodulation monitoring unit (NMU). Up to 10 electrodes (**Figure 9**), each with 16 contacts, are implanted in multiple regions of the basal ganglia and thalamus, targeting the most likely pathways for uncontrolled cortical stimulation. Test stimulation can be used to determine efficacy and any side effects of stimulation of each region. This is particularly helpful in the thalamus, for which the effects of stimulation are usually immediate. In the pallidum, effects of stimulation may require weeks or months to determine; therefore, test stimulation is primarily used to find regions that are free of adverse effects that might limit flexibility of stimulation.

Recording yields single-unit activity that can be correlated against surface electromyography (EMG) to determine regions that are more or less likely to be carrying dystonic signals. In particular, a region that does not change activity during dystonic contractions is unlikely to be a mediator of dystonia and unlikely to be a candidate target for DBS. Sanger et al. (170) have recorded so far from 20 children with acquired combined dystonia. Contrary to data from adults, in NHPs and children with primary dystonia, the group have found that baseline activity in the pallidum is low and increases with dystonic muscle contractions. In fact, all regions activate with dystonic spasms, including pallidum and multiple thalamic subnuclei (VIM, VPL, Vo, and VA). Although the pallidum inhibits the thalamus, activity in the pallidum is positively correlated with activity in the thalamus in all children. This suggests a loss of the normal inhibition and loss of specificity of activity within these regions. Overflow to contralateral muscles is evident within cerebellar projection pathways, and dystonic activity is always much higher and less focused than voluntary activity. Taken together, the results reported here suggest a generalized lack of specificity and both reversal of normal activity and hyperexcitability throughout the basal ganglia/thalamus circuit. Since the output of this circuit projects to motor cortex, these findings are consistent with the hypothesis of non-specific cortical drive as the mediator of dystonic postures.

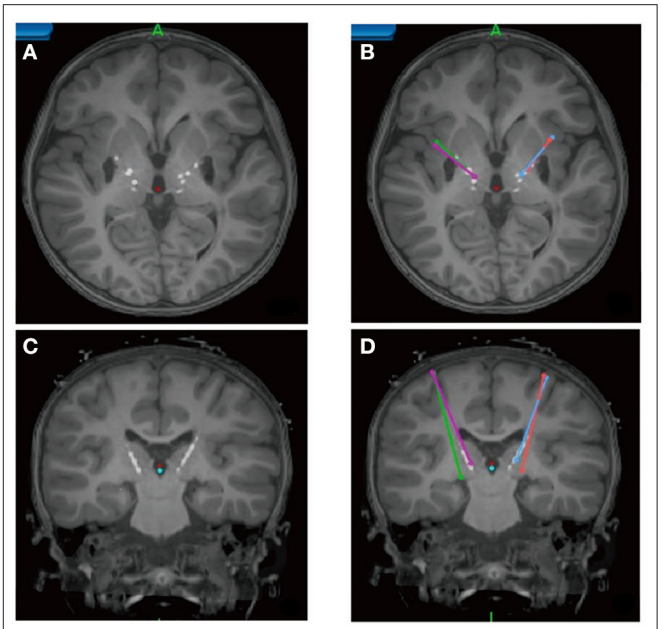

FIGURE 9 | Pediatric Deep Brain Stimulation Using Awake Recording and Stimulation for Target Selection in an Inpatient Neuromodulation Monitoring Unit (170). Axial **(A,B)** and coronal **(C,D)** MRI showing the position of temporary leads within the basal ganglia and thalamus. Stereotactic planning trajectories are shown in **(B,D)**.

Use of the NMU procedure by Sanger et al. (170) has allowed for finding more precise patient-specific targets for children. The group always implants four leads: usually two within the GPi and two within the optimal region of the thalamus for each child. Subsequent programming suggests that GPi DBS is the most effective for hypertonic components of dystonia, whereas thalamic DBS is the most effective for the hyperkinetic components of dystonia. Preliminary analysis of outcomes data shows significantly improved outcomes using the new procedure and four-lead DBS. This is a promising new procedure that will yield both improved outcomes for children with acquired combined dystonia, as well as detailed knowledge on the physiological mechanisms underlying this disabling condition.

CONCLUSIONS

This report summarizes the information presented in the first DBS initiative meeting held at the NELN of Tsinghua University. The collective group addressed foreseeable challenges in DBS therapy and recent clinical approaches with technological advancements. In-depth discussions were held on the connectome approach in DBS, novel developments in 3T MRI-compatible DBS devices and neural recording technologies for understanding disease pathophysiology, and pursuing new

clinical approaches and indications using such advancements. This meeting marks a unique milestone in developing global DBS research using state-of-the-art technologies for rapid clinical translation.

AUTHOR CONTRIBUTIONS

All authors listed have made a substantial, direct and intellectual contribution to the work, and approved it for publication.

REFERENCES

1. Kalin R, Stanton MS. Current clinical issues for MRI scanning of pacemaker and defibrillator patients. *Pacing Clin Electrophysiol.* (2005) 28:326–8 doi: 10.1111/j.1540-8159.2005.50024.x
2. Falowski S, Safriel Y, Ryan MP, Hargens L. The rate of magnetic resonance imaging in patients with deep brain stimulation. *Stereotact Funct Neurosurg.* (2016) 94:147–53. doi: 10.1159/000444760
3. Henderson JM, Tkach J, Phillips M, Baker K, Shellock FG, Rezai AR. Permanent neurological deficit related to magnetic resonance imaging in a patient with implanted deep brain stimulation electrodes for Parkinson's disease: case report. *Neurosurgery.* (2005) 57:E1063. doi: 10.1227/01.NEU.0000180810.16964.3E
4. Horn A, Wenzel G, Irmen F, Huebl J, Li N, Neumann WJ, et al. Deep brain stimulation induced normalization of the human functional connectome in Parkinson's disease. *Brain J Neurol.* (2019) 18:130–15. doi: 10.1093/brain/awz239
5. IEC 60601-2-33:2010+AMD1:2013+AMD2:2015 CSV: Medical electrical equipment - Part 2-33: Particular requirements for the basic safety and essential performance of magnetic resonanceequipment for medical diagnosis.
6. Shen L, Jiang C, Hubbard CS, Ren J, He C, Wang D, et al. Subthalamic nucleus deep brain stimulation modulates 2 distinct neurocircuits. *Ann Neurol.* (2020) 88:1178–93. doi: 10.1002/ana.25906
7. Brown P. Oscillatory nature of human basal ganglia activity: relationship to thepathophysiology of Parkinson's disease. *Mov Disord.* (2003) 18:357–63. doi: 10.1002/mds.10358
8. Eusebio A, Cagnan H, Brown P. Does suppression of oscillatory synchronisation medi-ate some of the therapeutic effects of DBS in patients with Parkinson's disease? *Front Integr Neurosci.* (2012) 6:47. doi: 10.3389/fnint.2012.00047
9. Kühn AA, Kupsch A, Schneider GH, Brown P. Reduction in subthalamic 8-35 Hz oscillatory activity correlates with clinical improvement in Parkinson's disease. *Eur J Neurosci.* (2006) 23:1956–60. doi: 10.1111/j.1460-9568.2006.04717.x
10. Neumann WJ, Jha A, Bock A, Huebl J, Horn A, Schneider GH, et al. Cortico-pallidal oscillatory connectivity in patients with dystonia. *Brain.* (2015) 138:1894–906. doi: 10.1093/brain/awv109
11. Chen Y, Gong C, Hao H, Guo Y, Xu S, Zhang Y, et al. Automatic sleep stage classification based on subthalamic local field potentials. *IEEE Trans Neural Syst Rehabil Eng.* (2019) 27:118–28. doi: 10.1109/TNSRE.2018.2890272
12. Farris S, Giroux M. Retrospective review of factors leading to dissatisfaction with subthalamic nucleus deep brain stimulation during long-term management. *Surg Neurol Int.* (2013) 4:69. doi: 10.4103/2152-7806.112612
13. Okun MS, Tagliati M, Pourfar M, Fernandez HH, Rodriguez RL, Alterman RL, Foote KD Management of referred deep brain stimulation failures: a retrospective analysis from 2 movement disorders centers. *Arch Neurol.* (2005) 62:1250–5. doi: 10.1001/archneur.62.8.noc40425
14. Chen Y, Hao H, Chen H, Tian Y, Li L. The study on a real-time remote monitoring system for Parkinson's disease patients with deep brain stimulators. *Annu Int Conf IEEE Eng Med Biol Soc.* (2014) 2014:1358–61. doi: 10.1109/EMBC.2014.6943851
15. Fasano A, Aquino CC, Krauss JK, Honey CR, Bloem BR. Axial disability and deep brain stimulation in patients with Parkinson disease. *Nat Rev Neurol.* (2015) 11:98–110. doi: 10.1038/nrneurol.2014.252
16. Fasano A, Romito LM, Daniele A, Piano C, Zinno M, Bentivoglio AR, et al. Motor and cognitive outcome in patients with Parkinson's disease 8 years after subthalamic implants. *Brain.* (2010) 133:2664–76. doi: 10.1093/brain/awq221
17. Fagundes VC, Rieder CR, da Cruz AN, Beber BC, Portuguez MW. Deep brain stimulation frequency of the subthalamic nucleus affects phonemic and action fluency in Parkinson's disease. *Parkinsons Dis.* (2016) 2016:6760243. doi: 10.1155/2016/6760243
18. Jia F, Hu W, Zhang J, Wagle Shukla A, Almeida L, Meng FG, et al. Variable frequency stimulation of subthalamic nucleus in Parkinson's disease: rationale and hypothesis. *Parkinsonism Relat Disord.* (2017) 39:27–30. doi: 10.1016/j.parkreldis.2017.03.015
19. Sui Y, Yue Y, Burdick JW. Correlational dueling bandits with application to clinical treatment in large decision spaces. In: Sierra C, editor. *Proceedings of the Twenty-Sixth International Joint Conference on Artificial Intelligence*. AAAI Press (2017). doi: 10.24963/ijcai.2017/389
20. Sui Y, Zhuang V, Burdick JW, Yue Y. Stagewise safe Bayesian optimization with Gaussian processes. In: *Thirtyb-fifth International Conference on Machine Learning*. (2018).
21. Wagner FB, Mignardot JB, Le Goff-Mignardot CG, Demesmaeker R, Komi S, Capogrosso M, et al. Targeted neurotechnology restores walking in humans with spinal cord injury. *Nature*. (2018) 563:65–71. doi: 10.1038/s41586-018-0649-2
22. Accolla EA, Herrojo Ruiz M, Horn A, Schneider, G.-H., Schmitz-Hubsch T, Draganski B, Kühn AA. Brain networks modulated by subthalamic nucleus deep brain stimulation. *Brain.* (2016) 139:2503–15. doi: 10.1093/brain/aww182
23. Horn A, Kühn AA, Merkl A, Shih L, Alterman R, Fox M. Probabilistic conversion of neurosurgical DBS electrode coordinates into MNI space. *NeuroImage*. (2017) 150:395–404. doi: 10.1016/j.neuroimage.2017.02.004
24. Horn A, Li N, Dembek TA, Kappel A, Boulay C, Ewert S, et al. Lead-DBS v2: Towards a comprehensive pipeline for deep brain stimulation imaging. *Neuroimage.* (2019) 184:293–316. doi: 10.1016/j.neuroimage.2018.08.068
25. Horn A, Reich M, Vorwerk J, Li N, Wenzel G, Fang Q, et al. Connectivity Predicts deep brain stimulation outcome in Parkinson disease. *Ann Neurol.* (2017) 82:67–78. doi: 10.1002/ana.24974
26. Joutsa J, Horn A, Hsu J, Fox MD. Localizing parkinsonism based on focal brain lesions. *Brain*. (2018) 141:2445–56. doi: 10.1093/brain/awy161
27. Lozano AM, Lipsman N. Probing and regulating dysfunctional circuits using deep brain stimulation. *Neuron*. (2013) 77:406–24. doi: 10.1016/j.neuron.2013.01.020
28. Sporns O, Tononi G, Kötter R. The human connectome: a structural description of the human brain. *PLoS Comp Biol.* (2005) 1:e42. doi: 10.1371/journal.pcbi.0010042
29. Fernandes HM, van Hartevelt TJ, Boccard SGJ, Owen SLF, Cabral J, Deco G, et al. Novel fingerprinting method characterises the necessary sufficient structural connectivity from deep brain stimulation electrodes for a successful outcome. *New J Phys.* (2015) 17:015001–15. doi: 10.1088/1367-2630/17/1/015001
30. van Hartevelt TJ, Cabral J, Deco G, Møller A, Green AL, Aziz TZ, Kringelbach ML. Neural plasticity in human brain connectivity: the effects of long term deep brain stimulation of the subthalamic nucleus in Parkinson's disease. *PLoS ONE*. (2014) 9:e86496. doi: 10.1371/journal.pone.0086496
31. Vanegas Arroyave N, Lauro PM, Huang L, Hallett M, Horovitz SG, Zaghloul KA, Lungu C. Tractography patterns of subthalamic nucleus deep brain stimulation. *Brain*. (2016) 139:1200–10. doi: 10.1093/brain/aww020
32. Ewert S, Plettig P, Li N, Chakravarty MM, Collins DL, Herrington TM, et al. Toward defining deep brain stimulation targets in MNI space: a subcortical atlas based on multimodal MRI, histology and structural connectivity. *NeuroImage*. (2018) 170:271–82. doi: 10.1016/j.neuroimage.2017.05.015
33. Horn A, Blankenburg F. Toward a standardized structural-functional group connectome in MNI space. *NeuroImage*. (2016) 124:310–22. doi: 10.1016/j.neuroimage.2015.08.048

34. Horn A, Ostwald D, Reisert M, Blankenburg F. The structural-functional connectome and the default mode network of the human brain. *NeuroImage*. (2014) 102:142–51. doi: 10.1016/j.neuroimage.2013.09.069
35. Darby RR, Horn A, Cushman F, Fox MD. Lesion network localization of criminal behavior. *Proc Natl Acad Sci USA*. (2017) 56:201706587–6. doi: 10.1073/pnas.1706587115
36. Weigand A, Horn A, Caballero R, Cooke D, Stern AP, Taylor SF, et al. Prospective validation that subgenual connectivity predicts antidepressant efficacy of transcranial magnetic stimulation sites. *Biol Psychiatry*. (2018) 84:28–37. doi: 10.1016/j.biopsych.2017.10.028
37. Al-Fatly B, Ewert S, Kübler D, Kroneberg D, Horn A, Kühn AA. Connectivity profile of thalamic deep brain stimulation to effectively treat essential tremor. *Brain J Neurol*. (2019) 18:130. doi: 10.1093/brain/awz236
38. Baldermann JC, Melzer C, Zapf A, Kohl S, Timmermann L, Tittgemeyer M, et al. Connectivity profile predictive of effective deep brain stimulation in obsessive-compulsive disorder. *Biol Psychiatry*. (2019) 85:735–43. doi: 10.1016/j.biopsych.2018.12.019
39. Ashkan K, Rogers P, Bergman H, Ughratdar I. Insights into the mechanisms of deep brain stimulation. *Nat Rev Neurol*. (2017) 13:548–54 doi: 10.1038/nrneurol.2017.105
40. Holtzheimer PE, Husain MM, Lisanby SH, Taylor SF, Whitworth LA, McClintock S, et al. Subcallosal cingulate deep brain stimulation for treatment-resistant depression: a multisite, randomised, sham-controlled trial. *Lancet Psychiatry*. (2017) 4:839–49. doi: 10.1016/S2215-0366(17)30371-1
41. Amunts K, Kedo O, Kindler M, Pieperhoff P, Mohlberg H, Shah NJ, et al. Cytoarchitectonic mapping of the human amygdala, hippocampal region and entorhinal cortex: intersubject variability and probability maps. *Anat Embryol (Berl)*. (2005) 210:343–52. doi: 10.1007/s00429-005-0025-5
42. Amunts K, Schleicher A, Bürgel U, Mohlberg H, Uylings HB, Zilles K. Broca's region revisited: cytoarchitecture and intersubject variability. *J Comparative Neurol*. (1999) 412:319–41. doi: 10.1002/(SICI)1096-9861(19990920)412:2<319::AID-CNE10>3.0.CO;2-7
43. Hill J, Dierker D, Neil J, Inder T, Knutsen A, Harwell J, et al. A surface-based analysis of hemispheric asymmetries and folding of cerebral cortex in term-born human infants. *J Neurosci*. (2010) 30:2268–76. doi: 10.1523/JNEUROSCI.4682-09.2010
44. Mueller S, Wang D, Fox MD, Yeo BT, Sepulcre J, Sabuncu MR, et al. Individual variability in functional connectivity architecture of the human brain. *Neuron*. (2013) 77:586–95. doi: 10.1016/j.neuron.2012.12.028
45. Wang D, Liu H. Functional connectivity architecture of the human brain: not all the same. *Neuroscientist*. (2014) 20:432–8. doi: 10.1177/1073858414543290
46. Buckner RL, Krienen FM. The evolution of distributed association networks in the human brain. *Trends Cognitive Sci*. (2013) 17:648–65. doi: 10.1016/j.tics.2013.09.017
47. Neumann WJ, Staub-Bartelt F, Horn A, Schanda J, Schneider GH, Brown P, et al. Long term correlation of subthalamic beta band activity with motor impairment in patients with Parkinson's disease. *Clin Neurophysiol*. (2017) 128:2286–91. doi: 10.1016/j.clinph.2017.08.028
48. Waters AC, Veerakumar A, Choi KS, Howell B, Tiruvadi V, Bijanki KR, et al. Test-retest reliability of a stimulation-locked evoked response to deep brain stimulation in subcallosal cingulate for treatment resistant depression. *Hum Brain Mapp*. (2018) 39:4844–56. doi: 10.1002/hbm.24327
49. Riva-Posse P, Choi KS, Holtzheimer PE, Crowell AL, Garlow SJ, Rajendra JK, et al. A connectomic approach for subcallosal cingulate deep brain stimulation surgery: prospective targeting in treatment-resistant depression. *Mol Psychiatry*. (2018) 23:843–9. doi: 10.1038/mp.2017.59
50. Fox MD, Qian T, Madsen JR, Wang D, Li M, Ge M, et al. Combining task-evoked and spontaneous activity to improve pre-operative brain mapping with fMRI. *Neuroimage*. (2016) 124:714–23. doi: 10.1016/j.neuroimage.2015.09.030
51. Langs G, Wang D, Golland P, Mueller S, Pan R, Sabuncu MR, et al. Identifying shared brain networks in individuals by decoupling functional and anatomical variability. *Cereb Cortex*. (2016) 26:4004–14. doi: 10.1093/cercor/bhv189
52. Wang D, Buckner RL, Fox MD, Holt DJ, Holmes AJ, Stoecklein S, et al. Parcellating cortical functional networks in individuals. *Nat Neurosci*. (2015) 18:1853–60. doi: 10.1038/nn.4164
53. Ray NJ, Jenkinson N, Wang S, Holland P, Brittain JS, Joint C, et al. Local field potential beta activity in the subthalamic nucleus of patients with Parkinson's disease is associated with improvements in bradykinesia after dopamine and deep brain stimulation. *Exp Neurol*. (2008) 213:108–13. doi: 10.1016/j.expneurol.2008.05.008
54. Qian X, Chen Y, Feng Y, Ma B, Hao H, Li, et al. A platform for long-term monitoring the deep brain rhythms. *Biomed Phys Eng Express*. (2017) 3:015009. doi: 10.1088/2057-1976/aa50d6
55. Chen Y, Gong C, Tian Y, Orlov N, Zhang J, Guo Y, et al. Neuromodulation effects of deep brain stimulation on beta rhythm: a longitudinal local field potential study. *Brain Stimul*. (2020) 13:1784–92. doi: 10.1016/j.brs.2020.09.027
56. Mayberg HS, Lozano AM, Voon V, McNeely HE, Seminowicz D, Hamani C, et al. Deep brain stimulation for treatment-resistant depression. *Neuron*. (2005) 45:651–60. doi: 10.1016/j.neuron.2005.02.014
57. Greenberg BD, Rauch SL, Haber SN. Invasive circuitry-based neurotherapeutics: stereotactic ablation deep brain stimulation for OCD. *Neuropsychopharmacology*. (2010) 35:317–36. doi: 10.1038/npp.2009.128
58. Mallet L, Polosan M, Jaafari N, Baup N, Welter ML, Fontaine D, et al. STOC Study Group. Subthalamic nucleus stimulation in severe obsessive-compulsive disorder. *N Engl J Med*. (2008) 359:2121–34. doi: 10.1056/NEJMoa0708514
59. Haber SN, Behrens TE. The neural network underlying incentive-based learning: implications for interpreting circuit disruptions in psychiatric disorders. *Neuron*. (2014) 83:1019–39. doi: 10.1016/j.neuron.2014.08.031
60. Hamani C, Mayberg H, Snyder B, Giacobbe P, Kennedy S, Lozano AM. Deep brain stimulation of the subcallosal cingulate gyrus for depression: anatomical location of active contacts in clinical responders and a suggested guideline for targeting. *J Neurosurg*. (2009) 111:1209–15. doi: 10.3171/2008.10.JNS08763
61. Lehman JF, Greenberg BD, McIntyre CC, Rasmussen SA, Haber SN. Rules ventral prefrontal cortical axons use to reach their targets: implications for diffusion tensor imaging tractography and deep brain stimulation for psychiatric illness. *J Neurosci*. (2011) 31:10392–402. doi: 10.1523/JNEUROSCI.0595-11.2011
62. Safadi Z, Grisot G, Jbabdi S, Behrens TE, Heilbronner SR, McLaughlin NCR, et al. Functional segmentation of the anterior limb of the internal capsule: linking white matter abnormalities to specific connections. *J Neurosci*. (2018) 38:2106–17. doi: 10.1523/JNEUROSCI.2335-17.2017
63. Kennedy SH, Giacobbe P, Rizvi SJ, Placenza FM, Nishikawa Y, Mayberg HS, et al. Deep brain stimulation for treatment-resistant depression: follow-up after 3 to 6 years. *Am J Psychiatry*. (2011) 168:502–10. doi: 10.1176/appi.ajp.2010.10081187
64. Greenberg BD, Gabriels LA, Malone DA Jr, Rezai AR, Friehs GM, Okun MS, et al. Deep brain stimulation of the ventral internal capsule/ventral striatum for obsessive-compulsive disorder: worldwide experience. *Mol Psychiatry*. (2010) 15:64–79. doi: 10.1038/mp.2008.55
65. Haynes WI, Haber SN. The organization of prefrontal-subthalamic inputs in primates provides an anatomical substrate for both functional specificity and integration: implications for Basal Ganglia models and deep brain stimulation. *J Neurosci*. (2013) 33:4804–14. doi: 10.1523/JNEUROSCI.4674-12.2013
66. Greenberg PE, Fournier AA, Sisitsky T, Pike CT, Kessler RC. The economic burden of adults with major depressive disorder in the United States (2005 and 2010). *J Clin Psychiatry*. (2015) 76:155–62. doi: 10.4088/JCP.14m09298
67. Tsolaki E, Espinoza R, Pouratian N. Using probabilistic tractography to target the subcallosal cingulate cortex in patients with treatment resistant depression. *Psychiatry Res*. (2017) 261:72–4. doi: 10.1016/j.pscychresns.2017.01.006
68. Dougherty DD, Rezai AR, Carpenter LL, Howland RH, Bhati MT, O'Reardon JP, et al. A randomized sham-controlled trial of deep brain stimulation of the ventral capsule/ventral striatum for chronic treatment-resistant depression. *Biol Psychiatry*. (2015) 78:240–8. doi: 10.1016/j.biopsych.2014.11.023

69. Wang TR, Moosa S, Dallapiazza RF, Elias JW, Lynch WJ. Deep brain stimulation for the treatment of drug addiction. *Neurosurg Focus*. (2018) 45:E11. doi: 10.3171/2018.5.FOCUS18163
70. Bari A, DiCesare J, Babayan D, Runcie M, Sparks H, Wilson B. Neuromodulation for substance addiction in human subjects: a review. *Neurosci Biobehav Rev*. (2018) 95:33–43. doi: 10.1016/j.neubiorev.2018.09.013
71. Bari AA, Mikell CB, Abosch A, Ben-Haim S, Buchanan RJ, Burton AW, et al. Charting the road forward in psychiatric neurosurgery: proceedings of the 2016 American Society for Stereotactic and Functional Neurosurgery workshop on neuromodulation for psychiatric disorders. *J Neurol Neurosurg Psychiatry*. (2018) 89:886–96. doi: 10.1136/jnnp-2017-317082
72. Williams LM. Precision psychiatry: a neural circuit taxonomy for depression and anxiety. *Lancet Psychiatry*. (2016) 3:472–80. doi: 10.1016/S2215-0366(15)00579-9
73. Holtzheimer PE, Kelley ME, Gross RE, Filkowski MM, Garlow SJ, Barrocas A, et al. Subcallosal cingulate deep brain stimulation for treatment-resistant unipolar and bipolar depression. *Arch Gen Psychiatry*. (2012) 69:150–8. doi: 10.1001/archgenpsychiatry.2011.1456
74. Mayberg HS. Targeted electrode-based modulation of neural circuits for depression. *J Clin Investigation*. (2009) 119:717–25. doi: 10.1172/JCI38454
75. Mayberg HS, Brannan SK, Tekell JL, Silva JA, Mahurin RK, McGinnis S, et al. Regional metabolic effects of fluoxetine in major depression: serial changes and relationship to clinical response. *Biol Psychiatry*. (2000) 48:830–43. doi: 10.1016/S0006-3223(00)01036-2
76. Mayberg HS. Limbic-cortical dysregulation: a proposed model of depression. *J Neuropsychiatry Clin Neurosci*. (1997) 9:471–81. doi: 10.1176/jnp.9.3.471
77. Mayberg HS, Liotti M, Brannan SK, McGinnis S, Mahurin RK, Jerabek PA, et al. Reciprocal limbic-cortical function and negative mood: converging PET findings in depression and normal sadness. *Am J Psychiatry*. (1999) 156:675–82. doi: 10.1176/ajp.156.5.675
78. Riva-Posse P, Choi KS, Holtzheimer PE, McIntyre CC, Gross RE, Chaturvedi A, et al. Defining critical white matter pathways mediating successful subcallosal cingulate deep brain stimulation for treatment-resistant depression. *Biol Psychiatry*. (2014) 76:963–9. doi: 10.1016/j.biopsych.2014.03.029
79. Choi KS, Noecker AM, Riva-Posse P, Rajendra JK, Gross RE, Mayberg HS, et al. Impact of brain shift on subcallosal cingulate deep brain stimulation. *Brain Stimul*. (2018) 11:445–53. doi: 10.1016/j.brs.2017.12.001
80. Chaturvedi A, Lujan J, McIntyre C. Artificial neural network based characterization of the volume of tissue activated during deep brain stimulation. *J Neural Eng*. (2013) 10:1–17. doi: 10.1088/1741-2560/10/5/056023
81. Lockhart IA, Mitchell SA, Kelly S. Safety and tolerability of donepezil, rivastigmine and galantamine for patients with Alzheimer's disease: systematic review of the 'real-world' evidence. *Dement Geriatr Cogn Disord*. (2009) 28:389–403. doi: 10.1159/000255578
82. Kesner RP. Brain stimulation: effects on memory. *Behav Neural Biol*. (1982) 36:315–67. doi: 10.1016/S0163-1047(82)90762-2
83. Hamani C, Dubiela FP, Soares JC, Shin D, Bittencourt S, Covolan L, et al. Anterior thalamus deep brain stimulation at high current impairs memory in rats. *Exp Neurol*. (2010) 225:154–62. doi: 10.1016/j.expneurol.2010.06.007
84. Wilburn MW, Kesner RP. Differential amnestic effects produced by electrical stimulation of the caudate nucleus and nonspecific thalamic system. *Exp Neurol*. (1972) 34:45–50. doi: 10.1016/0014-4886(72)90186-0
85. Hamani C, Temel Y. Deep brain stimulation for psychiatric disease: contributions and validity of animal models. *Sci Transl Med*. (2012) 4:142rv148. doi: 10.1126/scitranslmed.3003722
86. Stone SS, Teixeira CM, Devito LM, Zaslavsky K, Josselyn SA, Lozano AM, et al. Stimulation of entorhinal cortex promotes adult neurogenesis and facilitates spatial memory. *J Neurosci*. (2011) 31:13469–84. doi: 10.1523/JNEUROSCI.3100-11.2011
87. Suthana N, Haneef Z, Stern J, Mukamel R, Behnke E, Knowlton B, et al. Memory enhancement and deep-brain stimulation of the entorhinal area. *N Engl J Med*. (2012) 366:502–10. doi: 10.1056/NEJMoa1107212
88. Oh YS, Kim HJ, Lee KJ, Kim YI, Lim SC, Shon YM. Cognitive improvement after long-term electrical stimulation of bilateral anterior thalamic nucleus in refractory epilepsy patients. *Seizure*. (2012) 21:183–7. doi: 10.1016/j.seizure.2011.12.003
89. Brandling-Bennett EM, Bookheimer SY, Horsfall JL, Moftakhar P, Sedrak M, Barkulis CT, et al. A paradigm for awake intraoperative memory mapping during forniceal stimulation. *Neurocase*. (2012) 18:26–38. doi: 10.1080/13554794.2010.547509
90. Hamani C, McAndrews MP, Cohn M, Oh M, Zumsteg D, Shapiro CM, et al. Memory enhancement induced by hypothalamic/fornix deep brain stimulation. *Ann Neurol*. (2008) 63:119–23. doi: 10.1002/ana.21295
91. Laxton AW, Tang-Wai DF, McAndrews MP, Zumsteg D, Wennberg R, Keren R, et al. A phase I trial of deep brain stimulation of memory circuits in Alzheimer's disease. *Ann Neurol*. (2010) 68:521–34. doi: 10.1002/ana.22089
92. Lozano AM, Fosdick L, Chakravarty MM, Leoutsakos JM, Munro C, Oh E, et al. A phase II study of fornix deep brain stimulation in mild Alzheimer's disease. *J Alzheimers Dis*. (2016) 54:777–87. doi: 10.3233/JAD-160017
93. Kuhn J, Hardenacke K, Lenartz D, Gruendler T, Ullsperger M, Bartsch C, et al. Deep brain stimulation of the nucleus basalis of Meynert in Alzheimer's dementia. *Mol Psychiatry*. (2015) 20:353–60. doi: 10.1038/mp.2014.32
94. Gratwicke J, Zrinzo L, Kahan J, Peters A, Brechany U, McNichol A, et al. Bilateral nucleus basalis of Meynert deep brain stimulation for dementia with Lewy bodies: a randomised clinical trial. *Brain Stimul*. (2020) 13:1031–9. doi: 10.1016/j.brs.2020.04.010
95. Mann A, Gondard E, Tampellini D, Milsted JAT, Marillac D, Hamani C, et al. Chronic deep brain stimulation in an Alzheimer's disease mouse model enhances memory and reduces pathological hallmarks. *Brain Stimul*. (2018) 11:435–44. doi: 10.1016/j.brs.2017.11.012
96. Giladi N, McDermott MP, Fahn S, Przedborski S, Jankovic J, Stern M, et al. Freezing of gait in PD: prospective assessment in the DATATOP cohort. *Neurology*. (2001) 56:1712–21. doi: 10.1212/WNL.56.12.1712
97. Cotzias GC. L-Dopa for Parkinsonism. *N Engl J Med*. (1968) 278:630. doi: 10.1056/NEJM196803142781127
98. Langston JW, Ballard PA Jr. Parkinson's disease in a chemist working with 1-methyl-4-phenyl-1,2,5,6-tetrahydropyridine. *N Engl J Med*. (1983) 309:310. doi: 10.1056/NEJM198308043090511
99. Langston JW, Ballard P, Tetrud JW, Irwin I. Chronic Parkinsonism in humans due to a product of meperidine-analog synthesis. *Science*. (1983) 219:979–80. doi: 10.1126/science.6823561
100. Burns RS, Chiueh CC, Markey SP, Ebert MH, Jacobowitz DM, Kopin IJ. A primate model of parkinsonism: selective destruction of dopaminergic neurons in the pars compacta of the substantia nigra by N-methyl-4-phenyl-1,2,3,6-tetrahydropyridine. *Proc Natl Acad Sci U S A*. (1983) 80:4546–50. doi: 10.1073/pnas.80.14.4546
101. Crossman AR, Mitchell IJ, Sambrook MA. Regional brain uptake of 2-deoxyglucose in N-methyl-4-phenyl-1,2,3,6-tetrahydropyridine (MPTP)-induced parkinsonism in the macaque monkey. *Neuropharmacology*. (1985) 24:587–91 doi: 10.1016/0028-3908(85)90070-X
102. Bergman H, Wichmann T, DeLong MR. Reversal of experimental parkinsonism by lesions of the subthalamic nucleus. *Science*. (1990) 249:1436–8 doi: 10.1126/science.2402638
103. Aziz TZ, Peggs D, Sambrook MA, Crossman AR. Lesion of the subthalamic nucleus for the alleviation of 1-methyl-4-phenyl-1,2,3,6-tetrahydropyridine (MPTP)-induced parkinsonism in the primate. *Mov Disord*. (1991) 6:288–92. doi: 10.1002/mds.870060404
104. Nandi D, Liu X, Winter JL, Aziz TZ, Stein JF. Deep brain stimulation of the pedunculopontine region in the normal non-human primate. *J Clin Neurosci*. (2002) 9:170–4 doi: 10.1054/jocn.2001.0943
105. Nandi D, Aziz TZ, Giladi N, Winter J, Stein JF. Reversal of akinesia in experimental parkinsonism by GABA antagonist microinjections in the pedunculopontine nucleus. *Brain*. (2002) 125:2418–30. doi: 10.1093/brain/awf259
106. Mazzone P, Lozano A, Stanzione P, Galati S, Scarnati E, Peppe A, et al. Implantation of human pedunculopontine nucleus: a safe and clinically relevant target in Parkinson's disease. *Neuroreport*. (2005) 16:1877–81. doi: 10.1097/01.wnr.0000187629.38010.12
107. Plaha P, Gill SS. Bilateral deep brain stimulation of the pedunculopontine nucleus for Parkinson's disease. *Neuroreport*. (2005) 16:1883–7. doi: 10.1097/01.wnr.0000187637.20771.a0

108. Stefani A, Lozano AM, Peppe A, Stanzione P, Galati S, Tropepi D, et al. Bilateral deep brain stimulation of the pedunculopontine and subthalamic nuclei in severe Parkinson's disease. *Brain.* (2007) 130:1596–607. doi: 10.1093/brain/awl346
109. Yelnik J. PPN or PPD, what is the target for deep brain stimulation in Parkinson's disease? *Brain*. (2007) 130:e79. doi: 10.1093/brain/awm138
110. Zrinzo L, Hariz M. The peripeduncular nucleus: a novel target for deep brain stimulation? *Neuroreport*. (2007) 18:1631–2. doi: 10.1097/WNR.0b013e3282638603
111. Zrinzo L, Zrinzo LV, Hariz M. The pedunculopontine and peripeduncular nuclei: a tale of two structures. *Brain.* (2007) 130:e73. doi: 10.1093/brain/awm079
112. Zrinzo L, Zrinzo LV, Tisch S, Limousin PD, Yousry TA, Afshar F, et al. Stereotactic localization of the human pedunculopontine nucleus: atlas-based coordinates and validation of a magnetic resonance imaging protocol for direct localization. *Brain.* (2008) 131:1588–98. doi: 10.1093/brain/awn075
113. Ferraye MU, Debû B, Fraix V, Goetz L, Ardouin C, Yelnik J, et al. Effects of pedunculopontine nucleus area stimulation on gait disorders in Parkinson's disease. *Brain.* (2010) 133:205–14. doi: 10.1093/brain/awp229
114. Moro E, Hamani C, Poon YY, Al-Khairallah T, Dostrovsky JO, Hutchison WD, et al. Unilateral pedunculopontine stimulation improves falls in Parkinson's disease. *Brain.* (2010) 133:215–24. doi: 10.1093/brain/awp261
115. Jenkinson N, Nandi D, Muthusamy K, Ray NJ, Gregory R, Stein JF, et al. Anatomy, physiology, and pathophysiology of the pedunculopontine nucleus. *Mov Disord.* (2009) 24:319–28. doi: 10.1002/mds.22189
116. Mesulam MM, Geula C, Bothwell MA, Hersh LB. Human reticular formation: cholinergic neurons of the pedunculopontine and laterodorsal tegmental nuclei and some cytochemical comparisons to forebrain cholinergic neurons. *J Comp Neurol.* (1989) 283:611–33. doi: 10.1002/cne.902830414
117. Manaye KF, Zweig R, Wu D, Hersh LB, De Lacalle S, Saper CB, et al. Quantification of cholinergic and select non-cholinergic mesopontine neuronal populations in the human brain. *Neuroscience.* (1999) 89:759–70. doi: 10.1016/S0306-4522(98)00380-7
118. Rinne JO, Ma SY, Lee MS, Collan Y, Röyttä M. Loss of cholinergic neurons in the pedunculopontine nucleus in Parkinson's disease is related to disability of the patients. *Parkinsonism Relat Disord.* (2008) 14:553–7. doi: 10.1016/j.parkreldis.2008.01.006
119. Thevathasan W, Coyne TJ, Hyam JA, Kerr G, Jenkinson N, Aziz TZ, et al. Pedunculopontine nucleus stimulation improves gait freezing in Parkinson disease. *Neurosurgery.* (2011) 69:1248–53 doi: 10.1227/NEU.0b013e31822b6f71
120. Peppe A, Pierantozzi M, Chiavalon C, Marchetti F, Caltagirone C, Musicco M, et al. Deep brain stimulation of the pedunculopontine tegmentum and subthalamic nucleus: effects on gait in Parkinson's disease. *Gait Posture.* (2010) 32:512–8. doi: 10.1016/j.gaitpost.2010.07.012
121. Wang H, Gao H, Jiao T, Luo Z. A meta-analysis of the pedunculopontine nucleus deep-brain stimulation effects on Parkinson's disease. *Neuroreport.* (2016) 27:1336–44. doi: 10.1097/WNR.0000000000000697
122. Perez-Lloret S, Negre-Pages L, Damier P, Delval A, Derkinderen P, Destée A, et al. Prevalence, determinants, and effect on quality of life of freezing of gait in Parkinson disease. *JAMA Neurol.* (2014) 71:884–90. doi: 10.1001/jamaneurol.2014.753
123. Thevathasan W, Cole MH, Graepel CL, Hyam JA, Jenkinson N, Brittain J-S, et al. A spatiotemporal analysis of gait freezing and the impact of pedunculopontine nucleus stimulation. *Brain.* (2012) 135:1446–54. doi: 10.1093/brain/aws039
124. Jia F, Guo Y, Wan S, Chen H, Hao H, Zhang J, et al. Variable frequency stimulation of subthalamic nucleus for freezing of gait in Parkinson's disease. *Parkinsonism Relat Disord.* (2015) 21:1471–2. doi: 10.1016/j.parkreldis.2015.10.002
125. Weiss SA, Banks GP, McKhann GM Jr, Goodman RR, Emerson RG, Trevelyan AJ, et al. Ictal high frequency oscillations distinguish two types of seizure territories in humans. *Brain.* (2013) 136:3796–808. doi: 10.1093/brain/awt276
126. Fuentes R, Petersson P, Siesser WB, Caron MG, Nicolelis MAL. Spinal cord stimulation restores locomotion in animal models of Parkinson's disease. *Science.* (2009) 323:1578–82. doi: 10.1126/science.1164901
127. Santana MB, Halje P, Simplício H, Richter U, Freire MAM, Petersson P, et al. Spinal cord stimulation alleviates motor deficits in a primate model of Parkinson disease. *Neuron.* (2014) 84:716–22. doi: 10.1016/j.neuron.2014.08.061
128. de Andrade EM, Ghilardi MG, Cury RG, Barbosa ER, Fuentes R, Teixeira MJ, et al. Spinal cord stimulation for Parkinson's disease: a systematic review. *Neurosurg Rev.* (2016) 39:27–35. doi: 10.1007/s10143-015-0651-1
129. Pinto de Souza C, Hamani C, Oliveira Souza C, Lopez Contreras WO, Dos Santos Ghilardi MG, Cury RG, et al. Spinal cord stimulation improves gait in patients with Parkinson's disease previously treated with deep brain stimulation. *Mov Disord.* (2017) 32:278–82. doi: 10.1002/mds.26850
130. Samotus O, Parrent A, Jog M. Spinal cord stimulation therapy for gait dysfunction in advanced Parkinson's disease patients. *Mov Disord*. (2018) 33:783–92. doi: 10.1002/mds.27299
131. de Lima-Pardini AC, de Azevedo Neto RM, Coelho DB, Boffino CC, Shergill SS, de Oliveira Souza C, et al. An fMRI-compatible force measurement system for the evaluation of the neural correlates of step initiation. *Sci Rep.* (2017) 7:43088. doi: 10.1038/srep43088
132. de Lima-Pardini AC, Coelho DB, Souza CP, Souza CO, Ghilardi MGDS, Garcia T, et al. Effects of spinal cord stimulation on postural control in Parkinson's disease patients with freezing of gait. *Elife.* (2018) 7:e37727. doi: 10.7554/eLife.37727
133. de Souza CP, Dos Santos MGG, Hamani C, Fonoff ET. Spinal cord stimulation for gait dysfunction in Parkinson's disease: essential questions to discuss. *Mov Disord.* (2018) 33:1828–9. doi: 10.1002/mds.27508
134. Fonoff ET, Lima-Pardini AC, Coelho DB, Mônaco BA, Machado BM, Pinto de Souza C, et al. Spinal cord stimulation for freezing of gait: from the bench to the bedside. *Front Neurol.* (2019) 10:905. doi: 10.3389/fneur.2019.00905
135. Machado A, Baker KB. Upside down crossed cerebellar diaschisis: proposing chronic stimulation of the dentatothalamocortical pathway for post-stroke motor recovery. *Front Integr Neurosci.* (2012) 6:20. doi: 10.3389/fnint.2012.00020
136. Machado AG, Baker KB, Schuster D, Butler RS, Rezai A. Chronic electrical stimulation of the contralesional lateral cerebellar nucleus enhances recovery of motor function after cerebral ischemia in rats. *Brain Res.* (2009) 1280:107–16. doi: 10.1016/j.brainres.2009.05.007
137. Machado AG, Cooperrider J, Furmaga HT, Baker KB, Park HJ, Chen Z, et al. Chronic 30-Hz deep cerebellar stimulation coupled with training enhances post-ischemia motor recovery and peri-infarct synaptophysin expression in rodents. *Neurosurgery.* (2013) 73:344–53. doi: 10.1227/01.neu.0000430766.80102.ac
138. Baker KB, Schuster D, Cooperrider J, Machado AG. Deep brain stimulation of the lateral cerebellar nucleus produces frequency-specific alterations in motor evoked potentials in the rat *in vivo*. *Exp Neurol.* (2010) 226:259–64. doi: 10.1016/j.expneurol.2010.08.019
139. Cooperrider J, Furmaga H, Plow E, Park HJ, Chen Z, Kidd G, et al. Chronic deep cerebellar stimulation promotes long-term potentiation, microstructural plasticity, and reorganization of perilesional cortical representation in a rodent model. *J Neurosci.* (2014) 34:9040–50. doi: 10.1523/JNEUROSCI.0953-14.2014
140. Kupsch A, Benecke R, Müller J, Trottenberg T, Schneider GH, Poewe W, et al. Deep-Brain Stimulation for Dystonia Study Group. Pallidal deep-brain stimulation in primary generalized or segmental dystonia. *N Engl J Med.* (2006) 355:1978–90. doi: 10.1056/NEJMoa063618
141. Vidailhet M, Vercueil L, Houeto JL, Krystkowiak P, Benabid AL, Cornu P, et al. French Stimulation du Pallidum Interne dans la Dystonie (SPIDY) Study Group. Bilateral deep-brain stimulation of the globus pallidus in primary generalized dystonia. *N Engl J Med.* (2005) 352:459–67. doi: 10.1056/NEJMoa042187
142. Vidailhet M, Pollak P. Deep brain stimulation for dystonia: make the lame walk. *Ann Neurol.* (2005) 57:613–4. doi: 10.1002/ana.20491
143. Vidailhet M, Vercueil L, Houeto JL, Krystkowiak P, Lagrange C, Yelnik J, et al. French SPIDY Study Group. Bilateral, pallidal, deep-brain stimulation in primary generalised dystonia: a prospective 3 year follow-up study. *Lancet Neurol.* (2007). 6:223–9. doi: 10.1016/S1474-4422(07)70035-2
144. Volkmann J, Wolters A, Kupsch A, Müller J, Kühn AA, Schneider GH, et al. DBS study group for dystonia. Pallidal deep brain stimulation in patients with primary generalised or segmental

dystonia: 5-year follow-up of a randomised trial. *Lancet Neurol.* (2012) 11:1029–38. doi: 10.1016/S1474-4422(12)70257-0
145. Volkmann J, Mueller J, Deuschl G, Kühn AA, Krauss JK, Poewe W, et al. DBS study group for dystonia. Pallidal neurostimulation in patients with medication-refractory cervical dystonia: a randomised, sham-controlled trial. *Lancet Neurol.* (2014) 13:875–84. doi: 10.1016/S1474-4422(14)70143-7
146. Markun LC, Starr PA, Air EL, Marks WJ Jr, Volz MM, Ostrem JL. Shorter disease duration correlates with improved long-term deep brain stimulation outcomes in young-onset DYT1 dystonia. *Neurosurgery.* (2012) 71:325–30. doi: 10.1227/NEU.0b013e318258e21b
147. Walsh RA, Sidiropoulos C, Lozano AM, Hodaie M, Poon YY, Fallis M, et al. Bilateral pallidal stimulation in cervical dystonia: blinded evidence of benefit beyond 5 years. *Brain.* (2013) 136:761–9. doi: 10.1093/brain/awt009
148. Cif L, Vasques X, Gonzalez V, Ravel P, Biolsi B, Collod-Beroud G, et al. Long-term follow-up of DYT1 dystonia patients treated by deep brain stimulation: an open-label study. *Mov Disord.* (2010) 25:289–99. doi: 10.1002/mds.22802
149. Isaias IU, Alterman RL, Tagliati M. Outcome predictors of pallidal stimulation in patients with primary dystonia: the role of disease duration. *Brain.* (2008) 131:1895902. doi: 10.1093/brain/awn120
150. Brüggemann N, Kühn A, Schneider SA, Kamm C, Wolters A, Krause P, et al. Short- and long-term outcome of chronic pallidal neurostimulation in monogenic isolated dystonia. *Neurology.* (2015) 84:895–903. doi: 10.1212/WNL.0000000000001312
151. Lumsden DE, Kaminska M, Gimeno H, Tustin K, Baker L, Perides S, et al. Proportion of life lived with dystonia inversely correlates with response to pallidal deep brain stimulation in both primary and secondary childhood dystonia. *Dev Med Child Neurol.* (2013) 55:567–74. doi: 10.1111/dmcn.12117
152. Krause P, Brüggemann N, Völzmann S, Horn A, Kupsch A, Schneider GH, et al. Long-term effect on dystonia after pallidal deep brain stimulation (DBS) in three members of a family with a THAP1 mutation. *J Neurol.* (2015) 262:2739–44. doi: 10.1007/s00415-015-7908-z
153. Hammond C, Bergman H, Brown P. Pathological synchronization in Parkinson's disease: networks, models and treatments. *Trends in neurosciences.* (2007) Jul;30:357-64. doi: 10.1016/j.tins.2007.05.004
154. Barow E, Neumann WJ, Brücke C, Huebl J, Horn A, Brown P, et al. Deep brain stimulation suppresses pallidal low frequency activity in patients with phasic dystonic movements. *Brain.* (2014) Nov;137(Pt 11):3012-3024. doi: 10.1093/brain/awu258
155. Silberstein P, Kühn AA, Kupsch A, Trottenberg T, Krauss JK, Wöhrle JC, et al. Patterning of globus pallidus local field potentials differs between Parkinson's disease and dystonia. *Brain.* (2003) Dec;126(Pt 12):2597-608. doi: 10.1093/brain/awg267
156. Wang DD, de Hemptinne C, Miocinovic S, Qasim SE, Miller AM, Ostrem JL, et al. Subthalamic local field potentials in Parkinson's disease and isolated dystonia: An evaluation of potential biomarkers. *Neurobiol Dis.* (2016) 89:213–22. doi: 10.1016/j.nbd.2016.02.015
157. Neumann WJ, Horn A, Ewert S, Huebl J, Brücke C, Slentz C, et al. A localized pallidal physiomarker in cervical dystonia. *Ann Neurol.* (2017) 82:912–24. doi: 10.1002/ana.25095
158. Ostrem JL, Starr PA. Treatment of dystonia with deep brain stimulation. *Neurotherapeutics.* (2008) 5:320–30. doi: 10.1016/j.nurt.2008.01.002
159. Coubes P, Cif L, El Fertit H, Hemm S, Vayssiere N, Serrat S, et al. Electrical stimulation of the globus pallidus internus in patients with primary generalized dystonia: long-term results. *J Neurosurg.* (2004) 101:189–94. doi: 10.3171/jns.2004.101.2.0189
160. Krause M, Fogel W, Kloss M, Rasche D, Volkmann J, Tronnier V. Pallidal stimulation for dystonia. *Neurosurgery.* (2004) 55:1361–8; discussion 1368–70. doi: 10.1227/01.NEU.0000143331.86101.5E
161. Khan MF, Mewes K, Gross RE, Škrinjar O. Assessment of Brain Shift Related to Deep Brain Stimulation Surgery. *Stereotact Funct Neurosurg.* (2008) 86:44–53. doi: 10.1159/000108588
162. Rolston JD, Englot DJ, Starr PA, Larson PS. An unexpectedly high rate of revisions and removals in deep brain stimulation surgery: analysis of multiple databases. *Parkinsonism Relat Disord.* (2016) 33:72–7. doi: 10.1016/j.parkreldis.2016.09.014
163. Zaidel A, Spivak A, Shpigelman L, Bergman H, Israel Z. Delimiting subterritories of the human subthalamic nucleus by means of microelectrode recordings and a hidden Markov model. *Mov Disord.* (2009) 24:1785–93. doi: 10.1002/mds.22674
164. Valsky D, Marmor-Levin O, Deffains M, Marmor-Levin O, Deffains M, Eitan R, et al. Stop! border ahead: automatic detection of subthalamic exit during deep brain stimulation surgery. *Mov Disord.* (2017) 32:70–9. doi: 10.1002/mds.26806
165. Rabiner LR. A tutorial on hidden Markov models and selected applications in speech recognition. *Proc IEEE.* (1989) 77:257–86. doi: 10.1109/5.18626
166. Venkatraghavan L, Rakhman E, Krishna V, Sammartino F, Manninen P, Hutchison W. The effect of general anesthesia on the microelectrode recordings from pallidal neurons in patients with dystonia. *J Neurosurg Anesthesiol.* (2016) 28:256–61. doi: 10.1097/ANA.0000000000000200
167. Valsky D, Blackwell KT, Tamir I, Eitan R, Bergman H, Israel Z. Real-time machine learning classification of pallidal borders during deep brain stimulation surgery. *J Neural Eng.* (2020) 17:016021. doi: 10.1088/1741-2552/ab53ac
168. Sanger TD, Ferman D. Similarity of involuntary postures between different children with dystonia. *Mov Disord Clin Pract.* (2017) 4:870–4. doi: 10.1002/mdc3.12533
169. Graziano MSA, Taylor CSR, Moore T. Complex movements evoked by microstimulation of precentral cortex. *Neuron.* (2002) 34:841–51. doi: 10.1016/S0896-6273(02)00698-0
170. Sanger TD, Liker M, Arguelles E, Deshpande R, Maskooki A, Ferman D, et al. Pediatric deep brain stimulation using awake recording and stimulation for target selection in an inpatient neuromodulation monitoring unit. *Brain Sci.* (2018) 8:135. doi: 10.3390/brainsci8070135

Conflict of Interest: The authors declare that the research was conducted in the absence of any commercial or financial relationships that could be construed as a potential conflict of interest.

frontiers in Neuroscience

ORIGINAL RESEARCH
published: 15 March 2021
doi: 10.3389/fnins.2021.632697

Brain–Heart Interaction During Transcutaneous Auricular Vagus Nerve Stimulation

Kathrin Machetanz, Levan Berelidze, Robert Guggenberger and Alireza Gharabaghi**

Institute for Neuromodulation and Neurotechnology, University of Tübingen, Tübingen, Germany

Objectives: Transcutaneous auricular vagus nerve stimulation (taVNS) modulates brain activity and heart function. The induced parasympathetic predominance leads to an increase of heart rate variability (HRV). Knowledge on the corresponding cortical activation pattern is, however, scarce. We hypothesized taVNS-induced HRV increases to be related to modulation of cortical activity that regulates the autonomic outflow to the heart.

Materials and Methods: In thirteen healthy subjects, we simultaneously recorded 64-channel electroencephalography and electrocardiography during taVNS. Two taVNS stimulation targets were investigated, i.e., the cymba conchae and inner tragus, and compared to active control stimulation in the anatomical vicinity, i.e., at the crus helicis and outer tragus. We used intermitted stimulation bursts of 25 Hz applied at a periodicity of 1 Hz. HRV was estimated with different time-domain methodologies: standard deviation of RR (SDNN), the root mean squares of successive differences (RMSSD), the percentage of RR-intervals with at least 50 ms deviation from the preceding RR-interval (pNN50), and the difference of consecutive RR intervals weighted by their mean (rrHRV).

Results: The stimulation-induced HRV increases corresponded to frequency-specific oscillatory modulation of different cortical areas. All stimulation targets induced power modulations that were proportional to the HRV elevation. The most prominent changes that corresponded to HRV increases across all parameters and stimulation locations were frontal elevations in the theta-band. In the delta-band, there were frontal increases (RMSSD, pNN50, rrHRV, SDNN) and decreases (SDNN) across stimulation sites. In higher frequencies, there was a more divers activity pattern: Outer tragus/crus helicis stimulation increased oscillatory activity with the most prominent changes for the SDNN in frontal (alpha-band, beta-band) and fronto-parietal (gamma-band) areas. During inner tragus/cymba conchae stimulation the predominant pattern was a distributed power decrease, particularly in the fronto-parietal gamma-band.

Conclusion: Neuro–cardiac interactions can be modulated by electrical stimulation at different auricular locations. Increased HRV during stimulation is correlated with frequency-specific increases and decreases of oscillatory activity in different brain areas.

OPEN ACCESS

Edited by:
Jiande Chen,
University of Michigan, United States

Reviewed by:
Ying Zhu,
Northern Jiangsu People's Hospital (NJPH), China
Shaoyuan Li,
Acupuncture and Moxibustion Hospital, China Academy of Chinese Medical Sciences, China

****Correspondence:***
Kathrin Machetanz
kathrin.machetanz@med.uni-tuebingen.de
Alireza Gharabaghi
alireza.gharabaghi@uni-tuebingen.de

Specialty section:
This article was submitted to Autonomic Neuroscience, a section of the journal Frontiers in Neuroscience

Received: *23 November 2020*
Accepted: *17 February 2021*
Published: *15 March 2021*

Citation:
Machetanz K, Berelidze L, Guggenberger R and Gharabaghi A (2021) Brain–Heart Interaction During Transcutaneous Auricular Vagus Nerve Stimulation. Front. Neurosci. 15:632697. doi: 10.3389/fnins.2021.632697

When applying specific HRV measures, cortical patterns related to parasympathetic (RMSSD, pNN50, rrHRV) and sympathetic (SDNN) modulation can be identified. Thus, cortical oscillations may be used to define stimulation locations and parameters for research and therapeutic purposes.

Keywords: transcutaneous auricular vagus nerve stimulation (taVNS), non-invasive vagus nerve stimulation (nVNS), electroceutical, heart rate variability, electroencephalography, cortical oscillations

INTRODUCTION

The autonomic nervous system (ANS) plays a key role in many neurological, psychiatric, cardiovascular, immunological, and metabolic disorders (Kaniusas et al., 2019). Electroceutical neuromodulation of the ANS is, therefore, investigated as a potential therapeutic intervention, when pharmacological approaches remain unsuccessful. Stimulation of the vagal nerve, which represents an essential feedback-loop between brain and body via its afferent fibers (80%) and efferent (20%), modulates the ANS toward parasympathetic predominance (Kaniusas et al., 2019). Switching points of these loops are brainstem nuclei such as the nucleus of the solitary tract (NTS, afferent), nucleus spinalis of the trigeminal nerve (NSNT, afferent), nucleus ambiguous (NA, efferent), and dorsal motor nucleus (DMN, efferent). Specifically, electrical stimulation of the external ear, referred to as transcutaneous auricular vagus nerve stimulation (taVNS), modulates a peripheral branch of the vagal nerve and is considered as a safe and well tolerated intervention, which is increasingly explored for its physiological and behavioral effects (Redgrave et al., 2018). The influence of taVNS on the feedback-loop between the ANS and the central nervous system (CNS) may be captured by different measures such as functional magnetic resonance imaging (fMRI; Kraus et al., 2013; Frangos et al., 2015; Yakunina et al., 2016; Badran et al., 2018b; Tu et al., 2018; Sclocco et al., 2019), electroencephalography (Fallgatter et al., 2003; Leutzow et al., 2013; Hagen et al., 2014), electrocardiography (Antonino et al., 2017; Badran et al., 2018c), microneurography (Clancy et al., 2014), and pupillometry (Warren et al., 2019). Multi-modal bio-signal acquisition during taVNS may provide further insights on the neurophysiological systems' level effects, e.g., by the application of concurrent electroencephalographic and electrocardiographic recordings for the investigation of brain–heart interactions (Patron et al., 2019; Keute et al., 2021). During taVNS a shift in autonomic function toward parasympathetic predominance has been revealed by increases of heart rate variability (HRV; Clancy et al., 2014; De Couck et al., 2017; Sclocco et al., 2019); however, there are still open questions with regard to the auricular stimulation targets (Badran et al., 2018a; Burger and Verkuil, 2018), the impact on cortical brain areas and the underlying mechanisms (Leutzow et al., 2013, 2014; Polak et al., 2014) that influence the heart–brain-interaction (Silvani et al., 2016; Keute et al., 2021).

In this context, we investigated the two most often applied auricular stimulation locations, i.e., the cymba conchae and inner tragus, and the crus helicis and outer tragus as active control sites in their anatomical vicinity. We conjectured taVNS-induced HRV increases to be related to modulation of cortical activity that regulates the autonomic outflow to the heart. Since stimulation of cymba conchae and tragus has been shown to increase HRV (Clancy et al., 2014; De Couck et al., 2017), we expected differences with regard to the corresponding brain activity of these taVNS stimulation targets in comparison to the control sites that have less influence on HRV. Specifically, we conjectured these changes to occur in frontal areas which are characterized by neuro–cardiac coupling (Shoemaker et al., 2015; Ruiz Vargas et al., 2016; Patron et al., 2019).

MATERIALS AND METHODS

Subjects

Thirteen healthy subjects (age = 24 ± 3 [mean ± SD], 8 female) took part in this exploratory proof-of-concept study, which was a secondary data analysis of previous work on the impact of different auricular stimulation locations and parameters on HRV (Machetanz et al., under review). The electroencephalography data that we analyzed here has not been reported before. The experimental procedure and study-related information is identical to the previous report and is cited here accordingly when applicable (Machetanz et al., under review): Healthy, right-handed adults aged 18–80 years were included as participants. Exclusion criteria were checked beforehand and comprised an Edinburgh Handedness Inventory score below 75, any history of habitual drug or alcohol consumption, pregnancy, cardiac diseases, cognitive, or psychiatric impairments or neurological disorders. Furthermore, patients were asked to avoid substances that alter autonomic activity (e.g., caffeine or alcohol on the day of measurement for at least 2 h before the examination). Subjects gave their written informed consent before participation. The study was approved by the local ethics committee of the medical faculty of the University of Tübingen.

Experimental Procedure

Within one stimulation session, participants received taVNS to six different stimulation locations at either the right (n = 7; age = 24.3 ± 2.8; 3 females) or left ear (n = 6; age = 24 ± 3.1; 5 females). The stimulation locations were determined due to anatomical landmarks (e.g., separating the concha into cymba and cavum according to the crus of helix; **Figure 1**). There was no blinding of the participations or the examiner regarding the side of stimulation. However, subjects were not informed about the different stimulation localizations. Due to the low sample size, participants with right and left ear stimulation were pooled for the purpose of the present study.

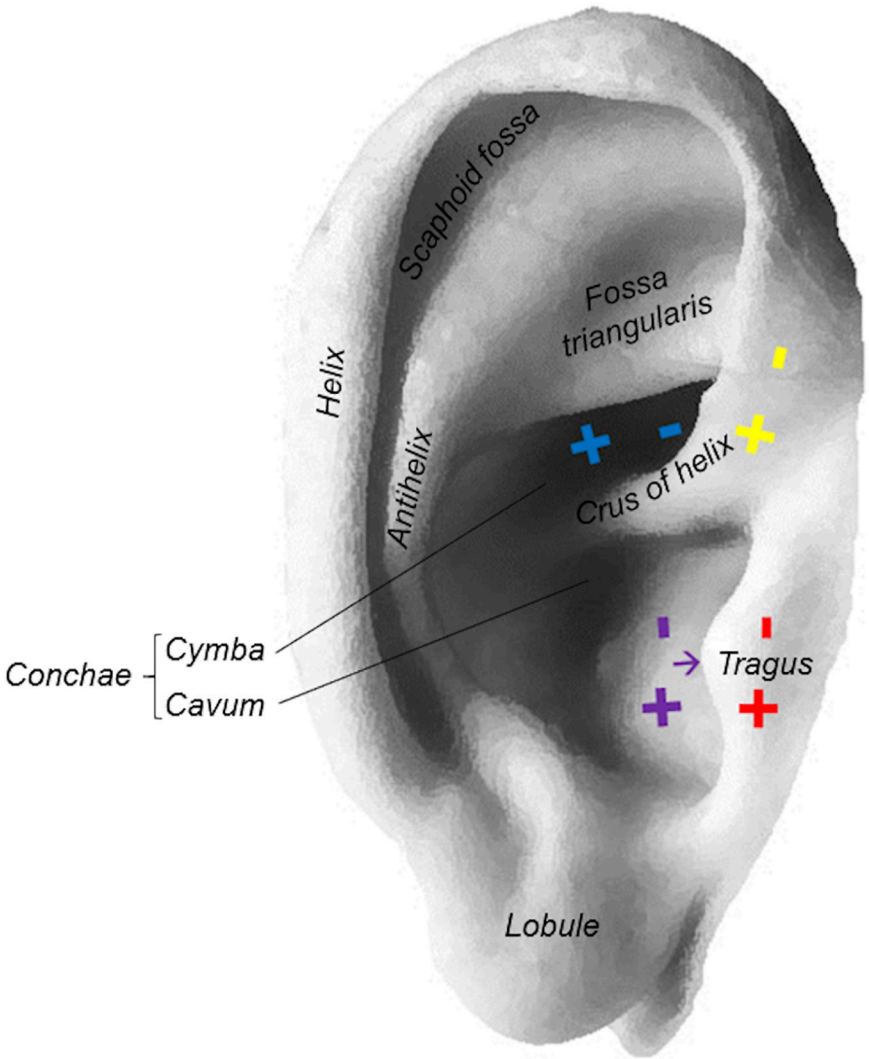

FIGURE 1 | Stimulation locations at the ear: cymba conchae (blue), inner tragus (purple), outer tragus (red), crus helicis (yellow).

At each stimulation location and parameter combination, we applied 30 bursts with a periodicity of 1 Hz, while each burst consisted of five pulses applied at 25 Hz. We started with the lowest electrical charge in three different charge-balanced parameter combinations [i.e., 100 μs (0.250 mA), 260 μs (0.096 mA), and 500 μs (0.050 mA)]. This resulted in 90 s (i.e., 3 × 30 s) of stimulation at the same charge and stimulation location. Then, the next higher charge was applied [i.e., 100 μs (0.500 mA), 260 μs (0.192 mA), and 500 μs (0.100 mA)]. After applying 2–3 different charges at one location, there was a short break of around 1 min before moving to the next location. Subsequently, the next stimulation round with higher charges ensued. Thereby, eight different electrical charges were evaluated by investigating three pulse durations and eight charge-balanced current intensities, i.e., 100 μs (0.250–2 mA in steps of 0.250 mA), 260 μs (0.096–0.769 mA in steps of 0.096 mA), and 500 μs (0.050–0.400 mA in steps of 0.050 mA).

Data Acquisition

The participants were positioned in a comfortable reclining chair, and electrocardiography (ECG), electroencephalography (EEG), and electrooculography (EOG) were recorded simultaneously. All signals were digitalized at a sampling frequency of 1,000 Hz (Brain Products Amplifiers, Brain Products GmbH, Gilching, Germany). Here, we analyzed the relationship between HRV obtained from a 3-channel ECG (electrodes at the left clavicle, sternum, and right olecranon) and EEG power spectrum from 64 Ag/AgCl electrodes (reference: FCz, ground: AFz) in accordance with the international 10–20 system (**Figure 2**). For artifact rejection, EOG was determined by Ag/AgCl electrodes above and below the left eye as well as a reference at the right olecranon.

For stimulation, we used a multichannel stimulator (STG-4000 series, multichannel systems, Harvard Bioscience Inc.) that was triggered by a customized python program and which allows current as well as voltage driven stimulation. Furthermore, a

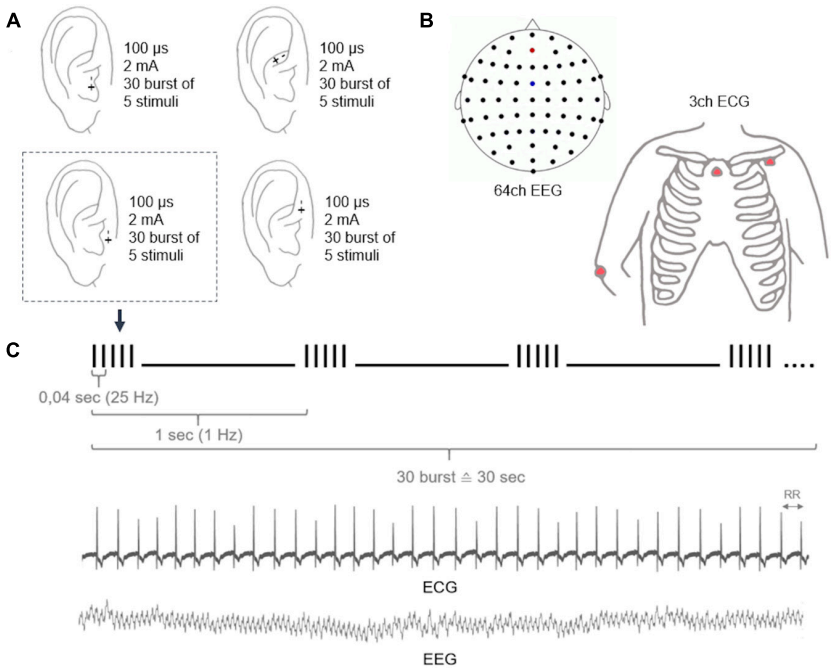

FIGURE 2 | Overview of the stimulation procedure during concurrent ECG/EEG recordings.

handheld bipolar spherical probe (GVB-gelimed GmbH) with a probe diameter of 2 mm and an inter-probe distance of 5 mm was applied. Throughout the experiment, participants were at rest; they were asked to relax and to indicate uncomfortable sensations whenever they occurred during stimulation. Stimulation was terminated, if the sensations became uncomfortable for the subjects. However, the stimulation intensity was not adjusted according to the individual perception threshold as applied in other studies (Clancy et al., 2014; Badran et al., 2018c; Borges et al., 2020), because (i) such adjustments were used inconsistently in previous studies and (ii) our aim was to stimulate the Aß-fibers and not the Aδ- and C-fibers, which primarily convey pain stimuli.

Data Analysis and Statistics

The ECG analysis of our previous study revealed that taVNS of the cymba conchae, and to a lesser extend also of the inner tragus, had the strongest influence on HRV increases (Machetanz et al., under review). Therefore, we chose the stimulation at these two locations as the verum intervention for our present EEG analysis. More specifically, we investigated the cortical oscillatory activity corresponding to HRV increases during taVNS of the cymba conchae and the inner tragus. For our proof-of-concept study, we restricted our analysis to stimulation with one parameter combination. Specifically, we investigated the cortical effects of stimulation with an amplitude of 2 mA and a pulse width of 100 µs, since our previous study revealed that this parameter combination was both effective in increasing HRV and comfortable for the participants. Moreover, a pulse width of 100 µs allows for a more selective fiber recruitment than longer pulse durations (Gorman and Mortimer, 1983; Helmers et al., 2012). Furthermore, a current intensity of 2 mA (which is lower than in other studies) allows for the activation of a restricted auricular region, i.e., the verum and the active sham condition can be applied in close vicinity without overlap of the stimulation areas (**Figure 1**). This allowed us to select stimulation of the crus helicis and outer tragus as active control conditions. More specifically, these stimulation locations are in the anatomical vicinity of the cymba conchae and inner tragus, respectively, but were shown to modulate the HRV significantly less (Machetanz et al., under review). We intentionally did not choose the common control site, i.e., the ear lobe, due to its distance to the cymba conchae and inner tragus. Thereby, we intended to avoid that the different density of perivascular sympathetic neurotransmitters that varies between lower and upper auricular zones would bias the stimulation effects (Cakmak, 2019).

The analysis of electrophysiological data was performed using MATLAB (MathWorks, Inc., Natick, MA, United States), Fieldtrip open-source toolbox[1] and other compatible toolboxes. EEG pre-processing included an automated artifact rejection by a linear regression of EOG data, a visual artifact rejection and epoching of the continuous EEG data into segments of 500 ms (350–850 ms after the first pulse). In a subsequent time-frequency analysis, the power spectrum of delta (0.5–3.5 Hz), theta (4–7 Hz), alpha (8–14 Hz), beta (15–30 Hz), and gamma (31–45 Hz) oscillatory activity was analyzed separately for each of the aforementioned segments using the methodology of a discrete prolate spheroidal sequence (DPSS; Percival and Walden, 1993).

For the ECG analysis, we used the MarcusVollmer/HRV toolbox.[2] The automated artifact rejection and R-peak detection was visually inspected to identify and correct for false positive

[1]http://fieldtrip.fcdonders.nl/

[2]https://marcusvollmer.github.io/HRV (v0.98; 02.09.2019).

and false negative findings. Subsequently, we applied different time-domain methodologies for HRV estimation by means of the toolbox, i.e., the standard deviation of RR (SDNN), the root mean squares of successive differences (RMSSD), and the pNN50 defined as the percentage of RR-intervals with at least 50 ms deviation from the preceding RR-interval. The SDNN is regarded as a parameter for the overall HRV (i.e., sympathetic and parasympathetic), while pNN50 and RMSSD are considered to reflect the parasympathetic nervous system. In addition, we analyzed the rrHRV which is based on the difference of consecutive RR intervals weighted by their mean, and which is particularly applicable for short RR sequences (Vollmer, 2015).

The study protocol followed a specific order of the applied parameters (see section "Experimental procedure"). Therefore, we controlled for a possible order effect of the performed examination runs by defining a general linear model with the run of each block as a categorical factor. Specifically, we regressed it out of the various HRV parameters and the 64 channels of the EEG power spectrum. Subsequently, we performed a correlation analysis for each EEG channel (of each power spectrum) with each HRV parameter (normalized for order) for the selected parameter conditions (2 mA, 100 μs; stimulation at cymba conchae/inner tragus and outer tragus/crus helicis), and determined the correlation matrix on the basis of pairwise Pearson correlations. Finally, the correlation coefficient (*R*-value) and the significance level (*P*-value) were graphically depicted in color-coded topoplots with a blue-to-yellow scale or black-to-white scale, respectively. The analyses were performed for the pooled trials of the inner tragus and cymbae conchae vs. the pooled trials of the crus helicis and outer tragus, and after concatenating left and right ear stimulation, to increase the number of trials for each condition (verum vs. active control).

RESULTS

The stimulation-induced HRV increases corresponded to frequency-specific oscillatory modulation of different cortical areas. All stimulation targets induced power modulations that were proportional to the HRV elevation (**Figure 3** and **Supplementary Tables 1, 2**).

The most prominent changes that corresponded to HRV increases across all measures (RMSSD, pNN50, rrHRV, and SDNN) and stimulation locations (cymba conchae/inner tragus, crus helicis/outer tragus) were significant frontal elevations (region of interest, ROI: Fp1, Fp2, AF3, AF4, Fpz, Fz) in the oscillatory theta-band. The mean *P*-value of a frontal region of interest (ROI; Fp1, Fp2, AF3, AF4, Fpz, Fz) was significant for RMSSD (*P*-value: 0.05 ± 0.06), pNN50 (0.04 ± 0.05) and rrHRV (0.04 ± 0.23) during cymba conchae/inner tragus stimulation; and also during crus helicis/outer tragus stimulation (*P*-value: $<0.001 \pm 0.001$; $<0.001 \pm 0.0004$; 0.001 ± 0.0005, respectively).

In the delta-band, there were frontal increases (RMSSD, pNN50, rrHRV, SDNN) and decreases (SDNN) across stimulation sites. However, these changes did not reach significance. In higher frequency bands, there was a more

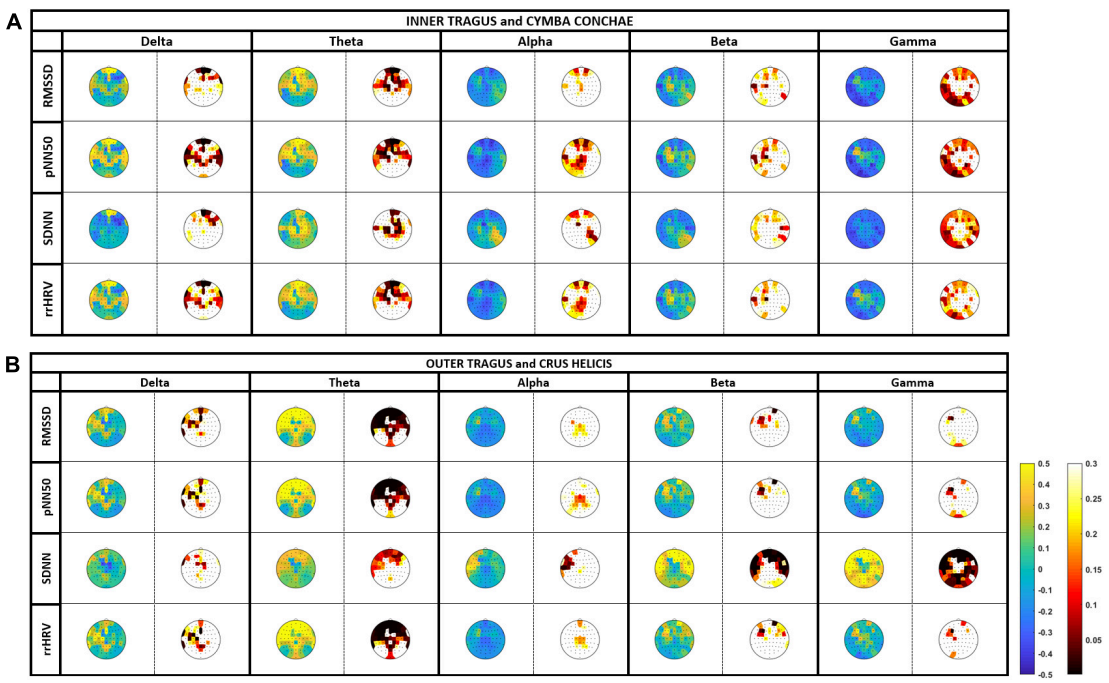

FIGURE 3 | Correlation between heart-rate variability (HRV) and cortical oscillatory activity (EEG): tVNS was applied at the cymba conchae/inner tragus and outer tragus/crus helicis with 2 mA and 100 μs. Oscillatory activity is estimated in the delta (0.5–3.5 Hz), theta (4–7 Hz), alpha (8–14 Hz), beta (15–30 Hz), and gamma (31–45 Hz). Color-coded topoplots show *r*-values (blue-to-yellow scale) and *p*-values (black-to-white scale) of the correlation analysis, where blue and black indicate power reduction and significance, respectively.

divers activity pattern: Outer tragus/crus helicis stimulation increased oscillatory activity with the most prominent changes for the SDNN measure in frontal (alpha-band, beta-band) and fronto-parietal (gamma-band) areas, which reached significance in the frontal ROI beta-band (P-value: 0.004 ± 0.01) and gamma-band (P-value: $<0.001 \pm 0.0004$). Inner tragus/cymba conchae stimulation led also to circumscribed alpha- and beta-band increases; however, the predominant pattern was a distributed power decrease, particularly in the fronto-parietal gamma-band.

DISCUSSION

Despite its wide range of potential therapeutic applications, there still exists controversy with regard to the underpinnings of taVNS. While the vagal influence on the ANS is established, the underlying anatomical and physiological mechanisms of the vagal CNS–ANS feedback loop are still incompletely understood (Cakmak, 2019; Kaniusas et al., 2019). In this context, the aim of this study was to evaluate corresponding changes of HRV and cortical activation patterns during taVNS. The present work showed, that the increase of HRV correlated with specific cortical activation patterns in different frequency bands.

Our results indicated a frontal increase in delta/theta oscillatory activity to be associated with an HRV increase during inner tragus and cymba conchae stimulation. This is in line with previous studies that revealed a neuro–cardiac coupling between HRV parameters and delta band activity in the frontal cortex as a cortical area promoting cardiac parasympathetic activity (Thayer et al., 2012; Patron et al., 2019; Keute et al., 2021). These studies showed higher cardiac control during stronger neuro–cardiac coupling. Interestingly, EEG correlates of 10 Hz vagus nerve stimulation for Crohn's disease showed acute increases of delta and theta activity as well (Kibleur et al., 2018). This observation is also supported by previous fMRI studies, which observed an association between increased vagal cardiac control and elevated activity in frontal areas (Shoemaker et al., 2015; Ruiz Vargas et al., 2016).

However, our data showed a frontal increase in delta/theta oscillatory activity also during active control stimulation at the outer tragus and crus helicis. This may be interpreted in different ways: The increase in delta/theta activity (that correlated with HRV) may not reflect specific vagal effects, but processes related to the general sensory afference induced by peripheral electrical stimulation (Hansen and Nielsen, 2004) or to changes of the attentional state (Aftanas and Golocheikine, 2001). Thereby, these findings may support the differentiation of autonomic, sensory and cognitive effects of auricular stimulation in future work. An alternative interpretation may suggest that stimulation at the active control locations was activating branches of the auricular branch of the vagus nerve – or other mechanisms that influence HRV – as well. Specifically, due to the proximity of the crus helicis and outer tragus to the cymba conchae and the inner tragus, respectively, electrical current may have been disseminated to more distantly located vagal fibers despite the relatively low stimulation intensity and narrow pulse width applied. An anatomical study of the auricular nerve supply in human cadavers revealed the most consistent vagal innervation patterns for the cymba conchae (Peuker and Filler, 2002), whereas, e.g., the crus helicis and fossa triangularis were innervated also by the lesser occipital nerve (LON), greater auricular nerve (GAN), and the auricotemporal nerve (ATN). However, although the outer tragus has been used as a location for taVNS in previous work (Badran et al., 2018b), the innervation of the tragus remains unclear due to inconsistent reporting (Peuker and Filler, 2002; Badran et al., 2018a; Burger and Verkuil, 2018). HRV-changes during cymba conchae and tragus stimulation (which are the two most investigated auricular stimulation targets) may be elicited by different mechanisms as stated elsewhere (Machetanz et al., under review): A fMRI study showed activation of vagal brainstem nuclei during stimulation of both targets, but with significant increases in comparison to control stimulation at the ear lobe for the cymba conchae only (Yakunina et al., 2016). On the other side, EEG recordings showed cortical evoked potentials, referred to as vagus somatosensory evoked potentials (VSEP), during inner tragus but not cymba conchae stimulation (Fallgatter et al., 2003). Notably, these EEG responses disappeared under a pharmacological neuromuscular block (Leutzow et al., 2013), which suggests rather a peripheral muscular than a central neural origin and has, therefore, initiated a debate with regard to the underlying mechanisms (Leutzow et al., 2014; Polak et al., 2014). In this context, two recent studies in humans (Clancy et al., 2014) and rats (Mahadi et al., 2019) suggested an alternative mechanisms of the observed HRV effects during tragus stimulation: microneurography recordings revealed a decrease of muscle sympathetic nerve activity (Clancy et al., 2014); recordings from the spinal sympathetic chain showed also an inhibition of sympathetic nerve activity, which disappeared after cervical nerve transections (Mahadi et al., 2019). These findings suggested that tragus stimulation effected HRV by potentially different autonomic mechanisms and pathways than cymba conchae stimulation. Furthermore, the influence of stimulation of auricular muscle zones, perivascular sympathetic neurotransmitters and the localization of perforatory artery zones should not be underestimated (Cakmak, 2019). Therefore, the similar activation pattern in frontal areas during stimulation of the classical tVNS targets and active control localizations could be induced by different mechanisms. Further studies with larger cohorts are necessary to better understand the observations.

In higher frequency bands, stimulation at tVNS targets (inner tragus/cymba conchae) and control localizations (outer tragus/crus helicis) showed a more divers and – in part – opposing pattern: Outer tragus/crus helicis stimulation increased oscillatory activity with the most prominent cortical changes correlating with HRV for the SDNN measure in frontal (alpha-, beta-band) and fronto-parietal (gamma-band) areas. Inner tragus/cymba conchae stimulation led also to circumscribed alpha- and beta-band increases; however, the predominant pattern was a distributed power decrease, particularly in the fronto-parietal gamma-band that correlated with HRV.

Notably, modulation of these higher frequency bands can be observed during somatosensory activation/processing as well as various cognitive functions (i.e., attention and memory; Herrmann et al., 2004; Jensen et al., 2007). Accordingly, in a case

of Crohn's disease, vagus nerve stimulation led to negative and positive correlation between HRV and gamma-band activity in frontal and parieto-occipital areas, respectively (Clarençon et al., 2014). In this context, previous studies showed also a divers and even contradictory picture. In tinnitus and epilepsy patients, for example, the previously increased gamma activity was reduced by vagus nerve stimulation (Willoughby et al., 2003; Hyvarinen et al., 2015); whereas, another study with epilepsy patients revealed a VNS-induced increase in gamma activity (Marrosu et al., 2005). These findings were interpreted as seizure-independent modulations of attention networks. Thus, the different effects of cymba conchae/inner tragus and outer tragus/crus helicis stimulation on gamma-band activity in the present study may reflect a different modulation of attention and/or the sympathetic system that is captured by the SDNN measure as well.

Limitations

This proof-of-concept study investigated EEG/ECG periods of 30 s only, since it was a secondary analysis of a screening session with different stimulation locations and parameters. Although even (ultra) short ECG recordings have been shown to be valid for HRV estimation (Percival and Walden, 1993; Kilner et al., 2005; Munoz et al., 2015; Shaffer and Ginsberg, 2017) and concurrent EEG/ECG evaluation (Patron et al., 2019), future studies may apply longer measurement periods including additional HRV parameters such as the LF/HF ration. Furthermore, on the basis of the present work, the long-tern effects of the novel intermitted taVNS paradigm on brain–heart interactions may be compared to standard continuous stimulation protocols. Moreover, future work would need to also consider trigeminal and sympathetic circuits by additional measures such as electromyography, microneurography, and pupillometry, and investigate larger sample sizes to allow for more detailed comparisons, e.g., between right vs. left ear stimulation.

CONCLUSION

Increased HRV during auricular stimulation is correlated with frequency-specific increases and decreases of oscillatory activity in different brain areas.

The HRV measures RMSSD, pNN50, and rrHRV, reflecting the parasympathetic nervous system, revealed consistent findings across frequency bands. With these measures, the most prominent changes that corresponded to HRV increases were frontal elevations in the oscillatory theta-band; they occurred across stimulation locations, i.e., during stimulation of cymba conchae/inner tragus and crus helicis/outer tragus.

The HRV measure SDNN, reflecting both the parasympathetic and sympathetic nervous system, differed from the other measures; the most prominent changes that corresponded to HRV were increased oscillatory activity in frontal (alpha-band, beta-band) and fronto-parietal (gamma-band) areas during outer tragus/crus helicis stimulation; while inner tragus/cymba conchae stimulation led predominantly to a distributed power decrease, particularly in the fronto-parietal gamma-band.

In summary, cortical oscillations may be used to define stimulation locations and parameters for research and therapeutic purposes.

DATA AVAILABILITY STATEMENT

The raw data of the presented study can be provided on request.

ETHICS STATEMENT

The studies involving human participants were reviewed and approved by Ethics Committee of the Medical Faculty of the University of Tübingen. The patients/participants provided their written informed consent to participate in this study.

AUTHOR CONTRIBUTIONS

KM contributed to the conception and design of the study, the acquisition, analysis and interpretation of data, and writing of the manuscript. LB and RG contributed to the data acquisition, analysis, interpretation of data, and review of the manuscript. AG was responsible for the conception and design of the study, interpretation of data, and writing of the manuscript. All authors contributed to the article and approved the submitted version.

FUNDING

This research study was supported by the German Federal Ministry of Education and Research (BMBF 13GW0359D, ENABLE). The funding had no involvement in study design, in the collection, analysis, and interpretation of data, in the writing of the report and in the decision to submit the article for publication.

ACKNOWLEDGMENTS

We acknowledge the support by the Open Access Publishing Fund of the University of Tübingen.

SUPPLEMENTARY MATERIAL

The Supplementary Material for this article can be found online at: https://www.frontiersin.org/articles/10.3389/fnins.2021.632697/full#supplementary-material

REFERENCES

Aftanas, L. I., and Golocheikine, S. A. (2001). Human anterior and frontal midline theta and lower alpha reflect emotionally positive state and internalized attention: High-resolution EEG investigation of meditation. *Neurosci. Lett.* 310, 57–60. doi: 10.1016/S0304-3940(01)02094-8

Antonino, D., Teixeira, A. L., Maia-Lopes, P. M., Souza, M. C., Sabino-Carvalho, J. L., Murray, A. R., et al. (2017). Non-invasive vagus nerve stimulation acutely improves spontaneous cardiac baroreflex sensitivity in healthy young men: A randomized placebo-controlled trial. *Brain Stimul.* 10, 875–881.

Badran, B. W., Brown, J. C., Dowdle, L. T., Mithoefer, O. J., LaBate, N. T., Coatsworth, J., et al. (2018a). Tragus or cymba conchae? Investigating the anatomical foundation of transcutaneous auricular vagus nerve stimulation (taVNS). *Brain Stimul.* 11, 947–948. doi: 10.1016/j.brs.2018.06.003

Badran, B. W., Dowdle, L. T., Mithoefer, O. J., LaBate, N. T., Coatsworth, J., Brown, J. C., et al. (2018b). Neurophysiologic effects of transcutaneous auricular vagus nerve stimulation (taVNS) via electrical stimulation of the tragus: A concurrent taVNS/fMRI study and review. *Brain Stimul.* 11, 492–500. doi: 10.1016/j.brs.2017.12.009

Badran, B. W., Mithoefer, O. J., Summer, C. E., LaBate, N. T., Glusman, C. E., Badran, A. W., et al. (2018c). Short trains of transcutaneous auricular vagus nerve stimulation (taVNS) have parameter-specific effects on heart rate. *Brain Stimul.* 11, 699–708. doi: 10.1016/j.brs.2018.04.004

Borges, U., Knops, L., Laborde, S., Klatt, S., and Raab, M. (2020). Transcutaneous Vagus Nerve Stimulation May Enhance Only Specific Aspects of the Core Executive Functions. A Randomized Crossover Trial. *Front. Neurosci.* 14:523. doi: 10.3389/fnins.2020.00523

Burger, A. M., and Verkuil, B. (2018). Transcutaneous nerve stimulation via the tragus: are we really stimulating the vagus nerve? *Brain Stimul.* 11, 945–946. doi: 10.1016/j.brs.2018.03.018

Cakmak, Y. O. (2019). Concerning Auricular Vagal Nerve Stimulation: Occult Neural Networks. *Front. Hum. Neurosci.* 13:421. doi: 10.3389/fnhum.2019.00421

Clancy, J. A., Mary, D. A., Witte, K. K., Greenwood, J. P., Deuchars, S. A., and Deuchars, J. (2014). Non-invasive Vagus nerve stimulation in healthy humans reduces sympathetic nerve activity. *Brain Stimul.* 7, 871–877. doi: 10.1016/j.brs.2014.07.031

Clarençon, D., Pellissier, S., Sinniger, V., Kibleur, A., Hoffman, D., Vercueil, L., et al. (2014). Long term effects of low frequency (10 Hz) vagus nerve stimulation on eeg and heart rate variability in crohn's disease: A case report. *Brain Stimul.* 7, 914–916. doi: 10.1016/j.brs.2014.08.001

De Couck, M., Cserjesi, R., Caers, R., Zijlstra, W. P., Widjaja, D., Wolf, N., et al. (2017). Effects of short and prolonged transcutaneous vagus nerve stimulation on heart rate variability in healthy subjects. *Auton. Neurosci. Basic Clin.* 203, 88–96. doi: 10.1016/j.autneu.2016.11.003

Fallgatter, A. J., Neuhauser, B., Herrmann, M. J., Ehlis, A. C., Wagener, A., Scheuerpflug, P., et al. (2003). Far field potentials from the brain stem after transcutaneous vagus nerve stimulation. *J. Neural Transm.* 110, 1437–1443. doi: 10.1007/s00702-003-0087-6

Frangos, E., Ellrich, J., and Komisaruk, B. R. (2015). Non-invasive access to the vagus nerve central projections via electrical stimulation of the external ear: FMRI evidence in humans. *Brain Stimul.* 8, 624–636. doi: 10.1016/j.brs.2014.11.018

Gorman, P. H., and Mortimer, J. T. (1983). The Effect of Stimulus Parameters on the Recruitment Characteristics of Direct Nerve Stimulation. *IEEE Trans. Biomed. Eng.* 30, 407–414. doi: 10.1109/TBME.1983.325041

Hagen, K., Ehlis, A. C., Schneider, S., Haeussinger, F. B., Fallgatter, A. J., and Metzger, F. G. (2014). Influence of different stimulation parameters on the somatosensory evoked potentials of the Nervus Vagus - How varied stimulation parameters affect VSEP. *J. Clin. Neurophysiol.* 31, 143–148. doi: 10.1097/WNP.0000000000000038

Hansen, N. L., and Nielsen, J. B. (2004). The effect of transcranial magnetic stimulation and peripheral nerve stimulation on corticomuscular coherence in humans. *J. Physiol.* 561(Pt 1), 295–306. doi: 10.1113/jphysiol.2004.071910

Helmers, S. L., Begnaud, J., Cowley, A., Corwin, H. M., Edwards, J. C., Holder, D. L., et al. (2012). Application of a computational model of vagus nerve stimulation. *Acta Neurol. Scand.* 126, 336–343. doi: 10.1111/j.1600-0404.2012.01656.x

Herrmann, C. S., Munk, M. H. J., and Engel, A. K. (2004). Cognitive functions of gamma-band activity: Memory match and utilization. *Trends Cogn. Sci.* 8, 347–355. doi: 10.1016/j.tics.2004.06.006

Hyvarinen, P., Yrttiaho, S., Lehtimaki, J., Ilmoniemi, R. J., Makitie, A., Ylikoski, J., et al. (2015). Transcutaneous Vagus Nerve Stimulation Modulates Tinnitus-Related Beta-and Gamma-Band Activity. *Ear Hear.* 36, e76–e85. doi: 10.1097/AUD.0000000000000123

Jensen, O., Kaiser, J., and Lachaux, J. P. (2007). Human gamma-frequency oscillations associated with attention and memory. *Trends Neurosci.* 30, 317–324. doi: 10.1016/j.tins.2007.05.001

Kaniusas, E., Kampusch, S., Tittgemeyer, M., Panetsos, F., Gines, R. F., Papa, M., et al. (2019). Current directions in the auricular vagus nerve stimulation I – A physiological perspective. *Front. Neurosci.* 13:854. doi: 10.3389/fnins.2019.00854

Keute, M., Machetanz, K., Berelidze, L., Guggenberger, R., and Gharabaghi, A. (2021). Neuro-cardiac coupling predicts transcutaneous auricular vagus nerve stimulation effects. *Brain Stimul.* 14, 209–216.

Kibleur, A., Pellissier, S., Sinniger, V., Robert, J., Gronlier, E., Clarençon, D., et al. (2018). Electroencephalographic correlates of low-frequency vagus nerve stimulation therapy for Crohn's disease. *Clin. Neurophysiol.* 129, 1041–1046. doi: 10.1016/j.clinph.2018.02.127

Kilner, J. M., Mattout, J., Henson, R., and Friston, K. J. (2005). Hemodynamic correlates of EEG: A heuristic. *Neuroimage.* 28, 280–286. doi: 10.1016/j.neuroimage.2005.06.008

Kraus, T., Kiess, O., Hösl, K., Terekhin, P., Kornhuber, J., and Forster, C. (2013). CNS BOLD fMRI effects of sham-controlled transcutaneous electrical nerve stimulation in the left outer auditory canal - A pilot study. *Brain Stimul.* 6, 798–804. doi: 10.1016/j.brs.2013.01.011

Leutzow, B., Lange, J., Gibb, A., Schroeder, H., Nowak, A., Wendt, M., et al. (2013). Vagal sensory evoked potentials disappear under the neuromuscular block - An experimental study. *Brain Stimul.* 6, 812–816. doi: 10.1016/j.brs.2013.03.005

Leutzow, B., Nowak, A., and Usichenko, T. I. (2014). On the origin of scalp responses - A comment on the letter of polak et al. *Brain Stimul.* 7, 625–626. doi: 10.1016/j.brs.2014.05.006

Machetanz, K., Berelidze, L., Guggenberger, R., and Gharabaghi, A. (under review). Transcutaneous auricular vagus nerve stimulation and heart rate variability: systematic analysis of parameters and targets. *Under rev.*

Mahadi, K. M., Lall, V. K., Deuchars, S. A., and Deuchars, J. (2019). Cardiovascular autonomic effects of transcutaneous auricular nerve stimulation via the tragus in the rat involve spinal cervical sensory afferent pathways. *Brain Stimul.* 12, 1151–1158. doi: 10.1016/j.brs.2019.05.002

Marrosu, F., Santoni, F., Puligheddu, M., Barberini, L., Maleci, A., Ennas, F., et al. (2005). Increase in 20-50 Hz (gamma frequencies) power spectrum and synchronization after chronic vagal nerve stimulation. *Clin. Neurophysiol.* 116, 2026–2036. doi: 10.1016/j.clinph.2005.06.015

Munoz, M. L., Van Roon, A., Riese, H., Thio, C., Oostenbroek, E., Westrik, I., et al. (2015). Validity of (Ultra-)Short recordings for heart rate variability measurements. *PLoS One.* 10:e0138921. doi: 10.1371/journal.pone.0138921

Patron, E., Mennella, R., Messerotti Benvenuti, S., and Thayer, J. F. (2019). The frontal cortex is a heart-brake: Reduction in delta oscillations is associated with heart rate deceleration. *Neuroimage.* 188, 403–410. doi: 10.1016/j.neuroimage.2018.12.035

Percival, D. B., and Walden, A. T. (1993). *Spectral Analysis for Physical Applications: Multitaper and Conventional Univariate Techniques*. Cambridge: Cambridge University Press, doi: 10.1017/cbo9780511622762

Peuker, E. T., and Filler, T. J. (2002). The nerve supply of the human auricle. *Clin. Anat.* 15, 35–37. doi: 10.1002/ca.1089

Polak, T., Metzger, F. G., Deckert, J., and Fallgatter, A. J. (2014). Central neural versus peripheral muscular origin of vagus somatosensory - Evoked potentials. *Brain Stimul.* 7, 624–625. doi: 10.1016/j.brs.2014.04.003

Redgrave, J., Day, D., Leung, H., Laud, P. J., Ali, A., Lindert, R., et al. (2018). Safety and tolerability of Transcutaneous Vagus Nerve stimulation in humans; a systematic review. *Brain Stimul.* 11, 1225–1238. doi: 10.1016/j.brs.2018.08.010

Ruiz Vargas, E., Sörös, P., Shoemaker, J. K., and Hachinski, V. (2016). Human cerebral circuitry related to cardiac control: A neuroimaging meta-analysis. *Ann. Neurol.* 79, 709–716. doi: 10.1002/ana.24642

Sclocco, R., Garcia, R. G., Kettner, N. W., Isenburg, K., Fisher, H. P., Hubbard, C. S., et al. (2019). The influence of respiration on brainstem and cardiovagal

response to auricular vagus nerve stimulation: A multimodal ultrahigh-field (7T) fMRI study. *Brain Stimul.* 12, 911–921. doi: 10.1016/j.brs.2019.02.003

Shaffer, F., and Ginsberg, J. P. (2017). An Overview of Heart Rate Variability Metrics and Norms. *Front. Public Heal.* 5:258. doi: 10.3389/fpubh.2017.00258

Shoemaker, J. K., Norton, K. N., Baker, J., and Luchyshyn, T. (2015). Forebrain organization for autonomic cardiovascular control. *Auton. Neurosci. Basic Clin.* 188, 5–9. doi: 10.1016/j.autneu.2014.10.022

Silvani, A., Calandra-Buonaura, G., Dampney, R. A. L., and Cortelli, P. (2016). Brain-heart interactions: Physiology and clinical implications. *Philos. Trans. R. Soc. A Math. Phys. Eng. Sci.* 374, 20150181. doi: 10.1098/rsta.2015.0181

Thayer, J. F., Åhs, F., Fredrikson, M., Sollers, J. J., and Wager, T. D. (2012). A meta-analysis of heart rate variability and neuroimaging studies: Implications for heart rate variability as a marker of stress and health. *Neurosci. Biobehav. Rev.* 36, 747–756. doi: 10.1016/j.neubiorev.2011.11.009

Tu, Y., Fang, J., Cao, J., Wang, Z., Park, J., Jorgenson, K., et al. (2018). A distinct biomarker of continuous transcutaneous vagus nerve stimulation treatment in major depressive disorder. *Brain Stimul.* 11, 501–508. doi: 10.1016/j.brs.2018.01.006

Vollmer, M. (2015). "A robust, simple and reliable measure of heart rate variability using relative RR intervals," in *2015 Computing in Cardiology Conference (CinC)*, (Nice), 609–612. doi: 10.1109/CIC.2015.7410984

Warren, C. M., Tona, K. D., Ouwerkerk, L., van Paridon, J., Poletiek, F., van Steenbergen, H., et al. (2019). The neuromodulatory and hormonal effects of transcutaneous vagus nerve stimulation as evidenced by salivary alpha amylase, salivary cortisol, pupil diameter, and the P3 event-related potential. *Brain Stimul.* 12, 635–642. doi: 10.1016/j.brs.2018.12.224

Willoughby, J. O., Fitzgibbon, S. P., Pope, K. J., Mackenzie, L., Medvedev, A. V., Clark, C. R., et al. (2003). Persistent abnormality detected in the non-ictal electroencephalogram in primary generalised epilepsy. *J. Neurol. Neurosurg. Psychiatry*. 74, 51–55. doi: 10.1136/jnnp.74.1.51

Yakunina, N., Kim, S. S., and Nam, E.-C. C. (2016). Optimization of Transcutaneous Vagus Nerve Stimulation Using Functional MRI. *Neuromodulation Technol. Neural Interface* 20, 290–300. doi: 10.1111/ner.12541

Conflict of Interest: The authors declare that the research was conducted in the absence of any commercial or financial relationships that could be construed as a potential conflict of interest.

frontiers in Neuroscience

REVIEW
published: 22 March 2021
doi: 10.3389/fnins.2021.650971

Therapeutic Potential of Vagus Nerve Stimulation for Inflammatory Bowel Diseases

Bruno Bonaz[1,2], Valérie Sinniger[1,2] and Sonia Pellissier[3†]*

[1] Division of Hepato-Gastroenterology, Centre Hospitalier Universitaire Grenoble Alpes, Grenoble, France, [2] Grenoble Institute of Neurosciences, Inserm U1216, University Grenoble Alpes, Grenoble, France, [3] Laboratoire Inter-Universitaire de Psychologie Personnalité, Cognition, Changement Social, University Grenoble Alpes, University Savoie Mont Blanc, Grenoble, France

The vagus nerve is a mixed nerve, comprising 80% afferent fibers and 20% efferent fibers. It allows a bidirectional communication between the central nervous system and the digestive tract. It has a dual anti-inflammatory properties via activation of the hypothalamic pituitary adrenal axis, by its afferents, but also through a vago-vagal inflammatory reflex involving an afferent (vagal) and an efferent (vagal) arm, called the cholinergic anti-inflammatory pathway. Indeed, the release of acetylcholine at the end of its efferent fibers is able to inhibit the release of tumor necrosis factor (TNF) alpha by macrophages via an interneuron of the enteric nervous system synapsing between the efferent vagal endings and the macrophages and releasing acetylcholine. The vagus nerve also synapses with the splenic sympathetic nerve to inhibit the release of TNF-alpha by splenic macrophages. It can also activate the spinal sympathetic system after central integration of its afferents. This anti-TNF-alpha effect of the vagus nerve can be used in the treatment of chronic inflammatory bowel diseases, represented by Crohn's disease and ulcerative colitis where this cytokine plays a key role. Bioelectronic medicine, via vagus nerve stimulation, may have an interest in this non-drug therapeutic approach as an alternative to conventional anti-TNF-alpha drugs, which are not devoid of side effects feared by patients.

Keywords: cholinergic anti-inflammatory pathway, heart rate variability, inflammatory bowel diseases, TNF, vagus nerve, vagus nerve stimulation

OPEN ACCESS

Edited by:
Helio Cesar Salgado, University of São Paulo, Brazil

Reviewed by:
Valentin A. Pavlov, Northwell Health, United States
Davide Martelli, University of Bologna, Italy
Ulf Andersson, Karolinska Institutet (KI), Sweden

****Correspondence:***
Bruno Bonaz
BBonaz@chu-grenoble.fr

†ORCID:
Sonia Pellissier
orcid.org/0000-0002-0033-2561

Specialty section:
This article was submitted to Autonomic Neuroscience, a section of the journal Frontiers in Neuroscience

Received: *08 January 2021*
Accepted: *01 March 2021*
Published: *22 March 2021*

Citation:
Bonaz B, Sinniger V and Pellissier S (2021) Therapeutic Potential of Vagus Nerve Stimulation for Inflammatory Bowel Diseases. Front. Neurosci. 15:650971. doi: 10.3389/fnins.2021.650971

INTRODUCTION

The vagus nerve, cited as the pneumogastric nerve or 10th cranial nerve, although referred in the singular is paired (right and left VN). It is the longest nerve in the body, extending from the

Abbreviations: ACh, acetylcholine; α7nAChR, alpha7 nicotinic ACh receptor; ACTH, adrenocorticotropic hormone; ANS, autonomic nervous system; CAN, central autonomic network; CAP, cholinergic anti-inflammatory pathway; CD, Crohn's disease; CNS, central nervous system; CRF, corticotrophin-releasing factor; CRP, C-reactive protein; DMNV, dorsal motor nucleus of the vagus; DSS, dextran sulfate sodium; HPA, hypothalamic pituitary adrenal; HRV, heart rate variability; IL, interleukin; IBD, inflammatory bowel diseases; LC, locus coeruleus; LPS, lipopolysaccharides; MDD, major depressive disorder; NE, norepinephrine; NTS, nucleus of the solitary tract; PVH, paraventricular nucleus of the hypothalamus; ta-VNS, transcutaneous auricular vagus nerve stimulation; TNBS, trinitrobenzensulfonic; TNF, tumor necrosis factor; UC, ulcerative colitis; VN, vagus nerve; VNS, vagus nerve stimulation.

medulla oblongata to the digestive tract. The VN is a mixed nerve containing afferent (sensory) and efferent (motor) nerve fibers. It ensures the innervation of many organs such as the pharynx, larynx, thoracic viscera (heart and lungs) and the digestive tract from the esophagus to the recto-colon. The VN is the main component of the cranial parasympathetic nervous system. The other parasympathetic component is represented by the sacral parasympathetic nucleus (S2–S4) at the origin of the pelvic nerves that provide innervation to the pelvic organs such as the bladder, genitals, and left recto-colon. These two components are part of the ANS (Langley, 1921) comprising the sympathetic and parasympathetic systems, which are classically antagonistic. Due to its mixed character, the VN ensures a bidirectional communication between the CNS and the viscera, in particular the digestive tract in the context of the brain–gut axis (Bonaz et al., 2017a). This reciprocal relationship ensures an integrated and coordinated functioning of digestive functions such as motility, sensitivity, secretion, permeability, immunity. The functioning of the digestive tract is most often unconscious (i.e., not perceived) but can, under certain conditions, become pathological (i.e., perceived as painful). Therapies targeting the VN, whether drugs, nutritional, complementary medicines, or using VN stimulation (VNS), known as Bioelectronic Medicine, could be used in the management of gastrointestinal disorders (Bonaz et al., 2017b). Bioelectronic medicine is based on neuromodulation of the nervous system restoring organ functions and health with less adverse effects than drugs, thus minimizing adherence issues (Olofsson and Tracey, 2017). In particular, due to its anti-inflammatory role, the VN could be used as a non-drug therapy in chronic IBD represented by CD and UC (Bonaz et al., 2016b). Indeed, the VN exerts a dual anti-inflammatory effect: both through its afferents, by stimulating the HPA axis and the release of glucocorticoids from the adrenal glands, and its efferents, through the CAP, more recently described.

FUNCTIONAL NEUROANATOMY OF THE VAGUS NERVE

The VN runs from the brainstem through the neck to many peripheral organs, including the lungs, heart, liver, stomach, intestines. The VN is a mixed nerve consisting of 80% afferent fibers, carrying information from the digestive tract to the CNS, and 20% efferent fibers involved in the control of gastrointestinal functions (Prechtl and Powley, 1990), as well as heart and lungs. Thus, the VN is a major component of the bidirectional communication between the brain and the gut through the brain–gut axis. We will now discuss only the GI functions of the VN.

Vagal Afferent Fibers

Vagal afferents inform the CNS, usually unconsciously, of the functional state of the gastrointestinal tract. These afferents originate from free endings in the different layers of the gut wall, including in the external muscle layers, myenteric plexus, and mucosal lamina propria and travel through the VN to the nucleus tractus solitarius (NTS) according to a viscerotopic distribution (Powley et al., 2019). The NTS, the main entry point of the digestive tract into the brain, is located in the medulla, just above the DMNV which is at the origin of vagal efferent fibers with the nucleus ambiguus (Jean, 1991). Thus, the NTS and the DMNV are closely connected. In fact, the dendrites of vagal motor neurons are connected with vagal afferents ending in the NTS, at the origin of vago-vagal reflex loops (**Figure 1**) (Travagli et al., 2006; Bonaz et al., 2019). Vagal afferent cell bodies are located in the nodose ganglia or jugular ganglia, at the base of the skull. Peripheral stimuli, via vagal afferents ending in the NTS, are transmitted to many regions of the CNS through projections of the NTS onto structures such as the parabrachial nucleus, an important sensory relay of the NTS, the hypothalamus, in particular the PVH, the limbic system including the amygdala, thalamus, hippocampus, and cerebral cortex including the insula and the prefrontal cortex (Norgren, 1978; Sawchenko, 1983; Cechetto, 1987). These different structures are part of the CAN described by Benarroch (1993). The CAN is at the origin of autonomic, behavioral, cognitive, and endocrine responses. It is capable of modulating the functioning of the ANS via descending pathways projecting onto sympathetic pre-ganglionic neurons in the spinal cord and onto the DMNV at the origin of vagal efferents. Vagal afferents are involved in detecting the presence of nutrients and their chemical composition in the digestive tract in the post-prandial period. They contain chemoreceptors, thermoreceptors, osmoreceptors, mechanoreceptors as opposed to afferent spinal fibers which essentially vehiculates pathways of visceral pain of digestive origin to the spinal cord (Berthoud and Neuhuber, 2000). Most of the nervous information coming from the viscera is not conscious but can become so in pathological conditions, particularly inflammatory. The VN is a major component of the pathways of interoception which is the sense of the body's internal physiological state (Craig, 2002), and interoceptive abnormalities are implicated in the pathophysiology of psychiatric disorders, neurodegenerative and neurological disorders, as well as in somatic disorders of brain-body interactions, including functional digestive disorders and IBD (Fournier et al., 2020; Bonaz et al., 2021).

Vagal Efferent Fibers

These fibers originate at the level of the medulla oblongata, from pre-ganglionic neurons located in the DMNV and travel through the VN toward the viscera synapsing with a second post-ganglionic neuron located in the target organ, namely the digestive wall. In the digestive tract, this second order neuron is an integral part of the enteric (or intrinsic) nervous system, a real "second brain" or "gut brain," able to ensure motor and secretory autonomy of the digestive tract (Furness et al., 2014). It is classically stated that the VN innervates the entire digestive tract up to the splenic angle (Netter, 1989). However, for others, it innervates the entire digestive tract in humans (Delmas and Laux, 1933) as well as in rats (Altschuler et al., 1993). The pelvic nerves classically innervate the left colon and the rectum as well as the bladder and genital organs. The sacral (S2–S4) parasympathetic nucleus is under the control of the Barrington's nucleus, also called the pontine micturition center (Valentino et al., 1999), which lies adjacent to, and interacts with the LC,

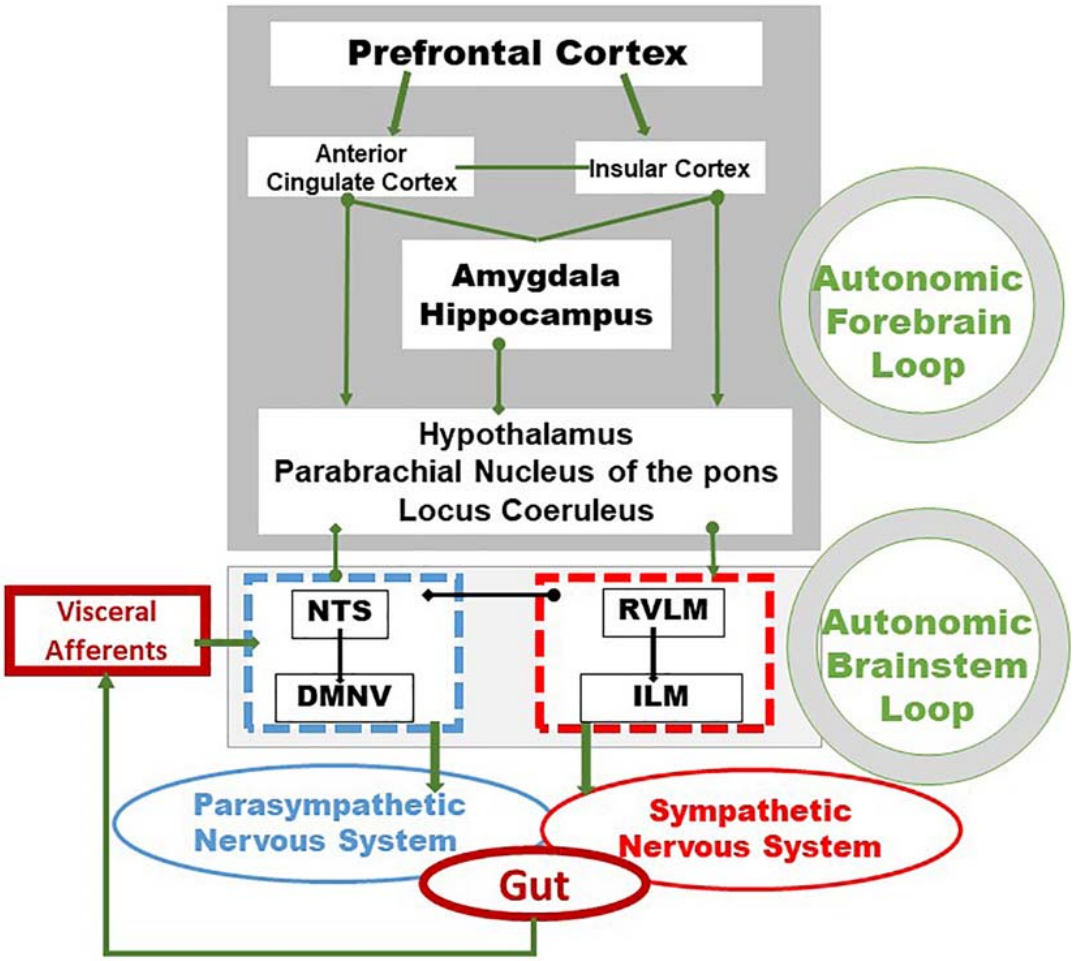

FIGURE 1 | Integrative pathways of the brain–gut axis. Vagal and splanchnic digestive afferents connect to the nucleus tractus solitarius, in close relationship with the dorsal motor nucleus of the vagus, from which vagal efferents originate, thus composing an autonomic loop of the brainstem, involved in the regulation of instinctual motility, acid secretion, food intake and satiety. This loop is modulated by the autonomic loop comprising the hypothalamus, the hippocampus, the amygdala, the anterior cingulate and the insular and prefrontal cortex. This last loop receives, coordinates and integrates visceral information enabling neuroendocrine, emotional, cognitive and behavioral responses. These two central loops explain how stress, sensations and thoughts can influence the functioning of the intestine and vice versa. Adapted from Bonaz et al. (2019). DMNV, dorsal motor nucleus of the vagus nerve; ILM, intermediolateralis nucleus; NTS, nucleus tractus solitarius; RVLM, rostral ventrolateral medulla.

the brain's principle noradrenergic projection center, involved in arousal, stress, autonomic function, cognition, and behavior (Benarroch, 2018). The neurotransmitter of the vagal and pelvic parasympathetic system is ACh for pre- and post-ganglionic neurons acting on nicotinic receptors at the pre-ganglionic level and muscarinic receptors at the post-ganglionic level.

Parasympathetic innervation of the gut is involved in the neuroimmune regulation of intestinal barrier through the recruitment of α7 nicotinic ACh receptor (α7nAChRs). It acts on enteroglial cells, interacting with innate immune cells (Fornai et al., 2018), myenteric neurons, making synaptic contacts with resident macrophage expressing α7nAChR. Vagal afferent fibers penetrate to the tips of jejunal villi and some of these nerves make intimate contact with intestinal mucosal mast cells. These data provide the microanatomical basis for direct neural communication between the CNS and mast cells in the gastrointestinal mucosa (Williams et al., 1997). Overall, the stimulation of vagal efferents could obviously "activate" these different gut cells and be one of the component of the CAP.

INFLAMMATORY BOWEL DISEASES

Inflammatory bowel diseases are organic diseases classically divided in CD and UC. CD can involve all the digestive tract, from the mouth to the anus, while UC involves the recto-colon only. IBD start early in life (between 15 and 30 years) and evolve by periods of flares alternating with periods of remission of variable duration (Chang, 2020). Symptoms are represented by abdominal pain, diarrhea, fever, weight loss, and extra-intestinal (skin, eyes, joints) manifestations. About 1.5 million Americans and 2.2 million people in Europe are

affected by IBD. There is a rising incidence of IBD in Western countries, supporting the hypothesis that "Westernization" of our lifestyle has led to the increased incidence and prevalence of IBD (Molodecky et al., 2012).

The pathophysiology of IBD is multifactorial involving genetic, immunologic, infectious and environmental factors (Chang, 2020). The theory is that genetically susceptible individuals experience an environmental trigger(s), resulting in an inappropriate immune response, potentially against gut microbes. Stress, through brain–gut interactions, as well as environmental factors, based on experimental and clinical data (Bonaz and Bernstein, 2013), has been proposed as a contributor. An imbalance of the ANS is observed in IBD, represented by a sympathetic dysfunction in CD (Lindgren et al., 1991) and a vagal dysfunction in UC (Lindgren et al., 1993). We have recently reported that this dysautonomia may be dependent on psychological adjustment in IBD. Indeed, the equilibrium of the ANS is differentially adapted according to the disease. This equilibrium is conjugated with positive affective and cognitive adjustment in IBD (Pellissier et al., 2010). Presently, there is no treatment to cure IBD. Current treatments suppress disease activity and there is generally a relapse of the disease after discontinuation of the treatment. TNF is a key cytokine that is involved in IBD and anti-TNF therapies have transformed the management of IBD (Peyrin-Biroulet, 2010). New compounds targeting other pro-inflammatory cytokines, such as IL-12, IL-23, anti-integrin therapies, and anti-Janus kinase (JAK) are available (Pagnini et al., 2019; D'Amico et al., 2020). Surgery is an alternative to a failure of treatment or a complication of IBD (perforation, abscess, stenosis) but the disease recurs after surgery. Anti-TNF therapies used in IBD have been shown to be effective but there is a 20–30% primary non-response rate (Ford et al., 2011) and the annual risk of loss of response to anti-TNF is 13% per patient-year for Infliximab (Gisbert and Panes, 2009) and 20% per patient-year for Adalimumab (Billioud et al., 2011). This secondary non-response is due to (i) the development of autoantibodies, in particular for Infliximab which is a chimeric molecule (75% human and 25% mouse), but also for Adalimumab (100% human) to a lesser degree, or (ii) a secondary failure of a well-dosed or under-dosed treatment using therapeutic drug monitoring (Ben-Horin and Chowers, 2011; Chaparro et al., 2012). Anti-TNF treatment currently represents the bulk of the cost of IBD treatment (van der Valk et al., 2014). Indeed, the median cost of a 1-year anti-TNF therapy raises up to $40,000 for CD patients (Targownik et al., 2019). In addition, biological therapies are not devoid of numerous side effects with a major impact on the patient's quality of life (Kerbleski and Gottlieb, 2009; Pereira et al., 2015; Murdaca et al., 2016). As a result, by fear of these side effects and the need for chronic treatment of these pathologies, patients are increasingly reluctant to take these treatments and to continue them once they are in remission. This explains, in particular, the 30–50% of non-adherence (Chan et al., 2017) and the growing interest of the patients for complementary medicines (Torres et al., 2019).

Consequently, a treatment targeting pro-inflammatory cytokines such as TNF-alpha and others, exploiting the CAP, with few side effects, devoid of problem of compliance, and cheaper than biologicals (i.e., anti-TNF-alpha) would be of great value. In this context, targeting the anti-inflammatory properties of the VN would be of interest (**Figure 2**). In particular, VNS, as a non-drug therapy could serve as an alternative to classical biological therapies. We have shown recently that there is a specific homeostatic link between vagal tone and TNF-alpha in CD patients since a low vagal tone was associated with a high level of TNF in the plasma (Pellissier et al., 2014). In addition, since stress is classically known to stimulate the sympathetic nervous system, which has a pro-inflammatory effect, and to inhibit the VN (Wood and Woods, 2007), and thus the CAP, VNS may help to restore an equilibrium of the sympatho-vagal balance.

ANTI-INFLAMMATORY PROPERTIES OF THE VAGUS NERVE

The VN has a double anti-inflammatory effect both via its afferents and efferents (Bonaz and Bernstein, 2013; Bonaz et al., 2017a).

Anti-inflammatory Properties of Vagal Afferents

The VN is a key element of the neuro-endocrine immune axis whose purpose is to ensure a homeostasis balance. The peripheral release of pro-inflammatory cytokines such as IL-1beta, IL-6, and TNF, activates vagal afferents via their interaction with receptors on the para-nodes (Goehler et al., 1997) (**Figure 2**). Zanos et al. (2018) have very recently shown that electrical signals recorded on the cervical VN can be decoded to discriminate between cytokine-specific signals. In animals, the induction of a septic shock by systemic or intraperitoneal injection of LPS, components of the wall of Gram-negative bacteria, leads to the release of these cytokines by blood and/or tissue macrophages, which in turn activates vagal afferents leading to fever, sleep and aphagia (Dantzer et al., 1998). This signal activates the HPA axis after being integrated at the level of the NTS and then transmitted to the hypothalamus via projections to the PVH, more particularly on CRF neurons, the main neuro-mediator of stress, located in the parvocellular zone of the PVH (Rivest et al., 2000) (**Figure 2**). These CRF neurons project themselves into the pituitary gland, whose activation will release ACTH that will stimulate the release of glucocorticoids (cortisol) by the adrenal glands with well-known anti-inflammatory properties. Most of neuromodulation studies focus on vagal regulation of inflammation via the peripheral efferent pathway toward the viscera. However, abdominal vagal afferent neurostimulation suppresses systemic inflammation in rats, and the efferent neural pathway for this action is in the splanchnic sympathetic nerves (Komegae et al., 2018). Vagal stimulation also modulates arthritic joint inflammation through an afferent pathway mediated by the LC where central stimulation is followed by activation of joint sympathetic nerve terminals releasing NE. The vagal control of arthritic joint inflammation is dampened by selective adrenergic beta-blockers. These results reveals a novel neuro-immune brain map with afferent vagal signals controlling side-specific articular

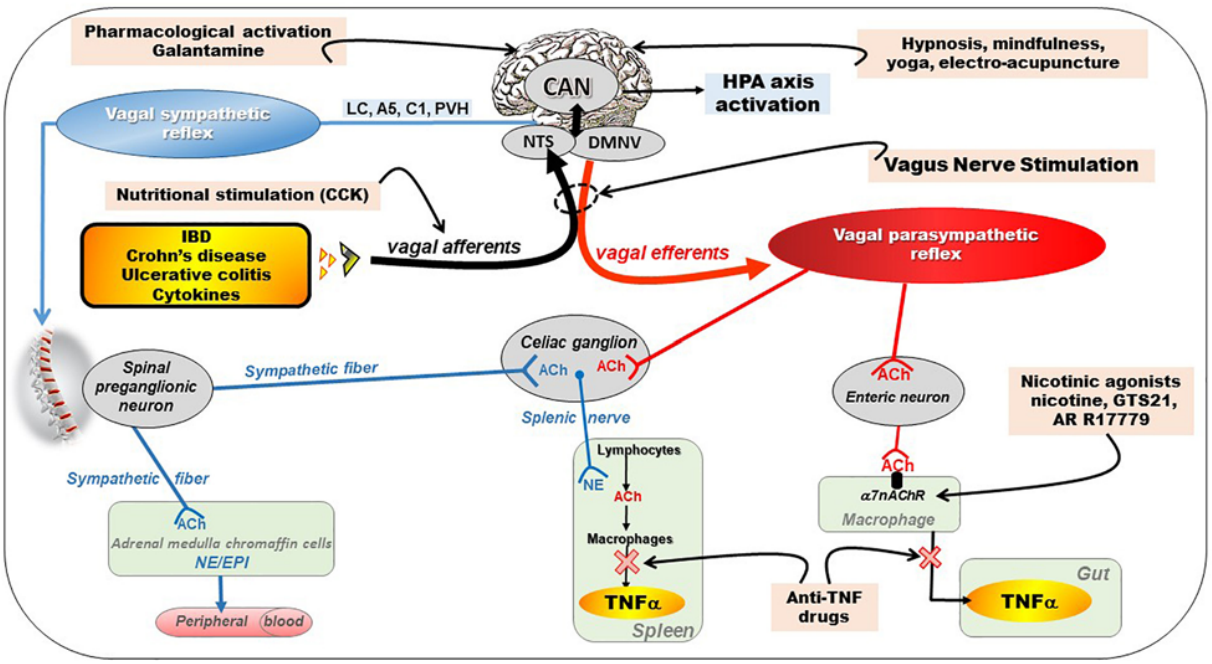

FIGURE 2 | Different pathways of the anti-inflammatory properties of the vagus nerve: (1) through activation of the HPA axis via vagal afferents and through vago-parasympathetic efferents (red), (2) through sympathetic efferents (blue) arising from thoraco-lumbar spinal preganglionic neurons through the vago-sympathetic pathway where vagal afferents activate central descending pathways (e.g., LC, A5, C1, PVH) targeting spinal pre-ganglionic neurons. Targeting the VN for its anti-inflammatory properties (pink) in chronic inflammatory diseases (orange) such as inflammatory bowel diseases appears as potentially effective therapeutics. Adapted from Bonaz et al. (2017a). A5, A5 noradrenergic group (in the brainstem); ACh, acetylcholine; C1, C1 adrenergic group (in the brainstem); CAN, central autonomic network; CCK, cholecystokinin; DMNV, dorsal motor nucleus of the vagus nerve; EPI, epinephrine; HPA, hypothalamic–pituitary–adrenal; IBD, inflammatory bowel diseases; LC, locus coeruleus; NE, norepinephrine; NTS, nucleus tractus solitarius; PVH, paraventricular nucleus of the hypothalamus; TNFα, tumor necrosis factor-alpha; α7nAChR, alpha7nicotinic acetylcholine receptor.

inflammation through specific inflammatory-processing brain centers and joint sympathetic innervations (Bassi et al., 2017).

Anti-inflammatory Properties of Vagal Efferents

In 2000, Kevin Tracey's team described, for the first time, the CAP (Borovikova et al., 2000; Pavlov et al., 2003). This group showed that a septic shock in rats, induced by iv injection of LPS, was prevented by low frequency neurostimulation of the distal end cut of the VN thus stimulating vagal efferents (Borovikova et al., 2000). The authors concluded that there was an inflammatory reflex in which stimulation of vagal afferents by pro-inflammatory cytokines resulted in activation of vagal efferents that inhibited the release of these cytokines by tissue macrophages, in particular TNF but also other proinflammatory cytokines such as IL6, IL1β but not the anti-inflammatory cytokine IL-10. The VN has therefore anti-inflammatory properties through the inhibition of pro-inflammatory cytokines (**Figure 2**). This group also characterized the cholinergic receptor of macrophages involved in this effect, which was not muscarinic but α7nAChR. Indeed, the effect of VNS was abolished in animals knock out for this receptor (Wang et al., 2003). Intracellular mechanisms downstream of α7nAChR activate the JAK2–signal transducer and activator of transcription 3 pathway, sequester Nuclear Factor-kB (NF-κB), and inhibit activation of the inflammasome (Guarini et al., 2003; de Jonge et al., 2005; Lu et al., 2014). This anti-TNF effect of the VN has, of course, therapeutic applications in pathologies where this cytokine is involved such as IBD. However, this effect of the VN is not direct via vagal efferent endings on macrophages but indirect through the interaction of the VN with nNOS, VIP and ChAT enteric neurons located within the gut muscularis with nerve endings in close proximity of the resident macrophages (Cailotto et al., 2014). Tracey's group also showed that the spleen, an important source of ACh, where it was first isolated, and TNF in the body, was also involved in the anti-inflammatory effect of the VN. This effect involves a connection between vagal efferent endings and the spleen (Rosas-Ballina et al., 2008), through the celiac sympathetic ganglion, inducing the release of NE by noradrenergic endings in the spleen (**Figure 2**). They recently showed that cholinergic neurons in the DMNV, which project to the celiac superior mesenteric ganglia, significantly increase splenic nerve activity and inhibit TNF production (Kressel et al., 2020). So there is a vago-sympathetic excitatory pathway while the VN and the sympathetic nervous system have generally antagonistic effects. Indeed, NE acts on beta2 receptors of splenic lymphocytes to release ACh by these lymphocytes: this is the non-neuronal cholinergic pathway by opposition to the neuronal (i.e., vagal) cholinergic pathway (**Figure 2**). ACh

then binds to α7nAChR of splenic macrophages to inhibit the release of TNF by these macrophages (Olofsson et al., 2012). These activated T lymphocytes do not just inhibit macrophages locally. They may also move and behave like "mobile neurons" and downregulate inflammation in areas not innervated by the VN. The characteristics of these CHAT-containing T cells have been well outlined by the Tracey's group (Rosas-Ballina et al., 2011; Olofsson et al., 2016). However, the innervation of the spleen by the VN via this interaction with the splenic nerve is questioned by some authors, notably by the work of Martelli et al. (2014). For this author, the efferent anti-inflammatory pathway is not the VN but the sympathetic system, notably the splanchnic sympathetic nerve and its anti-inflammatory effect is distributed across abdominal organs (Martelli et al., 2019). The sympathetic nervous system originates in the thoracolumbar spinal pre-ganglionic neurons (T1-L2) and synapses with post-ganglionic neurons at the origin of splanchnic sympathetic nerves distributed to the viscera, with a mirror distribution of the parasympathetic system (**Figure 2**). These pre-ganglionic spinal sympathetic neurons are under the control of central nuclei such as the PVH, Kölliker-Fuse nucleus, pontine noradrenergic groups A5, the LC (A6), the chemosensitive region of the ventral medulla, and possibly the region of the A1 catecholamine cell group (Loewy, 1981). These neural groups are part of the CAN and send descending projections to modulate these pre-ganglionic sympathetic neurons. In particular, Abe et al. (2017) showed, in an experimental model of renal inflammation, that C1 was involved in an anti-inflammatory reflex involving only the splanchnic nerve.

In fact, contrasting the vagal anti-inflammatory pathway with the splanchnic pathway is a reductive view since both pathways can act in concert to play a pivotal role in the crosstalk with the immune system, a fortiori if they are activated by VNS (Brinkman et al., 2019). In particular, because of its mixed, essentially afferent, character, the VN via its central projections on the NTS and then on the CAN is able to activate A5, A6, and C1 which will secondarily activate the splanchnic sympathetic nerves via their descending projections to the spinal cord. Our group has shown in particular that low-frequency (5Hz) VNS in rats, supposed to activate only vagal efferents, also activated vagal afferents (Reyt et al., 2010). Lomarev et al. (2002) have also shown that, compared to 5 Hz, 20 Hz VNS produced more acute activity changes from rest in regions similar to our initial VNS synchronized fMRI feasibility study in depression. There is therefore a bidirectional activation of vagal fibers by VNS, even at low frequency, involving a peripheral vagal and sympathetic action via a vago-vagal and vago-sympathetic reflex through the CNS (Bonaz et al., 2019).

THE VAGUS NERVE AT THE INTERFACE OF THE MICROBIOTA–GUT–BRAIN AXIS

The human intestine contains 10^{13} to 10^{14} microorganisms, which is much more than the cells in our body and 100 times more genes than our genome. The weight of the microbiota is about 1 kg in adults, approximately the weight of the human brain. In healthy subjects, two species of bacteria, Bacteroides and Firmicutes, dominate the bacterial composition, with smaller amounts of actinobacteria, proteobacteria and verrucomicrobia. At the species level, each individual presents a very specific signature. In addition to bacteria, the intestinal microbiota contains methanogenic archaea, eukaryotes (mainly yeasts) and numerous phages (Eckburg et al., 2005; Reyes et al., 2010). Recently, it has been shown that the microbiota, the gut, and the brain communicate via the microbiota–gut–brain axis (Cryan et al., 2019) and that a disruption of this axis is involved in the pathophysiology of neurodegenerative diseases (Cryan and Dinan, 2012; Forsythe et al., 2016). A dysbiosis is observed in various pathological conditions of the gastrointestinal tract, such as IBD (Sundin et al., 2017), and fecal transplantation is presently under investigation in clinical trials (Levy and Allegretti, 2019). However, the question is whether it is a cause or consequence of an abnormal communication between the gut and the brain. The VN is a key component of this microbiota–gut–brain axis (Bonaz et al., 2018) (**Figure 3**). Indeed, it is able to detect metabolites of the microbiota through its afferents and to transfer this intestinal information to the CAN, then generating an adapted or inappropriate response from the CAN to the intestine and the microbiota (Bonaz et al., 2018). It can also be activated indirectly by the microbiota via the interaction of the microbiota with digestive endocrine cells that will release serotonin acting on 5-HT3 receptors of vagal afferents. The VN, via the CAP, could modulate the intestinal microbiota by decreasing intestinal permeability and modulating local immunity (Bonaz et al., 2018). One can imagine that, an indicator such as HRV, easy to assess through the detection of heartbeat intervals, could be used to explore the microbiota–gut–brain axis homeostasis. Indeed, HRV is probably not a direct index of "the true" vagal tone (Marmerstein et al., 2021) since it is an indirect assessment of the parasympathetic modulation on the heart so that the metrics of the HRV would rather reflect different aspects of the neurophysiologic regulation of the heart rhythm (Reyes del Paso et al., 2013; Thomas et al., 2019). Presently, HRV is the final output of several regulatory loops resulting from afferent signals integrated at the level of the CNS influencing the efferent vagally mediated modulations on the heart (Thayer and Lane, 2009). In that way, HRV can be used to mark and follow the activity of the neurophysiological pathways involved in adaptation, homeostasis and health (Thayer et al., 2012). A recent meta-analysis underlines that HRV metrics such as the high frequency band (HF-HRV) and the standard deviation of RR intervals (SDNN) are the most robustly associated with inflammation (Williams et al., 2019). Finally, targeting the VN through VNS, even if the mechanism is not clear yet, could have therapeutic implications in the modulation of the microbiota–gut–brain axis.

STRESS AND THE VAGUS NERVE

Besides its well-known effects on gastrointestinal motility (Tache et al., 2001), stress increases intestinal permeability, modifies the intestinal flora, and intestinal immunity (Tache and Bonaz,

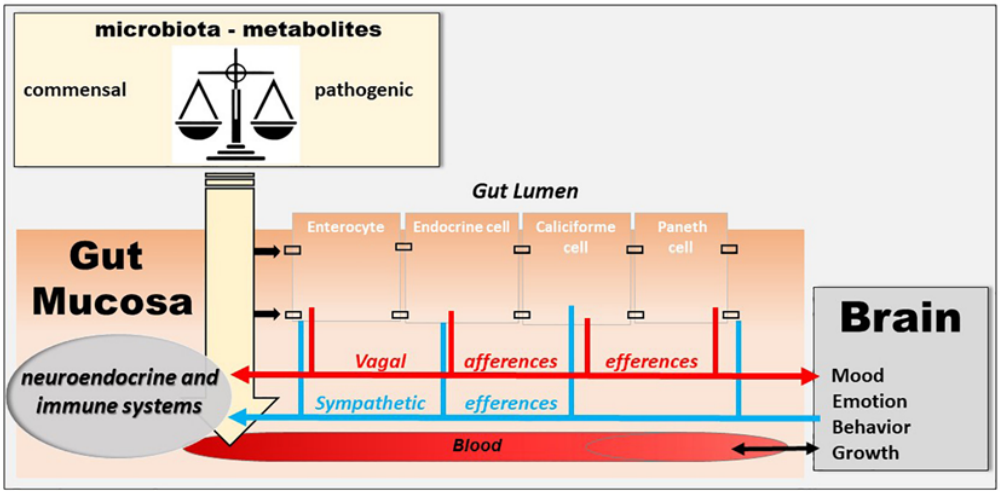

FIGURE 3 | The microbiota–gut–brain axis. The microbiota exerts an effect on the gut-brain axis, impacting the biochemistry of the peripheral and central nervous system. Commensal and/or pathogenic bacteria and their metabolites are translocated across the intestinal barrier and act on both the digestive immune system and vagal afferents. Similarly, the brain acts on the various organs, including the digestive tract, and can thus regulate the survival and proliferation of the intestinal microbiota.

2007; Larauche et al., 2009a,b). If the role of stress is well known in functional digestive disorders such as irritable bowel syndrome (Pellissier and Bonaz, 2017), recent data have shown its role in IBD (Bonaz and Bernstein, 2013). Furthermore, stress modifies the activity of the ANS. Classically, stress leads to vagal inhibition and activation of the sympathetic system, thus favoring the body's ability to cope with a "threat to its homeostasis" and in fact strengthens the defenses through the pro-inflammatory reaction (Tache and Bonaz, 2007). Any vagal hypotonia with or without sympathetic hypertonia can therefore promote an inflammatory process. In patients at the pre-rheumatoid arthritis stage, those who had vagal hypotonia developed rheumatoid arthritis more easily afterward (Roura et al., 2016). Moreover, several arguments are in favor with such a causal association in IBD. First, a low level of HRV as indexed by the RMSSD metric, at onset of newly diagnosed UC patients predicts the systemic inflammatory response over 3 years of follow-up (Gunterberg et al., 2016). Second, there is a positive association between vagotomy and later IBD, and this particularly for CD revealing the role of VN integrity in the prevention of IBD (Liu et al., 2020). Thus, we can assume that the level of vagal tone is predictive of the development of an inflammatory disorder in people at risk. We also showed in patients with CD in remission, that a low resting vagal tone correlated with elevated circulating TNF (Pellissier et al., 2014) (**Figure 4**). The systemic inflammation observed during IBD or other chronic inflammatory pathologies is capable of leading to vagal hypotonia, which in turn maintains this inflammatory state. Moreover, chronic inflammation, by its central impact, can lead to a depressive state which itself can promote an inflammatory flare-up of the disease (Mikocka-Walus et al., 2016a,b; Bullmore, 2018). Two meta-analysis have shown that the levels of proinflammatory cytokines, such as TNF, IL-6, IL-1, and CRP, increase during depressive episodes (Hiles et al., 2012; Kohler et al., 2017). Chronic infection or stress may inhibit the negative feedback of the HPA axis, triggers the activation of microglia in the brain, and increases the permeability of the blood–brain barrier, resulting in excessive activation of proinflammatory cytokines (Song and Wang, 2011). Increased proinflammatory cytokines may cause MDD by activating the HPA axis, which results in a depletion of serotonin with an increased activity of the indoleamine-2,3-dioxygenase enzyme in the tryptophan–kynurenine system (Schiepers et al., 2005). Anti-inflammatory agents improve depressive symptoms compared to placebo as add-on in MDD patients and as monotherapy (Köhler-Forsberg et al., 2019). There is a link between depression and inflammation as a vicious circle: depression promotes inflammation and vice-versa. Depression increases the risk of IBD, which may be mitigated by the use of anti-depressants in the treatment of depression (Frolkis et al., 2019). Recently, it has been shown that individuals with IBD have a higher prevalence of depression than matched controls as early as 9 years before diagnosis (Blackwell et al., 2020). Depression in the absence of prior gastrointestinal symptoms was not associated with a future diagnosis of IBD but those patients with depression diagnosed after already experiencing gastrointestinal symptoms are at increased risk of later being diagnosed with IBD. The excess prevalence of depression prior to a diagnosis of IBD may be a consequence of diagnostic delay and untreated gastrointestinal symptoms. Antidepressant drugs have also shown a definite interest in the management of IBD (Macer et al., 2017). Therefore, any therapy, whether drug-based or not such as VNS, capable of restoring vagal activity, has a potential interest in IBD, but also in other chronic non-digestive inflammatory pathologies such as depression. There is a reduced HRV in depression with a high risk of cardiovascular disease (Sgoifo et al., 2015). Recently, it has been shown that transcranial direct current stimulation as an adjunct therapy is effective in alleviating unipolar and bipolar depression.

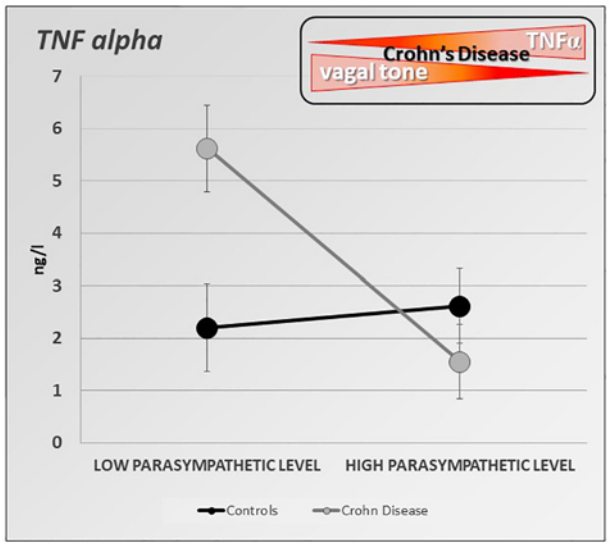

FIGURE 4 | Specific inverse relationship between the resting parasympathetic vagal tone and TNF-alpha plasma level in Crohn's disease (CD) patients. CD patients with high parasympathetic vagal tone exhibit a lower level of TNF-alpha than those with low parasympathetic vagal tone. Parasympathetic vagal tone was assessed by power spectral analysis of HRV and TNF-alpha level was assessed by ELISA-based technic. Data expressed as mean ± sem (adapted from Pellissier et al., 2014).

Moreover, the amplitude of the increase in parasympathetic signaling, as indexed by the RR interval lengthening, during the first session, predicts the clinical response after 10-sessions (Lin et al., 2021).

HOW TO USE THE ANTI-INFLAMMATORY PROPERTIES OF THE VAGUS NERVE FOR THERAPEUTIC PURPOSES?

Targeting the VN for anti-inflammatory purposes can be done in different ways (Bonaz and Bernstein, 2013; Bonaz et al., 2017a) (**Figure 2**).

Pharmacological Stimulation of Alpha7 Nicotinic Receptors

Pharmacologic stimulation can be performed with α7nAChR agonists such as GTS-21, AR-R17779 which have been used in post-operative ileus models, following intestinal macrophagic activation at the origin of ileus, as well as in experimental pancreatitis (van Westerloo et al., 2006; The et al., 2007). GTS-21, is able to inhibit proinflammatory cytokines *in vitro* and *in vivo* and improve survival in murine endotoxemia and severe sepsis (Pavlov et al., 2007). Hyperoxia-induced acute lung injury is attenuated by GTS-21 by inhibiting extracellular high mobility group box 1-mediated inflammatory responses (Sitapara et al., 2020).

Nutritional Stimulation

Cholecystokinin, a satiety hormone released at the duodenal level by I cells by the arrival of fat during the meal, acts on vagal afferents receptors. Activation of these receptors by cholecystokinin stimulates vagal afferents and an inflammatory reflex via activation of the CAP. This has been demonstrated in a model of hemorrhagic shock resulting in systemic release of proinflammatory cytokines such as TNF and IL-6 and inducing intestinal permeability through a loss of intestinal barrier function. The ingestion of high-fat enteral nutrition inhibited the release of these cytokines and reduced intestinal permeability. This effect was prevented either by vagotomy or by antagonists targeting cholecystokinin receptors or α7nAChR (Luyer et al., 2005).

Fasting

Fasting has a well-known anti-inflammatory effect, especially in IBD. This effect could be conveyed by ghrelin, an orexigenic peptide released during fasting by P/D1 cells of the gastric fundus, considered to be a leptin antagonist and also known for its gastric pro-kinetic properties (Mao et al., 2015). Plasma ghrelin levels increase during fasting and decrease after ingesting glucose and lipid, but not protein. The efferent VN contributes to the fasting-induced increase in ghrelin secretion. Ghrelin secreted by the stomach stimulates vagal afferents and promotes food intake (Nonogaki, 2008). As an illustration, mice invalidated for ghrelin have a suppression of the CAP demonstrated by a reduction in VN activity and an increase in plasma levels of the pro-inflammatory cytokines IL-1beta and IL-6. This effect is prevented by the administration of ghrelin or nicotine, which activate this anti-inflammatory pathway (Mao et al., 2015). Ghrelin stimulates the VN since vagotomy dampens its effects (Zhou et al., 2020). Ghrelin protects animals from renal ischemia-reperfusion injury through the VN (Rajan et al., 2012).

Stimulation of Central Cholinergic Pathways

Galantamine, a selective acetylcholinesterase inhibitor which has shown potential for the treatment of Alzheimer's disease, is able to cross the blood–brain barrier, after peripheral administration (Metz and Pavlov, 2020). Galantamine stimulates the central cholinergic system, activates the VN and inhibits the peripheral release of TNF during endotoxic shock in animals. This effect is prevented by a centrally acting muscarinic antagonist, or in α7nAChR knockout mice (Pavlov et al., 2009). These findings show that inhibition of brain acetylcholinesterase suppresses systemic inflammation through a central muscarinic receptor-mediated and vagal- and α7nAChR-dependent mechanism. Galantamine also improves experimental colitis in mice; this effect is suppressed by vagotomy, splenectomy or splenic denervation (Ji et al., 2014). Using forebrain-selective genetic ablation of ACh release and vagotomy, selective stimulation of ACh action on the M1 muscarinic ACh receptor (M1 mAChR), as well as selective optogenetic stimulation of basal forebrain cholinergic neurons innervating brain regions with abundant M1 mAChR localization, Lehner et al. (2019) have

shown that forebrain cholinergic neurons regulate innate immune responses and inflammation. Thus, targeting forebrain cholinergic signaling should be of interest in cholinergic dysfunction diseases.

Physical Activity

Exercise reduces systemic inflammatory activity (Heffernan et al., 2009). Regular physical activity reduces the risk of developing chronic diseases involving inflammation. Its mechanism of action is not well known but it may involve the CAP, as high levels of physical activity are associated with increased vagal tone and low levels of CRP, a systemic inflammatory marker (Lujan and DiCarlo, 2013). Physical activity therefore has a potential anti-inflammatory effect in inflammatory pathologies whether used in isolation or in combination with treatment. Physical activity, by enhancing parasympathetic tone and activating the CAP, is a therapeutic strategy to restrain chronic inflammation and prevent many chronic diseases (Lujan and DiCarlo, 2013). The anti-inflammatory effect of physical activity has also been associated with an enhancement of the sympathetic output (Weippert et al., 2013).

Complementary Techniques

Hypnosis stimulates the VN as shown in the study of HRV under hypnosis; HRV decreased during hypnosis but increased post-hypnosis (Yuksel et al., 2013). The efficacy of hypnosis is well known in patients with irritable bowel syndrome and some data are available in IBD, where its use is believed to improve patients with UC (Mawdsley et al., 2008) and prolong clinical remission (Keefer et al., 2013). *Mindfulness meditation ("mindfulness")* is able of activating the VN and may have anti-inflammatory as well as anti-stress properties by increasing HRV (Azam et al., 2015; Lumma et al., 2015). There are possible effects of mindfulness meditation on specific markers of inflammation, cell-mediated immunity, and biological aging, but these results are tentative and require further replication (Black and Slavich, 2016). Regular practice of *yoga* also increases vagal tone (Tyagi and Cohen, 2016). In a model of chronic obstructive pulmonary disease, *electro-acupuncture* can reduce the lung inflammatory response and improve lung function in this model, which may be related to its involvement in the regulation of the CAP (Zhang et al., 2018).

Vagus Nerve Stimulation for Anti-inflammatory Purposes in Chronic Inflammatory Bowel Diseases

Vagus nerve stimulation is a new therapeutic pathway for TNF-mediated chronic inflammatory diseases (Bonaz et al., 2016a,b) within the framework of Bioelectronic Medicine, whose goal is to use miniaturized stimulators to administer electrical nerve signals for non-drug therapeutic purposes (Olofsson and Tracey, 2017). VNS is already approved for the treatment of drug-refractory epilepsy and depression (Bonaz et al., 2013).

Experimental Data

The first data on the anti-inflammatory effect of the VN during digestive inflammation was reported by Miceli and Jacobson (2003). They showed that prior administration of anticholinesterase drugs such as neostigmine, which does not cross the blood–brain barrier, or physostigmine, which does, improved an experimental 2,4,6-trinitrobenzene sulfonic acid (TNBS)-colitis in rats in a model mimicking CD. This effect was more convincing for physostigmine, thus in favor of a predominant central mechanism. Vagotomy aggravated experimental colitis in mice, which is in favor of the protective role of the VN (Ghia et al., 2007). However, intestine-specific vagal nerve denervation had no effect in DSS-induced colitis (Willemze et al., 2018). Our group showed, for the first time, in the non-vagotomized vigilant rat, that low frequency (5 Hz) VNS, 3 h per day for five consecutive days, resulted in an improvement of TNBS-colitis in rats (Meregnani et al., 2011). VNS reduced the degree of body weight loss and inflammatory markers as observed above the lesion by histological score and myeloperoxidase quantification. This anti-inflammatory effect was also demonstrated by the improvement of a multivariate index of colitis (including body weight, temperature and locomotor activity, macroscopic area of lesions, histological, and biological parameters such as myeloperoxidase activity, cytokine and cytokine-related mRNAs). We have also shown that low-frequency stimulation (5 Hz), supposed to stimulate vagal efferents, also stimulated vagal afferents, as demonstrated in a brain imaging (MRI) study in rats where low-frequency neurostimulation led to deactivation in the NTS, the gateway to vagal afferents, and its projection sites (Reyt et al., 2010). Low-frequency VNS therefore stimulates both vagal efferents and afferents, which implies that it stimulates the two anti-inflammatory pathways of the VN: the CAP and the HPA axis, and also probably the anti-inflammatory sympathetic pathway (Martelli et al., 2016; Komegae et al., 2018). Our data were confirmed later by the study of Sun et al. (2013) who also performed chronic VNS *in vivo* in rats with TNBS-colitis, as well as LPS-induced inflammatory response in human epithelial colorectal adenocarcinoma cells (Caco-2) by ACh *in vitro*. They showed that clinical activity index, histological scores, biological inflammation using myeloperoxydase activity, iNOS, TNF and IL-6 levels were significantly decreased by chronic VNS and that vagal activity, measured by HRV, was improved. In addition, both VNS and ACh reduced the phosphorylation of MAPKs and prevented the nuclear translocation of NF-κB p65. Jin et al. (2017) also found an improvement of TNBS-colitis in rats both at the clinical, biological (MPOA, TNF, IL1-beta, IL-6) and histological level. In addition, they showed that the addition of electroacupuncture to VNS may enhanced the anti-inflammatory effect of VNS. Both VNS plus electroacupuncture and VNS alone substantially increased vagal activity, measured by HRV, and decreased sympathetic activity compared with sham ($P < 0.001$, $P < 0.001$, respectively). More recently, Meroni et al. (2018) performed VNS in mice following intracolonic oxazolone administration. This model represents a model of sepsis and may resemble a severe type of UC, resulting in a severe destruction of the colonic mucosa and a rapid drop in body temperature leading to a 65% mortality rate at day 5. Severe infiltration of neutrophils and monocytes was detected 6h after oxazolone administration which was associated with a Th2-type

inflammatory response. VNS significantly improved survival rate which correlated with decreased levels of HMGB1 and reduced colonic (IL-6 and CXCL1 mRNA) and serum cytokine levels (IL-6, TNF, and CXCL1) compared to sham treated mice. Chen et al. (2018) performed a dextran sodium sulfate (DSS) colitis in mice mimicking UC. They showed that VNS improved DSS-colitis but also alleviated cerebral cortical microinfarct induced by a two-photon laser and this neuroprotection was associated with the suppression of blood–brain barrier permeability, neuroinflammation and oxidative stress.

Clinical Data

In a translational approach from bench to bedside, we conducted, for the first time, a pilot study of VNS in patients with moderate to severe CD as an alternative to anti-TNF drug therapy or in treatment-naïve patients (ClinicalTrials.gov Identifier: NCT01569503). Nine patients were implanted with a VNS device and electrode (Cyberonics, Houston, TX, United States). Two patients were in failure of immunosuppressant (azathioprine) at the time of implantation and the other seven patients were naïve of treatment. Under general anesthesia, an electrode (Model 302) was wrapped around the left VN in the neck and connected to a bipolar pulse generator (Model 102) subcutaneously implanted in the chest wall. The day of the surgery, the device was switched on at 0.25 mA (duty cycle 30 s ON/5 min OFF, pulse width 250–500 μs -depending on patient tolerance-, 10 Hz frequency) and progressively increased up to 1.25 mA as patient tolerance permitted. VNS was continuously performed for 12 months. The first patient was implanted in April 2012 and the last in March 2016. Two patients were removed from the study after 3 months of neurostimulation for a worsening of their disease: the first patient underwent an ileo-cecal resection but, because of an initially beneficial effect and a drug treatment rejection, chose to continue neurostimulation until the end of the study. The second patient was treated with a combination of Infliximab and azathioprine and also wanted to keep on an active VNS. Six patients were in remission only under neurostimulation with a 1-year follow-up, the last patient was in flare. The first patient implanted in April 2012, was in relapse under azathioprine for an ileal CD with a history of ileo-cecal resection. We reported the results of this pilot study at 6-months follow-up in seven implanted patients (Bonaz et al., 2016a) and at 1 year in the all (n = 9) implanted (Sinniger et al., 2020). Briefly, of the seven patients who completed the 12-month VNS, five achieved clinical remission (CD activity index, CDAI < 150) and all the patients reached the CDAI-70 response (CDAI decrease from baseline by 70 points). Similarly the Crohn's disease endoscopic score of severity (CDEIS) decreased in five patients from 60 to 100%. No adverse events related to the device were observed except discomfort to the intensity/output current levels. Our results are in accordance with the preliminary results of D'Haens study (D'Haens et al., 2018) who observed clinical and endoscopic improvement for half of the 16 CD patients under either VNS monotherapy (biologics refractory patients) or VNS adjunctive therapy for 4 months.

A 12-month VNS could reduce inflammatory markers like CRP (in four patients whose three reaching normal value), fecal calprotectin (in three patients), and cytokines like TNF, IL6, IL12, and IL23, all being archetypal pro-inflammatory cytokines implicated in CD (**Figure 5**) (Sinniger et al., 2020). VNS was also able to increase or sustain plasma anti-inflammatory TGF-β1 in six patients, probably through its active regulatory role on Th17/Treg balance as demonstrated by Bettelli et al. (2006) and Tanaka and Kishimoto (2012) and also through its regulatory role in monocyte-driven inflammatory responses resulting in a reduction in TNF and a production of IL10 (Lee et al., 2013). Some plasma inflammatory markers have been correlated with gut mucosa metabolic markers; this is the case for CRP, which correlated with taurine, a metabolite produced by CRP-activated leucocytes and involved in the cytoprotection and homeostatic maintenance of cells during inflammatory/oxidative processes. We also showed a correlation between TNF and lactate, alanine and β-hydroxybutyrate that could reflect a metabolite shift occurring within the gut mucosa during the 12-months VNS, both being either involved in activation/deactivation and in the redox state of the immune cells, or as an alternative source of energy.

This pilot study requires of course confirmation in a larger randomized double-blinded control study and, overall, a

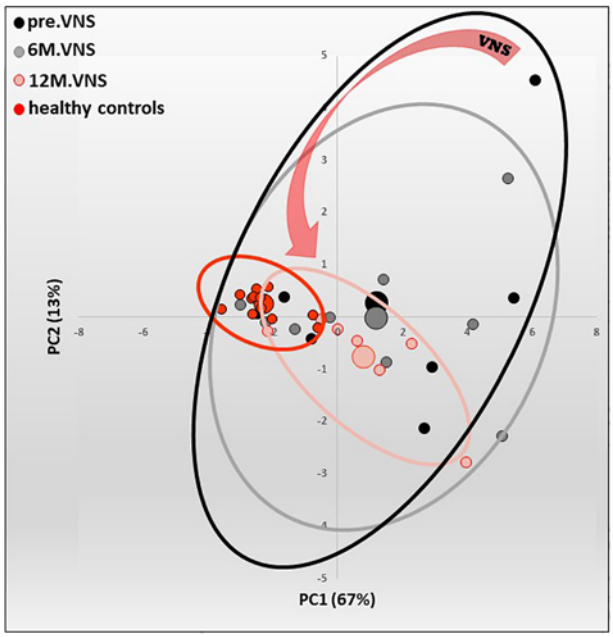

FIGURE 5 | Pilot study of vagus nerve stimulation (VNS) in patients with moderate to severe Crohn's Disease (CD). Twelve-month-VNS effect on cytokinergic profile. A plasma cytokinergic profile for controls (red), before (black), 6-month (gray) and 12-month (pink) VNS has been assessed using PCA analysis of plasma multicytokines assay for all CD patients [IL1b, IL2, IL6, IL10, IL12(p70), IL17A, IL21, IL23, MIP1α, IFNγ, GM-CSF, TNFα, TGFβ1 and MCP1]. The control values are well grouped, while profiles before VNS are very scattered, indicating that CD patients have their own cytokinergic profile. After 6 months, and even more after 12 months of VNS, the points are tightened, indicating that cytokine levels evolve through a more "common" profile. Ellipses are centered on the barycenter (big dots) of each group. Adapted from Sinniger et al. (2020).

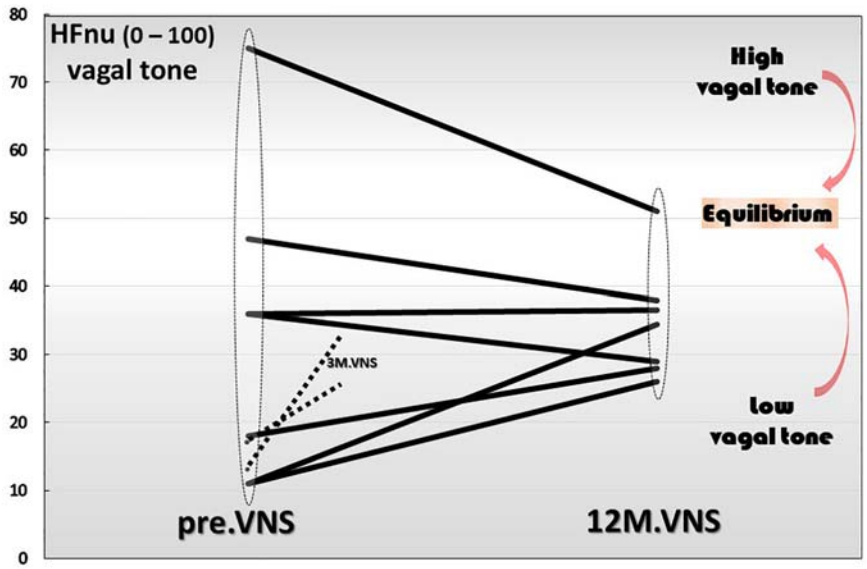

FIGURE 6 | Twelve-month-vagus nerve stimulation (VNS) effect on vagal tone. High frequencies are expressed in normal units (HFnu) and are extracted from heart rate variability analysis.

long-lasting follow-up of the patients to confirm these promising results (Cheng et al., 2020).

The Question of the Regulatory Role of VNS

Finally yet importantly, we have also shown that a 1-year chronic VNS exerts a modulatory role on vagal tone (**Figure 6**). Indeed, the trajectory toward the return to vagal equilibrium under VNS is dependent of the initial level of the HF-HRV. Interestingly, we observed in this clinical trial, that a very low HF-HRV on inclusion, increases until the equilibrium under VNS, a moderate level of HF-HRV was stabilized while an abnormally high resting HF-HRV on inclusion was decreased and brought back to equilibrium. Consequently, we can see that chronic VNS, on the long term, bring the autonomic regulation to homeostasis. At this stage, the question that arises is that of the mechanism by which this regulatory effect occurs, which has so far, never been observed before. A central mechanism through a change in the network balance within the CAN is most likely. There are several arguments in favor of this hypothesis. First, if we look at the kinetics of the evolution of the HRV over time, we can see that the return to equilibrium began at the third month of VNS (Sinniger et al., 2020). Second, we must also keep in mind that the assessment of HRV is mainly an evaluation of the ability of the central loops to regulate the functioning of the ANS, the HRV being the output (**Figure 1**). Hence, VNS logically must imply a mechanism that takes time to set up. VNS, used in the treatment of drug-refractory epilepsy, drives a 50% reduction frequency in 40–60% of the patients, with an increasing efficacy up to 10 years, showing that this treatment is a slow-acting therapy (Elliott et al., 2011). Third, electroencephalographic studies performed along with VNS over 1-year follow-up, revealed differences on power spectral bands between acute and chronic VNS. Acute VNS increased delta and theta bands on frontal, temporal and occipital sites while 1 year chronic VNS decreased power in the alpha band in correlation with the improvement of bowel mucosal inflammation, anxiety state and vagal tone. This suggests that chronic VNS has a regulatory action through the CNS and probably the CAN via afferent vagal fibers (Kibleur et al., 2018). This regulation-modulation mechanism of VNS on the return to equilibrium of the ANS but also that of the cytokines is quite original and rare in therapy outside of the example of thymoregulatory drugs like lithium. This requires serious consideration of this fundamental question by continuing investigations in this field.

CONCLUSION

Targeting the anti-inflammatory properties of the VN with VNS could be of interest in the management of patients with CD through a non-drug therapy. VNS is an alternative to biologics such as anti-TNF but also other pro-inflammatory cytokines such as IL-6, IL-12, IL-23, as observed in our study, or even as an alternative to any drug treatment: this was the case in five of our first seven patients who were naïve of treatment on inclusion. In addition, the CAP is an intrinsic anti-inflammatory non-drug pathway, which protects against the potential iatrogenic effects of treatments. VNS, on the other hand, is devoid of major side effects and cheaper than biologics (the electrode and neurostimulator cost ∼ 11,000 euros).

Non-invasive neurostimulation by the transcutaneous auricular route (ta-VNS) is an alternative to invasive neurostimulation, as used in our pilot study (Butt et al., 2020). The aim of ta-VNS is to stimulate the ear *concha* (*concha auriculae*), part of the ear which is 100% innervated by the auricular branch of the VN (Peuker and Filler, 2002) whose

stimulation would activate the "inflammatory reflex." The tragus and the cavity of the concha are 45% innervated by the auricular branch of the VN. A recent functional brain imaging study showed that neurostimulation of this region of the ear induced brain activation of the NTS and its numerous projection sites, as observed with invasive VNS (Badran et al., 2018). Ta-VNS is under clinical investigation in a double blind placebo-controlled study in adult patients with UC (ClinicalTrials.gov Identifier: NCT03908073) and pediatric patients with IBD (CD and UC) (ClinicalTrials.gov Identifier: NCT03863704). It is also possible to stimulate the VN at the left cervical level with the Gammacore device marketed by Electrocore LLC (Basking Ridge, NJ, United States) represented by two round stainless steel disks serving as a contact surface with the skin. This device, recommended in the treatment of headaches, epilepsy, and depression (Ben-Menachem et al., 2015), delivers a stimulation lasting 2 min with a frequency of 20 Hz. There is presently no clinical trial registered with this technique in Clinical.Trial.gov.

The optimal parameters of VNS to achieve efficacious inflammation-related symptomatic relief by recruiting the appropriate fibers within the VN are still unknown. Specific combinations of pulse width, pulse amplitude, and frequency produced significant increases of the proinflammatory cytokine TNF, while other parameters selectively lowered serum TNF levels, as compared to sham-stimulated mice (Bonaz, 2020; Tsaava et al., 2020). VN morphology influences fiber responses to electrical stimulation. Specifically, nerve diameter (and thus, electrode-fiber distance), fascicle diameter, fascicular organization, and perineurium thickness all significantly affect the responses of nerve fibers to electrical signals delivered through a cuff electrode (Pelot et al., 2020). Miniaturization of the VNS device is also warranted. In the same way, instead of an electrode, a VNS device which would act as an electrode by clipping it around the VN would be of interest (see setpointmedical.com; MØ1-ØØ1123). Another important progress would be a device able to record HRV and trigger VNS in case of low HRV to restore a normal tone. A VNS system, AspireSRTM, already approved in Europe, and created by Cyberonics Inc. analyzes relative changes of heart rate, particularly ictal tachycardia, and responds to seizures automatically. Consequently, all the technical and anatomical points developed above should be taken into consideration in future clinical studies and may influence the results of these studies.

AUTHOR CONTRIBUTIONS

BB wrote the first draft of the manuscript. VS and SP completed the writing of the manuscript and built the figures. All authors contributed to the article and approved the submitted version.

FUNDING

This review was supported by INSERM and DGOS ("Appel à Projet Translationnel 2011") and the DRCI from the Grenoble Hospital, France.

ACKNOWLEDGMENTS

The pilot study of VNS in patients with CD was supported by the French National Institute of Health and Medical Research (INSERM), the French Ministry of Health (DGOS call for Translational Project 2011) and the Grenoble University Hospital [Department of Clinical Research and Innovation (DRCI)]. The electroencephalographic study was performed on the IRMaGe technical platform in Grenoble (Dr. Olivier David, head of the EEG technical platform). The authors would like to thank (1) Mr. Nicolas Gonnet, Mr. David Tartry and Mrs. Mélanie Arnaud (clinical research associates) for organizing the clinical trial, (2) Mrs. Astrid Kibleur, Ph.D., for the implementation and analysis of the electroencephalograms, (3) Mrs. Florence Fauvelle, Ph.D., for the metabolomic data acquisition and spectra processing (INSERM, US17, MRI facility IRMaGe), (4) Mrs. Françoise Bardin for the formatting of the manuscript.

REFERENCES

Abe, C., Inoue, T., Inglis, M. A., Viar, K. E., Huang, L., Ye, H., et al. (2017). C1 neurons mediate a stress-induced anti-inflammatory reflex in mice. *Nat. Neurosci.* 20, 700–707. doi: 10.1038/nn.4526

Altschuler, S. M., Escardo, J., Lynn, R. B., and Miselis, R. R. (1993). The central organization of the vagus nerve innervating the colon of the rat. *Gastroenterology* 104, 502–509.

Azam, M. A., Katz, J., Fashler, S. R., Changoor, T., Azargive, S., and Ritvo, P. (2015). Heart rate variability is enhanced in controls but not maladaptive perfectionists during brief mindfulness meditation following stress-induction: A stratified-randomized trial. *Int. J. Psychophysiol.* 98, 27–34. doi: 10.1016/j.ijpsycho.2015.06.005

Badran, B. W., Dowdle, L. T., Mithoefer, O. J., LaBate, N. T., Coatsworth, J., Brown, J. C., et al. (2018). Neurophysiologic effects of transcutaneous auricular vagus nerve stimulation (taVNS) via electrical stimulation of the tragus: A concurrent taVNS/fMRI study and review. *Brain Stimul.* 11, 492–500. doi: 10.1016/j.brs.2017.12.009

Bassi, G. S., Dias, D. P. M., Franchin, M., Talbot, J., Reis, D. G., Menezes, G. B., et al. (2017). Modulation of experimental arthritis by vagal sensory and central brain stimulation. *Brain Behav. Immun.* 64, 330–343. doi: 10.1016/j.bbi.2017.04.003

Benarroch, E. E. (1993). The central autonomic network: functional organization, dysfunction, and perspective. *Mayo Clin. Proc.* 68, 988–1001. doi: 10.1016/s0025-6196(12)62272-1

Benarroch, E. E. (2018). Locus coeruleus. *Cell Tissue Res.* 373, 221–232. doi: 10.1007/s00441-017-2649-1

Ben-Horin, S., and Chowers, Y. (2011). Review article: loss of response to anti-TNF treatments in Crohn's disease. *Aliment. Pharmacol. Ther.* 33, 987–995. doi: 10.1111/j.1365-2036.2011.04612.x

Ben-Menachem, E., Revesz, D., Simon, B. J., and Silberstein, S. (2015). Surgically implanted and non-invasive vagus nerve stimulation: a review of efficacy, safety and tolerability. *Eur. J. Neurol.* 22, 1260–1268. doi: 10.1111/ene.12629

Berthoud, H. R., and Neuhuber, W. L. (2000). Functional and chemical anatomy of the afferent vagal system. *Auton. Neurosci.* 85, 1–17. doi: 10.1016/S1566-0702(00)00215-0

Bettelli, E., Carrier, Y., Gao, W., Korn, T., Strom, T. B., Oukka, M., et al. (2006). Reciprocal developmental pathways for the generation of pathogenic effector TH17 and regulatory T cells. *Nature* 441, 235–238. doi: 10.1038/nature04753

Billioud, V., Sandborn, W. J., and Peyrin-Biroulet, L. (2011). Loss of response and need for adalimumab dose intensification in Crohn's disease: a systematic review. *Am. J. Gastroenterol.* 106, 674–684. doi: 10.1038/ajg.2011.60

Black, D. S., and Slavich, G. M. (2016). Mindfulness meditation and the immune system: a systematic review of randomized controlled trials. *Ann. N Y. Acad. Sci.* 1373, 13–24. doi: 10.1111/nyas.12998

Blackwell, J., Saxena, S., Petersen, I., Hotopf, M., Creese, H., Bottle, A., et al. (2020). Depression in individuals who subsequently develop inflammatory bowel disease: a population-based nested case-control study. *Gut* 2020:322308. doi: 10.1136/gutjnl-2020-322308

Bonaz, B. (2020). Parameters matter: modulating cytokines using nerve stimulation. *Bioelectron. Med.* 6:12. doi: 10.1186/s42234-020-00049-1

Bonaz, B. L., and Bernstein, C. N. (2013). Brain-gut interactions in inflammatory bowel disease. *Gastroenterology* 144, 36–49. doi: 10.1053/j.gastro.2012.10.003

Bonaz, B., Bazin, T., and Pellissier, S. (2018). The Vagus Nerve at the Interface of the Microbiota-Gut-Brain Axis. *Front. Neurosci.* 12:49. doi: 10.3389/fnins.2018.00049

Bonaz, B., Lane, R. D., Oshinsky, M. L., Kenny, P. J., Sinha, R., Mayer, E. A., et al. (2021). Diseases, Disorders, and Comorbidities of Interoception. *Trends Neurosci.* 44, 39–51. doi: 10.1016/j.tins.2020.09.009

Bonaz, B., Picq, C., Sinniger, V., Mayol, J. F., and Clarencon, D. (2013). Vagus nerve stimulation: from epilepsy to the cholinergic anti-inflammatory pathway. *Neurogastroenterol. Motil.* 25, 208–221. doi: 10.1111/nmo.12076

Bonaz, B., Sinniger, V., Hoffmann, D., Clarencon, D., Mathieu, N., Dantzer, C., et al. (2016a). Chronic vagus nerve stimulation in Crohn's disease: a 6-month follow-up pilot study. *Neurogastroenterol. Motil.* 28, 948–953. doi: 10.1111/nmo.12792

Bonaz, B., Sinniger, V., and Pellissier, S. (2016b). Anti-inflammatory properties of the vagus nerve: potential therapeutic implications of vagus nerve stimulation. *J. Physiol.* 594, 5781–5790. doi: 10.1113/JP271539

Bonaz, B., Sinniger, V., and Pellissier, S. (2017a). The Vagus Nerve in the Neuro-Immune Axis: Implications in the Pathology of the Gastrointestinal Tract. *Front. Immunol.* 8:1452. doi: 10.3389/fimmu.2017.01452

Bonaz, B., Sinniger, V., and Pellissier, S. (2019). Vagus Nerve Stimulation at the Interface of Brain-Gut Interactions. *Cold Spring Harb. Perspect. Med.* 9:a034199. doi: 10.1101/cshperspect.a034199

Bonaz, B., Sinniger, V., Pellissier, S., and Clarencon, D. (2017b). "VNS for the treatment of inflammatory disorders of the gastrointestinal tract," in *Electroceuticals: Advances in Electrostimulation Therapies*, ed. A. Majid (Switzerland: Springer Nature), 205–230.

Borovikova, L. V., Ivanova, S., Nardi, D., Zhang, M., Yang, H., Ombrellino, M., et al. (2000). Role of vagus nerve signaling in CNI-1493-mediated suppression of acute inflammation. *Auton. Neurosci.* 85, 141–147. doi: 10.1016/S1566-0702(00)00233-2

Brinkman, D. J., Ten Hove, A. S., Vervoordeldonk, M. J., Luyer, M. D., and de Jonge, W. J. (2019). Neuroimmune Interactions in the Gut and Their Significance for Intestinal Immunity. *Cells* 8:8070670. doi: 10.3390/cells8070670

Bullmore, E. (2018). *The inflamed mind: a radical new approach to depression*. London: Picador.

Butt, M. F., Albusoda, A., Farmer, A. D., and Aziz, Q. (2020). The anatomical basis for transcutaneous auricular vagus nerve stimulation. *J. Anat.* 236, 588–611. doi: 10.1111/joa.13122

Cailotto, C., Gomez-Pinilla, P. J., Costes, L. M., van der Vliet, J., Di Giovangiulio, M., Nemethova, A., et al. (2014). Neuro-anatomical evidence indicating indirect modulation of macrophages by vagal efferents in the intestine but not in the spleen. *PLoS One* 9:e87785. doi: 10.1371/journal.pone.0087785

Cechetto, D. F. (1987). Central representation of visceral function. *Fed. Proc.* 46, 17–23.

Chan, W., Chen, A., Tiao, D., Selinger, C., and Leong, R. (2017). Medication adherence in inflammatory bowel disease. *Intest. Res.* 15, 434–445. doi: 10.5217/ir.2017.15.4.434

Chang, J. T. (2020). Pathophysiology of Inflammatory Bowel Diseases. *N. Engl. J. Med.* 383, 2652–2664. doi: 10.1056/NEJMra2002697

Chaparro, M., Guerra, I., Munoz-Linares, P., and Gisbert, J. P. (2012). Systematic review: antibodies and anti-TNF-alpha levels in inflammatory bowel disease. *Aliment. Pharmacol. Ther.* 35, 971–986. doi: 10.1111/j.1365-2036.2012.05057.x

Chen, X., He, X., Luo, S., Feng, Y., Liang, F., Shi, T., et al. (2018). Vagus Nerve Stimulation Attenuates Cerebral Microinfarct and Colitis-induced Cerebral Microinfarct Aggravation in Mice. *Front. Neurol.* 9:798. doi: 10.3389/fneur.2018.00798

Cheng, J., Shen, H., Chowdhury, R., Abdi, T., Selaru, F., and Chen, J. D. Z. (2020). Potential of Electrical Neuromodulation for Inflammatory Bowel Disease. *Inflamm. Bowel Dis.* 26, 1119–1130. doi: 10.1093/ibd/izz289

Craig, A. D. (2002). How do you feel? Interoception: the sense of the physiological condition of the body. *Nat. Rev. Neurosci.* 3, 655–666. doi: 10.1038/nrn894

Cryan, J. F., and Dinan, T. G. (2012). Mind-altering microorganisms: the impact of the gut microbiota on brain and behaviour. *Nat. Rev. Neurosci.* 13, 701–712. doi: 10.1038/nrn3346

Cryan, J. F., O'Riordan, K. J., Cowan, C. S. M., Sandhu, K. V., Bastiaanssen, T. F. S., Boehme, M., et al. (2019). The Microbiota-Gut-Brain Axis. *Physiol. Rev.* 99, 1877–2013. doi: 10.1152/physrev.00018.2018

D'Amico, F., Peyrin-Biroulet, L., Danese, S., and Fiorino, G. (2020). New drugs in the pipeline for the treatment of inflammatory bowel diseases: what is coming? *Curr. Opin. Pharmacol.* 55, 141–150. doi: 10.1016/j.coph.2020.10.015

Dantzer, R., Bluthe, R. M., Gheusi, G., Cremona, S., Laye, S., Parnet, P., et al. (1998). Molecular basis of sickness behavior. *Ann. N Y. Acad. Sci.* 856, 132–138. doi: 10.1111/j.1749-6632.1998.tb08321.x

de Jonge, W. J., van der Zanden, E. P., The, F. O., Bijlsma, M. F., van Westerloo, D. J., Bennink, R. J., et al. (2005). Stimulation of the vagus nerve attenuates macrophage activation by activating the Jak2-STAT3 signaling pathway. *Nat. Immunol.* 6, 844–851. doi: 10.1038/ni1229

Delmas, J., and Laux, G. (1933). *Anatomie médico-chirurgicale du système nerveux végétatif: (sympathique & parasympathique)*. Paris: Masson.

D'Haens, G. R., Cabrijan, Z., Eberhardson, M., van den Berg, R. M., Löwenberg, M., Fiorino, G., et al. (2018). Mo1906 - The Effects of Vagus Nerve Stimulation in Biologic refractory Crohn's Disease: A Prospective Clinical Trial. *Gastroenterology* 154(Suppl. 1), S–847. doi: 10.1016/S0016-5085(18)32870-1

Eckburg, P. B., Bik, E. M., Bernstein, C. N., Purdom, E., Dethlefsen, L., Sargent, M., et al. (2005). Diversity of the human intestinal microbial flora. *Science* 308, 1635–1638. doi: 10.1126/science.1110591

Elliott, R. E., Morsi, A., Tanweer, O., Grobelny, B., Geller, E., Carlson, C., et al. (2011). Efficacy of vagus nerve stimulation over time: review of 65 consecutive patients with treatment-resistant epilepsy treated with VNS > 10 years. *Epilepsy Behav.* 20, 478–483. doi: 10.1016/j.yebeh.2010.12.042

Ford, A. C., Sandborn, W. J., Khan, K. J., Hanauer, S. B., Talley, N. J., and Moayyedi, P. (2011). Efficacy of biological therapies in inflammatory bowel disease: systematic review and meta-analysis. *Am. J. Gastroenterol.* 106, 644–659. doi: 10.1038/ajg.2011.73

Fornai, M., van den Wijngaard, R. M., Antonioli, L., Pellegrini, C., Blandizzi, C., and de Jonge, W. J. (2018). Neuronal regulation of intestinal immune functions in health and disease. *Neurogastroenterol. Motil.* 30:e13406. doi: 10.1111/nmo.13406

Forsythe, P., Kunze, W., and Bienenstock, J. (2016). Moody microbes or fecal phrenology: what do we know about the microbiota-gut-brain axis? *BMC Medicine* 14:58. doi: 10.1186/s12916-016-0604-8

Fournier, A., Mondillon, L., Luminet, O., Canini, F., Mathieu, N., Gauchez, A. S., et al. (2020). Interoceptive Abilities in Inflammatory Bowel Diseases and Irritable Bowel Syndrome. *Front. Psychiatry* 11:229. doi: 10.3389/fpsyt.2020.00229

Frolkis, A. D. I, Vallerand, A., Shaheen, A. A., Lowerison, M. W., Swain, M. G., Barnabe, C., et al. (2019). Depression increases the risk of inflammatory bowel disease, which may be mitigated by the use of antidepressants in the treatment of depression. *Gut* 68, 1606–1612. doi: 10.1136/gutjnl-2018-317182

Furness, J. B., Callaghan, B. P., Rivera, L. R., and Cho, H. J. (2014). The enteric nervous system and gastrointestinal innervation: integrated local and central control. *Adv. Exp. Med. Biol.* 817, 39–71. doi: 10.1007/978-1-4939-0897-4_3

Ghia, J. E., Blennerhassett, P., El-Sharkawy, R. T., and Collins, S. M. (2007). The protective effect of the vagus nerve in a murine model of chronic relapsing colitis. *Am. J. Physiol. Gastrointest Liver Physiol.* 293, G711–G718. doi: 10.1152/ajpgi.00240.2007

Gisbert, J. P., and Panes, J. (2009). Loss of response and requirement of infliximab dose intensification in Crohn's disease: a review. *Am. J. Gastroenterol.* 104, 760–767. doi: 10.1038/ajg.2008.88

Goehler, L. E., Relton, J. K., Dripps, D., Kiechle, R., Tartaglia, N., Maier, S. F., et al. (1997). Vagal paraganglia bind biotinylated interleukin-1 receptor antagonist: a possible mechanism for immune-to-brain communication. *Brain Res. Bull.* 43, 357–364.

Guarini, S., Altavilla, D., Cainazzo, M. M., Giuliani, D., Bigiani, A., Marini, H., et al. (2003). Efferent vagal fibre stimulation blunts nuclear factor-kappaB activation and protects against hypovolemic hemorrhagic shock. *Circulation* 107, 1189–1194. doi: 10.1161/01.cir.0000050627.90734.ed

Gunterberg, V., Simren, M., Ohman, L., Friberg, P., Jones, M. P., Van Oudenhove, L., et al. (2016). Autonomic nervous system function predicts the inflammatory response over three years in newly diagnosed ulcerative colitis patients. *Neurogastroenterol. Motil.* 28, 1655–1662. doi: 10.1111/nmo.12865

Heffernan, K. S., Jae, S. Y., Vieira, V. J., Iwamoto, G. A., Wilund, K. R., Woods, J. A., et al. (2009). C-reactive protein and cardiac vagal activity following resistance exercise training in young African-American and white men. *Am. J. Physiol. Regul. Integr. Comp. Physiol.* 296, R1098–R1105. doi: 10.1152/ajpregu.90936.2008

Hiles, S. A., Baker, A. L., de Malmanche, T., and Attia, J. (2012). A meta-analysis of differences in IL-6 and IL-10 between people with and without depression: exploring the causes of heterogeneity. *Brain Behav. Immun.* 26, 1180–1188. doi: 10.1016/j.bbi.2012.06.001

Jean, A. (1991). [The nucleus tractus solitarius: neuroanatomic, neurochemical and functional aspects]. *Arch. Int. Physiol. Biochim. Biophys.* 99, A3–A52. doi: 10.3109/13813459109145916

Ji, H., Rabbi, M. F., Labis, B., Pavlov, V. A., Tracey, K. J., and Ghia, J. E. (2014). Central cholinergic activation of a vagus nerve-to-spleen circuit alleviates experimental colitis. *Mucosal Immunol.* 7, 335–347. doi: 10.1038/mi.2013.52

Jin, H., Guo, J., Liu, J., Lyu, B., Foreman, R. D., Yin, J., et al. (2017). Anti-inflammatory effects and mechanisms of vagal nerve stimulation combined with electroacupuncture in a rodent model of TNBS-induced colitis. *Am. J. Physiol. Gastrointest Liver Physiol.* 313, G192–G202. doi: 10.1152/ajpgi.00254.2016

Keefer, L., Taft, T. H., Kiebles, J. L., Martinovich, Z., Barrett, T. A., and Palsson, O. S. (2013). Gut-directed hypnotherapy significantly augments clinical remission in quiescent ulcerative colitis. *Aliment. Pharmacol. Ther.* 38, 761–771. doi: 10.1111/apt.12449

Kerbleski, J. F., and Gottlieb, A. B. (2009). Dermatological complications and safety of anti-TNF treatments. *Gut* 58, 1033–1039. doi: 10.1136/gut.2008.163683

Kibleur, A., Pellissier, S., Sinniger, V., Robert, J., Gronlier, E., Clarencon, D., et al. (2018). Electroencephalographic correlates of low-frequency vagus nerve stimulation therapy for Crohn's disease. *Clin. Neurophysiol.* 129, 1041–1046. doi: 10.1016/j.clinph.2018.02.127

Kohler, C. A., Freitas, T. H., Maes, M., de Andrade, N. Q., Liu, C. S., Fernandes, B. S., et al. (2017). Peripheral cytokine and chemokine alterations in depression: a meta-analysis of 82 studies. *Acta Psychiatr. Scand.* 135, 373–387. doi: 10.1111/acps.12698

Köhler-Forsberg, O., Lydholm, C., Hjorthøj, C., Nordentoft, M., Mors, O., and Benros, M. E. (2019). Efficacy of anti-inflammatory treatment on major depressive disorder or depressive symptoms: meta-analysis of clinical trials. *Acta Psychiatr. Scand.* 139, 404–419. doi: 10.1111/acps.13016

Komegae, E. N., Farmer, D. G. S., Brooks, V. L., McKinley, M. J., McAllen, R. M., and Martelli, D. (2018). Vagal afferent activation suppresses systemic inflammation via the splanchnic anti-inflammatory pathway. *Brain Behav. Immun.* 73, 441–449. doi: 10.1016/j.bbi.2018.06.005

Kressel, A. M., Tsaava, T., Levine, Y. A., Chang, E. H., Addorisio, M. E., Chang, Q., et al. (2020). Identification of a brainstem locus that inhibits tumor necrosis factor. *Proc. Natl. Acad. Sci. U S A.* 117, 29803–29810. doi: 10.1073/pnas.2008213117

Langley, J. N. (1921). *The autonomic nervous system*. Oxford: Heffer W. & Sons Limited.

Larauche, M., Gourcerol, G., Wang, L., Pambukchian, K., Brunnhuber, S., Adelson, D. W., et al. (2009a). Cortagine, a CRF1 agonist, induces stresslike alterations of colonic function and visceral hypersensitivity in rodents primarily through peripheral pathways. *Am. J. Physiol. Gastrointest Liver Physiol.* 297, G215–G227. doi: 10.1152/ajpgi.00072.2009

Larauche, M., Kiank, C., and Tache, Y. (2009b). Corticotropin releasing factor signaling in colon and ileum: regulation by stress and pathophysiological implications. *J. Physiol. Pharmacol.* 60(Suppl. 7), 33–46.

Lee, J. C., Espeli, M., Anderson, C. A., Linterman, M. A., Pocock, J. M., Williams, N. J., et al. (2013). Human SNP links differential outcomes in inflammatory and infectious disease to a FOXO3-regulated pathway. *Cell* 155, 57–69. doi: 10.1016/j.cell.2013.08.034

Lehner, K. R., Silverman, H. A., Addorisio, M. E., Roy, A., Al-Onaizi, M. A., Levine, Y., et al. (2019). Forebrain Cholinergic Signaling Regulates Innate Immune Responses and Inflammation. *Front. Immunol.* 10:585. doi: 10.3389/fimmu.2019.00585

Levy, A. N., and Allegretti, J. R. (2019). Insights into the role of fecal microbiota transplantation for the treatment of inflammatory bowel disease. *Therap. Adv. Gastroenterol.* 12:1756284819836893. doi: 10.1177/1756284819836893

Lin, Y. Y., Chang, C. C., Huang, C. C., Tzeng, N. S., Kao, Y. C., and Chang, H. A. (2021). Efficacy and neurophysiological predictors of treatment response of adjunct bifrontal transcranial direct current stimulation (tDCS) in treating unipolar and bipolar depression. *J. Affect. Disord.* 280(Pt A), 295–304. doi: 10.1016/j.jad.2020.11.030

Lindgren, S., Lilja, B., Rosen, I., and Sundkvist, G. (1991). Disturbed autonomic nerve function in patients with Crohn's disease. *Scand. J. Gastroenterol.* 26, 361–366. doi: 10.3109/00365529108996495

Lindgren, S., Stewenius, J., Sjolund, K., Lilja, B., and Sundkvist, G. (1993). Autonomic vagal nerve dysfunction in patients with ulcerative colitis. *Scand. J. Gastroenterol.* 28, 638–642. doi: 10.3109/00365529309096103

Liu, B., Wanders, A., Wirdefeldt, K., Sjolander, A., Sachs, M. C., Eberhardson, M., et al. (2020). Vagotomy and subsequent risk of inflammatory bowel disease: a nationwide register-based matched cohort study. *Aliment. Pharmacol. Ther.* 51, 1022–1030. doi: 10.1111/apt.15715

Loewy, A. D. (1981). Descending pathways to sympathetic and parasympathetic preganglionic neurons. *J. Auton. Nerv. Syst.* 3, 265–275. doi: 10.1016/0165-1838(81)90068-0

Lomarev, M., Denslow, S., Nahas, Z., Chae, J. H., George, M. S., and Bohning, D. E. (2002). Vagus nerve stimulation (VNS) synchronized BOLD fMRI suggests that VNS in depressed adults has frequency/dose dependent effects. *J. Psychiatr. Res.* 36, 219–227. doi: 10.1016/s0022-3956(02)00013-4

Lu, B., Kwan, K., Levine, Y. A., Olofsson, P. S., Yang, H., Li, J., et al. (2014). alpha7 nicotinic acetylcholine receptor signaling inhibits inflammasome activation by preventing mitochondrial DNA release. *Mol. Med.* 20, 350–358. doi: 10.2119/molmed.2013.00117

Lujan, H. L., and DiCarlo, S. E. (2013). Physical activity, by enhancing parasympathetic tone and activating the cholinergic anti-inflammatory pathway, is a therapeutic strategy to restrain chronic inflammation and prevent many chronic diseases. *Med. Hypothes.* 80, 548–552. doi: 10.1016/j.mehy.2013.01.014

Lumma, A. L., Kok, B. E., and Singer, T. (2015). Is meditation always relaxing? Investigating heart rate, heart rate variability, experienced effort and likeability during training of three types of meditation. *Int. J. Psychophysiol.* 97, 38–45. doi: 10.1016/j.ijpsycho.2015.04.017

Luyer, M. D., Greve, J. W., Hadfoune, M., Jacobs, J. A., Dejong, C. H., and Buurman, W. A. (2005). Nutritional stimulation of cholecystokinin receptors inhibits inflammation via the vagus nerve. *J. Exp. Med.* 202, 1023–1029. doi: 10.1084/jem.20042397

Macer, B. J., Prady, S. L., and Mikocka-Walus, A. (2017). Antidepressants in Inflammatory Bowel Disease: A Systematic Review. *Inflamm. Bowel Dis.* 23, 534–550. doi: 10.1097/MIB.0000000000001059

Mao, Y., Tokudome, T., Kishimoto, I., Otani, K., Nishimura, H., Yamaguchi, O., et al. (2015). Endogenous ghrelin attenuates pressure overload-induced cardiac hypertrophy via a cholinergic anti-inflammatory pathway. *Hypertension* 65, 1238–1244. doi: 10.1161/HYPERTENSIONAHA.114.04864

Marmerstein, J. T., McCallum, G. A., and Durand, D. M. (2021). Direct measurement of vagal tone in rats does not show correlation to HRV. *Sci. Rep.* 11:1210. doi: 10.1038/s41598-020-79808-8

Martelli, D., Farmer, D. G. S., McKinley, M. J., Yao, S. T., and McAllen, R. M. (2019). Anti-inflammatory reflex action of splanchnic sympathetic nerves is distributed across abdominal organs. *Am. J. Physiol. Regul. Integr. Comp. Physiol.* 316, R235–R242. doi: 10.1152/ajpregu.00298.2018

Martelli, D., Farmer, D. G., and Yao, S. T. (2016). The splanchnic anti-inflammatory pathway: could it be the efferent arm of the inflammatory reflex? *Exp. Physiol.* 101, 1245–1252. doi: 10.1113/EP085559

Martelli, D., Yao, S. T., McKinley, M. J., and McAllen, R. M. (2014). Reflex control of inflammation by sympathetic nerves, not the vagus. *J. Physiol.* 592, 1677–1686. doi: 10.1113/jphysiol.2013.268573

Mawdsley, J. E., Jenkins, D. G., Macey, M. G., Langmead, L., and Rampton, D. S. (2008). The effect of hypnosis on systemic and rectal mucosal measures of inflammation in ulcerative colitis. *Am. J. Gastroenterol.* 103, 1460–1469. doi: 10.1111/j.1572-0241.2008.01845.x

Meregnani, J., Clarencon, D., Vivier, M., Peinnequin, A., Mouret, C., Sinniger, V., et al. (2011). Anti-inflammatory effect of vagus nerve stimulation in a rat model of inflammatory bowel disease. *Auton. Neurosci.* 160, 82–89. doi: 10.1016/j.autneu.2010.10.007

Meroni, E., Stakenborg, N., Gomez-Pinilla, P. J., De Hertogh, G., Goverse, G., Matteoli, G., et al. (2018). Functional characterization of oxazolone-induced colitis and survival improvement by vagus nerve stimulation. *PLoS One* 13:e0197487. doi: 10.1371/journal.pone.0197487

Metz, C. N., and Pavlov, V. A. (2020). Treating disorders across the lifespan by modulating cholinergic signaling with galantamine. *J. Neurochem.* 2020:15243. doi: 10.1111/jnc.15243

Miceli, P. C., and Jacobson, K. (2003). Cholinergic pathways modulate experimental dinitrobenzene sulfonic acid colitis in rats. *Auton. Neurosci.* 105, 16–24. doi: 10.1016/S1566-0702(03)00023-7

Mikocka-Walus, A., Knowles, S. R., Keefer, L., and Graff, L. (2016a). Controversies Revisited: A Systematic Review of the Comorbidity of Depression and Anxiety with Inflammatory Bowel Diseases. *Inflamm. Bowel Dis.* 22, 752–762. doi: 10.1097/MIB.0000000000000620

Mikocka-Walus, A., Pittet, V., Rossel, J. B., von Kanel, R., and Swiss, I. B. D. C. S. G. (2016b). Symptoms of Depression and Anxiety Are Independently Associated With Clinical Recurrence of Inflammatory Bowel Disease. *Clin. Gastroenterol. Hepatol.* 14:e821. doi: 10.1016/j.cgh.2015.12.045

Molodecky, N. A. I, Soon, S., Rabi, D. M., Ghali, W. A., Ferris, M., Chernoff, G., et al. (2012). Increasing incidence and prevalence of the inflammatory bowel diseases with time, based on systematic review. *Gastroenterology* 142, 46–54e42. doi: 10.1053/j.gastro.2011.10.001

Murdaca, G., Spano, F., Contatore, M., Guastalla, A., Penza, E., Magnani, O., et al. (2016). Immunogenicity of infliximab and adalimumab: what is its role in hypersensitivity and modulation of therapeutic efficacy and safety? *Expert Opin. Drug Saf.* 15, 43–52. doi: 10.1517/14740338.2016.1112375

Netter, F. H. (1989). *Atlas of Human Anatomy*. New Jersey, NJ: Ciba-Geigy Corporation.

Nonogaki, K. (2008). Ghrelin and feedback systems. *Vitam. Horm.* 77, 149–170. doi: 10.1016/S0083-6729(06)77007-8

Norgren, R. (1978). Projections from the nucleus of the solitary tract in the rat. *Neuroscience* 3, 207–218. doi: 10.1016/0306-4522(78)90102-1

Olofsson, P. S., and Tracey, K. J. (2017). Bioelectronic medicine: technology targeting molecular mechanisms for therapy. *J. Intern. Med.* 282, 3–4. doi: 10.1111/joim.12624

Olofsson, P. S., Katz, D. A., Rosas-Ballina, M., Levine, Y. A., Ochani, M., Valdes-Ferrer, S. I., et al. (2012). alpha7 nicotinic acetylcholine receptor (alpha7nAChR) expression in bone marrow-derived non-T cells is required for the inflammatory reflex. *Mol. Med.* 18, 539–543. doi: 10.2119/molmed.2011.00405

Olofsson, P. S., Steinberg, B. E., Sobbi, R., Cox, M. A., Ahmed, M. N., Oswald, M., et al. (2016). Blood pressure regulation by CD4(+) lymphocytes expressing choline acetyltransferase. *Nat. Biotechnol.* 34, 1066–1071. doi: 10.1038/nbt.3663

Pagnini, C., Pizarro, T. T., and Cominelli, F. (2019). Novel Pharmacological Therapy in Inflammatory Bowel Diseases: Beyond Anti-Tumor Necrosis Factor. *Front. Pharmacol.* 10:671. doi: 10.3389/fphar.2019.00671

Pavlov, V. A., Ochani, M., Yang, L. H., Gallowitsch-Puerta, M., Ochani, K., Lin, X., et al. (2007). Selective alpha7-nicotinic acetylcholine receptor agonist GTS-21 improves survival in murine endotoxemia and severe sepsis. *Crit. Care Med.* 35, 1139–1144. doi: 10.1097/01.CCM.0000259381.56526.96

Pavlov, V. A., Parrish, W. R., Rosas-Ballina, M., Ochani, M., Puerta, M., Ochani, K., et al. (2009). Brain acetylcholinesterase activity controls systemic cytokine levels through the cholinergic anti-inflammatory pathway. *Brain Behav. Immun.* 23, 41–45. doi: 10.1016/j.bbi.2008.06.011

Pavlov, V. A., Wang, H., Czura, C. J., Friedman, S. G., and Tracey, K. J. (2003). The cholinergic anti-inflammatory pathway: a missing link in neuroimmunomodulation. *Mol. Med.* 9, 125–134.

Pellissier, S., and Bonaz, B. (2017). The Place of Stress and Emotions in the Irritable Bowel Syndrome. *Vitam. Horm.* 103, 327–354. doi: 10.1016/bs.vh.2016.09.005

Pellissier, S., Dantzer, C., Canini, F., Mathieu, N., and Bonaz, B. (2010). Psychological adjustment and autonomic disturbances in inflammatory bowel diseases and irritable bowel syndrome. *Psychoneuroendocrinology* 35, 653–662. doi: 10.1016/j.psyneuen.2009.10.004

Pellissier, S., Dantzer, C., Mondillon, L., Trocme, C., Gauchez, A. S., Ducros, V., et al. (2014). Relationship between vagal tone, cortisol, TNF-alpha, epinephrine and negative affects in Crohn's disease and irritable bowel syndrome. *PLoS One* 9:e105328. doi: 10.1371/journal.pone.0105328

Pelot, N. A., Goldhagen, G. B., Cariello, J. E., Musselman, E. D., Clissold, K. A., Ezzell, J. A., et al. (2020). Quantified Morphology of the Cervical and Subdiaphragmatic Vagus Nerves of Human, Pig, and Rat. *Front. Neurosci.* 14:601479. doi: 10.3389/fnins.2020.601479

Pereira, R., Lago, P., Faria, R., and Torres, T. (2015). Safety of Anti-TNF Therapies in Immune-Mediated Inflammatory Diseases: Focus on Infections and Malignancy. *Drug Dev. Res.* 76, 419–427. doi: 10.1002/ddr.21285

Peuker, E. T., and Filler, T. J. (2002). The nerve supply of the human auricle. *Clin. Anat.* 15, 35–37. doi: 10.1002/ca.1089

Peyrin-Biroulet, L. (2010). Anti-TNF therapy in inflammatory bowel diseases: a huge review. *Minerva Gastroenterol. Dietol.* 56, 233–243.

Powley, T. L., Jaffey, D. M., McAdams, J., Baronowsky, E. A., Black, D., Chesney, L., et al. (2019). Vagal innervation of the stomach reassessed: brain-gut connectome uses smart terminals. *Ann. N Y. Acad. Sci.* 1454, 14–30. doi: 10.1111/nyas.14138

Prechtl, J. C., and Powley, T. L. (1990). The fiber composition of the abdominal vagus of the rat. *Anat. Embryol.* 181, 101–115.

Rajan, D., Wu, R., Shah, K. G., Jacob, A., Coppa, G. F., and Wang, P. (2012). Human ghrelin protects animals from renal ischemia-reperfusion injury through the vagus nerve. *Surgery* 151, 37–47. doi: 10.1016/j.surg.2011.06.027

Reyes del Paso, G. A., Langewitz, W., Mulder, L. J., van Roon, A., and Duschek, S. (2013). The utility of low frequency heart rate variability as an index of sympathetic cardiac tone: a review with emphasis on a reanalysis of previous studies. *Psychophysiology* 50, 477–487. doi: 10.1111/psyp.12027

Reyes, A., Haynes, M., Hanson, N., Angly, F. E., Heath, A. C., Rohwer, F., et al. (2010). Viruses in the faecal microbiota of monozygotic twins and their mothers. *Nature* 466, 334–338. doi: 10.1038/nature09199

Reyt, S., Picq, C., Sinniger, V., Clarencon, D., Bonaz, B., and David, O. (2010). Dynamic Causal Modelling and physiological confounds: a functional MRI study of vagus nerve stimulation. *Neuroimage* 52, 1456–1464. doi: 10.1016/j.neuroimage.2010.05.021

Rivest, S., Lacroix, S., Vallières, L., Nadeau, S., Zhang, J., and Laflamme, N. (2000). How the Blood Talks to the Brain Parenchyma and the Paraventricular Nucleus of the Hypothalamus During Systemic Inflammatory and Infectious Stimuli. *Proc. Soc. Exp. Biol. Med.* 223, 22–38. doi: 10.1111/j.1525-1373.2000.22304.x

Rosas-Ballina, M., Ochani, M., Parrish, W. R., Ochani, K., Harris, Y. T., Huston, J. M., et al. (2008). Splenic nerve is required for cholinergic antiinflammatory pathway control of TNF in endotoxemia. *Proc. Natl. Acad. Sci. U S A.* 105, 11008–11013. doi: 10.1073/pnas.0803237105

Rosas-Ballina, M., Olofsson, P. S., Ochani, M., Valdes-Ferrer, S. I., Levine, Y. A., Reardon, C., et al. (2011). Acetylcholine-synthesizing T cells relay neural signals in a vagus nerve circuit. *Science* 334, 98–101. doi: 10.1126/science.1209985

Roura, E., Koopmans, S. J., Lalles, J. P., Le Huerou-Luron, I., de Jager, N., Schuurman, T., et al. (2016). Critical review evaluating the pig as a model for human nutritional physiology. *Nutr. Res. Rev.* 29, 60–90. doi: 10.1017/S0954422416000020

Sawchenko, P. E. (1983). Central connections of the sensory and motor nuclei of the vagus nerve. *J. Auton. Nerv. Syst.* 9, 13–26.

Schiepers, O. J., Wichers, M. C., and Maes, M. (2005). Cytokines and major depression. *Prog. Neuropsychopharmacol. Biol. Psychiatry* 29, 201–217. doi: 10.1016/j.pnpbp.2004.11.003

Sgoifo, A., Carnevali, L., Alfonso Mde, L., and Amore, M. (2015). Autonomic dysfunction and heart rate variability in depression. *Stress* 18, 343–352. doi: 10.3109/10253890.2015.1045868

Sinniger, V., Pellissier, S., Fauvelle, F., Trocme, C., Hoffman, D., Vercueil, L., et al. (2020). A 12-month pilot study outcomes of vagus nerve stimulation in Crohn's disease. *Neurogastroenterol. Motil.* 32:e13911. doi: 10.1111/NMO.13911

Sitapara, R. A., Gauthier, A. G., Valdes-Ferrer, S. I., Lin, M., Patel, V., Wang, M., et al. (2020). The alpha7 nicotinic acetylcholine receptor agonist, GTS-21, attenuates hyperoxia-induced acute inflammatory lung injury by alleviating the accumulation of HMGB1 in the airways and the circulation. *Mol. Med.* 26:63. doi: 10.1186/s10020-020-00177-z

Song, C., and Wang, H. (2011). Cytokines mediated inflammation and decreased neurogenesis in animal models of depression. *Prog. Neuropsychopharmacol. Biol. Psychiatry* 35, 760–768. doi: 10.1016/j.pnpbp.2010.06.020

Sun, P., Zhou, K., Wang, S., Li, P., Chen, S., Lin, G., et al. (2013). Involvement of MAPK/NF-kappaB signaling in the activation of the cholinergic anti-inflammatory pathway in experimental colitis by chronic vagus nerve stimulation. *PLoS One* 8:e69424. doi: 10.1371/journal.pone.0069424

Sundin, J., Ohman, L., and Simren, M. (2017). Understanding the Gut Microbiota in Inflammatory and Functional Gastrointestinal Diseases. *Psychosom. Med.* 79, 857–867. doi: 10.1097/PSY.0000000000000470

Tache, Y., and Bonaz, B. (2007). Corticotropin-releasing factor receptors and stress-related alterations of gut motor function. *J. Clin. Invest.* 117, 33–40. doi: 10.1172/JCI30085

Tache, Y., Martinez, V., Million, M., and Wang, L. (2001). Stress and the gastrointestinal tract III. Stress-related alterations of gut motor function: role of brain corticotropin-releasing factor receptors. *Am. J. Physiol. Gastrointest. Liver Physiol.* 280, G173–G177. doi: 10.1152/ajpgi.2001.280.2.G173

Tanaka, T., and Kishimoto, T. (2012). Targeting interleukin-6: all the way to treat autoimmune and inflammatory diseases. *Int. J. Biol. Sci.* 8, 1227–1236. doi: 10.7150/ijbs.4666

Targownik, L. E., Benchimol, E. I., Witt, J., Bernstein, C. N., Singh, H., Lix, L., et al. (2019). The Effect of Initiation of Anti-TNF Therapy on the Subsequent Direct Health Care Costs of Inflammatory Bowel Disease. *Inflamm. Bowel Dis.* 25, 1718–1728. doi: 10.1093/ibd/izz063

Thayer, J. F., Ahs, F., Fredrikson, M., Sollers, J. J. III, and Wager, T. D. (2012). A meta-analysis of heart rate variability and neuroimaging studies: implications for heart rate variability as a marker of stress and health. *Neurosci. Biobehav. Rev.* 36, 747–756. doi: 10.1016/j.neubiorev.2011.11.009

Thayer, J. F., and Lane, R. D. (2009). Claude Bernard and the heart-brain connection: further elaboration of a model of neurovisceral integration. *Neurosci. Biobehav. Rev.* 33, 81–88. doi: 10.1016/j.neubiorev.2008.08.004

The, F. O., Boeckxstaens, G. E., Snoek, S. A., Cash, J. L., Bennink, R., Larosa, G. J., et al. (2007). Activation of the cholinergic anti-inflammatory pathway ameliorates postoperative ileus in mice. *Gastroenterology* 133, 1219–1228. doi: 10.1053/j.gastro.2007.07.022

Thomas, B. L., Claassen, N., Becker, P., and Viljoen, M. (2019). Validity of Commonly Used Heart Rate Variability Markers of Autonomic Nervous System Function. *Neuropsychobiology* 78, 14–26. doi: 10.1159/000495519

Torres, J., Ellul, P., Langhorst, J., Mikocka-Walus, A., Barreiro-de Acosta, M., Basnayake, C., et al. (2019). European Crohn's and Colitis Organisation Topical Review on Complementary Medicine and Psychotherapy in Inflammatory Bowel Disease. *J. Crohns Colitis* 13, 673e–685e. doi: 10.1093/ecco-jcc/jjz051

Travagli, R. A., Hermann, G. E., Browning, K. N., and Rogers, R. C. (2006). Brainstem circuits regulating gastric function. *Annu. Rev. Physiol.* 68, 279–305. doi: 10.1146/annurev.physiol.68.040504.094635

Tsaava, T., Datta-Chaudhuri, T., Addorisio, M. E., Masi, E. B., Silverman, H. A., Newman, J. E., et al. (2020). Specific vagus nerve stimulation parameters alter serum cytokine levels in the absence of inflammation. *Bioelectron. Med.* 6:8. doi: 10.1186/s42234-020-00042-8

Tyagi, A., and Cohen, M. (2016). Yoga and heart rate variability: A comprehensive review of the literature. *Int. J. Yoga* 9, 97–113. doi: 10.4103/0973-6131.183712

Valentino, R. J., Miselis, R. R., and Pavcovich, L. A. (1999). Pontine regulation of pelvic viscera: pharmacological target for pelvic visceral dysfunctions. *Trends Pharmacol. Sci.* 20, 253–260.

van der Valk, M. E., Mangen, M. J., Leenders, M., Dijkstra, G., van Bodegraven, A. A., Fidder, H. H., et al. (2014). Healthcare costs of inflammatory bowel disease have shifted from hospitalisation and surgery towards anti-TNFalpha therapy: results from the COIN study. *Gut* 63, 72–79. doi: 10.1136/gutjnl-2012-303376

van Westerloo, D. J. I, Giebelen, A., Florquin, S., Bruno, M. J., Larosa, G. J., Ulloa, L., et al. (2006). The vagus nerve and nicotinic receptors modulate experimental pancreatitis severity in mice. *Gastroenterology* 130, 1822–1830. doi: 10.1053/j.gastro.2006.02.022

Wang, H., Yu, M., Ochani, M., Amella, C. A., Tanovic, M., Susarla, S., et al. (2003). Nicotinic acetylcholine receptor alpha7 subunit is an essential regulator of inflammation. *Nature* 421, 384–388. doi: 10.1038/nature01339

Weippert, M., Behrens, K., Rieger, A., Stoll, R., and Kreuzfeld, S. (2013). Heart rate variability and blood pressure during dynamic and static exercise at similar heart rate levels. *PLoS One* 8:e83690. doi: 10.1371/journal.pone.0083690

Willemze, R. A., Welting, O., van Hamersveld, H. P., Meijer, S. L., Folgering, J. H. A., Darwinkel, H., et al. (2018). Neuronal control of experimental colitis occurs via sympathetic intestinal innervation. *Neurogastroenterol. Motil.* 30:13163. doi: 10.1111/nmo.13163

Williams, D. P., Koenig, J., Carnevali, L., Sgoifo, A., Jarczok, M. N., Sternberg, E. M., et al. (2019). Heart rate variability and inflammation: A meta-analysis of human studies. *Brain Behav. Immun.* 80, 219–226. doi: 10.1016/j.bbi.2019.03.009

Williams, R. M., Berthoud, H. R., and Stead, R. H. (1997). Vagal afferent nerve fibres contact mast cells in rat small intestinal mucosa. *Neuroimmunomodulation* 4, 266–270. doi: 10.1159/000097346

Wood, S. K., and Woods, J. H. (2007). Corticotropin-releasing factor receptor-1: a therapeutic target for cardiac autonomic disturbances. *Expert Opin. Ther. Targets* 11, 1401–1413. doi: 10.1517/14728222.11.11.1401

Yuksel, R., Ozcan, O., and Dane, S. (2013). The effects of hypnosis on heart rate variability. *Int. J. Clin. Exp. Hypn.* 61, 162–171. doi: 10.1080/00207144.2013.753826

Zanos, T. P., Silverman, H. A., Levy, T., Tsaava, T., Battinelli, E., Lorraine, P. W., et al. (2018). Identification of cytokine-specific sensory neural signals by decoding murine vagus nerve activity. *Proc. Natl. Acad. Sci. U S A.* 115, E4843–E4852. doi: 10.1073/pnas.1719083115

Zhang, X. F., Xiang, S. Y., Geng, W. Y., Cong, W. J., Lu, J., Jiang, C. W., et al. (2018). Electro-acupuncture regulates the cholinergic anti-inflammatory pathway in a rat model of chronic obstructive pulmonary disease. *J. Integr. Med.* 16, 418–426. doi: 10.1016/j.joim.2018.10.003

Zhou, M., Aziz, M., Ochani, M., and Wang, P. (2020). Correction of immunosuppression in aged septic rats by human ghrelin and growth hormone through the vagus nerve-dependent inhibition of TGF-beta production. *Mol. Med.* 26:71. doi: 10.1186/s10020-020-00195-x

Conflict of Interest: The authors declare that the research was conducted in the absence of any commercial or financial relationships that could be construed as a potential conflict of interest.

frontiers in Neuroscience

ORIGINAL RESEARCH
published: 25 March 2021
doi: 10.3389/fnins.2021.632234

Peripheral Electrical Stimulation Modulates Cortical Beta-Band Activity

*Laura J. Arendsen[1], Robert Guggenberger[1], Manuela Zimmer[1], Tobias Weigl[2] and Alireza Gharabaghi[1]**

[1] Institute for Neuromodulation and Neurotechnology, University of Tübingen, Tübingen, Germany, [2] Department of Anesthesiology and Intensive Care Medicine, University Hospital Bonn, Bonn, Germany

Low-frequency peripheral electrical stimulation using a matrix electrode (PEMS) modulates spinal nociceptive pathways. However, the effects of this intervention on cortical oscillatory activity have not been assessed yet. The aim of this study was to investigate the effects of low-frequency PEMS (4 Hz) on cortical oscillatory activity in different brain states in healthy pain-free participants. In experiment 1, PEMS was compared to sham stimulation. In experiment 2, motor imagery (MI) was used to modulate the sensorimotor brain state. PEMS was applied either during MI-induced oscillatory desynchronization (concurrent PEMS) or after MI (delayed PEMS) in a cross-over design. For both experiments, PEMS was applied on the left forearm and resting-state electroencephalography (EEG) was recording before and after each stimulation condition. Experiment 1 showed a significant decrease of global resting-state beta power after PEMS compared to sham (p = 0.016), with a median change from baseline of −16% for PEMS and −0.54% for sham. A cluster-based permutation test showed a significant difference in resting-state beta power comparing pre- and post-PEMS (p = 0.018) that was most pronounced over bilateral central and left frontal sensors. Experiment 2 did not identify a significant difference in the change from baseline of global EEG power for concurrent PEMS compared to delayed PEMS. Two cluster-based permutation tests suggested that frontal beta power may be increased following both concurrent and delayed PEMS. This study provides novel evidence for supraspinal effects of low-frequency PEMS and an initial indication that the presence of a cognitive task such as MI may influence the effects of PEMS on beta activity. Chronic pain has been associated with changes in beta activity, in particular an increase of beta power in frontal regions. Thus, brain state-dependent PEMS may offer a novel approach to the treatment of chronic pain. However, further studies are warranted to investigate optimal stimulation conditions to achieve a reduction of pain.

Keywords: sensorimotor rhythm, state-dependent stimulation, nociception, peripheral electrical stimulation, electroencephalography

OPEN ACCESS

Edited by:
Luming Li,
Tsinghua University, China

Reviewed by:
Eduardo López-Larraz,
Bitbrain, Spain
Francesco Maria Petrini,
SensArs Neuroprosthetics Sarl, Switzerland

***Correspondence:**
Alireza Gharabaghi
alireza.gharabaghi@uni-tuebingen.de

Specialty section:
This article was submitted to Neuroprosthetics, a section of the journal Frontiers in Neuroscience

Received: *22 November 2020*
Accepted: *08 March 2021*
Published: *25 March 2021*

Citation:
Arendsen LJ, Guggenberger R, Zimmer M, Weigl T and Gharabaghi A (2021) Peripheral Electrical Stimulation Modulates Cortical Beta-Band Activity. Front. Neurosci. 15:632234. doi: 10.3389/fnins.2021.632234

INTRODUCTION

In various pain conditions evidence has been found for central sensitization (Coderre et al., 1993; Banic et al., 2004; Latremoliere and Woolf, 2009; Woolf, 2011). Central sensitization broadly refers to hypersensitivity of the central nociceptive system, i.e., greater spinal excitability. Moreover, supra-spinal regions (the brainstem and higher brain centers) are important modulators of spinal excitability (Gwilym et al., 2009; Ossipov et al., 2010; Heinricher, 2016). Thus, modulating the excitability of the central nociceptive system offers a promising target for neurostimulation techniques to reduce pain.

Peripheral electrical stimulation (PES) is commonly used to facilitate motor rehabilitation and treat pain via the induction of plastic changes in corticospinal excitability (Klein et al., 2004; Chipchase et al., 2011; Dimyan and Cohen, 2011). For example, low frequency PES has been demonstrated to reduce pain perception and the spinal and cortical response to nociceptive stimuli (Jung et al., 2009, 2012; Rottmann et al., 2010). However, evidence for the clinical efficacy of PES interventions such as transcutaneous electrical nerve stimulation (TENS), a commonly used PES intervention to treat pain, is inconclusive (Catley et al., 2015; Johnson et al., 2015), leaving room for improvement.

Brain state-dependent stimulation, a novel development in the field of neurostimulation, could be of interest for the application of PES to reduce pain. Motor imagery (MI), the cognitive task of imagining a movement, is commonly used to modulate the sensorimotor brain state. MI results in sensorimotor desynchronization of alpha and beta oscillations (Fadiga et al., 1999; Pfurtscheller et al., 2006) and has a top-down influence on cortico-spinal excitability (Oishi et al., 1994; Li et al., 2004; Aoyama and Kaneko, 2011). Using MI to modulate the sensorimotor brain state, state-dependency of transcranial magnetic stimulation (TMS) and PES has been demonstrated for the motor system (Kraus et al., 2016a,b, 2018; Guggenberger et al., 2018, 2020; Ziegler et al., 2019). Stimulation applied concurrently with MI enhanced the modulation of corticospinal excitability, as reflected by an increase of the amplitude of the motor-evoked potential (MEP) (Saito et al., 2013; Kaneko et al., 2014; Kraus et al., 2016a,b). This was not the case when stimulation was applied after MI. Moreover, only when combined TMS and peripheral stimulation was applied concurrently with MI, a significant modulation of corticospinal excitability was present; this was not the case when the combined stimulation was applied after MI (Kraus et al., 2018). Thus, applying PES sensorimotor state-dependently may offer an opportunity to optimize the efficacy of low-frequency PES to modulate the excitability of the central nociceptive system and reduce pain. However, whereas previous work has predominantly examined the impact of MI combined with PES on cortico-spinal excitability of the motor system, the influence of MI and PES on the cortical response, especially in the context of nociceptive processing, is less understood.

The type of electrode used for PES is also of importance; the type of electrode influences the effect of PES on the nociceptive system (Steenbergen et al., 2012; Mücke et al., 2014). Larger surface electrodes conventionally used for TENS affect deeper tissues and activate tactile afferents. One of the main theories used to explain the effects of TENS on pain is the gate control theory of pain (Melzack and Wall, 1965). This theory proposes that a type of "gate" exists in the dorsal horn of the spinal cord that controls the transmission of large (non-nociceptive) and small (nociceptive) sensory afferents to the brain. This gate can be opened by noxious stimuli and closed by non-noxious stimuli. Following this, stimulation of large diameter tactile afferents by TENS it thought to reduce pain by inhibiting the transmission of noxious information in the spinal cord (Sluka and Walsh, 2003; Johnson et al., 2015).

In contrast, concentric electrodes preferentially activate nociceptive afferents in superficial skin layers (Kaube et al., 2000; Mücke et al., 2014). The use of repetitive electrical stimulation targeting the nociceptive fibers is thought to inhibit nociceptive processing and reduce pain via a long-term depression (LTD)-like phenomenon. Repetitive activation of synaptic connections can lead to long-term potentiation (LTP) or LTD of synaptic transmission (Madison et al., 1991; Siegelbaum and Kandel, 1991). This also applies to the transmission of noxious input. For example, it has been demonstrated that repetitive stimulation of nociceptive Aδ fibers produces LTD of C-fiber-evoked field potentials in rats (Liu et al., 1998). In humans, the induction of an LTD-like modulation of nociceptive processing and pain perception has also been demonstrated with a conditioning protocol consisting of low-frequency electrical stimuli. Using a concentric electrode, low-frequency PES has been shown to lead to a prolonged reduction of experimentally induced pain (Klein et al., 2004) that is accompanied by a reduction of the cortical evoked response to pain (Jung et al., 2009, 2012).

More recently, a new type of PES electrode has been developed that contains a matrix or grid of pin electrodes (Bomedus GmbH, Germany). Like the concentric electrode, the matrix electrode is designed to preferentially activate nociceptive afferents in the superficial skin layers, but with its larger size it allows for the stimulation of a larger skin area (Mücke et al., 2014). Compared to the concentric electrode, the matrix electrode was particularly effective in reducing deep pain sensitivity (Mücke et al., 2014). However, the cortical effects of low-frequency PES with the matrix electrode (PEMS) have not been investigated yet.

Oscillatory neural activity has been identified as a promising target for the development of novel pain therapies (Jensen et al., 2008). Chronic pain is associated with changes in oscillatory neural activity. Most commonly, an increase in theta activity is reported, and also an increase in alpha and beta activity (Sarnthein et al., 2006; Stern et al., 2006; Lim et al., 2016; Pinheiro et al., 2016; Ploner et al., 2017). Moreover, a recent recommendation in the development of safe and effective neurotherapeutics for pain emphasized the importance of the identification of objective biomarkers to help define pathophysiological subtypes of pain, evaluate target engagement of a therapy and predict therapeutic response (Davis et al., 2020). Electroencephalography (EEG)-based biomarkers of pain could be particularly useful to not only classify chronic pain, but

also to individualize pain treatment and to serve as targets for neurotherapeutics. However, more work is required to identify accurate and clinically relevant EEG-based biomarkers (Ploner and May, 2018). Therefore, in this study we investigated the effects of low-frequency PEMS on cortical oscillatory activity in the theta, alpha and beta band. In a first experiment, two 10-min blocks of PEMS were compared to sham stimulation. In a second experiment, sensorimotor state-dependency of the effect of PEMS on cortical oscillatory activity was assessed, by comparing PEMS applied during MI (concurrent stimulation) to PEMS applied after MI (delayed stimulation). To assess the effect on cortical oscillatory activity, resting-state EEG was recorded before and after each stimulation condition. Finally, previous research has also demonstrated a significant positive relationship between the self-reported kinesthetic vividness of MI and the MI-induced change in corticomotor excitability (Williams et al., 2012; Vasilyev et al., 2017; Moriuchi et al., 2020) and intracortical excitability (Lebon et al., 2012). Therefore, the Kinesthetic and Visual Imaging Questionnaire (KVIQ) (Malouin et al., 2007) was included in experiment 2 to assess the participants' MI ability, to explore if any relationship was present between visual and kinesthetic MI ability and the change in cortical oscillatory activity following state-dependent PEMS.

MATERIALS AND METHODS

Participants

The study protocol was approved by the Ethical Committee of the Medical Faculty of the University of Tübingen. All participants provided written informed consent prior to participation. A screening questionnaire was completed to ensure that all participants met the inclusion criteria of the study. All participants were aged 18 or older, free of any neurological conditions and chronic pain conditions, had no history of drug misuse or sleep deprivation, and did not use any medication that could influence the assessments. Potential participants were excluded if they had participated in another neurostimulation study in the last 48 h. Right-handedness was confirmed with the Edinburgh Handedness Inventory (Oldfield, 1971). Participants were instructed to not consume any caffeinated drinks on the day of a study visit.

Experiment 1 consisted of two study visits. In a within-subject design, 26 participants completed the first session and twenty of these participants also completed the second session. Experiment 2 consisted of a single session that was completed by twenty participants. For the statistical analysis of experiment 1, the datasets of 2 of the 20 participants that completed both experimental sessions were excluded, resulting in a total of 18 datasets (mean age ± SD = 23.28 ± 5.00 years; 10 female); one dataset was excluded due to missing data and one dataset was excluded due to poor data quality. For experiment 2, the datasets of 2 participants were excluded from the statistical analysis, resulting in a total of 18 datasets (mean age ± SD = 23.78 ± 4.43 years; 10 female); one dataset was excluded due to technical issues and one dataset was excluded due to poor data quality.

Procedure

Experiment 1

In a within-subject design, participants attended the lab for two study visits to undergo two stimulation conditions in a non-randomized order: verum stimulation (visit 1) and sham stimulation (visit 2), with a minimum of 2 weeks in between study visits. For each visit, first 5 min of resting-state EEG was recorded. This was followed by two 10-min blocks of PEMS/sham stimulation with a 10-min break between blocks, in line with the treatment recommendations of the device manufacturer (Bomedus GmbH). Another 5 min of resting-state EEG was recorded after the two stimulation blocks (**Figure 1**). Each 5-min resting-state recording consisted of ten 30-s intervals of eyes open (EO) and eyes closed (EC). Participants received auditory cues to instruct them to open/close their eyes and were asked to focus on the fixation cross on the computer screen for the EO condition to minimize eye movements.

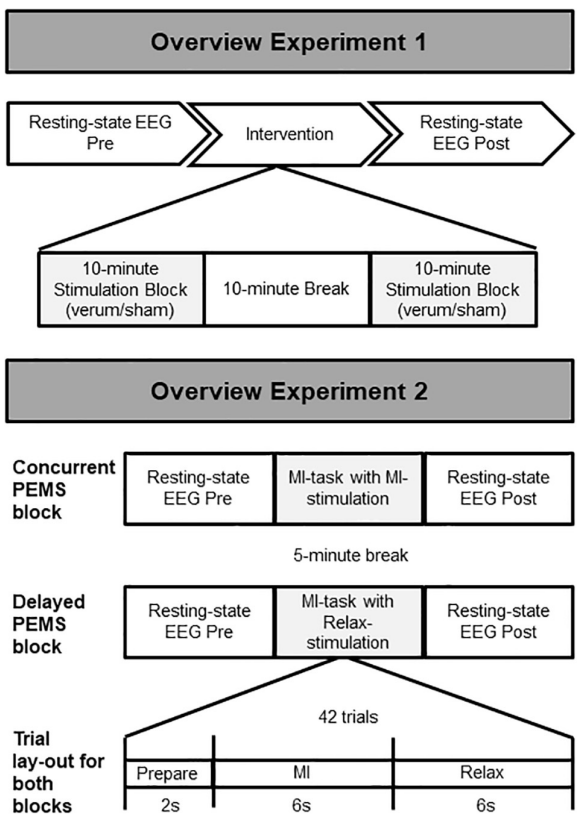

FIGURE 1 | Overview of the study procedure. Experiment 1: Two stimulation conditions (verum and sham) were delivered during two separate stimulation sessions (session 1 = verum, session 2 = sham). The same overall procedure was followed for each session, starting with 5-min recording of resting-state EEG, followed by a total of 20 min of PEMS (verum) or sham stimulation, and finally another 5-min recording of resting-state EEG. Experiment 2: Two stimulation conditions (concurrent and delayed PEMS) were delivered during a single session, in two separate blocks. Order of stimulation conditions was randomized. In the concurrent PEMS condition, PEMS was applied during the MI phase of the trial. In the delayed PEMS condition, PEMS was applied during the Relax phase of the trial.

Experiment 2

Experiment 2 consisted of a single study visit. Two stimulation conditions were applied in separate blocks in a randomized order (**Figure 1**). Each block consisted of 42 trials of MI; participants were asked to imagine extension of the fingers of the left hand. Participants received visual and auditory cues as guidance for the MI task. For each MI trial, a 2-s preparation phase ("Ready"), was followed by a 6-s MI phase ("Imagine"), and finally a 6-s rest phase ("Relax"). For one stimulation condition PEMS was applied during the MI phase of each trial (concurrent PEMS), for the other stimulation condition PEMS was applied after MI during the rest phase of each trial (delayed PEMS). Each stimulation block had a duration of ∼10 min and there was a 5-min break between blocks. Five minutes of resting-state EEG was recorded before and after each stimulation block. Participants were asked to keep their eyes opened and focused on the fixation cross on the computer screen for the entire 5-min recording. In addition, all participants completed the Kinesthetic and Visual Imaging Questionnaire (KVIQ) (Malouin et al., 2007) to assess their ability to feel and visualize imagined movements.

PES With the Matrix Electrode (PEMS)

For both experiments PES was applied using a matrix array electrode (Bomedus GmbH, Germany) that was placed over the left Extensor Digitorum Communis (EDC) muscle. A circular matrix electrode was used with a diameter of 15 cm (**Figure 2**). The Bomedus stimulator used, (The Small Fiber Activator; Bomedus GmbH) generated monopolar rectangular pulses with a width of 200 μs and a frequency of 4 Hz. A bandage was wrapped around the matrix electrode to ensure optimal contact between the electrode and the skin.

PEMS Experiment 1

For the verum stimulation condition PEMS was applied continuously (for two blocks of 10 min) at an intensity just below pain threshold, which resulted in a sensation of intense prickling under the electrode. To identify the pain threshold intensity participants were asked to gradually increase the stimulation intensity themselves and to select an intensity as high as possible before becoming painful. Participants were allowed to increase/decrease the intensity during the stimulation as well, to ensure that a sensation of intense prickling (but no pain) remained present throughout.

No stimulation was applied during the sham condition. Here participants were asked to gradually increase the stimulation intensity themselves until they first detected a prickling sensation. Then an intensity was chosen that was just below the sensory threshold. Subjects were informed that during this session the stimulation would be applied at an intensity just below the sensory threshold and would thus not be noticeable. As soon as the experiment started, the stimulator was automatically turned off, without the participant knowing.

PEMS Experiment 2

For experiment 2, PEMS was applied intermittently either during the 6-s MI phase of each trial (the concurrent PEMS condition) or the 6-s rest phase of each trial (the delayed PEMS condition).

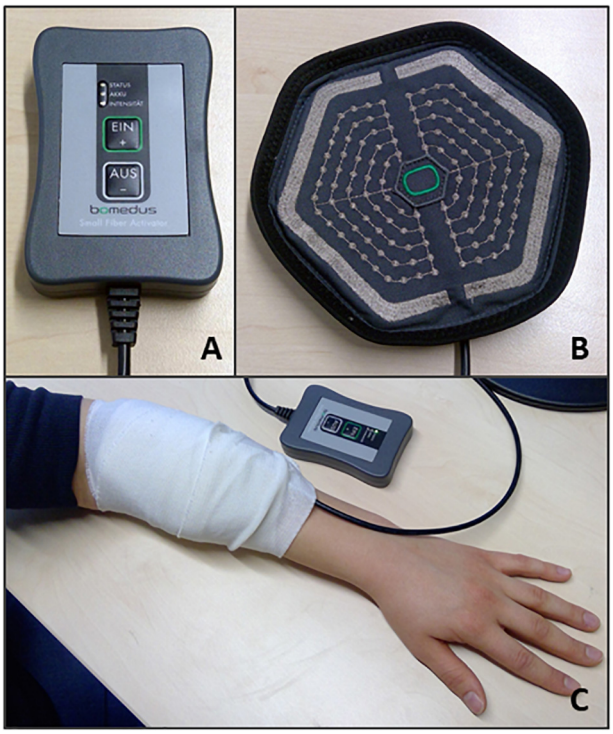

FIGURE 2 | PEMS set up. The following equipment was used to deliver the PEMS for both experiments: **(A)** The PEMS stimulator (The Small Fiber Activator; Bomedus GmbH); **(B)** A circular matrix electrode (Bomedus GmbH). **(C)** Shows the placement of the matrix electrode on the left forearm. A bandage was wrapped around the electrode to ensure optimal contact between the electrode and the skin.

Stimulation intensity was set individually, following the same procedure as for the verum stimulation (experiment 1) to ensure participants experienced a strong prickling (but not painful) sensation during the stimulation. The stimulation intensity was set separately before each of the two blocks of the experiment.

EEG Recordings

Electroencephalography was recorded using a 64-channel actiCAP combined with BrainAmp DC amplifiers (Brain Products GmbH, Germany). Impedances were kept below 25 kΩ. The AFz electrode location was used as the ground electrode and the FCz electrode location as the reference electrode.

Kinesthetic and Visual Imaging Questionnaire

For experiment 2, all participants completed the Kinesthetic and Visual Imaging Questionnaire (KVIQ) (Malouin et al., 2007). The questionnaire includes two subscales, the Visual Imagery Scale (VIS) and the Kinesthetic Imagery Scale (KIS) that contain 10 items each. For each item participants are asked to first perform a movement (e.g., elbow flexion) and then imagine performing the same movement. Next, participants rate on a 5-point scale: (i) the clarity of the visual image (1 = no image, 5 = image as clear as seeing); or (ii) the intensity of the sensations associated

with the imagined movement (1 = no sensation, 5 = as intense as executing the action). In line with Malouin et al. (2008), items involving limb movement were tested on both sides. This resulted in a total of 17 ratings for each scale and a maximum sum score of 85 for each scale.

EEG Analysis

All EEG recordings were analyzed in MATLAB (The Mathworks, Inc., Natick, MA, United States) using custom built code and the Fieldtrip toolbox (Oostenveld et al., 2011). For both experiments the same pre-processing and frequency analysis procedure was applied. For each recording, a 1 Hz high-pass filter (4th order Butterworth) was applied on the continuous data and the signal was re-referenced to the average reference. Next, the continuous EEG data was segmented into consecutive 1-s epochs. Any bad channels were interpolated. Finally, epochs containing artifacts were rejected using an automated artifact detection procedure. Any epochs containing data with a range >200 μV were rejected. The re-referencing to an average-reference was repeated after the artifact rejection procedure to ensure that for the final re-referencing the interpolated channels were included instead of the original noisy channels.

Whereas for experiment 1 resting-state EEG with EO and EC was collected, it was decided to only use the EO data for further analysis, since the closing of the eyes affects the power of ongoing alpha activity and pooling across EO and EC resting-state data would introduce variance of alpha activity. This also ensured that for both experiments the same type of resting-state data was analyzed (i.e., EO data only), as experiment 2 only included EO resting-state data. Frequency analysis was performed using the Fieldtrip toolbox (Oostenveld et al., 2011). Average EEG power was calculated using the fast Fourier transform (FFT) with a single Hanning taper for three frequency bands of interest: the theta (4–7 Hz), alpha (8–13 Hz), and beta band (15–30 Hz). For both experiments, average EEG power for the theta, alpha, and beta band was calculated for the resting-state EEG recorded before and after each stimulation condition. Finally, a change from baseline score was calculated for each stimulation condition and each frequency band of interest ((EEG power post – EEG power pre)/EEG power pre) and used for the statistical analysis. For experiment 1, this resulted in a comparison of the change from baseline score for verum stimulation versus sham stimulation for theta, alpha, and beta power separately. For experiment 2, this resulted in a comparison of the change from baseline score for concurrent PEMS (PEMS during the MI phase) versus delayed PEMS (PEMS after MI, during the rest phase).

Statistical Analysis

To assess a statistical difference between verum and sham stimulation (experiment 1) and concurrent and delayed stimulation (experiment 2), non-parametric tests were used. Non-parametric tests were chosen over parametric tests as there was evidence that the assumption of normality was not met, based on the Kolmogorov-Smirnov tests of normality and the kurtosis and skewness z-scores. Additionally, non-parametric permutation tests were used as they allow for the estimation of the statistical significance of spatial clusters. For experiment 1, the Kolmogorov-Smirnov tests of normality and the kurtosis and skewness z-scores were calculated for the difference scores in change from baseline for theta, alpha, and beta power comparing verum and sham stimulation. The same was applied for experiment 2, here for the difference scores comparing concurrent and delayed stimulation. For experiment 1 and 2 together a total of 18 tests were calculated to assess normality. More than 50% (61%) of these tests had a $p < 0.05$. For the PEMS stimulation levels applied, no strong evidence for a violation of the assumption of normality was present. For experiment 1, the kurtosis and skewness z-scores and the Kolmogorov-Smirnov test of normality were calculated for the difference score of the PEMS level of block 1 and block 2. For experiment 2, the kurtosis and skewness z-scores and the Kolmogorov-Smirnov test of normality were calculated for the difference score of the PEMS level of concurrent and delayed stimulation. Here, out of the total of 6 tests performed, less than 50% (33%) of tests had a $p < 0.05$. Therefore, for the descriptive statistics parametric tests were used.

Global EEG Power Changes

For both experiments, first, global EEG power changes were assessed (i.e., EEG power averaged over all EEG electrodes) using SPSS version 26 (IBM Corp, Armonk, NY, United States). Wilcoxon signed-rank tests were used to test for a significant difference in the change from baseline scores of global EEG power for (1) verum versus sham stimulation, and (2) concurrent PEMS versus delayed PEMS. This was done for global theta, alpha, and beta power separately, resulting in the calculation of three Wilcoxon signed-rank tests for each experiment. The exact 2-sided significance was reported.

Cluster-Based Permutation Tests

In a second step, cluster-based permutation tests (Maris and Oostenveld, 2007) were carried out using the Fieldtrip toolbox (Oostenveld et al., 2011) in MATLAB, to identify clusters where a significant difference in EEG power was present for each stimulation condition. Cluster-based permutation tests offers a more data-driven approach to identify patterns in oscillatory neural activity without strong prior assumptions and are well suited to control for the problem of multiple comparisons (Maris and Oostenveld, 2007). As there was no previous research available on the effects of PEMS on oscillatory neural activity to inform a specific frequency range and/or scalp region of interest in the present study, here we included the full range of EEG frequencies (4–30 Hz, i.e., the theta, alpha, and beta band together) and each individual EEG electrode for each cluster-based permutation test, instead of running a test for each frequency band separately.

The general cluster-based permutation test procedure that was applied for all tests in this study was as follows: (1) for every frequency-electrode pair (64 electrodes, frequency range 4–30 Hz) a repeated measures t-statistic was calculated (e.g., to compare EEG power before and after verum stimulation), to be used later to calculate the cluster-level test statistic; (2) samples were selected using the uncorrected threshold of $p < 0.05$ and the selected samples were clustered in connected sets based

on spatial and spectral adjacency; (3) cluster-level statistics were calculated by taking the sum of the t-values within each identified cluster; (4) to calculate the significance probability for the cluster-level test statistic the Monte Carlo method was used. A permutation was performed 2000 times (i.e., 2000 random partitions) to generate a random-partition-based cluster-level test statistic and (5) corrected p-values were calculated by comparing the values of the cluster-level statistics of the observed data against the distribution of the cluster-level test statistic based on the 2000 permutations.

For experiment 1, two cluster-based permutation tests were carried out to compare EEG power for the pre- and post-stimulation resting-state recordings. For the verum and sham condition separately, a comparison of resting-state EEG power pre- and post-stimulation was carried out to assess any significant changes following stimulation. The same approach was used for experiment 2, for the concurrent PEMS and delayed PEMS condition, i.e., two tests were carried out to assess any pre-post EEG power differences for each stimulation condition separately. Because we performed two statistical tests for each experiment, we used Bonferroni-correction for multiple comparison, rendering an effective alpha-threshold of 0.025. Finally, for each cluster-based permutation test, a Cohen's d effect size for dependent samples was calculated for each cluster with an uncorrected p-value < 0.05 (i.e., each cluster that was significant before correction for multiple comparison), by dividing the mean difference by the standard deviation of the difference (Lakens, 2013). To do this, the clustered channels which exhibited a difference were selected and the mean EEG power and standard deviation were calculated for these channels across the clustered frequencies which exhibited a difference.

Correlations

For experiment 2, a number of correlations were calculated to assess whether a change in EEG power in response to PEMS was related to the participant's MI capability. The sum score for the KIS and VIS were each correlated with the change from baseline scores for global theta, alpha, and beta power, for the concurrent PEMS and the delayed PEMS condition separately. I.e., 6 correlations were calculated for the VIS subscale and 6 correlations for the KIS subscale. The Bonferroni corrected significance level of 0.0083 was used.

RESULTS

Descriptive Statistics

The PEMS stimulator used in both experiments (The Small Fiber Activator; Bomedus GmbH), has a maximum output current of 40 mA and comes with 30 pre-set stimulation levels of which the participants could select their individual stimulation level.

For experiment 1, taking into account any adjustments made by the participants during the stimulation, the average stimulation level [mean (SD)] for verum stimulation was 14.94 (5.70) for stimulation block 1 and 15.86 (5.62) for stimulation block 2. A repeated measures t-test showed that there was no significant difference in stimulation level for block 1 compared to block 2 ($t = -1.94$, $p = 0.069$, $N = 18$).

For experiment 2, the average stimulation level used was 21.22 (7.62) for the concurrent PEMS condition and 20.39 (7.84) for the delayed PEMS condition. A repeated measures t-test showed that there was no significant difference in stimulation level between the two conditions ($t = 1.16$, $p = 0.26$, $N = 18$).

Global EEG Power

For experiment 1, the Wilcoxon signed rank tests comparing the change from baseline scores of global EEG power ((EEG power post – EEG power pre)/EEG power pre) for sham versus verum stimulation, showed a significant difference in the change from baseline for beta power ($Z = -2.37$, $p = 0.016$, $N = 18$). For beta power, the median change from baseline was −16% for verum stimulation and −0.54% for sham stimulation (**Figure 3**). No significant difference between verum and sham was found for the theta band ($Z = -0.94$, $p = 0.37$) or the alpha band ($Z = -0.59$, $p = 0.56$). The median change from baseline was 13% and 7.80% for the theta band and −18% and −5.88% for the alpha band, for verum and sham stimulation, respectively.

For experiment 2, the Wilcoxon signed rank tests comparing the change from baseline of global EEG power for concurrent PEMS versus delayed PEMS, did not identify a significant change of global power in any of the frequency bands (theta: $Z = -0.46$, $p = 0.67$; alpha: $Z = -0.54$, $p = 0.61$; and beta: $Z = -0.065$, $p = 0.97$). The median change from baseline was −0.57% and 2.83% for the theta band, 0.97% and −5.89% for the alpha band, and 0.41% and 4.63% for the beta band, for concurrent and delayed PEMS, respectively.

Cluster-Based Permutation Tests

Experiment 1: Verum and Sham Stimulation

The non-parametric cluster-based permutation test for the verum stimulation condition, assessing a difference in resting-state EEG power before and after verum stimulation, indicated a significant difference ($p = 0.018$). This corresponded to a negative cluster in the beta frequency band that was most pronounced over bilateral central and left frontal sensors (**Figure 4**). The Cohen's d effect size for this cluster was 0.41 (for EEG power averaged across the frequency range of 23–26 Hz and including the following 27 clustered electrodes: FT7, F5, F7, FC1, FC3, FC5, C1, C2, C4, CPz, CP1, CP3, CP4, CP5, CP6, T8, TP7, TP8, TP9, P1, P2, P4, P5, P6, P7, P8, and POz). The non-parametric cluster-based permutation test for sham stimulation did not show any significant difference for pre- and post-sham EEG power.

Experiment 2: Concurrent and Delayed PEMS

The non-parametric cluster-based permutation test for the concurrent PEMS condition, suggested a trend of a difference in resting-state EEG power comparing before and after concurrent stimulation ($p = 0.029$). This corresponded to a positive cluster in the beta frequency range that was most pronounced over frontal sensors (**Figure 5**). However, this did not survive correction for multiple comparisons, i.e., this was not significant using the corrected significance level of 0.025. The Cohen's d effect size for this cluster was 0.28 (for EEG power averaged across

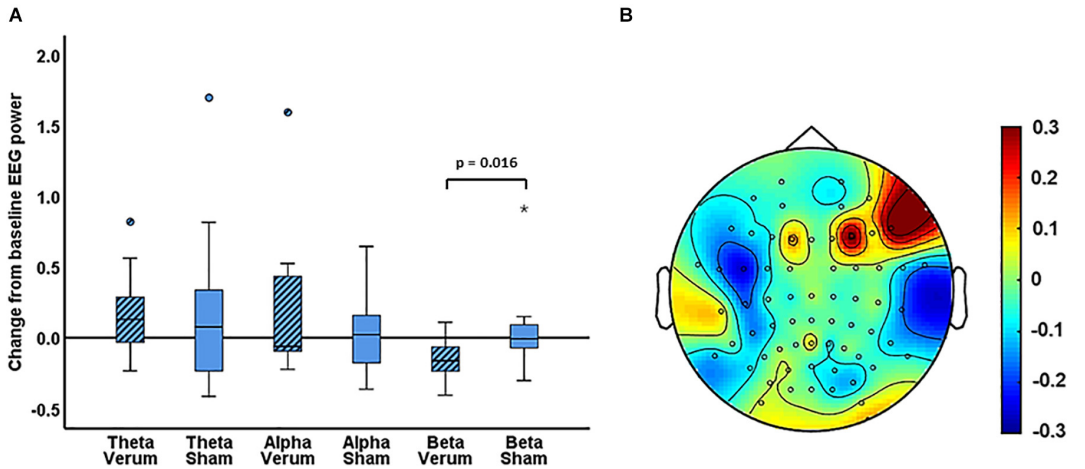

FIGURE 3 | (A) Boxplots of the change from baseline scores ((EEG power post – EEG power pre)/EEG power pre) for the verum and sham PEMS condition, and for the theta, alpha, and beta band, separately. The ° and the * in the figure indicate outliers. **(B)** A topography plot of the average change from baseline of beta power for the PEMS condition (verum stimulation).

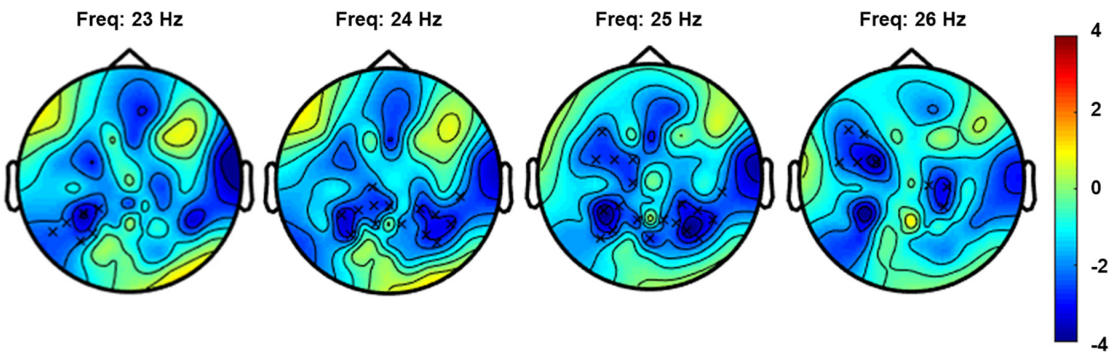

FIGURE 4 | Topoplot for the cluster-based permutation test that compared resting-state EEG power (4–30 Hz) before and after verum stimulation. The plot shows the negative cluster (indicated by the "x" markers) that demonstrated a significant difference between EEG power before and after PEMS, plotted on top of the *t*-statistic of the difference as calculated for every frequency-electrode pair (repeated-measures *t*-test). The cluster showed a significant difference most pronounced over bilateral central and left frontal regions and in the frequency range of 23–26 Hz.

the frequency range of 17–21 Hz and including the following 11 clustered electrodes: AF3, AF4, AF7, AF8, Fp2, F1, F4, F5, F7, F8, and FC3).

The non-parametric cluster-based permutation test for delayed PEMS similarly suggested a trend of a difference in resting-state EEG power comparing before and after delayed stimulation ($p = 0.039$). This corresponded to a positive cluster in the beta frequency range that was most pronounced over frontal sensors (**Figure 5**). However, again, this did not survive correction for multiple comparisons, i.e., this was not significant using the corrected significance level of 0.025. The Cohen's *d* effect size for this cluster was 0.39 (for EEG power averaged across the frequency range of 16–25 Hz and including the following 9 clustered electrodes: AF3, AF4, AF8, F1, F2, F3, F4, F5, and FC4).

Correlations

For the two subscales of the KVIQ, the average sum score was 62.94 (12.31) with a range of 36–76 for the VIS and the average sum score for the KIS was 60.61 (15.31) with a range of 20–76. For the concurrent PEMS condition, a correlation between the VIS sum score and the change from baseline score of beta power was identified ($R = -0.60$, $p = 0.009$). However, this did not survive correction for multiple comparisons (the corrected significance level was 0.0083). No significant correlations were found for the delayed PEMS condition. For the KIS subscale, no significant correlations were found either (**Table 1**).

DISCUSSION

Cortical oscillatory activity has been proposed as a promising target for the development of novel pain neurotherapeutics (Jensen et al., 2008; Ploner and May, 2018). A novel neurostimulation approach delivering low-frequency PES via a matrix electrode, has been shown particularly effective to reduce deep pain sensitivity (Mücke et al., 2014) and has

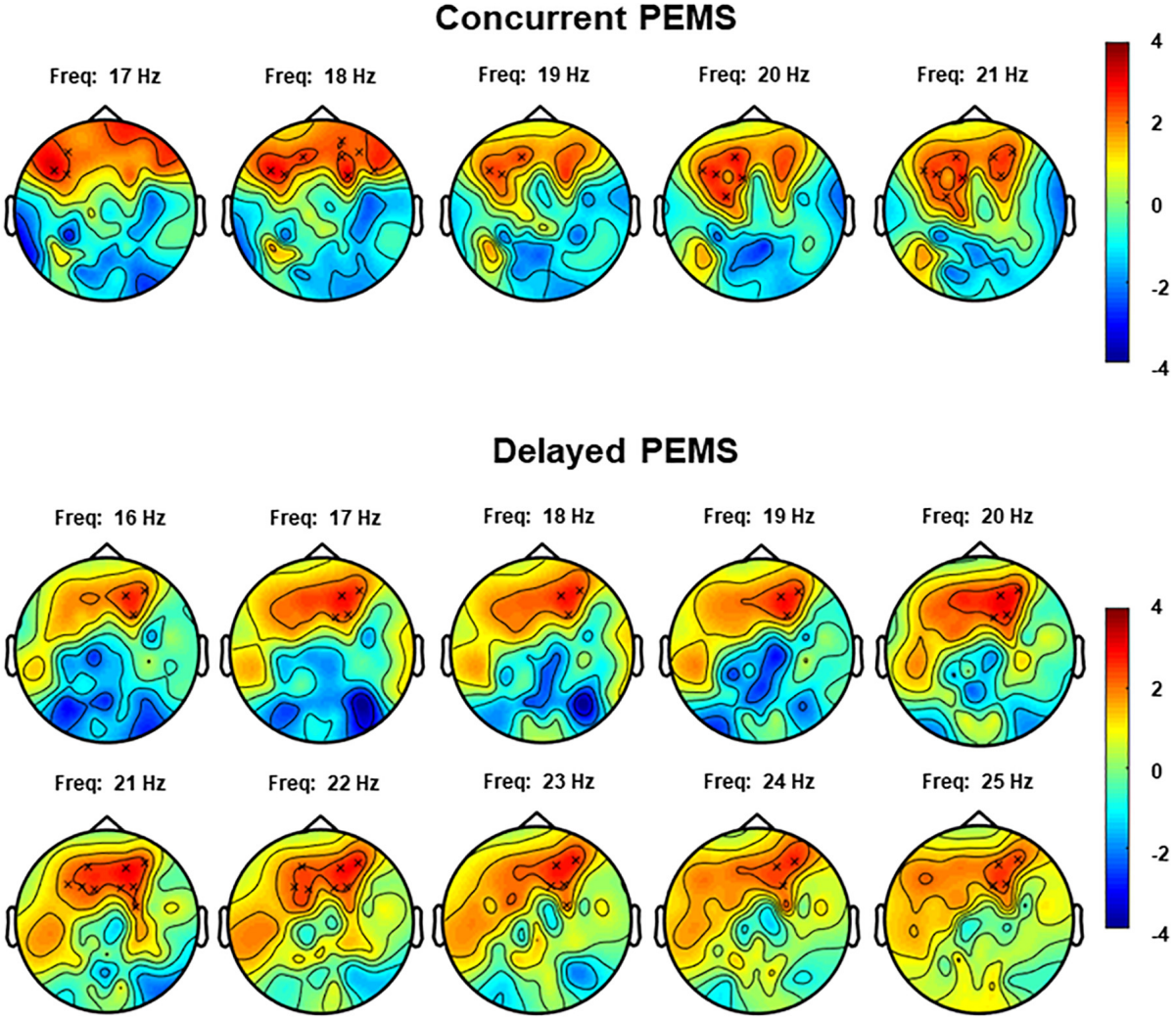

FIGURE 5 | Topoplots for the cluster-based permutation test that compared resting-state EEG power (4–30 Hz) before and after concurrent and delayed stimulation. Each plot shows the largest positive cluster (indicated by the "x" markers) that demonstrated a difference between EEG power before and after PEMS, plotted on top of the t-statistic of the difference as calculated for every frequency-electrode pair (repeated-measures *t*-test). The cluster showed a difference most pronounced over frontal regions and in the frequency range of 17–21 Hz for concurrent PEMS and 16–25 Hz for delayed PEMS.

been applied to reduce pain in patients with ongoing cancer pain (Mücke et al., 2018). The present study investigated for the first time the effects of PEMS on cortical oscillatory activity. Experiment 1 showed that low-frequency PEMS (4 Hz) resulted in a significantly larger reduction of global beta power compared to sham stimulation; the median change from baseline was −16% for PEMS and −0.54% for sham. No significant difference was identified for the theta and alpha frequency band. The cluster-based permutation test comparing resting-state EEG power before and after PEMS also resulted in a significant difference, which corresponded to a negative cluster in the beta frequency band most pronounced over bilateral central and left frontal sensors. This study provides initial evidence that low-frequency PEMS results in a widespread reduction of resting-state beta power following 20 min of stimulation, most prominent over central and frontal scalp regions.

Previously, a small number of studies also showed changes in oscillatory neural activity for PES, with varying outcomes. One study that investigated the effects of high-frequency-low-intensity TENS and low-frequency-high intensity TENS in 80 healthy pain-free participants showed that only the low-frequency-high-intensity TENS resulted in a long-lasting enhancement of ongoing alpha activity in the primary sensorimotor cortex compared to sham (Peng et al., 2019). Another study showed that following 20 min of conventional TENS at 70 Hz an increase of posterior theta power was present in patients with fibromyalgia (Yüksel et al., 2019). In addition, an increase in anterior alpha power and a decrease in posterior alpha power was found. However, it should be noted that this study did not include a sham condition. Insausti-Delgado et al. (2021) showed that neuromuscular electrical stimulation (NMES) over the wrist extensors resulted in an event-related

TABLE 1 | Overview of the results of the correlation analysis.

	VIS sum score (N = 18)	KIS sum score (N = 18)
Concurrent PEMS – theta	r = 0.092, p = 0.72	r = 0.55, p = 0.017
Concurrent PEMS – alpha	r = 0.005, p = 0.98	r = 0.22, p = 0.38
Concurrent PEMS – beta	r = −0.60, p = 0.009	r = −0.26, p = 0.30
Delayed PEMS – theta	r = 0.074, p = 0.77	r = 0.19, p = 0.44
Delayed PEMS – alpha	r = 0.15, p = 0.55	r = 0.087, p = 0.73
Delayed PEMS – beta	r = −0.47, p = 0.052	r = −0.43, p = 0.072

Correlations were calculated for the sum score of the VIS and the KIS, and the change from baseline scores of EEG power in the theta, alpha, and beta range, both for the concurrent and delayed PEMS condition. A correlation between the VIS sum score and the change from baseline score of beta power was identified for the concurrent PEMS condition. However, this did not survive correction for multiple comparisons (the corrected significance level was 0.0083).

desynchronization of sensorimotor alpha and beta oscillations, which was influenced by stimulation intensity. During high-intensity NMES (above motor threshold) a significantly larger alpha and beta desynchronization was present than during low- and medium-intensity stimulation (below motor threshold). Finally, Tu-Chan et al. (2017) investigated the potential of somatosensory electrical stimulation to improve hand function in individuals with acquired brain injury. In this pilot study, TENS was applied simultaneously over the median, ulnar, and radial nerve at an intensity that induced a clear and strong sensation but no pain or visible muscle contractions. A single 2-h session resulted in a significant improvement of hand function and a significant reduction of resting-state delta and theta power. Moreover, the improvement of finger movement was significantly correlated with the combined change of theta and alpha power over ipsilesional sensorimotor regions.

In the present study, we applied low-frequency PES with a matrix electrode to preferentially stimulate the nociceptive afferents in the superficial skin layer and found an increase in resting-state beta power over central and frontal scalp regions, following 20 min of PEMS. Thus, this study provides initial evidence for a role of beta oscillations in the cortical effects of PEMS. Moreover, the combined findings of the present study and the previous studies identifying a change in oscillatory neural activity in response to TENS and NMES, suggest that the choice of PES electrode (e.g., targeting tactile/nociceptive afferents) may have an influence on the effect of PES on cortical oscillatory activity, along with the applied stimulation parameters such as stimulation frequency and intensity. However, further studies are necessary to directly compare different electrode types, stimulation frequencies and intensities (Nilsson et al., 2003; Jung et al., 2009).

Secondly, the present study also offered an initial exploration of state dependency of the effects of PEMS on cortical oscillatory activity. Using MI to modulate sensorimotor brain activity, we assessed state-dependency of PES by comparing two stimulation conditions: (1) concurrent PEMS, i.e., PEMS applied during a state of MI-induced oscillatory desynchronization (sensorimotor activation); and (2) delayed PEMS, i.e., PEMS applied directly after MI during a state of oscillatory synchronization/rebound (sensorimotor deactivation) (Pfurtscheller and Neuper, 1997; Fadiga et al., 1999; Pfurtscheller et al., 2005, 2006). This study did not identify a significant difference between concurrent and delayed PEMS for the change from baseline of global theta/alpha/beta power, i.e., the timing of intermittent bursts of low-frequency PEMS with respect to the underlying sensorimotor brain state, did not influence the change from baseline of global cortical oscillatory activity. In addition, no significant correlations between kinesthetic and visual MI ability (KVIQ) and changes in oscillatory neural activity following state-dependent PEMS were identified. In previous studies, sensorimotor state-dependency of the effects of TMS and peripheral stimulation on corticospinal excitability (Saito et al., 2013; Kaneko et al., 2014; Kraus et al., 2016a) and intracortical motor circuits has been demonstrated (Guggenberger et al., 2018; Kraus et al., 2018; Ziegler et al., 2019).

Whereas sensorimotor state-dependency of PES has been shown for studies targeting the motor system, the present study did not show a similar state-dependency of the effects of PES on resting-state cortical oscillatory activity, when using a matrix electrode that preferentially stimulates nociceptive afferents in the skin. This is somewhat in contrast with the findings of Corbet et al. (2018), who showed that the online effects of MI on sensorimotor desynchronization were enhanced when MI was combined with NMES at sensory threshold intensity. When sensory threshold NMES was applied without MI, no significant sensorimotor desynchronization was present. However, these findings were based on changes in sensorimotor activation during the MI task, whereas the present study assessed changes comparing resting-state activity before and after stimulation. Thus, further investigation of the online effects of sensorimotor state-dependent PES could be a useful direction for future studies.

The combined findings of experiment 1 and 2, however, do suggest that adding the cognitive task of MI to PEMS may have a more general influence on the effects of PEMS on oscillatory activity. Whereas the cluster-based permutation tests for experiment 1 showed a decrease of central and frontal resting-state beta power following 20 min of continuous PEMS, this was not the case in experiment 2. Here, PEMS was applied intermittently and together with a MI task. Moreover, the cluster-based permutation tests from experiment 2 provided preliminary evidence to suggest an increase of beta power over frontal scalp regions, both after concurrent and delayed PEMS ($p < 0.05$), albeit this finding did not survive correction for multiple comparisons. Thus, the combined findings of experiment 1 and 2 suggest a potential influence of the attentional or cognitive state, induced by the MI task, on low-frequency PEMS.

Further support for an influence of attentional/cognitive factors on PEMS effects comes from the finding that PEMS compared to sham modulated beta power not only in central but also frontal regions and the initial indication that PEMS combined with MI modulates beta power in frontal regions in particular. Although traditionally, beta oscillations have been associated with sensorimotor function and motor control, more recently, beta oscillations have been investigated in a wider range of cortical areas and have been implicated in a wider range of cognitive functions (Spitzer and Haegens, 2017). In particular,

beta oscillations have been associated with top-down processing functions (Engel and Fries, 2010). For example, coherence in the beta frequency range between the frontal and parietal cortex was found in particular for top-down control of attention (compared to bottom-up control of attention) in monkeys (Buschman and Miller, 2007). In another study, humans showed a dissociation in beta oscillatory changes using a motor go/no-go paradigm (Alegre et al., 2004). A central decrease followed by an increase of beta activity was associated with movement preparation and execution, whereas a frontal increase of beta was associated with decision making and motor inhibition. Similarly, Wagner et al. (2016) showed that two distinct beta oscillatory networks were involved in motor adjustments during gait adaptation: suppression of beta power in central and parietal regions (motor execution) and an increase of beta power in prefrontal regions (cognitive top-down control).

Finally, some previous studies have also demonstrated an influence of attention and cognitive state on the effects of neurostimulation. For example, Sarkar et al. (2014) found that transcranial direct current stimulation (tDCS) over the prefrontal cortex improved reaction times for a simple arithmetic task in individuals with high anxiety related to mathematics, whereas individuals with a low anxiety level had impaired reaction times. Another study showed that the effect of tDCS applied over the parietal cortex on visual working memory was influenced both by task difficulty and participants' working memory capacity (Jones and Berryhill, 2012). For pain, it has been shown that the effect of alternating current stimulation (tACS) at alpha frequency on pain perception is influenced by expectations about pain (Arendsen et al., 2018); a reduction of pain was found when participants were uncertain about the intensity of an upcoming painful stimulus, but not when the intensity of an upcoming stimulus was predictable. However, it should be emphasized that no definitive conclusions can be drawn based on the comparison of the results of experiment 1 and 2, since the two experiments had differences in some stimulation parameters (experiment 1: a total of ∼20 min of continuous stimulation; experiment 2: ∼10 min of intermittent stimulation) that may have influenced the findings. Thus, well-controlled studies are recommended to further investigate the potential influence of a cognitive task on the effects of low-frequency PEMS.

The present study in pain-free participants showed a modulation of resting-state oscillatory activity in the beta band specifically. Chronic pain is associated with changes in cortical oscillatory activity in a variety of frequency bands, including the beta band. In particular, an increase of beta power in frontal regions has been demonstrated (Sarnthein et al., 2006; Stern et al., 2006; Lim et al., 2016; Ploner et al., 2017). PES using the matrix electrode to modulate frontal beta power may therefore offer a novel direction in the application of PES to reduce chronic pain. The initial suggestion of this study, that the effects of low-frequency PEMS may be influenced by the presence of a cognitive task (albeit in pain-free participants), is also of interest to the application of PES interventions to reduce chronic pain. To improve the efficacy of neurostimulation interventions to manage chronic pain, it is important to take into account inter- and intra-individual factors such as cognitive, psychological, and neurophysiological state (Li et al., 2015; Fertonani and Miniussi, 2017). Thus, further investigations on the influence of adding a cognitive task such as MI to PES interventions to reduce chronic pain should be considered. In addition, adding a cognitive task such as MI introduces an element of active participation to any intervention. Active patient engagement in the therapeutic context is key in achieving lasting clinical improvements (Lequerica and Kortte, 2010; Blank et al., 2014). Ultimately, improving our understanding of the influence of these attentional/cognitive factors on the effects of PES may improve the efficacy of PES interventions to reduce chronic pain. However, future investigations should also include measures of pain experience, to assess whether the modulation of beta activity in associated with a reduction in pain. Whereas the potential of PEMS to reduce pain in healthy pain-free participants has been demonstrated previously (Mücke et al., 2014), no simultaneous assessment of changes in oscillatory neural activity and pain experience following PEMS has been carried out yet. Confirming a relationship between the modulation of beta power and pain experience would be an important next step in the confirmation of beta power as a potential biomarker for low-frequency PEMS, and in line with the recent recommendations of the importance of identifying objective biomarkers for the development of safe and effective neurotherapeutics for pain (Davis et al., 2020).

Another factor deserving further investigation is whether any effects following (state-dependent) PES remain present for a longer period after stimulation. The present study focused on changes in oscillatory neural activity in the period immediately after PEMS and did not include any longer-term assessments of change in oscillatory neural activity (e.g., 30 min after stimulation). Some previous studies investigating cortical effects of low-frequency PES have shown a longer-term reduction of SEP amplitude (up to 30–60 min post-stimulation) (Jung et al., 2009, 2012). However, less is known about any longer-lasting effects of PES on oscillatory neural activity, especially for PES combined with MI. Previous studies demonstrated an online effect of PES combined with MI on corticospinal excitability (Saito et al., 2013; Kaneko et al., 2014) and sensorimotor desynchronization (Corbet et al., 2018). When a combined TMS and peripheral stimulation protocol was applied sensorimotor state-dependently, a modulation of corticospinal excitability and cortical motor maps survived a depotentiation task with voluntary muscle contraction after the stimulation indicating robustness (Guggenberger et al., 2018; Kraus et al., 2018). When considering the implementation of state-dependent low-frequency PES as a pain intervention, it is critical that we gain a better understanding of any longer-lasting effects of PES and the specific stimulation parameters that are most effective to inducing a plastic change in central nociception and the perception of pain.

Finally, a recent study showed that MI together with NMES at sensory threshold resulted in a larger desynchronization of sensorimotor oscillatory activity and a significant enhancement of brain connectivity patterns (compared to MI accompanied by visual feedback) (Corbet et al., 2018). A significantly higher connectivity was found for MI with NMES in the fronto-parietal network, including the associative somatosensory cortex, premotor cortex and supplementary motor area, and the primary

motor cortex. These observations confirmed previous findings applying MI with visual or proprioceptive feedback (Vukeliæ and Gharabaghi, 2015): Both feedback modalities activated a distributed functional connectivity network of coherent oscillations. However, proprioceptive feedback was more suitable than visual feedback to entrain the motor network architecture (e.g., beta-band and theta-band activity in bilateral fronto-central regions and left parieto-occipital regions, respectively) during the interplay between motor imagery and feedback processing, thus resulting in better volitional control of regional brain activity. Therefore, the inclusion of connectivity analysis would be recommended for future studies investigating the cortical effects of brain state-dependent PES, to gain further insight on the effects of PES on the interaction between somatosensory and motor brain regions.

CONCLUSION

This study investigated the effects of low-frequency PEMS on cortical oscillatory activity in the theta, alpha and beta band. Secondly, sensorimotor state-dependency of the effect of PEMS on cortical oscillatory activity was assessed using a MI task. Low-frequency PEMS (4 Hz) resulted in a significantly larger reduction of global beta power compared to sham stimulation after the stimulation period. This reduction was most pronounced over central and frontal scalp regions. Furthermore, there was some initial evidence to suggest an influence of MI on the effect of PEMS. Following PEMS combined with a MI task no decrease of global beta power was present. Instead, the results provide preliminary evidence for an increase of frontal beta power following both concurrent and delayed PEMS, although there was no significant difference between these two conditions. This study provides novel evidence for supraspinal effects of low-frequency PEMS and an initial indication that the presence of a cognitive task such as MI may influence the effects of PEMS on beta activity.

DATA AVAILABILITY STATEMENT

The raw data supporting the conclusions of this article will be made available by the authors, without undue reservation.

ETHICS STATEMENT

The studies involving human participants were reviewed and approved by the Ethical Committee of the Medical Faculty of the University of Tübingen. The patients/participants provided their written informed consent to participate in this study.

AUTHOR CONTRIBUTIONS

AG, TW, and RG: conceptualization and study design. MZ: recruitment and data collection. LA, RG, and MZ: analysis. LA: writing – original draft preparation. All authors writing – review and editing.

FUNDING

This research study was supported by the German Federal Ministry of Education and Research (BMBF 13GW0214, INSPIRATION). We also acknowledge support by the Open Access Publishing Fund of the University of Tübingen.

REFERENCES

Alegre, M., Gurtubay, I. G., Labarga, A., Iriarte, J., Valencia, M., and Artieda, J. (2004). Frontal and central oscillatory changes related to different aspects of the motor process: A study in go/no-go paradigms. *Exp. Brain Res.* 159, 14–22. doi: 10.1007/s00221-004-1928-8

Aoyama, T., and Kaneko, F. (2011). The effect of motor imagery on gain modulation of the spinal reflex. *Brain Res.* 1372, 41–48. doi: 10.1016/j.brainres.2010.11.023

Arendsen, L. J., Hugh-Jones, S., and Lloyd, D. M. (2018). Transcranial alternating current stimulation at alpha frequency reduces pain when the intensity of pain is uncertain. *J. Pain* 19, 807–818.

Banic, B., Petersen-Felix, S., Andersen, O. K., Radanov, B. P., Villiger, P. M., Arendt-Nielsen, L., et al. (2004). Evidence for spinal cord hypersensitivity in chronic pain after whiplash injury and in fibromyalgia. *Pain* 107, 7–15. doi: 10.1016/j.pain.2003.05.001

Blank, A. A., French, J. A., Pehlivan, A. U., and O'Malley, M. K. (2014). Current trends in robot-assisted upper-limb stroke rehabilitation: Promoting patient engagement in therapy. *Curr. Phys. Med. Rehabilit. Rep.* 2, 184–195. doi: 10.1007/s40141-014-0056-z

Buschman, T. J., and Miller, E. K. (2007). Top-down versus bottom-up control of attention in the prefrontal and posterior parietal cortices. *Science* 315, 1860–1862.

Catley, M. J., Gibson, W., Wand, B. M., Meads, C., and O'Connell, N. E. (2015). Transcutaneous Electrical Nerve Stimulation (TENS) for chronic pain - an overview of Cochrane reviews. *Cochr. Database Systemat. Rev.* 4:CD011890. doi: 10.1002/14651858.CD011890

Chipchase, L. S., Schabrun, S. M., and Hodges, P. W. (2011). Peripheral electrical stimulation to induce cortical plasticity: A systematic review of stimulus parameters. *Clin. Neurophysiol.* 122, 456–463. doi: 10.1016/j.clinph.2010.07.025

Coderre, T. J., Katz, J., Vaccarino, A. L., and Melzack, R. (1993). Contribution of central neuroplasticity to pathological pain: Review of clinical and experimental evidence. *Pain* 52, 259–285. doi: 10.1016/0304-3959(93)90161-H

Corbet, T., Iturrate, I., Pereira, M., Perdikis, S., Millán, J., and del, R. (2018). Sensory threshold neuromuscular electrical stimulation fosters motor imagery performance. *NeuroImage* 176, 268–276. doi: 10.1016/j.neuroimage.2018.04.005

Davis, K. D., Aghaeepour, N., Ahn, A. H., Angst, M. S., Borsook, D., Brenton, A., et al. (2020). Discovery and validation of biomarkers to aid the development of safe and effective pain therapeutics: challenges and opportunities. *Nat. Rev. Neurol.* 16, 381–400. doi: 10.1038/s41582-020-0362-2

Dimyan, M. A., and Cohen, L. G. (2011). Neuroplasticity in the context of motor rehabilitation after stroke. *Nat. Rev. Neurol.* 7, 76–85. doi: 10.1038/nrneurol.2010.200

Engel, A. K., and Fries, P. (2010). Beta-band oscillations-signalling the status quo? *Curr. Opin. Neurobiol.* 20, 156–165. doi: 10.1016/j.conb.2010.02.015

Fadiga, L., Buccino, G., Craighero, L., Fogassi, L., Gallese, V., and Pavesi, G. (1999). Corticospinal excitability is specifically modulated by motor imagery: A magnetic stimulation study. *Neuropsychologia* 37, 147–158. doi: 10.1016/S0028-3932(98)00089-X

Fertonani, A., and Miniussi, C. (2017). Transcranial electrical stimulation: What we know and do not know about mechanisms. *Neuroscientist* 23, 109–123. doi: 10.1177/1073858416631966

Guggenberger, R., Kraus, D., Naros, G., Leão, M. T., Ziemann, U., and Gharabaghi, A. (2018). Extended enhancement of corticospinal connectivity with concurrent cortical and peripheral stimulation controlled by sensorimotor desynchronization. *Brain Stimulat.* 11, 1331–1335.

Guggenberger, R., Raco, V., and Gharabaghi, A. (2020). State-Dependent Gain Modulation of Spinal Motor Output. *Front. Bioengine. Biotechnol.* 8:523866. doi: 10.3389/fbioe.2020.523866

Gwilym, S. E., Keltner, J. R., Warnaby, C. E., Carr, A. J., Chizh, B., Chessell, I., et al. (2009). Psychophysical and functional imaging evidence supporting the presence of central sensitization in a cohort of osteoarthritis patients. *Arthritis Care Res.* 61, 1226–1234. doi: 10.1002/art.24837

Heinricher, M. M. (2016). "Pain Modulation and the Transition from Acute to Chronic Pain," in *Translational Research in Pain and Itch. Advances in Experimental Medicine and Biology*, Vol. 904, eds C. Ma and Y. Huang (Berlin: Springer), doi: 10.1007/978-94-017-7537-3_8

Insausti-Delgado, A., López-Larraz, E., Omedes, J., and Ramos-Murguialday, A. (2021). Intensity and Dose of Neuromuscular Electrical Stimulation Influence Sensorimotor Cortical Excitability. *Front. Neurosci.* 14:593360. doi: 10.3389/fnins.2020.593360

Jensen, M. P., Hakimian, S., Sherlin, L. H., and Fregni, F. (2008). New insights into neuromodulatory approaches for the treatment of pain. *J. Pain* 9, 193–199. doi: 10.1016/j.jpain.2007.11.003

Johnson, M. I., Paley, C. A., Howe, T. E., and Sluka, K. A. (2015). Transcutaneous electrical nerve stimulation for acute pain. *Cochr. Database Systemat. Rev.* 6:CD006142.

Jones, K. T., and Berryhill, M. E. (2012). Parietal contributions to visual working memory depend on task difficulty. *Front. Psychiatry* 3:1–11. doi: 10.3389/fpsyt.2012.00081

Jung, K., Lelic, D., Rottmann, S., Drewes, A. M., Petrini, L., and Ellrich, J. (2012). Electrical low-frequency stimulation induces central neuroplastic changes of pain processing in man. *Eur. J. Pain* 16, 509–521. doi: 10.1016/j.ejpain.2011.08.006

Jung, K., Rottmann, S., and Ellrich, J. (2009). Long-term depression of spinal nociception and pain in man: Influence of varying stimulation parameters. *Eur. J. Pain* 13, 161–170. doi: 10.1016/j.ejpain.2008.04.001

Kaneko, F., Hayami, T., Aoyama, T., and Kizuka, T. (2014). Motor imagery and electrical stimulation reproduce corticospinal excitability at levels similar to voluntary muscle contraction. *J. NeuroEngine. Rehabilit.* 11:94. doi: 10.1186/1743-0003-11-94

Kaube, H., Katsarava, Z., Käufer, T., Diener, H. C., and Ellrich, J. (2000). A new method to increase nociception specificity of the human blink reflex. *Clin. Neurophysiol.* 111, 413–416. doi: 10.1016/S1388-2457(99)00295-3

Klein, T., Magerl, W., Hopf, H. C., Sandkühler, J., and Treede, R. D. (2004). Perceptual correlates of nociceptive long-term potentiation and Long-term depression in humans. *J. Neurosci.* 24, 964–971. doi: 10.1523/jneurosci.1222-03.2004

Kraus, D., Naros, G., Bauer, R., Khademi, F., Leão, M. T., Ziemann, U., et al. (2016a). Brain state-dependent transcranial magnetic closed-loop stimulation controlled by sensorimotor desynchronization induces robust increase of corticospinal excitability. *Brain Stimulat.* 9, 415–424. doi: 10.1016/j.brs.2016.02.007

Kraus, D., Naros, G., Bauer, R., Leão, M. T., Ziemann, U., and Gharabaghi, A. (2016b). Brain–robot interface driven plasticity: Distributed modulation of corticospinal excitability. *NeuroImage* 125, 522–532. doi: 10.1016/j.neuroimage.2015.09.074

Kraus, D., Naros, G., Guggenberger, R., Leão, M. T., Ziemann, U., and Gharabaghi, A. (2018). Recruitment of additional corticospinal pathways in the human brain with state-dependent paired associative stimulation. *J. Neurosci.* 38, 1396–1407. doi: 10.1523/jneurosci.2893-17.2017

Lakens, D. (2013). Calculating and reporting effect sizes to facilitate cumulative science: a practical primer for *t*-tests and ANOVAs. *Front. Psychol.* 4:863. doi: 10.3389/fpsyg.2013.00863

Latremoliere, A., and Woolf, C. J. (2009). Central sensitization: A generator of pain hypersensitivity by central neural plasticity. *J. Pain* 10, 895–926. doi: 10.1016/j.jpain.2009.06.012

Lebon, F., Byblow, W. D., Collet, C., Guillot, A., and Stinear, C. M. (2012). The modulation of motor cortex excitability during motor imagery depends on imagery quality. *Eur. J. Neurosci.* 35, 323–331. doi: 10.1111/j.1460-9568.2011.07938.x

Lequerica, A. H., and Kortte, K. (2010). Therapeutic engagement: A proposed model of engagement in medical rehabilitation. *Am. J. Phys. Med. Rehabilit.* 89, 415–422. doi: 10.1097/phm.0b013e3181d8ceb2

Li, L. M., Uehara, K., and Hanakawa, T. (2015). The contribution of interindividual factors to variability of response in transcranial direct current stimulation studies. *Front. Cell. Neurosci.* 9:181. doi: 10.3389/fncel.2015.00181

Li, S., Kamper, D. G., Stevens, J. A., and Rymer, W. Z. (2004). The effect of motor imagery on spinal segmental excitability. *J. Neurosci.* 24, 9674–9680. doi: 10.1523/jneurosci.2781-04.2004

Lim, M., Kim, J. S., Kim, D. J., and Chung, C. K. (2016). Increased low- and high-frequency oscillatory activity in the prefrontal cortex of fibromyalgia patients. *Front. Hum. Neurosci.* 10:111. doi: 10.3389/fnhum.2016.00111

Liu, X.-G., Morton, G. R., Azkue, J. J., Zimmermann, M., and Sandkühler, J. (1998). Long-term depression of C-fibre-evoked spinal field potentials by stimulation of primary afferent Aδ-fibres in the adult rat. *Eur. J. Neurosci.* 10, 3069–3075. doi: 10.1046/j.1460-9568.1998.00310.x

Madison, D. V., Malenka, R. C., and Nicoll, R. A. (1991). Mechanisms underlying long-term potentiation of synaptic transmission. *Annu. Rev. Neurosci.* 14, 379–397. doi: 10.1146/annurev.ne.14.030191.002115

Malouin, F., Richards, C. L., Durand, A., and Doyon, J. (2008). Clinical assessment of motor imagery after stroke. *Neurorehabilit. Neural Repair* 22, 330–340. doi: 10.1177/1545968307313499

Malouin, F., Richards, C. L., Jackson, P. L., Lafleur, M. F., Durand, A., and Doyon, J. (2007). The kinesthetic and visual imagery questionnaire (KVIQ) for assessing motor imagery in persons with physical disabilities: A reliability and construct validity study. *J. Neurol. Phys. Ther.* 31, 20–29. doi: 10.1097/01.NPT.0000260567.24122.64

Maris, E., and Oostenveld, R. (2007). Nonparametric statistical testing of EEG- and MEG-data. *J. Neurosci. Methods* 164, 177–190. doi: 10.1016/j.jneumeth.2007.03.024

Melzack, R., and Wall, P. D. (1965). Pain mechanisms - a new theory. *Science* 150, 971–979.

Moriuchi, T., Nakashima, A., Nakamura, J., Anan, K., Nishi, K., Matsuo, T., et al. (2020). The Vividness of Motor Imagery Is Correlated With Corticospinal Excitability During Combined Motor Imagery and Action Observation. *Front. Hum. Neurosci.* 14:581652. doi: 10.3389/fnhum.2020.581652

Mücke, M., Tils, M., Conrad, R., Kravchenko, D., Cuhls, H., Radbruch, L., et al. (2018). Matrix stimulation in cancer pain: Methodology, safety and effectiveness. *Eur. J. Pain* 22, 58–71. doi: 10.1002/ejp.1089

Mücke, Martin, Cuhls, H., Radbruch, L., Weigl, T., and Rolke, R. (2014). Evidence of heterosynaptic LTD in the human nociceptive system: Superficial skin neuromodulation using a matrix lectrode reduces deep pain sensitivity. *PLoS One* 9:e107718. doi: 10.1371/journal.pone.0107718

Nilsson, H. J., Psouni, E., and Schouenborg, J. (2003). Long term depression of human nociceptive skin senses induced by thin fibre stimulation. *Eur. J. Pain* 7, 225–233. doi: 10.1016/S1090-3801(02)00120-9

Oishi, K., Kimura, M., Yasukawa, M., Yoneda, T., and Maeshima, T. (1994). Amplitude reduction of H-reflex during mental movement simulation in elite athletes. *Behav. Brain Res.* 62, 55–61.

Oldfield, R. C. (1971). The assessment and analysis of handedness: The Edinburgh inventory. *Neuropsychologia* 9, 97–113. doi: 10.1016/0028-3932(71)90067-4

Oostenveld, R., Fries, P., Maris, E., and Schoffelen, J. M. (2011). FieldTrip: Open source software for advanced analysis of MEG, EEG, and invasive electrophysiological data. *Computat. Intellig. Neurosci.* 2011:156869.

Ossipov, M. H., Dussor, G. O., and Porreca, F. (2010). Central modulation of pain. *J. Clin. Investig.* 120, 3779–3787. doi: 10.1172/JCI43766.reduced

Peng, W. W., Tang, Z. Y., Zhang, F. R., Li, H., Kong, Y. Z., Iannetti, G. D., et al. (2019). Neurobiological mechanisms of TENS-induced analgesia. *NeuroImage* 195, 396–408. doi: 10.1016/j.neuroimage.2019.03.077

Pfurtscheller, G., and Neuper, C. (1997). Motor imagery activates primary sensorimotor area in humans. *Neurosci. Lett.* 239, 65–68. doi: 10.1016/S0304-3940(97)00889-6

Pfurtscheller, G., Brunner, C., Schlögl, A., Lopes, and da Silva, F. H. (2006). Mu rhythm (de)synchronization and EEG single-trial classification of different motor imagery tasks. *NeuroImage* 31, 153–159. doi: 10.1016/j.neuroimage.2005.12.003

Pfurtscheller, G., Neuper, C., Brunner, C., Lopes, and Da Silva, F. (2005). Beta rebound after different types of motor imagery in man. *Neurosci. Lett.* 378, 156–159. doi: 10.1016/j.neulet.2004.12.034

Pinheiro, E. S. D. S., De Queirós, F. C., Montoya, P., Santos, C. L., Do Nascimento, M. A., Ito, C. H., et al. (2016). Electroencephalographic patterns in chronic pain: A systematic review of the literature. *PLoS One* 11:e0149085. doi: 10.1371/journal.pone.0149085

Ploner, M., Sorg, C., and Gross, J. (2017). Brain Rhythms of Pain. *Trends Cognit. Sci.* 21, 100–110. doi: 10.1016/j.tics.2016.12.001

Ploner, M., and May, E. S. (2018). Electroencephalography and magnetoencephalography in pain research - Current state and future perspectives. *Pain* 159, 206–211. doi: 10.1097/j.pain.0000000000001087

Rottmann, S., Jung, K., Vohn, R., and Ellrich, J. (2010). Long-term depression of pain-related cerebral activation in healthy man: An fMRI study. *Eur. J. Pain* 14, 615–624. doi: 10.1016/j.ejpain.2009.10.006

Saito, K., Yamaguchi, T., Yoshida, N., Tanabe, S., Kondo, K., and Sugawara, K. (2013). Combined effect of motor imagery and peripheral nerve electrical stimulation on the motor cortex. *Exp. Brain Res.* 227, 333–342. doi: 10.1007/s00221-013-3513-5

Sarkar, A., Dowker, A., and Kadosh, R. C. (2014). Cognitive enhancement or cognitive cost: Trait-specific outcomes of brain stimulation in the case of mathematics anxiety. *J. Neurosci.* 34, 16605–16610. doi: 10.1523/JNEUROSCI.3129-14.2014

Sarnthein, J., Stern, J., Aufenberg, C., Rousson, V., and Jeanmonod, D. (2006). Increased EEG power and slowed dominant frequency in patients with neurogenic pain. *Brain* 129, 55–64. doi: 10.1093/brain/awh631

Siegelbaum, S. A., and Kandel, E. R. (1991). Learning-related synaptic plasticity: LTP and LTD. *Curr. Opin. Neurobiol.* 1, 113–120. doi: 10.1016/0959-4388(91)90018-3

Sluka, K. A., and Walsh, D. (2003). Transcutaneous electrical nerve stimulation: Basic science mechanisms and clinical effectiveness. *J. Pain* 4, 109–121. doi: 10.1054/jpai.2003.434

Spitzer, B., and Haegens, S. (2017). Beyond the Status Quo: A Role for Beta Oscillations in Endogenous Content (Re) Activation. *Cognit. Behav.* 4, 1–15.

Steenbergen, P., Buitenweg, J. R., Trojan, J., van der Heide, E. M., van den Heuvel, T., Flor, H., et al. (2012). A system for inducing concurrent tactile and nociceptive sensations at the same site using electrocutaneous stimulation. *Behav. Res. Methods* 44, 924–933. doi: 10.3758/s13428-012-0216-y

Stern, J., Jeanmonod, D., and Sarnthein, J. (2006). Persistent EEG overactivation in the cortical pain matrix of neurogenic pain patients. *NeuroImage* 31, 721–731. doi: 10.1016/j.neuroimage.2005.12.042

Tu-Chan, A. P., Natraj, N., Godlove, J., Abrams, G., and Ganguly, K. (2017). Effects of somatosensory electrical stimulation on motor function and cortical oscillations. *J. NeuroEngine. Rehabilit.* 14:113. doi: 10.1186/s12984-017-0323-1

Vasilyev, A., Liburkina, S., Yakovlev, L., Perepelkina, O., and Kaplan, A. (2017). Assessing motor imagery in brain-computer interface training: Psychological and neurophysiological correlates. *Neuropsychologia* 97, 56–65. doi: 10.1016/j.neuropsychologia.2017.02.005

Vukelić, M., and Gharabaghi, A. (2015). Oscillatory entrainment of the motor cortical network during motor imagery is modulated by the feedback modality. *NeuroImage* 111, 1–11. doi: 10.1016/j.neuroimage.2015.01.058

Wagner, J., Makeig, S., Gola, M., Neuper, C., and Müller-Putz, G. (2016). Distinct β band oscillatory networks subserving motor and cognitive control during gait adaptation. *J. Neurosci.* 36, 2212–2226. doi: 10.1523/JNEUROSCI.3543-15.2016

Williams, J., Pearce, A. J., Loporto, M., Morris, T., and Holmes, P. S. (2012). The relationship between corticospinal excitability during motor imagery and motor imagery ability. *Behav. Brain Res.* 226, 369–375. doi: 10.1016/j.bbr.2011.09.014

Woolf, C. J. (2011). Central sensitization: Implications for the diagnosis and treatment of pain. *Pain* 152, S2–S15. doi: 10.1016/j.pain.2010.09.030

Yüksel, M., Ayaş, Ş., Cabioğlu, M. T., Yilmaz, D., and Cabioğlu, C. (2019). Quantitative Data for Transcutaneous Electrical Nerve Stimulation and Acupuncture Effectiveness in Treatment of Fibromyalgia Syndrome. *Evid. Based Complemen. Alternat. Med.* 2019:9684649. doi: 10.1155/2019/9684649

Ziegler, L., Schulte, R., and Gharabaghi, A. (2019). Combined endogenous and exogenous disinhibition of intracortical circuits augments plasticity induction in the human motor cortex. *Brain Stimulat.* 12, 1027–1040. doi: 10.1016/j.brs.2019.03.009

Conflict of Interest: TW is the founder and CEO of Bomedus GmbH, the company that developed the stimulation device used in this study.

The remaining authors declare that the research was conducted in the absence of any commercial or financial relationships that could be construed as a potential conflict of interest.

The reviewer EL-L declared a past co-authorship with one of the authors AG to the handling editor.

frontiers in Neuroscience

ORIGINAL RESEARCH
published: 07 April 2021
doi: 10.3389/fnins.2021.632768

Neuroskeletal Effects of Chronic Bioelectric Nerve Stimulation in Health and Diabetes

*Alec T. Beeve[1,2], Ivana Shen[2], Xiao Zhang[1,2], Kristann Magee[2], Ying Yan[3], Matthew R. MacEwan[3] and Erica L. Scheller[1,2]**

[1] Department of Biomedical Engineering, Washington University in St. Louis, St. Louis, MO, United States, [2] Department of Internal Medicine, Division of Bone and Mineral Diseases, Washington University School of Medicine in St. Louis, St. Louis, MO, United States, [3] Department of Neurosurgery, Washington University School of Medicine in St. Louis, St. Louis, MO, United States

Background/Aims: Bioelectric nerve stimulation (eStim) is an emerging clinical paradigm that can promote nerve regeneration after trauma, including within the context of diabetes. However, its ability to prevent the onset of diabetic peripheral neuropathy (DPN) has not yet been evaluated. Beyond the nerve itself, DPN has emerged as a potential contributor to sarcopenia and bone disease; thus, we hypothesized that eStim could serve as a strategy to simultaneously promote neural and musculoskeletal health in diabetes.

Methods: To address this question, an eStim paradigm pre-optimized to promote nerve regeneration was applied to the sciatic nerve, which directly innervates the tibia and lower limb, for 8 weeks in control and streptozotocin-induced type 1 diabetic (T1D) rats. Metabolic, gait, nerve and bone assessments were used to evaluate the progression of diabetes and the effect of sciatic nerve eStim on neuropathy and musculoskeletal disease, while also considering the effects of cuff placement and chronic eStim in otherwise healthy animals.

Results: Rats with T1D exhibited increased mechanical allodynia in the hindpaw, reduced muscle mass, decreased cortical and cancellous bone volume fraction (BVF), reduced cortical bone tissue mineral density (TMD), and decreased bone marrow adiposity. Type 1 diabetes also had an independent effect on gait. Placement of the cuff electrode alone resulted in altered gait patterns and unilateral reductions in tibia length, cortical BVF, and bone marrow adiposity. Alterations in gait patterns were restored by eStim and tibial lengthening was favored unilaterally; however, eStim did not prevent T1D-induced changes in muscle, bone, marrow adiposity or mechanical sensitivity. Beyond this, chronic eStim resulted in an independent, bilateral reduction in cortical TMD.

Conclusion: Overall, these results provide new insight into the pathogenesis of diabetic neuroskeletal disease and its regulation by eStim. Though eStim did not prevent neural or musculoskeletal complications in T1D, our results demonstrate that clinical applications of peripheral neuromodulation ought to consider the impact of device

OPEN ACCESS

Edited by:
Jiande Chen,
University of Michigan, United States

Reviewed by:
Megan Killian,
University of Michigan, United States
Liudmila Leppik,
Goethe University Frankfurt, Germany

***Correspondence:**
Erica L. Scheller
scheller@wustl.edu;
scheller@umich.edu

Specialty section:
This article was submitted to Autonomic Neuroscience, a section of the journal Frontiers in Neuroscience

Received: *24 November 2020*
Accepted: *16 March 2021*
Published: *07 April 2021*

Citation:
Beeve AT, Shen I, Zhang X, Magee K, Yan Y, MacEwan MR and Scheller EL (2021) Neuroskeletal Effects of Chronic Bioelectric Nerve Stimulation in Health and Diabetes. Front. Neurosci. 15:632768. doi: 10.3389/fnins.2021.632768

placement and eStim on long-term skeletal health in both healthy individuals and those with metabolic disease. This includes monitoring for compounded bone loss to prevent unintended consequences including decreased bone mineral density and increased fracture risk.

Keywords: bone, nerves, neuropathy, electrical stimulation, muscle, type 1 diabetes (T1D), gait, bone marrow adiposity

INTRODUCTION

Therapeutic use of electrical stimuli, or bioelectric medicine, is ancient. For centuries, humans have exploited the responses of the body to electrical stimuli for medical treatment, starting with pain and expanding to increasingly complex disorders from hearing loss to paralysis (Chang, 2021). Bioelectric medicine has also provided solutions to musculoskeletal disease and injury. For example, electrical current delivered to nearby bone fractures can enhance healing outcomes (Aleem et al., 2016), and long, thin electrodes implanted near the spine or peripheral nerves can relieve chronic back or joint pain (Kapural et al., 2016; Ilfeld et al., 2019; Deer et al., 2021). Additionally, electrical stimulation of peripheral nerves (eStim) offers a unique opportunity to utilize the interconnectedness and regulatory function of the nervous system to treat diverse conditions throughout the body. For example, one of the most widely applied therapeutics in bioelectric medicine today is vagus nerve stimulation. Promising results have been shown for both rheumatoid arthritis and obesity in using eStim to harness the anti-inflammatory and satiety-mediating functions of the vagus nerve (Koopman et al., 2016; Apovian et al., 2017).

In the past two decades, eStim paradigms that enhance the regenerative capacity of nerves in rodents and humans post-injury have also been established. In rats and mice, both motor and sensory nerves demonstrate upregulated regeneration-associated genes with application of eStim (Brushart et al., 2005; Geremia et al., 2007; Gordon and English, 2016). In humans, one application of post-surgical eStim similarly improves functional nerve regeneration after repair of digital nerve transection and median nerve crush injury (i.e., carpal tunnel syndrome) (Gordon et al., 2010; Wong et al., 2015). Studies in mice and rats suggest that the neuroregenerative effects of eStim post-injury persist even in the metabolically challenged state of streptozotocin (STZ)-induced type 1 diabetes (T1D) (Lin et al., 2015; Singh et al., 2015).

In this study, we hypothesized that a neuroregenerative eStim paradigm may be sufficient to halt the progression of diabetic peripheral neuropathy (DPN), contributing to restoration of function. Considering correlations between neural and musculoskeletal health in diabetes (Melendez-Ramirez et al., 2010; Forbes and Cooper, 2013; Jaiswal et al., 2017; Beeve et al., 2019), we also hypothesized that eStim would provide a simultaneous benefit for innervated downstream organs, including muscle and bone, in both control and diabetic rats. To test this hypothesis, we utilized a fully implantable, wireless system for sciatic nerve stimulation that has previously been employed to promote nerve regeneration (MacEwan et al., 2018). This technology enabled us to deliver weekly 1 h eStim treatments for 8 weeks with a silicone nerve cuff electrode. Coupled with metabolic, neural and musculoskeletal analyses, our experimental design allowed us to determine the *in vivo* effect of chronic eStim on nerve, muscle and bone in the context of health and diabetes. This work was completed as part of the National Institutes of Health SPARC consortium (Stimulating Peripheral Activity to Relieve Conditions) in the United States.

MATERIALS AND METHODS

eStim Device Fabrication

Fully implantable sciatic nerve cuff stimulators were fabricated as previously described (MacEwan et al., 2018). Braided Pt/Ir leads (10IR9/49T, Medwire, Sigmund Cohn Corp.) were threaded through 8 mm of silicone tubing (inner diameter 1.5 mm) using a custom plastic rig (**Figures 1A,B**). Exposed wires on the external surface of the silicone cuff were insulated with medical-grade silicone elastomer (A-564, Factor II). Cuff leads were then soldered to a thin-film wireless receiver coil and embedded in the same medical silicone (**Figure 1A**). As the average diameter of the rat sciatic nerve is approximately 1 mm (Isaacs et al., 2014; Onode et al., 2019), it was neither expected nor intended that the cuff would constrict the sciatic nerve at any stage of development.

Animals

The procedures in this investigation were approved by the Washington University Animal Studies Committee (Saint Louis, MO, United States). Male Lewis rats (7 weeks, Strain 004) were obtained from Charles River and housed on a 12-hour light/dark cycle while fed *ad libitum* (LabDiet, 53WU, PicoLab Rodent Diet 20).

eStim Device Implantation

All surgeries were conducted under anesthesia with 2% isoflurane. All animals were implanted unilaterally with a device onto the right side at 12-weeks of age. An incision was made on the lateral surface of the right thigh to expose the sciatic nerve. The silicone cuff was placed around the nerve and closed with one stitch of 6-O nylon suture (McKesson, REF S1698GX), and the receiver was placed subcutaneously proximal to the cuff (**Figure 1C**, dotted circle). Device function was verified at the time of surgery by activating the device with a superimposed transmitter coil (**Figure 1C**, white coil) and the implant site muscle and skin layers were closed with 5-O Vicryl (Ethicon, J303H) and 4-O Nylon (McKesson, REF S662GX) suture, respectively. Animals received a single 1.0 mg/kg dose

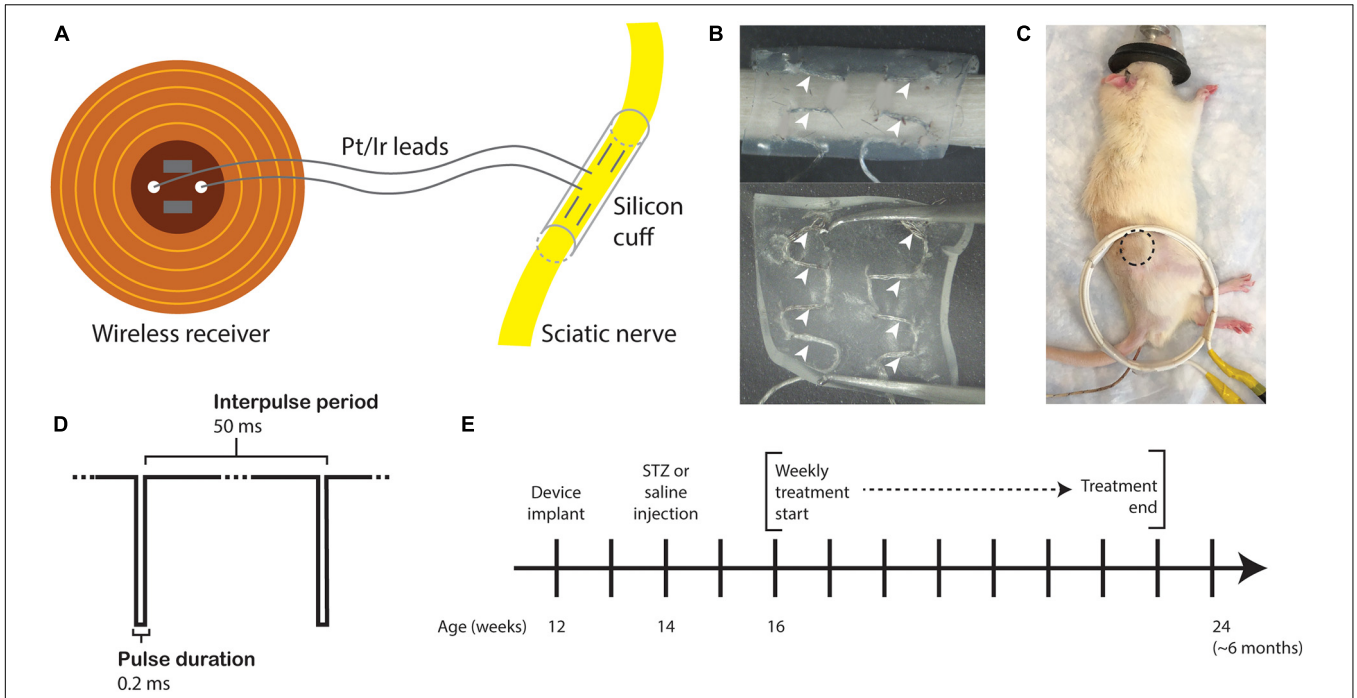

FIGURE 1 | Study design. **(A)** Drawing of the sciatic nerve cuff stimulator. **(B)** Outer surface (top) and inner surface (bottom) of the silicone cuff threaded with Pt/Ir electrode leads. White arrowheads indicate horizontally threaded regions in which the electrode wire is exposed to the nerve. **(C)** Rat under anesthesia for eStim treatment with location of implanted receiver indicated (dotted circle) with external power-transmitting coil (white coil). A rectal probe was inserted for thermal monitoring (wire under tail). **(D)** Stimulus waveform. **(E)** Experimental timeline.

of buprenorphine sustained-release (ZooPharm) subcutaneously 1 h before surgery for post-operative analgesia.

Induction of Diabetes

Type 1 diabetes was induced in rats at 14-weeks of age, 2 weeks before beginning eStim treatments. A 2 week delayed-onset treatment paradigm was selected to allow for early progression of disease, mirroring clinical intervention for diabetic complications such as neuropathy and bone loss that begins after diagnosis of disease and/or onset of symptoms. Animals were fasted for 24 h on aspen bedding, after which a single 65 mg/kg dose of STZ was administered by IP injection. Controls received saline vehicle. After injection, fasting was continued for 2 h prior to returning food and 10% sucrose filter-sterilized water was provided *ad libitum* for 24 h. After 24 h, the rats were returned to cobb bedding and filtered water. Body mass and tail blood glucose were monitored daily after STZ injection with an electronic scale and with a tail prick by blood glucometer (Bayer Contour Next) for 3 days post-injection. Blood glucose and body mass were subsequently recorded weekly for all animals. Rats exhibiting successive reductions in weight and bradykinesia were given biweekly 2 mL subcutaneous saline injections, wet food and hydrogel until stable body mass was restored.

eStim Treatment Regimen

Beginning at 16-weeks of age and continuing for 8 weeks total, those animals assigned to the stimulation group were treated weekly for 1 h with a supramaximal cathodic square pulse, 0.2 ms pulse duration, and 20 Hz frequency (**Figure 1D**). Animals were anesthetized with 2% isoflurane and placed on a heating pad throughout treatment. These parameters were previously shown to enhance neural regrowth post-transection (Geremia et al., 2007; MacEwan et al., 2018). Sham animals received only anesthesia, also weekly for 1 h. Body temperature was monitored in all animals with a rectal thermometer probe (Extech Instruments Easy View 10, **Figure 1B**, wire under tail). Treatments began 2 weeks post-STZ and continued for 8 weeks prior to end point analysis at 24 weeks of age (**Figure 1E**). There were four experimental groups in this study: control sham, control eStim, T1D sham, and T1D eStim.

At the start of the experiment, all animals showed maximal activation of muscles in the lower limb at a stimulation amplitude of 8–9 V. Maximal muscular activation was defined visually by pointed toes and clenched paw and by palpating twitches in the tibialis anterior and gastrocnemius muscles (**Supplementary Video 1**). Upon implantation of a neuroprosthetic device, it was expected that some fibrotic encapsulation would occur that might affect the magnitude of muscle activation over time. Therefore, muscular contraction was assessed visually and by palpation during each week of eStim for each animal to ensure that the stimulations achieved this maximally activated effect. If the effect was not achieved by the initial stimulus intensity, it was increased by raising first the voltage and then the pulse duration in order to maintain the maximally activated muscle contraction observed at the start of the experiment.

Single Frame Motion Analysis

Single frame motion analysis (SFMA) was performed at 10- and 23-weeks of age. Animals were trained to walk across a 3-foot-long, 3.5-inch wide wooden plank to their home cage by placing them on the plank at increasingly distant positions from their home cage. Tickling was used as a reward for task completion (Cloutier et al., 2018). Once animals were adequately trained to walk from the most distant end of the plank to their home cage without pausing, the animals were recorded from behind (iPhone X). Video analysis was performed in MATLAB using a custom guided-user interface designed to measure the first-quadrant angle between the horizontal axis and the foot-to-base vector – this parameter is called the foot-to-base angle (FBA) (Fey et al., 2010). The horizontal axis was determined by the edge of the home cage. The foot-to-base vector was measured by drawing a line between the heel and the midplantar surface at a frame just before pushoff. The angle was measured for every frame available for each foot while the animal was actively walking.

Von Frey

The up-down method was used to assess mechanical allodynia in all animals at 23-weeks of age (Chaplan et al., 1994). Animals were placed on a chicken-wire metal grid fixed to a wooden frame. The frame was elevated 1.5-feet above a countertop to allow for testing and viewing the plantar surface of the paw. A mouse cage was placed over the animal to restrain motion. Animals were allowed to acclimate for 5 min, at which point they were no longer actively exploring their environment. Manual von Frey monofilaments ranged from 8 to 300 g force. A response was recorded as hindpaw withdrawal upon or subsequent to application of the filament. Filaments were applied on alternating sides as described previously, and after a response, animals were allowed to reacclimate for 1 min before the applying the next filament.

In vivo Computed Tomography: Cortical Bone

All animals were scanned *in vivo* at 12- and 24-weeks of age. Animals were anesthetized with 1–2% isoflurane and placed into the scanning bed. A piece of VetWrap bandage was taped over the animal's torso to reduce loss of body heat. The top limb was placed into a rig to straighten and stabilize the leg during the scan with the foot secured. *In vivo* scans were conducted on the mid-diaphysis: a 3 mm region (200 slices) centered halfway between the proximal end of the tibia and the tibiofibular junction (VivaCT40; Scanco Medical; 70 kVp; 114 uA; 15 μm voxel size). After the first limb was scanned, the animal was rotated on the bed and the scan process was repeated for the contralateral limb. The total time under anesthesia exceeded no more than 1 h. Analysis was performed using the Scanco software. The entire 3 mm ROI at the mid-diaphysis was contoured and analyzed at a threshold of 250 with sigma and support values of 0.8 and 1, respectively. Bone volume fraction (BV/TV), cortical thickness (mm), tissue mineral density (mg HA/cm^3), total area (mm^2), bone area (mm^2), medullary area (mm^2), and pMOI (mm^4) were extracted for data analysis.

Ex vivo Computed Tomography: Cancellous Bone

Prior to sectioning for histology, explanted tibias were embedded in 2% agarose, and a 6 mm region was scanned starting at the growth plate (VivaCT40; Scanco Medical; 70 kVp; 114 uA; 15 μm voxel size). Analysis was performed using the Scanco software. From 2 mm (133 slices) below the growth plate, an ROI of 1.5 mm (100 slices) was contoured and analyzed at a threshold of 240 with 0.8 sigma and 1 support. Total volume (mm^3), bone volume (mm^3), bone volume fraction (BV/TV), structural model index (SMI), connectivity density, trabecular number, trabecular thickness (mm), trabecular separation (mm), and tissue mineral density (mg HA/cm^3) were extracted for analysis.

Histology and Bone Marrow Adipocyte Analysis

At the end point (24 weeks), rats were euthanized *via* carbon dioxide overdose followed by pneumothorax. Tissues were collected and weighed on an electronic scale. Collected tissues were fixed in 10% neutral buffered formalin (Fisher Scientific 23-245684) for 24 h prior to processing as detailed below. Tibia length was measured with digital calipers (iKKEGOL).

All histology was performed by the WUSM Musculoskeletal Histology and Morphometry core. Prior to embedding, tibias were dehydrated in a reverse gradient to 70% ethanol. Tibias were bisected transversely at the 50% site between the proximal end and the tibiofibular junction and approximately 2 mm below the growth plate to achieve cross-sections corresponding to our regions of CT analysis. Bones were fully decalcified in 14% EDTA (Sigma-Aldrich E5134), pH 7.4 prior to paraffin embedding, sectioning (10 μm thickness) and staining with hematoxylin and eosin. Images were taken on a Hamamatsu 2.0-HT Nano Zoomer System with NDP.scan 2.5 image software at 20× in bright field mode.

The acquired images were exported as TIFF files under 10× magnification and were processed in Fiji to measure average adipocyte cell size and number. Briefly, the scale in Fiji was first set to be consistent with the original image (1.084 pixels/μm). The image was then converted to 8-bit and the cortical bone was specifically selected by thresholding. A median filter with a radius of 10 pixels was applied. The image was then inverted and the area of bone marrow cavity was selected and measured using the "Wand tool" and the "Measure" command. A threshold of 230 to 255 was applied to the original 8-bit image and everything outside the bone marrow cavity was cleared using the "Clear Outside" command. A median filter with a radius of two pixels was applied to the image and the non-adipocyte structures were selected and eliminated using the "Analyze Particles" tool by setting the circularity to 0–0.2. The cleaned image was further processed using the "Watershed" tool and the adipocyte size and number were finally determined using the "Analyze Particles" tool by setting the size to 200 to 4000 μm^2 and circularity to 0.50–1.00. The average adipocyte cell size and number per bone marrow area were calculated using Excel.

Statistics

Statistical analyses for this study were performed in GraphPad Prism. Tests included two-way ANOVA, three-way ANOVA, and mixed effects analyses. Specific information on statistical tests is detailed in the figure legends. A p-value of less than 0.050 was considered statistically significant. Quantitative assessments including bone length, organ mass, microcomputed tomography, behavioral assessments, and bone marrow adiposity measurements were performed by individuals blinded to the experimental groups.

RESULTS

Regulation of Blood Glucose, Body, and Tissue Mass by T1D and eStim

Blood glucose and body mass were monitored longitudinally to confirm diabetic induction and sustained hyperglycemia throughout the study. In T1D rats, blood glucose increased from 106 ± 7 to 503 ± 70 mg/dL post-injection with STZ (**Figure 2A**). Sustained hyperglycemia was maintained throughout the course of the experiment (**Figure 2A**). By contrast, control animals remained normoglycemic (**Figure 2A**). From the time of T1D onset at 14-weeks of age to the final week of treatment, body mass increased by $28 \pm 4\%$ in control animals and decreased by $23 \pm 4\%$ in diabetic animals relative to baseline (**Figure 2B**). As expected, unilateral sciatic nerve eStim for 1 h per week did not influence body mass or blood glucose in healthy or diabetic animals, relative to sham, anesthesia-only controls (**Figures 2A,B**).

At the end point, tissues including liver, gonadal white adipose tissue (gWAT), and spleen were dissected and weighed to gauge overall health. Type 1 diabetes resulted in reduced absolute liver and gWAT mass (**Figures 2C,E**). When normalized to body weight, liver mass was elevated by 37% in T1D rats (**Figure 2D**) and the relative quantity of gWAT was reduced by 78% (**Figure 2F**). Bioelectric nerve stimulation resulted in reduced absolute liver mass, but normalization to body weight eliminated this effect (**Figures 2C,D**). Bioelectric nerve stimulation did not alter gWAT (**Figures 2E,F**). Type 1 diabetes caused absolute decreases in spleen mass that were proportional to body size and not impacted by eStim (data not shown). Overall, this confirmed that intermittent, unilateral stimulation of the sciatic nerve did not cause overt global changes in peripheral tissues.

Stimulation of the sciatic nerve causes unilateral muscle contraction (**Supplementary Video 1**). We hypothesized that this may be sufficient to increase muscle mass in healthy animals and to rescue muscle atrophy in those with T1D. In previous studies, type II (fast-twitch) muscle fibers and type I (slow-twitch) fibers were differentially regulated by T1D in the STZ-induced model (Rutschmann et al., 1984; Cotter et al., 1989). Thus, muscles of predominately type I [soleus (SOL)], type II [tibialis anterior (TA), extensor digitorum longus (EDL), plantaris (PL)] and mixed type fiber compositions [lateral and medial gastrocnemius (LGC/MGC)] were selected for analysis (**Figure 3A**). Rats with T1D had reduced hindlimb muscle mass relative to controls (**Figures 3B–F**). Specifically, in diabetic animals, muscle masses were bilaterally reduced by 32% in the soleus (**Figure 3B**); by 56, 60, and 54% in the tibialis anterior, EDL, and plantaris, respectively (**Figures 3C–E**); and by 53% in the gastrocnemius (**Figure 3F**). Consistent with previous reports (Rutschmann et al., 1984; Cotter et al., 1989), muscles containing a significant population of type II fibers were more severely affected by diabetes than muscles with predominately type I fibers. In addition to the effect of diabetes, we also considered the effects of sciatic nerve cuff placement and eStim using three-way ANOVA (T1D × Cuff × eStim). The placement of a sciatic nerve cuff did not independently influence muscle mass. In addition, contrary to our expectations, eStim treatment did not significantly alter or improve muscle mass in control rats or those with T1D (**Figures 3B–F**).

Gait Alterations and Mechanical Allodynia With T1D, Sciatic Nerve Cuff, and eStim

As the sciatic nerve is involved in locomotion, its manipulation could result in gait changes. For example, FBA is reduced in rodents with sciatic nerve damage (Fey et al., 2010). To assess this, single-frame motion analysis was conducted at 10- and 23-weeks of age. Foot-to-base angle was measured as the first-quadrant angle between the line from midplantar surface to heel and the perpendicular (home cage edge) (**Figure 4A**; Fey et al., 2010; Kruspe et al., 2014). At baseline, prior to surgery, FBA was not significantly different between the left and right limbs (**Figure 4B**). At the end point, T1D resulted in a bilateral reduction of FBA by −12%, independent of cuff placement or eStim (**Figure 4C**). Foot-to-base angle was further reduced unilaterally on the cuffed side of non-stimulated animals by $-12 \pm 10\%$ in controls and by $-13 \pm 14\%$ in diabetics (**Figure 4C**). In stimulated animals, however, this effect was suppressed. The FBA of the cuffed limb was partially restored in control and diabetic eStim groups to -3 ± 7 and $-3 \pm 13\%$, respectively, relative to the control side (**Figure 4C**). Overall, these results show a unilateral, detrimental effect of sciatic nerve cuffing on gait that is partially restored by eStim.

Rodent models of T1D exhibit mechanical allodynia, representative of sensory DPN (Morrow, 2004). We hypothesized that application of neuroregenerative eStim would oppose the progression of DPN, resulting in normalization of mechanical sensitivity. Cuff placement can also independently cause unilateral sensitivity if placed too tightly around the nerve (Mosconi and Kruger, 1996; Austin et al., 2012). Thus, we measured mechanical allodynia at 23-weeks of age (one week before end point) using manual von Frey filaments applied to the mid-plantar surface of the hindpaw [**Figure 4D**, red oval; (Chaplan et al., 1994)]. As expected, diabetic animals exhibited, on average, a 56% reduction in the response threshold bilaterally compared to controls, indicative of increased sensitivity to mechanical stimuli (**Figure 4E**, three-way ANOVA, T1D $p = 0.0026$). However, contrary to our expectations, eStim treatment did not alter the mechanical sensitivity of the controls or rescue the mechanical allodynia of those with T1D (**Figure 4E**,

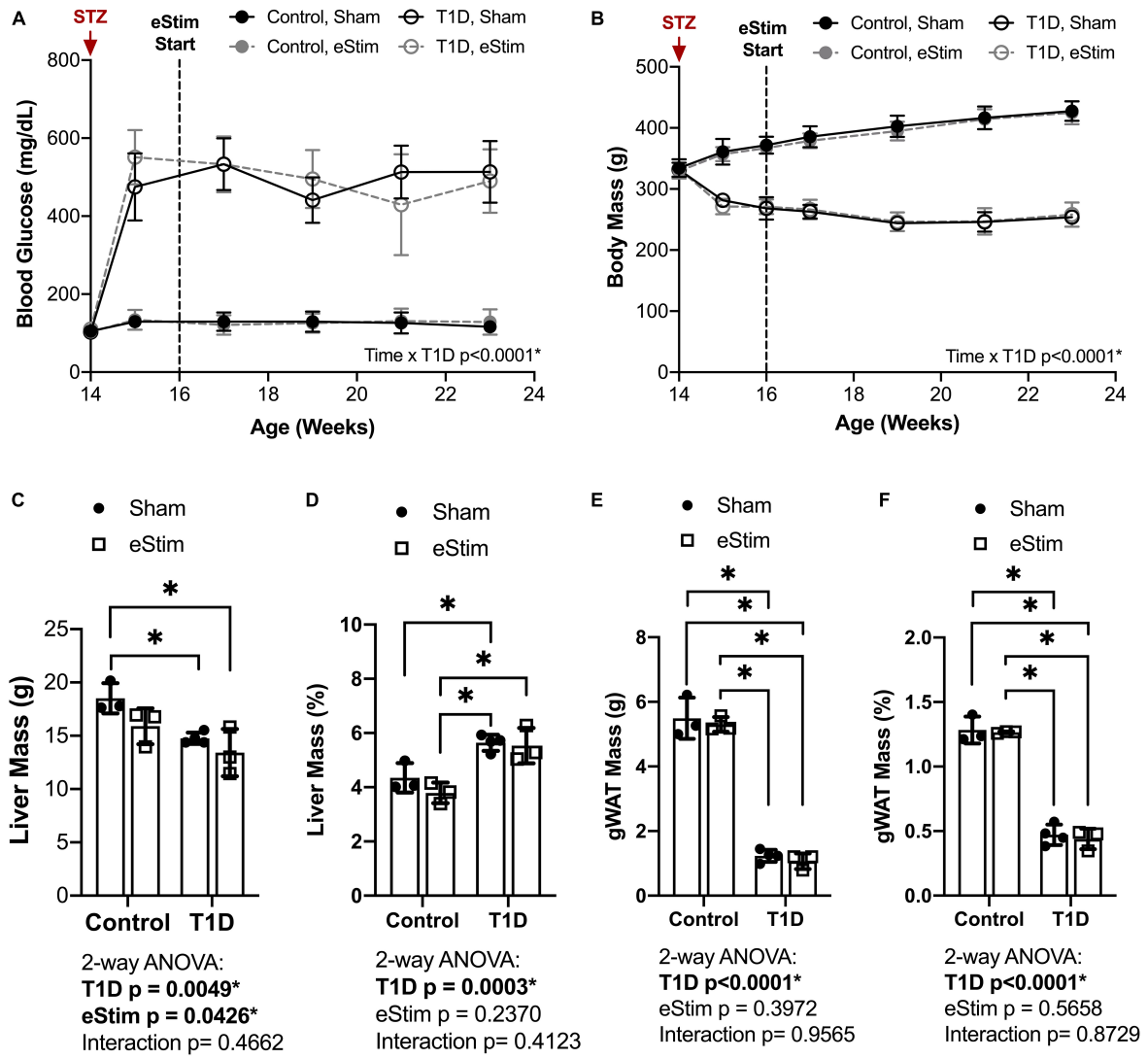

FIGURE 2 | Blood glucose and body and organ mass. Blood glucose and body mass were evaluated starting at the time of STZ induction (14-week of age) up to the final week of treatment (24-week of age). **(A)** Blood glucose. **(B)** Body mass. **(C)** Liver mass at end point. **(D)** Liver mass normalized to body mass. **(E)** Gonadal white adipose tissue (gWAT) mass at end point. **(F)** gWAT mass normalized to body mass. Statistics for blood glucose and body mass were performed by mixed effects and three-way ANOVA analyses, respectively, as a single missing value was present in the blood glucose data; Control, sham $n = 7$; Control, eStim $n = 6$; Diabetic, sham $n = 8$; Diabetic, eStim $n = 5$; $^*p < 0.050$. Statistics for organ masses was performed by two-way ANOVA with Sidak's multiple comparisons test; Control, sham $n = 3$; Control, eStim $n = 3$; Diabetic, sham $n = 4$; Diabetic, eStim $n = 3$; $^*p < 0.050$.

three-way ANOVA, eStim $p = 0.6957$). The presence of the unilateral sciatic nerve cuff also did not impact the mechanical sensitivity in the cuffed limb in either control or diabetic animals, confirming the absence of overt nerve constriction or irritation in our model (three-way ANOVA, Cuff $p = 0.6964$).

Changes in Bone and Bone Marrow Adiposity With T1D, Sciatic Nerve Cuff, and eStim

Bone Length

Sensory neurotransmitters such as calcitonin gene related peptide (CGRP) have previously been shown to promote bone formation in developing animals (Xu et al., 2020). By contrast, T1D can limit bone growth (Silva et al., 2009). We hypothesized that chronic nerve activation would promote bone formation in both control and T1D animals due to increased local release of anabolic neurotransmitters and activation of muscle contraction. To assess the effects of T1D, cuff placement, and eStim on skeletal growth, left and right side tibial lengths were measured with digital calipers and compared using three-way ANOVA (T1D × Cuff × eStim). Tibial length was decreased bilaterally by 5% in rats with T1D when compared to controls, independent of cuff placement or eStim (**Figure 5A**, T1D $p < 0.0001$). In addition, the cuffed limb was slightly shorter than the non-surgical limb in sham-treated animals (−0.3 and −0.5%

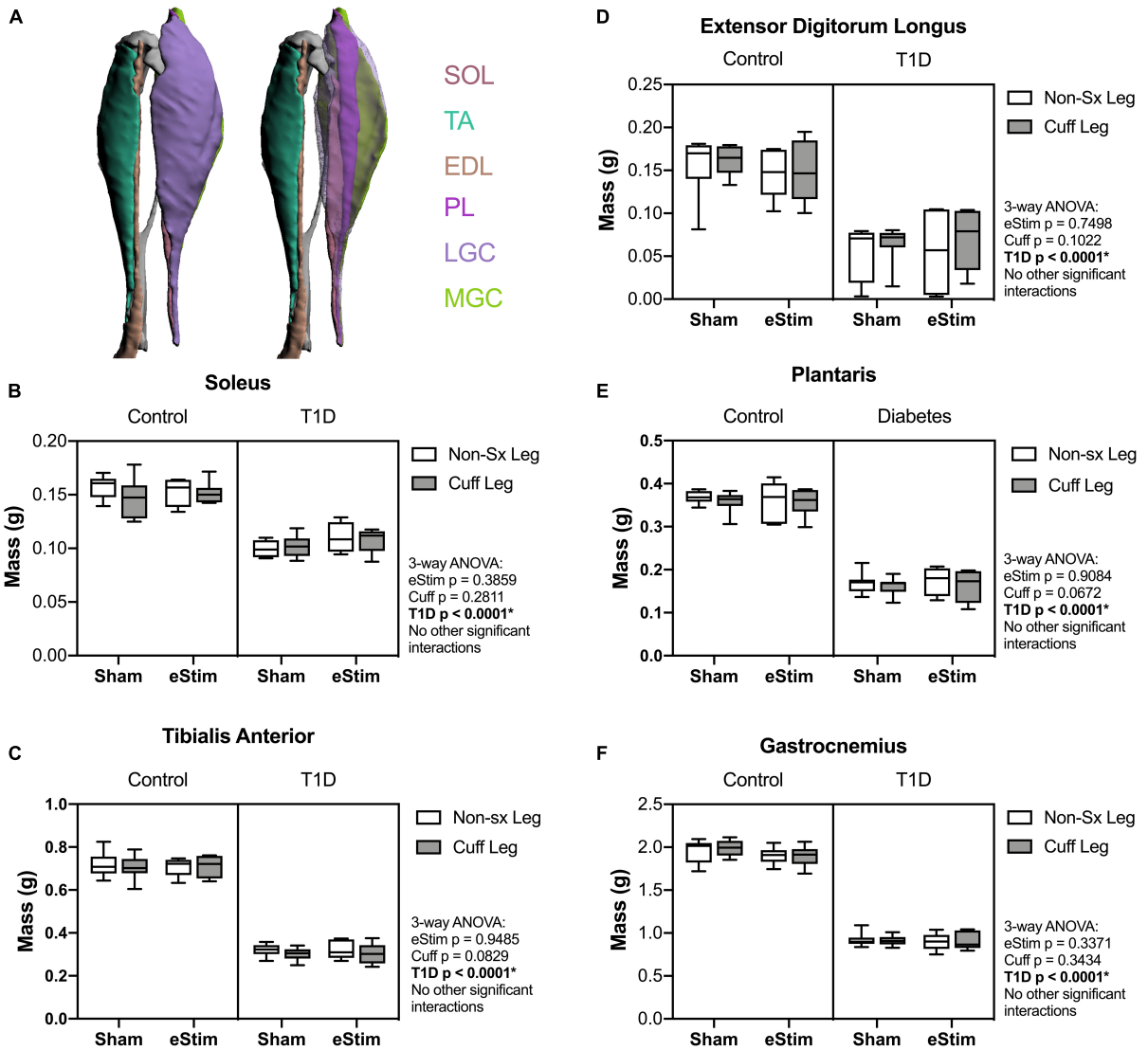

FIGURE 3 | Muscle mass. At end point, muscles surrounding the tibia **(A)** were dissected and weighed. **(B)** Soleus (SOL) muscle mass. **(C)** Tibialis anterior (TA) muscle mass. **(D)** Lateral and medial gastrocnemius (LGC, MGC) combined muscle mass. **(E)** Extensor digitorumlongus (EDL) muscle mass. **(F)** Plantaris (PL) muscle mass. Control, sham $n = 7$; Control, eStim $n = 6$; Diabetic, sham $n = 8$; Diabetic, eStim $n = 5$; three-way ANOVA with repeated measures (Non-sx Leg vs. Cuff Leg); *$p < 0.050$. Panel A generated from Charles et al. (2016).

in control and diabetic animals, respectively; **Figure 5A**). By contrast, in animals treated with unilateral chronic eStim the cuffed limb was slightly longer (+0.3 and +1.6% in control and diabetic animals, respectively) (**Figure 5A**), indicating an interaction between sciatic nerve cuffing and eStim on longitudinal bone growth (three-way ANOVA, Cuff × eStim $p = 0.0243$).

Cortical Bone

As mentioned above, sensory nerves in bone are thought to release anabolic neuropeptides near bone-forming cells (Tomlinson et al., 2016; Brazill et al., 2019); thus, we expected that DPN prevention and/or neural activation by eStim would increase bone mass. Cortical bone was analyzed by *in vivo* microcomputed tomography at 12-weeks (baseline) and 24-weeks of age (end point) in a 3 mm section of the mid-diaphysis, centered between the proximal end of the tibia and the tibia-fibula junction (**Figure 5B**). At baseline, prior to cuff implantation, the left and right limbs exhibited no difference in bone size or morphology (data not shown), although cortical TMD was 0.8% lower, on average, in the right limb (the limb to be cuffed) relative to the left at baseline ($p = 0.0412$).

At end point, rats with T1D demonstrated a 19% reduction in cortical bone volume fraction (BVF), a 26% decrease in cortical thickness, and a 4% decrease in cortical TMD relative to non-diabetic controls (**Figures 5C–E**). Reduced bone quantity in diabetic animals was driven by a 24% reduction in bone area, a 7% decrease in total area, and a 16% increase in marrow area

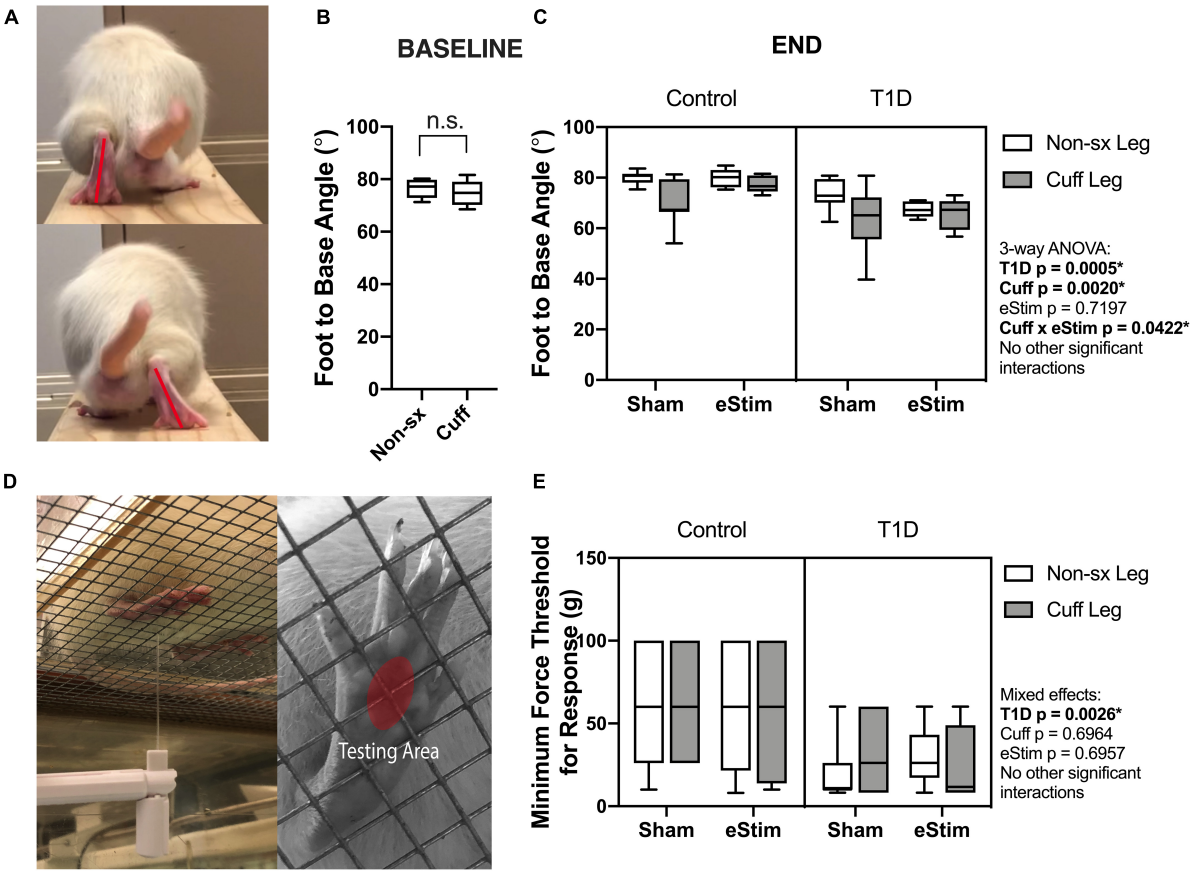

FIGURE 4 | Neuromuscular behavioral assessments. **(A)** Foot to base angle (FBA) was measured using single frame motion analysis (SFMA). **(B)** Baseline FBA measurements at 10 weeks of age. **(C)** End point FBA measurements at 23-week of age. Manual von Frey filaments were also applied to the midplantar surface of the hindpaw (indicated by a red circle) **(D)**. **(E)** Minimum force threshold for response at end point. Statistics for baseline FBA measurements was performed by paired *t*-test. Control, sham $n = 7$; Control, eStim $n = 6$; Diabetic, sham $n = 8$; Diabetic, eStim $n = 5$; three-way ANOVA with repeated measures (Non-sx Leg vs. Cuff Leg); $^*p < 0.050$.

(**Figures 5F–H**). Sciatic nerve cuffing over 12 weeks had a small negative effect on cortical BVF in the cuffed limb (ranging from −0.4 to −1.5%), independent of eStim or T1D (**Figure 5C**). This effect was also reflected by a unilateral 1 to 3% reduction in bone area in the cuffed limb relative to the non-surgical control side (**Figure 5G**). The only observed effect of eStim on cortical bone was a 0.6 and 1.6% bilateral reduction in TMD in control and diabetic animals, respectively, relative to non-stimulated, sham controls (**Figure 5E**). In summary, T1D resulted in reduced cortical bone quantity and mineral density that was not rescued by eStim. In fact, eStim and sciatic nerve cuffing introduced additional cortical bone deficits in both control and diabetic animals including bilaterally reduced TMD (as a result of eStim) and unilaterally reduced bone mass (as a result of sciatic nerve cuffing).

Cancellous Bone

Long bones are filled with spongy, cancellous bone that is concentrated largely at the metaphyses. This bone has a high turnover rate and is susceptible to systemic change, including well-documented decreases in rodents with T1D (Silva et al., 2009). To assess the effects of T1D, cuff placement and eStim on metaphyseal cancellous bone, we analyzed a 1.5 mm region starting 2 mm below the growth plate (**Figure 6A**). Consistent with previous reports, cancellous BVF was reduced by 31% in rats with T1D (**Figure 6B**). This was associated with a 10% increase in trabecular number and a 25% decrease in trabecular thickness (**Figures 6C,D**). Animals with T1D exhibited a trending 20% reduction in connectivity density (data not shown; three-way ANOVA, $p = 0.0651$) and a significant increase in structure model index (SMI) (**Figure 6E**; 2.6 vs. 3.1; SMI = 0 for plates, 3 for rods and 4 for solid spheres). Cancellous bone mineral density (BMD) was not significantly different between groups (data not shown). Unlike the effects observed with T1D, cancellous bone quantity, morphology, and mineralization were not modified by sciatic nerve cuffing or chronic eStim.

Bone Marrow Adiposity

In addition to bone, the skeleton is filled with a unique population of adipocytes that are collectively known as the bone marrow adipose tissue (BMAT). Bone marrow adipose tissue is an emerging regulator of hematopoietic, metabolic

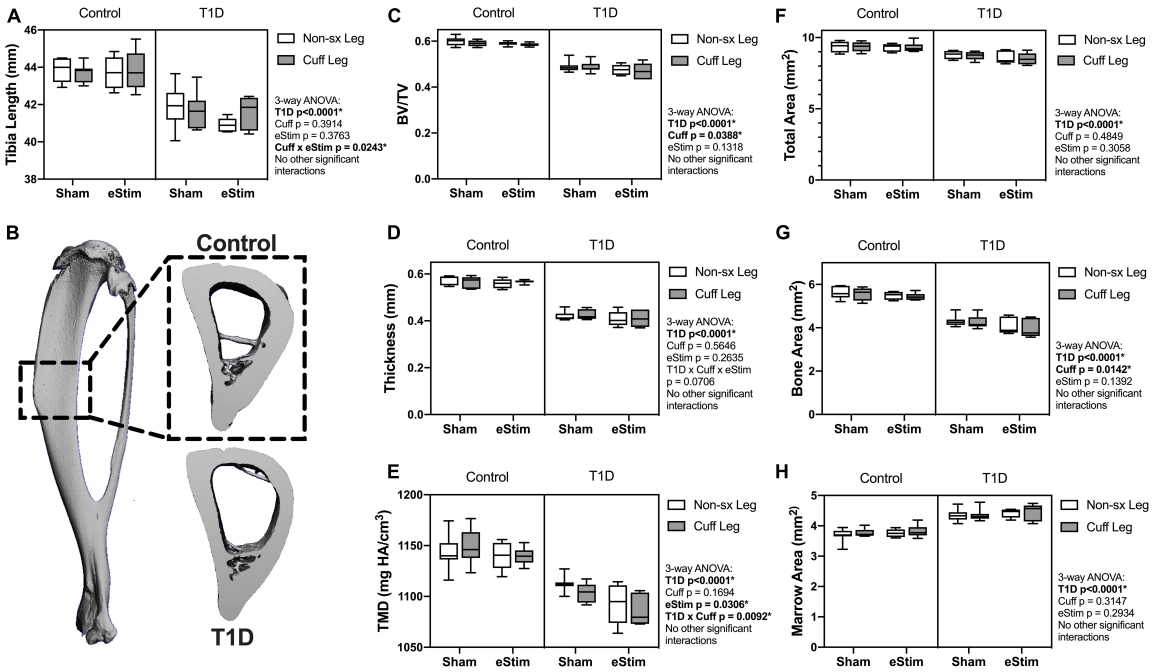

FIGURE 5 | Tibia length and cortical bone. **(A)** End point tibial length as assessed after dissection using digital calipers. Cortical bone was evaluated at 24-week of age by μCT in a 3 mm region centered midway between the proximal end of the tibia and the tibia-fibula junction **(B)**. **(C)** Cortical bone volume fraction (BV/TV). **(D)** Cortical thickness. **(E)** Cortical tissue mineral density (TMD). **(F)** Cortical total area. **(G)** Cortical bone area. **(H)** Cortical marrow area. Control, sham $n = 7$; Control, eStim $n = 6$; Diabetic, sham $n = 8$; Diabetic, eStim $n = 5$; three-way ANOVA with repeated measures (Non-sx Leg vs. Cuff Leg); $^*p < 0.050$.

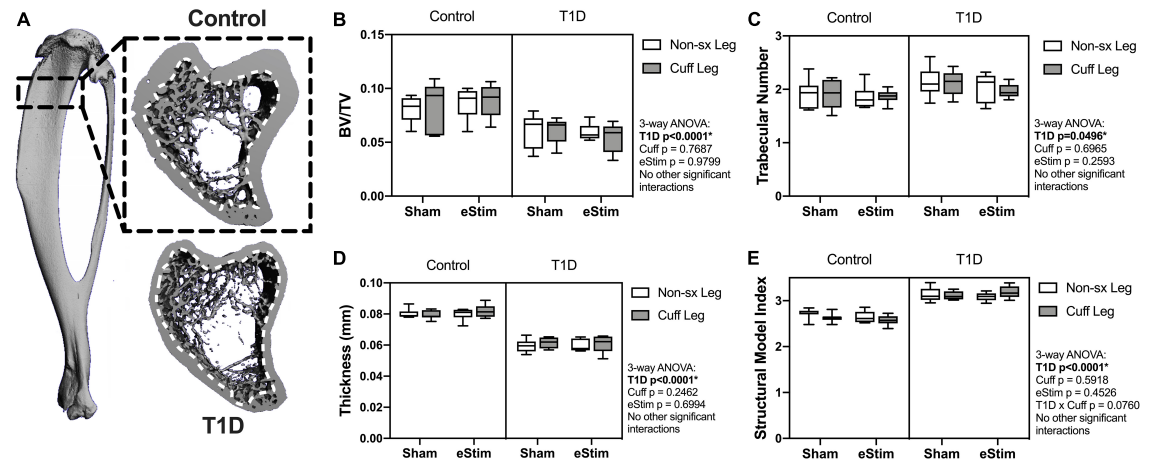

FIGURE 6 | Cancellous bone. Cancellous bone was analyzed 2 mm below the growth plate in a 1.5 mm region **(A)**, dotted line represents contour inside of which bone was analyzed. **(B)** Cancellous bone volume fraction (BV/TV). **(C)** Trabecular number. **(D)** Trabecular thickness. **(E)** Structural model index (SMI). Control, sham $n = 7$; Control, eStim $n = 6$; Diabetic, sham $n = 8$; Diabetic, eStim $n = 5$; three-way ANOVA with repeated measures (Non-sx Leg vs. Cuff Leg); $^*p < 0.050$.

and skeletal health (Scheller et al., 2016). The ability of nerve stimulation to regulate bone marrow adipocytes *in vivo* remains unknown. In this study, bone marrow adipocytes were analyzed in the metaphysis approximately 2 mm below the growth plate (**Figures 7A–C**) and in the diaphysis approximately 2 mm above the peak of the tibial crest (**Figures 7D–F**), matching our regions of skeletal morphologic assessment in **Figures 5**, **6**, respectively. Type 1 diabetes and sciatic nerve cuff placement both had independent effects on BMAT (**Figure 7**); however, the effect of sciatic nerve cuffing was region-specific. In the metaphysis, T1D resulted in a 59% reduction in BMA number, a 63% decrease in BMA density, and a 30% reduction in BMA size (**Figures 7A–C** and data not shown). Neither sciatic nerve cuffing nor eStim resulted in a change in metaphyseal BMAT. In the diaphysis,T1D similarly, resulted in a 39% reduction in BMA number, a 59% decrease in BMA density, and a 19% reduction in BMA size

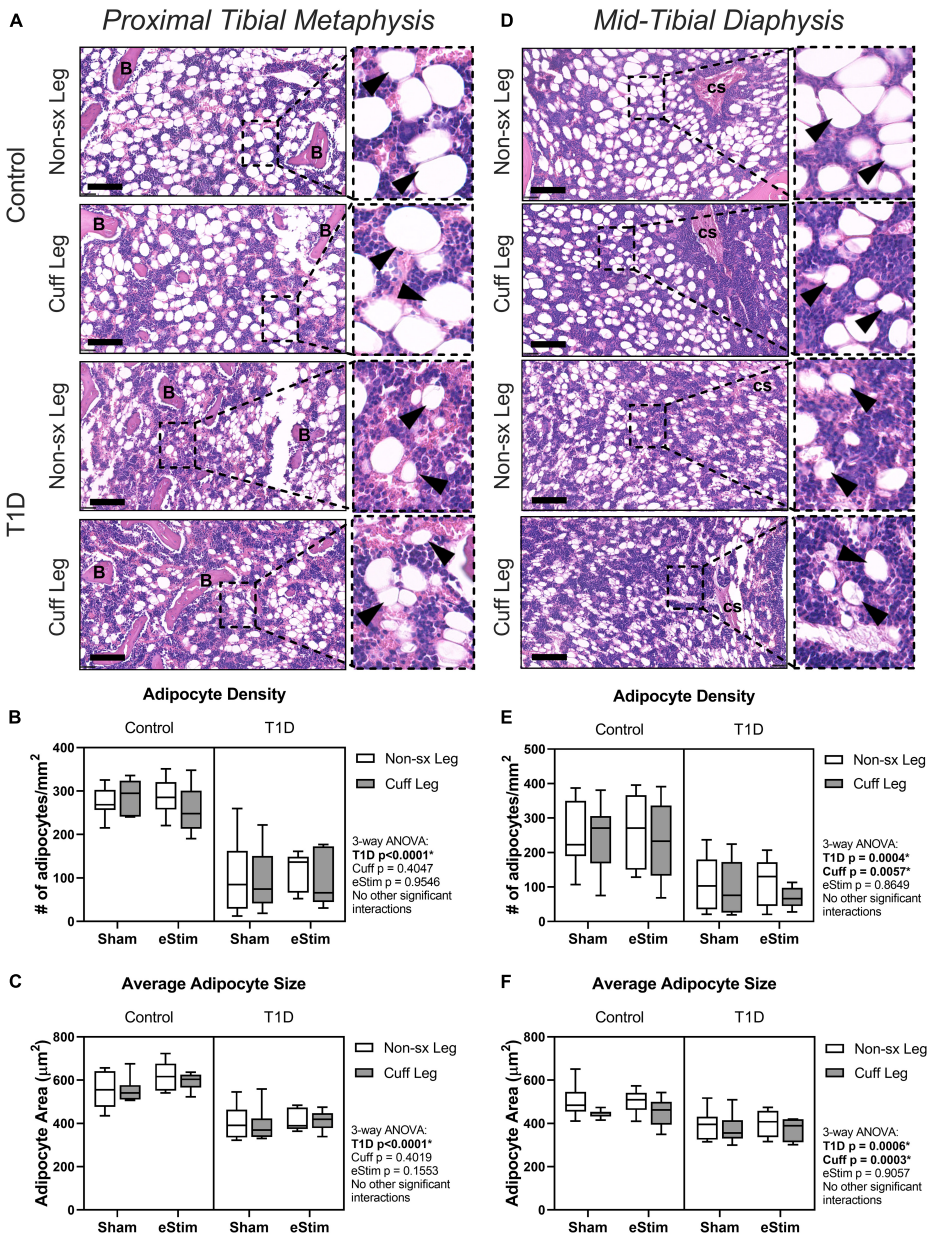

FIGURE 7 | Bone marrow adipose tissue. Bone marrow adiposity was analyzed in the metaphysis 2 mm below the growth plate and in the mid-diaphysis. **(A)** BMAT histology in the metaphysis in healthy and control animals. **(B)** Adipocyte density in the metaphysis. **(C)** Average adipocyte size in the metaphysis. **(D)** BMAT histology in the diaphysis in health and control animals. **(E)** Adipocyte density in the diaphysis. **(F)** Average adipocyte size in the diaphysis. B = bone; cs = central venous sinus. Scale = 100 μm. (Control, sham $n = 7$; Control, eStim $n = 6$; Diabetic, sham $n = 8$; Diabetic, eStim $n = 5$) three-way ANOVA with repeated measures (Non-sx Leg vs. Cuff Leg); $^*p < 0.050$.

(**Figures 7D–F** and data not shown). However, contrary to the metaphyseal data, sciatic nerve cuffing alone also caused a 5–32% reduction in BMA number, a 5–38% reduction in BMA density, and a 4–12% reduction in adipocyte cell size relative to the contralateral limb (**Figures 7D–F** and data not shown). These cuff-side effects on bone marrow adiposity were driven primarily by changes in the non-diabetic control group and align spatially with previously reported differences in the innervation of the bone marrow adipocyte population along the length of the limb (Wee et al., 2019). Bioelectric stimulation did not modify the effects of T1D or cuff placement on bone marrow adiposity.

DISCUSSION

Despite promising results showing the pro-regenerative benefits of eStim (Geremia et al., 2007; Wong et al., 2015; Gamble et al., 2016), studies to date have not addressed its utility to

prevent the onset of neuropathic symptoms and musculoskeletal decline in the context of metabolic diseases like T1D. Our experimental design allowed us to address the above questions using a fully implantable, wireless sciatic nerve stimulation device in a rat model of T1D while also considering the effects of cuff placement and chronic eStim in otherwise healthy animals.

Rodent models of T1D are characterized by progressive increases in mechanical sensitivity in addition to deficits in bone quantity, muscle mass and neuromuscular function (Cotter et al., 1989; Morrow, 2004; Silva et al., 2009). Similar to previous studies, we observed a significant decrease in hindlimb muscle mass, reduced withdrawal threshold to mechanical stimuli in the hindpaw, changes in gait, and substantial decreases in bone in animals with T1D. These results are entirely consistent with previous studies with one exception. Previous reports of STZ-induced T1D in rodents have demonstrated an increase in bone marrow adiposity and a decrease in peripheral fat mass (Botolin et al., 2005; Martin and McCabe, 2007). While we did observe a significant reduction in peripheral fat, we did not observe an increase in tibial bone marrow adipocyte density or size in either the metaphysis or diaphysis of rats after 10 weeks of STZ-induced T1D. In fact, contrary to prior results, both adipocyte density and size were substantially reduced in diabetic rats. Previous findings were observed in mice at 4- to 6-weeks post-induction; thus, our results may indicate a differential effect on bone marrow adiposity with sustained T1D that warrants further investigation.

In our study we also assessed the effect of chronic placement of a silicone sciatic nerve cuff for 12 weeks. We found that cuff placement contributed to independent changes in gait, tibial length, cortical bone and bone marrow adiposity. Cuff placement can be used as a model of chronic constriction injury (CCI) and neuropathic pain, but the largest inner diameter used in CCI models is approximately half of that used in our device (0.86 vs. 1.5 mm) (Mosconi and Kruger, 1996; Balasubramanyan et al., 2006; Austin et al., 2012). In addition, we did not see a unilateral increase in mechanical sensitivity induced by the placement of a sciatic nerve cuff, a typical indicator of neuropathy in CCI studies. Thus, it is unlikely that the effects on gait and bone were caused by overt nerve constriction. Instead, we anticipate that these results reflect local changes in nerve swelling, fibrosis and inflammation that occur after implantation of a local neuroprosthesis, contributing to the observed changes in gait and tibia length and unilateral reductions in cortical bone mass and bone marrow adiposity. Indeed, upon dissection, we observed that the sciatic nerve cuff implanted in all animals, regardless of glycemic condition or eStim, was enveloped in fibrotic tissue that fixed the cuff in place. To reduce activation of inflammatory responses and improve flexibility, more sophisticated designs for chronic neural implants are available. Extraneural electrodes like the one used herein are preferred (Günter et al., 2019), but helical or spiral cuff designs can provide more flexibility and relieve any tension or strain on the nerve (Naples et al., 1988; Christie et al., 2017). Noninvasive transcutaneous stimulation of the sciatic nerve is also possible, though reportedly ineffective for neuroregeneration (Baptista et al., 2008). Additional research is needed to investigate whether more flexible electrode designs would limit the undesirable effects on bone as observed in this study.

Beyond consideration of the effects of T1D and cuff placement, the primary goal of this study was to isolate the impact of chronic, intermittent eStim on nerve and bone health and on the progression of DPN. Contrary to our initial hypotheses, we did not observe an effect of eStim on muscle mass, bone quantity, or mechanical sensitivity in healthy animals or a rescue in those with T1D. However, we did find that treatment with eStim opposed unilateral cuff-induced effects on tibial length and gait. This suggests that intermittent application of a local bioelectric stimulus can counteract some of the negative side-effects of cuff placement. Previously, the device used herein was shown to evoke longitudinally consistent electromyogram amplitudes in the gluteal, tibialis anterior, and plantaris muscles over 14 weeks of implantation in healthy animals (Gamble et al., 2016). However, inclusion of additional functional assays such as *in vivo* joint torque measurements or more comprehensive gait analyses may provide additional insight into alterations in gait and bone caused by sciatic nerve cuffing and opposed by eStim. Local, stimulation-induced release of anabolic neuropeptides at the growth plate may also be involved in promoting unilateral tibial lengthening (Brazill et al., 2019). Additionally, bioelectric nerve stimulation has been shown to drive changes in muscular gene expression (Brownson et al., 1988); which may also underlie functional changes observed in gait independent of muscle mass. Future investigation is required to determine if eStim modulates endochondral ossification at the skeletal growth plate and aspects of muscle function, including underlying gene expression. In addition to the possible direct effects of eStim on the growth plate and muscle, inhibition of local neuroinflammation may also contribute to the outcomes. While we did observe fibrosis around the sciatic nerve cuff in all animals regardless of eStim, we acknowledge that it remains possible that eStim locally suppressed inflammation or fibrosis in more subtle ways than were grossly observable. Local neuroinflammatory suppression, in turn, may have indirectly contributed to the restoration of gait and tibial lengthening.

Contrary to its mild restorative effects, treatment with eStim unexpectedly resulted in a 1–2% bilateral reduction in cortical bone tissue mineral density, independent of T1D. The mechanism underlying this effect remains unknown. However, we hypothesize that nerve action potentials produced by the device used here may have travelled bidirectionally along the axon, resulting in bilateral reductions in skeletal mineralization through activation of central neural relays. Additional studies may address whether this effect was centrally mediated by eStim responses in the spinal cord or brain, or by treatment-induced systemic stress factors otherwise insufficient to alter body mass or blood glucose.

Limitations

The eStim paradigm employed here was previously optimized to enhance neuroregeneration in a post-injury setting

(Geremia et al., 2007; Singh et al., 2015; MacEwan et al., 2018), but it was unknown if this paradigm could be leveraged to prevent neuropathy or other musculoskeletal deficits associated with chronic metabolic disease. While it restored cuff-induced imbalances in gait and promoted unilateral tibial lengthening, eStim did not prevent T1D-associated mechanical allodynia, osteopenia, or sarcopenia. To the extent that our assays could measure, we did not observe a benefit of eStim therapy for nerve function in T1D animals. However, our interpretation is limited by assay specificity. Von Frey and gait analyses are indicative of large diameter sensory and/or motor fiber dysfunction. While our analyses show that eStim did not prevent large fiber neuropathy, it is left to future investigation to determine whether eStim can protect against small-fiber neuropathy. Our study was also limited to a discrete selection of eStim parameters and dosing regimens. It remains possible that increasing the number of weekly sessions or otherwise optimizing the eStim parameters could provide additional therapeutic benefit for nerve, muscle or bone. For example, in a more muscle-targeted approach, shorter, daily eStim bouts with implementation of a resting phase have been shown to protect bone in the context of disuse osteopenia (Lam and Qin, 2008; Lam et al., 2011; Tamaki et al., 2017). Additionally, peripheral pain is a common application of eStim clinically, in which parameters are typically optimized to block aberrant nerve activity, at either the peripheral or spinal level (Mobbs et al., 2007; Kumar et al., 2008). As such, it would be worthwhile to assess bone health in pre-clinical and clinical models that block neuronal activation, in addition to those designed for activation. Last, the present study was limited to male rats only. Sex differences have been reported in growth, metabolism, neuropathy, and sarcopenia in STZ-induced diabetic rodents (Vital et al., 2006; Pesaresi et al., 2011; Choi et al., 2013; Pesaresi et al., 2018; Virgen-Ortiz et al., 2018). Bone structural phenotypes are gender-independent in the STZ model (Martin and McCabe, 2007), but sexual dimorphism in eStim interaction with this phenotype may exist. Thus, it remains unknown whether the eStim regimen employed here would be therapeutic in female rats.

CONCLUSION

Overall, the stimulation parameters and treatment regimen selected for this study were insufficient to prevent T1D-induced osteopenia, sarcopenia, and neuropathy. However, our results indicate that cuff device placement on peripheral nerves can unilaterally reduce cortical bone mass and tibial length and regulate bone marrow adiposity. In addition, while bioelectric nerve stimulation restored cuff-induced gait imbalances and unilaterally favored tibial lengthening, it also caused bilateral reductions in cortical bone mineral density. Altogether, this suggests that skeletal health should be monitored in long-term clinical applications of neuromodulation devices to prevent unintended consequences including decreased bone mineral density and increased fracture risk.

DATA AVAILABILITY STATEMENT

The original contributions presented in the study are included in the article/**Supplementary Material**, further inquiries can be directed to the corresponding author.

ETHICS STATEMENT

The animal study was reviewed and approved by Institutional Animal Care and Use Committee, Washington University in Saint Louis, MO, United States.

AUTHOR CONTRIBUTIONS

AB: conceptualization, data curation, formal analysis, investigation, methodology, project administration, visualization, validation, writing, reviewing, and editing. IS: data curation, formal analysis, investigation, visualization, reviewing, and editing. XZ: data curation, formal analysis, investigation, methodology, validation, visualization, reviewing, and editing. KM: data curation, project administration, investigation, supervision, reviewing, and editing. YY: investigation, methodology, resources, supervision, reviewing, and editing. MM: conceptualization, methodology, resources, reviewing, and editing. ES: conceptualization, formal analysis, funding acquisition, methodology, project administration, resources, supervision, visualization, writing, reviewing, and editing. All authors contributed to the article and approved the submitted version.

FUNDING

This project was supported by funding from the National Institutes of Health, including U01-DK116317 (ES), T32-AR060719 (AB), S10-RR0227552 (Nanozoomer Shared Instrument Grant), and P30-AR074992 (Musculoskeletal Research Center cores). This project was completed as part of the NIH SPARC consortium.

ACKNOWLEDGMENTS

We would like to give special thanks to Priscilla Stecher for her help executing treatments in initial pilot studies and Nathan Birenbaum for his practical guidance in eStim device fabrication. We would also like to thank Matt Ward for providing practical and theoretical training on electrical peripheral nerve stimulation and Gretchen Meyer for training and assistance in dissecting hindlimb muscles.

SUPPLEMENTARY MATERIAL

The Supplementary Material for this article can be found online at: https://www.frontiersin.org/articles/10.3389/fnins.2021.632768/full#supplementary-material

REFERENCES

Aleem, I. S., Aleem, I., Evaniew, N., Busse, J. W., Yaszemski, M., Agarwal, A., et al. (2016). Efficacy of electrical stimulators for bone healing: a meta-analysis of randomized sham-controlled trials. *Sci. Rep.* 6:31724. doi: 10.1038/srep31724

Apovian, C. M., Shah, S. N., Wolfe, B. M., Ikramuddin, S., Miller, C. J., Tweden, K. S., et al. (2017). Two-Year outcomes of vagal nerve blocking (vBloc) for the treatment of obesity in the recharge trial. *Obes. Surg.* 27, 169–176. doi: 10.1007/s11695-016-2325-7

Austin, P. J., Wu, A., and Moalem-Taylor, G. (2012). Chronic constriction of the sciatic nerve and pain hypersensitivity testing in rats. *J. Vis. Exp.* 61:339. doi: 10.3791/3393

Balasubramanyan, S., Stemkowski, P. L., Stebbing, M. J., and Smith, P. A. (2006). Sciatic chronic constriction injury produces cell-type-specific changes in the electrophysiological properties of rat substantia gelatinosa neurons. *J. Neurophysiol.* 96, 579–590. doi: 10.1152/jn.00087.2006

Baptista, A. F., Gomes, J. R. S., Oliveira, J. T., Santos, S. M. G., Vannier-Santos, M. A., and Martinez, A. M. B. (2008). High- and low-frequency transcutaneous electrical nerve stimulation delay sciatic nerve regeneration after crush lesion in the mouse. *J. Peripher. Nerv. Syst.* 13, 71–80. doi: 10.1111/j.1529-8027.2008.00160.x

Beeve, A. T., Brazill, J. M., and Scheller, E. L. (2019). Peripheral neuropathy as a component of skeletal disease in diabetes. *Curr. Osteoporos. Rep.* 17, 256–269. doi: 10.1007/s11914-019-00528-8

Botolin, S., Faugere, M.-C., Malluche, H., Orth, M., Meyer, R., and McCabe, L. R. (2005). Increased bone adiposity and peroxisomal proliferator-activated receptor-gamma2 expression in type I diabetic mice. *Endocrinology* 146, 3622–3631. doi: 10.1210/en.2004-1677

Brazill, J. M., Beeve, A. T., Craft, C. S., Ivanusic, J. J., and Scheller, E. L. (2019). Nerves in bone: evolving concepts in pain and anabolism. *J. Bone Miner. Res.* 34, 1393–1406. doi: 10.1002/jbmr.3822

Brownson, C., Isenberg, H., Brown, W., Salmons, S., and Edwards, Y. (1988). Changes in skeletal muscle gene transcription induced by chronic stimulation. *Muscle Nerve* 11, 1183–1189. doi: 10.1002/mus.880111113

Brushart, T. M., Jari, R., Verge, V., Rohde, C., and Gordon, T. (2005). Electrical stimulation restores the specificity of sensory axon regeneration. *Exp. Neurol.* 194, 221–229. doi: 10.1016/j.expneurol.2005.02.007

Chang, E. H. (2021). Changing the tune using bioelectronics. *Bioelectron. Med.* 7:2. doi: 10.1186/s42234-021-00063-x

Chaplan, S. R., Bach, F. W., Pogrel, J. W., Chung, J. M., and Yaksh, T. L. (1994). Quantitative assessment of tactile allodynia in the rat paw. *J. Neurosci. Methods* 53, 55–63. doi: 10.1016/0165-0270(94)90144-9

Charles, J. P., Cappellari, O., Spence, A. J., Hutchinson, J. R., and Wells, D. J. (2016). Musculoskeletal geometry, muscle architecture and functional specialisations of the mouse hindlimb. *PLoS One* 11:e0147669. doi: 10.1371/journal.pone.0147669

Choi, M., Choi, J.-W., Chaudhari, H. N., Aseer, K. R., Mukherjee, R., and Yun, J. W. (2013). Gender-dimorphic regulation of skeletal muscle proteins in streptozotocin-induced diabetic rats. *Cell Physiol. Biochem.* 31, 408–420. doi: 10.1159/000343378

Christie, B. P., Freeberg, M., Memberg, W. D., Pinault, G. J. C., Hoyen, H. A., Tyler, D. J., et al. (2017). Long-term stability of stimulating spiral nerve cuff electrodes on human peripheral nerves. *J. Neuroeng. Rehabil.* 14:70. doi: 10.1186/s12984-017-0285-3

Cloutier, S., LaFollette, M. R., Gaskill, B. N., Panksepp, J., and Newberry, R. C. (2018). Tickling, a technique for inducing positive affect when handling rats. *J. Vis. Exp.* 135:57190. doi: 10.3791/57190

Cotter, M., Cameron, N. E., Lean, D. R., and Robertson, S. (1989). Effects of long-term streptozotocin diabetes on the contractile and histochemical properties of rat muscles. *Q. J. Exp. Physiol.* 74, 65–74. doi: 10.1113/expphysiol.1989.sp003240

Deer, T. R., Gilmore, C. A., Desai, M. J., Li, S. C., DePalma, M. J., Hopkins, T. J., et al. (2021). Percutaneous peripheral nerve stimulation of the medial branch nerves for the treatment of chronic axial back pain in patients after radiofrequency ablation. *Pain Med.* 22, 548–560. doi: 10.1093/pm/pnaa432

Fey, A., Schachner, M., and Irintchev, A. (2010). A novel motion analysis approach reveals late recovery in C57BL/6 mice and deficits in NCAM-deficient mice after sciatic nerve crush. *J. Neurotrauma.* 27, 815–828. doi: 10.1089/neu.2009.1217

Forbes, J. M., and Cooper, M. E. (2013). Mechanisms of diabetic complications. *Physiol. Rev.* 93, 137–188. doi: 10.1152/physrev.00045.2011

Gamble, P., Stephen, M., MacEwan, M., and Ray, W. Z. (2016). Serial assessment of functional recovery following nerve injury using implantable thin-film wireless nerve stimulators. *Muscle Nerve* 54, 1114–1119. doi: 10.1002/mus.25153

Geremia, N. M., Gordon, T., Brushart, T. M., Al-Majed, A. A., and Verge, V. M. K. (2007). Electrical stimulation promotes sensory neuron regeneration and growth-associated gene expression. *Exp. Neurol.* 205, 347–359. doi: 10.1016/j.expneurol.2007.01.040

Gordon, T., Amirjani, N., Edwards, D. C., and Chan, K. M. (2010). Brief post-surgical electrical stimulation accelerates axon regeneration and muscle reinnervation without affecting the functional measures in carpal tunnel syndrome patients. *Exp. Neurol.* 223, 192–202. doi: 10.1016/j.expneurol.2009.09.020

Gordon, T., and English, A. W. (2016). Strategies to promote peripheral nerve regeneration: electrical stimulation and/or exercise. *Eur. J. Neurosci.* 43, 336–350. doi: 10.1111/ejn.13005

Günter, C., Delbeke, J., and Ortiz-Catalan, M. (2019). Safety of long-term electrical peripheral nerve stimulation: review of the state of the art. *J Neuroeng. Rehabil.* 16:13. doi: 10.1186/s12984-018-0474-8

Ilfeld, B. M., Ball, S. T., Gabriel, R. A., Sztain, J. F., Monahan, A. M., Abramson, W. B., et al. (2019). A feasibility study of percutaneous peripheral nerve stimulation for the treatment of postoperative pain following total knee arthroplasty. *Neuromodulation* 22, 653–660. doi: 10.1111/ner.12790

Isaacs, J., Mallu, S., Yan, W., and Little, B. (2014). Consequences of oversizing: nerve-to-nerve tube diameter mismatch. *J. Bone Joint Surg. Am.* 96, 1461–1467. doi: 10.2106/JBJS.M.01420

Jaiswal, M., Divers, J., Dabelea, D., Isom, S., Bell, R. A., Martin, C. L., et al. (2017). Prevalence of and risk factors for diabetic peripheral neuropathy in youth with type 1 and type 2 diabetes: SEARCH for diabetes in youth study. *Diabetes Care* 40, 1226–1232. doi: 10.2337/dc17-0179

Kapural, L., Yu, C., Doust, M. W., Gliner, B. E., Vallejo, R., Sitzman, B. T., et al. (2016). Comparison of 10-khz high-frequency and traditional low-frequency spinal cord stimulation for the treatment of chronic back and leg pain: 24-month results from a multicenter, randomized, controlled pivotal trial. *Neurosurgery* 79, 667–677. doi: 10.1227/NEU.0000000000001418

Koopman, F. A., Chavan, S. S., Miljko, S., Grazio, S., Sokolovic, S., Schuurman, P. R., et al. (2016). Vagus nerve stimulation inhibits cytokine production and attenuates disease severity in rheumatoid arthritis. *Proc. Natl. Acad. Sci. U.S.A.* 113, 8284–8289. doi: 10.1073/pnas.1605635113

Kruspe, M., Thieme, H., Guntinas-Lichius, O., and Irintchev, A. (2014). Motoneuron regeneration accuracy and recovery of gait after femoral nerve injuries in rats. *Neuroscience* 280, 73–87. doi: 10.1016/j.neuroscience.2014.08.051

Kumar, K., Taylor, R. S., Jacques, L., Eldabe, S., Meglio, M., Molet, J., et al. (2008). The effects of spinal cord stimulation in neuropathic pain are sustained: a 24-month follow-up of the prospective randomized controlled multicenter trial of the effectiveness of spinal cord stimulation. *Neurosurgery* 63, 762–770; discussion 770. doi: 10.1227/01.NEU.0000325731.46702.D9

Lam, H., Hu, M., and Qin, Y.-X. (2011). Alteration of contraction-to-rest ratio to optimize trabecular bone adaptation induced by dynamic muscle stimulation. *Bone* 48, 399–405. doi: 10.1016/j.bone.2010.09.018

Lam, H., and Qin, Y.-X. (2008). The effects of frequency-dependent dynamic muscle stimulation on inhibition of trabecular bone loss in a disuse model. *Bone* 43, 1093–1100. doi: 10.1016/j.bone.2008.07.253

Lin, Y.-C., Kao, C.-H., Chen, C.-C., Ke, C.-J., Yao, C.-H., and Chen, Y.-S. (2015). Time-course effect of electrical stimulation on nerve regeneration of diabetic rats. *PLoS One* 10:e0116711. doi: 10.1371/journal.pone.0116711

MacEwan, M. R., Gamble, P., Stephen, M., and Ray, W. Z. (2018). Therapeutic electrical stimulation of injured peripheral nerve tissue using implantable thin-film wireless nerve stimulators. *J. Neurosurg.* 130, 486–495. doi: 10.3171/2017.8.JNS163020

Martin, L. M., and McCabe, L. R. (2007). Type I diabetic bone phenotype is location but not gender dependent. *Histochem. Cell Biol.* 128, 125–133. doi: 10.1007/s00418-007-0308-4

Melendez-Ramirez, L. Y., Richards, R. J., and Cefalu, W. T. (2010). Complications of type 1 diabetes. *Endocrinol. Metab. Clin. North Am.* 39, 625–640. doi: 10.1016/j.ecl.2010.05.009

Mobbs, R. J., Nair, S., and Blum, P. (2007). Peripheral nerve stimulation for the treatment of chronic pain. *J. Clin. Neurosci* 14, 216–221; discussion 222. doi: 10.1016/j.jocn.2005.11.007

Morrow, T. J. (2004). Animal models of painful diabetic neuropathy: the STZ rat model. . *Curr. Protoc. Neurosci.* Chapter 9:Unit9.18. doi: 10.1002/0471142301.ns0918s29

Mosconi, T., and Kruger, L. (1996). Fixed-diameter polyethylene cuffs applied to the rat sciatic nerve induce a painful neuropathy: ultrastructural morphometric analysis of axonal alterations. *Pain* 64, 37–57. doi: 10.1016/0304-3959(95)00077-1

Naples, G. G., Mortimer, J. T., Scheiner, A., and Sweeney, J. D. (1988). A spiral nerve cuff electrode for peripheral nerve stimulation. *IEEE Trans. Biomed. Eng.* 35, 905–916. doi: 10.1109/10.8670

Onode, E., Uemura, T., Takamatsu, K., Shintani, K., Yokoi, T., Okada, M., et al. (2019). Nerve capping with a nerve conduit for the treatment of painful neuroma in the rat sciatic nerve. *J. Neurosurg.* 132, 856–864. doi: 10.3171/2018.10.JNS182113

Pesaresi, M., Giatti, S., Cavaletti, G., Abbiati, F., Calabrese, D., Bianchi, R., et al. (2011). Sex differences in the manifestation of peripheral diabetic neuropathy in gonadectomized rats: a correlation with the levels of neuroactive steroids in the sciatic nerve. *Exp. Neurol.* 228, 215–221. doi: 10.1016/j.expneurol.2011.01.005

Pesaresi, M., Giatti, S., Spezzano, R., Romano, S., Diviccaro, S., Borsello, T., et al. (2018). Axonal transport in a peripheral diabetic neuropathy model: sex-dimorphic features. *Biol. Sex Differ.* 9:6. doi: 10.1186/s13293-018-0164-z

Rutschmann, M., Dahlmann, B., and Reinauer, H. (1984). Loss of fast-twitch isomyosins in skeletal muscles of the diabetic rat. *Biochem. J.* 221, 645–650. doi: 10.1042/bj2210645

Scheller, E. L., Cawthorn, W. P., Burr, A. A., Horowitz, M. C., and MacDougald, O. A. (2016). Marrow adipose tissue: trimming the fat. *Trends Endocrinol. Metab.* 27, 392–403. doi: 10.1016/j.tem.2016.03.016

Silva, M. J., Brodt, M. D., Lynch, M. A., McKenzie, J. A., Tanouye, K. M., Nyman, J. S., et al. (2009). Type 1 diabetes in young rats leads to progressive trabecular bone loss, cessation of cortical bone growth, and diminished whole bone strength and fatigue life. *J. Bone Miner. Res.* 24, 1618–1627. doi: 10.1359/jbmr.090316

Singh, B., Krishnan, A., Micu, I., Koshy, K., Singh, V., Martinez, J. A., et al. (2015). Peripheral neuron plasticity is enhanced by brief electrical stimulation and overrides attenuated regrowth in experimental diabetes. *Neurobiol. Dis.* 83, 134–151. doi: 10.1016/j.nbd.2015.08.009

Tamaki, H., Yotani, K., Ogita, F., Hayao, K., Nakagawa, K., Sugawara, K., et al. (2017). Electrical stimulation of denervated rat skeletal muscle ameliorates bone fragility and muscle loss in early-stage disuse musculoskeletal atrophy. *Calcif. Tissue Int.* 100, 420–430. doi: 10.1007/s00223-017-0250-y

Tomlinson, R. E., Li, Z., Zhang, Q., Goh, B. C., Li, Z., Thorek, D. L. J., et al. (2016). NGF-TrkA signaling by sensory nerves coordinates the vascularization and ossification of developing endochondral bone. *Cell Rep.* 16, 2723–2735. doi: 10.1016/j.celrep.2016.08.002

Virgen-Ortiz, A., Apolinar-Iribe, A., and Muñiz, J. (2018). Gender-effect on the contractile properties of skeletal muscle in streptozotocin-induced diabetic rats. *J. Musculoskelet. Neuronal. Interact.* 18, 255–261.

Vital, P., Larrieta, E., and Hiriart, M. (2006). Sexual dimorphism in insulin sensitivity and susceptibility to develop diabetes in rats. *J. Endocrinol.* 190, 425–432. doi: 10.1677/joe.1.06596

Wee, N. K. Y., Lorenz, M. R., Bekirov, Y., Jacquin, M. F., and Scheller, E. L. (2019). Shared autonomic pathways connect bone marrow and peripheral adipose tissues across the central neuraxis. *Front. Endocrinol. (Lausanne)* 10:668. doi: 10.3389/fendo.2019.00668

Wong, J. N., Olson, J. L., Morhart, M. J., and Chan, K. M. (2015). Electrical stimulation enhances sensory recovery: a randomized controlled trial. *Ann. Neurol.* 77, 996–1006. doi: 10.1002/ana.24397

Xu, J., Wang, J., Chen, X., Li, Y., Mi, J., and Qin, L. (2020). The effects of calcitonin gene-related peptide on bone homeostasis and regeneration. *Curr. Osteoporos. Rep.* 18, 621–632. doi: 10.1007/s11914-020-00624-0

Conflict of Interest: The authors declare that the research was conducted in the absence of any commercial or financial relationships that could be construed as a potential conflict of interest.

frontiers in Neuroscience

ORIGINAL RESEARCH
published: 12 April 2021
doi: 10.3389/fnins.2021.637274

Removal of Electrocardiogram Artifacts From Local Field Potentials Recorded by Sensing-Enabled Neurostimulator

*Yue Chen[1], Bozhi Ma[1], Hongwei Hao[1] and Luming Li[1,2,3,4]**

[1] National Engineering Laboratory for Neuromodulation, Tsinghua University, Beijing, China, [2] Precision Medicine & Healthcare Research Center, Tsinghua-Berkeley Shenzhen Institute, Tsinghua University, Shenzhen, China, [3] International Data Group (IDG)/McGovern Institute for Brain Research at Tsinghua University, Beijing, China, [4] Institute of Epilepsy, Beijing Institute for Brain Disorders, Beijing, China

Sensing-enabled neurostimulators are an advanced technology for chronic observation of brain activities, and show great potential for closed-loop neuromodulation and as implantable brain-computer interfaces. However, local field potentials (LFPs) recorded by sensing-enabled neurostimulators can be contaminated by electrocardiogram (ECG) signals due to complex recording conditions and limited common-mode-rejection-ratio (CMRR). In this study, we propose a solution for removing such ECG artifacts from local field potentials (LFPs) recorded by a sensing-enabled neurostimulator. A synchronized monopolar channel was added as an ECG reference, and two pre-existing methods,i.e., template subtraction and adaptive filtering, were then applied. ECG artifacts were successfully removed and the performance of the method was insensitive to residual stimulation artifacts. This approach to removal of ECG artifacts broadens the range of applications of sensing-enabled neurostimulators.

Keywords: local field potential, ECG, artifact, removal, sensing-enabled neurostimulator

OPEN ACCESS

Edited by:
Valdir Andrade Braga, Federal University of Paraíba, Brazil

Reviewed by:
Timothy Denison, University of Oxford, United Kingdom
Ali Moin, University of California, Berkeley, United States

***Correspondence:**
Luming Li
lilm@tsinghua.edu.cn

Specialty section:
This article was submitted to Autonomic Neuroscience, a section of the journal Frontiers in Neuroscience

Received: *03 December 2020*
Accepted: *17 February 2021*
Published: *12 April 2021*

Citation:
Chen Y, Ma B, Hao H and Li L (2021) Removal of Electrocardiogram Artifacts From Local Field Potentials Recorded by Sensing-Enabled Neurostimulator. Front. Neurosci. 15:637274. doi: 10.3389/fnins.2021.637274

INTRODUCTION

Recently, sensing-enabled neurostimulation has emerged as a technology for long-term observation of brain activities and has paved the way for development of closed-loop neuromodulators and implantable brain-computer interfaces (Stanslaski et al., 2012; Qian et al., 2014; Martini et al., 2020; Ramirez-Zamora et al., 2020). Using sensing-enabled neurostimulators, a seminal series of studies made enormous advances in the mechanisms of deep brain stimulation (DBS) (Trager et al., 2016; Neumann et al., 2017), the effects of closed-loop neuromodulation (Meidahl et al., 2017; Velisar et al., 2019), and the feasibility of implantable brain-computer interfaces (Vansteensel et al., 2016; Golshan et al., 2020). By integrating recordings of LFPs, sensing-enabled neurostimulators have opened a real window into chronic brain activities (Shen, 2014). However, it is difficult to faithfully record LFPs due to electrocardiogram (ECG) and stimulation artifacts (Sorkhabi et al., 2020). Previous studies using sensing-enabled neurostimulators reported considerable data loss due to

ECG contamination (Quinn et al., 2015; Trager et al., 2016; Anidi et al., 2018; Hell et al., 2018; Swann et al., 2018). The research of Quinn et al. (2015) showed that six of the sixteen recordings were excluded because of ECG artifacts. In some cases, ECG artifacts could develop in the LFPs recorded during longitudinal follow-ups (Trager et al., 2016). The researchers had to choose those LFP channels free of ECG contamination (Swann et al., 2018), which limited the precision of the targeted recording positions.

ECG artifacts can be attributed to an inadequate common-mode-rejection-ratio (CMRR) of the recording module in a sensing-enabled neurostimulator. For LFP recording, signals were usually differentiated between pairs of contacts on the electrode. The ECG spikes are regarded as common-mode signals that can be rejected by differentiating. To eliminate ECG artifacts, previous studies have shown that the CMRR has to be greater than 60 dB (Sorkhabi et al., 2020). However, achieving a high and stable CMRR is very challenging for implantable devices because power consumption and size of the neurostimulators are very limited. Furthermore, after implantation, a slight leakage of fluid into the neurostimulator can break the symmetry of the differentiated channels, which alters the CMRR (Quinn et al., 2015).

Although there are ample algorithms for removal of ECG artifacts from electrophysiological signals, few can be applied to LFP recordings. Template subtraction calculates the average waveform of ECG artifacts and subtracts it from each spike in contaminated recordings (Zhou et al., 2007; Marker and Maluf, 2014). A previous study used a raw ECG signal and template subtraction to remove the ECG artifacts from LFPs recorded by sensing-enabled neurostimulators (Canessa et al., 2016). Adaptive filtering is another popular method for removing ECG artifacts (Lu et al., 2009; Sweeney et al., 2012). It estimates the noise component and subtracts it from the original recording. Both methods usually require a synchronized ECG waveform for reference. Independent component analysis (ICA) is a widely used blind-source separation method that dispenses with the need for an ECG reference (Mak et al., 2010; Sweeney et al., 2012). However, the recordings of sensing-enabled neurostimulators are usually made without an ECG reference, and the number of LFP channels is too limited (for example, two channels) to perform ICA. Therefore, these methods are unsuitable for removal of ECG artifacts from most LFP recordings. Although there are some blind-source separation methods for single-channel recordings (Sweeney et al., 2012), their robustness is inconclusive due to residual DBS artifacts.

In this study, we propose a method for the removal of ECG artifacts from LFPs. A sensing-enabled neurostimulator was used to record simulated LFPs contaminated with ECG artifacts in saline solution. We modified the recording montages to add a synchronized ECG reference channel. Using the reference channel, we used template subtraction and adaptive filtering to remove ECG artifacts from simulated LFPs. We evaluated the performance of the proposed method of ECG artifact removal and explored the effects of DBS artifacts. The results show that using modified recording montages allows ECG artifacts to be successfully removed, thus revealing the LFP signals.

MATERIALS AND METHODS

Instrumentation Design and Implementation

Sensing-Enabled Neurostimulator

The LFP recording instrumentation is illustrated in **Figure 1**. A sensing-enabled neurostimulator (G102RS, Beijing PINS Medical Co., Ltd.) which can be fully implanted for DBS therapy was used. Before sampling, signals were first filtered by a built-in 0.3–250 Hz band-pass filter. Then the signals were sampled by the neurostimulator and wirelessly transmitted to the external PC platform through radio frequency communication. The transmission rate was 250 kbps and the delay was less than 10 ms. The wireless communication distance was approximately 2 m. A rechargeable battery was incorporated into the neurostimulator to ensure long-term recording.

Modification of Recording Montages

For LFP recording, signals were usually differentiated between pairs of contacts in the electrode, i.e., bipolar recording. For example, in **Figure 2**, the signal was differentiated between contact 1 and contact 3 in the DBS electrode after the passive filter

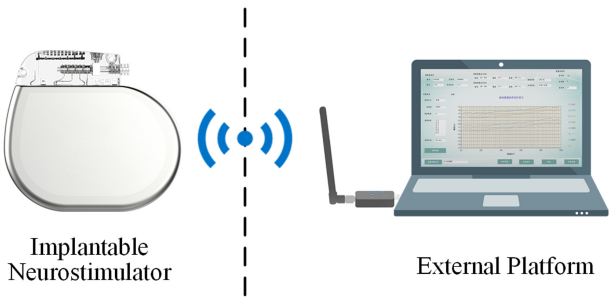

FIGURE 1 | Illustration of the sensing-enabled neurostimulator system.

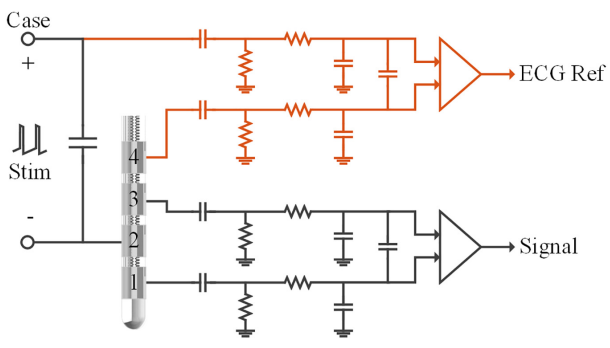

FIGURE 2 | Schematic of the recording module in the sensing-enabled neurostimulator. LFPs were recorded in the bipolar recording channel (between contacts 1 and 3). The ECG signals were recorded in the monopolar recording channel (between the titanium case and contact 4). The capacitors and resistors in each chain formed passive band-pass filters (0.3–250Hz) of the analog-front-end circuits. Monopolar stimulation was delivered between the titanium case and contact 2.

network. Monopolar stimulation was synchronously delivered between the titanium case of the neurostimulator (anode, implanted in the chest) and the therapeutic contact 2 (cathode). Potentials generated by the stimulation and the ECG source were approximately the same at contacts 1 and 3. Thus, both of the ECG potentials and stimulation pulses could be regarded as common-mode signals in the bipolar recording chain.

To achieve efficient ECG artifact removal, we developed recording montages by adding a channel for the ECG reference in the neurostimulator. As shown in **Figure 2** (red lines), a monopolar recording channel was differentiated between the titanium case and another contact in the DBS electrode. In this monopolar channel, ECG signals were synchronously recorded with the LFPs in the bipolar recording channel. Although the monopolar recording montage may yield larger DBS artifacts, recording ECG signals is possible as long as the analog-to-digital converter is not saturated. In the following sections, we describe tests of the feasibility of synchronized bipolar and monopolar recordings during stimulation and evaluate the benefits of the modified recording montages for removal of ECG artifacts.

Data Recording

Simulated Recording Setup

As shown in **Figure 3**, to simulate signal recordings after implantation, the neurostimulator's titanium case and the DBS electrodes were fully immersed in an ASTM phantom (ASTM, 2011) filled with saline solution at room temperature. The DBS electrodes (model L301, Beijing PINS Medical Co., Ltd.) have four platinum-iridium cylindrical contacts. The contacts were 1.3 mm in diameter, 1.5 mm in length, and spaced 0.5 mm apart. Two Ag/Cl disc-electrodes beside the DBS electrodes delivered a 23 Hz sinusoidal signal that simulated an LFP, which was chosen for the following reasons: (1) the beta band (13–35 Hz) of LFPs recorded by sensing-enabled neurostimulators is the most relevant band for revealing the mechanisms of DBS and for developing a closed-loop stimulation strategy (Trager et al., 2016; Meidahl et al., 2017; Neumann et al., 2017; Velisar et al., 2019), and (2) based on previous clinical experience, ECGs mainly contaminate the low-frequency band (below 100 Hz) in these specific LFPs, especially in the beta band. For the relevant signals in the high-frequency band (above 100 Hz), a high-pass filter could remove the ECG artifacts (Redfern et al., 1993; Zhou and Kuiken, 2006; Marker and Maluf, 2014). The method proposed in the current study aims to extract LFPs in the ECG-contaminated frequency band, i.e., the low-frequency band. Thus, a 23 Hz tone should be sufficient for validation of the method. Two additional Ag/Cl disc-electrodes beside the titanium case delivered a standard ECG waveform generated from a digital function generator. The period of the ECG signal was set to 750 ms.

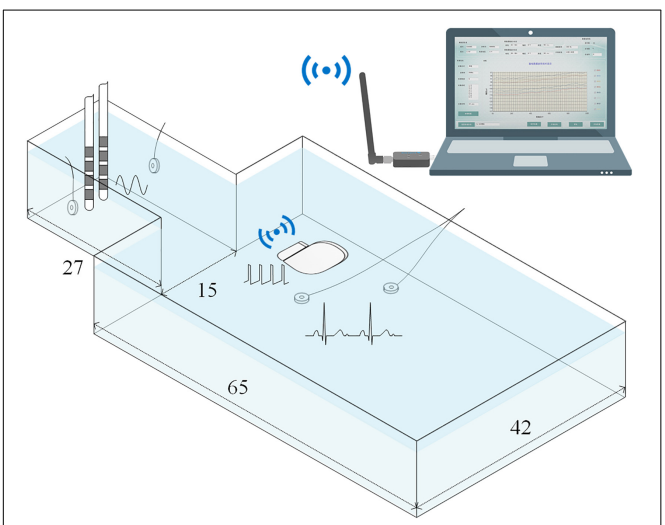

FIGURE 3 | Illustration of the simulated recording setup. The titanium case and the DBS electrodes were fully immersed in the phantom that was filled with saline solution.Phantom size is expressed in centimeters. A 23Hz sinusoidal signal and a standard ECG waveform were delivered by two pairs of Ag/Cl disc-electrodes. The recordings were wirelessly transmitted toa computer.

Stimulation and Recording

Electrode contacts 1 and 3 were configured as the bipolar montage for LFP recording. The sensing-enabled neurostimulator case and electrode contact 2 were configured as the monopolar montage for ECG reference recording. The bipolar and monopolar recordings were synchronized by the sensing-enabled neurostimulator. The sampling rate was 1,000 Hz. Monopolar stimulation was delivered between the case and contact 2 in the DBS electrodes. In a real recording scenario after the implantation of the sensing-enabled neurostimulators, no power line noise could be sensed. However, in the saline simulation, strong power line noises could be sensed by the neurostimulator. To avoid cross-interference (differential harmonics) between stimulation and the power frequency (50 Hz), the stimulation frequency was set to 150 Hz. The stimulation pulse width was 60 μs. To study the effects of DBS artifacts, the stimulation amplitude was set to off, 0.5, 1.0, 1.5, 2.0, 2.5, and 3.0 V. A segment of clean LFP was recorded after the ECG source and stimulation were both turned off. Under each condition, data was recorded for at least 300 s.

Data Preprocessing

All recordings were first filtered by a 1 Hz high-pass filter (digital Butterworth) to suppress the baseline fluctuations and then filtered by a 470 Hz low-pass filter (digital Butterworth) to exclude higher aliasing frequencies. For recordings of a clean LFP, the power frequency of 50 Hz and its harmonics at 100 Hz were filtered by an adaptive trap filter (Keshtkaran and Yang, 2014). For the recordings of ECG-contaminated LFP, DBS artifacts combined with the power frequency inferences were filtered out. To retain the information in the frequency domain as much as possible, we used a custom-designed adaptive trap filter to remove the DBS artifacts. For recordings of the ECG reference signal, data was filtered by the adaptive filter used for the power frequency and then filtered by a 100 Hz low-pass filter (3rd-order digital Butterworth).

ECG Artifact Removal

In this study, a monopolar channel was added for ECG recording. We took advantage of two pre-existing methods, i.e., template subtraction and adaptive filtering, to evaluate the effectiveness of ECG artifact removal. MATLAB (version 2016a) was used for all the calculations.

Template Subtraction

The template subtraction method extracts an ECG artifact template from the contaminated LFP recordings and subtracts the template in each ECG artifacts spike. The method mainly involved three steps: (1) ECG spike detection, (2) ECG artifact template extraction, and (3) ECG artifact template subtraction. For ECG spike detection, we applied an accurate QRS complex detector proposed by Pan and Tompkins (1985) and Hamilton and Tompkins (1986) to the ECG reference channel. The detected R-waves were used to align the ECG artifacts in the contaminated LFPs. A template was extracted by averaging the ECG artifacts and filtered by a 100 Hz low-pass filter (3rd-order digital Butterworth). The filtered template was then subtracted from the ECG-contaminated LFPs.

Adaptive Filtering

The general methodology of adaptive filtering is to estimate the ECG artifacts from the contaminated LFPs by minimizing the errors between the output and the ECG reference. In this study, we took advantage of the built-in frequency domain adaptive filter toolbox (dsp.FrequencyDomainAdaptiveFilter) in MATLAB to design the adaptive filter. The length of the coefficient vector of the adaptive filter was 64 and the block length of the coefficients updates was 1,000. The frequency-domain adaptive filter iterated the coefficients vector after transformation of the inputs to the frequency domain using discrete Fourier transforms. For detailed algorithms, please see Shynk (1992). The input was the ECG reference and the desired signal was the contaminated LFP. The outputs were the estimated ECG artifacts. The estimated ECG artifacts were then subtracted from the contaminated LFP recordings.

Performance Evaluation

Power spectral density (PSD) was estimated by the Welch's method. The frequency resolution of the PSDs was 1 Hz and the overlap of the Hamming window was 50%. Logarithmic PSDs were plotted for comparison between the clean LFP, the contaminated LFPs, and the cleaned LFPs. To quantitatively evaluate artifact removal, the signal-noise-ratio (SNR) and the root mean square logarithmic error (RMSLE) of the PSDs were calculated.

The SNR was defined as the ratio of the average power in the signal and noise bands. The SNR was calculated as:

$$SNR = 10\log_{10}\frac{Power_{signal}}{Power_{noise}} \quad (1)$$

where $Power_{signal}$ represents the average power of the signal in the band of 22–23 Hz, $Power_{noise}$ represents the average power of the ECG contamination in the band of 1–100 Hz, excluding 22–23 Hz. A larger SNR indicates better ECG artifact removal.

Because the spectrum was not uniformly distributed across the band, we used the RMSLE to evaluate the difference between the PSDs of cleaned LFPs and the simulated clean LFP. By logarithmic transformation, RMSLE evaluates the differences between small values (such as the power of the noise) similarly to differences between big values (such as the power of the signal). The RMSLE was calculated as:

$$RMSLE = \sqrt{\frac{1}{N}\sum_{f_1}^{f_2}\left(psd_{sin}(f) - psd(f)\right)^2} \quad (2)$$

where $psd_{sin}(f)$ represents the logarithmic PSD of the clean LFP, $psd(f)$ represents the logarithmic PSD of the contaminated or cleaned LFPs. f_1 and f_2 indexes the relevant band for analysis, which is 1–100 Hz (i.e., N = 100). A smaller RMSLE indicates better performance of ECG artifact removal.

RESULTS

Simulated LFP Recordings

In this study, we synchronously recorded bipolar and monopolar channels for ECG artifact removal. Examples of the recordings are shown in **Figure 4A**. The top axis in **Figure 4A** is the time series of bipolar recordings. The dark line is the clean LFP and the gray line is the contaminated LFP. The residual DBS (2.5 V, 150 Hz, 60 μs) artifacts in the contaminated LFP are more than two orders of magnitude greater than in the clean LFP. The ECG artifacts could hardly be distinguished in the time series. The bottom axis in **Figure 4A** is the time series of the monopolar recording synchronized with the contaminated LFP. Although the DBS artifacts were greater in the monopolar recording, a clear ECG waveform could be distinguished. **Figure 4B** shows the PSD of the clean LFP. **Figure 4C** shows the PSD of the contaminated LFP. The fundamental frequency of the DBS artifacts was 150 Hz and the harmonic frequencies were 300 and 450 Hz. Other aliasing frequencies superposed with the power frequency were integer multiples of 50 Hz.

ECG Artifact Removal

ECG Recording Performance

To extract clear ECG spikes, monopolar recordings were filtered by a fixed 100 Hz low-pass filter (3rd-order digital Butterworth). To study whether the ECG spikes in the monopolar recordings could be consistently restored in the presence of different DBS artifacts, we compared the amplitudes of the extracted spikes. The spikes were aligned according to the detected R-waves. **Figure 5A** shows the averaged spikes extracted under different stimulation amplitudes. **Figure 5B** shows the peak-to-peak amplitudes of each ECG spike and the peak-to-peak amplitudes of the DBS artifacts in the original monopolar recordings. Compared with the mean value in the DBS off state (5.57 ± 0.60 mV, mean ± SD), the amplitudes of the spikes decreased slightly in the DBS on state (4.54 ± 0.66 mV, $p < 0.001$, N = 266). Although the amplitudes of the DBS artifacts increased from 2.50 ± 1.8 mV (0.5 V DBS) to 9.65 ± 0.29 mV (3.0 V DBS), no significant changes were found

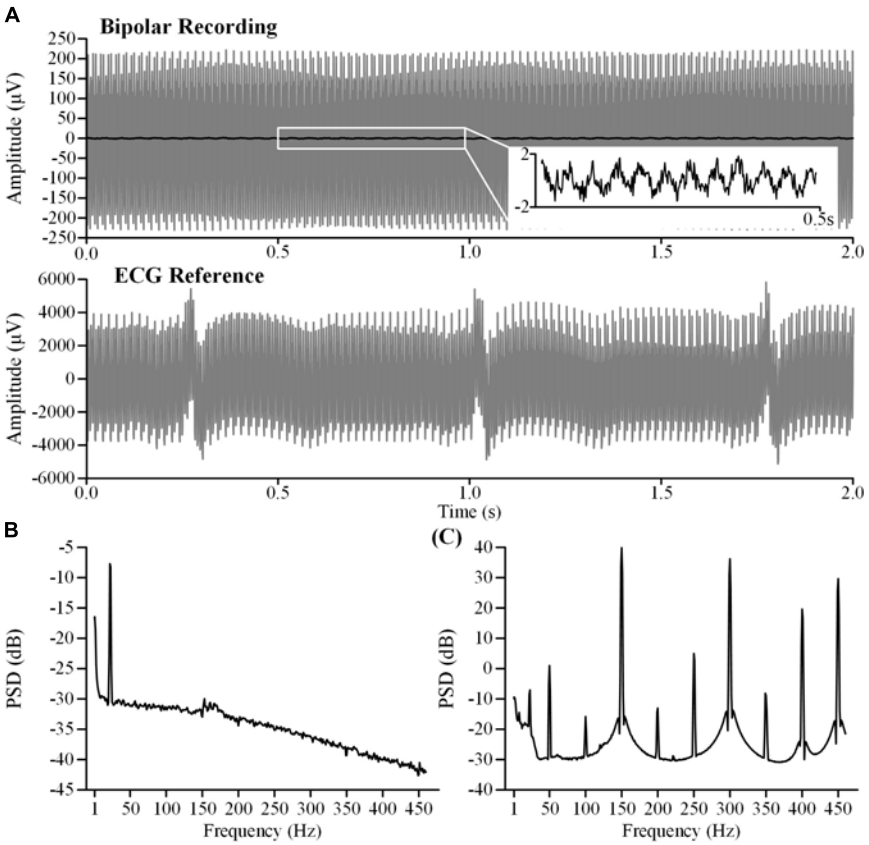

FIGURE 4 | Characteristics of the original recordings. **(A)** The top axis is the bipolar recording of the clean LFP (dark line) and the contaminated LFP (gray line). The bottom axis is the monopolar recording of theECG reference. The contaminated LFP and the ECG reference were synchronously recorded during stimulation (2.5 V, 150 Hz, 60μs). **(B)** The PSD of the clean LFP. **(C)** The PSD of the contaminated LFP.

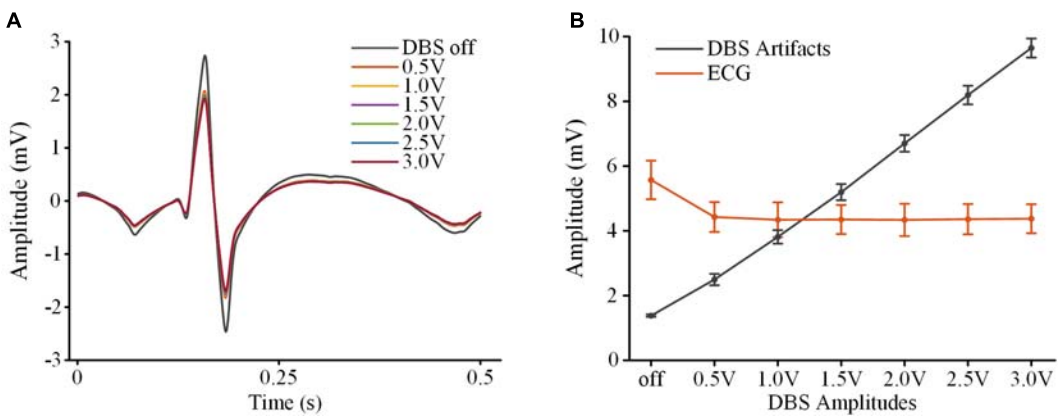

FIGURE 5 | Extraction of ECG spikes from monopolar recordings. **(A)** The averaged ECG spikes in DBS off and DBS on states. **(B)** The peak-to-peak values of the ECG spikes and DBS artifacts. The dots are mean values and the error bars are standard deviations.

between the amplitudes of the ECG spikes ($p > 0.064$, $N = 266$). The results indicated that by using a simple fixed 100 Hz low-pass filter, ECG spikes could be extracted from the monopolar recordings under different stimulation amplitudes. The robust performance of spike extraction provided a foundation for ECG artifact removal.

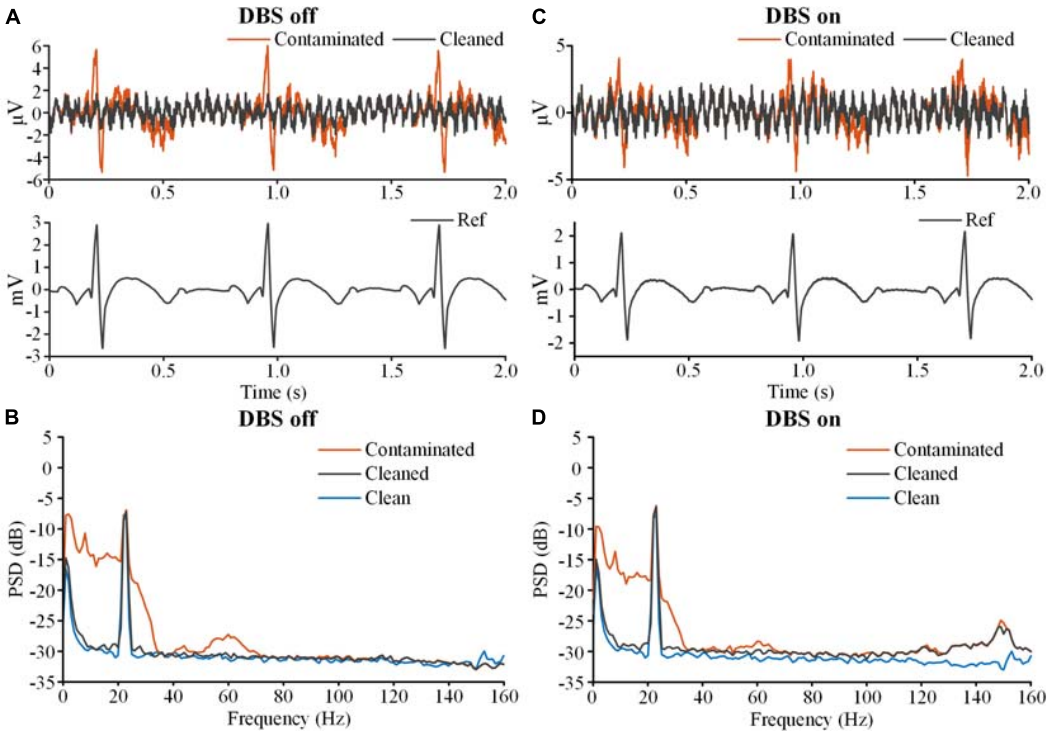

FIGURE 6 | The results of ECG artifact removal using template subtraction. **(A)** The results of ECG removal with the DBS off. The bipolar recordings before (contaminated, red line) and after (cleaned, gray line) ECG removal were plotted on the top axis. The monopolar recording of the ECG reference was plotted on the bottom axis. **(B)** The PSDs of the bipolar recording before and after ECG removal. The blue line is the PSD of the clean LFP. **(C)** The results of ECG removal fromthe recording with the DBS on. **(D)** The PSDs of the bipolar recordings before and after ECG removal.

Performance of ECG Artifact Removal

To validate the feasibility of using the monopolar channel as a reference for ECG artifact removal, we tested two pre-existing methods, i.e., template subtraction and adaptive filtering. Performance of ECG artifact removal using each method was evaluated in the DBS off and on states.

Figure 6 shows the results of template subtraction. In **Figure 6A**, the red line on the top axis is the ECG-contaminated LFP recorded in the DBS off state and the gray line is the cleaned LFP. The bottom axis shows the distinct R-waves in the synchronized monopolar channel. Using the monopolar channel as an ECG reference, the template subtraction method removed the ECG artifacts in the contaminated LFP. **Figure 6B** shows the PSDs of the ECG-contaminated LFP (red line) and cleaned LFP (gray line). The ECG artifacts mainly contaminated the band below 100 Hz. After removing the artifacts, the PSD of the cleaned LFP was overlaid with the PSD of the simulated clean LFP (blue line). In **Figure 6C**, an ECG-contaminated LFP recorded in the DBS on state (2.5 V, 150 Hz, 60 μs) and the corresponding cleaned LFP are plotted on the top axis. After removing the DBS artifacts, the monopolar recording reflected distinct R-waves (bottom axis). Using the monopolar channel as an ECG reference, the ECG artifacts were successfully removed. **Figure 6D** shows the PSDs of the contaminated (red line) and cleaned (gray line) LFPs in the DBS on state. The ECG-contaminated band below 100 Hz was restored in the cleaned LFP. We found a slightly elevated noise floor in the PSD of the cleaned LFP, which partially resulted from the ECG signal generator. In addition, some noise came from residual stimulation artifacts. Although the stimulation artifacts were largely removed, some harmonics and aliasing components remained, such as at 250, 300, 400, and 450 Hz. Spectrum estimation of these residual stimulation artifacts would unavoidably introduce leakage of the power to a broadband range.

Figure 7 shows the results of adaptive filtering. **Figures 7A,B** show recordings in the DBS off state, and **Figures 7C,D** show recordings in the DBS on state (2.5 V, 150 Hz, 60 μs). The ECG-contaminated band below 100 Hz was restored in the cleaned LFPs. Therefore, both template subtraction and adaptive filtering could remove the ECG artifacts.

To quantitatively evaluate the performance of the method, SNRs and RMSLEs of the PSDs were calculated. **Table 1** shows the SNR and RMSLE of the cleaned LFPs. Compared with the ECG-contaminated LFPs, the SNRs of the cleaned LFPs were greatly improved, with values close to the SNR of the clean LFP (20.87 dB). The RMSLEs also decreased, indicating that the differences in the PSDs between the cleaned LFP and the simulated clean LFP decreased after ECG artifact removal. Neither SNR nor RMSLE were significantly influenced by increasing the stimulation amplitude.

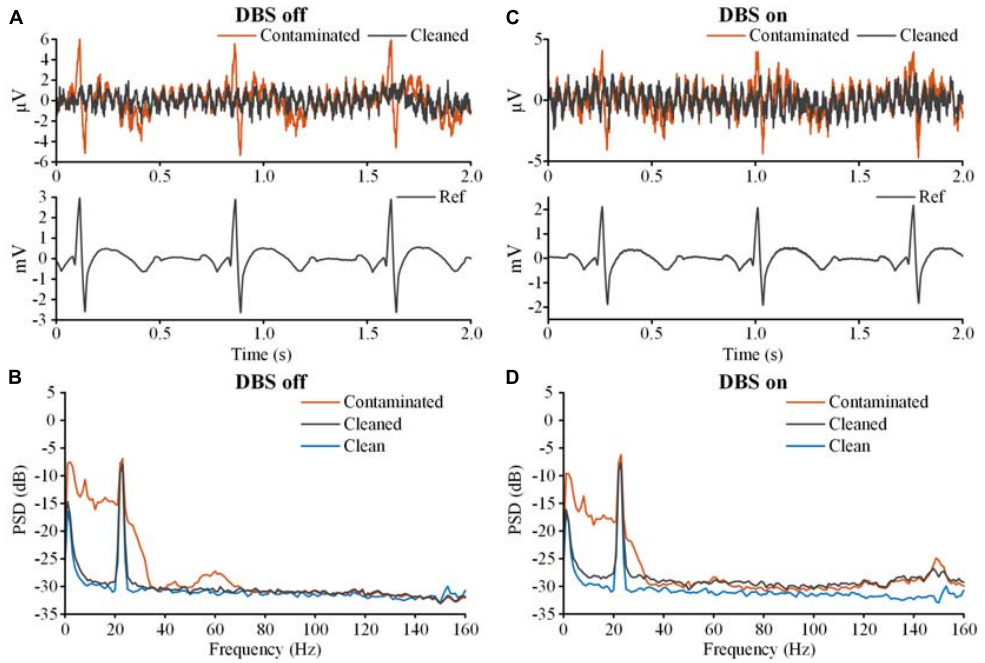

FIGURE 7 | The results of ECG artifact removal using adaptive filtering. **(A)** The results of ECG removal of the recording with the DBS off. The bipolar recordings before (contaminated, red line) and after (cleaned, gray line) ECG removal were plotted on the top axis. The monopolar recording of the ECG reference was plotted on the bottom axis. **(B)** The PSDs of the bipolar recording before and after ECG removal. The blue line is the PSD of the clean LFP. **(C)** The results of ECG removal from the recording with the DBS on. **(D)** The PSDs of the bipolar recordings before and after ECG removal.

Performance Under Residual DBS Artifacts

In section "ECG Artifact Removal," the DBS artifacts under different stimulation amplitudes were precisely filtered. However, due to complex recording conditions and various filtering methods, DBS artifacts could remain in the LFPs at varying levels. Therefore, it is crucially important to evaluate the performance in a background of residual DBS artifacts.

Figure 8A shows the contaminated LFP in the stimulation on state (gray lines, 2.5 V, 150 Hz, 60 μs) without filtering DBS artifacts. The recordings were aligned according to the ECG spikes detected in the monopolar channel. By overlapping the recordings, the envelope of the ECG artifacts could be distinguished (dashed red lines). The white line in **Figure 8A** shows the average waveform of the overlapped recordings. Using this template, the ECG artifacts were subtracted from the contaminated LFP. **Figure 8B** shows the PSDs of the contaminated LFP (red line) and ECG-cleaned LFP (gray line). The ECG-contaminated band was restored while the DBS artifacts remained. **Figure 8C** shows the ECG templates extracted from the contaminated LFPs. The performance of template extraction was stable across 0.5–3.0 V DBS without additional filtering of the DBS artifacts.

Table 2 shows a quantitative evaluation of the ECG removal performance without filtering the DBS artifacts. To exclude the effects of increasing the DBS artifacts, SNR and RSMLE were calculated for the band below 40 Hz. Compared with the ECG-contaminated LFPs, both the SNR and RMSLE of the cleaned LFPs were improved. SNR of the cleaned LFPs was close to the value of the simulated clean LFP (18.70 dB). From 1.0 V DBS to 3.0 V DBS, the SNR of the cleaned LFPs decreased from 18.29 to 17.62 dB and the RSMLE increased from 0.98 to 1.9 dB, indicating an attenuation of performance. However, this attenuation of the performance was very slight compared with the increase on the DBS artifacts from 1.0 V DBS (211.01 μV) to 3.0 V DBS (516.18 μV). The results indicate that the ECG artifacts in the contaminated LFPs can be suppressed to a significant extent even in the presence of residual DBS artifacts.

TABLE 1 | Performance evaluation using signal-noise-ratio (SNR) and root mean square logarithmic error (RMSLE).

Stimulation[#] (V)	SNR (dB)		RMSLE (dB)	
	TS*	AF*	TS*	AF*
Off	19.88 (8.93)	19.16 (8.22)	0.94 (−6.60)	0.94 (−6.59)
0.5	18.97 (5.89)	18.91 (5.82)	1.58 (−5.09)	1.37 (−5.30)
1.0	20.69 (7.17)	19.64 (6.11)	1.02 (−5.33)	1.26 (−5.09)
1.5	20.57 (6.92)	19.25 (5.61)	1.10 (−5.14)	1.34 (−4.90)
2.0	20.48 (6.73)	19.60 (5.85)	1.14 (−5.01)	1.35 (−4.80)
2.5	20.52 (6.58)	19.14 (5.19)	1.17 (−4.87)	1.85 (−4.20)
3.0	20.53 (6.41)	19.35 (5.23)	1.32 (−4.64)	1.60 (−4.36)

The values in the brackets are the differences with the contaminated local field potentials (LFPs).

[#]*Thedeep brain stimulation (DBS) artifacts in the recordings were removed.*

**TS, template subtraction; AF, adaptive filtering.*

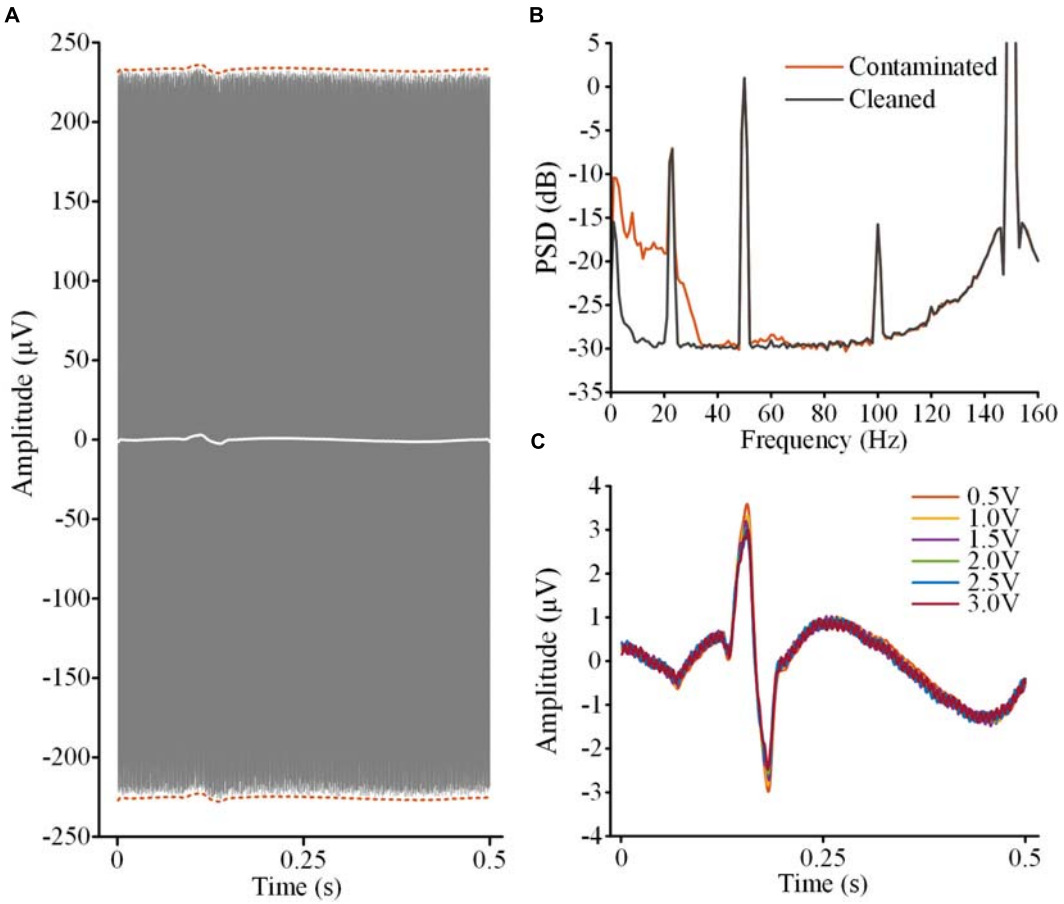

FIGURE 8 | ECG artifact removal without extra filtering of DBS artifacts. **(A)** The gray lines are the overlapped contaminated LFPs aligned according to the R-waves detected in the monopolar channel. The dashed red lines indicate the envelope of the ECG artifacts. The white line is the averaged waveform of the aligned recordings. **(B)** PSDs of the contaminated LFP and ECG-cleaned LFP. **(C)** The templates of the ECG artifacts in the contaminated LFPs with different DBS amplitudes.

TABLE 2 | Performance evaluation of electrocardiogram (ECG) artifact removal without extra filtering deep brain stimulation (DBS) artifacts.

Stimulation (V)	SNR (dB)	RMSLE (dB)
0.5	16.02 (6.77)	1.74 (−8.01)
1.0	18.29 (8.58)	0.98 (−8.35)
1.5	18.01 (8.17)	1.10 (−8.02)
2.0	17.75 (7.81)	1.29 (−7.66)
2.5	17.82 (7.73)	1.32 (−7.50)
3.0	17.62 (7.30)	1.90 (−6.77)

Signal-noise-ratio (SNR) androot mean square logarithmic error (RMSLE) were calculated for the band below 40 Hz. The values in the brackets are the differences with the contaminated local field potentials(LFPs).

DISCUSSION

In this study, we proposed an approach to removing ECG artifacts from the signals recorded by sensing-enabled neurostimulators. A simultaneous monopolar montage was added and distinct R-waves could be recorded in the time series. Using the monopolar recording as an ECG reference, conventional ECG filtering methods, including template subtraction and adaptive filtering, could effectively remove ECG artifacts in the bipolar LFP recordings. The performance of this method was not significantly influenced by the magnitude of residual DBS artifacts. Combining the monopolar and bipolar recordings, the method could remove ECG artifacts without additional complex signal processing.

Using Simultaneous Monopolar Recording as an ECG Reference

Removing ECG artifacts is a common challenge in the field of electrophysiological signal processing. There have been many algorithms proposed in previous studies, such as template subtraction (Zhou et al., 2007; Marker and Maluf, 2014), adaptive filtering (Lu et al., 2009; Sweeney et al., 2012), ICA (Mak et al., 2010), and other blind-source separation methods (Sweeney et al., 2012). Most of the methods proved effective for multi-channel EEG and

electromyography recording. Some methods were specifically designed for single-channel recording (Sweeney et al., 2012). However, most of the pre-existing methods cannot be directly applied to the signals recorded by implanted sensing-enabled neurostimulators. For sensing-enabled neurostimulators, the electrophysiological signals (LFPs) are usually independently recorded without ECG reference. Thus, the methods of template subtraction or adaptive filtering, both of which require reference signals, are not suitable. The number of synchronized channels of sensing-enabled neurostimulators is usually very limited. For recording in the DBS on state, the sensing-enabled DBS usually records only a few synchronized channels due to limited electrodes. Thus, the method of ICA which needs multi-channel recordings is not fully applicable to the LFPs recorded during DBS. Although there are some single-channel blind-source separation methods (Sweeney et al., 2012), the cost of the algorithms is usually higher and the robustness of the performance is inconclusive due to residual DBS artifacts. Lack of an ECG reference and recording channels makes it difficult to remove ECG artifacts in the LFPs recorded by sensing-enabled neurostimulators.

There are two kinds of recording montages in sensing-enabled neurostimulators, i.e., the bipolar montage and the monopolar montage. The bipolar montage differentiates the potentials between pairs of contacts in the DBS electrode while the monopolar montage differentiates the potentials between one contact in the DBS electrode and the titanium case of the neurostimulator (Stanslaski et al., 2012; Qian et al., 2014, 2017). Previous studies reported that the monopolar montage is considerably affected by remote volume conductivity (Marmor et al., 2017). Thus, it is possible to record ECG references using a monopolar montage.

In this study, we demonstrated the feasibility of recording ECG reference signals using the monopolar montage of a sensing-enabled neurostimulator. Our results showed that although the DBS artifacts were large, a clear R-waveform could be extracted in the monopolar channel. However, the peak-to-peak amplitudes of ECG artifacts in bipolar recordings *in vivo* might be unstable due to respiration or motion. Previous literature reported that respiration or even relatively slow motion over time would induce baseline wander in the ECG signals (Satija et al., 2018; Chatterjee et al., 2020). The peak-to-peak amplitudes of ECG spikes vary by 15% due to baseline wander (Friesen et al., 1990; Satija et al., 2018). For rapid motion artifacts, the effect is usually over a short duration and the fluctuation could be 500 percent of the peak-to-peak amplitudes of ECG spikes (Friesen et al., 1990; Satija et al., 2018). In **Figure 6C**, the coefficient of variation of the ECG peak-to-peak amplitudes in bipolar recordings was 13.07% (std/mean) and the value of the ECG spikes in monopolar recordings was 0.7%. To estimate the influence of these variations, we added amplitude-modulated white noise to the recordings. The coefficients of variation increased to 21.62% in bipolar recordings and 16.37% in monopolar recordings. Both variations in the bipolar and monopolar recordings were above the typical value reported in the literature. The methods of template subtraction and adaptive filtering were applied to remove ECG-artifacts in the noisy recordings. The results showed that the ECG artifacts could still largely be removed (see **Supplementary Material** for details).

The primary benefit of the current study is to make conventional ECG removal methods that require ECG reference signals applicable to LFPs recorded by sensing-enabled neurostimulators. The method proposed in our study may help researchers to extract real LFPs to study chronic deep brain neural activities and DBS mechanisms. Most such research is conducted retrospectively. Where real-time analysis is needed, such as in closed-loop stimulation, a template could only be extracted in a short window. In a previous study using the template subtraction method for real-time ECG artifact removal, 30 ECG spikes were used to update the template (Abbaspour and Fallah, 2014). We tested time windows of 30, 20, and 10 s, respectively, and found that the template was valid in the 30 s window (see **Supplementary Material** for details). Because the interval of the simulated ECG spikes was 0.75 s, the results indicate that at least 40 ECG spikes would be necessary for extracting a valid template. In real-time scenarios, the templates could be accumulated and the performance could be improved by introducing overlap and padding techniques for each window. Alternatively, we could use the method of adaptive filtering for real-time analysis. Future studies should focus on development and refinement of detailed real-time algorithms based on specific real-time scenarios.

Effects of DBS Artifacts

The magnitudes of the stimulation pulses in the monopolar recording chain were asymmetric. The asymmetry would induce large DBS artifacts in the ECG reference channel. Consequently, different magnitudes of residual DBS artifacts might influence detection of ECG spikes. Previous studies have shown that as long as the amplifiers are not saturated, the real signals in an asymmetric montage can still be restored (Kent and Grill, 2012; Qian et al., 2017). In our study, we compared the amplitudes of the ECG spikes under different DBS amplitudes. The results showed that although the DBS artifacts increased greatly from 0.5 V DBS to 3.0 V DBS, no significant difference was found between the amplitudes of extracted ECG spikes. Robust R-waves could be extracted from the monopolar recordings. This result provided the foundation for the removal of ECG artifacts.

In the bipolar channel of the sensing-enabled neurostimulator, the amplitudes of DBS artifacts could be more than two orders of magnitude greater than the ECG artifacts and LFP signals. In our study, we precisely filtered the DBS artifacts to restore the time series. However, residual DBS artifacts were usually unavoidable in LFP recordings due to complex recording conditions and different filtering methods. To evaluate the effects of residual DBS artifacts on the removal of ECG artifacts, we studied the performance of the method without extra filtering of the DBS artifacts. The results showed that even in the presence of large DBS artifacts, ECG artifacts were suppressed significantly,

indicating that the method was not sensitive to residual DBS artifacts. This finding emphasizes the robustness of the method and limits restrictions on its algorithms.

Limitations and Future Work

Removal of ECG artifacts in our study was only tested using the conventional fixed-template subtraction method and a simple adaptive filter. The performance could be improved by optimizing the extraction template and design of the adaptive filter. The current method was only tested on simulated signals recorded in saline solution. Although we have tested and verified the methods using physiological ECG levels, the performance of the method could still be influenced by chronic changes in the recording impedance, leakage of fluid, and different *in-vivo* electromagnetic environments. The performance needs to be confirmed for real *in-vivo* recordings in future studies. In addition, we should estimate whether the algorithms can be integrated into an embedded system. The goal of the current study was to provide an ECG reference for use with current methods and thus to reduce the complexity of the related algorithms. Based on our survey of the computation efficiency and storage resource of the current sensing-enabled neurostimulators, both of the approaches proposed in this study could be completed within 400–500 ms. This is sufficient for real-time analysis. Thus, this method holds potential for development of algorithms for real-time removal of ECG artifacts in an embedded system. However, there is still plenty of work that needs to be done in future embedded development, especially for addressing the trade-off between power consumption and analytical performance in specific applications.

DATA AVAILABILITY STATEMENT

The raw data supporting the conclusions of this article will be made available by the authors, without undue reservation, to any qualified researcher.

AUTHOR CONTRIBUTIONS

YC, BM, and LL designed the research. YC conducted the research, collected the data, and wrote the initial manuscript. BM, HH, and LL revised the manuscript. All authors read and approved the final manuscript.

FUNDING

This study was supported by the National Natural Science Foundation of China Grants 81527901 and 61901243, and the Shenzhen International Cooperative Research Project GJHZ20180930110402104.

ACKNOWLEDGMENTS

We thank Tiangang Long and Changqing Jiang for their help in the preparation of the ASTM phantom.

SUPPLEMENTARY MATERIAL

The Supplementary Material for this article can be found online at: https://www.frontiersin.org/articles/10.3389/fnins.2021.637274/full#supplementary-material

REFERENCES

Abbaspour, S., and Fallah, A. (2014). Removing ECG artifact from the surface EMG signal using adaptive subtraction technique. *J. Biomed. Phys. Eng. Anal.* 4, 33–38.

Anidi, C., O'Day, J. J., Anderson, R. W., Afzal, M. F., Syrkin-Nikolau, J., Velisar, A., et al. (2018). Neuromodulation targets pathological not physiological beta bursts during gait in Parkinson's disease. *Neurobiol. Dis.* 120, 107–117. doi: 10.1016/j.nbd.2018.09.004

ASTM (2011). *F2182-11a: Standard Test Method for Measurement of Radio Frequency Induced Heating on or Near Passive Implants During Magnetic Resonance Imaging*. West Conshohocken, PA: ASTM International.

Canessa, A., Pozzi, N. G., Arnulfo, G., Brumberg, J., Reich, M. M., Pezzoli, G., et al. (2016). Striatal dopaminergic innervation regulates subthalamic beta-oscillations and cortical-subcortical coupling during movements: preliminary evidence in subjects with Parkinson's disease. *Front. Hum. Neurosci.* 10:611. doi: 10.3389/fnhum.2016.00611

Chatterjee, S., Thakur, R. S., Yadav, R. N., Gupta, L., and Raghuvanshi, D. K. (2020). Review of noise removal techniques in ECG signals. *IET Signal Process.* 14, 569–590. doi: 10.1049/iet-spr.2020.0104

Friesen, G. M., Jannett, T. C., Jadallah, M. A., Yates, S. L., Quint, S. R., and Nagle, H. T. (1990). A comparison of the noise sensitivity of nine QRS detection algorithms. *IEEE Trans. Biomed. Eng.* 37, 85–98. doi: 10.1109/10.43620

Golshan, H. M., Hebb, A. O., and Mahoor, M. H. (2020). LFP-Net: a deep learning framework to recognize human behavioral activities using brain STN-LFP signals. *J. Neurosci. Methods* 335:108621. doi: 10.1016/j.jneumeth.2020.108621

Hamilton, P. S., and Tompkins, W. J. (1986). Quantitative investigation of QRS detection rules using the MIT/BIH arrhythmia database. *IEEE Trans. Biomed. Eng.* 33, 1157–1165. doi: 10.1109/TBME.1986.325695

Hell, F., Plate, A., Mehrkens, J. H., and Bötzel, K. (2018). Subthalamic oscillatory activity and connectivity during gait in Parkinson's disease. *NeuroImage Clin.* 19, 396–405. doi: 10.1016/j.nicl.2018.05.001

Kent, A., and Grill, W. (2012). Recording evoked potentials during deep brain stimulation: development and validation of instrumentation to suppress the stimulus artefact. *J. Neural Eng.* 9:036004. doi: 10.1088/1741-2560/9/3/036004

Keshtkaran, M. R., and Yang, Z. (2014). A fast, robust algorithm for power line interference cancellation in neural recording. *J. Neural Eng.* 11:026017. doi: 10.1088/1741-2560/11/2/026017

Lu, G., Brittain, J.-S., Holland, P., Yianni, J., Green, A. L., Stein, J. F., et al. (2009). Removing ECG noise from surface EMG signals using adaptive filtering. *Neurosci. Lett.* 462, 14–19. doi: 10.1016/j.neulet.2009.06.063

Mak, J. N., Hu, Y., and Luk, K. D. K. (2010). An automated ECG-artifact removal method for trunk muscle surface EMG recordings. *Med. Eng. Phys.* 32, 840–848. doi: 10.1016/j.medengphy.2010.05.007

Marker, R. J., and Maluf, K. S. (2014). Effects of electrocardiography contamination and comparison of ECG removal methods on upper trapezius electromyography recordings. *J. Electromyogr. Kinesiol.* 24, 902–909. doi: 10.1016/j.jelekin.2014.08.003

Marmor, O., Valsky, D., Joshua, M., Bick, A. S., Arkadir, D., Tamir, I., et al. (2017). Local vs. volume conductance activity of field potentials in the human

subthalamic nucleus. *J. Neurophysiol.* 117, 2140–2151. doi: 10.1152/jn.00756.2016

Martini, M. L., Oermann, E. K., Opie, N. L., Panov, F., Oxley, T., and Yaeger, K. (2020). Sensor modalities for brain-computer interface technology: a comprehensive literature review. *Neurosurgery* 86, E108–E117. doi: 10.1093/neuros/nyz286

Meidahl, A. C., Tinkhauser, G., Herz, D. M., Cagnan, H., Debarros, J., and Brown, P. (2017). Adaptive deep brain stimulation for movement disorders: the long road to clinical therapy. *Mov. Disord.* 32, 810–819. doi: 10.1002/mds.27022

Neumann, W. J., Staub Bartelt, F., Horn, A., Schanda, J., Schneider, G.-H., Brown, P., et al. (2017). Long term correlation of subthalamic beta band activity with motor impairment in patients with Parkinson's disease. *Clin. Neurophysiol.* 128, 2286–2291. doi: 10.1016/j.clinph.2017.08.028

Pan, J., and Tompkins, W. J. (1985). A real-time QRS detection algorithm. *IEEE Trans. Biomed. Eng.* 32, 230–236. doi: 10.1109/TBME.1985.325532

Qian, X., Chen, Y., Feng, Y., Ma, B., Hao, H., and Li, L. (2017). A method for removal of deep brain stimulation artifact from local field potentials. *IEEE Trans. Neural Syst. Rehabil. Eng.* 25, 2217–2226. doi: 10.1109/TNSRE.2016.2613412

Qian, X., Hao, H., Ma, B., Wen, X., Hu, C., and Li, L. (2014). Implanted rechargeable electroencephalography (EEG) device. *Electron. Lett.* 50, 1419–1421. doi: 10.1049/el.2014.1820

Quinn, E. J., Blumenfeld, Z., Velisar, A., Koop, M. M., Shreve, L. A., Trager, M. H., et al. (2015). Beta oscillations in freely moving Parkinson's subjects are attenuated during deep brain stimulation. *Mov. Disord.* 30, 1750–1758. doi: 10.1002/mds.26376

Ramirez-Zamora, A., Giordano, J., Gunduz, A., Alcantara, J., Cagle, J. N., Cernera, S., et al. (2020). Proceedings of the seventh annual deep brain stimulation think tank: advances in neurophysiology, adaptive DBS, virtual reality, neuroethics and technology. *Front. Hum. Neurosci.* 14:54. doi: 10.3389/fnhum.2020.00054

Redfern, M. S., Hughes, R. E., and Chaffin, D. B. (1993). High-pass filtering to remove electrocardiographic interference from torso EMG recordings. *Clin. Biomech.* 8, 44–48. doi: 10.1016/S0268-0033(05)80009-9

Satija, U., Ramkumar, B., and Manikandan, M. S. (2018). A review of signal processing techniques for electrocardiogram signal quality assessment. *IEEE Rev. Biomed. Eng.* 11, 36–52. doi: 10.1109/RBME.2018.2810957

Shen, H. (2014). Neuroscience: tuning the brain. *Nature* 507, 290–292. doi: 10.1038/507290a

Shynk, J. J. (1992). Frequency-domain and multirate adaptive filtering. *IEEE Signal Process. Mag.* 9, 14–37. doi: 10.1109/79.109205

Sorkhabi, M. M., Benjaber, M., Brown, P., and Denison, T. (2020). "Physiological artifacts and the implications for brain-machine-interface design," in *Proceedings of the 2020 IEEE International Conference on Systems, Man, and Cybernetics (SMC)*, (Toronto, ON: IEEE), 1498–1498.

Stanslaski, S., Afshar, P., Cong, P., Giftakis, J., Stypulkowski, P., Carlson, D., et al. (2012). Design and validation of a fully implantable, chronic, closed-loop neuromodulation device with concurrent sensing and stimulation. *IEEE Trans. Neural Syst. Rehabil. Eng.* 20, 410–421. doi: 10.1109/TNSRE.2012.2183617

Swann, N. C., de Hemptinne, C., Miocinovic, S., Qasim, S., Ostrem, J. L., Galifianakis, N. B., et al. (2018). Chronic multisite brain recordings from a totally implantable bidirectional neural interface: experience in 5 patients with Parkinson's disease. *J. Neurosurg.* 128, 605–616. doi: 10.3171/2016.11.JNS161162

Sweeney, K. T., Ward, T. E., and McLoone, S. F. (2012). Artifact removal in physiological signals—Practices and possibilities. *IEEE Trans. Inform. Technol. Biomed.* 16, 488–500. doi: 10.1109/TITB.2012.2188536

Trager, M. H., Koop, M. M., Velisar, A., Blumenfeld, Z., Nikolau, J. S., Quinn, E. J., et al. (2016). Subthalamic beta oscillations are attenuated after withdrawal of chronic high frequency neurostimulation in Parkinson's disease. *Neurobiol. Dis.* 96, 22–30. doi: 10.1016/j.nbd.2016.08.003

Vansteensel, M. J., Pels, E. G., Bleichner, M. G., Branco, M. P., Denison, T., Freudenburg, Z. V., et al. (2016). Fully implanted brain–computer interface in a locked-in patient with ALS. *N. Engl. J. Med.* 375, 2060–2066. doi: 10.1056/NEJMoa1608085

Velisar, A., Syrkin-Nikolau, J., Blumenfeld, Z., Trager, M., Afzal, M., Prabhakar, V., et al. (2019). Dual threshold neural closed loop deep brain stimulation in Parkinson disease patients. *Brain Stimul.* 12, 868–876. doi: 10.1016/j.brs.2019.02.020

Zhou, P., and Kuiken, T. A. (2006). Eliminating cardiac contamination from myoelectric control signals developed by targeted muscle reinnervation. *Physiol. Meas.* 27, 1311–1327. doi: 10.1088/0967-3334/27/12/005

Zhou, P., Lock, B., and Kuiken, T. A. (2007). Real time ECG artifact removal for myoelectric prosthesis control. *Physiol. Meas.* 28, 397–413. doi: 10.1088/0967-3334/28/4/006

Conflict of Interest: LL, HH, and BM serve on the scientific advisory board for Beijing Pins Medical Co., Ltd., and were listed as inventors in issued patents and patent applications on the deep brain stimulator used in this work.

The remaining author declares that the research was conducted in the absence of any commercial or financial relationships that could be construed as a potential conflict of interest.

frontiers in Neuroscience

REVIEW
published: 22 April 2021
doi: 10.3389/fnins.2021.645472

Strategies to Refine Gastric Stimulation and Pacing Protocols: Experimental and Modeling Approaches

Leo K. Cheng[1,2,3], Nipuni D. Nagahawatte[1], Recep Avci[1], Peng Du[1], Zhongming Liu[4,5] and Niranchan Paskaranandavadivel[1]*

[1] Auckland Bioengineering Institute, University of Auckland, Auckland, New Zealand, [2] Department of General Surgery, Vanderbilt University Medical Center, Nashville, TN, United States, [3] Riddet Institute, Palmerston North, New Zealand, [4] Department of Biomedical Engineering, University of Michigan, Ann Arbor, MI, United States, [5] Department of Electrical Engineering and Computer Science, University of Michigan, Ann Arbor, MI, United States

Gastric pacing and stimulation strategies were first proposed in the 1960s to treat motility disorders. However, there has been relatively limited clinical translation of these techniques. Experimental investigations have been critical in advancing our understanding of the control mechanisms that innervate gut function. In this review, we will discuss the use of pacing to modulate the rhythmic slow wave conduction patterns generated by interstitial cells of Cajal in the gastric musculature. In addition, the use of gastric high-frequency stimulation methods that target nerves in the stomach to either inhibit or enhance stomach function will be discussed. Pacing and stimulation protocols to modulate gastric activity, effective parameters and limitations in the existing studies are summarized. Mathematical models are useful to understand complex and dynamic systems. A review of existing mathematical models and techniques that aim to help refine pacing and stimulation protocols are provided. Finally, some future directions and challenges that should be investigated are discussed.

Keywords: stimulation, pacing, gastric motility, slow wave, biophysical model, mathematical model

OPEN ACCESS

Edited by:
Tamas Ordog,
Mayo Clinic, United States

Reviewed by:
Kenneth Louis Koch,
Wake Forest Baptist Medical Center, United States
Conor McCann,
University College London, United Kingdom

****Correspondence:***
Leo K. Cheng
l.cheng@auckland.ac.nz

Specialty section:
This article was submitted to Autonomic Neuroscience, a section of the journal Frontiers in Neuroscience

Received: *23 December 2020*
Accepted: *22 March 2021*
Published: *22 April 2021*

Citation:
Cheng LK, Nagahawatte ND, Avci R, Du P, Liu Z and Paskaranandavadivel N (2021) Strategies to Refine Gastric Stimulation and Pacing Protocols: Experimental and Modeling Approaches. Front. Neurosci. 15:645472. doi: 10.3389/fnins.2021.645472

INTRODUCTION

Bioelectricity is a key regulator of bodily function. The coordinated contraction and relaxation of the muscles necessary for controlling movement are initiated by electrical signals propagating through the nerves and muscles. Disorders in the electrical signals and patterns can result in dysmotility. An improved understanding of how intrinsic bioelectrical events, and externally introduced electrical signals, interact with our nerves and muscles is critical for refining existing, and developing new therapies. The foundations of electrophysiology can be attributed to Galvani's studies on frog muscles and hearts in the 1790s (Piccolino, 1997). It was not long afterward that the first reports of using electrical stimulation to treat cardiac conditions occurred in the 1800s, despite the underlying science being uncertain (Green, 1872; McWilliam, 1889). Subsequently, in the 1920s, the first external cardiac pacemakers were reported independently by Lidwell and Hyman (Aquilina, 2006; Mond et al., 2012). Hyman was the first to coin the term "artificial pacemaker," a term that is still widely used to date.

Bioelectrical signals were first measured from the gastrointestinal tract in the 1920s (Alvarez, 1922b). In his seminal studies, Alvarez established that rhythmic electrical events occurred 3 cycles per minutes (cpm) in the human stomach. These electrical events were omnipresent, and occurred even in the absence of any visible contractions (Alvarez, 1922a). Despite substantial effort devoted to investigate the normal and impaired bioelectrical activity along the gastrointestinal tract over the last century, our understanding of gastrointestinal electrophysiology and the application of electrical pulses to treat disorders has lagged the cardiac field (Cheng, 2015; Avci et al., 2020). This is partly because the gastrointestinal tract has a number of cooperating and overlapping mechanisms that coordinate the mechanical contractions to aid in the breakdown, mixing and transportation of luminal contents (Huizinga and Lammers, 2009). One of the key contributors is bioelectrical events, known as slow waves, that are generated by interstitial cells of Cajal (ICC) (Huizinga et al., 1995). Loss of ICC and disordered slow wave patterns have been associated with a number of functional gastrointestinal and motility disorders (see section "Gastric Functional Motility Disorders"). Therefore, the use of external electrical impulses to restore function is an attractive approach.

Electrical stimulation of the stomach was first reported in 1963 as a potential therapy for paralytic ileus–the loss of peristaltic activity that frequently occurs following abdominal surgery (Bilgutay et al., 1963). Investigators have also applied electrical impulses to treat gastroparesis by improving the rate of gastric emptying (McCallum et al., 1998), or to treat obesity, by delaying the rate of gastric emptying (Sarna et al., 1976; Liu et al., 2006a). However, the results have generally been inconsistent and variable. This variability can be associated with a number of key problems: (i) lack of understanding of the mechanisms of action, (ii) large variation in the pulses sequences applied, (iii) lack of high-quality human trials, and (iv) lack of unbiased methods for quantifying the efficacy of a therapy.

In recent years, there has been renewed interest in the use of electrical impulses to modulate the bioelectrical activity for acute and chronic disorders. Neurology and cardiology have received the most attention, but it has also been applied for pain management and for the treatment of functional gastrointestinal motility disorders. This review will focus on the application of electrical impulses directly on the stomach musculature and techniques used to optimize the pacing parameters. In addition, some future directions for stimulation, pacing and modeling efforts are discussed.

GASTRIC FUNCTIONAL MOTILITY DISORDERS

Gastric motility disorders are complex and often present with overlapping symptoms and phenotypes of disorders. Some functional motility disorders that are associated with disordered slow wave activity, along with obesity and post-operative ileus are discussed below.

Gastroparesis

Gastroparesis is a chronic symptomatic gastric motility disorder, defined as delayed gastric emptying of a solid meal in the absence of mechanical obstruction. Symptoms or signs of gastroparesis include nausea, vomiting, early satiety, fullness, anorexia, and/or weight loss (Camilleri et al., 2013). Definitive diagnosis for gastroparesis includes retention of greater than 10% of a solid-meal as determined by scintigraphy after 4 h (Abell et al., 2008). Gastroparesis is not a common disease, with its prevalence reported at 0.2% in the United States (Syed et al., 2020). However, delayed emptying has been estimated to be 1.8% in the community and suggests that gastroparesis may be undiagnosed in many subjects in the population. Patients with severe gastroparesis may require long-term enteral or parenteral nutritional support, as well as frequent and prolonged hospital admissions (Wang et al., 2008).

Gastroparesis is associated with loss and degradation of the ICC network (Farrugia, 2008; Grover et al., 2011). The NIH Gastroparesis Clinical Research Consortium[1] has collected and analyzed full-thickness gastric biopsies from gastroparetic patients undergoing gastric stimulator implantation and reported a 48% reduction in ICC numbers in diabetic gastroparesis patients compared to age matched controls (2.8 vs. 5.3 cells/high powered field) (Grover et al., 2011). The degradation of ICC numbers and network integrity are associated with disordered slow wave and motility patterns (see section "High Resolution Slow Wave Mapping"). Therefore, a variety of electrical therapies have been proposed to treat gastroparesis (Paskaranandavadivel et al., 2020). Therapies have reported to both improve symptoms (McCallum et al., 2010, 2013; Ducrotte et al., 2020), and in some cases improve gastric emptying rates (McCallum et al., 1998) (see section "Gastric Stimulation and Pacing" for further details).

Chronic Unexplained Nausea and Vomiting

Chronic unexplained nausea and vomiting patients have symptoms similar to gastroparesis patients (Pasricha et al., 2011). However, they have normal gastric emptying (less than 10% retention of a solid meal after a 4 h period). These patients have been reported to have a moderate reduction in ICC numbers compared with controls, with gastroparesis patients having the greatest reduction in ICC numbers (5.6 vs. 3.5 vs. 2.3 cell bodies/high powered field) (Angeli et al., 2015). In addition, compared with gastroparesis, patients with chronic unexplained nausea and vomiting have less smooth muscle fibrosis (Bashashati et al., 2017). Disordered slow wave patterns have also been reported in these patients (see section "High Resolution Slow Wave Mapping").

Functional Dyspepsia

Functional dyspepsia is defined by the Rome IV guidelines when a subject has presented with post-prandial fullness, early satiety, epigastric pain and epigastric burning (Futagami et al., 2018). It is also associated with impaired accommodation of the proximal

[1] https://repository.niddk.nih.gov/studies/gpcrc/

stomach, early distension and impaired motility of the antrum post-prandial (Bortolotti et al., 1995; Gilja et al., 1996). The reported prevalence of functional dyspepsia is variable from 5 to 40%, with varying severities in symptoms (Enck et al., 2017).

Cutaneous electrogastrography studies have detected slow wave frequencies outside the normal range (i.e., greater or less than 2–4 cpm) in functional dyspepsia subjects. In one study, abnormal frequencies were detected in 83% of the subjects (Sha et al., 2009). A recent high resolution (HR) electrogastrography study was able to detect spatial slow wave abnormalities in 44% of subjects along with a higher proportion of aberrant propagation directions (Gharibans et al., 2019). In addition, abnormal spatial parameters were found to be correlated with severity of upper gastrointestinal symptoms. Electrical therapies using implanted and transcutaneous methods have successfully been applied to relieve symptoms (Lu et al., 2013; Zhu et al., 2021).

Obesity

Obesity is a significant risk factor for a range of diseases from diabetes, cardiovascular disease to cancer (Sowers, 2003). It is also associated with a host of gastrointestinal symptoms from abdominal pain, bloating, diarrhea, and frequency vomiting (Delgado-Aros et al., 2004). Its prevalence has significantly increased, with reports of 20–40% of the population being obese across various countries (Hales et al., 2020). Typical management involves physical activity, modifying eating patterns, reducing caloric intake, drug therapy and counseling (Turner et al., 2018). In severe cases, bariatric surgery is considered, where the stomach capacity is reduced to limit food intake or bypassed to reduce nutrient uptake. Electrical therapies have been proposed as a treatment for obesity. However, mixed results have been reported, with some human trials reporting promising results (Cigaina, 2004; Favretti et al., 2004; Yao et al., 2005; Liu et al., 2006a), but longer term studies have failed to show sustained weigh loss over an extended period (Johannessen et al., 2017).

Post-operative Ileus

Post-operative ileus, a transient impairment of gastrointestinal motility, is a common occurrence after abdominal surgery and has limited treatment options (Iyer et al., 2009). It is associated with delayed recovery, prolonged hospital stays, significant increases in health costs and increased risks of morbidity (Iyer et al., 2009). Patients may experience abdominal pain, nausea, vomiting, bloating, and are unable to eat or pass stool for multiple days (Vather et al., 2013). Due to these needs, post-operative ileus was proposed as one of the initial targets for electrical therapy (Bilgutay et al., 1963; Hocking et al., 1992).

ELECTRICAL CONDUCTION SYSTEM OF THE STOMACH

The cause, diagnosis and treatments of GI functional motility disorders as described in section "Gastric Functional Motility Disorders" remain poorly understood. A number of these disorders are linked with impaired electrophysiology of the GI tract. Therefore, an improved understanding of the electrical conduction system in the GI tract, in both health and disease, will assist in the development of new and the refinement of existing therapies.

Slow waves are a key input that are generated and propagated by ICC (Huizinga et al., 1995). ICC are named after Nobel laureate Santiago Ramón y Cajal. In the late 19th century, Cajal described a new type of nerve-like branching networks interleaved among neurons embedded within the smooth muscle linings in the GI tract (Cajal, 1911). However, their developmental origin and function remained unclear for many decades (Huizinga et al., 1995). Subsequently, Thuneberg sparked a revival in ICC research by proposing that ICC were the intestinal pacemaker cells (Thuneberg, 1982) and showed that injury of ICC resulted in loss of slow wave activity (Liu et al., 1994).

Individually, ICC have different intrinsic frequencies, however, *in vivo* they form an integrated network and entrain to the dominant highest frequency (Hinder and Kelly, 1977; Hirst and Edwards, 2006). For example, stomach ICC have been found to have a gradient of intrinsic activity (Xue et al., 1995; Hirst and Edwards, 2006). However, in the normal, intact human stomach, all activity is entrained to a dominant frequency of 3 cpm (Hinder and Kelly, 1977; O'Grady et al., 2010a). If distal regions are either partially or totally isolated, they autonomously generate slow waves at a lower intrinsic frequency (Sarna et al., 1972; Hinder and Kelly, 1977). In addition, if tissue samples are excised and left for an extended period of time, the slow wave frequency can increase significantly higher than the normal *in vivo* frequency. For example, in the cat stomach the frequency increased from 4.1 to 12.0 cpm (Xue et al., 1995) and in excised human tissue samples, frequency was reported to be as high as 7.4 cpm in the antrum, while the excised fundus (normally devoid of cyclic activity) had a frequency of 5.1 cpm (Rhee et al., 2011). Therefore, *in vivo* slow wave recordings are likely to be a more accurate representation of intrinsic physiology (Angeli et al., 2013; Sarna, 2013; Huizinga, 2017).

Slow waves depolarize the neighboring smooth muscle cells, either through gap junctions or peg-and-socket coupling (Torihashi et al., 2002; Huizinga et al., 2010). Under the right combination of neuro-hormonal conditions, the depolarized smooth muscle cells are able to generate contractions based on a series of intracellular Ca^{2+} release mechanisms (Karaki and Weiss, 1984). The sustained plateau of depolarization of smooth muscle membrane can also lead to bursts of action potentials or spikes that are associated with Ca^{2+} entry and contractile activity (Ver Donck et al., 2006; Lee et al., 2007).

Importantly, the stomach is not completely autonomous (Travagli and Anselmi, 2016). Slow wave activity is coordinated by the ICC, but the resulting motility is also modulated through extrinsic nerve innervation (Powley et al., 2019), and the enteric nervous system (Furness, 2012; Furness et al., 2014). In this regard, the vagus plays a central role in extrinsic neural control of the stomach. The nucleus tractus solitarius is the primary viscerosensory nucleus of the vagus, which gathers vagal afferent input and modulates the dorsal motor nucleus of the vagus to alter visceromotor output. The left vagal fibers are understood to innervate the proximal region of the stomach where the

gastric pacemaker is located (Pagani et al., 1988). Additionally, the vagus nerve can modulate antral motility, pyloric opening, and gastric emptying (Lu et al., 2018, 2020). Neuropathy has also been known to accompany a number of gastrointestinal diseases, particularly when accompanied by diabetes (Vinik et al., 2003). Animal models of impaired gastrointestinal functions have also shown damage to both extrinsic and intrinsic nerves, as well as reduced ICC (Young and Edwards, 2005). The readers are referred to Furness et al. (2014) for a detailed review of the vagal control of gut motility, and Phillips et al. (2006) for a detailed review of neuropathy affecting the gastrointestinal tract.

SLOW WAVE ACTIVITY IN THE STOMACH

Slow Wave Recordings

The earliest recordings of gastrointestinal slow wave activity can be attributed to the foundational work of Alvarez (1922b,c). Initially, measurements were obtained from individual locations, either on the surface of the stomach or on the body surface. Such recordings allowed the normal frequency of the slow wave events to be established. The term tachygastria was first introduced in 1974, referring to activity with an abnormally high frequency (Code and Marlett, 1974). Bradygastria, a term for low frequency slow wave activity, was soon reported in human studies (You and Chey, 1984; Abell and Malagelada, 1985). Examples of normal, bradygastric and tachygastric slow wave traces are shown in **Figure 1**. The frequency bands of gastric slow wave activity types have now been formally defined, with normal activity generally defined to be within 2.5–3.75 cpm and bradygastria and tachygastria, below or above this range (Parkman et al., 2003; Koch, 2011).

Subsequently, more electrodes were introduced and by placing the electrodes along the central axis of the stomach, it was possible to track the propagation of the slow wave from electrode to electrode (Kelly et al., 1969; Hinder and Kelly, 1977). Using these techniques, propagation direction and speed were able to be deduced. However, it is now clear that such sparse or low resolution slow wave recordings can at times be misleading due to spatial aliasing, especially when activity is dysrhythmic (Cheng et al., 2013; O'Grady et al., 2019).

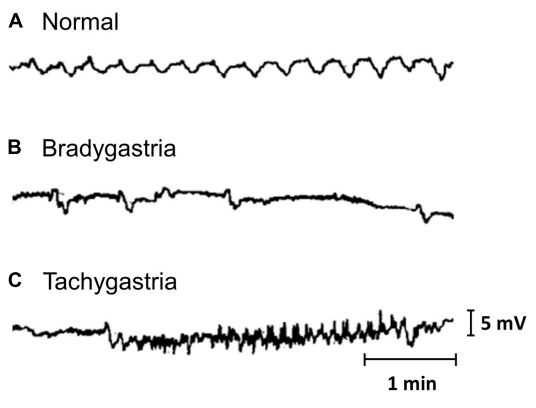

FIGURE 1 | Gastric mucosal slow wave traces of **(A)** normal, **(B)** bradygastric, and **(C)** tachygastric activity. Modified from Abell and Malagelada (1985).

High Resolution Slow Wave Mapping

High resolution mapping utilizes hundreds of spatially dense electrodes, typically arranged in a two-dimensional grid, to map the spatio-temporal pattern of slow wave activity. Adapting techniques that had previously been used to map the electrical activity in the heart (Durrer et al., 1970; Pullan et al., 2003), HR mapping was first applied to the gastrointestinal tract by Lammers et al. (1993), to map the slow wave activity in the rabbit duodenum. Similar methods have now been applied to map the slow wave patterns in the stomach of a variety of animal species (Lammers et al., 1998, 2009; Du et al., 2009a; Egbuji et al., 2010), and the human stomach in both health and disease (O'Grady et al., 2010a, 2012a; Angeli et al., 2015). HR mapping studies have identified regional variations in gastric slow wave activity, most notably a region of high amplitude and high velocity in the distal antrum of the human stomach (Berry et al., 2016). It is postulated that this distal antral wave acceleration, along with coordination with the pylorus, plays a major role in retropulsion of contents to allow both efficient mixing and breakdown on contents, along with antral flow of contents into the intestine (Berry et al., 2016; Ishida et al., 2019).

As discussed in section "Gastric Functional Motility Disorders," a loss of ICC numbers and a breakdown in the ICC network integrity has been reported in gastroparesis patients (Grover et al., 2011). Furthermore, HR mapping studies in gastroparetic and chronic unexplained nausea and vomiting patients undergoing Enterra stimulator implantation (Medtronic Inc., Minneapolis, MN, United States) reported a range of abnormal slow wave propagation patterns including, ectopic pacemakers and conduction blocks (O'Grady et al., 2012a; Angeli et al., 2015). Mechanism of slow wave dysrhythmias can be classified into disorders of: (i) conduction and (ii) initiation (O'Grady et al., 2014). Ectopic pacemakers are an example of an initiation disorder, where a secondary pacemaker may compete with the primary or normal pacemaker. In this case, the ectopic pacemaker may initiate retrograde waves that eventually collide with waves generated by the natural pacemaker located in the upper/mid-corpus leading to uncoordinated or uncoupled activity in different regions of the stomach (Berry et al., 2017). A conduction block is an example of a conduction abnormality. In this case, a region of tissue may have a zone of abnormally slow propagation, or force the slow wave to propagate around the conduction block zone. This may then result in secondary forms of dysrhythmias, including reentrant activity and rapid circumferential activation (Lammers et al., 2008; O'Grady et al., 2011). Rapid circumferential propagation is present in a range of gastric dysrhythmias, elevating extracellular amplitudes and organizing transverse wavefronts that may help to reset activity back into an ordered band (O'Grady et al., 2012b). One important finding from the HR mapping studies was that abnormalities of slow wave initiation and conduction

occurred at a frequency similar to normal slow wave patterns (around 3 cpm). As a result, such spatial abnormalities could be missed using techniques that lack sufficient spatial resolution (Buist et al., 2006).

By combining HR mapping with pacing or stimulation techniques, it is possible to monitor and track the electrophysiological response of the organ. The first study to report such techniques was conducted in the isolated rabbit duodenum (see **Figure 2A**; Lammers et al., 1993). Similar techniques have been applied to pigs to investigate the effects of different pacing parameters (O'Grady et al., 2010b), to test the efficacy of new pacemaker designs (Wang et al., 2018; Alighaleh et al., 2019) and to assess acute slow wave response in patients undergoing Enterra stimulator implantation (Angeli et al., 2016). As Enterra Therapy uses high-frequency stimulation protocols, its mechanism of action is likely via nerves. Despite using a variety of stimulation parameters, including protocols that attempted to mimic pacing parameters within hardware limitations (e.g., amplitude 19 mA, pulse-width 0.45 ms, frequency 130 Hz, on period 1 s, off period 17 s), no changes in slow wave patterns were observed during these acute studies (Angeli et al., 2016). Initial work on mapping the slow wave response with pacing protocols has been applied to human studies (Alighaleh et al., 2018). An example of such results is shown in **Figure 2B**, where pacing electrodes were integrated into the center of the HR electrode array and a new pacemaker region was initiated slightly above the pacing electrodes (identified by the dark orange area). Further work is required to assess regional electrophysiological characteristics and long-term outcomes.

GASTRIC STIMULATION AND PACING

Electrical pulses applied to the stomach can take many forms, which typically consist of a series of rectangular pulses applied as a constant current or voltage at a prescribed frequency. They can be broadly grouped into two categories: (i) pacing methods that are typically low frequency and high energy and (ii) stimulation methods that are typically high frequency and low energy. **Figure 3** illustrates some of the types of electrical pulses that have been applied to the stomach. Key parameters that define the electrical pulses include the amplitude, pulse width, frequency at which pulses are applied. In some cases, stimulation pulses are modulated or comprised of trains of shorter pulses.

Gastric Pacing

Pacing methods involve the application of high energy pulses applied at a frequency close to the intrinsic slow wave frequency. These methods attempt to entrain or modulate the underlying slow wave activity of the stomach, hence they primarily target the ICC to alter slow wave patterns, and therefore motility patterns.

The pulse sequences used for two human gastric pacing protocols (Hocking et al., 1992; McCallum et al., 1998) are visually compared in **Figure 4**. Pacing methods were initially trialed in dog studies and showed the ability to either increase or decrease the slow wave frequency (intrinsic frequency 5.0 cpm, modulated range 4.2–8 cpm) in response to the pacing (Kelly and La Force, 1972). Subsequently, human studies were reported by two groups in 1992 (Hocking et al., 1992; Miedema et al., 1992). Hocking et al. (1992) were one of the first to apply pacing protocols to the stomach applying a pulse at 2 mA for 300 ms

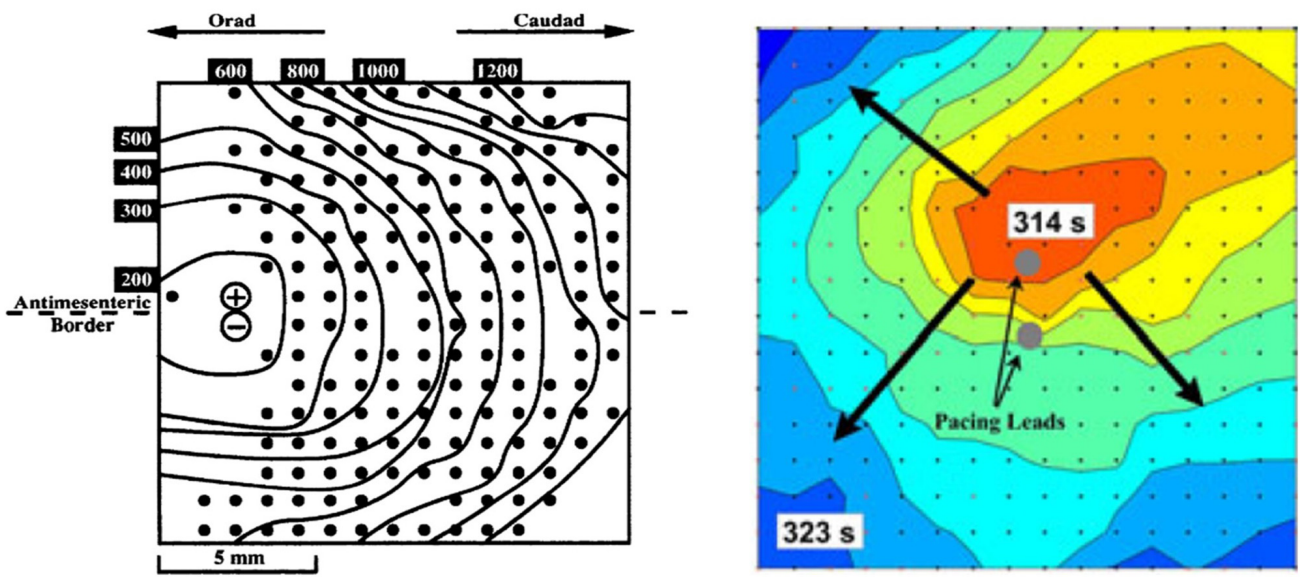

FIGURE 2 | Combining HR mapping and pacing techniques allows the slow wave response to be tracked and quantified. **(A)** Pacing on the left side of a rabbit duodenum preparation and resultant propagation across the mapped area, **(B)** Pacing from the center of a 60 mm^2 electrode array (red is early activation, and blue is late activation), and corresponding radial propagation from the pacing leads (gray circles). Modified from Lammers et al. (1993) and Alighaleh et al. (2018).

at between 0.3 and 1.6 cpm higher than the intrinsic slow wave frequency. They were able to entrain and increase the slow wave frequency but were unable to improve gastric emptying. However, other studies have reported that gastric emptying could be enhanced with gastric pacing (Eagon and Kelly, 1993; McCallum et al., 1998). McCallum et al. (1998) applied 4 mA for 300 ms at 110% of the intrinsic frequency of baseline slow waves to gastroparesis patients and were able to correct tachygastric slow waves and also improve gastric emptying rates.

On the other hand, Sarna et al. (1976) demonstrated that gastric emptying could be delayed by pacing from the distal antrum in dogs. Therefore, the use of pacing protocols to treat obesity has also been investigated (Cigaina et al., 1996). Such methods aim to limit food intake by reducing rates of gastric emptying. Although exact mechanisms remain uncertain, likely contributors include inhibiting antral contractions or initiating retrograde slow wave to disrupt the intrinsic slow wave activity. Trials in a small human cohort have shown promising results (Cigaina, 2004; Favretti et al., 2004; Yao et al., 2005; Liu et al., 2006a).

Table 1 summarizes the pacing protocols used in both human and animal studies. A typical range of effective pacing parameters reported in the literature across species can be summarized as 2–5 mA of amplitude and 300–500 ms pulse width with a frequency similar to intrinsic frequency. Applying correct pulse width and amplitude is essential for an effective pacing. In humans, 4–5 mA current and 300 ms pulse width applied at a frequency similar to, or larger than, the intrinsic frequency were reported to be the most effective parameters. On the other hand, lower amplitudes (e.g., 0.5–1 mA) and pulse widths (e.g., 3 or 30 ms) were reported to fail to entrain slow wave activity (Lin et al., 1998, 2011). The amplitude and pulse width parameters used in other species such as pig, dog, and rats were relatively comparable with human studies. Since the baseline slow wave activity is to be modulated via pacing, the frequency of applied pulse is also a critical factor for effective pacing and likely vary between subjects and species.

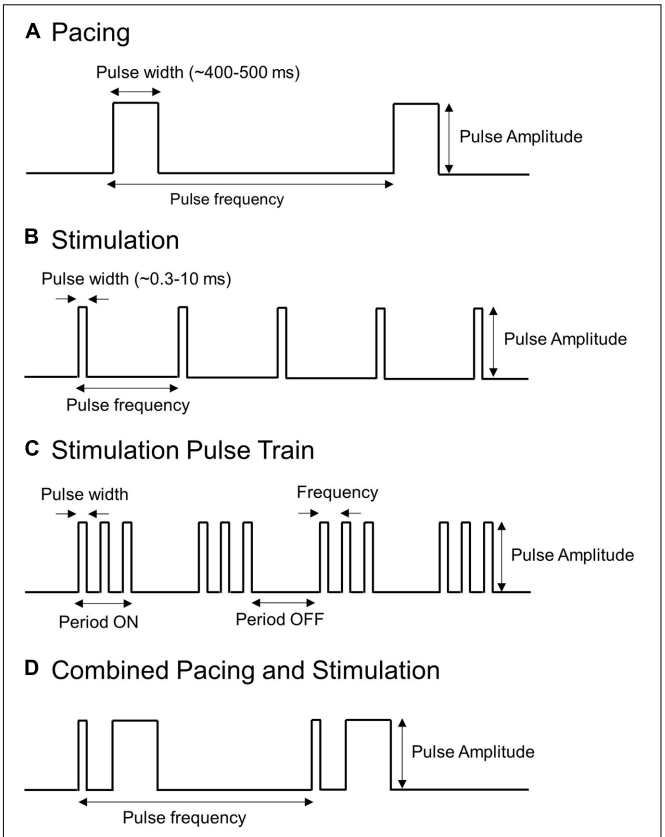

FIGURE 3 | Types of pulses used to stimulate or pace the stomach. Shown are **(A)** Long pulses associated with pacing (high-energy and low frequency), **(B,C)** Short pulses or trains of short pulses associated with stimulation (low energy and high frequency), and **(D)** a hybrid pacing and stimulation approach that combines short and long pulses.

Gastric Stimulation

Stimulation methods apply higher frequency pulses at lower energy level compared with pacing techniques. They do not seek to entrain the underlying slow wave patterns but instead target the neural pathways that also have a role in modulation of motility patterns.

Bilgutay et al. (1963) were one of the first to report the concept of gastric electrical stimulation where a pulse sequence with amplitudes of 7–10 mA at 50 Hz for 5 s periods was applied in each minute (see **Figure 4D**). They reported results from 5 case studies out of 40 patients with paralytic ileus. Using their methods, stimulation was successful in generating peristalsis in post-operative ileus following a variety of abdominal operations. Stimulation resulted in early return of bowel activity, reduced the time for intravenous administration of fluids and electrolytes, allowed oral intake to resume sooner, and reduced the passing of flatulence from 55 to 20 h.

Familoni et al. (1997a) performed one of the early stimulation studies in dogs. They used short pulses of 0.3 ms duration and 2 mA amplitude, and were able to both entrain the slow wave activity and elicit contractions. When the pulses were applied at 20 or 30 cpm (0.33 or 0.5 Hz) the motility patterns were significantly enhanced. Similar techniques were then attempted on a refractory gastroparesis patient (Familoni et al., 1997b). They found that stimulation at a frequency much greater than the intrinsic frequency (i.e., at 12 cpm) resulted in improved emptying and symptoms in that patient. As a result of these promising results, the World-wide Anti-Vomiting Electrical Stimulation study (WAVESS) was performed (Abell et al., 2002, 2003). During the initial double blinded phase of WAVESS, there was a significant reduction in the frequency of vomiting. After 12 months, there was a greater than 50% reduction in vomiting in more than 70% of subjects, and vomiting and nausea severity scores were significantly improved (Abell et al., 2003). As a result, the Enterra Therapy system was developed and approved for use under humanitarian device exception by the FDA.

For detailed meta-analysis of past high-frequency stimulation trials for treating gastroparesis refer to Table 1 in O'Grady et al. (2009) and Table 1 in Chu et al. (2012). As part of these analyses only two randomized, control trials were reported and both were classified as "medium quality" (Abell et al.,

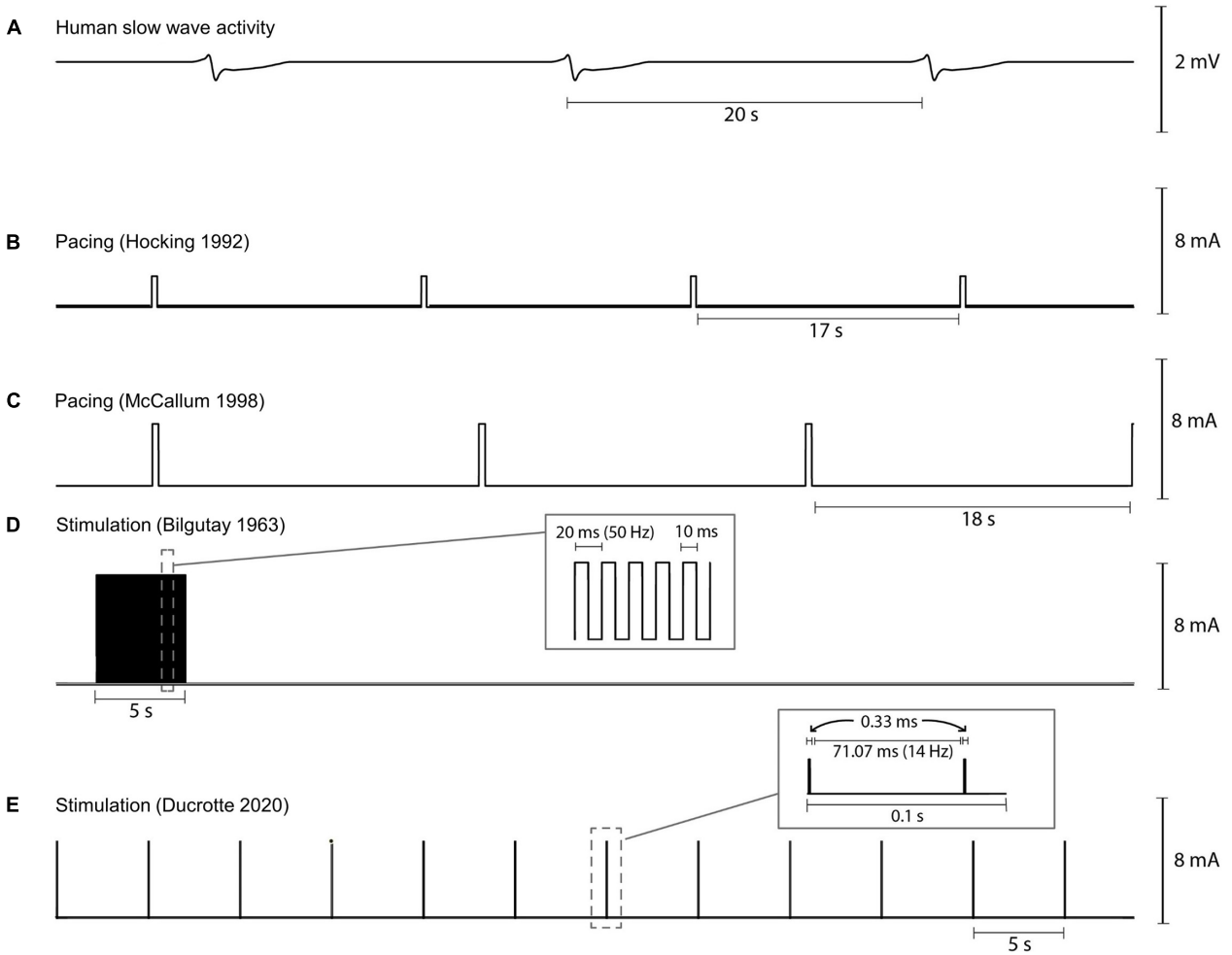

FIGURE 4 | Illustration of variability in pacing and stimulation pulses used by various researchers for human gastric pacing studies. **(A)** Normal gastric slow wave activity occurring at 3 cpm, **(B,C)** gastric pacing parameters as applied by Hocking et al. (1992) (2 mA, 350 ms, IF + 0.5 cpm) and McCallum et al. (1998) (4 mA, 350 ms, 110% IF), and **(D,E)** gastric stimulation parameters as applied by Bilgutay et al. (1963) (7 mA, 50 Hz, 5 s on period, 55 s off period) and Ducrotte et al. (2020) (5 mA, 14 Hz, 0.1 s on period, 5 s off period). IF: intrinsic frequency.

2003; McCallum et al., 2010). Recently, Ducrotte et al. (2020) completed a comprehensive randomized control study evaluating the standard Enterra Therapy pulse sequence of 5 mA, 14 Hz pulse train applied for 0.1 s, followed by a 5 s off period (see **Figure 4E**). It should be noted that the pulse train only consisted of 2 impulses separated by 71 ms because of the short 0.1 s on period. The study determined that the stimulator was effective in reducing the frequency of vomiting and nausea in a subset of patients. However, overall after 4 months of gastric stimulation, neither gastric emptying nor quality of life was improved. Nevertheless, patients with medically resistant symptoms may benefit from gastric stimulation to relieve nausea and vomiting. In this study, stimulation reduced episodes of vomiting from 1 per week to 1 per month in approximately 30% of subjects. Temporary stimulation methods have been proposed by some centers to help improve patient selection, and to personalize stimulation parameters and lead placement (Abell et al., 2011; Elfvin et al., 2011; Corvinus et al., 2018).

Gastric stimulation protocols have also been applied to treat obesity by reducing motility, delaying emptying and increasing satiety. Pre-clinical trials showed that stimulation was able to delay gastric emptying, distention, and reduce food intake and eventually led to weight loss (Song et al., 2015). Initial trials in humans showed encouraging results (Favretti et al., 2004; Bohdjalian et al., 2006), but randomized trials have failed to show clinical benefit over a prolonged period (Shikora et al., 2009; Paulus et al., 2020).

Table 2 summarizes types of stimulation parameters that have been applied in both animal and human studies. There is a large variability in the stimulation parameters compared to gastric pacing protocols (see **Table 1**). The typical range of pulse amplitude is 2–10 mA, but there was high level of variability in pulse width (typical range 0.2–10 ms), frequency (typical range 0.2–50 Hz), and on/off periods (typical range 0.1–5 s on period/3–55 s off period). A high degree of variation in the stimulation parameters is noted in these studies and it is hypothesized that

TABLE 1 | Protocols used for gastric pacing.

References	Species	Amplitude	Pulse Width	(Applied) Frequency
Miedema et al., 1992	Human	4 V	60 ms	IF + 0.5 cpm
Hocking et al., 1992	Human	2 mA	300 ms	IF + (0.3–1.6) cpm
Lin et al., 1998	Human	4 mA	300 ms	110% IF
McCallum et al., 1998	Human	4 mA	300 ms	110% IF
Yao et al., 2005	Human	5 mA	500 ms	9 cpm
Lin et al., 2011	Human	4 mA	350 ms	110% IF
		2 and 0.5 mA*	150 and 150 ms	110% IF
Kelly and La Force, 1972	Dog	1–8 mA	100–2000 ms	2–12 cpm
Sarna and Daniel, 1973	Dog	1–25 V	100 ms	4.8–7.3 cpm
Bellahsene et al., 1992	Dog	2 mA	300 ms	IF (approximately 5 cpm)
Song et al., 2005	Dog	5 mA	550 ms	110% IF
		1 and 0.6 mA*	200 ms	110% IF
Xu et al., 2008	Dog	4 mA	300–500 ms (Modulated at 50 Hz)	110% IF
		1 and 0.5 mA*	200–400 ms (modulated at 50 Hz)	110% IF
O'Grady et al., 2010b	Pig	4 mA	400 ms	Similar to, or faster than IF
Wang et al., 2018	Pig	5 and 8 mA	500, 900 ms	2.7–6 cpm
Alighaleh et al., 2019	Pig	4 mA	400 ms	110% IF
Yin et al., 2006	Mouse	3 mA	20–150 ms	110% IF

IF: intrinsic frequency.
**: two channel pacing.*

different sets of parameters target different functional responses. Typically, activation of vagal afferents is achieved at a stimulation frequency of 20–30 Hz and frequencies higher than 50 Hz can potentially cause damage to the nerves (Bonaz et al., 2013). On the other hand, lower than 5 Hz frequency is understood to be more effective at targeting the vagal efferents (Bonaz, 2018). Therefore, parameters with excitatory or inhibitory effects need be accordingly chosen for an effective stimulation. For instance, trains of short pulses were reported to be more effective on nausea and vomiting as it was mediated by vagal pathway (Chen et al., 2003). Similarly, parameters that inhibit antral contractions via the sympathetic pathway would be more effective to treat obesity (e.g., amplitude 10 mA, width 0.6 s, 2 s period, 3 s off period, frequency 40 Hz) (Zhu and Chen, 2005). The effect of different stimulation protocols has also been evaluated using transcutaneous auricular vagal nerve stimulation. In an acute setting, auricular stimulation has been shown to normalize gastric activity when stimulating at 10 Hz, whereas slow wave activity was inhibited when stimulation was applied at 80 Hz (Sukasem et al., 2020).

Alternative Approaches

Alternative approaches for pacing and stimulation include combining stimulation and pacing methods, use of multiple stimulation electrodes, synchronizing the applied pulses with the intrinsic activity, and direct stimulation of the vagus nerve.

Gastric pacing is able to entrain gastric slow waves and normalize gastric dysrhythmias and, in some cases, improve gastric emptying (see section "Gastric Pacing"). However, pacing methods do not improve symptoms of nausea and vomiting (Zhang and Chen, 2006). On the other hand, gastric stimulation has been shown to improve symptoms of nausea and vomiting but not to improve gastric emptying (O'Grady et al., 2009; Ducrotte et al., 2020). The ability to improve both emptying rates and treat symptoms is a key therapeutic goal. Therefore, dual pulse approaches that incorporate both pacing and stimulation methods have been proposed (Liu et al., 2004, 2006b). In rats, stimulation with short pulses (e.g., 0.3 ms) and pacing with long pulses (e.g., 550 ms) were reported to improve gastric emptying and alter slow waves patterns (Liu et al., 2004). Similarly, when applied in a canine study, both gastric dysrhythmias and symptoms were normalized by the dual pulse approach (Liu et al., 2006b).

The use of multiple sites for stimulation or pacing has been proposed to influence a larger region of the stomach (Song et al., 2005; Lin et al., 2011). Such approaches have successfully modulated a larger region of the stomach using two pairs for leads utilizing lower levels of total energy compared to a single lead approach. By implanting up to six rings of stimulating electrodes circumferentially around the stomach and stimulating sequentially, it was possible to induce circumferential contraction patterns and increase gastric emptying (Mintchev et al., 2000).

In most studies, pacing and stimulation are performed at a fixed frequency or in an "open-loop" fashion irrespective of the underlying slow wave frequency. In many gastric pacing studies, the intrinsic frequency is determined in a baseline recording period, and then pacing applied at a slightly higher frequency (see **Table 1**). However, the timing at which these pulses are applied is still irrespective of the underlying activity. Studies have proposed "closed-loop" or synchronized methods which sense the underlying activity and then stimulate at appropriate times (Wang et al., 2020a,b). Experimentally, the synchronized methods were able to either induce or enhance antral contractions and increase rates of gastric emptying (Zhu et al., 2007).

Obesity has also been a target for gastric stimulation and pacing (see section "Obesity") and some human trials have reported promising results (Cigaina, 2004; Favretti et al., 2004; Yao et al., 2005; Liu et al., 2006a). The most comprehensive study has used vagal nerve stimulation to provide a significant benefit for obesity via the Maestro Rechargeable system or VBLOC (Johannessen et al., 2017). A double-blinded randomized controlled study with 53 subjects receiving the therapy and 31 in a sham group has shown that vagal nerve stimulation resulted in a significantly greater weight loss. At 12 months, the percentage

TABLE 2 | Protocols used for gastric stimulation.

References	Species	Amplitude	Pulse Width	Frequency	On/Off Period
Bilgutay et al., 1963	Human	7–10 mA	10 ms	50 Hz	5 s/55 s
Moran and Nabseth, 1965	Human	10 mA	10 ms	50 Hz	5 s/55 s
Familoni et al., 1997b	Human	2 mA	0.3 ms	0.2 Hz	Not specified
De Luca et al., 2004	Human	10 mA	0.208 ms	40 Hz	2 s/3 s
Abell et al., 2002	Human	5 mA	0.330 ms	14 Hz	∼0.07 s/∼5 s
Angeli et al., 2016	Human	5–19.2 mA	0.33, 0.45 ms	14–130 Hz	0.1–4 s/1–17 s
Ducrotte et al., 2020	Human	5 mA	0.33 ms	14 Hz	0.1 s/5 s
Grundfest-Broniatowski et al., 1990	Dog	2–15 mA	2–50 ms	6, 20 Hz	Not specified
Familoni et al., 1997a	Dog	2 mA	0.3 ms	0.075–0.5 Hz	30 min on
Qin et al., 2007	Rat	6 mA	0.3, 3 ms	14, 40 Hz	0.1, 2 s/3, 5 s
Tang et al., 2006	Rat	6 mA	0.3, 3 ms	20, 40 Hz	0.1, 2 s/3, 4.9 s

excess weight loss was 33% for those that received the VBLOC therapy compared to 19% in the sham group (Morton et al., 2016). Despite promising outcomes from these stimulation and pacing approaches, further controlled studies are required to establish reliability.

MATHEMATICAL MODELS

As described in section "Gastric Stimulation and Pacing," a large variation of stimulation or pacing parameters are used and there is no consensus of parameters that result in the best functional outcomes. Given the range of different gastric electrical stimulation protocols and the inherent dynamic responses to stimulation, a stable platform is required to optimize the protocols in order to minimize the number of animal and human subject trials. An *in silico* Virtual Stomach model is an attractive strategy for systematically evaluating the electrophysiological and functional responses to stimulation protocols (Cheng et al., 2013; Du et al., 2013). Readers are encouraged to follow a previous review of the state-of-art in multi-scale modeling development of gastrointestinal electrophysiology (Corrias et al., 2013; Du et al., 2018). However, there has been relatively limited use of mathematical models to investigate the influence of external stimulation.

One of the earliest modeling studies that investigated the effects of gastric stimulation utilized a conoidal dipole model of whole-organ gastric slow wave activity, and four rings of stimulating electrodes (2 s bipolar trains of 50 Hz, 15 V) were capable of entraining contractions in the distal region of the stomach (Mintchev and Bowes, 1997). While the study assumed a relatively simple geometry of the stomach, the effects of the stimulation protocols were validated in canine subjects. The conoidal model was then refined to incorporate acetylcholine as the neurogenic pathway to drive mechanical response to stimulation (Rashev et al., 2002). The simulation results suggested that rectangular bipolar stimulating trains are potentially more effective in depolarization of smooth muscle cells because of the increased likelihood of matching externally facilitated cell depolarization with invoked release of acetylcholine (Rashev et al., 2002).

A series of automata or rule-based models were also developed to investigate the effects of pacing or slow wave abnormalities in dogs, pigs, and rats (Familoni et al., 2005; Du et al., 2009b; Lammers et al., 2011). One of the key features of the rule-based models was the ability to impose precise definitions of the relative and absolute refractory periods so the expected propagations and their responses to stimulation could be simulated quickly and the system can be adopted to model a closed-loop operation (Wang et al., 2020a). However, a limitation of this approach is the plasticity of the response of the individual automata, which means frequency dependent responses to stimulation, such as frequency restitution cannot be easily modeled (Wang et al., 2017).

Advances in computational power have enabled the development of biophysically based models that are able to more accurately represent the underlying physiology. These models have been used to investigate the slow wave propagation over detailed tissue block representations and the whole stomach (Corrias et al., 2013; Du et al., 2018). A recent study has included anatomically realistic representations of a human stomach and fiber architecture to investigate pacing parameters on slow wave entrainment (Sathar et al., 2015).

Vagal nerve stimulation has been shown to offer therapeutic benefit for modulating gastric function (see section "Electrical Conduction System of the Stomach") (Payne et al., 2019; Ward et al., 2020). However, mathematical models of the enteric nervous system have largely focused on interaction with the small intestine (Chambers et al., 2014; O'Sullivan-Greene et al., 2018). By modeling vagal afferent signaling of intestinal inflammation, O'Sullivan-Greene et al. (2018) showed that the information delivered to the central nervous system can be predicted and potentially be used in feedback control of stimulators. In order to parameterize and personalize vagal stimulation models various detailed physiological metrics may be required. One study has investigated the influence of neurostimulation strategies for enhancing small intestine motility patterns (Barth et al., 2017) and determined that stimulation at 0.5 Hz was effective in modulating the intrinsic pacemaker activity of ICC, increasing peristalsis, and reducing overall colonic transit time. Translating these methods to the stomach and incorporating it into patient-specific stimulator may allow for improved benefit.

FUTURE DIRECTIONS AND CONCLUSION

Significant advances have been made in our understanding of the mechanisms underlying gastric motility since the first electrical recordings reported in the 1920s (Alvarez, 1922c). Significant research has also been devoted to the application of electrical stimuli to modulate gastric function. However, gaps remain in our knowledge and clinical acceptance remains limited (Yin and Chen, 2008; Paskaranandavadivel et al., 2020).

Recently, significant research programs have been initiated by the NIH, DARPA and companies to address these short comings (Reardon, 2014; Waltz, 2016). The SPARC program initiated by the NIH[2] has a primary goal to transform our understanding of nerve-organ interactions to advance bioelectronic medicine in a number of organ systems. In the following sections, we discuss possible future directions for gastric stimulation and pacing, modeling efforts as well as other applications in the gastrointestinal tract. It is expected that techniques can be readily translated to other sections of the gastrointestinal tract and organ systems (Avci et al., 2020).

Future Directions for Stimulation and Pacing

Electrical stimulation and pacing techniques have been successfully applied to treat a number of conditions, with cardiac electrophysiology disorders being the most noted. A number of key challenges need to be addressed before electrical stimulation and pacing can be more widely applied clinically to treat gastrointestinal disorders. Most importantly, there have been limited randomized controlled trials that have carefully evaluated the efficacy of various approaches.

As discussed in section "Gastric Stimulation and Pacing," there remains a wide variety of stimulation and pacing protocols. In addition, there is variability in the electrode types and electrode placements used. Greater certainty in "optimal" pulse parameters and electrode placements would help to standardize methods. However, it is likely that parameters will need to be specifically personalized for individual subjects prior to implantation and improved selection of patients that will response to such treatments will help to improve overall response rates (Abell et al., 2011).

To achieve this, methods to sense and stimulate the stomach which do not require surgical intervention have also been investigated. Such approaches have already been applied to the Enterra Therapy, whereby a temporary stimulation phase can be trialed to tune parameters and evaluate outcomes prior to eventual stimulator implantation (Ayinala et al., 2005; Abell et al., 2011). Studies have also placed electrodes endoscopically to record the slow wave activity from the mucosal surface of the stomach for up to 5 days (Coleski and Hasler, 2004; Paskaranandavadivel et al., 2019). Attempts have also been made to develop miniature, wireless stimulators that can be deployed endoscopically on the mucosal surface, avoiding the need for surgical implantation (Deb et al., 2012; Kim et al., 2020). Trials have proven successful on pigs, and these techniques await clinical translation.

Entrainment mapping techniques described in section "High Resolution Slow Wave Mapping" show great promise for quantifying the efficacy of pacing techniques to alter slow wave patterns. However, to date, they have only been evaluated in short term studies in pigs (O'Grady et al., 2010b). More detailed evaluation in human subjects with functional motility disorders are urgently needed, as well as evaluation in conjunction with gastric function.

Future Directions for Modeling

Mathematical models provide an ideal technique to test hypotheses and aid in the interpretation of experimental recordings. Modeling techniques have been widely used in the cardiac field (Pullan et al., 2003; Henriquez, 2014). Over the years, detailed mathematical models of cardiac activity that bridges cellular, tissue and organ level activity have been developed (Trew et al., 2006). These models have been instrumental for guiding the development on new drugs and therapies (Brennan et al., 2009; Bear et al., 2018).

Mathematical models of gastric slow wave activity are also maturing rapidly (Cheng and Farrugia, 2013; Cheng et al., 2013; Du et al., 2013). However, the use of mathematical modeling to study other aspects of the stomach, such as neural regulation, biomechanics and luminal flow patterns is relatively new. A number of ICC and smooth muscle cell models have been developed to simulate normal and abnormal function (Lees-Green et al., 2011; Mah et al., 2020). Anatomically realistic models have been developed over which slow wave function can be simulated (Cheng et al., 2007, 2013). More recently, mathematical models have provided key insights into how intrinsic slow wave frequencies, tissue conductivities and external stimuli influence the initiation, maintenance and termination of gastric slow wave re-entry (Gizzi et al., 2010; Du et al., 2014). As discussed in section "Mathematical Models," further models incorporating enteric nervous system function are required, along with integration with existing models of slow wave activity.

The use of biomechanics to model stomach function is an emerging research area (Brandstaeter et al., 2019). This is in part due to the large deformations that the smooth muscle can undergo and the relatively complex shape and regional variation of the stomach. Most studies on the gastrointestinal tract have focused on modeling the biomechanics of the esophagus and small intestine, possibly due to their simpler uniform tubular structure (Gregersen and Kassab, 1996; Kou et al., 2017). A limited number of studies have investigated the passive and active mechanical properties of the stomach wall (Jia et al., 2015; Aydin et al., 2017; Tomalka et al., 2017). However, further studies are required to investigate the variation in different regions of the stomach and in different species (Bauer et al., 2020). The most comprehensive anatomically realistic stomach model incorporated electro-mechanical coupling, with explicit representation of ICC and smooth muscle cell activity (Klemm et al., 2020). Mechanic-electrical feedback-mechanism was also

[2]https://sparc.science/

included that takes into account the mechanical response due to stretch of the stomach wall.

Computational fluid dynamics (CFD) models provide a method to interpret and quantify the consequences of gastric motility patterns. Significant advances have been made since the initial two-dimensional models were developed (Pal et al., 2004, 2007). Subsequently, anatomically realistic three-dimensional models have been introduced and the influence of enhanced contraction patterns in the distal antrum were investigated (Ferrua and Singh, 2010; Berry et al., 2016). Most recent models have incorporated gastric emptying into the models (Harrison et al., 2018; Ishida et al., 2019). Despite significant advances in CFD models, a number of challenges remain (Brandstaeter et al., 2019). All models to date, have utilized idealized and simplified representations of the stomach anatomy and contraction patterns. More advanced models have used experimental slow wave data to derive contraction patterns, although these remain relatively simplified (Berry et al., 2016; Ishida et al., 2019). Most models assume a rigid wall that deforms in a pre-determined manner. In addition, to reduce the complexity of the stimulations, the contents of the stomach assume simple fluids and generally do not attempt to model the breakdown of solid particles. Only a few models have attempted to model gastric emptying, in part because the interaction between the gastric contractions and pylorus function is poorly understood (Imai et al., 2013; Yokrattanasak et al., 2016). Recent MRI studies have shown the ability to accurately capture dynamic data from the stomach (Bharucha et al., 2011; Lu et al., 2017; Menys et al., 2019). This data provides the opportunity to incorporate more realistic boundary conditions for CFD modeling and provide an integrated understanding of the complex interactions between gastric motility patterns, mixing and emptying (Hosseini et al., 2020).

CONCLUSION

Since initially being proposed in the 1960s, significant advances have been made towards the use of electrical therapies for modulating gastric function. However, widespread clinical usage remains limited when compared to the large number of therapies approved to treat cardiac electrophysiology disorders. A number of key challenges remain to be addressed. These include the development of methods to reliably quantify functional responses to electrical therapies, and the convergence of the range of pacing and stimulation protocols that are able to sustain long-term responses. The use of mathematical modeling techniques has the potential to help reduce the number of pulse parameters that need to be tested and optimized in animal and clinical trials. The customization of therapies to a specific individual may also help to provide improved long-term outcomes.

AUTHOR CONTRIBUTIONS

All authors drafted and edited the manuscript text. LC, NN, and NP prepared the figures and tables.

FUNDING

This work was funded, in part, by the Marsden Fund Council managed by Royal Society Te Apārangi, Health Research Council of New Zealand, the Medical Technologies Centre of Research Excellence (MedTech CoRE), the Riddet Institute Centre of Research Excellence, and the National Institutes of Health (NIH) (R01 HD088662, SPARC OT2OD030538).

REFERENCES

Abell, T., McCallum, R., Hocking, M., Koch, K., Abrahamsson, H., Leblanc, I., et al. (2003). Gastric electrical stimulation for medically refractory gastroparesis. *Gastroenterology* 125, 421–428. doi: 10.1016/s0016-5085(03)00878-3

Abell, T. L., Camilleri, M., Donohoe, K., Hasler, W. L., Lin, H. C., Maurer, A. H., et al. (2008). Consensus recommendations for gastric emptying scintigraphy: a joint report of the American neurogastroenterology and motility society and the society of nuclear medicine. *Am. J. Gastroenterol.* 103, 753–763. doi: 10.1111/j.1572-0241.2007.01636.x

Abell, T. L., Johnson, W. D., Kedar, A., Runnels, J. M., Thompson, J., Weeks, E. S., et al. (2011). A double-masked, randomized, placebo-controlled trial of temporary endoscopic mucosal gastric electrical stimulation for gastroparesis. *Gastrointest. Endosc.* 74, 496–503.e3. doi: 10.1016/j.gie.2011.05.022

Abell, T. L., and Malagelada, J. R. (1985). Glucagon-evoked gastric dysrhythmias in humans shown by an improved electrogastrographic technique. *Gastroenterology* 88, 1932–1940. doi: 10.1016/0016-5085(85)90022-8

Abell, T. L., Van Cutsem, E., Abrahamsson, H., Huizinga, J. D., Konturek, J. W., Galmiche, J. P., et al. (2002). Gastric electrical stimulation in intractable symptomatic gastroparesis. *Digestion* 66, 204–212. doi: 10.1159/000068359

Alighaleh, S., Cheng, L. K., Angeli, T. R., Amiri, M., Sathar, S., O'Grady, G., et al. (2019). A novel gastric pacing device to modulate slow waves and assessment by high-resolution mapping. *IEEE Trans. Biomed. Eng.* 66, 2823–2830. doi: 10.1109/TBME.2019.2896624

Alighaleh, S., Cheng, L. K., O'Grady, G., Angeli, T. R., Sathar, S., Bartlett, A., et al. (2018). High-resolution entrainment mapping for human gastric pacing: design and initial results. *Neurogastroenterol. Motil.* 31:423. doi: 10.1111/nmo.13423

Alvarez, W. C. (1922a). Action currents in stomach and intestine. *Am. J. Physiol. Content* 58, 476–493. doi: 10.1152/ajplegacy.1922.58.3.476

Alvarez, W. C. (1922b). New methods of studying gastric peristalsis. *JAMA* 79, 1281–1285. doi: 10.1001/jama.1922.02640160001001

Alvarez, W. C. (1922c). The electrogastrogram and what it shows. *JAMA* 78, 1116–1119. doi: 10.1001/jama.1922.02640680020008

Angeli, T. R., Cheng, L. K., Du, P., Wang, T. H.-H., Bernard, C. E., Vannucchi, M.-G., et al. (2015). Loss of interstitial cells of cajal and patterns of gastric dysrhythmia in patients with chronic unexplained nausea and vomiting. *Gastroenterology* 149, 56–66.e5. doi: 10.1053/j.gastro.2015.04.003

Angeli, T. R., Du, P., Midgley, D., Paskaranandavadivel, N., Sathar, S., Lahr, C., et al. (2016). Acute slow wave responses to high-frequency gastric electrical stimulation in patients with gastroparesis defined by high-resolution mapping. *Neuromodulation* 19, 864–871. doi: 10.1111/ner.12454

Angeli, T. R., Du, P., Paskaranandavadivel, N., Janssen, P. W. M., Beyder, A., Lentle, R. G., et al. (2013). The bioelectrical basis and validity of gastrointestinal extracellular slow wave recordings. *J. Physiol.* 591, 4567–4579. doi: 10.1113/jphysiol.2013.254292

Aquilina, O. (2006). A brief history of cardiac pacing. *Images Paediatr. Cardiol.* 8, 17–81.

Avci, R., Miller, K. J. W., Paskaranandavadivel, N., Bradshaw, L. A., Huckabee, M.-L., and Cheng, L. K. (2020). Bioelectrical signals for the diagnosis and

therapy of functional gastrointestinal disorders. *Appl. Sci.* 10:8102. doi: 10.3390/app10228102

Aydin, R. C., Brandstaeter, S., Braeu, F. A., Steigenberger, M., Marcus, R. P., Nikolaou, K., et al. (2017). Experimental characterization of the biaxial mechanical properties of porcine gastric tissue. *J. Mech. Behav. Biomed. Mater.* 74, 499–506. doi: 10.1016/j.jmbbm.2017.07.028

Ayinala, S., Batista, O., Goyal, A., Al-Juburi, A., Abidi, N., Familoni, B. O., et al. (2005). Temporary gastric electrical stimulation with orally or PEG-placed electrodes in patients with drug refractory gastroparesis. *Gastrointest. Endosc.* 61, 455–461.

Barth, B. B., Henriquez, C. S., Grill, W. M., and Shen, X. (2017). Electrical stimulation of gut motility guided by an in silico model. *J. Neural Eng.* 14:066010. doi: 10.1088/1741-2552/aa86c8

Bashashati, M., Moraveji, S., Torabi, A., Sarosiek, I., Davis, B. R., Diaz, J., et al. (2017). Pathological findings of the Antral and pyloric smooth muscle in patients with gastroparesis-like syndrome compared to Gastroparesis: similarities and differences. *Dig. Dis. Sci.* 62, 2828–2833. doi: 10.1007/s10620-017-4629-4

Bauer, M., Morales-Orcajo, E., Klemm, L., Seydewitz, R., Fiebach, V., Siebert, T., et al. (2020). Biomechanical and microstructural characterisation of the porcine stomach wall: location- and layer-dependent investigations. *Acta Biomater.* 102, 83–99. doi: 10.1016/j.actbio.2019.11.038

Bear, L. R., LeGrice, I. J., Sands, G. B., Lever, N. A., Loiselle, D. S., Paterson, D. J., et al. (2018). How accurate is inverse electrocardiographic mapping? a systematic in vivo evaluation. *Circ. Arrhythm. Electrophysiol.* 11:e006108. doi: 10.1161/CIRCEP.117.006108

Bellahsene, B. E., Lind, C. D., Schirmer, B. D., Updike, O. L., and McCallum, R. W. (1992). Acceleration of gastric emptying with electrical stimulation in a canine model of gastroparesis. *Am. J. Physiol. Gastrointest. Liver Physiol.* 262, 826. doi: 10.1152/ajpgi.1992.262.5.g826

Berry, R., Cheng, L. K., Du, P., Paskaranandavadivel, N., Angeli, T. R., Mayne, T., et al. (2017). Patterns of abnormal gastric pacemaking after sleeve gastrectomy defined by laparoscopic high-resolution electrical mapping. *Obes. Surg.* 27, 1929–1937. doi: 10.1007/s11695-017-2597-6

Berry, R., Miyagawa, T., Paskaranandavadivel, N., Du, P., Angeli, T. R., Trew, M. L., et al. (2016). Functional physiology of the human terminal antrum defined by high-resolution electrical mapping and computational modeling. *Am. J. Physiol. Gastrointest. Liver Physiol.* 311, G895–G902. doi: 10.1152/ajpgi.00255.2016

Bharucha, A. E., Manduca, A., Lake, D. S., Fidler, J., Edwards, P., Grimm, R. C., et al. (2011). Gastric motor disturbances in patients with idiopathic rapid gastric emptying. *Neurogastroenterol. Motil.* 23, 617–e252. doi: 10.1111/j.1365-2982.2011.01710.x

Bilgutay, A. M., Wingrove, R., Griffen, W. O., Bonnabeau, R. C., and Lillehei, C. W. (1963). Gastro-intestinal pacing: a new concept in the treatment of ileus. *Ann. Surg.* 158, 338–348. doi: 10.1097/00000658-196315830-00003

Bohdjalian, A., Prager, G., Aviv, R., Policker, S., Schindler, K., Kretschmer, S., et al. (2006). One-year experience with Tantalus: a new surgical approach to treat morbid obesity. *Obes. Surg.* 16, 627–634. doi: 10.1381/096089206776945101

Bonaz, B. (2018). Is-there a place for vagus nerve stimulation in inflammatory bowel diseases? *Bioelectron. Med.* 4:4. doi: 10.1186/s42234-018-0004-9

Bonaz, B., Picq, C., Sinniger, V., Mayol, J. F., and Clarençon, D. (2013). Vagus nerve stimulation: from epilepsy to the cholinergic anti-inflammatory pathway. *Neurogastroenterol. Motil.* 25, 208–221. doi: 10.1111/nmo.12076

Bortolotti, M., Bolondi, L., Santi, V., Sarti, P., Brunelli, F., and Barbara, L. (1995). Patterns of gastric emptying in dysmotility-like dyspepsia. *Scand. J. Gastroenterol.* 30, 408–410. doi: 10.3109/00365529509093299

Brandstaeter, S., Fuchs, S. L., Aydin, R. C., and Cyron, C. J. (2019). Mechanics of the stomach: a review of an emerging field of biomechanics. *GAMM Mitteilungen* 42:201900001.

Brennan, T., Fink, M., and Rodriguez, B. (2009). Multiscale modelling of drug-induced effects on cardiac electrophysiological activity. *Eur. J. Pharm. Sci.* 36, 62–77. doi: 10.1016/j.ejps.2008.09.013

Buist, M. L., Cheng, L. K., Sanders, K. M., and Pullan, A. J. (2006). Multiscale modelling of human gastric electric activity: can the electrogastrogram detect functional electrical uncoupling? *Exp. Physiol.* 91, 383–390. doi: 10.1113/expphysiol.2005.031021

Cajal, S. (1911). *Histologie du Système Nerveux de l'homme et des Vertébrés*. Paris: Maloine.

Camilleri, M., Parkman, H. P., Shafi, M. A., Abell, T. L., and Gerson, L. (2013). Clinical guideline: management of gastroparesis. *Am. J. Gastroenterol.* 108, 18–37. doi: 10.1038/ajg.2012.373

Chambers, J. D., Thomas, E. A., and Bornstein, J. C. (2014). Mathematical modelling of enteric neural motor patterns. *Clin. Exp. Pharmacol. Physiol.* 41, 155–164. doi: 10.1111/1440-1681.12209

Chen, J. D. Z., Qian, L., Ouyang, H., and Yin, J. (2003). Gastric electrical stimulation with short pulses reduces vomiting but not dysrhythmias in dogs. *Gastroenterology* 124, 401–409. doi: 10.1053/gast.2003.50048

Cheng, L. K. (2015). Slow wave conduction patterns in the stomach: from Waller's foundations to current challenges. *Acta Physiol.* 213, 384–393. doi: 10.1111/apha.12406

Cheng, L. K., Du, P., and O'Grady, G. (2013). Mapping and modeling gastrointestinal bioelectricity: from engineering bench to bedside. *Physiology* 28, 310–317. doi: 10.1152/physiol.00022.2013

Cheng, L. K., and Farrugia, G. (2013). *New Advances in Gastrointestinal Motility Research*. Berlin: Springer, doi: 10.1007/978-94-007-6561-0_1

Cheng, L. K., Komuro, R., Austin, T. M., Buist, M. L., and Pullan, A. J. (2007). Anatomically realistic multiscale models of normal and abnormal gastrointestinal electrical activity. *World J. Gastroenterol.* 13, 1378–1383. doi: 10.3748/wjg.v13.i9.1378

Chu, H., Lin, Z., Zhong, L., McCallum, R. W., and Hou, X. (2012). Treatment of high-frequency gastric electrical stimulation for gastroparesis. *J. Gastroenterol. Hepatol.* 27, 1017–1026. doi: 10.1111/j.1440-1746.2011.06999.x

Cigaina, V. (2004). Long-term follow-up of gastric stimulation for obesity: the Mestre 8-year experience. *Obes. Surg.* 14(Suppl. 1), S14–S22. doi: 10.1007/BF03342133

Cigaina, V., Saggioro, A., Rigo, V., Pinato, G., and Ischai, S. (1996). Long-term effects of gastric pacing to reduce feed intake in swine. *Obes. Surg.* 6, 250–253. doi: 10.1381/096089296765556854

Code, C. F., and Marlett, J. A. (1974). Canine tachygastria. *Mayo Clin. Proc.* 49, 325–332.

Coleski, R., and Hasler, W. L. (2004). Directed endoscopic mucosal mapping of normal and dysrhythmic gastric slow waves in healthy humans. *Neurogastroenterol. Motil.* 16, 557–565. doi: 10.1111/j.1365-2982.2004.00542.x

Corrias, A., Du, P., and Buist, M. L. (2013). "Modelling Tissue electrophysiology in the GI tract: past, present and future," in *New Advances in Gastrointestinal Motility Research*, eds L. K. Cheng, A. J. Pullan, and G. Farrugia (Cham: Springer), 167–195. doi: 10.1007/978-94-007-6561-0_10

Corvinus, F. M., Heinrich, S., Neumann, H., Hadzijusufovic, E., Babic, B., Lang, H., et al. (2018). Minimally-invasive temporary gastric stimulation: a pilot study to predict the outcome of electronic gastric stimulation with the Enterra^{TM} system. *Dig. Liver Dis.* 50, 1030–1034. doi: 10.1016/j.dld.2018.05.023

De Luca, M., Segato, G., Busetto, L., Favretti, F., Aigner, F., Weiss, H., et al. (2004). Progress in implantable gastric stimulation: summary of results of the European multi-center study. *Obes. Surg.* 14(Suppl. 1), S33–S39. doi: 10.1007/BF03342136

Deb, S., Tang, S.-J., Abell, T. L., Rao, S. M. N., Huang, W.-D., To, S. D. F., et al. (2012). An endoscopic wireless gastrostimulator (with video). *Gastrointest. Endosc.* 75, 411–415. doi: 10.1016/j.gie.2011.09.052

Delgado-Aros, S., Locke, G. R., Camilleri, M., Talley, N. J., Fett, S., Zinsmeister, A. R., et al. (2004). Obesity is associated with increased risk of gastrointestinal symptoms: a population-based study. *Am. J. Gastroenterol.* 99, 1801–1806. doi: 10.1111/j.1572-0241.2004.30887.x

Du, P., Calder, S., Angeli, T. R., Sathar, S., Paskaranandavadivel, N., O'Grady, G., et al. (2018). Progress in mathematical modeling of gastrointestinal slow wave abnormalities. *Front. Physiol.* 8:1136. doi: 10.3389/fphys.2017.01136

Du, P., O'Grady, G., Egbuji, J. U., Lammers, W. J., Budgett, D., Nielsen, P., et al. (2009a). High-resolution mapping of in vivo gastrointestinal slow wave activity using flexible printed circuit board electrodes: methodology and validation. *Ann. Biomed. Eng.* 37, 839–846. doi: 10.1007/s10439-009-9654-9

Du, P., O'Grady, G., Windsor, J. A., Cheng, L. K., and Pullan, A. J. (2009b). A tissue framework for simulating the effects of gastric electrical stimulation and in vivo validation. *IEEE Trans. Biomed. Eng.* 56, 2755–2761. doi: 10.1109/TBME.2009.2027690

Du, P., O'Grady, G., Gao, J., Sathar, S., and Cheng, L. K. (2013). Toward the virtual stomach: progress in multiscale modeling of gastric electrophysiology

and motility. *Wiley Interdiscip. Rev. Syst. Biol. Med.* 5, 481–493. doi: 10.1002/wsbm.1218

Du, P., Paskaranandavadivel, N., O'Grady, G., Tang, S.-J., and Cheng, L. K. (2014). A theoretical study of the initiation, maintenance and termination of gastric slow wave re-entry. *Math. Med. Biol.* 2014:dqu023.

Ducrotte, P., Coffin, B., Bonaz, B., Fontaine, S., Bruley Des Varannes, S., Zerbib, F., et al. (2020). Gastric electrical stimulation reduces refractory vomiting in a randomized crossover trial. *Gastroenterology* 158, 506–514.e2. doi: 10.1053/j.gastro.2019.10.018

Durrer, D., van Dam, R. T., Freud, G. E., Janse, M. J., Meijler, F. L., and Arzbaecher, R. C. (1970). Total excitation of the isolated human heart. *Circulation* 41, 899–912.

Eagon, J. C., and Kelly, K. A. (1993). Effects of gastric pacing on canine gastric motility and emptying. *Am. J. Physiol.* 265, G767–G774.

Egbuji, J. U., O'Grady, G., Du, P., Cheng, L. K., Lammers, W. J., Windsor, J. A., et al. (2010). Origin, propagation and regional characteristics of porcine gastric slow wave activity determined by high-resolution mapping. *Neurogastroenterol. Motil.* 22, e292–e300. doi: 10.1111/j.1365-2982.2010.01538.x

Elfvin, A., Göthberg, G., Lönroth, H., Saalman, R., and Abrahamsson, H. (2011). Temporary percutaneous and permanent gastric electrical stimulation in children younger than 3 years with chronic vomiting. *J. Pediatr. Surg.* 46, 655–661. doi: 10.1016/j.jpedsurg.2010.10.028

Enck, P., Azpiroz, F., Boeckxstaens, G., Elsenbruch, S., Feinle-Bisset, C., Holtmann, G., et al. (2017). Functional dyspepsia. *Nat. Rev. Dis. Prim.* 3:17081. doi: 10.1038/nrdp.2017.81

Familoni, B. O., Abell, T. L., Gan, Z., and Voeller, G. (2005). Driving gastric electrical activity with electrical stimulation. *Ann. Biomed. Eng.* 33, 356–364. doi: 10.1007/s10439-005-1738-6

Familoni, B. O., Abell, T. L., Nemoto, D., Voeller, G., and Johnson, B. (1997a). Efficacy of electrical stimulation at frequencies higher than basal rate in canine stomach. *Dig. Dis. Sci.* 42, 892–897. doi: 10.1023/a:1018804128695

Familoni, B. O., Abell, T. L., Voeller, G., Salem, A., and Gaber, O. (1997b). Electrical stimulation at a frequency higher than basal rate in human stomach. *Dig. Dis. Sci.* 42, 885–891. doi: 10.1023/a:1018852011857

Farrugia, G. (2008). Interstitial cells of Cajal in health and disease. *Neurogastroenterol. Motil.* 20(Suppl. 1), 54–63. doi: 10.1111/j.1365-2982.2008.01109.x

Favretti, F., De Luca, M., Segato, G., Busetto, L., Ceoloni, A., Magon, A., et al. (2004). Treatment of morbid obesity with the Transcend Implantable Gastric Stimulator (IGS): a prospective survey. *Obes. Surg.* 14, 666–670. doi: 10.1381/096089204323093462

Ferrua, M. J., and Singh, R. P. (2010). Modeling the fluid dynamics in a human stomach to gain insight of food digestion. *J. Food Sci.* 75, R151–R162. doi: 10.1111/j.1750-3841.2010.01748.x

Furness, J. B. (2012). The enteric nervous system and neurogastroenterology. *Nat. Rev. Gastroenterol. Hepatol.* 9, 286–294. doi: 10.1038/nrgastro.2012.32

Furness, J. B., Callaghan, B. P., Rivera, L. R., and Cho, H. J. (2014). The enteric nervous system and gastrointestinal innervation: integrated local and central control. *Adv. Exp. Med. Biol.* 817, 39–71. doi: 10.1007/978-1-4939-0897-4_3

Futagami, S., Yamawaki, H., Agawa, S., Higuchi, K., Ikeda, G., Noda, H., et al. (2018). New classification Rome IV functional dyspepsia and subtypes. *Transl. Gastroenterol. Hepatol.* 3:70. doi: 10.21037/tgh.2018.09.12

Gharibans, A. A., Coleman, T. P., Mousa, H., and Kunkel, D. C. (2019). Spatial Patterns from high-resolution electrogastrography correlate with severity of symptoms in patients with functional Dyspepsia and Gastroparesis. *Clin. Gastroenterol. Hepatol.* 17, 2668–2677. doi: 10.1016/j.cgh.2019.04.039

Gilja, O. H., Hausken, T., Wilhelmsen, I., and Berstad, A. (1996). Impaired accommodation of proximal stomach to a meal in functional dyspepsia. *Dig. Dis. Sci.* 41, 689–696. doi: 10.1007/BF02213124

Gizzi, A., Cherubini, C., Migliori, S., Alloni, R., Portuesi, R., and Filippi, S. (2010). On the electrical intestine turbulence induced by temperature changes. *Phys. Biol.* 7:16011. doi: 10.1088/1478-3975/7/1/016011

Green, T. (1872). On death from chloroform: its prevention by galvanism. *Br. Med. J.* 1, 551–553. doi: 10.1136/bmj.1.595.551

Gregersen, H., and Kassab, G. (1996). Biomechanics of the gastrointestinal tract. *Neurogastroenterol. Motil.* 8, 277–297. doi: 10.1111/j.1365-2982.1996.tb00267.x

Grover, M., Farrugia, G., Lurken, M. S., Bernard, C. E., Faussone-Pellegrini, M.-S., Smyrk, T. C., et al. (2011). Cellular changes in diabetic and idiopathic gastroparesis. *Gastroenterology* 140, 1575–1585.e8. doi: 10.1053/j.gastro.2011.01.046

Grundfest-Broniatowski, S., Davies, C. R., Olsen, E., Jacobs, G., Kasick, J., Chou, S. M., et al. (1990). Electrical control of gastric emptying in denervated and reinnervated canine stomach: a pilot study. *Artif. Organs* 14, 254–259. doi: 10.1111/j.1525-1594.1990.tb02966.x

Hales, C. M., Carroll, M. D., Fryar, C. D., and Ogden, C. L. (2020). *Prevalence of Obesity and Severe Obesity Among Adults: United States, 2017-2018. NCHS Data Brief, 1-8.* Available online at: https://www.cdc.gov/nchs/data/databriefs/db360-h.pdf (accessed December 23, 2020).

Harrison, S. M., Cleary, P. W., and Sinnott, M. D. (2018). Investigating mixing and emptying for aqueous liquid content from the stomach using a coupled biomechanical-SPH model. *Food Funct.* 9, 3202–3219. doi: 10.1039/c7fo01226h

Henriquez, C. S. (2014). A brief history of tissue models for cardiac electrophysiology. *IEEE Trans. Biomed. Eng.* 61, 1457–1465. doi: 10.1109/TBME.2014.2310515

Hinder, R. A., and Kelly, K. A. (1977). Human gastric pacesetter potential. Site of origin, spread, and response to gastric transection and proximal gastric vagotomy. *Am. J. Surg.* 133, 29–33.

Hirst, G. D. S., and Edwards, F. R. (2006). Electrical events underlying organized myogenic contractions of the guinea pig stomach. *J. Physiol.* 576, 659–665. doi: 10.1113/jphysiol.2006.116491

Hocking, M. P., Vogel, S. B., and Sninsky, C. A. (1992). Human gastric myoelectric activity and gastric emptying following gastric surgery and with pacing. *Gastroenterology* 103, 1811–1816.

Hosseini, S., Avci, R., Paskaranandavadivel, N., Palmada, N., Suresh, V., and Cheng, L. K. (2020). "A novel method for time-dependent numerical modeling of gastric motility directly from magnetic resonance imaging," in *Proceedings of the 42nd Annual International Conference of the IEEE Engineering in Medicine & Biology Society (EMBC)*, New York, NY, doi: 10.1109/EMBC44109.2020.9175607

Huizinga, J. D. (2017). The powerful advantages of extracellular electrical recording. *Nat. Rev. Gastroenterol. Hepatol.* 14, 372–372. doi: 10.1038/nrgastro.2017.16

Huizinga, J. D., and Lammers, W. J. (2009). Gut peristalsis is governed by a multitude of cooperating mechanisms. *Am. J. Physiol. Gastrointest. Liver Physiol.* 296, G1–G8. doi: 10.1152/ajpgi.90380.2008

Huizinga, J. D., Lammers, W. J. E. P., Mikkelsen, H. B., Zhu, Y., and Wang, X.-Y. (2010). Toward a concept of stretch coupling in smooth muscle: a thesis by Lars Thuneberg on contractile activity in neonatal interstitial cells of Cajal. *Anat. Rec.* 293, 1543–1552. doi: 10.1002/ar.21214

Huizinga, J. D., Thuneberg, L., Klüppel, M., Malysz, J., Mikkelsen, H. B., and Bernstein, A. (1995). W/kit gene required for interstitial cells of Cajal and for intestinal pacemaker activity. *Nature* 373, 347–349. doi: 10.1038/373347a0

Imai, Y., Kobayashi, I., Ishida, S., Ishikawa, T., Buist, M. L., and Yamaguchi, T. (2013). Antral recirculation in the stomach during gastric mixing. *Am. J. Physiol. Gastrointest. Liver Physiol.* 304, G536–G542. doi: 10.1152/ajpgi.00350.2012

Ishida, S., Miyagawa, T., O'Grady, G., Cheng, L. K., and Imai, Y. (2019). Quantification of gastric emptying caused by impaired coordination of pyloric closure with antral contraction: a simulation study. *J. R. Soc. Interf.* 16:20190266. doi: 10.1098/rsif.2019.0266

Iyer, S., Saunders, W. B., and Stemkowski, S. (2009). Economic burden of postoperative ileus associated with colectomy in the United States. *J. Manag. Care Pharm.* 15, 485–494. doi: 10.18553/jmcp.2009.15.6.485

Jia, Z. G., Li, W., and Zhou, Z. R. (2015). Mechanical characterization of stomach tissue under uniaxial tensile action. *J. Biomech.* 48, 651–658. doi: 10.1016/j.jbiomech.2014.12.048

Johannessen, H., Revesz, D., Kodama, Y., Cassie, N., Skibicka, K. P., Barrett, P., et al. (2017). Vagal blocking for obesity control: a possible mechanism-of-action. *Obes. Surg.* 27, 177–185. doi: 10.1007/s11695-016-2278-x

Karaki, H., and Weiss, G. B. (1984). Calcium channels in smooth muscle. *Gastroenterology* 87, 960–970.

Kelly, K. A., Code, C. F., and Elveback, L. R. (1969). Patterns of canine gastric electrical activity. *Am. J. Physiol.* 217, 461–470.

Kelly, K. A., and La Force, R. C. (1972). Pacing the canine stomach with electric stimulation. *Am. J. Physiol.* 222, 588–594. doi: 10.1152/ajplegacy.1972.222.3.588

Kim, S. H., Kim, H. B., Chun, H. J., Choi, H. S., Kim, E. S., Keum, B., et al. (2020). Minimally invasive gastric electrical stimulation using a newly developed wireless gastrostimulator: a pilot animal study. *J. Neurogastroenterol. Motil.* 26, 410–416. doi: 10.5056/jnm20063

Klemm, L., Seydewitz, R., Borsdorf, M., Siebert, T., and Böl, M. (2020). On a coupled electro-chemomechanical model of gastric smooth muscle contraction. *Acta Biomater.* 109, 163–181. doi: 10.1016/j.actbio.2020.04.007

Koch, K. L. (2011). The electrifying stomach. *Neurogastroenterol. Motil.* 23, 815–818. doi: 10.1111/j.1365-2982.2011.01756.x

Kou, W., Griffith, B. E., Pandolfino, J. E., Kahrilas, P. J., and Patankar, N. A. (2017). A continuum mechanics-based musculo-mechanical model for esophageal transport. *J. Comput. Phys.* 348, 433–459. doi: 10.1016/j.jcp.2017.07.025

Lammers, W. J., Al-Bloushi, H. M., Al-Eisaei, S. A., Al-Dhaheri, F. A., Stephen, B., John, R., et al. (2011). Slow wave propagation and plasticity of interstitial cells of Cajal in the small intestine of diabetic rats. *Exp. Physiol.* 96, 1039–1048. doi: 10.1113/expphysiol.2011.058941

Lammers, W. J., Al-Kais, A., Singh, S., Arafat, K., and El-Sharkawy, T. Y. (1993). Multielectrode mapping of slow-wave activity in the isolated rabbit duodenum. *J. Appl. Physiol.* 74, 1454–1461.

Lammers, W. J., Stephen, B., Adeghate, E., Ponery, S., and Pozzan, O. (1998). The slow wave does not propagate across the gastroduodenal junction in the isolated feline preparation. *Neurogastroenterol. Motil.* 10, 339–349.

Lammers, W. J., Ver Donck, L., Stephen, B., Smets, D., and Schuurkes, J. A. J. (2008). Focal activities and re-entrant propagations as mechanisms of gastric tachyarrhythmias. *Gastroenterology* 135, 1601–1611. doi: 10.1053/j.gastro.2008.07.020

Lammers, W. J. E. P., Ver Donck, L., Stephen, B., Smets, D., and Schuurkes, J. A. J. (2009). Origin and propagation of the slow wave in the canine stomach: the outlines of a gastric conduction system. *Am. J. Physiol. Gastrointest. Liver Physiol.* 296, G1200–G1210. doi: 10.1152/ajpgi.90581.2008

Lee, H.-T., Hennig, G. W., Fleming, N. W., Keef, K. D., Spencer, N. J., Ward, S. M., et al. (2007). The mechanism and spread of pacemaker activity through myenteric interstitial cells of Cajal in human small intestine. *Gastroenterology* 132, 1852–1865. doi: 10.1053/j.gastro.2007.02.049

Lees-Green, R., Du, P., O'Grady, G., Beyder, A., Farrugia, G., and Pullan, A. J. (2011). Biophysically based modeling of the interstitial cells of cajal: current status and future perspectives. *Front. Physiol.* 2:29. doi: 10.3389/fphys.2011.00029

Lin, Z., Sarosiek, I., Forster, J., Ross, R. A., Chen, J. D. Z., and McCallum, R. W. (2011). Two-channel gastric pacing in patients with diabetic gastroparesis. *Neurogastroenterol. Motil.* 23, 912–e396. doi: 10.1111/j.1365-2982.2011.01754.x

Lin, Z. Y., McCallum, R. W., Schirmer, B. D., and Chen, J. D. (1998). Effects of pacing parameters on entrainment of gastric slow waves in patients with gastroparesis. *Am. J. Physiol.* 274, G186–G191.

Liu, J., Hou, X., Song, G., Cha, H., Yang, B., and Chen, J. D. Z. (2006a). Gastric electrical stimulation using endoscopically placed mucosal electrodes reduces food intake in humans. *Am. J. Gastroenterol.* 101, 798–803. doi: 10.1111/j.1572-0241.2006.00493.x

Liu, J., Qiao, X., and Chen, J. D. Z. (2006b). Therapeutic potentials of a novel method of dual-pulse gastric electrical stimulation for gastric dysrhythmia and symptoms of nausea and vomiting. *Am. J. Surg.* 191, 255–261. doi: 10.1016/j.amjsurg.2005.11.005

Liu, J., Qiao, X., Micci, M.-A., Pasricha, P. J., and Chen, J. D. Z. (2004). Improvement of gastric motility with gastric electrical stimulation in STZ-induced diabetic rats. *Digestion* 70, 159–166. doi: 10.1159/000081516

Liu, L. W., Thuneberg, L., and Huizinga, J. D. (1994). Selective lesioning of interstitial cells of Cajal by methylene blue and light leads to loss of slow waves. *Am. J. Physiol.* 266, G485–G496.

Lu, K.-H., Cao, J., Oleson, S., Ward, M. P., Phillips, R. J., Powley, T. L., et al. (2018). Vagus nerve stimulation promotes gastric emptying by increasing pyloric opening measured with magnetic resonance imaging. *Neurogastroenterol. Motil.* 30:e13380. doi: 10.1111/nmo.13380

Lu, K.-H., Cao, J., Oleson, S. T., Powley, T. L., and Liu, Z. (2017). Contrast-enhanced magnetic resonance imaging of gastric emptying and motility in rats. *IEEE Trans. Biomed. Eng.* 64, 2546–2554. doi: 10.1109/TBME.2017.2737559

Lu, K.-H., Cao, J., Phillips, R., Powley, T. L., and Liu, Z. (2020). Acute effects of vagus nerve stimulation parameters on gastric motility assessed with magnetic resonance imaging. *Neurogastroenterol. Motil.* 32:e13853. doi: 10.1111/nmo.13853

Lu, P. L., Teich, S., Di Lorenzo, C., Lorenzo, C. D., Skaggs, B., Alhajj, M., et al. (2013). Improvement of quality of life and symptoms after gastric electrical stimulation in children with functional dyspepsia. *Neurogastroenterol. Motil.* 25, 567–e456. doi: 10.1111/nmo.12104

Mah, S. A., Avci, R., Cheng, L. K., and Du, P. (2020). Current applications of mathematical models of the interstitial cells of Cajal in the gastrointestinal tract. *Wiley Interdiscip. Rev. Syst. Biol. Med.* 13, e1507. doi: 10.1002/wsbm.1507

McCallum, R. W., De, Z., Chen, J., Lin, Z., Schirmer, B. D., Williams, R. D., et al. (1998). Gastric pacing improves emptying and symptoms in patients with gastroparesis. *Gastroenterology* 114, 456–461. doi: 10.1016/S0016-5085(98)70528-1

McCallum, R. W., Sarosiek, I., Parkman, H. P., Snape, W., Brody, F., Wo, J., et al. (2013). Gastric electrical stimulation with Enterra therapy improves symptoms of idiopathic gastroparesis. *Neurogastroenterol. Motil.* 25, 815–e636. doi: 10.1111/nmo.12185

McCallum, R. W., Snape, W., Brody, F., Wo, J., Parkman, H. P., and Nowak, T. (2010). Gastric electrical stimulation with Enterra therapy improves symptoms from diabetic gastroparesis in a prospective study. *Clin. Gastroenterol. Hepatol.* 8, 947–954. doi: 10.1016/j.cgh.2010.05.020

McWilliam, J. A. (1889). Electrical stimulation of the heart in man. *Br. Med. J.* 1, 348–350. doi: 10.1136/bmj.1.1468.348

Menys, A., Hoad, C., Spiller, R., Scott, S. M., Atkinson, D., Marciani, L., et al. (2019). Spatio-temporal motility MRI analysis of the stomach and colon. *Neurogastroenterol. Motil.* 31:e13557. doi: 10.1111/nmo.13557

Miedema, B. W., Sarr, M. G., and Kelly, K. A. (1992). Pacing the human stomach. *Surgery* 111, 143–150.

Mintchev, M., and Bowes, K. (1997). Computer model of gastric electrical stimulation. *Ann. Biomed. Eng.* 25, 726–730. doi: 10.1007/bf02684849

Mintchev, M. P., Sanmiguel, C. P., Amaris, M., and Bowes, K. L. (2000). Microprocessor-controlled movement of solid gastric content using sequential neural electrical stimulation. *Gastroenterology* 118, 258–263. doi: 10.1016/s0016-5085(00)70207-1

Mond, H. G., Wickham, G. G., and Sloman, J. G. (2012). The Australian history of cardiac pacing: memories from a bygone era. *Hear. Lung Circ.* 21, 311–319. doi: 10.1016/j.hlc.2011.09.004

Moran, J. M., and Nabseth, D. C. (1965). Electrical stimulation of the bowel. a controlled clinical study. *Arch. Surg.* 91, 449–451. doi: 10.1001/archsurg.1965.01320150079011

Morton, J. M., Shah, S. N., Wolfe, B. M., Apovian, C. M., Miller, C. J., Tweden, K. S., et al. (2016). Effect of vagal nerve blockade on moderate obesity with an obesity-related comorbid condition: the ReCharge study. *Obes. Surg.* 26, 983–989. doi: 10.1007/s11695-016-2143-y

O'Grady, G., Angeli, T. R., Du, P., Lahr, C., Lammers, W. J., Windsor, J. A., et al. (2012a). Abnormal initiation and conduction of slow-wave activity in gastroparesis, defined by high-resolution electrical mapping. *Gastroenterology* 143, 589–598.e1-3. doi: 10.1053/j.gastro.2012.05.036

O'Grady, G., Du, P., Paskaranandavadivel, N., Angeli, T. R., Lammers, W. J., Asirvatham, S. J., et al. (2012b). Rapid high-amplitude circumferential slow wave propagation during normal gastric pacemaking and dysrhythmias. *Neurogastroenterol. Motil.* 24, e299–e312. doi: 10.1111/j.1365-2982.2012.01932.x

O'Grady, G., Angeli, T. R., Paskaranandavadivel, N., Erickson, J. C., Wells, C. I., Gharibans, A. A., et al. (2019). Methods for high-resolution electrical mapping in the gastrointestinal tract. *IEEE Rev. Biomed. Eng.* 12, 287–302. doi: 10.1109/RBME.2018.2867555

O'Grady, G., Du, P., Cheng, L. K., Egbuji, J. U., Lammers, W. J., Windsor, J. A., et al. (2010a). Origin and propagation of human gastric slow-wave activity defined by high-resolution mapping. *Am. J. Physiol. Gastrointest. Liver Physiol.* 299, G585–G592. doi: 10.1152/ajpgi.00125.2010

O'Grady, G., Du, P., Lammers, W. J., Egbuji, J. U., Mithraratne, P., Chen, J. D. Z., et al. (2010b). High-resolution entrainment mapping of gastric pacing: a new analytical tool. *Am. J. Physiol. Gastrointest. Liver Physiol.* 298, G314–G321. doi: 10.1152/ajpgi.00389.2009

O'Grady, G., Egbuji, J. U., Du, P., Cheng, L. K., Pullan, A. J., and Windsor, J. A. (2009). High-frequency gastric electrical stimulation for the treatment

of gastroparesis: a meta-analysis. *World J. Surg.* 33, 1693–1701. doi: 10.1007/s00268-009-0096-1

O'Grady, G., Egbuji, J. U., Du, P., Lammers, W. J., Cheng, L. K., Windsor, J. A., et al. (2011). High-resolution spatial analysis of slow wave initiation and conduction in porcine gastric dysrhythmia. *Neurogastroenterol. Motil.* 23, e345–e355. doi: 10.1111/j.1365-2982.2011.01739.x

O'Grady, G., Wang, T. H.-H., Du, P., Angeli, T. R., Lammers, W. J., and Cheng, L. K. (2014). Recent progress in gastric dysrhythmia: pathophysiology, clinical significance and future horizons. *Clin. Exp. Pharmacol. Physiol.* 41, 854–862. doi: 10.1111/1440-1681.12288

O'Sullivan-Greene, E., Kameneva, T., Trevaks, D., Shafton, A., Payne, S. C., McAllen, R., et al. (2018). Modeling experimental recordings of vagal afferent signaling of intestinal inflammation for neuromodulation. *J. Neural Eng.* 15:aad96d.

Pagani, F. D., Norman, W. P., and Gillis, R. A. (1988). Medullary parasympathetic projections innervate specific sites in the feline stomach. *Gastroenterology* 95, 277–288. doi: 10.1016/0016-5085(88)90481-7

Pal, A., Brasseur, J. G., and Abrahamsson, B. (2007). A stomach road or "Magenstrasse" for gastric emptying. *J. Biomech.* 40, 1202–1210. doi: 10.1016/j.jbiomech.2006.06.006

Pal, A., Indireshkumar, K., Schwizer, W., Abrahamsson, B., Fried, M., and Brasseur, J. G. (2004). Gastric flow and mixing studied using computer simulation. *Proc. Biol. Sci.* 271, 2587–2594. doi: 10.1098/rspb.2004.2886

Parkman, H. P., Hasler, W. L., Barnett, J. L., and Eaker, E. Y. (2003). Electrogastrography: a document prepared by the gastric section of the American motility society clinical gi motility testing task force. *Neurogastroenterol. Motil.* 15, 89–102.

Paskaranandavadivel, N., Angeli, T. R., Manson, T., Stocker, A., McElmurray, L., O'Grady, G., et al. (2019). Multi-day, multi-sensor ambulatory monitoring of gastric electrical activity. *Physiol. Meas.* 40:025011. doi: 10.1088/1361-6579/ab0668

Paskaranandavadivel, N., Avci, R., Nagahawatte, N., Farajidavar, A., and Cheng, L. K. (2020). ""Electroceutical approaches for Gastroparesis," in *Obesity and Diabetes*, eds J. Faintuch and S. Faintuch (Cham: Springer International Publishing), 967–982. doi: 10.1007/978-3-030-53370-0_72

Pasricha, P. J., Colvin, R., Yates, K. P., Hasler, W. L., Abell, T. L., Unalp-Arida, A., et al. (2011). Characteristics of patients with chronic unexplained nausea and vomiting and normal gastric emptying. *Clin. Gastroenterol. Hepatol.* 9, 567–576.e1-4. doi: 10.1016/j.cgh.2011.03.003

Paulus, G. F., van Avesaat, M., van Rijn, S., Alleleyn, A. M. E., Swain, J. M., Abell, T. L., et al. (2020). Multicenter, Phase 1, open prospective trial of gastric electrical stimulation for the treatment of obesity: first-in-human results with a novel implantable system. *Obes. Surg.* 30, 1952–1960. doi: 10.1007/s11695-020-04422-6

Payne, S. C., Furness, J. B., and Stebbing, M. J. (2019). Bioelectric neuromodulation for gastrointestinal disorders: effectiveness and mechanisms. *Nat. Rev. Gastroenterol. Hepatol.* 16, 89–105. doi: 10.1038/s41575-018-0078-6

Phillips, L. K., Rayner, C. K., Jones, K. L., and Horowitz, M. (2006). An update on autonomic neuropathy affecting the gastrointestinal tract. *Curr. Diab. Rep.* 6, 417–423. doi: 10.1007/s11892-006-0073-0

Piccolino, M. (1997). Luigi Galvani and animal electricity: two centuries after the foundation of electrophysiology. *Trends Neurosci.* 20, 443–448.

Powley, T. L., Jaffey, D. M., McAdams, J., Baronowsky, E. A., Black, D., Chesney, L., et al. (2019). Vagal innervation of the stomach reassessed: brain-gut connectome uses smart terminals. *Ann. N. Y. Acad. Sci.* 1454, 14–30. doi: 10.1111/nyas.14138

Pullan, A. J., Buist, M. L., Sands, G. B., Cheng, L. K., and Smith, N. P. (2003). Cardiac electrical activity-from heart to body surface and back again. *J. Electrocardiol.* 36, 63–67. doi: 10.1016/j.jelectrocard.2003.09.016

Qin, C., Chen, J. D. Z., Zhang, J., and Foreman, R. D. (2007). Modulatory effects and afferent pathways of gastric electrical stimulation on rat thoracic spinal neurons receiving input from the stomach. *Neurosci. Res.* 57, 29–39. doi: 10.1016/j.neures.2006.09.003

Rashev, P. Z., Bowes, K. L., and Mintchev, M. P. (2002). Three-dimensional object-oriented modeling of the stomach for the purpose of microprocessor-controlled functional stimulation. *IEEE Trans. Inf. Technol. Biomed.* 6, 296–309. doi: 10.1109/TITB.2002.806095

Reardon, S. (2014). Electroceuticals spark interest. *Nature* 511:18. doi: 10.1038/511018a

Rhee, P.-L., Lee, J. Y., Son, H. J., Kim, J. J., Rhee, J. C., Kim, S., et al. (2011). Analysis of pacemaker activity in the human stomach. *J. Physiol.* 589, 6105–6118. doi: 10.1113/jphysiol.2011.217497

Sarna, S. K. (2013). The gold standard for interpretation of slow wave frequency in in vitro and in vivo recordings by extracellular electrodes. *J. Physiol.* 591, 4373–4374. doi: 10.1113/jphysiol.2013.260976

Sarna, S. K., Bowes, K. L., and Daniel, E. E. (1976). Gastric pacemakers. *Gastroenterology* 70, 226–231. doi: 10.1016/S0016-5085(76)80014-5

Sarna, S. K., and Daniel, E. E. (1973). Electrical stimulation of gastric electrical control activity. *Am. J. Physiol.* 225, 125–131. doi: 10.1152/ajplegacy.1973.225.1.125

Sarna, S. K., Daniel, E. E., and Kingma, Y. J. (1972). Effects of partial cuts on gastric electrical control activity and its computer model. *Am. J. Physiol.* 223, 332–340. doi: 10.1152/ajplegacy.1972.223.2.332

Sathar, S., Trew, M. L., O'Grady, G., and Cheng, L. K. (2015). A multiscale tridomain model for simulating bioelectric gastric pacing. *IEEE Trans. Biomed. Eng.* 62, 2685–2692. doi: 10.1109/TBME.2015.2444384

Sha, W., Pasricha, P. J., and Chen, J. D. Z. (2009). Rhythmic and spatial abnormalities of gastric slow waves in patients with functional dyspepsia. *J. Clin. Gastroenterol.* 43, 123–129. doi: 10.1097/MCG.0b013e318157187a

Shikora, S. A., Bergenstal, R., Bessler, M., Brody, F., Foster, G., Frank, A., et al. (2009). Implantable gastric stimulation for the treatment of clinically severe obesity: results of the SHAPE trial. *Surg. Obes. Relat. Dis.* 5, 31–37. doi: 10.1016/j.soard.2008.09.012

Song, G., Hou, X., Yang, B., Liu, J., Qian, W., and Chen, J. D. Z. (2005). Two-channel gastric electrical stimulation accelerates delayed gastric emptying induced by vasopressin. *Dig. Dis. Sci.* 50, 662–668. doi: 10.1007/s10620-005-2553-5

Song, G.-Q., Zhu, H., Lei, Y., Yuan, C., Starkebaum, W., Yin, J., et al. (2015). Gastric electrical stimulation optimized to inhibit gastric motility reduces food intake in dogs. *Obes. Surg.* 25, 1047–1055. doi: 10.1007/s11695-014-1491-8

Sowers, J. R. (2003). Obesity as a cardiovascular risk factor. *Am. J. Med.* 115, 37–41. doi: 10.1016/j.amjmed.2003.08.012

Sukasem, A., Cakmak, Y. O., Khwaounjoo, P., Gharibans, A., and Du, P. (2020). The effects of low-and high-frequency non-invasive transcutaneous auricular vagal nerve stimulation (taVNS) on gastric slow waves evaluated using in vivo high-resolution mapping in porcine. *Neurogastroenterol. Motil.* 32:e13852. doi: 10.1111/nmo.13852

Syed, A. R., Wolfe, M. M., and Calles-Escandon, J. (2020). Epidemiology and diagnosis of Gastroparesis in the United States: a population-based study. *J. Clin. Gastroenterol.* 54, 50–54. doi: 10.1097/MCG.0000000000001231

Tang, M., Zhang, J., and Chen, J. D. Z. (2006). Central mechanisms of gastric electrical stimulation involving neurons in the paraventricular nucleus of the hypothalamus in rats. *Obes. Surg.* 16, 344–352. doi: 10.1381/096089206776116372

Thuneberg, L. (1982). Interstitial cells of Cajal: intestinal pacemaker cells? *Adv. Anat. Embryol. Cell Biol.* 71, 1–130.

Tomalka, A., Borsdorf, M., Böl, M., and Siebert, T. (2017). Porcine stomach smooth muscle force depends on history-effects. *Front. Physiol.* 8:802. doi: 10.3389/fphys.2017.00802

Torihashi, S., Fujimoto, T., Trost, C., and Nakayama, S. (2002). Calcium oscillation linked to pacemaking of interstitial cells of Cajal: requirement of calcium influx and localization of TRP4 in caveolae. *J. Biol. Chem.* 277, 19191–19197. doi: 10.1074/jbc.M201728200

Travagli, R. A., and Anselmi, L. (2016). Vagal neurocircuitry and its influence on gastric motility. *Nat. Rev. Gastroenterol. Hepatol.* 13, 389–401. doi: 10.1038/nrgastro.2016.76

Trew, M. L., Caldwell, B. J., Sands, G. B., Hooks, D. A., Tai, D. C.-S., Austin, T. M., et al. (2006). Cardiac electrophysiology and tissue structure: bridging the scale gap with a joint measurement and modelling paradigm. *Exp. Physiol.* 91, 355–370. doi: 10.1113/expphysiol.2005.031054

Turner, M., Jannah, N., Kahan, S., Gallagher, C., and Dietz, W. (2018). Current knowledge of obesity treatment guidelines by health care professionals. *Obesity* 26, 665–671. doi: 10.1002/oby.22142

Vather, R., Trivedi, S., and Bissett, I. (2013). Defining postoperative ileus: results of a systematic review and global survey. *J. Gastrointest. Surg.* 17, 962–972. doi: 10.1007/s11605-013-2148-y

Ver Donck, L., Lammers, W. J., Moreaux, B., Smets, D., Voeten, J., Vekemans, J., et al. (2006). Mapping slow waves and spikes in chronically instrumented conscious dogs: implantation techniques and recordings. *Med. Biol. Eng. Comput.* 44, 170–178. doi: 10.1007/s11517-005-0018-9

Vinik, A. I., Maser, R. E., Mitchell, B. D., and Freeman, R. (2003). Diabetic autonomic neuropathy. *Diabetes Care* 26, 1553–1579. doi: 10.2337/diacare.26.5.1553

Waltz, E. (2016). A spark at the periphery. *Nat. Biotechnol.* 34, 904–908. doi: 10.1038/nbt.3667

Wang, L., Malik, A., Roop, P. S., Cheng, L. K., Paskaranandavadivel, N., and Ai, W. (2020a). A novel approach for model-based design of gastric pacemakers. *Comput. Biol. Med.* 116:103576. doi: 10.1016/j.compbiomed.2019.103576

Wang, L., Malik, A., Roop, P. S., Cheng, L. K., Paskaranandavadivel, N., and Ai, W. (2020b). "Design of a closed-loop gastric pacemaker for modulating dysrhythmic conduction patterns via extracellular potentials," in *Proceedings of the 42nd Annual International Conference of the IEEE Engineering in Medicine & Biology Society (EMBC)*, Piscataway, NJ.

Wang, R., Abukhalaf, Z., Javan-Khoshkholgh, A., Wang, T. H.-H., Sathar, S., Du, P., et al. (2018). A miniature configurable wireless system for recording gastric electrophysiological activity and delivering high-energy electrical stimulation. *IEEE J. Emerg. Sel. Top Circ. Syst.* 8, 221–229. doi: 10.1109/JETCAS.2018.2812105

Wang, T. H.-H., Du, P., Angeli, T. R., Paskaranandavadivel, N., Erickson, J. C., Abell, T. L., et al. (2017). Relationships between gastric slow wave frequency, velocity, and extracellular amplitude studied by a joint experimental-theoretical approach. *Neurogastroenterol. Motil.* 30:e13152. doi: 10.1111/nmo.13152

Wang, Y. R., Fisher, R. S., and Parkman, H. P. (2008). Gastroparesis-related hospitalizations in the United States: trends, characteristics, and outcomes, 1995-2004. *Am. J. Gastroenterol.* 103, 313–322. doi: 10.1111/j.1572-0241.2007.01658.x

Ward, M. P., Gupta, A., Wo, J. M., Rajwa, B., Furness, J. B., Powley, T. L., et al. (2020). An emerging method to noninvasively measure and identify vagal response markers to enable bioelectronic control of gastroparesis symptoms with gastric electrical stimulation. *J. Neurosci. Methods* 336:108631. doi: 10.1016/j.jneumeth.2020.108631

Xu, J., Ross, R. A., McCallum, R. W., and Chen, J. D. Z. (2008). Two-channel gastric pacing with a novel implantable gastric pacemaker accelerates glucagon-induced delayed gastric emptying in dogs. *Am. J. Surg.* 195, 122–129. doi: 10.1016/j.amjsurg.2007.04.007

Xue, S., Valdez, D. T., Tremblay, L., Collman, P. I., and Diamant, N. E. (1995). Electrical slow wave activity of the cat stomach: its frequency gradient and the effect of indomethacin. *Neurogastroenterol. Motil.* 7, 157–167. doi: 10.1111/j.1365-2982.1995.tb00221.x

Yao, S., Ke, M., Wang, Z., Xu, D., Zhang, Y., and Chen, J. D. Z. (2005). Retrograde gastric pacing reduces food intake and delays gastric emptying in humans: a potential therapy for obesity? *Dig. Dis. Sci.* 50, 1569–1575. doi: 10.1007/s10620-005-2899-8

Yin, J., and Chen, J. D. Z. (2008). Implantable gastric electrical stimulation: ready for prime time? *Gastroenterology* 134, 665–667. doi: 10.1053/j.gastro.2008.01.068

Yin, J., Hou, X., and Chen, J. D. Z. (2006). Roles of interstitial cells of Cajal in intestinal transit and exogenous electrical pacing. *Dig. Dis. Sci.* 51, 1818–1823. doi: 10.1007/s10620-006-9313-z

Yokrattanasak, J., De Gaetano, A., Panunzi, S., Satiracoo, P., Lawton, W. M., and Lenbury, Y. (2016). A simple, realistic stochastic model of gastric emptying. *PLoS One* 11:e0153297. doi: 10.1371/journal.pone.0153297

You, C. H., and Chey, W. Y. (1984). Study of Electromechanical Activity of the Stomach in Humans and in Dogs With Particular Attention to Tachygastria. *Gastroenterology* 86, 1460–1468. doi: 10.1016/S0016-5085(84)80159-6

Young, A. A., and Edwards, G. L. (2005). "Effects of diabetes mellitus on gastrointestinal function in animal models," in *Gastrointestinal Function in Diabetes Mellitus*, eds M. Horowitz and M. Samsom (Chichester: John Wiley & Sons, Ltd), 29–95. doi: 10.1002/0470013877.ch2

Zhang, J., and Chen, J. D. Z. (2006). Systematic review: applications and future of gastric electrical stimulation. *Aliment. Pharmacol. Ther.* 24, 991–1002. doi: 10.1111/j.1365-2036.2006.03087.x

Zhu, H., and Chen, J. D. Z. (2005). Implantable gastric stimulation inhibits gastric motility via sympathetic pathway in dogs. *Obes. Surg.* 15, 95–100. doi: 10.1381/0960892052993549

Zhu, H., Sallam, H., Chen, D. D., and Chen, J. D. Z. (2007). Therapeutic potential of synchronized gastric electrical stimulation for gastroparesis: enhanced gastric motility in dogs. *AJP Regul. Integr. Comp. Physiol.* 293, R1875–R1881. doi: 10.1152/ajpregu.00821.2006

Zhu, Y., Xu, F., Lu, D., Rong, P., Cheng, J., Li, M., et al. (2021). Transcutaneous auricular vagal nerve stimulation improves functional dyspepsia by enhancing vagal efferent activity. *Am. J. Physiol. Gastrointest. Liver Physiol.* (in press). doi: 10.1152/ajpgi.00426.2020

Conflict of Interest: LC, PD, and NP hold intellectual property/patent applications in the field of mapping gastrointestinal electrophysiology.

The remaining authors declare that the research was conducted in the absence of any commercial or financial relationships that could be construed as a potential conflict of interest.

The handling editor declared a past co-authorship with one of the authors PD.

frontiers in Neuroscience

ORIGINAL RESEARCH
published: 02 July 2021
doi: 10.3389/fnins.2021.645393

Neuro-Immune Modulation Effects of Sacral Nerve Stimulation for Visceral Hypersensitivity in Rats

Xue Jin[1†], Payam Gharibani[2†], Jieyun Yin[1] and Jiande D. Z. Chen[1]*

[1] Division of Gastroenterology and Hepatology, Department of Medicine, Johns Hopkins University School of Medicine, Baltimore, MD, United States, [2] Division of Neuroimmunology, Department of Neurology, Johns Hopkins University School of Medicine, Baltimore, MD, United States

Background: Visceral hypersensitivity (VH) is one of the underlying pathophysiologies of irritable bowel syndrome. Mast cell overactivation has been found to be one of the main causes of VH. We investigated the effects and mechanisms of actions of sacral nerve stimulation (SNS) on visceral pain in a rodent model of VH.

Methods: The VH was established by an intrarectal infusion of AA in 10-day-old pups. Rats were chronically implanted with electrodes for SNS and recording electromyogram (EMG) and electrocardiogram. The acute study was performed in 2-randomized sessions with SNS (14 Hz, 330 μs, 40% motor threshold or MT, 30 min) or sham-SNS. Later on, rats were randomized into SNS/sham-SNS groups and a chronic study was performed with 2 h-daily SNS or sham-SNS for 21 days. Visceromotor reflexes were assessed by abdominal EMG and withdrawal reflex (AWR). Colon tissues were collected to study colonic acetylcholine (ACh), the enteric neurons (ChAT, nNOS, and PGP9.5), mast cells activity [Tryptase, prostaglandins E2 (PGE2), and cyclooxygenases-2 (COX2)] and pain markers [nerve growth factor (NGF) and Sub-P].

Key Results: Sacral nerve stimulation significantly improved visceromotor reflexes assessed by the EMG and AWR, compared with sham-SNS. SNS normalized the protein expressions of ChAT and nNOS and regulated mast cells activity by downregulating Tryptase, COX2, and PGE2. Neonatal AA administration upregulated NGF and Sub-P; chronic SNS significantly decreased these pain biomarkers. Concurrently, chronic SNS increased ACh in colon tissues and vagal efferent activity.

Conclusions: Sacral nerve stimulation reduces VH in rats and this ameliorating effect might be attributed to the suppression of mast cell overactivation in the colon tissue via the modulation of autonomic nervous system functions.

Keywords: sacral nerve stimulation, visceral hypersensitivity, enteric neurons, mast cells, autonomic functions

OPEN ACCESS

Edited by:
Luming Li,
Tsinghua University, China

Reviewed by:
Guang-Yin Xu,
Soochow University, China
Richard J. Traub,
University of Maryland, Baltimore, United States
Luke Grundy,
Flinders University, Australia

****Correspondence:***
Jiande D. Z. Chen
cjiande@umich.edu

† These authors have contributed equally to this work and share first authorship

Specialty section:
This article was submitted to Autonomic Neuroscience, a section of the journal Frontiers in Neuroscience

Received: *23 December 2020*
Accepted: *01 June 2021*
Published: *02 July 2021*

Citation:
Jin X, Gharibani P, Yin J and Chen JDZ (2021) Neuro-Immune Modulation Effects of Sacral Nerve Stimulation for Visceral Hypersensitivity in Rats. Front. Neurosci. 15:645393. doi: 10.3389/fnins.2021.645393

INTRODUCTION

Visceral pain is a complex disorder sensed by internal organs which is by far the most common type of complaint in gastrointestinal (GI) diseases (Pusceddu and Gareau, 2018). It exerts massive pressure on the healthcare system and impacts the overall quality of life in patients (Hungin et al., 2003; Pusceddu and Gareau, 2018). Most abdominal pain is due to the functional GI disorders,

such as irritable bowel syndrome (IBS) and functional dyspepsia (Locke et al., 1997). The most prevalent form of visceral pain is attributed to IBS which affects 3–22% of the general population (Boyce et al., 2000).

Several elements contribute to the pathophysiologies of IBS, such as dysmotility, visceral hypersensitivity (VH), increased intestinal permeability and psychological stress (Whorwell, 2015; Lee and Lee, 2016). However its pathogenesis is still poorly understood, and the treatment outcome is not satisfactory. Low-grade inflammation has been shown to be one of the causes of IBS (Ohman and Simren, 2010) which involves the enteric nervous system (ENS) and immune cells, such as mast cells with direct cross-interactions on each other (De Winter et al., 2012; Karhausen et al., 2013; Jin et al., 2017; Lennon et al., 2018). More attentions have been drawn to the roles of mast cells in GI functions. Mast cells within the GI tract regulate nociception, innate and adaptive immunity, vascular and epithelial permeability, peristalsis, ion secretion, fibrosis and also tissue repair (Bischoff and Kramer, 2007; Boeckxstaens, 2018). Moreover, mast cells can serve as an end effector and release several mediators such as Tryptase/histamine, prostaglandins E2 (PGE2), tumor necrosis alpha (TNF-α) to provoke inflammation, change the permeability (De Winter et al., 2012) and induce VH (Jacob et al., 2005). Hyperplasia and overactivation of the mast cells were shown to induce the main hallmark symptoms of IBS such as abdominal pain, discomfort, bloating and abnormal bowel functions (O'Sullivan et al., 2000; Robles et al., 2019). Compelling evidence has shown that mast cells might be involved in the generation of IBS symptoms, particularly VH (Boeckxstaens, 2018). Targeting mast cells to improve VH has partially exhibited good efficacy in symptom improvement. Accordingly, a more comprehensive approach in treatment is necessary (Camilleri, 2013; Boeckxstaens, 2018).

Electrical stimulation of the peripheral nervous system has been proposed for reducing inflammation and pain in some GI diseases (Locke et al., 1997; Hungin et al., 2003; Whorwell, 2015; Pusceddu and Gareau, 2018), and as such sacral nerve stimulation (SNS) has been approved by the FDA for treating fecal incontinence and overactive bladder (Thin et al., 2013). In a series of animal studies, we have also shown that SNS with appropriate parameters could improve several other GI dysfunctions, such as delayed colonic transit (Peters et al., 2007) and bowel mucosal inflammation (Falletto et al., 2009; Lundby et al., 2011; Jiang et al., 2019b; Tu et al., 2020b). Few studies explored the potential of SNS for VH in animal models (Fassov et al., 2014; Langlois et al., 2015; Jiang et al., 2019a). However, the mode of action needs to be more elucidated. Jiang et al. (2019b) demonstrated that SNS with appropriate parameters could improve VH via the autonomic pathway. While we have also shown that SNS could ameliorate the colonic permeability in animal mode of IBD (Tu et al., 2020b), its mechanisms of action involved in the ameliorating effect of SNS on VH needs further investigation. Thus, in this study, we induced VH by administrating acetic acid (AA) in a neonatal stage, which is a widely accepted IBS animal model. We hypothesized that SNS could ameliorate VH by reducing mucosal mast cell overactivity mediated via the autonomic pathway. The aim of this study was to show that SNS could suppress visceral pain (assessed by visceromotor reflexes) by modulating enteric neurons and regulating mast cells activity in a rodent model of AA-induced VH.

MATERIALS AND METHODS

Animals and Ethics Statement

We used a total number of 20 male Sprague-Dawley (SD) rats in this study in accordance with the guidelines of the Johns Hopkins University for the Care and Use of the laboratory Animals (ACUC's approved protocol #RA17M292). Six-day-old pups (Charles River, United States) were housed in one cage with one mother and weaned when they were 4 weeks old. The animal room was under controlled conditions with regulated temperature (20–22°C), 50% humidity, and a 12-h light/12-h dark cycle and free access to water and solid food *ad libitum*.

The rats were randomized into three groups: SNS group (n = 6), sham-SNS group (n = 6) and control group (n = 8). The animal model of VH was stablished according to previous studies (Al-Chaer et al., 2000; Yin et al., 2010b). Briefly, at the age of 10 days old, the pups in SNS and sham-SNS groups received an infusion of 0.2 ml of 0.5% AA solution in saline (0.09%) into the colon 2 cm from the anus. The control group received only saline using the identical administration method. The rats in the SNS and sham-SNS groups underwent all surgical and experimental procedures outlined in **Figure 1**. The control rats were only subjected to the electromyogram (EMG)/abdominal withdrawal reflex (AWR) and blood sample collected at Week 10 and Week 13 and colon tissue collection at Week 13.

Surgical Procedure

The surgical procedure was performed during 8–9 weeks of age for implanting electrodes for three purposes: (Pusceddu and Gareau, 2018) SNS, (Hungin et al., 2003) recording electromyography (EMG) and (Locke et al., 1997) recording electrocardiogram (ECG).

SNS Electrodes Implantation

Rats were anesthetized with 2% isoflurane (Abbott Laboratories, Abbott Park, IL, United States) with a 1–2 liter/min oxygen flow. In our previous study, we showed that unilateral but not bilateral SNS improved the inflammation in colitis (Zhang et al., 2020). Therefore, in this study we used unilateral SNS on right sacral nerve of S3 to investigate the possible analgesic effects of SNS. Briefly, as we reported previously (Jiang et al., 2019b; Tu et al., 2020b), a dorsal midline incision was made to expose the right sacral nerve. One pair of electrodes (Cardiac pacing wire, A&E Medical, Farmingdale, NJ, United States) were placed around the right sacral nerve (S3) behind the sacral foramen and fixed by a surgical knot (oval cathode 2–3 mm in length in each electrode). To isolate the exposed wires from

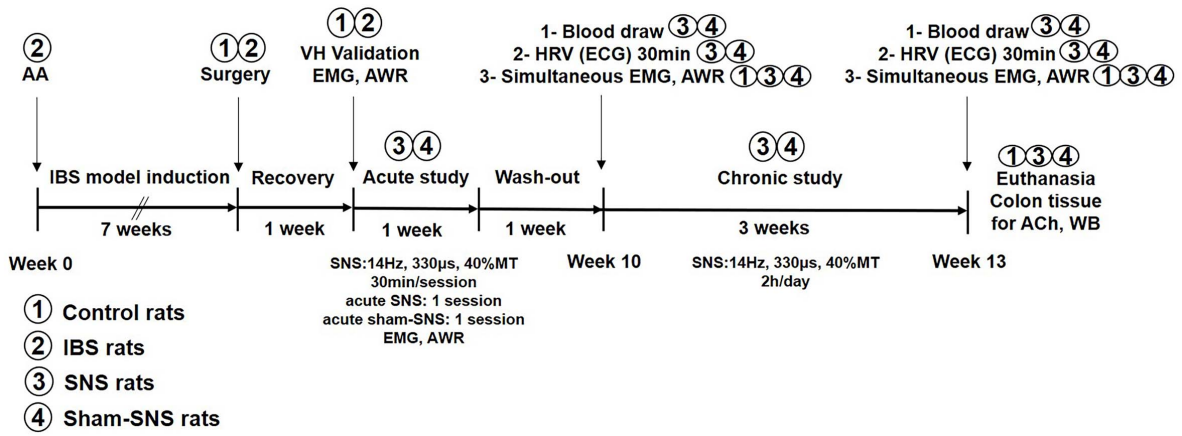

FIGURE 1 | Experimental design and the effects of acute and chronic SNS and sham-SNS on visceral hypersensitivity. EMG and AWR were assessed using colorectal distention test in hypersensitive and control (normal rats). Animal groups are presented by numbers.

the adjacent tissues, we used the dental cement on the wires (Griffin et al., 2011).

EMG Electrodes Implantation

An oblique incision was made on the abdominal skin and the tips of two cardiac pacing wires (A&E Medical, Farmingdale, NJ, United States) were implanted at the external oblique muscles in the lower left abdomen to record EMG (Jiang et al., 2019b).

ECG Electrodes Implantation

Electrodes were implanted for recording the ECG for measuring heart rate variability (HRV). Briefly, three electrodes (A&E Medical, Farmingdale, NJ, United States) were implanted subcutaneously (two of them under the skin in the chest wall of the chest, and the other one under the skin of abdomen). In order to do that, three skin incisions were made, and the tips of three cardiac pacing wires (A&E Medical, Farmingdale, NJ, United States) were implanted at muscles, underneath the incision sites. All abovementioned electrode connecting wires were subcutaneously tunneled through the back and externalized at the back of neck. The skin incisions were closed with sutures.

Control and sham-SNS animals underwent the same surgical procedures for the placement of electrodes. The rats were given a 7-day recovery following the surgery.

Experimental Protocols

In this study, the experiments were accomplished at two different steps. In the first step, we validated the success of VH in our animal model. Then, acute and chronic SNS were performed with electrical current produced by a universal pulse generator (Model DS8000, World Precision Instruments, Sarasota, FL, United States) through the chronically implanted SNS electrodes. The experimental design is shown in **Figure 1** and described as follows.

Measurement of Visceromotor Reflexes

The EMG of external oblique muscles as well as AWR were assessed in response to the colorectal distention (CRD) for assessing visceromotor reflex, as previously reported (Al-Chaer et al., 2000; Jiang et al., 2019b).

Recording and Measurement of EMG

Under a mild anesthesia with 1% isoflurane, a 5 cm-flexible balloon (made from a finger of a surgical glove) attached to a Tygon tube was inserted into the rat anus and advanced for about 8 cm from anal verge to the descending colon and held in place by taping the tube to the tail. Rats were allowed to adapt for 30 min in a small Lucite cubicle (20 × 8 × 8 cm) before the CRD test. An EMG100C amplifier (MP100, BIOPAC Systems, Inc., Santa Barbara, CA, United States) was used to record the EMG signal during the whole process (before, during and after CRD). To test the visceromotor reflex via the EMG, the balloon was rapidly inflated to a constant pressure of 20, 40, 60, and 80 mmHg determined by a sphygmomanometer. Each distention lasted for 20 s and was followed by a 2 min rest (pressure at 0 mmHg). Then the distention was repeated for one more time. The EMG signals were amplified and digitized at a frequency of 2000 Hz using the accompanying software (ACQKNOWLEDGE, BIOPAC System, Inc., Santa Barbara, CA, United States). The area under the curve (AUC) of the EMG signal during each 20 s of distention was calculated using an in-house written computer program. Meanwhile, the AUC of the EMG 20 s before, 20 s during and 20 s after each distention were calculated. The change of the EMG at each distention pressure was calculated by the AUC during the distention subtracting the mean value of the AUC before each distention. The final results were presented by the mean value of the EMG change in 2 repeated sessions (Yin et al., 2010b).

Recording and Measurement of AWR

The AWR was assessed by two colleagues who were blinded to the study protocol. It was assessed simultaneously during the graded CRD for the EMG recording and scored from 1 to 4 as follows: 1: no behavioral response to CRD; 2: contraction of abdominal muscles; 3: lifting of abdomen; and 4: body arching and lifting of pelvic structures (Al-Chaer et al., 2000).

Assessments of Autonomic Functions

Recording and Measurement of Heart Rate Variability

As shown in **Figure 1**, the ECG was recorded before the initiation of chronic SNS (week 10) and at the end of the treatment (week 13) for 30 min period in the fasting state using a special one-channel amplifier with a cutoff frequency of 100 Hz (Fetrode Amplifier, model 2283 ft/I, UFI, Morro Bay, CA, United States). An HRV signal was derived using a previously validated software (Yin et al., 2010a) by identifying R waves, calculating R-R intervals, interpolating the R-R interval data and sampling at a frequency of 8 Hz. The overall power spectrum of the HRV signal was then calculated and the total power in each of 2 frequency sub-bands was assessed, including low frequency (LF) and high frequency (HF) (Yin et al., 2010a). The power in the LF band (0.3–0.8 Hz) represents mainly sympathetic activity and the power in the HF band (0.8–4.0 Hz) stands purely for vagal activity (Tu et al., 2020c). The ratio LF/HF reflects the balance between sympathetic activity and vagal activity.

Measurements of Endocrine Hormones, Norepinephrine and Pancreatic Polypeptide

Blood samples were drawn in the fasting state before the initiation of chronic SNS (week 10) and at the end of the treatment (week 13, see **Figure 1**). Plasma pancreatic polypeptide (PP) (CSB-E12747r, CUSABIO, United States) and norepinephrine (NE) (ab47831, Abcam, Cambridge, United Kingdom) were measured by ELISA, according to the manufacturer's protocols.

Measurement of Acetylcholine Release in Colon

At the end of experiment, colonic acetylcholine (ACh) was measured as described previously (Tu et al., 2020b) in all rats, including the control rats. Briefly, the colonic tissues were dissected, and the mucosal layer was scarped on an ice-cold dish with clean tools as quickly as possible to prevent degradation by endogenous proteases. Tissue samples were homogenized in 0.01 M PBS using a glass tissue homogenizer and centrifuged at 5,000 × *g* for 10 min. The resulting supernatants were collected, and the protein concentrations were measured using the Bradford Protein Assay (Bio-Rad). The content of ACh in colonic tissue samples was assessed using an ACh assay kit (Abbexa Ltd., Catalog No abx051982) according to the manufacturer's protocol (Sun et al., 2013).

Validation of Animal Model of Visceral Hypersensitivity

This experiment (marked as "VH validation" in **Figure 1**) was performed to validate if the VH model was induced successfully. The AA-treated rats (n = 12) and saline-treated controls (n = 8) were tested 8 weeks after AA or saline administration. The EMG and AWR were recorded and analyzed at baseline and during CRD at different pressures (20, 40, 60, and 80 mmHg). The AWR was graded at the same time by two colleagues who were blinded to the study protocols.

Effect of Acute and Chronic SNS on Visceral Hypersensitivity

In this experiment, we investigated if acute SNS was able to improve the visceromotor reflexes in AA-treated rats and then, how chronic SNS might have ameliorating effects in the AA-treated rats. During week 9 (marked as "acute study" in **Figure 1**), all 12 AA-treated rats were subjected to two randomized sessions of SNS or sham-SNS with an interval of 3 days. In each session, the EMG and AWR were simultaneously recorded immediately after 30-min SNS (14 Hz, 330 μs, 40% motor threshold or MT) (Jiang et al., 2019b) or sham-SNS (identical with SNS except there was no actual stimulation). The MT was defined as the lowest level of SNS capable of causing a contraction in the tail muscle that can be seen by bare eyes (Tu et al., 2020b).

In the chronic study, the 12 AA-treated rats were randomized into SNS group (n = 6) and sham-SNS group (n = 6). The SNS group (n = 6) received daily SNS (14 Hz, 330 μs, 40%MT, 2 h) for 3 weeks, whereas, the sham-SNS group (n = 6) received daily sham-SNS (identical with SNS except there was no actual stimulation). Following measurements were made sequentially (see **Figure 1**) in the fasting state before and after the chronic treatment: after, the collection of blood samples from tail vein, a 30-min ECG recording (for HRV) was made and then the EMG and AWR responses to CRD were simultaneously assessed. The control group (n = 8) received no treatment.

At the end of the entire study, all animals (including controls) were sacrificed, and colon tissues were collected for the mechanistic assessment.

Mechanisms of Chronic SNS on Visceral Hypersensitivity

At the end of the study, all rats terminated by an overdose of isoflurane (adjusting the isoflurane flow rate to 5% until breathing stopped) and opening the abdominal cavity and chest for tissue collection. Colon tissue samples (middle third: 8–12 cm proximal to the anus as total length of 4 cm) were collected for assessing key biomarkers in ENS (PGP9.5, ChAT, and nNOS) as well as mast cells [Tryptase, PGE2, and cyclooxygenases-2 (COX2)] and pain markers [nerve growth factor (NGF) and Substance-P] by western blot (WB).

Western Blot Analysis

The colon tissue samples were lysed in a RIPA buffer containing a 2% phosphatase-inhibitor (Thermo Fisher Scientific, Waltham, MA, United States) and a 1% mammalian-protease inhibitor (Sigma-Aldrich). 50 μg of extracted proteins were run a single track of 10% sodium dodecyl sulfate–polyacrylamide gel electrophoresis (SDS-PAGE), and the separated proteins were transferred electrophoretically onto cellulose membranes. The membranes were blocked in 5% non-fat dry milk for 60 min, and then incubated with primary antibodies against nNOS (1:1000; Cell Signaling, Boston, MA, United States), Sub-P (1:100; Novus biologicals, Centennial, CO, United States), ChAT (1:100), NGF (1:200), COX2 (1:300), Tryptase (1:500), PGP9.5 (1:1000) and GAPDH (1:10,000) (all Abcam, Cambridge, United Kingdom), and PGE2 polyclonal antibody (1 : 200; Bioss Inc., Woburn,

MA, United States) (Chia et al., 2017) overnight at 4°C. The membranes were washed 3× with TBS-T (TBS mixed with 0.1% Tween-20) and then, they were incubated with ECL AP-conjugated anti-rabbit/mouse IgG (1:3,000; GE Healthcare, United Kingdom) for 90 min in room temperature. Quantitative western blot results were obtained by densitometric analysis using image processing and analysis in Java (Image J, NIH, Bethesda, MD, United States). The percent change of relative intensity was calculated against control samples.

Statistical Analysis

All results are expressed as mean ± SE. Differences between multiple groups were evaluated by Analysis of variance (One-way or Two-way ANOVA). For EMG and AWR, Two-way ANOVA was used to compare the difference between baseline and animal model of IBS or after treatments. While One-way ANOVA was used for HRV and ACh, Student's unpaired *t*-test was performed for NE/PP and western-blot. *P* value ≤ 0.05 was considered significant. All statistical analysis was performed by using GraphPad Prism 8.3.

RESULTS

Acetic Acid Induced Visceral Hypersensitivity

In order to carry out the SNS experiment, firstly we validated if VH was induced successfully in rats treated with AA. Compared with the control ($n = 8$) rats, the abdominal visceromotor (EMG) and AWR were increased significantly in the AA-treated rats ($n = 12$) responding to CRD. The area under the curve of EMG in the AA-treated rats was increased from 5.32 ± 0.92 to 13.92 ± 0.1; 10.44 ± 1.7 to 20.8 ± 1.8; 15.3 ± 1.9 to 30.8 ± 2.3; and 18.86 ± 1.6 to 36.32 ± 3.08 compared to the control at 20, 40, 60, and 80 mmHg CRD, respectively (**Figures 2A,C,D**, $p < 0.03$; Two-way ANOVA, Bonferroni). AWR scores in the AA-treated rats were increased from 1.31 ± 0.09 to 3.5 ± 0.1; 2.25 ± 0.13 to 3.9 ± 0.05; 2.75 ± 0.12 to 4.0 ± 0.0; and 3.12 ± 0.08 to 4.0 ± 0.0 compared to the control rats at 20, 40, 60, and 80 mmHg CRD, respectively (**Figure 2B**, $p < 0.001$; Two-way ANOVA, Bonferroni). Thus, it was confirmed that VH was induced successfully in AA-treated rats.

Ameliorating Effects of Acute SNS on Visceromotor Reflexes

As shown in **Figure 1**, following the validation of our animal model of VH, we tested the effects of acute SNS (14 Hz, 330 μs, 40%MT, 30 min) or sham-SNS on EMG and AWR during CRD. Acute SNS significantly reduced EMG and AWR in AA-treated rats compared to the sham-SNS. SNS was able to decrease the area under the curve of EMG by 41.81% (13.26 ± 0.91 to 7.71 ± 0.34), 51.0% (20.29 ± 1.52 to 9.95 ± 0.67), 48.12% (27.91 ± 1.93 to 14.48 ± 1.53), and 52.6% (31.7 ± 2.88 to 15.02 ± 0.71) at 20, 40, 60, and 80 mmHg CRD, respectively compared to the sham-SNS (**Figure 3A**, $n = 12$, $p < 0.05$; Two-way ANOVA, Bonferroni). Similarly, AWR scores were also decreased by 23.66% (3.37 ± 0.1 to 2.5 ± 0.1), 26.3% (3.95 ± 0.04 to 2.91 ± 0.08), 21.87% (4.0 ± 0.0 to 3.12 ± 0.1), and 12.5% (4.0 ± 0.0 to 3.5 ± 0.1) at 20, 40, 60, and 80 mmHg CRD, respectively compared to the sham-SNS (**Figure 3B**, $n = 12$, $p < 0.001$; Two-way ANOVA, Bonferroni). However, it can be seen from the figure that the AWR was a less sensitive measure of visceromotor reflexes as its score almost reached the maximum at CRD of 40 mmHg.

Mechanisms of Chronic SNS on Visceral Hypersensitivity

Chronis SNS was performed for 2 h/day for a period of 3 weeks with the same parameters. The EMG and AWR were recorded during CRD before and after the chronic SNS. Meanwhile, we collected blood and recorded the ECG to assess the effects of chronic SNS on the autonomic system function (experimental design: **Figure 1**).

Chronic SNS Ameliorated Visceromotor Reflexes in Visceral Hypersensitive Rats

Compared to the sham-SNS, chronic SNS decreased the area under the curve of EMG by 49.17% (12.1 ± 1.57 to 6.15 ± 0.88), 66.5% (20.73 ± 2.59 to 6.94 ± 0.69), 63.76% (27.18 ± 1.5 to 9.85 ± 1.5), and 65.08% (33.3 ± 3.39 to 11.64 ± 1.38) at 20, 40, 60, and 80 mmHg CRD, respectively (**Figures 3C,E–G**, $p < 0.04$; Two-way ANOVA, Tukey). EMG in sham-SNS group but not in SNS was significantly higher compared with control group. AWR scores were also reduced by 50.0% (3 ± 0.18 to 1.5 ± 0.18), 46.51% (3.58 ± 0.15 to 1.92 ± 0.08), 33.3% (3.75 ± 0.11 to 2.5 ± 0.18), and 29.16% (4 ± 0 to 2.83 ± 0.1) at 20, 40, 60, and 80 mmHg CRD, respectively compared to the sham-SNS (**Figure 3D**, $p < 0.02$; Two-way ANOVA, Tukey). Interestingly, chronic SNS was able to normalize both EMG and AWR at different pressure of CRD, comparable to the normal rats (control).

Chronic SNS Improved the Autonomic Nervous System Functions

Autonomic nervous system functions were measured via assessing the HRV derived from the ECG as well as measuring the release of endocrine hormones of NE and PP in the blood drawn from vein (**Figure 4**).

The heart rate variability derived from ECG

As shown in **Figure 4A**, following 3-week treatment, SNS could significantly decrease the sympathetic activity (LF) from 0.41 ± 0.05 to 0.34 ± 0.04 ($p < 0.05$) compared to the sham-SNS. On the other hand, chronic SNS increased the vagal activity (HF) from 0.59 ± 0.05 to 0.66 ± 0.04 ($p < 0.05$). LF and HF showed no changes in value in our animal model of VH compared to the control ($p > 0.05$). 3-week chronic SNS, could significantly reduce LF/HF value compared to the control and sham-SNS groups (SNS: 0.51 ± 0.08, sham-SNS: 0.66 ± 0.024, baseline: 0.69 ± 0.03; $p < 0.001$; One-Way ANOVA, Tukey).

Endocrine hormones of NE and PP

Sympathetic (norepinephrine, NE) and vagal (pancreatic polypeptide, PP) endocrine hormones, were measured by Elisa, before and after the chronic treatment in both SNS and

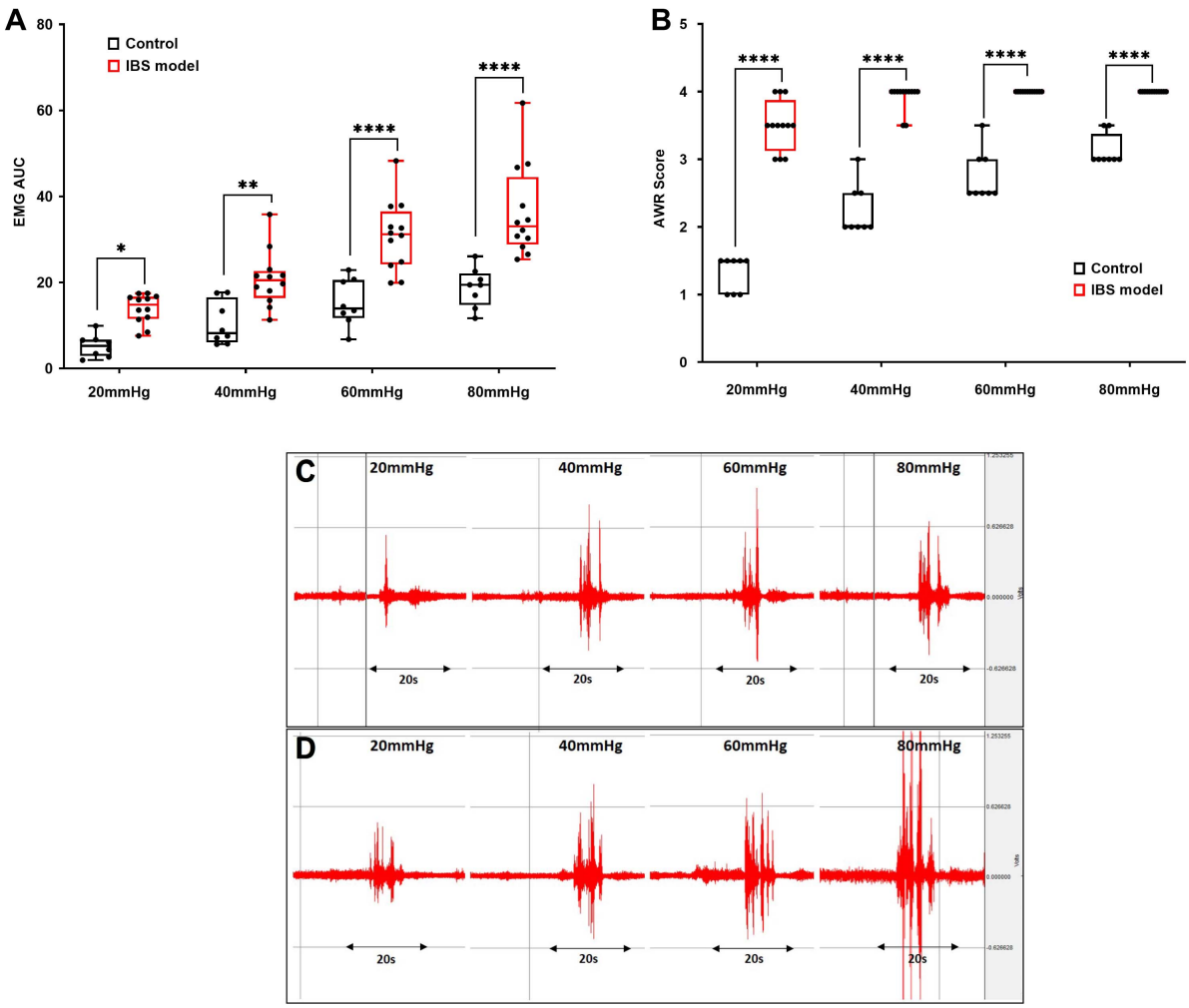

FIGURE 2 | Validation of animal model of visceral hypersensitivity (IBS model). EMG and AWR were assessed using colorectal distention test in hypersensitive (n = 12) and control (normal) rats (n = 8). **(A,C,D)** EMG in acetic acid-treated rats were significantly higher at 20, 40, 60, and 80 mmHg than control (*$p < 0.03$, **$p < 0.005$, ****$p < 0.0001$; Two-way ANOVA, Bonferroni). **(C,D)** Representative EMG examples of control **(C)** and IBS **(D)** rats at 20, 40, 60, and 80 mmHg. Each CRD was carried out for 20 s. **(B)** AWR scores in acetic acid-treated rats were significantly higher at different colorectal distention pressures compared to the control. Values were represented as the means ± SE, (****$p < 0.0001$; Two-way ANOVA, Bonferroni). IBS: inflammatory bowel disease; EMG: electromyogram; AWR: abdominal withdraw reflex; AUC: area under the curve; CRD: colorectal distention.

sham-SNS groups. As shown in **Figures 4B,C**, while plasma NE was significantly decreased compared to the sham-SNS, PP conversely increased after the 3-week SNS treatment. While SNS notably increased the PP value from 63.6 ± 5.09 pg/ml in sham-SNS to 83.33 ± 5.83 pg/ml in SNS treatment group ($p < 0.03$; Student t-test), plasma NE was reduced from 0.53 ± 0.05 ng/ml in sham-SNS to 0.36 ± 0.059 ng/ml in SNS treatment group ($p < 0.05$; Student t-test).

ACh release in colon tissue

Acetylcholine is known to play an important role in the cholinergic anti-inflammatory pathway. AA administration induced endogenous increase of ACh in colon tissue (sham-SNS: 32.48 ± 2.80) compared with the control group (normal rats) (17.80 ± 1.48) ($p < 0.05$; One-Way ANOVA, Tukey). Despite this, the SNS treatment increased further the ACh release in SNS group (51.06 ± 9.20) ($p = 0.04$, vs. sham-SNS, respectively; One-Way ANOVA, Tukey) (**Figure 5**).

Restoring Effects of Chronic SNS on Enteric Nervous System Functions

After a 3-week SNS or sham-SNS treatment, rats were sacrificed, and the middle third of the colon was harvested to investigate the treatment impacts on neuronal as well as pain related biomarkers. Normal rats were used as control.

ENS markers: ChAT, nNOS, and PGP9.5

Figure 6 shows the protein expression of ChAT, nNOS, and PGP9.5 in colon tissues of all treatment groups. The neonatal AA treatment induced adverse effects in the protein expressions of ChAT, nNOS, and PGP9.5 in the rats that were not treated with chronic SNS. While the AA treatment

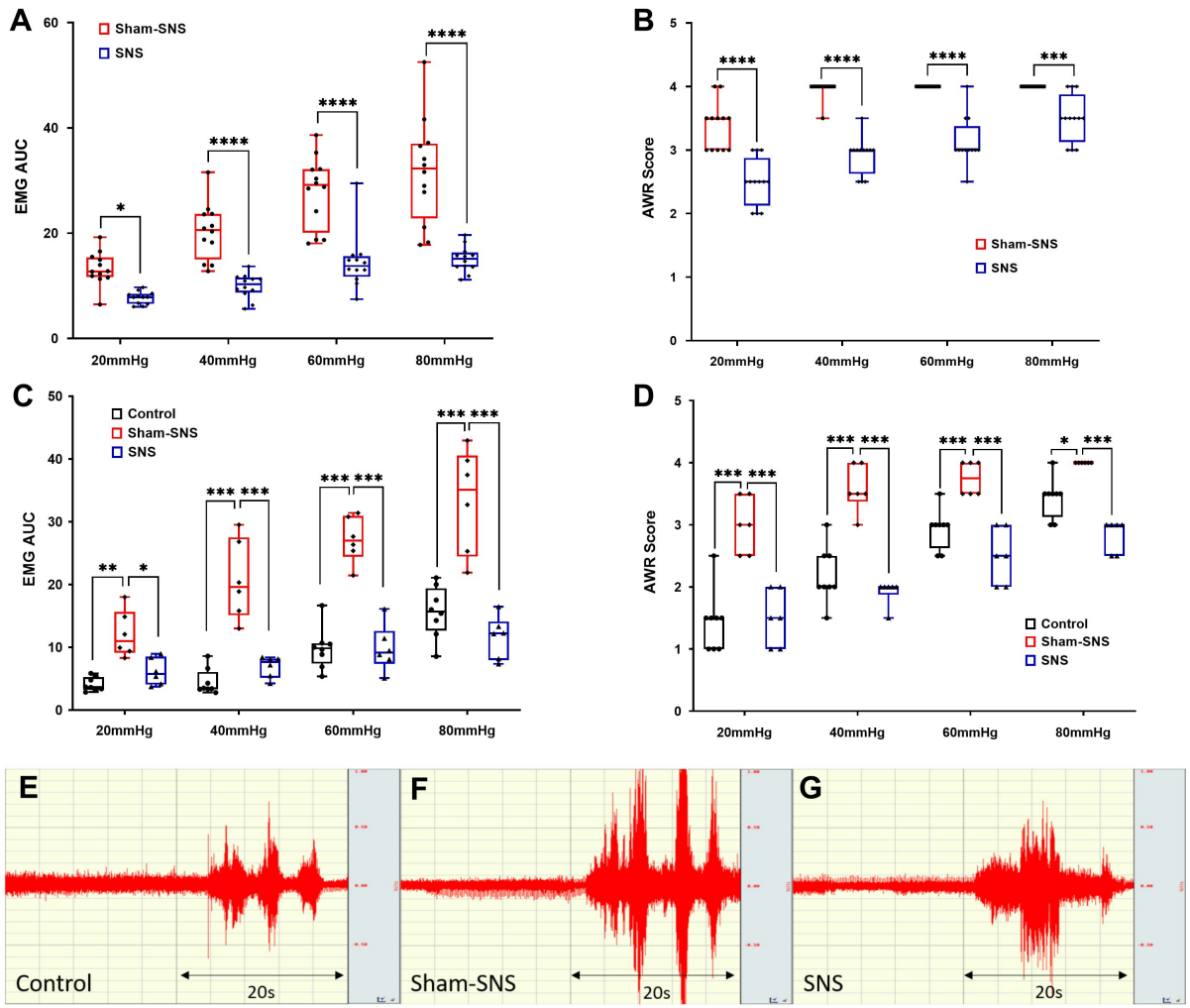

FIGURE 3 | The effects of acute and chronic SNS and sham-SNS on visceral hypersensitivity. EMG and AWR were assessed using colorectal distention test in hypersensitive and control (normal rats). **(A,B)** Effects of acute SNS (14 Hz, 330 μs, 40% motor threshold, 30 min) on EMG and AWR of SNS and sham-SNS groups (n = 12). In animal model of hypersensitivity, EMG and AWR were significantly lower in SNS-treated rats compared to sham-SNS (*$p < 0.05$, ***$p < 0.001$, ****$p < 0.0001$; EMG: Two-way ANOVA, Bonferroni). **(C,D)** Effects of chronic SNS (14 Hz, 330 μs, 40% motor threshold, 3 weeks, 2 h/day, n = 6) on EMG and AWR of SNS and sham-SNS groups (n = 6). Chronic SNS significantly reduced the EMG and AWR compared to sham-SNS and normalized the values comparable to the control (n = 8) (*$p < 0.02$, **$p < 0.002$, ***$p < 0.003$, ****$p < 0.0001$; Two-Way ANOVA, Tukey). **(E–G)** EMG tracing of CRD at 80 mmHg for 20 s in control, sham-SNS and SNS groups following chronic treatment. Values were represented as the means ± SE. AA, acetic acid; SNS, sacral nerve stimulation; HRV, heart rate variability; WB, western blot; IHC, immunohistochemistry; EMG, electromyogram; AUC, area under the curve; AWR, abdominal withdraw reflex; CRD, colorectal distention.

decreased the protein expression of ChAT by 50.29% in the sham-SNS group (p = 0.009 vs. control); SNS was able to normalize the expressions of this protein (p = 0.002 vs. sham-SNS; $p > 0.05$ vs. control) (**Figures 6A,E**). Conversely, nNOS protein expression that was upregulated more that 2-folds in the sham-SNS group (p = 0.0002 vs. control), was significantly diminished by the SNS treatment (p = 0.01 vs. sham-SNS; Student t-test) (**Figures 6B,F**). On the other hand, as shown in **Figures 6C,G**, the protein expression of PGP9.5 was downregulated by almost 33.1% in the sham-SNS group compared to the control (p = 0.046; Student t-test), however, chronic SNS was not able to alter its expression after a 3-week treatment (**Figures 6C,G**).

Molecular Mechanisms of SNS on Visceral Sensation

Mast cell markers: PGE2, COX2, and Tryptase

As shown in **Figure 7**, the neonatal AA treatment upregulated the protein expressions of PGE2, COX2 and Tryptase in the colon tissues in sham-SNS group compared to the control (all $p \leq 0.03$; One-Way ANOVA, Tukey). Interestingly, SNS was able to normalize these protein expressions comparable to the control (PGE2: p = 0.016, COX2: p = 0.021, Tryptase: p = 0.03 vs. sham-SNS, respectively; Student t-test).

Pain markers: NGF and substance-P

As shown in **Figure 8**, the neonatal AA treatment upregulated the protein expressions of NGF and Sub-P more than two-folds

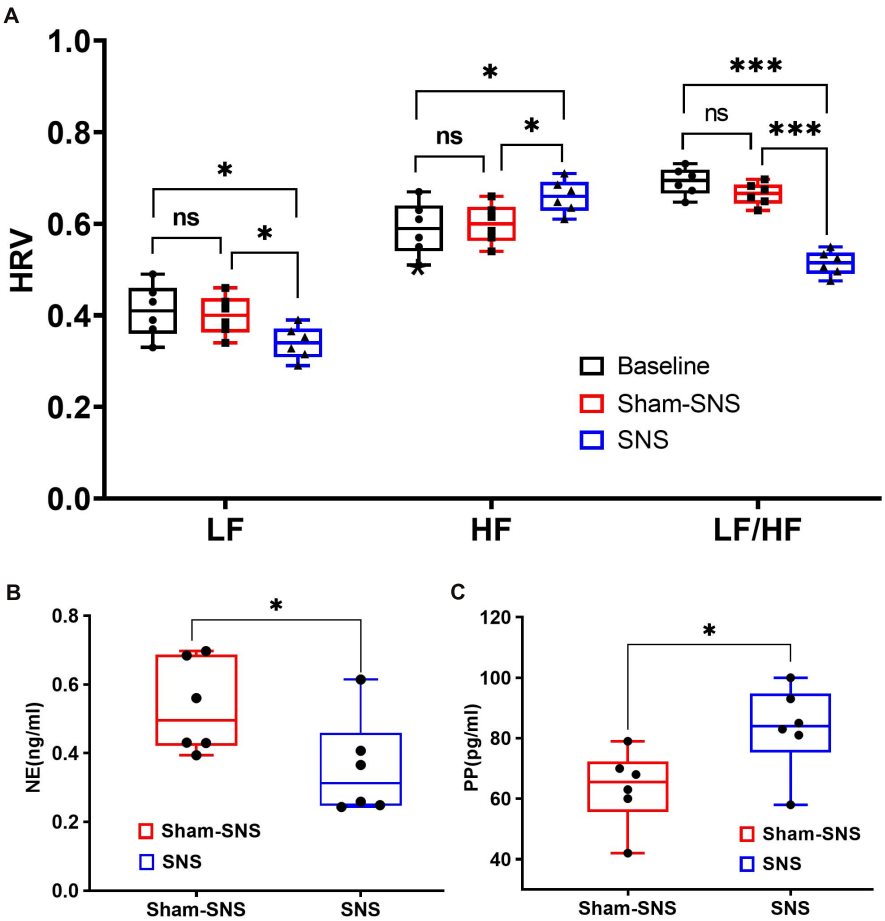

FIGURE 4 | Effects of chronic SNS and sham-SNS on autonomic functions. **(A)** Upper panel shows the effects of chronic SNS and sham-SNS on vagal and sympathetic activities of visceral hypersensitive rats. HF and LF were measured by heart rate variability derived from ECG recording. HF (0.8–4.0 Hz) represents vagal activity, while LF (0.3–0.8 Hz) represents sympathetic activity. LF/HF ratio reflects the balance between sympathetic and vagal activity. Chronic SNS (but not sham-SNS) for 2 h/day for 14 days, significantly increased vagal activity (HF) and decreased sympathetic activity (LF) and the balance between sympathetic and parasympathetic activity (LF/HF) (ns: not significant, $^{*}p < 0.05$, $^{***}p < 0.001$; One-Way ANOVA, Tukey). The unit for both LF and HF was the decibel. **(B,C)** Lower panel show the effects of chronic SNS on endocrine hormones NE and PP before and after treatment. **(B)** Represents the endocrine hormone NE showing the level of sympathetic activities in SNS and sham-SNS groups. **(C)** Represents the endocrine hormone PP showing the level of vagal activities in SNS and sham-SNS groups. NE and PP dramatically changed after 3-week SNS treatment compared to sham-SNS (all significantly changed; $^{*}p < 0.05$; Student *t*-test). Values were represented as the means ± SE ($n = 6$). Baseline: represents HRV before treatment initiation. SNS, sacral nerve stimulation; HRV, heart rate variability; HF, high frequency; LF, low frequency; NE, norepinephrine; PP, pancreatic polypeptide.

in the colon tissues in sham-SNS group compared to the control (both $p \leq 0.003$; One-Way ANOVA, Tukey). Interestingly, SNS was able to downregulate NGF and Sub-P protein expressions compared to the sham-SNS ($p = 0.007$ and $p = 0.03$, respectively; Student *t*-test).

DISCUSSION

In this study, we found that (1) SNS was able to improve the sympathovagal balance and the endocrine hormones, PP and NE, and through that (2) SNS reduced VH possibly by modulating the interactions between the enteric neurons and mast cells as: (i) SNS could regulate the enteric neurons to increase ACh release as well as upregulating the ratio of ChAT protein expression over nNOS; (ii) SNS reduced the mast cells overactivation by the normalization of the protein expressions of Tryptase, PGE2 and COX2; (iii) SNS downregulated the pain markers of NGF and Sub-P; and finally (3) SNS improved the treatment outcome verified by reduced visceromotor reflex (EMG and AWR) during CRD. To the best of our knowledge, this was the first study to report that SNS with appropriate parameters was effective in suppressing VH by modulating the ENS and mast cells via the autonomic pathway in visceral hypersensitive rats. The schematic figure shown in **Figure 9** illustrates the above mechanisms involved in the analgesic effect of SNS.

While IBS has been treated with a variety of medications, the effectiveness of commonly used clinical medications is not always adequate due to the complexity of its symptoms and etiology. Moreover, lack of effective treatments for IBS casts a

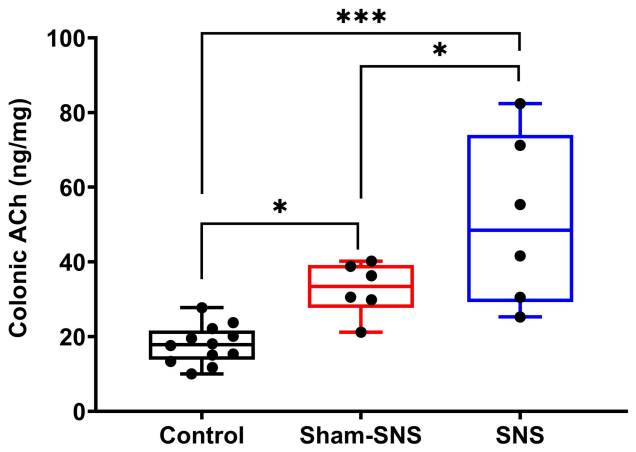

FIGURE 5 | Effects of chronic SNS and sham-SNS on colonic ACh release. ACh in colon tissues was significantly increased in SNS group. Values were represented as the means ± SE (control: $n = 6$, SNS and sham-SNS: $n = 6$). SNS, sacral nerve stimulation (*$p < 0.05$, ***$p < 0.0001$; One-Way ANOVA, Tukey).

large socioeconomic cost (Enck et al., 2016; Grundy et al., 2019). Traditional analgesics, such as non-steroidal anti-inflammatory drugs (NSAIDs) and opioids, are unsuitable for treatment due to potentially severe side effects, such as increasing dependency and tolerance, and/or inducing constipation (Grundy et al., 2019). Electroacupuncture has been shown in clinical trials to effectively improve functional GI disorders including IBS and functional dyspepsia (Ouyang and Chen, 2004; Takahashi, 2006). While electroacupuncture compared to other treatments is considered a safer alternative with less side-effects, its mechanisms of actions on VH have not been well-studied.

In contrast to somatic nociception, the gut nociception is more complex due to the presence of two extrinsic innervation systems (vagal and spinal), intertwined with intrinsic innervation structure, called the ENS (Knowles and Aziz, 2009). The colon and rectum are innervated by spinal sensory afferents from two distinct regions: the lumbar splanchnic and sacral pelvic nerves pathways (Grundy et al., 2019). The innervation for nociception is contributing to receiving stimulus in the mucosa/muscular layers and then to transducing the pain to the dorsal horn of spinal cord via dorsal root ganglia of T10–L2 and L5–S1 (Chichlowski and Rudolph, 2015). Then the pain message is relayed by spinothalamic and spinoparabrachial pathway to the supraspinal centers (Al-Chaer and Traub, 2002; Grundy et al., 2019) at the cingulate cortex, medial thalamus, amygdala, hypothalamus, periaqueductal gray, and the solitary tract (Jones et al., 2006). While these centers are important components of the brain for pain perception, spinal afferent has been extensively studied in basic and clinical research as a classical method for visceral pain treatment by the spinal cord stimulation (Coffin et al., 2004; Yampolsky et al., 2012). In this study, our focus was on the ameliorating effects of SNS on VH that might be mediated by the regulation of the autonomic nervous functions on the colon. This effect might take place via two pathways: the local sacral

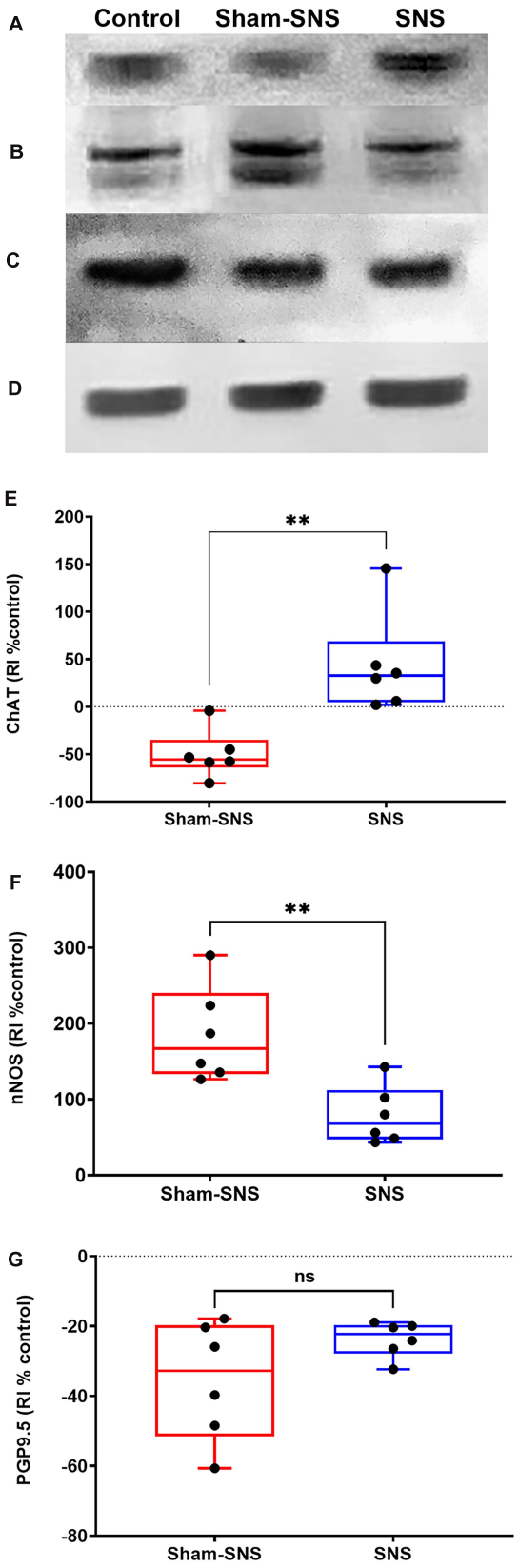

FIGURE 6 | Continued

FIGURE 6 | Effects of chronic SNS and sham-SNS on protein expression of ChAT **(A,E)**, nNOS **(B,F)**, PGP9.5 **(C,G)**, and GAPDH **(D)** in middle third of colon of visceral hypersensitive rats in comparison with the control (normal rats). **(A)** Illustrates ChAT immunoblot (72 kDa), while panel **(E)** displays the percent change of protein expression of ChAT in colon tissue compared to control group. SNS markedly upregulated ChAT protein expression in colon tissue after 3 weeks treatment. Panel **(B)** shows nNOS immunoblot (170 kDa), while panel **(F)** represents the percent change of protein expression of nNOS in colon tissue compared to control group. nNOS that was upregulated in sham-SNS group was downregulated after a 3-week SNS. Panel **(C)** show PGP9.5 immunoblot (25 kDa), while panel **(G)** illustrates the percent change of protein expression of PGP9.5 in colon tissue compared to control group. PGP9.5 protein expression did not alter by 3-week SNS. Values were represented as the means ± SE ($n = 6$) as percentage of relative intensity normalized to internal control (GAPDH, 36 kDa). SNS, sacral nerve stimulation, RI, relative intensity $^{**}p < 0.01$; Student hbox*t*-test).

splanchnic nerve pathway and the sacral afferent-brain stem-vagal efferent pathway. In fact, in a previous study we showed that there was a possible sacral afferent-brain stem-vagal efferent pathway that could transmit SNS to the brain and then via the vagal efferents to the colon tissue (Tu et al., 2020b).

It was reported that the autonomic functions could play an important role in visceromotor reflex and VH (Jiang et al., 2019b; Tu et al., 2020a). As vagus nerve has been more and more validated to have a major role in regulating visceral sensitivity (Swartz and Holmes, 2014; Inoue et al., 2016; Tu et al., 2020a), the vagus nerve neuromodulation is closely pursued in the treatment of visceral pain (Chen et al., 2008). From one hand, suppression of sympathetic activity by SNS might not only block the spinal afferent signal carrying pain to the brain, but also desensitize the spinal sensory pathway in both nociceptors and dorsal root ganglion levels (Xia et al., 2011; He et al., 2017). On the other hand, SNS might take actions via both vagal nerve and local splanchnic nerves to send a signal to the colon and to suppress neurotransmitters associated with VH, such as NGF and Sub-P (Coffin et al., 2004; Chen et al., 2008; Ohman and Simren, 2010; Li et al., 2016) and/or special cells highly associated with VH such as mast cells (Bischoff and Kramer, 2007; Boeckxstaens, 2018). While Jiang et al. (2019b) showed that the neonatal treatment of AA led to sympathetic overactivity and vagal suppression in rats, we found no changes in sympathovagal balance in our animal model induced by AA. However, consistent with their study, we demonstrated that chronic SNS could effectively alter the autonomic functions. Chronic SNS could interestingly increase vagal activity (HF) and suppress sympathetic activity (LF). The values of LF and LF/HF ratio were lower in SNS-treated rats in comparison to the baseline and sham-SNS treated rats. In addition, plasma NE (a sympathetic indicator) and PP (a marker of vagal activation) showed the same trend (Cooper et al., 2015). Consistent with the HRV results, SNS enhanced circulating PP and reduced NE. Based on previous results (Tu et al., 2020b) and the findings of this study, we speculated that the ameliorating effect on VH was mediated through the regulation of the autonomic nervous function via the CNS afferents and vagal efferents as well as local pelvic splanchnic efferents.

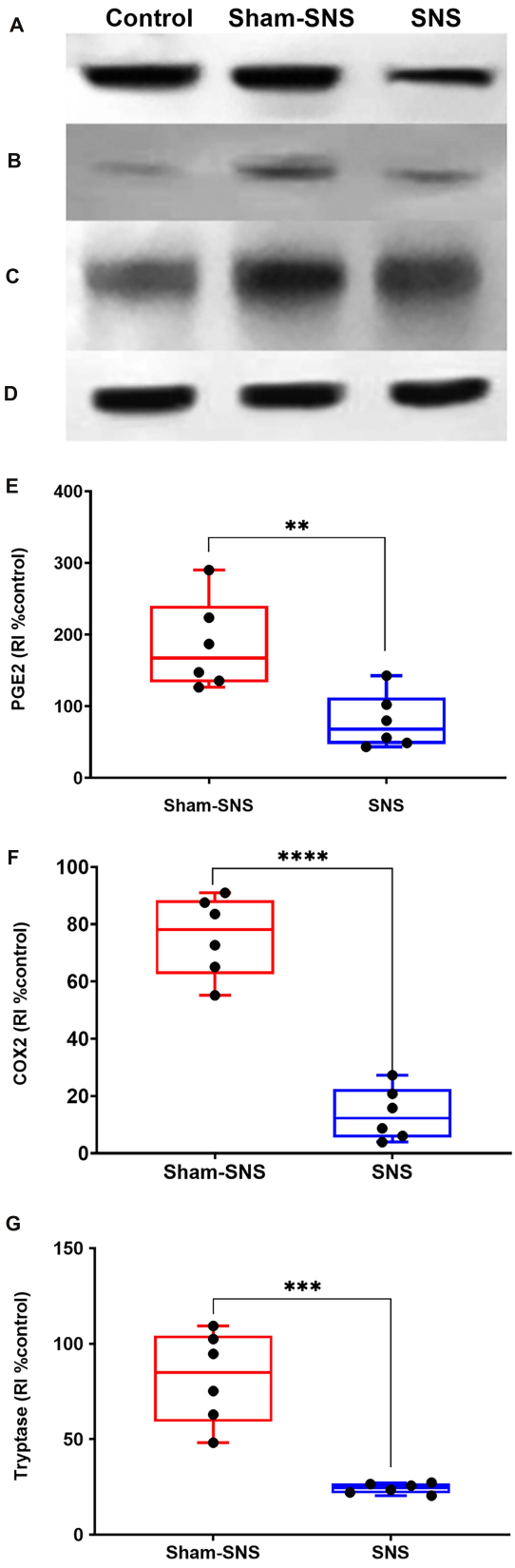

FIGURE 7 | Continued

FIGURE 7 | Effects of chronic SNS and sham-SNS on protein expression of PGE2 **(A,E)**, COX2 **(B,F)**, Tryptase **(C,G)**, and GAPDH **(D)** in middle third of colon of visceral hypersensitive rats in comparison with the control (normal rats). Panel **(A)** shows PGE2 immunoblot (42 kDa) and panel **(E)** displays the percent change of protein expression of PGE2 in colon tissue compared to control group. SNS markedly downregulated PGE2 protein expression in colon tissue after 3 weeks treatment. Panel **(B)** shows COX2 immunoblot (75 kDa) and panel **(F)** exhibits the percent change of protein expression of COX2 in colon tissue compared to control group. COX2 that was upregulated in sham-SNS group was downregulated after a 3-week SNS. Panel **(C)** shows Tryptase immunoblot (52 kDa) and panel **(G)** presents the percent change of protein expression of Tryptase in colon tissue compared to control group. Tryptase protein that was upregulated in sham-SNS group was down-regulated after a 3-week SNS. Values were represented as the means ± SE ($n = 6$) as percentage of relative intensity to normalized to internal control (GAPDH, 36 kDa). SNS, sacral nerve stimulation, RI, relative intensity (**$p < 0.01$, ***$p < 0.001$, ****$p < 0.0001$; Student t-test).

In recent years, VH has been linked to low-grade inflammatory involving the ENS and mast cells with direct cross-interactions on each other (De Winter et al., 2012; Karhausen et al., 2013; Jin et al., 2017; Lennon et al., 2018). VH, as one of the hallmarks of IBS associated with abdominal pain, is referred to a decreased pain threshold and/or an exaggerated response following nociceptor stimulus (Chichlowski and Rudolph, 2015). A few possible pathogeneses of this phenomenon could be (Pusceddu and Gareau, 2018) over-sensitization of primary sensory neurons, Hungin et al. (2003) hyper-excitability of spinal ascending neurons, and (Locke et al., 1997) changes in the central perception of a painful stimulus (Sengupta, 2009). Few studies have shown that mucosal afferents can become mechanically hypersensitive in chronic VH (Brierley et al., 2009; Hughes et al., 2009). Moreover, others have shown that mast cells play a key role in IBS (Adam et al., 2013; Heron and Dubayle, 2013; Zhang et al., 2016; Robles et al., 2019) and also for VH (Ohman and Simren, 2010; Zhang et al., 2016). Mast cells hyperplasia and/or overactivation has been shown to be a common feature in IBS patients (Robles et al., 2019). Vivinus-Nebot et al. (2012) reported that the severity of IBS is significantly correlated with the quantity of colonic mast cells and spontaneous release of tryptase/histamine. Furthermore, Barbara et al. (2004) showed that the close proximity of mast cells to nerves significantly correlated with the severity and frequency of abdominal pain/discomfort. Mast cells within the GI tract, communicate with extrinsic afferents to regulate nociception (Bischoff and Kramer, 2007; Boeckxstaens, 2018). Colonic mucosal biopsies from IBS patients showed an increase release of mast cells' mediators, such as histamine, tryptase and the proinflammatory cytokine correlated with the severity and frequency of abdominal pain. These mediators have been shown to act on receptors expressed by colonic afferents to induce over-sensitization via TRPV1 and NaV1.7-dependent mechanisms (Grundy et al., 2019). The neonatal treatment of AA as an inducer of VH in rats has been shown to alter immune responses and correlate with the over-activity of mast cells in rats (Yang et al., 2019). Targeting mast cells deactivators (cromoglycate and ketotifen) and antagonists of histamine and serotonin receptors,

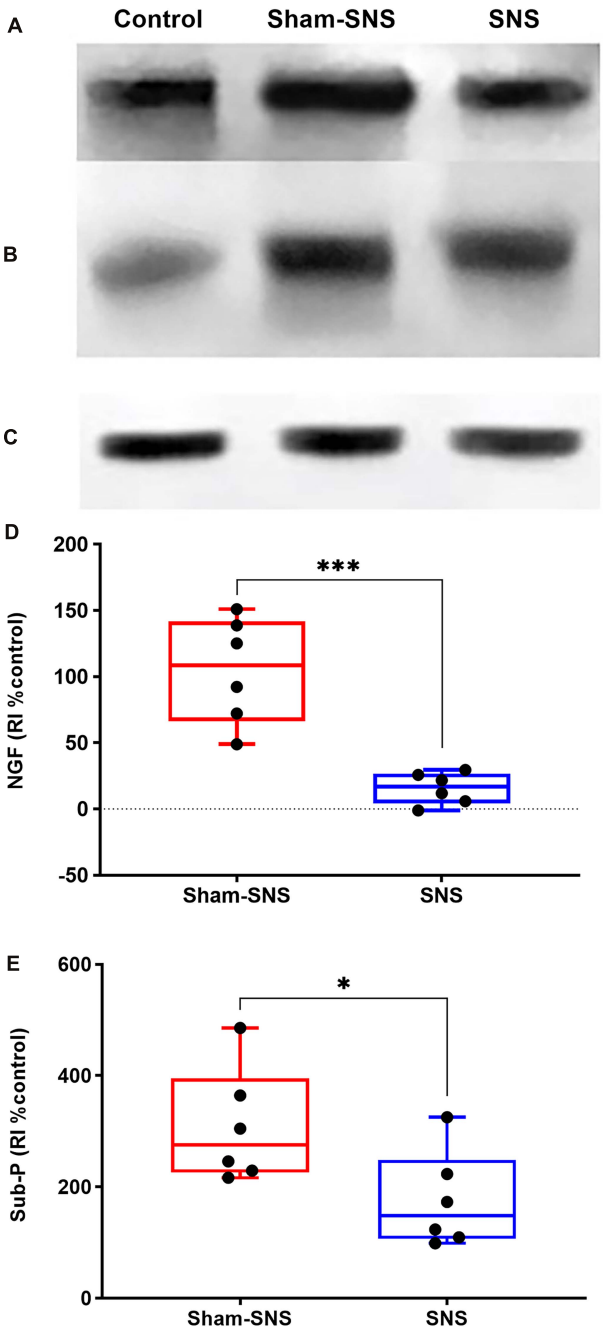

FIGURE 8 | Effects of chronic SNS and sham-SNS on protein expression of NGF **(A,D)**, Sub-P **(B,E)**, and GAPDH **(C)** in middle third of colon of visceral hypersensitive rats in comparison with the control (normal rats). Panel **(A)** shows NGF immunoblot (140 kDa) and panel **(D)** represents the percent change of protein expression of NGF in colon tissue compared to control group. SNS markedly downregulated NGF protein expression in colon tissue after 3 weeks treatment. Panel **(B)** shows Sub-P immunoblot (50 kDa) and panel **(E)** displays the percent change of protein expression of Sub-P in colon tissue compared to control group. Sub-P that was upregulated in sham-SNS group was downregulated after a 3-week SNS. Values were represented as the means ± SE ($n = 6$) as percentage of relative intensity normalized to internal control (GAPDH, 36 kDa). NGF, nerve growth factor; Sub-P, substance-P; SNS, sacral nerve stimulation, RI, relative intensity (*$p < 0.05$, ***$p < 0.001$; Student t-test).

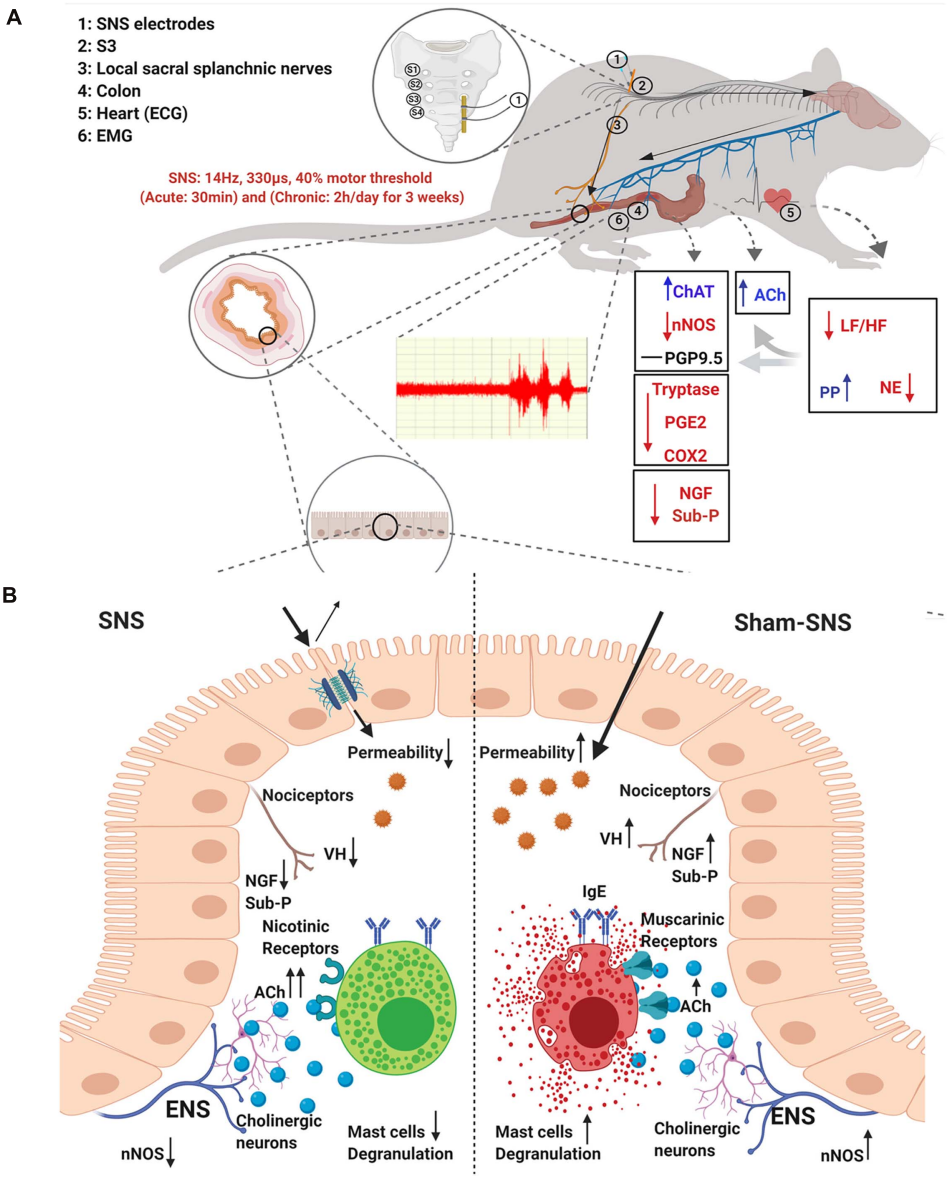

FIGURE 9 | Schematic figure of the possible mechanism of effects of SNS on VH. **(A)** Possible extrinsic afferent circuitry. **(B)** Possible intrinsic mechanism.

have been tried in IBS patients in several studies, and partially exhibited good efficacy in symptom improvement (Camilleri, 2013; Boeckxstaens, 2018).

In this study, we found that SNS increased ACh and ChAT in the colon tissue, suggesting an cholinergic anti-inflammatory pathway involved in the observed analgesic effect of SNS, similar to what has been discovered in vagal nerve stimulation (Bonaz et al., 2013, 2016; Jin et al., 2017; Tu et al., 2020b). Although chronic SNS was not able to alter the number of ganglionic neurons (PGP9.5 positive cells) compared with sham-SNS in colon, it could efficiently change the level of protein expression of ChAT and nNOS. While the protein expression of ChAT was enhanced in colon tissue, nNOS showed a decrease following chronic SNS treatment. This data supported our previous findings to showing the ameliorating effect of SNS on ENS neuronal functions in a rodent model of inflammatory bowel disease (Tu et al., 2020b).

Regarding the effects of ACh on the mast cells, interestingly, mast cells have both muscarinic and nicotinic cholinergic receptors (Masini et al., 1983; Kindt et al., 2008). In spite of that, studies have shown different outcomes describing the functional effects of ACh on the mast cells. Initial investigations reported that ACh via muscarinic receptors could activate the mast cells for degranulation (Fantozzi et al., 1978; Blandina et al., 1980; Masini et al., 1985). Other investigators, however, failed to show an effect of ACh on mast cell degranulation (Kazimierczak et al., 1980; Leung and Pearce, 1984). Masini et al. (1985) demonstrated that

abundance of IgE could increase the sensitivity of mast cells to ACh via muscarinic receptor and induced more degranulation. On the other hand, nicotinic receptors (nAChR) seem to mediate an anti-inflammatory effect in the presence of ACh. In fact, nicotine was shown to inhibit antigen-IgE-induced degranulation of mast cells, an effect that was mirrored by the nAChR subunit agonist, GTS-21 (Kageyama-Yahara et al., 2008). This was also shown by other investigators demonstrating a potential therapeutic effect for the cholinergic anti-inflammatory pathway in an experimental murine model of food allergy. Yamamoto et al. (2014) showed vagal stimulation by 2-deoxy-D-glucose and drug treatment with nAChR agonists could alleviate the food allergic symptoms in the gut. Previously, we showed that SNS could reduce the colonic permeability by overexpression of tight-junction's proteins in mucosa which leads to less allergen exposure and thus IgE to mucosa (Tu et al., 2020b). Gathering with our findings that shows a downregulation in Tryptase and PGE2 expression in colon tissue, this data can support that ACh in absence of IgE might activate the nicotinic receptor to suppress the overactivation of mast cells to reduce the inflammation. On the other hand, as a mutual interaction between mast cells and neurons, it was shown that activated mast cells in rodents could release histamine/Tryptase and that can act on H3 receptor of ENS to suppress the release of ACh from enteric neurons (Frieling et al., 1993; Liu et al., 2000; Buhner and Schemann, 2012). Interestingly, our findings showed that SNS was able to suppress the mast cells activation by downregulation of Tryptase, PGE2, and cyclooxygenases-2 (COX2) and thus increase the ACh release via ENS neurons. Furthermore, it has been demonstrated in both animal models and humans that mast cell mediators in particular histamine, proteases (Tryptase) and PGE2 has substantial effects on sensitization of extrinsic afferent neurons (Jiang et al., 2011; Peiris et al., 2011; Buhner and Schemann, 2012). PGE2 is an important prostaglandin in inflammatory and immune responses (Agard et al., 2013). It was revealed that upon stimulation by various proinflammatory stimuli such as TNF-α, IL-1β, PGE2 synthesis is upregulated by the expression of COX2 (Brierley and Linden, 2014). PGE2 is an essential molecule to regulate the activation of several immune cells, particularly those involved in innate immunity such as macrophages, neutrophils, natural killer cells, and dendritic cells (Agard et al., 2013). Grabauskas et al. (2020) showed that inflammatory mediators such as protease (Tryptase) and histamine activate COX2 to increase the synthesis of PGE2 from arachnoid acid by the mast cells and furthermore, demonstrated that administration of EP2 antagonist prevents the development of VH in a rodent IBS model (Agard et al., 2013; Grabauskas et al., 2020). Alongside with this, they also revealed that this process was enhanced by Sub-P and NGF released from intrinsic sensory nerves which in turn increases the synthesis of arachnoid acid, the substrate for COX2 as well as decreasing visceral pain threshold (Jiang et al., 2019a; Grabauskas et al., 2020).

Nerve growth factor is one member of the neurotrophic factor family with an important regulatory role in the survival, growth, differentiation and function of neurons (Aloe, 2011). Moreover, NGF was shown to be associated with several pathophysiological factors of VH, such as impaired barrier function and a lowered threshold to noxious stimuli (Stanzel et al., 2008; Thin et al., 2013). The NGF expression was also shown to be up-regulated in other inflammatory diseases such as asthma (Frossard et al., 2004), arthritis (Manni and Aloe, 1998) and psoriasis (Raychaudhuri and Raychaudhuri, 2004), suggesting a role for this neurotrophin in inflammatory diseases. It was reported that the level of NGF was significantly higher in both IBS patients and animal models with VH (Tsang et al., 2012; Xu et al., 2017). Some scholars found that NGF participated in the VH process by regulating neuroplasticity and neurosynaptic transmitter secretion, which led to a decrease of visceral pain threshold (Tsang et al., 2012; Winston and Sarna, 2016). Jiang et al. (2019a) showed that SNS was able to downregulate NGF as well as tyrosine kinase A (TrkA), a high affinity receptor for NGF via MAPK/ERK pathway, PI3K/Akt pathway and PLC pathway. Sub-P and NGF as inflammatory mediators can activate specific receptors on sensory afferents, which leads to a localized membrane depolarization and change in membrane potential that can be sufficient to activate voltage-gated ion channels, leading to action potential generation and transmission to the central nervous system (Grundy et al., 2019). Interestingly, alongside with their study, we showed that chronic SNS was able to downregulate both Sub-P and NGF. The protein expression of NGF was still overexpressed at the end of the study in the sham-SNS group but normalized in the SNS-treated group. This data seemed to suggest that SNS might reduce NGF and inflammation by decreasing sympathetic innervation in the mucosal layer. As mast cells were also reported to synthesize NGF (Skaper, 2001), the reduction in the NGF expression might reflect a reduced mast cell activity with chronic SNS. *In vivo* animal studies have suggested that Sub-P is involved in the regulation of intestinal VH (Hallgren et al., 1998; Keita et al., 2010). Indeed, sub-P was found to increase mucosal permeability through producing nitric oxide and increasing inflammation (Youakim and Ahdieh, 1999; Ma et al., 2004). We found that the neonatal AA treatment increased Sub-P by more than two folds in the colon tissue, which was remarkably reduced with SNS.

There were a few limitations in this study such as the use of only male rats. Further studies are needed to investigate if SNS is able to ameliorate the VH in females as not only IBS is predominant in women, but also there are sex differences in mast cell functions. Nevertheless, this study showed that chronic SNS is able to ameliorate visceral pain in an animal model of AA-induced VH by suppressing mast cell overactivity possibly via modulation of the interaction between the enteric nervous system and mast cells, mediated by the autonomic pathway.

DATA AVAILABILITY STATEMENT

The raw data supporting the conclusions of this article will be made available by the authors, without undue reservation.

ETHICS STATEMENT

The animal study was reviewed and approved by Nancy Athor, Director–ACUC Johns Hopkins University.

AUTHOR CONTRIBUTIONS

JC and JY: study concept and design, analysis and interpretation of data, critical revision of the manuscript for important intellectual content, study supervision, and obtaining funding. XJ and PG: study design, performing the research, acquisition of data, analysis and interpretation of data, drafting of the manuscript, and statistical analysis. All authors contributed to the article and approved the submitted version.

FUNDING

This study was partially sponsored by the DARPA BTO ElectRx Program under the auspices of Doug Weber and Eric Van Gieson Contract No. N66001-15-2-4059.

REFERENCES

Adam, B., Tsopelas, C., Liebregts, T., Bartholomeusz, F. D., and Holtmann, G. (2013). Host immune response determines visceral hyperalgesia in a rat model of post-inflammatory irritable bowel syndrome. *J. Gastroenterol.* 48, 1119–1127. doi: 10.1007/s00535-012-0729-2

Agard, M., Asakrah, S., and Morici, L. A. (2013). PGE(2) suppression of innate immunity during mucosal bacterial infection. *Front. Cell. Infect. Microbiol.* 3:45. doi: 10.3389/fcimb.2013.00045

Al-Chaer, E. D, and Traub, R. J. (2002). Biological basis of visceral pain: recent developments. *Pain* 96, 221–225. doi: 10.1016/s0304-3959(02)00046-5

Al-Chaer, E. D., Kawasaki, M., and Pasricha, P. J. (2000). A new model of chronic visceral hypersensitivity in adult rats induced by colon irritation during postnatal development. *Gastroenterology* 119, 1276–1285. doi: 10.1053/gast.2000.19576

Aloe, L. (2011). Rita Levi-Montalcini and the discovery of NGF, the first nerve cell growth factor. *Arch. Italiennes Biol.* 149, 175–181. doi: 10.4449/aib.v149i2.1377

Barbara, G., Stanghellini, V., De Giorgio, R., Cremon, C., Cottrell, G. S., Santini, D., et al. (2004). Activated mast cells in proximity to colonic nerves correlate with abdominal pain in irritable bowel syndrome. *Gastroenterology* 126, 693–702. doi: 10.1053/j.gastro.2003.11.055

Bischoff, S. C., and Kramer, S. (2007). Human mast cells, bacteria, and intestinal immunity. *Immunol. Rev.* 217, 329–337. doi: 10.1111/j.1600-065X.2007.00523.x

Blandina, P., Fantozzi, R., Mannaioni, P. F., and Masini, E. (1980). Characteristics of histamine release evoked by acetylcholine in isolated rat mast cells. *J. Physiol.* 301, 281–293. doi: 10.1113/jphysiol.1980.sp013205

Boeckxstaens, G. E. (2018). The Emerging Role of Mast Cells in Irritable Bowel Syndrome. *Gastroenterol. Hepatol.* 14, 250–252.

Bonaz, B., Picq, C., Sinniger, V., Mayol, J. F., and Clarencon, D. (2013). Vagus nerve stimulation: from epilepsy to the cholinergic anti-inflammatory pathway. *Neurogastroenterol. Motil. Offic. J. Eur. Gastrointest. Motil. Soc.* 25, 208–221.

Bonaz, B., Sinniger, V., Hoffmann, D., Clarencon, D., Mathieu, N., Dantzer, C., et al. (2016). Chronic vagus nerve stimulation in Crohn's disease: a 6-month follow-up pilot study. *Neurogastroenterol. Motil. Offic. J. Eur. Gastrointest. Motil. Soc.* 28, 948–953.

Boyce, P. M., Koloski, N. A., and Talley, N. J. (2000). Irritable bowel syndrome according to varying diagnostic criteria: are the new Rome II criteria unnecessarily restrictive for research and practice? *Am. J. Gastroenterol.* 95, 3176–3183. doi: 10.1111/j.1572-0241.2000.03197.x

Brierley, S. M., and Linden, D. R. (2014). Neuroplasticity and dysfunction after gastrointestinal inflammation. *Nat. Rev. Gastroenterol. Hepatol.* 11, 611–627. doi: 10.1038/nrgastro.2014.103

Brierley, S. M., Hughes, P. A., Page, A. J., Kwan, K. Y., Martin, C. M., O'Donnell, T. A., et al. (2009). The ion channel TRPA1 is required for normal mechanosensation and is modulated by algesic stimuli. *Gastroenterology* 137, 2084–95e3. doi: 10.1053/j.gastro.2009.07.048

Buhner, S., and Schemann, M. (2012). Mast cell-nerve axis with a focus on the human gut. *Biochim. Biophys. Acta* 1822, 85–92. doi: 10.1016/j.bbadis.2011.06.004

Camilleri, M. (2013). Current and future pharmacological treatments for diarrhea-predominant irritable bowel syndrome. *Exp. Opin. Pharmacother.* 14, 1151–1160. doi: 10.1517/14656566.2013.794223

Chen, S. L., Wu, X. Y., Cao, Z. J., Fan, J., Wang, M., Owyang, C., et al. (2008). Subdiaphragmatic vagal afferent nerves modulate visceral pain. *Am. J. Physiol. Gastrointest. Liver Physiol.* 294, G1441–G1449. doi: 10.1152/ajpgi.00588.2007

Chia, Y. Y., Liu, C. C., Feng, G. M., Tseng, C. A., Hung, K. C., Chen, C. C., et al. (2017). The Antinociceptive Effect of Light-Emitting Diode Irradiation on Incised Wounds Is Correlated with Changes in Cyclooxygenase 2 Activity, Prostaglandin E2, and Proinflammatory Cytokines. *Pain Res. Manage.* 2017:4792489. doi: 10.1155/2017/4792489

Chichlowski, M., and Rudolph, C. (2015). Visceral pain and gastrointestinal microbiome. *J. Neurogastroenterol. Motil.* 21, 172–181. doi: 10.5056/jnm15025

Coffin, B., Bouhassira, D., Sabate, J. M., Barbe, L., and Jian, R. (2004). Alteration of the spinal modulation of nociceptive processing in patients with irritable bowel syndrome. *Gut* 53, 1465–1470. doi: 10.1136/gut.2003.031310

Cooper, T. M., McKinley, P. S., Seeman, T. E., Choo, T. H., Lee, S., and Sloan, R. P. (2015). Heart rate variability predicts levels of inflammatory markers: Evidence for the vagal anti-inflammatory pathway. *Brain Behav. Immun.* 49, 94–100.

De Winter, B. Y., van den Wijngaard, R. M., and de Jonge, W. J. (2012). Intestinal mast cells in gut inflammation and motility disturbances. *Biochim. Biophys. Acta* 1822, 66–73. doi: 10.1016/j.bbadis.2011.03.016

Enck, P., Aziz, Q., Barbara, G., Farmer, A. D., Fukudo, S., Mayer, E. A., et al. (2016). Irritable bowel syndrome. *Nat. Rev. Dis. Primers* 2:16014. doi: 10.1038/nrdp.2016.14

Falletto, E., Masin, A., Lolli, P., Villani, R., Ganio, E., Ripetti, V., et al. (2009). Is sacral nerve stimulation an effective treatment for chronic idiopathic anal pain? *Dis. Colon Rectum* 52, 456–462.

Fantozzi, R., Masini, E., Blandina, P., Mannaioni, P. F., and Bani-Sacchi, T. (1978). Release of histamine from rat mast cells by acetylcholine. *Nature* 273, 473–474. doi: 10.1038/273473a0

Fassov, J. L., Lundby, L., Laurberg, S., Buntzen, S., and Krogh, K. (2014). A randomized, controlled, crossover study of sacral nerve stimulation for irritable bowel syndrome. *Ann. Surg.* 260, 31–36. doi: 10.1097/SLA.0000000000000559

Frieling, T., Cooke, H. J., and Wood, J. D. (1993). Histamine receptors on submucous neurons in guinea pig colon. *Am. J. Physiol.* 264(1 Pt 1), G74–G80. doi: 10.1152/ajpgi.1993.264.1.G74

Frossard, N., Freund, V., and Advenier, C. (2004). Nerve growth factor and its receptors in asthma and inflammation. *Eur. J. Pharmacol.* 500, 453–465. doi: 10.1016/j.ejphar.2004.07.044

Grabauskas, G., Wu, X., Gao, J., Li, J. Y., Turgeon, D. K., and Owyang, C. (2020). Prostaglandin E2, Produced by Mast Cells in Colon Tissues From Patients With Irritable Bowel Syndrome, Contributes to Visceral Hypersensitivity in Mice. *Gastroenterology* 158, 2195–207e6. doi: 10.1053/j.gastro.2020.02.022

Griffin, K. M., Pickering, M., O'Herlihy, C., O'Connell, P. R., and Jones, J. F. (2011). Sacral nerve stimulation increases activation of the primary somatosensory cortex by anal canal stimulation in an experimental model. *Br. J. Surg.* 98, 1160–1169. doi: 10.1002/bjs.7536

Grundy, L., Erickson, A., and Brierley, S. M. (2019). Visceral Pain. *Annu. Rev. Physiol.* 81, 261–284. doi: 10.1146/annurev-physiol-020518-114525

Hallgren, A., Flemstrom, G., and Nylander, O. (1998). Interaction between neurokinin A, VIP, prostanoids, and enteric nerves in regulation of duodenal function. *Am. J. Physiol.* 275(1 Pt 1), G95–G103.

He, Y. Q., Lang, X. Q., Lin, L., Ji, L., Yuan, X. Y., Chen, Q., et al. (2017). P2X3 receptor-mediated visceral hyperalgesia and neuronal sensitization following exposure to PTSD-like stress in the dorsal root ganglia of rats.

Neurogastroenterol. Motil. Offic. J. Eur. Gastrointest. Motil. 29:12976. doi: 10.1111/nmo.12976

Heron, A., and Dubayle, D. (2013). A focus on mast cells and pain. *J. Neuroimmunol.* 264, 1–7. doi: 10.1016/j.jneuroim.2013.09.018

Hughes, P. A., Brierley, S. M., Martin, C. M., Brookes, S. J., Linden, D. R., and Blackshaw, L. A. (2009). Post-inflammatory colonic afferent sensitisation: different subtypes, different pathways and different time courses. *Gut* 58, 1333–1341. doi: 10.1136/gut.2008.170811

Hungin, A. P., Whorwell, P. J., Tack, J., and Mearin, F. (2003). The prevalence, patterns and impact of irritable bowel syndrome: an international survey of 40,000 subjects. *Alimentary Pharmacol. Therapeut.* 17, 643–650. doi: 10.1046/j.1365-2036.2003.01456.x

Inoue, T., Abe, C., Sung, S. S., Moscalu, S., Jankowski, J., Huang, L., et al. (2016). Vagus nerve stimulation mediates protection from kidney ischemia-reperfusion injury through alpha7nAChR+ splenocytes. *J. Clin. Investigat.* 126, 1939–1952. doi: 10.1172/JCI83658

Jacob, C., Yang, P. C., Darmoul, D., Amadesi, S., Saito, T., Cottrell, G. S., et al. (2005). Mast cell tryptase controls paracellular permeability of the intestine. Role of protease-activated receptor 2 and beta-arrestins. *J. Biol. Chem.* 280, 31936–31948. doi: 10.1074/jbc.M506338200

Jiang, L., Ye, B., Wang, Y., Yu, T., and Xu, H. (2019a). Effect and mechanisms of sacral nerve stimulation on visceral hypersensitivity mediated by nerve growth factor. *J. Cell. Mol. Med.* 23, 8019–8024. doi: 10.1111/jcmm.14660

Jiang, L., Zhang, N., Zhang, S., and Chen, J. D. (2019b). Sacral nerve stimulation with optimized parameters improves visceral hypersensitivity in rats mediated via the autonomic pathway. *Mol. Pain* 15:1744806919880651. doi: 10.1177/1744806919880651

Jiang, W., Adam, I. J., Kitsanta, P., Tiernan, J., Hill, C., Shorthouse, A., et al. (2011). 'First-in-man': characterising the mechanosensitivity of human colonic afferents. *Gut* 60, 281–282. doi: 10.1136/gut.2010.229799

Jin, H., Guo, J., Liu, J., Lyu, B., Foreman, R. D., Yin, J., et al. (2017). Anti-inflammatory effects and mechanisms of vagal nerve stimulation combined with electroacupuncture in a rodent model of TNBS-induced colitis. *Am. J. Physiol. Gastrointest. Liver Physiol.* 313, G192–G202.

Jones, M. P., Dilley, J. B., Drossman, D., and Crowell, M. D. (2006). Brain-gut connections in functional GI disorders: anatomic and physiologic relationships. *Neurogastroenterol. Motil. Offic. J. Eur. Gastrointest. Motil. Soc.* 18, 91–103. doi: 10.1111/j.1365-2982.2005.00730.x

Kageyama-Yahara, N., Suehiro, Y., Yamamoto, T., and Kadowaki, M. (2008). IgE-induced degranulation of mucosal mast cells is negatively regulated via nicotinic acetylcholine receptors. *Biochem. Biophys. Res. Commun.* 377, 321–325. doi: 10.1016/j.bbrc.2008.10.004

Karhausen, J., Qing, M., Gibson, A., Moeser, A. J., Griefingholt, H., Hale, L. P., et al. (2013). Intestinal mast cells mediate gut injury and systemic inflammation in a rat model of deep hypothermic circulatory arrest. *Crit. Care Med.* 41, e200–e210. doi: 10.1097/CCM.0b013e31827cac7a

Kazimierczak, W., Adamas, B., and Maslinski, C. (1980). Failure of acetylcholine to release histamine from rat mast cells. *Agents Actions* 10(1 Pt 2), 1–3. doi: 10.1007/BF02024170

Keita, A. V., Soderholm, J. D., and Ericson, A. C. (2010). Stress-induced barrier disruption of rat follicle-associated epithelium involves corticotropin-releasing hormone, acetylcholine, substance P, and mast cells. *Neurogastroent. Motil.* 22, e221–e222. doi: 10.1111/j.1365-2982.2010.01471.x

Kindt, F., Wiegand, S., Niemeier, V., Kupfer, J., Loser, C., Nilles, M., et al. (2008). Reduced expression of nicotinic alpha subunits 3, 7, 9 and 10 in lesional and nonlesional atopic dermatitis skin but enhanced expression of alpha subunits 3 and 5 in mast cells. *Br. J. Dermatol.* 159, 847–857. doi: 10.1111/j.1365-2133.2008.08774.x

Knowles, C. H., and Aziz, Q. (2009). Basic and clinical aspects of gastrointestinal pain. *Pain* 141, 191–209. doi: 10.1016/j.pain.2008.12.011

Langlois, L., Meleine, M., Ouelaa, W., Caremel, R., Bridoux, V., Benard, M., et al. (2015). Acute sacral nerve stimulation reduces visceral mechanosensitivity in Rat through spinal opioid pathway. *Neurogastroenterol. Motil. Offic. J. Eur. Gastrointest. Motil. Soc.* 27, 816–823. doi: 10.1111/nmo.12555

Lee, K. N., and Lee, O. Y. (2016). The Role of Mast Cells in Irritable Bowel Syndrome. *Gastroenterol. Res. Pract.* 2016:2031480. doi: 10.1155/2016/2031480

Lennon, E. M., Borst, L. B., Edwards, L. L., and Moeser, A. J. (2018). Mast Cells Exert Anti-Inflammatory Effects in an IL10(-/-) Model of Spontaneous Colitis. *Mediat. Inflamm.* 2018:7817360. doi: 10.1155/2018/7817360

Leung, K. B., and Pearce, F. L. (1984). A comparison of histamine secretion from peritoneal mast cells of the rat and hamster. *Br. J. Pharmacol.* 81, 693–701. doi: 10.1111/j.1476-5381.1984.tb16136.x

Li, Q., Winston, J. H., and Sarna, S. K. (2016). Noninflammatory upregulation of nerve growth factor underlies gastric hypersensitivity induced by neonatal colon inflammation. *Am. J. Physiol. Regulat. Integrat. Comparat. Physiol.ogy* 310, R235–R242. doi: 10.1152/ajpregu.00342.2015

Liu, S., Xia, Y., Hu, H., Ren, J., Gao, C., and Wood, J. D. (2000). Histamine H3 receptor-mediated suppression of inhibitory synaptic transmission in the submucous plexus of guinea-pig small intestine. *Eur. J. pharmacol.* 397, 49–54. doi: 10.1016/s0014-2999(00)00228-4

Locke, G. R. III, Talley, N. J., Fett, S. L., Zinsmeister, A. R., and Melton, L. J. III (1997). Prevalence and clinical spectrum of gastroesophageal reflux: a population-based study in Olmsted County, Minnesota. *Gastroenterology* 112, 1448–1456. doi: 10.1016/s0016-5085(97)70025-8

Lundby, L., Møller, A., Buntzen, S., Krogh, K., Vang, K., Gjedde, A., et al. (2011). Relief of fecal incontinence by sacral nerve stimulation linked to focal brain activation. *Dis. Colon Rectum* 54, 318–323.

Ma, T. Y., Iwamoto, G. K., Hoa, N. T., Akotia, V., Pedram, A., Boivin, M. A., et al. (2004). TNF-alpha-induced increase in intestinal epithelial tight junction permeability requires NF-kappa B activation. *Am. J. Physiol. Gastrointest. Liver Physiol.* 286, G367–G376. doi: 10.1152/ajpgi.00173.2003

Manni, L., and Aloe, L. (1998). Role of IL-1 beta and TNF-alpha in the regulation of NGF in experimentally induced arthritis in mice. *Rheumatol. Int.* 18, 97–102.

Masini, E., Fantozzi, R., Blandina, P., Brunelleschi, S., and Mannaioni, P. F. (1983). Muscarinic cholinergic receptor binding in rat mast cells. *Agents Actions* 13, 327–332. doi: 10.1007/BF01971484

Masini, E., Fantozzi, R., Conti, A., Blandina, P., Brunelleschi, S., and Mannaioni, P. F. (1985). Mast cell heterogeneity in response to cholinergic stimulation. *Int. Arch. Allergy Appl. Immunol.* 77, 184–185. doi: 10.1159/000233780

Ohman, L., and Simren, M. (2010). Pathogenesis of IBS: role of inflammation, immunity and neuroimmune interactions. *Nat. Rev. Gastroenterol. Hepatol.* 7, 163–173. doi: 10.1038/nrgastro.2010.4

O'Sullivan, M., Clayton, N., Breslin, N. P., Harman, I., Bountra, C., McLaren, A., et al. (2000). Increased mast cells in the irritable bowel syndrome. *Neurogastroenterol. Motil. Offic. J. Eur. Gastrointest. Motil. Soc.* 12, 449–457. doi: 10.1046/j.1365-2982.2000.00221.x

Ouyang, H., and Chen, J. D. (2004). Review article: therapeutic roles of acupuncture in functional gastrointestinal disorders. *Alimentary Pharmacol. Therapeut.* 20, 831–841. doi: 10.1111/j.1365-2036.2004.02196.x

Peiris, M., Bulmer, D. C., Baker, M. D., Boundouki, G., Sinha, S., Hobson, A., et al. (2011). Human visceral afferent recordings: preliminary report. *Gut* 60, 204–208. doi: 10.1136/gut.2010.221820

Peters, K. M., Feber, K. M., and Bennett, R. C. (2007). A prospective, single-blind, randomized crossover trial of sacral vs pudendal nerve stimulation for interstitial cystitis. *BJU Int.* 100, 835–839.

Pusceddu, M. M., and Gareau, M. G. (2018). Visceral pain: gut microbiota, a new hope? *J. Biomed. Sci.* 25:73. doi: 10.1186/s12929-018-0476-7

Raychaudhuri, S. P., and Raychaudhuri, S. K. (2004). Role of NGF and neurogenic inflammation in the pathogenesis of psoriasis. *Progress Brain Res.* 146, 433–437. doi: 10.1016/S0079-6123(03)46027-5

Robles, A., Perez Ingles, D., Myneedu, K., Deoker, A., Sarosiek, I., Zuckerman, M. J., et al. (2019). Mast cells are increased in the small intestinal mucosa of patients with irritable bowel syndrome: A systematic review and meta-analysis. *Neurogastroenterol. Motil. Offic. J. Eur. Gastrointest. Motil. Soc.* 31, e13718. doi: 10.1111/nmo.13718

Sengupta, J. N. (2009). Visceral pain: the neurophysiological mechanism. *Handb. Exp. Pharmacol.* 194, 31–74. doi: 10.1007/978-3-540-79090-7_2

Skaper, S. D. (2001). Nerve growth factor: a neurokine orchestrating neuroimmune-endocrine functions. *Mol. Neurobiol.* 24, 183–199. doi: 10.1385/MN:24:1-3:183

Stanzel, R. D., Lourenssen, S., and Blennerhassett, M. G. (2008). Inflammation causes expression of NGF in epithelial cells of the rat colon. *Exp. Neurol.* 211, 203–213. doi: 10.1016/j.expneurol.2008.01.028

Sun, P., Zhou, K., Wang, S., Li, P., Chen, S., Lin, G., et al. (2013). Involvement of MAPK/NF-κB signaling in the activation of the cholinergic anti-inflammatory pathway in experimental colitis by chronic vagus nerve stimulation. *PLoS One* 8:e69424. doi: 10.1371/journal.pone.0069424

Swartz, E. M., and Holmes, G. M. (2014). Gastric vagal motoneuron function is maintained following experimental spinal cord injury. *Neurogastroenterol. Motil. Offic. J. Eur. Gastrointest. Motil. Soc.* 26, 1717–1729. doi: 10.1111/nmo.12452

Takahashi, T. (2006). Acupuncture for functional gastrointestinal disorders. *J. Gastroenterol.* 41, 408–417. doi: 10.1007/s00535-006-1773-6

Thin, N. N., Horrocks, E. J., Hotouras, A., Palit, S., Thaha, M. A., Chan, C. L., et al. (2013). Systematic review of the clinical effectiveness of neuromodulation in the treatment of faecal incontinence. *Br. J. Surg.* 100, 1430–1447.

Tsang, S. W., Zhao, M., Wu, J., Sung, J. J., and Bian, Z. X. (2012). Nerve growth factor-mediated neuronal plasticity in spinal cord contributes to neonatal maternal separation-induced visceral hypersensitivity in rats. *Eur. J. Pain* 16, 463–472. doi: 10.1016/j.ejpain.2011.07.005

Tu, L., Gharibani, P., Yang, Y., Zhang, B., Ji, F., Yin, J., et al. (2020a). A Novel Approach in Spinal Cord Stimulation for Enhancing Gastric Motility: A Preliminary Study on Canines. *J. Neurogastroenterol. Motil.* 26, 147–159. doi: 10.5056/jnm19101

Tu, L., Gharibani, P., Yin, J., and Chen, J. D. Z. (2020b). Sacral nerve stimulation ameliorates colonic barrier functions in a rodent model of colitis. *Neurogastroenterol. Motil. Offic. J. Eur. Gastrointest. Motil. Soc.* 2020, e13916. doi: 10.1111/nmo.13916

Tu, L., Gharibani, P., Zhang, N., Yin, J., and Chen, J. D. (2020c). Anti-inflammatory effects of sacral nerve stimulation: a novel spinal afferent and vagal efferent pathway. *Am. J. Physiol. Gastrointest. Liver Physiol.* 318, G624–G634. doi: 10.1152/ajpgi.00330.2019

Vivinus-Nebot, M., Dainese, R., Anty, R., Saint-Paul, M. C., Nano, J. L., Gonthier, N., et al. (2012). Combination of allergic factors can worsen diarrheic irritable bowel syndrome: role of barrier defects and mast cells. *Am. J. Gastroenterol.* 107, 75–81. doi: 10.1038/ajg.2011.315

Whorwell, P. J. (2015). IBS in 2014: Developments in pathophysiology, diagnosis and management. *Nat. Rev. Gastroenterol. Hepatol.* 12, 72–74. doi: 10.1038/nrgastro.2014.225

Winston, J. H., and Sarna, S. K. (2016). Enhanced sympathetic nerve activity induced by neonatal colon inflammation induces gastric hypersensitivity and anxiety-like behavior in adult rats. *Am. J. Physiol. Gastrointest. Liver physiol.* 311, G32–G39. doi: 10.1152/ajpgi.00067.2016

Xia, C. M., Colomb, D. G. Jr., Akbarali, H. I., and Qiao, L. Y. (2011). Prolonged sympathetic innervation of sensory neurons in rat thoracolumbar dorsal root ganglia during chronic colitis. *Neurogastroenterol. Motil. Offic. J. Eur. Gastrointest. Motil. Soc.* 23, 801–e339. doi: 10.1111/j.1365-2982.2011.01728.x

Xu, X. J., Zhang, Y. L., Liu, L., Pan, L., and Yao, S. K. (2017). Increased expression of nerve growth factor correlates with visceral hypersensitivity and impaired gut barrier function in diarrhoea-predominant irritable bowel syndrome: a preliminary explorative study. *Alimentary Pharmacol. Therapeut.* 45, 100–114. doi: 10.1111/apt.13848

Yamamoto, T., Kodama, T., Lee, J., Utsunomiya, N., Hayashi, S., Sakamoto, H., et al. (2014). Anti-allergic role of cholinergic neuronal pathway via alpha7 nicotinic ACh receptors on mucosal mast cells in a murine food allergy model. *PLoS One* 9:e85888. doi: 10.1371/journal.pone.0085888

Yampolsky, C., Hem, S., and Bendersky, D. (2012). Dorsal column stimulator applications. *Surg. Neurol. Int.* 3(Suppl. 4), S275–S289. doi: 10.4103/2152-7806.103019

Yang, J., Shang, B., Shi, H., Zhu, S., Lu, G., and Dai, F. (2019). The role of toll-like receptor 4 and mast cell in the ameliorating effect of electroacupuncture on visceral hypersensitivity in rats. *Neurogastroenterol. Motil. Offic. J. Eur. Gastrointest. Motil. Soc.* 31, e13583. doi: 10.1111/nmo.13583

Yin, J., Chen, J., and Chen, J. D. (2010a). Ameliorating effects and mechanisms of electroacupuncture on gastric dysrhythmia, delayed emptying, and impaired accommodation in diabetic rats. *Am. J. Physiol. Gastrointest. Liver Physiol.* 298, G563–G570. doi: 10.1152/ajpgi.00252.2009

Yin, J., Wang, W., Winston, J. H., Zhang, R., and Chen, J. D. (2010b). Ameliorating effects of mirtazapine on visceral hypersensitivity in rats with neonatal colon sensitivity. *Neurogastroenterol. Motil. Offic. J. Eur. Gastrointest. Motil. Soc.* 22, 1022.–1028. doi: 10.1111/j.1365-2982.2010.01526.x

Youakim, A., and Ahdieh, M. (1999). Interferon-gamma decreases barrier function in T84 cells by reducing ZO-1 levels and disrupting apical actin. *Am. J. Physiol.* 276(5 Pt 1), G1279–G1288.

Zhang, L., Song, J., and Hou, X. (2016). Mast Cells and Irritable Bowel Syndrome: From the Bench to the Bedside. *J. Neurogastroenterol. Motil.* 22, 181–192. doi: 10.5056/jnm15137

Zhang, N., Zhang, H., Jiang, L., Zhang, S., Yin, J., Schramm, L., et al. (2020). A novel method of sacral nerve stimulation for colonic inflammation. *Neurogastroenterol. Motil. Offic. J. Eur. Gastrointest. Motil. Soc.* 32:e13825. doi: 10.1111/nmo.13825

Conflict of Interest: The authors declare that the research was conducted in the absence of any commercial or financial relationships that could be construed as a potential conflict of interest.

frontiers in Neuroscience

ORIGINAL RESEARCH
published: 26 October 2021
doi: 10.3389/fnins.2021.620750

Prediction of Deep Brain Stimulation Outcome in Parkinson's Disease With Connectome Based on Hemispheric Asymmetry

Jingqi Wang[1†], Ruihong Shang[1†], Le He[2], Rongsong Zhou[3], Zhensen Chen[4], Yu Ma[3] and Xuesong Li[1*]*

[1] School of Computer Science and Technology, Beijing Institute of Technology, Beijing, China, [2] Department of Biomedical Engineering, Center for Biomedical Imaging Research, School of Medicine, Tsinghua University, Beijing, China, [3] Department of Neurosurgery, Tsinghua University Yuquan Hospital, Beijing, China, [4] Department of Radiology, University of Washington, Seattle, WA, United States

OPEN ACCESS

Edited by:
Leo Cheng,
The University of Auckland,
New Zealand

Reviewed by:
Kazutaka Takahashi,
University of Chicago, United States
Ningfei Li,
Charité—Universitätsmedizin Berlin,
Germany

***Correspondence:**
Yu Ma
mayu@tsinghua.edu.cn
Xuesong Li
lixuesong@bit.edu.cn

[†] These authors have contributed equally to this work

Specialty section:
This article was submitted to Neuroprosthetics, a section of the journal Frontiers in Neuroscience

Received: 27 October 2020
Accepted: 28 September 2021
Published: 26 October 2021

Citation:
Wang J, Shang R, He L, Zhou R, Chen Z, Ma Y and Li X (2021) Prediction of Deep Brain Stimulation Outcome in Parkinson's Disease With Connectome Based on Hemispheric Asymmetry. Front. Neurosci. 15:620750. doi: 10.3389/fnins.2021.620750

Parkinson's disease (PD) is a neurodegenerative disease that is associated with motor and non-motor symptoms and caused by lack of dopamine in the substantia nigra of the brain. Subthalamic nucleus deep brain stimulation (STN-DBS) is a widely accepted therapy of PD that mainly inserts electrodes into both sides of the brain. The effect of STN-DBS was mainly for motor function, so this study focused on the recovery of motor function for PD after DBS. Hemispherical asymmetry in the brain network is considered to be a potential indicator for diagnosing PD patients. This study investigated the value of hemispheric brain connection asymmetry in predicting the DBS surgery outcome in PD patients. Four types of brain connections, including left intra-hemispheric (LH) connection, right intra-hemispheric (RH) connection, inter-hemispheric homotopic (Ho) connection, and inter-hemispheric heterotopic (He) connection, were constructed based on the resting state functional magnetic resonance imaging (rs-fMRI) performed before the DBS surgery. We used random forest for selecting features and the Ridge model for predicting surgical outcome (i.e., improvement rate of motor function). The functional connectivity analysis showed that the brain has a right laterality: the RH networks has the best correlation (r = 0.37, p = 5.68E-03) between the predicted value and the true value among the above four connections. Moreover, the region-of-interest (ROI) analysis indicated that the medioventral occipital cortex (MVOcC)–superior temporal gyrus (STG) and thalamus (Tha)–precentral gyrus (PrG) contributed most to the outcome prediction model for DBS without medication. This result provides more support for PD patients to evaluate DBS before surgery.

Keywords: hemispheric asymmetry, functional connectivity, important feature, resting state functional magnetic resonance imaging (rfMRI), Parkinson's disease, improvement of motor function, subthalamic nucleus deep brain stimulation (STN-DBS)

INTRODUCTION

Parkinson's disease (PD) is a common degenerative disease of the nervous system, including motor symptoms such as retardation, tremor, and muscle rigidity and non-motor symptoms. Subthalamic nucleus deep brain stimulation (STN-DBS) is a widely accepted therapy for PD, especially when the dopaminergic replacement therapy is unsatisfactory (Kleiner-Fisman et al., 2006). This technique was also used in the pallidum and the STN (Benabid, 2003). DBS can significantly reduce the freeing of gait (Xie et al., 2012), tremor, dyskinesia, or postural instability (Weaver et al., 2005) and thereby improve the quality of life. DBS can also reduce the non-motor symptoms (Hwynn et al., 2011) in PD patients. However, DBS could not ensure a significant therapeutic effect on each patient. In spite of a careful patient selection before the operation, some patients may still show limited or no improvement of their motor functions after surgery. On the other hand, DBS surgery is expensive at the moment. Therefore, how to evaluate the possible therapeutic improvement of each patient especially before the surgery is a question that deserves serious consideration.

A growing number of studies suggest that the variability in treatment response may be linked to cortical blood flow changes (Campbell et al., 2008; Quraan et al., 2014). Research showed that cortical blood flow change abnormalities in patients with schizophrenia may be related to the treatment response to stress symptoms (Masuda et al., 2000). Early scalp acupuncture treatment can speed up the cortical blood flow of patients with acute ischemic stroke, thereby promoting the recovery of motor function (Li et al., 2005). Resting-state functional magnetic resonance imaging (rs-fMRI) is related to cortical blood flow, and the method of analyzing rs-fMRI is usually to construct a brain network. Therefore, the brain network is shown to have great potential in predicting the treatment outcome (van Waarde et al., 2015; Kawahara et al., 2017). Human brain networks can be characterized by estimating interregional synchronization of neural function with rs-fMRI. This study focuses on rs-fMRI instead of task-related fMRI data. There are many measurements (small-worldness, clustering coefficient, local efficiency, modularity, and rich-hub) (Kaiser, 2008) to assess information exchange and processing of the human brain networks, which can be measured after the brain network is converted into a weighted graph. Analyses of functional networks could provide complementary insights into brain organization under pathological conditions. For example, compared to healthy controls, PD patients have lower clustering coefficient and local efficiency (Luo et al., 2015b) and have impaired corticostriatal network pathways and related neural circuits (Hacker et al., 2012).

The dopaminergic denervation of the striatum in PD occurs asymmetrically at the beginning and becomes bilateral gradually along with the disease progression (Hornykiewicz, 1966). As such, the accompanying motor dysfunction symptoms (bradykinesia, tremor, and rigidity) usually begin on the side contralateral to the most affected nigrostriatal pathway and later spread to the opposite side. This study of the striatum in PD indicated that the hemispheric asymmetry of functional connectivity is an important factor that may affect brain network organization, which has been demonstrated in healthy subjects (Tian et al., 2011), patients with Alzheimer's disease and mild cognitive impairment (Yang et al., 2017), and patients with neuropsychiatric disorders (Sun et al., 2015). It has been well documented that the brain network of PD patients tend to show asymmetry (Luo et al., 2015a).

Machine learning as a powerful data-driven method has been widely used in outcome prediction, including outcome of the DBS surgery (Bermudez et al., 2019; Habets et al., 2020). In this paper, we aimed at creating a machine learning model based on functional connectivity profiles to predict the possible improvements of motor function before the DBS surgery. This model could help us pick out the unsuitable patients. More importantly, the machine learning methods may reveal the potential components that limit the effect of the surgery and help physician improve the technique. This study involves the assessment of preoperative rs-fMRI for predicting the DBS-based improvements of motor function as measured by the Unified Parkinson's Disease Rating Scale (UPDRS-III) score. Four brain networks were constructed for topological analysis, including intrahemisphere connectivity [left-hemispheric (LH) network and right-hemispheric (RH) network] and inter-hemisphere connectivity [homotopic (Ho: the edges link the geometrically corresponding regions in the two hemispheres) network and heterotopic (He: the edges link the geometrically non-corresponding regions in the two hemispheres) network]. The random forest algorithm (Liaw and Wiener, 2002) was used for feature selection, and the Ridge model was used to predict the improvement of motor function after the DBS surgery in each brain (LH, RH, Ho, and He) network. Pearson analysis was performed on the predicted improvement rate and the real improvement rate to obtain Pearson's r and Pearson's p-values, which were used to evaluate the correlation between brain asymmetry and the improvement rate after DBS surgery. In order to study whether this correlation is affected by age and gender, we divided patients into younger and older groups and divided them into male and female groups.

MATERIALS AND METHODS

Participants

This study was approved by the Ethics Committee of Tsinghua University Yuquan Hospital. All participants gave written informed consent. This study included 55 patients whose age ranged from 29 to 77 in Tsinghua University Yuquan Hospital, Beijing, China, who were diagnosed with idiopathic PD according to the UK PD Society Brain Bank criteria. The exclusion criteria included (1) severe suicidal tendency; (2) pregnant or lactating women; (3) a history of physical diseases that can affect the assessment of PD such as intracranial tumors and communicating hydrocephalus; (4) a history of organic brain disorders such as cerebellum injury, neurological disorders such as repeated strokes, severe dementia at an early stage accompanied by memory, language, and behavior disorders, and other psychiatric disorders; and (5) a history of substance abuse,

including tobacco, alcohol, or other psychoactive substances. All participants were right dominant based on screening questions.

The DBS surgery outcome was measured in a medication-off condition where levodopa should not be taken 12 h presurgery or postsurgery by the motor section of the UPDRS-III scale (Antonini et al., 2013). This scale was proposed by a team with more than 10 years' experience. All patients were on levodopa prior to the study. A small number of patients may have mild confusion after taking levodopa for 1 h. These symptoms will disappear within 12 h of stopping the medicine. UPDRS-III is one of the four scales of UPDRS, a clinical scoring system, which is used to judge the motor function of the pre-operation and post-operation of each participant. There are 27 items in UPDRS-III, and each item is divided into a four-level index, from 0 to 4, where 0 is normal and 4 is serious. It is often used to assess the patient's progress. For the 55 selected PD patients, the UPDRS-III score was measured twice before and 6 months after the DBS surgery. At least two doctors took the measurement and averaged each time. Among them, presurgical scoring and postsurgical scoring were performed routinely, independent of the study and blind to the analysis outcomes. The physicians who program the DBS and the people who measure these scores after surgery were blinded to the analysis. The mean preoperative and postoperative scores were 43.79 ± 11.78 and 15.35 ± 10.67, and all patients had lower scores after surgery, with a lower UPDRS-III score and higher degree of motor function. The improvement of motor function after DBS surgery is assessed by the △UPDRS-III rate = $(\text{UPDRS-III}_{\text{presurgery}} - \text{UPDRS-III}_{\text{postsurgery}})/\text{UPDRS-III}_{\text{presurgery}}$. The mean △UPDRS-III rate of 55 tested PD patients is $65.62\% \pm 20.48\%$.

Surgical Procedure

DBS surgery was performed using a Leksell stereotaxic frame (Elekta AB, Stockholm, Sweden) under local anesthesia. During the surgery, the micro-electrodes and STN-DBS electrodes (PINS L301, Beijing, China) were placed in the left and right hemispheres of the brain. The microelectrodes were used to record, and then STN-DBS were implanted bilaterally for stimulation to evaluate and confirm the site where the best clinical effect can be obtained. After confirming the placement of the lead, a pulse generator (G102R, PINS, Beijing, China) was used to connect the electrodes and was implanted subcutaneously into the right subclavian region. The optimal stimulation patterns with the highest UPDRS score and maximum improvement rate were selected according to the actual situation of the patient.

Image Acquisition

The rs-fMRI, high-resolution T1-weighted structural MRI data and T2-weighted structural MRI data were acquired on each participant at Tsinghua University using a 3T Philips Achieva rs-fMRI scanner equipped with a 32-channel head coil. Imaging parameters of rs-fMRI were 35 axial slices; repetition time (TR) = 2,000 ms; scan length in time = 8 min; echo time (TE) = 30 ms; flip angle (FA) = 90°; slice thickness = 4 mm; acquisition matrix = 64 × 64; field of view (FOV) = 224 × 224 mm^2. Imaging parameters of T1-weighted MRI were as follows: TR/TE = 7.46 ms/3.73 ms, FOV = 256 × 256 mm^2, acquisition matrix = 256 × 256 × 160, slice thickness = 1.0 mm.

The rs-fMRI (8 min) was performed 2–3 days before the operation, and the participants were asked not to take levodopa for more than 12 h before the scanning to keep medication off. Patients were instructed to relax with their eyes closed and to not fall asleep during the scan.

The purpose of the research is to use preoperative images to evaluate postoperative effects, and rs-fMRI can do the prediction and other analyses. Due to the acquisition conditions, only rs-fMRI before DBS surgery can be acquired, so the UPDRS-III score was used to indicate the improvement of the PD patient's motor function after the DBS surgery. In brief, rs-fMRI before DBS surgery was used to evaluate the improvement rate of motor function after the DBS surgery.

Image Preprocessing and Brain Network Construction

In the preprocessing of the rs-fMRI data, the first 10 volumes of each participant were discarded to ensure magnetization equilibrium, slice timing was corrected with the first slice, and head motion was corrected by aligning all image volumes with the first volume. In human rs-fMRI data, a 0.01–0.1 Hz band pass filter was commonly used to keep only the interesting frequencies and discard potential noise sources, including the heart rate and respiration rate, which were ∼1.3 and ∼0.2 Hz, respectively. Higher-frequency signals were considered as noise or physiological signals, which are not neuron signal. In order to perform the group analysis, the functional images were co-registered to the same participant's T1-weighted structural image, which was normalized to the Montreal Neurological Institute template space.

GRETNA software was used to construct the whole-brain functional network (246 × 246) (Wang et al., 2015) for each participant. The nodes of the brain networks come from the brain segmentation based on the Brainnetome Atlas (BNA) (Fan et al., 2016), which parcellated the whole brain into 210 (105 for each hemisphere) cortical and 36 subcortical regions of interest (ROIs). Then the Pearson correlation coefficients of the rs-fMRI signal between each two ROIs were computed to acquire a whole-brain functional network.

Four brain networks were constructed for topological analysis, i.e., LH network, RH network, Ho network, and He network, as illustrated in **Figure 1**.

Connectome-Based Predictive Modeling

For each of the four aforementioned networks (i.e., LH, RH, Ho, and He), the Ridge model was trained to predict the improvement rate of motor function after DBS. For each network, upper triangle elements were used for the input of the Ridge model. Ridge regression has been used as a statistical tool to address the small sample size issue since the 1970s (Hoerl and Kennard, 1970). With the regression coefficient being limited, Ridge regression is free from overfitting and high variances associated with correlated coefficients. Therefore, Ridge regression has many advantages over the traditional

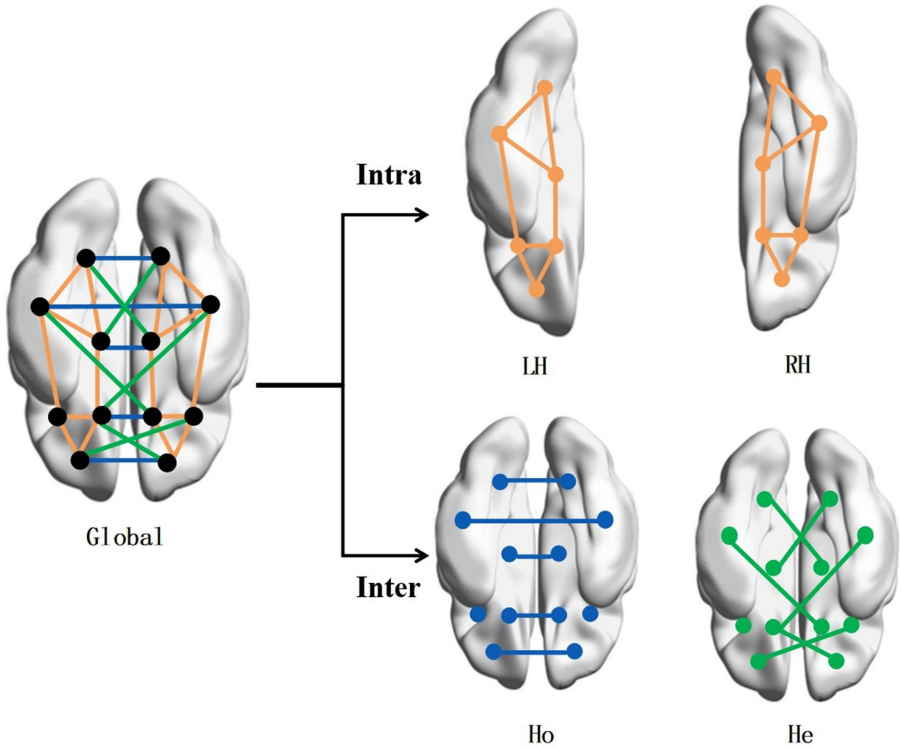

FIGURE 1 | Brain network construction. To study the correlation of brain symmetry on the off-rate of DBS, the brain network is built by intra- and inter-hemispheric connectivity. The connection types include intra-left-hemispheric (LH), intra-right-hemispheric (RH), inter-hemispheric homotopic (Ho), and inter-hemispheric heterotopic (He).

multiple-regression models, and it can effectively deal with a large number of predictor variables that are far more than the number of subjects (Li et al., 2006).

Since brain signals are rich and redundant, it is necessary to perform a feature selection strategy to narrow the range of features (i.e., functional connections) for each network. Here, we use the random forest algorithm (Liaw and Wiener, 2002) to select important features for each brain (LH/RH/Ho/He) network. The random forest algorithm is time-efficient in training and can detect the mutual influence between connections as features and therefore is suitable for selecting the most important connections in this study. In this paper, the random forest feature extraction algorithm of the network (LH/RH/Ho/He) is given from the connection information of all cortical region pairs in each network. After the feature vector (upper triangle elements) of the training set was input into the random forest, the importance of each feature (i.e., connection) can be obtained, and only the features with higher importance were retained. Then the retained feature set was applied into the testing set.

The random forest algorithm in this paper was used to extract d times from the d features of the LH, RH, Ho, and He networks with replacement, obtain a sample set, and input it into a decision tree, which is repeated 20 times. In this way, 20 sample sets were each input into 20 decision trees. In the extraction process, the data that were not extracted each time were used as out-of-bag data (OOB). This part of the data can be used for the screening of important features: first, the OOB data error (errOOB1) was calculated, and then noise was added randomly to the feature X of all samples of the OOB data to calculate the OOB error (errOOB2) with noise. The importance of the feature was assessed by $X = \sum \frac{(\text{errOOB2} - \text{errOOB1})}{20}$, and then features with an importance higher than 0.005 were selected. The selected features were less affected by noise, and the prediction was more stable. In the Ridge model, for each topic, we used the percentage UPDRS improvement score and the numerical connection values of the above-mentioned cortical region pairs found from the random forest search (i.e., weights). These were used to train the classifier in a nested leave-one-out cross-validation (LOOCV) approach. And the "leave one" here meant leaving a subject in the training-and-test split. The leave-one-out method was also used for group analysis.

We adopted nested cross-validation including an inner fivefold cross-validation and outer LOOCV to measure prediction accuracy. The structural risk minimization of the Ridge model was equal to the sum of the loss function and regularization (L2 norm). The optimal solution was obtained when the loss function value was as small as possible. The inner fivefold cross-validation was used to determine the optimal parameters (e.g., α and max_iter) for the Ridge model by the grid search method, and LOOCV was used to evaluate the generalizability of the model. α balances the relationship between

the two parts of the $J(\theta) = MSE(y, \widehat{y}; \theta) + \alpha \frac{1}{2} \sum_{i=1}^{n} \theta_i^2$ in the loss function (MSE was the mean square error, which was a function of network performance), so that the error is as small as possible, and max_iter is the number of repetitions of the process of calculating the loss function of the full sample and performing a unified gradient update. The R-squared value of the Ridge formulation is slightly lower than that of ordinary regression analysis, but the significance of the regression coefficient is often significantly higher than that of ordinary regression. The R-squared value is between 0 and 1. The closer to 1, the better the fitting effect. In the four networks, the R-squared value of LH is 0.67, the R-squared value of RH is 0.72, the R-squared value of Ho is 0.64, and the R-squared value of He is 0.5. The features come from a vector of (N, d), where N is the number of people and each person is a d-dimensional vector. This d-dimensional vector comes from the network (LH, RH, Ho, and He) of each person. There are d column vectors that are d features. The importance features are selected by random forest. The selected features and actual △UPDRS-III rate of patients were used as input in each training procedure of inner and outer loops. The weighting of each feature (i.e., connection) was determined via the model training and then used to predict the △UPDRS-III rate of patients. Then, two indicators (i.e., Pearson's r and Pearson's p) were utilized to measure the performance of predicting the model in each network.

Group Analysis

The age of the participants ranged from 29 to 77 (mean age = 58.15 ± 10.13) years. Studies have indicated age-based variations in rs-fMRI networks such that in 20–80-year age groups, some aspects of sensory and cognitive resting state networks show weakening with age (Varangis et al., 2019). To study the effect of age and gender on the correlation between brain asymmetry and the improvement of motor function after DBS surgery, we grouped patients by age and gender. There were 53 participants in the group analysis, excluding one patient with incomplete data and a 29-year-old patient to narrow the age span (previously 55 patients). The 53 patients were divided into two groups as evenly as possible according to age: 26 people aged 34–58 and 27 patients aged 59–77. Also, these 53 patients were divided into two groups according to gender: 29 males and 24 females. We used the leave-one-out method on feature selection and the classifier for age and gender group analyses. Inter-group feature selection was performed instead of intra-group.

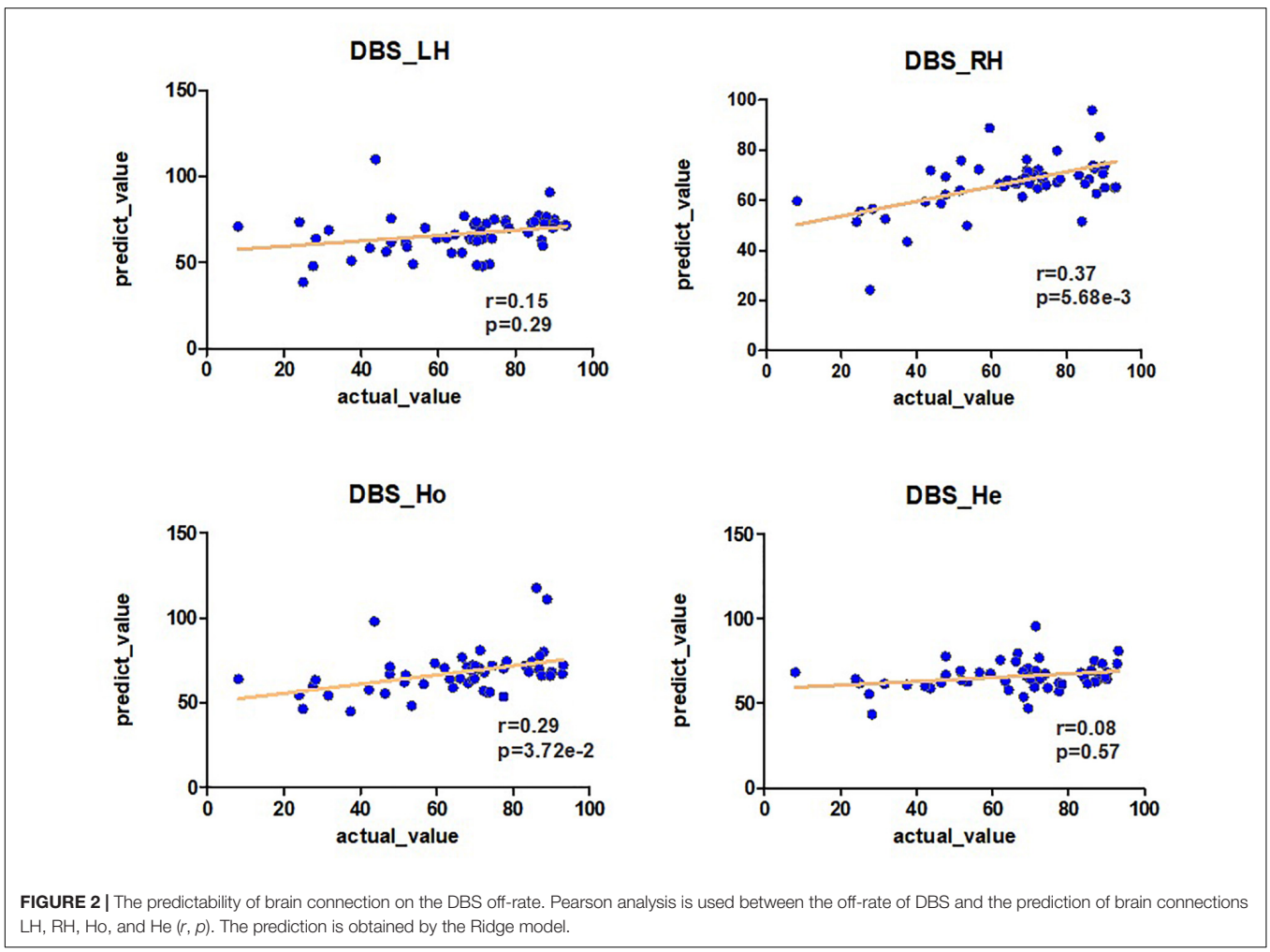

FIGURE 2 | The predictability of brain connection on the DBS off-rate. Pearson analysis is used between the off-rate of DBS and the prediction of brain connections LH, RH, Ho, and He (r, p). The prediction is obtained by the Ridge model.

TABLE 1 | The top 10 connections in LH **(A)** and RH **(B)** with higher importance in the prediction of the improvement rate in the UPDRS-III score after DBS surgery in the medication-off condition.

(A)				
ID	**Node name**	**ID**	**Node name**	**LH normalized connection value**
18	Cingulate gyrus (CG)	18	Cingulate gyrus (CG)	1
17	Insular gyrus (INS)	4	Orbital gyrus (OrG)	0.9
14	Inferior parietal lobule (IPL)	4	Orbital gyrus (OrG)	0.8
18	Cingulate gyrus (CG)	1	Superior frontal gyrus (SFG)	0.7
18	Cingulate gyrus (CG)	14	Inferior parietal lobule (IPL)	0.6
16	Postcentral gyrus (PoG)	15	Precuneus (PCun)	0.5
3	Inferior frontal gyrus (IFG)	11	Parahippocampal gyrus (PhG)	0.4
14	Inferior parietal lobule (IPL)	4	Orbital gyrus (OrG)	0.3
2	Middle frontal gyrus (MFG)	9	Inferior temporal gyrus (ITG)	0.2
23	Basal ganglia (BG)	3	Inferior frontal gyrus (IFG)	0.1
(B)				
ID	**Node name**	**ID**	**Node name**	**RH normalized connections value**
19	Medioventral occipital cortex (MVOcC)	7	Superior temporal gyrus (STG)	1
24	Thalamus (Tha)	5	Precentral gyrus (PrG)	0.9
11	Parahippocampal gyrus (PhG)	5	Precentral gyrus (PrG)	0.8
23	Basal ganglia (BG)	1	Superior frontal gyrus (SFG)	0.7
7	Superior temporal gyrus (STG)	13	Superior parietal lobule (SPL)	0.6
10	Fusiform gyrus (FuG)	5	Precentral gyrus (PrG)	0.5
24	Thalamus (Tha)	14	Inferior parietal lobule (IPL)	0.4
17	Insular gyrus (INS)	5	Precentral gyrus (PrG)	0.3
23	Basal ganglia (BG)	14	Inferior parietal lobule (IPL)	0.2
24	Thalamus (Tha)	8	Middle temporal gyrus (MTG)	0.1

1–6: Frontal; 7–12: Temporal; 13–16: Parietal; 17: Insular Lobe; 18: Limbic Lobe; 19, 20: Occipital Lobe; 21–24: Subcortical Nuclei.

The *r*- and *p*-values obtained by Pearson analysis were used as the evaluation of correlation.

RESULTS

Predicting Improvement in Motor Function After DBS

The *r*- and *p*-values were observed in the LH network (r = 0.15, p = 0.29), RH network (r = 0.37, p = 5.68E-03), Ho network (r = 0.29, p = 3.72E-02), and He network (r = 0.08, p = 0.57) as shown in **Figure 2** and **Table 1**. The above results were obtained by using the leave-one-out method in both the feature selection and the classifier.

For group analysis (age and gender), we used the leave-one-out method on both feature screening and classifiers. Inter-group feature screening was performed. Among the two groups divided by age mentioned by the participants, the results were as follows: r = 0.41, p = 0.04 for the younger group and r = 0.4, p = 0.04 for the older group in the LH network; r = 0.58, p = 1.35E-03 for the younger group and r = 0.43, p = 0.02 for the older group in the RH network; r = 0.42, p = 3.37E-02 for the younger group and r = 0.09, p = 0.66 for the older group in the Ho network; and r = 0.42, p = 2.9E-02 for the younger group and r = 0.34, p = 8.66E-02 for the older group in the He network as shown in **Supplementary Table 1A**. Patients were also grouped by gender (male and female), the results were as follows: r = 0.49, p = 8.71E-03 for the male group and r = 0.16, p = 0.47 for the female group in the LH network; r = 0.59, p = 7.18E-04 for the male group and r = 0.47, p = 1.5E-02 for the female group in the RH network; r = 0.21, p = 0.33 for the male group and r = 0.26, p = 0.18 for the female group in the Ho network; and r = 0.10, p = 0.60 for the male group and r = 0.69, p = 2.1E-04 for the female group in the He network as shown in **Supplementary Table 2A**. The comparisons of the results obtained by inter-group and intra-group feature selection in age and gender groups were shown in **Supplementary Tables 1, 2**.

For better interpretation, the four subcortical areas listed were lateralized. We grouped the 246 ROIs into 48 gyri (24 left gyri and 24 right gyri) defined by BNA and calculated the top 10 predictive connections between 24 hemispherical gyri in the LH/RH network. The gyri of each brain hemisphere were further divided into seven lobes, and the predictive connections selected by the Ridge model from the perspective of lobes are shown in **Figure 3**.

In predicting the DBS outcome, the connectome-based model showed the best correlation between the predicted value and the true value in the RH network, and the connection between medioventral occipital cortex (MVOcC) and superior temporal gyrus (STG) provided the largest contribution in the prediction. The top 10 predictive connections (measured by *r*) of the LH network and RH network are shown in **Table 2**, and the predictive connections of the Ho network and He network are shown in **Figure 4**.

DISCUSSION

In this study, we combine an rs-fMRI graph-based network with a machine learning prediction model to predict the DBS outcome based on brain hemispheric asymmetry. Previous studies on the DBS of PD mainly focused on the accuracy of surgery such as the Lead-DBS v2 method with precise electrode positioning (Horn et al., 2019), stimulation such as closed-loop DBS (Rosin et al., 2011), and treatment such as an omics method for prospective targeted therapy for refractory depression (Rivaposse et al., 2018), etc. In addition, research involving the prediction of brain asymmetry in PD patients had different statistical indicators from this study that were based on the value of voxel-mirrored homotopic connectivity to assess the asymmetry of the hemispheric function and its morphology (Gan et al., 2020), and there were also different prediction methods from this study using the human connectome as a connectivity profile (Horn et al., 2017). The brain asymmetry study that similarly

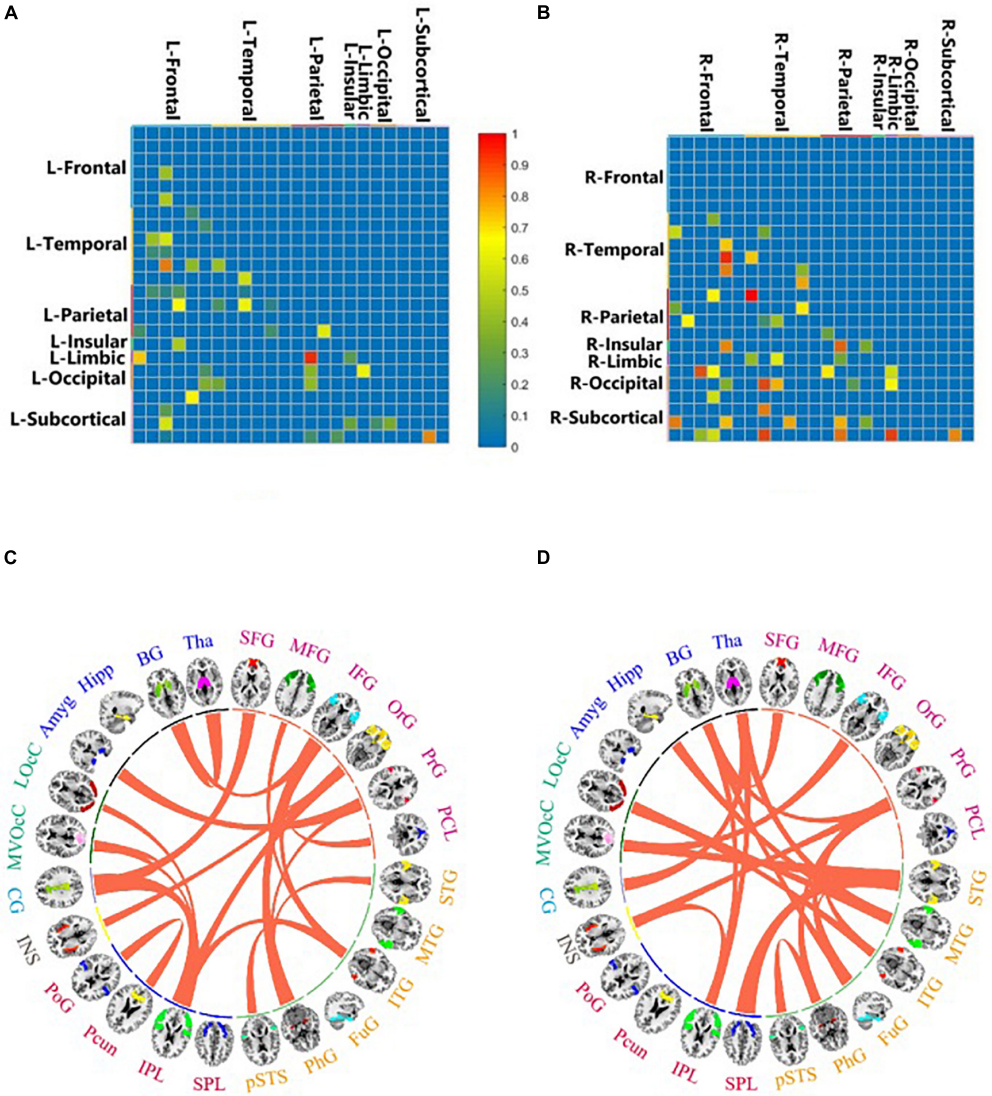

FIGURE 3 | Important brain connections by feature selection of LH **(A,C)** and RH **(B,D)**. The value is the important connection corresponding to the important feature selected by random forest. It ranges from 0 to 1, which is proportional to the importance of the brain connection. Important brain connections by prediction of LH **(C)** and RH **(D)**. This value is the important connection obtained by using the Ridge model for prediction. The important connections between 24 brain areas are connected by curves.

TABLE 2 | The correlation of the four networks for the improvement of motor function after DBS surgery.

	LH	RH	Ho	He
r, *p*	$r = 0.15$, $p = 0.29$	$r = 0.37$, $p = 5.68E-03$	$r = 0.29$, $p = 3.72E-02$	$r = 0.08$, $p = 0.57$

uses machine learning was the analysis of depression (Jiang et al., 2019), not an analysis of PD.

On the basis of stable prediction, further brain analysis could be conducted assisted by this preoperative predicting model. We were able to characterize networks associated with the outcome of DBS surgery therapy in 55 PD patients. Our findings might provide a potential neural biomarker that can detect the hemispheric asymmetry in brain networks for predicting the DBS outcome before surgery.

From the perspective of asymmetry, the degree of intra-nodes and inter-hemispheres reveals that network asymmetry is widely distributed in the human brain functional network. At the functional connection level, the DBS operation recovery of PD showed a rightward advantage in the brain. The RH and Ho networks had significantly predictive effects. It was also found that the symptoms of PD such as hallucinating, dreaming, and frequent dozing may be related to right-hemisphere dysfunction (Stavitsky et al., 2008), and late-stage PD patients exhibited greater atrophy in the bilateral occipital and right-hemisphere—predominant cortical areas

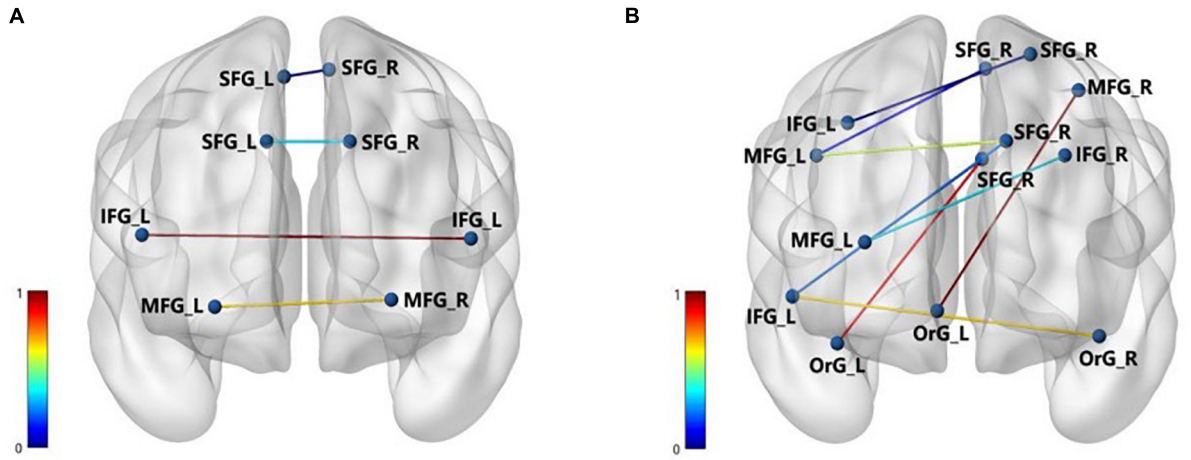

FIGURE 4 | The important brain connections of Ho **(A)** and He **(B)**. The nodes represent the corresponding brain area, and the edges are the important connection between the areas. The normalized values of the edges indicate the importance of brain connection.

(Claassen et al., 2016). Reduced structural connectivity in the right hemisphere of PD patients was also found with freezing of gait (Fling et al., 2013). STN-DBS with two electrodes provided the opportunity to modify stimulation parameters for each hemisphere (Lizarraga et al., 2017), which may alleviate the hemispheric asymmetry in PD patients.

In two groups divided by age, the results of inter-group feature selection showed that all four networks (LH, RH, Ho, and He) of the older group had a low correlation between the predicted value and the true value on the improvement of motor function after DBS surgery. The correlation of the RH network in both groups was higher than that of the LH network reflected by *r*-, *p*-values, and the contrast for laterality for the RH network was much clearer for the older group. As for two groups divided by gender, the RH network was most predictive in the male group, and the He network was most predictive in the female group, which significantly correlated with the improvement rate of DBS surgery in participants. Both male and female groups had significant laterality in the RH network. The male group had higher *r*-values in the LH and RH networks compared with the female group, while the female group had higher *r*-values in the Ho and He networks compared with the male group.

The connection between the MVOcC-STG and thalamus (Tha)–precentral gyrus (PrG) had the greatest contribution to the prediction of surgical outcome in the predictive model based on the RH network. It was reported that MVOcC was metabolically and structurally altered in PD (Ellmore et al., 2020). Compared with that in the HC group, STG exhibited significant reduction of nodal efficiency in PD patients with mild cognitive impairment (Wang et al., 2019), and the functional connectivity between left supramarginal–STG (Wiesman et al., 2016) in PD patients was reduced. The change in activity of Tha neurons in the motor circuits was identified as the most marked differences in PD (Halliday, 2009), and Tha was also considered as a suitable stimulation position for PD patients (Caparroslefebvre et al., 1994), which was centrally located in the pathway of the model of the basal ganglia motor circuit and can inhibit movement (Alexander et al., 1991; Kocabicak et al., 2012). The fibers from cerebellar deep nuclei to PrG were implicated in speech deterioration of PD patients (Fenoy et al., 2016). These ROIs are related to the symptoms of PD, indicating the effectiveness of the predictive model.

In the Ho and He networks, the top 10 predictive connections (measured by *r*) were all distributed in the inferior frontal gyrus (IFG), middle frontal gyrus (MFG), and superior frontal gyrus. These results indicated that the frontal lobe of the Ho and He networks played an important role in predicting the DBS outcome. It was widely accepted that the changes in cognitive function in PD were most closely related to the frontal lobe (Obeso et al., 2012). For the brain functional connection, the connections between the dorsolateral prefrontal cortex (DLPFC) and the IFG, superior frontal gyrus (SFG), and MFG in PD patients were significantly reduced (Dong et al., 2020). The frontal lobe "N30" status indicated the severity of PD movement and can effectively respond to dopamine deficiency (Claassen et al., 2016). "N30" resulted from distinct oscillating and phasic generators in the frontal cortex, and the "N30" component of somatosensory evoked potentials has been recognized as a crucial index of brain sensorimotor processing and has been increasingly used clinically (Cebolla et al., 2011). From the perspective of brain biomarkers, the accumulation of Lewy body in the frontal lobe was related to the risk of PD (Crane et al., 2016). In terms of the improvement rate of UPDRS-III for PD patients, the frontal cortex thickness and cortical atrophy in the frontal lobe may be an obvious predictor of poor prognosis of PD patients after STN-DBS (Muthuraman et al., 2017).

In the LH network, the top 10 predictive connections (measured by *r*) were almost distributed in the inferior parietal lobule (IPL), postcentral gyrus (PoG), and precuneus (Pcun), which indicated that the parietal lobe of the LH network may show great correlation for predicting the outcome after DBS.

Previous studies have shown that PD-related cognitive patterns (PDCPs) were characterized by reduced metabolism in the frontal and parietal regions (Huang et al., 2007), which also confirmed the above-mentioned correlation between the frontal lobe of the He and Ho networks in PD patients. For the motor sequence learning task for PD, it was found that a longitudinal decline in activation was related to learning of motor function in the parietal lobe region (Carbon and Eidelberg, 2006). In the case of ON and OFF STN-DBS, gait images can induce activity in the auxiliary movement area and the upper right parietal lobule (Weiss et al., 2015).

There are several limitations in our study. Firstly, the sample size is relatively small for machine learning techniques, which may limit the predictive performance of the generated model. Besides, the existing asymmetry in the cortical structure may bring bias to the experiment. Although symmetrical templates were used, the influence of methodological asymmetry cannot be completely eliminated.

CONCLUSION

In this study, we predicted the DBS outcome based on brain hemispheric asymmetry in 55 PD patients. By using random forest to select the important connections and the Ridge model with suitable parameters to predict the improvement rate in UPDRS-III, we proved that the RH network can better predict the improvement rate among the four intra- and inter-brain networks (LH, RH, Ho, and He). Besides, the ROI analysis showed that MVOcC-STG and Tha-PrG of the RH network contributed most in predicting the improvement rate in DBS surgery in the medication-off condition, which has a clinical significance for the presurgical analysis of DBS.

DATA AVAILABILITY STATEMENT

The raw data supporting the conclusions of this article will be made available by the authors, without undue reservation.

ETHICS STATEMENT

The studies involving human participants were reviewed and approved by the Ethics Committee of Tsinghua University Yuquan Hospital. The patients/participants provided their written informed consent to participate in this study. Written informed consent was obtained from the individual(s) for the publication of any potentially identifiable images or data included in this article.

AUTHOR CONTRIBUTIONS

RS and JW conduct experiments and wrote the manuscript. LH: search information and conduct experiments. RZ conduct experiments and get the original data set. ZC participate in the writing and revision of the manuscript. YM conduct experiments, obtain original data set, and supervise the completion of the project. XL determine the subject, participate in experimental design, and assist in writing the manuscript. All authors contributed to the article and approved the submitted version.

FUNDING

This study was supported by the Capital Health Research and Development of Special (Grant number: 2020-2-4141).

ACKNOWLEDGMENTS

We acknowledge Beihang University and Capital Medical University Advanced Innovation Center for Big Data-Based Precision Medicine Plan (BHME-201907) and Beijing Institute of Technology Research Fund Program for Young Scholars for their support.

SUPPLEMENTARY MATERIAL

The Supplementary Material for this article can be found online at: https://www.frontiersin.org/articles/10.3389/fnins.2021.620750/full#supplementary-material

REFERENCES

Alexander, G. E., Crutcher, M. D., and Delong, M. R. (1991). Basal ganglia-thalamocortical circuits: parallel substrates for motor, oculomotor, "prefrontal" and "limbic" functions. *Prog. Brain Res.* 85, 119–146. doi: 10.1016/s0079-6123(08)62678-3

Antonini, A., Abbruzzese, G., Ferini-Strambi, L., Tilley, B., Huang, J., Stebbins, G. T., et al. (2013). Validation of the Italian version of the movement disorder society—unified Parkinson's disease rating scale. *Neurol. Sci.* 34, 683–687.

Benabid, A. L. (2003). Deep brain stimulation for Parkinson's disease. *Curr. Opin. Neurobiol.* 13, 696–706.

Bermudez, C., Rodriguez, W., Huo, Y., Hainline, A. E., Li, R., Shults, R., et al. (2019). Towards machine learning prediction of deep brain stimulation (DBS) intra-operative efficacy maps. *Proc. SPIE Int. Soc. Opt. Eng.* 10949:1094922.

Campbell, M. C., Karimi, M., Weaver, P. M., Wu, J., Perantie, D. C., Golchin, N. A., et al. (2008). Neural correlates of STN DBS-induced cognitive variability in Parkinson disease. *Neuropsychologia* 46, 3162–3169. doi: 10.1016/j.neuropsychologia.2008.07.012

Caparroslefebvre, D., Ruchoux, M. M., Blond, S., Petit, H., and Percheron, G. (1994). Long-term thalamic stimulation in Parkinson's disease Postmortem anatomoclinical study. *Neurology* 44, 1856–1856. doi: 10.1212/wnl.44.10.1856

Carbon, M., and Eidelberg, D. (2006). Functional imaging of sequence learning in Parkinson's disease. *J. Neurol. Sci.* 248, 72–77. doi: 10.1016/j.jns.2006.05.005

Cebolla, A. M., Palmero-Soler, E., Dan, B., and Cheron, G. (2011). Frontal phasic and oscillatory generators of the N30 somatosensory evoked potential. *Neuroimage* 54, 1297–1306. doi: 10.1016/j.neuroimage.2010.08.060

Claassen, D. O., Mcdonell, K. E., Donahue, M. J., Rawal, S., Wylie, S. A., Neimat, J. S., et al. (2016). Cortical asymmetry in Parkinson's disease: early susceptibility of the left hemisphere. *Brain Behav.* 6:e00573.

Crane, P. K., Gibbons, L. E., Dams-O'connor, K., Trittschuh, E., Leverenz, J. B., Keene, C. D., et al. (2016). Association of traumatic brain injury with late-life neurodegenerative conditions and neuropathologic findings. *JAMA Neurol.* 73, 1062–1069. doi: 10.1001/jamaneurol.2016.1948

Dong, W., Qiu, C., Jiang, X., Shen, B., Zhang, L., Liu, W., et al. (2020). Can the executive control network be used to diagnose Parkinson's disease and as an efficacy indicator of deep brain stimulation? *Parkinsons Dis.* 2020:6348102.

Ellmore, T. M., Suescun, J., Castriotta, R. J., and Schiess, M. C. (2020). A study of the relationship between uric acid and substantia nigra brain connectivity in patients with REM sleep behavior disorder and Parkinson's disease. *Front. Neurol.* 11:815. doi: 10.3389/fneur.2020.00815

Fan, L., Hai, L., Zhuo, J., Yu, Z., Wang, J., Chen, L., et al. (2016). The human brainnetome atlas: a new brain atlas based on connectional architecture. *Cereb. Cortex* 26, 3508–3526. doi: 10.1093/cercor/bhw157

Fenoy, A. J., Mchenry, M. A., and Schiess, M. C. (2016). Speech changes induced by deep brain stimulation of the subthalamic nucleus in Parkinson disease: involvement of the dentatorubrothalamic tract. *J. Neurosurg.* 126, 2017–2027. doi: 10.3171/2016.5.jns16243

Fling, B. W., Cohen, R. G., Mancini, M., Nutt, J. G., Fair, D. A., and Horak, F. B. (2013). Asymmetric pedunculopontine network connectivity in parkinsonian patients with freezing of gait. *Brain* 136, 2405–2418. doi: 10.1093/brain/awt172

Gan, C., Wang, M., Si, Q., Yuan, Y., and Zhang, K. (2020). Altered interhemispheric synchrony in Parkinson's disease patients with levodopa-induced dyskinesias. *npj Parkinsons Dis.* 6:14.

Habets, J. G. V., Janssen, M. L. F., Duits, A. A., Sijben, L. C. J., Mulders, A. E. P., De Greef, B., et al. (2020). Machine learning prediction of motor response after deep brain stimulation in Parkinson's disease-proof of principle in a retrospective cohort. *PeerJ* 8:e10317. doi: 10.7717/peerj.10317

Hacker, C. D., Perlmutter, J. S., Criswell, S. R., Ances, B. M., and Snyder, A. Z. (2012). Resting state functional connectivity of the striatum in Parkinson's disease. *Brain* 135, 3699–3711. doi: 10.1093/brain/aws281

Halliday, G. M. (2009). Thalamic Changes in Parkinson's Disease. *Parkinsonism Relat. Disord.* 15, S152–S155.

Hoerl, A. E., and Kennard, R. W. (1970). Ridge regression: biased estimation for nonorthogonal problems. *Technometrics* 12, 55–67.

Horn, A., Li, N., Dembek, T. A., Kappel, A., Boulay, C., Ewert, S., et al. (2019). Lead-DBS v2: towards a comprehensive pipeline for deep brain stimulation imaging. *Neuroimage* 184, 293–316. doi: 10.1016/j.neuroimage.2018.08.068

Horn, A., Reich, M. M., Vorwerk, J., Li, N., Wenzel, G., Fang, Q., et al. (2017). Connectivity predicts deep brain stimulation outcome in Parkinson disease. *Ann. Neurol.* 82, 67–78. doi: 10.1002/ana.24974

Hornykiewicz, O. (1966). Dopamine (3-hydroxytyramine) and brain function. *Pharmacol. Rev.* 18, 925–964.

Huang, C., Mattis, P., Tang, C., Perrine, K., Carbon, M., and Eidelberg, D. (2007). Metabolic brain networks associated with cognitive function in Parkinson's disease. *Neuroimage* 34, 714–723. doi: 10.1016/j.neuroimage.2006.09.003

Hwynn, N., Ul Haq, I., Malaty, I. A., Resnick, A. S., Dai, Y., Foote, K. D., et al. (2011). Effect of deep brain stimulation on Parkinsons nonmotor symptoms following unilateral DBS: a pilot study. *Parkinsons Dis.* 2011:507416. doi: 10.4061/2011/507416

Jiang, X., Shen, Y., Yao, J., Zhang, L., Xu, L., Feng, R., et al. (2019). Connectome analysis of functional and structural hemispheric brain networks in major depressive disorder. *Transl. Psychiatry* 9:136. doi: 10.1038/s41398-019-0467-9

Kaiser, M. (2008). Mean clustering coefficients: the role of isolated nodes and leafs on clustering measures for small-world networks. *N. J. Phys.* 10:083042. doi: 10.1088/1367-2630/10/8/083042

Kawahara, J., Brown, C. J., Miller, S. P., Booth, B. G., Chau, V., Grunau, R. E., et al. (2017). BrainNetCNN: Convolutional neural networks for brain networks; towards predicting neurodevelopment. *Neuroimage* 146, 1038–1049. doi: 10.1016/j.neuroimage.2016.09.046

Kleiner-Fisman, G., Herzog, J., Fisman, D. N., Tamma, F., Lyons, K. E., Pahwa, R., et al. (2006). Subthalamic nucleus deep brain stimulation: summary and meta-analysis of outcomes. *Mov. Disord.* 21(Suppl. 14), S290–S304. doi: 10.1002/mds.20962

Kocabicak, E., Tan, S., and Temel, Y. (2012). Deep brain stimulation of the subthalamic nucleus in Parkinson's disease: why so successful? *Surg. Neurol. Int.* 3:312. doi: 10.4103/2152-7806.103024

Li, D. R., Wu, G. C., Lin, J. L., Wang, X. L., Lai, B. H., and Zou, G. Y. (2005). Changes of cerebral blood flow and limb motor function in patients with acute ischemic stroke after scalp acupuncture treatment. *Zhong. Linchuang Kangfu* 9, 138–139.

Li, L., Zhao, W., and Wang, Z. (2006). Advantage of ridge regression over LS in solving multicollinearity. *J. Bohai Univ.* 27, 32–34.

Liaw, A., and Wiener, M. (2002). Classification and regression by randomForest. *R News* 2, 18–22.

Lizarraga, K. J., Luca, C. C., De Salles, A., Gorgulho, A., Lang, A. E., and Fasano, A. (2017). Asymmetric neuromodulation of motor circuits in Parkinson's disease: the role of subthalamic deep brain stimulation. *Surg. Neurol. Int.* 8:261. doi: 10.4103/sni.sni_292_17

Luo, C. Y., Guo, X. Y., Song, W., Chen, Q., Cao, B., Yang, J., et al. (2015b). Functional connectome assessed using graph theory in drug-naive Parkinson's disease. *J. Neurol.* 262, 1557–1567. doi: 10.1007/s00415-015-7750-3

Luo, C. Y., Guo, X., Song, W., Zhao, B., Cao, B., Yang, J., et al. (2015a). Decreased resting-state interhemispheric functional connectivity in Parkinson's disease. *Biomed Res. Int.* 2015:692684. doi: 10.1155/2015/692684

Masuda, D., Nohara, R., Tamaki, N., Hosokawa, R., Inada, H., Hikai, T., et al. (2000). Evaluation of coronary blood flow reserve by 13N-NH3 positron emission computed tomography (PET) with dipyridamole in the treatment of hypertension with the ACE inhibitor (Cilazapril). *Ann. Nucl. Med.* 14, 353–360. doi: 10.1007/BF02988695

Muthuraman, M., Deuschl, G., Koirala, N., Riedel, C., Volkmann, J., and Groppa, S. (2017). Effects of DBS in parkinsonian patients depend on the structural integrity of frontal cortex. *Sci. Rep.* 7:43571. doi: 10.1038/srep43571

Obeso, I., Casabona, E., Bringas, M. L., Alvarez, L., and Jahanshahi, M. (2012). Semantic and phonemic verbal fluency in Parkinson's disease: influence of clinical and demographic variables. *Behav. Neurol.* 25, 111–118. doi: 10.1155/2012/673610

Quraan, M. A., Protzner, A. B., Daskalakis, Z. J., Giacobbe, P., Tang, C. W., Kennedy, S. H., et al. (2014). EEG power asymmetry and functional connectivity as a marker of treatment effectiveness in DBS surgery for depression. *Neuropsychopharmacology* 39, 1270–1281. doi: 10.1038/npp.2013.330

Rivaposse, P., Choi, K. S., Holtzheimer, P. E., Crowell, A., Garlow, S. J., Rajendra, J., et al. (2018). A connectomic approach for subcallosal cingulate deep brain stimulation surgery: prospective targeting in treatment-resistant depression. *Mol. Psychiatry* 23, 843–849. doi: 10.1038/mp.2017.59

Rosin, B., Slovik, M., Mitelman, R., Rivlin-Etzion, M., Haber, S. N., Israel, Z., et al. (2011). Closed-loop deep brain stimulation is superior in ameliorating parkinsonism. *Neuron* 72, 370–384. doi: 10.1016/j.neuron.2011.08.023

Stavitsky, K., Mcnamara, P., Durso, R., Harris, E., Auerbach, S., and Cronin-Golomb, A. (2008). Hallucinations, dreaming and frequent dozing in Parkinson's disease: impact of right-hemisphere neural networks. *Cogn. Behav. Neurol.* 21, 143. doi: 10.1097/WNN.0b013e318185e698

Sun, Y., Chen, Y., Collinson, S. L., Bezerianos, A., and Sim, K. (2015). Reduced hemispheric asymmetry of brain anatomical networks is linked to schizophrenia: a connectome study. *Cereb. Cortex* 27, 602–615. doi: 10.1093/cercor/bhv255

Tian, L., Wang, J., Yan, C., and He, Y. (2011). Hemisphere-and gender-related differences in small-world brain networks: a resting-state functional MRI study. *Neuroimage* 54, 191–202. doi: 10.1016/j.neuroimage.2010.07.066

van Waarde, J., Scholte, H., van Oudheusden, L., Verwey, B., Denys, D., and van Wingen, G. (2015). A functional MRI marker may predict the outcome of electroconvulsive therapy in severe and treatment-resistant depression. *Mol. Psychiatry* 20, 609–614. doi: 10.1038/mp.2014.78

Varangis, E., Habeck, C. G., Razlighi, Q. R., and Stern, Y. (2019). The effect of aging on resting state connectivity of predefined networks in the brain. *Front. Aging Neurosci.* 11:234. doi: 10.3389/fnagi.2019.00234

Wang, J., Wang, X., Xia, M., Liao, X., Evans, A., and He, Y. (2015). GRETNA: a graph theoretical network analysis toolbox for imaging connectomics. *Front. Hum. Neurosci.* 9:386. doi: 10.3389/fnhum.2015.00386

Wang, W., Mei, M., Gao, Y., Huang, B., Qiu, Y., Zhang, Y., et al. (2019). Changes of brain structural network connection in Parkinson's disease patients with mild

cognitive dysfunction: a study based on diffusion tensor imaging. *J. Neurol.* 267, 933–943. doi: 10.1007/s00415-019-09645-x

Weaver, F., Follett, K., Hur, K., Ippolito, D., and Stern, M. (2005). Deep brain stimulation in Parkinson disease: a metaanalysis of patient outcomes. *J. Neurosurg.* 103, 956–967. doi: 10.3171/jns.2005.103.6.0956

Weiss, P. H., Herzog, J., Potter-Nerger, M., Falk, D., Herzog, H., Deuschl, G., et al. (2015). Subthalamic nucleus stimulation improves Parkinsonian gait via brainstem locomotor centers. *Mov. Disord.* 30, 1121–1125. doi: 10.1002/mds.26229

Wiesman, A. I., Heinrichsgraham, E. C., Mcdermott, T. J., Santamaria, P. M., Gendelman, H. E., and Wilson, T. W. (2016). Quiet connections: reduced fronto-temporal connectivity in nondemented Parkinson's disease during working memory encoding. *Hum. Brain Mapp.* 37, 3224–3235. doi: 10.1002/hbm.23237

Xie, T., Kang, U. J., and Warnke, P. (2012). Effect of stimulation frequency on immediate freezing of gait in newly activated STN DBS in Parkinson's disease. *J. Neurol. Neurosurg. Psychiatry* 83, 1015–1017. doi: 10.1136/jnnp-2011-302091

Yang, C., Zhong, S., Zhou, X., Wei, L., Wang, L., and Nie, S. (2017). The abnormality of topological asymmetry between hemispheric brain white matter networks in Alzheimer's disease and mild cognitive impairment. *Front. Aging Neurosci.* 9:261. doi: 10.3389/fnagi.2017.00261

Conflict of Interest: The authors declare that the research was conducted in the absence of any commercial or financial relationships that could be construed as a potential conflict of interest.

Publisher's Note: All claims expressed in this article are solely those of the authors and do not necessarily represent those of their affiliated organizations, or those of the publisher, the editors and the reviewers. Any product that may be evaluated in this article, or claim that may be made by its manufacturer, is not guaranteed or endorsed by the publisher.

frontiers in Neuroscience

BRIEF RESEARCH REPORT
published: 22 December 2021
doi: 10.3389/fnins.2021.632822

Measurement of Lead Localization Accuracy Based on Magnetic Resonance Imaging

Changgeng He[1], Feng Zhang[1], Linze Li[1], Changqing Jiang[1] and Luming Li[1,2,3,4]**

[1] National Engineering Laboratory for Neuromodulation, School of Aerospace Engineering, Tsinghua University, Beijing, China, [2] Precision Medicine and Healthcare Research Center, Tsinghua-Berkeley Shenzhen Institute, Tsinghua University, Shenzhen, China, [3] IDG/McGovern Institute for Brain Research at Tsinghua University, Beijing, China, [4] Institute of Epilepsy, Beijing Institute for Brain Disorders, Beijing, China

Post-implantation localization of deep brain stimulation (DBS) lead based on a magnetic resonance (MR) image is widely used. Existing localization methods use artifact center method or template registration method, which may lead to a considerable deviation of $>$ 2 mm, and result in severe side effects or even surgical failure. Accurate measurement of lead position can instantly inform surgeons of the imprecise implantation. This study aimed to identify the influencing factors in DBS lead post-implantation localization approach, analyze their influence, and describe a localization approach that uses the individual template method to reduce the deviation. We verified that reconstructing direction should be parallel or perpendicular to lead direction, instead of the magnetic field. Besides, we used simplified relationship between magnetic field angle and deviation error to correct the localization results. The mean localization error can be reduced after correction and favors the feasibility of direct localization of DBS lead using MR images. We also discussed influence of *in vivo* noise on localization frequency and the possibility of using only MR images to localize the contacts.

Keywords: deep brain stimulation, magnetic resonance imaging, lead localization, artifact, template

OPEN ACCESS

Edited by:
Michela Chiappalone, Italian Institute of Technology (IIT), Italy

Reviewed by:
Xiaohong Sui, Shanghai Jiao Tong University, China
Teppei Matsui, Okayama University, Japan

****Correspondence:***
Changqing Jiang
jiangcq13@tsinghua.edu.cn
Luming Li
lilm@tsinghua.edu.cn

Specialty section:
This article was submitted to Brain Imaging Methods, a section of the journal Frontiers in Neuroscience

Received: *26 November 2020*
Accepted: *04 November 2021*
Published: *22 December 2021*

Citation:
He C, Zhang F, Li L, Jiang C and Li L (2021) Measurement of Lead Localization Accuracy Based on Magnetic Resonance Imaging. Front. Neurosci. 15:632822. doi: 10.3389/fnins.2021.632822

INTRODUCTION

Deep brain stimulation (DBS) is a widely used treatment for various neurological and neuropsychiatric diseases, including Parkinson's disease, epilepsy, and depression (Benabid, 2003; Stefurak et al., 2003; Huys et al., 2016). Its clinical outcomes depend on the regulation of disease-specific pathological neural circuits through precise stimulation of the artfully selected targets (Knight et al., 2015). Accurate implantation of stimulating leads is required in order to have a favorable clinical outcome. In addition, the spatial relationship between the leads and target nuclei, as well as the surrounding neural elements, should also be determined to guide the programming in order to optimize clinical efficacy and reduce side effects (Butson et al., 2007; Chaturvedi et al., 2010). It can also help elucidate the therapeutic mechanism of DBS and its related fundamental brain functions.

Postoperative magnetic resonance imaging (MRI) is generally used to localize implanted leads (Pollo et al., 2004; Starr et al., 2010). It could provide simultaneous and direct visualization of the leads and the surrounding brain tissues. In addition, results can be readily fused with those from other MRI modalities, such as functional MRI, in order to provide powerful means of investigating

the DBS and disease mechanisms (Schönecker et al., 2014; Ashkan et al., 2017). Safety concerns once hindered its use in clinics, which led to the proposal of alternative approaches, such as fusion of computed tomography (CT) and preoperative MRI techniques (Thani et al., 2011; Engelhardt et al., 2019). Nowadays, after continuous efforts to address these concerns and with the new designs of the DBS device (Jiang et al., 2013; Zhao et al., 2020), not only 1.5 T but also 3.0 T MRI is now deemed relatively safe under certain controlled conditions (Jiang et al., 2014; Mo et al., 2016). An increasing number of clinical centers are performing MRI after DBS implantation as a routine procedure (Lozano et al., 2019).

With less obvious safety concerns, accuracy of direct lead localization on MR images becomes the major question. The metallic contacts of the lead can induce large artifacts on the images due to the magnetic susceptibility difference between the contacts and surrounding brain tissues (Schenck, 1996), which would hinder the identification of the actual contact positions. Generally, the contact artifacts are treated as ellipses symmetrical to the lead axis and whose centers are deemed coincidence with those of the contacts (Pollo et al., 2004). However, this is not the exact case when the lead is inclined from the main field direction of the MRI. Not only are the shapes of the artifacts rather irregular but also the centers would deviate from the true positions of the contacts (Matsui et al., 2007; Lee et al., 2010). Moreover, a number of factors, such as reconstruction direction, sequence type, and scan parameters, would also affect the appearance of the artifact, making it even challenging to address the problem (Liu et al., 2001).

The average template method is widely used in postoperative MR localization (Horn and Kühn, 2015). However, this method may ignore some details of the electrode artifacts. Therefore, the registration result may not be as good as the personalized template.

In order to evaluate the accuracy of direct lead localization on postoperative MR images, phantom experiments were conducted under 3.0 T MRI in this study. The DBS lead was placed at a variety of orientations, and both T1- and T2-weighted images were acquired. Positions of the contacts directly derived from the artifacts were compared with those calculated based on fiducial marks, which were more accurate measurements, to get the localization error. Our design guaranteed that the calculation of contact center coordinate is accurate and provide a reliable reference to estimate the localization error in the traditional method, which was not considered in previous studies. Through these analyses, whether and how MR images alone can be used as a reliable lead localization method was discussed.

MATERIALS AND METHODS

Deep Brain Stimulation Lead

The lead PINS L301 (PINS Medical, Inc., Beijing, China) was used in the experiments. Four cylindrical-stimulating contacts (distal contact 0 to proximal contact 3) made of platinum–iridium alloy was established in the distal end. Each contact was 1.5 mm in length and 1.27 mm in diameter. The space between the two adjacent contacts was 0.5 mm. The proximal end of the lead bore the four connecting contacts. Both ends were interconnected by helical platinum–iridium alloy cables covered with polyurethane sheath.

Experiment Setup

A cuboid-shaped phantom with inner dimensions of $280 \times 170 \times 150$ mm^3 was made and filled with a solution consisting of 5 g/L of CuSO4 and 0.9 g/L of NaCl. It was placed flat with the long axis parallel to the main field B0 and calibrated with a spirit level.

To hold the lead at various orientations, a rotatable fixture was designed as presented in **Figures 1A,B**. The lead was clamped on the ring of the rotatable fixture with a cover block. A nylon wire was tied to the tip of the lead and fixed to a knob fixture at the center of the arc in order to maintain the lead straight. A coordinate system could be established with the origin located at the center of the knob fixture and Z-axis aligning with B0. By adjusting the cover block position and the knob fixture orientation, the lead could be deflected to an angle θ of 0°, 15°, and 30° relative to the Y–Z plane. Its inclination angle φ relative to the horizontal plane could be adjusted to 0°, 15°, 30°, and 45° by fixation to location holes on the sidewalls with nylon screws. The angle α of the lead axis relative to the B0 direction can be calculated by

$$\alpha = \cos^{-1}(\cos\varphi \cos\theta) \quad (1)$$

The phantom and fixtures were made of PMMA, which had little artifact in MR images, so that the profiles could serve as fiducials to determine the lead positions. Before scanning, air bubbles were removed to prevent their influence on images.

Magnetic Resonance Data Acquisition

T1-weighted three-dimensional turbo field echo (T1w-3D-TFE) and T2-weighted turbo spin echo (T2w-TSE) sequences were scanned on a 3.0 T MRI scanner (Philips Ingenia, Netherlands, software version 6.0.541.1), with a 32-channel head coil (NMRB 375, Philips, Netherlands). The parameters for the T1w-3D-TFE sequence were repetition time (TR) of 10.2 ms, echo time (TE) of 4.7 ms, field of view (FOV) of 224 mm, matrix of 224×224, and slice thickness of 1 mm, resulting in a final voxel size of $1 \times 1 \times 1$ mm^3. The parameters for the T2w-TSE sequence were TR of 2,111 ms, TE of 90 ms, FOV of 280 mm, matrix of 720×720, and slice thickness of 2 mm, resulting in a final voxel size of $0.39 \times 0.39 \times 2$ mm^3.

Contact Localization

The center of contact 0 was localized longitudinally and transversely from T1 and T2 images, respectively. All reconstructed images were bilinear, upsampled to a resolution of 0.1 mm before processing.

In order to locate the contacts in the image, we created a fixture coordinate system. We used multiple cross-section images to establish the rotatable fixture coordinate system. The cross section parallel to the rotatable fixture was used to determine the axis of the knob fixture in the image slice. We used the Hough transform to calculate the center of the

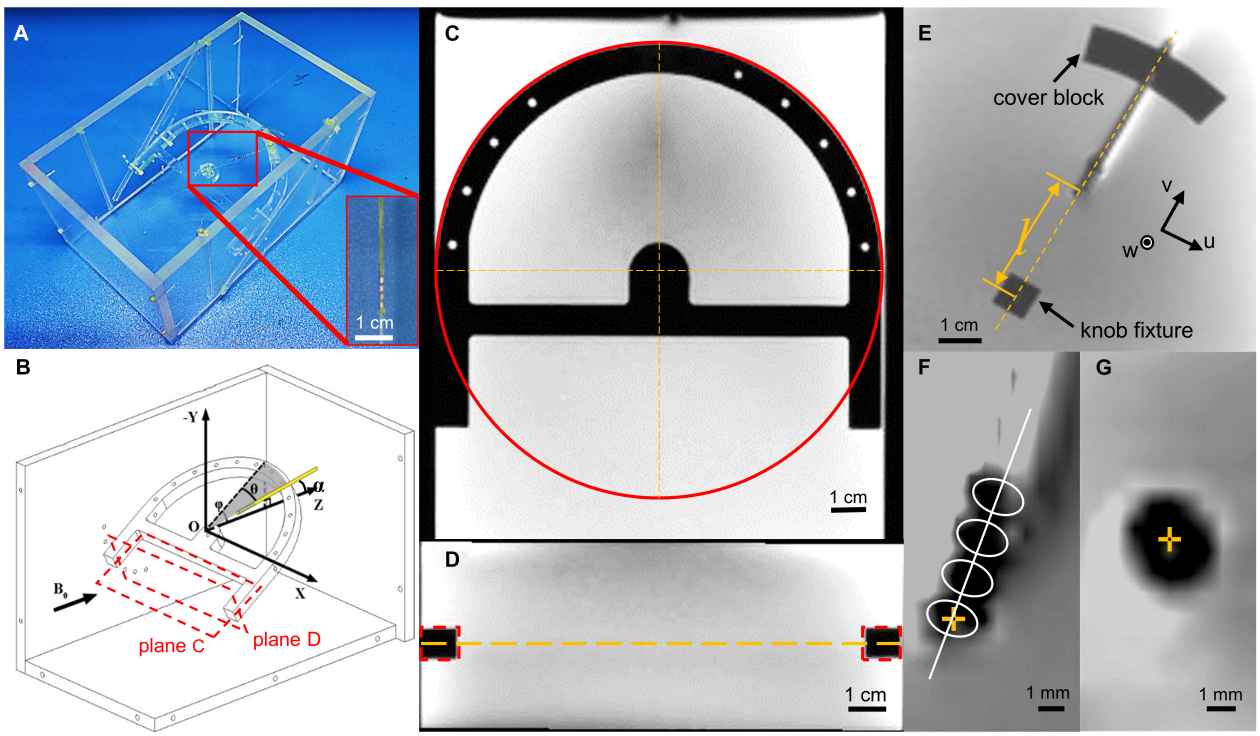

FIGURE 1 | Illustration of the experiment layout. **(A)** Photo of the phantom layout with the lead terminal tied to the nylon wire and fixed on a cubic fixture. **(B)** The schematic map of the experiment layout. Black vector stands for the direction of the main field. Plane **(C,D)** stands for the cross sections in **(C,D)**. **(C)** Demonstration of how we calculate the fixture coordinate system center in a slice and axis direction. The red circle stands for the Hough transformation, which gives us the coordinate of the fixture center. **(D)** Demonstration of how we calculate the slice that contains the coordinate system center. There d-dotted rectangle stands for the cross section of the fixture, which gives the center slice position, which contains the lead. **(E)** Magnetic resonance (MR) image of the lead, cover block, and knob fixture, and depiction of the u and v axes, whereas the w-axis is perpendicular to the u–v plane. Length l indicates the distance between contact 0 and the center of the knob fixture, measured using an image measuring instrument. **(F)** The template used to directly identify the contact center in the coronal view. The center of contact 0 is highlighted with a yellow cross mark. **(G)** The contact center is in transverse view, highlighted with a yellow cross.

half-ring structure and the bar direction of the rotatable fixture (**Figure 1C**). The cross-section perpendicular to the rotatable fixture and parallel to the x-axis was used to calculate the slice, which contains the lead (**Figure 1D**). The center of the knob fixture was selected as our origin of the fixture coordinate system, and the axis is determined by the bar direction and fixture symmetry axis. After the coordinate system is set, we calculate the coordinates of the contact with parameters measured with a microscope. As with the fiducial approach, the longitudinal position of contact 0 was determined by offsetting the center of the knob fixture O along the lead axis by the distance l between the center of contact 0 and O, which was precisely premeasured when the lead was fixed on the fixtures using an image measurement instrument (Optiv Advance 332, Hexagon AB, Sweden). For direct identification, a template-based approach was used. A template consisting of a series of four identical ellipses equally spaced by 2.0 mm with their axes perpendicular to the lead axis was used, as presented in **Figure 1D**. The position of contact 0 with the highest correlation between the projections of the artifact and the template was searched along the lead axis. The longitudinal position deviation of contact 0 between the two methods was then calculated and denoted by dL.

On the transverse T2 images, the position of contact 0 was either fiducially determined from the intersection of the lead axis and the image plane, or directly identified by picking the center of the hypointense artifact as presented in **Figures 1E–G**. The deviation between the two methods was denoted by dT.

We computed contrast-to-noise ratio (CNR) and analyzed the influence of CNR on localization error. Coronal view images were selected to study this influence since they were frequently used in localization. We calculated CNR in both phantom and *in vivo* conditions, and simulated *in vivo* condition by adding artificial noise to the phantom data. The noise is sampled from location where there is no contrast media, where the signal should be zero, and all signals can be considered noise (National Electrical Manufacturers Association, 2008). After calculating the standard deviation from the noise, we derived CNR from both phantom and *in vivo* data. Artificial Gaussian noise was added to the phantom data so that they have the same CNR as the *in vivo* data. Then we compared the localization error between the phantom data and simulated *in vivo* data.

Template Data Processing

Deviation From the Real Position

The lead was registered to a template using the imregister function in MATLAB (MathWorks, Natick, MA, United States) software. The center of contact after registration was chosen as the focus. The deviation was calculated for the registration results of both the mean template and individual template registration methods. We selected an individual template by choosing the closest direction in our experiment setup, and the mean template is the average of all 12 templates generated in the phantom experiment. The deviation is defined by the difference between the real position and registration calculated position. The real position was calculated using the lead fixture as reference. The registration calculated position was derived by the near template registration algorithm.

Correlation Coefficient Calculation

We compute 12 × 12 pairwise correlation coefficient matrixes for direction correlation, template volume correlation, and template volume correlation after registration in order to measure their similarity.

Statistical Analysis of the Phantom Experiment

Coordinate values were expressed as mean ± standard deviation (SD). Two-way analysis of variance (ANOVA) was conducted to investigate the influence of the θ and φ angles on the localization deviation, including their interaction effect. The statistical significance level was set at 0.05. All calculations were performed using the MATLAB software (MathWorks, Natick, MA, United States).

RESULTS

Longitudinal Localization of the Lead Contact

The regions of the T1w-3D-TFE images containing the lead contacts at various lead orientations are shown in **Figures 2A,B**, which were reconstructed along the lead axis and along the B0 direction, respectively. The hypointense artifacts of the four contacts could be clearly seen in **Figure 2A**, but were hard to distinguish from **Figure 2B**. It indicated the importance of the reconstruction direction on the accuracy of lead localization, and contact positions were determined from **Figure 2A** by both the fiducial-based and direct identification approaches, and marked in the figure. The directly identified positions of contact 0 deviated from the fiducial results by 0.51 to 1.93 mm at various orientations, as shown in **Figure 2D**. Two-way ANOVA revealed that both θ and φ had significant influence on dL (p = 0.003 and 0.017, respectively). It could further be seen from **Figure 2C** that dL showed an increase with the angle α, which combined θ and φ according to Equation (1).

Transverse Localization of the Lead Contacts

The regions of the T2w-TSE images containing the lead contacts are shown in **Figures 3A,B**, which were reconstructed perpendicular to the lead axis and the B0 direction, respectively. The profiles of the artifact were relatively regular in **Figure 3A**, but were severely distorted in many of the images in **Figure 3B**, especially in those with large α angles. Thus, transverse contact positions were determined from and marked in **Figure 3A**. There was a slight difference of 0.75 ± 0.29 mm between the directly identified and fiducial-derived positions, as shown in **Figure 3D**. Neither φ nor θ angle showed significant impact on dT, which was consistent with the influence of α, as shown in **Figure 3C**.

Contrast-to-Noise Ratio Influence on Localization Error

We estimated the CNR and noticed that the CNR is different between the phantom data and clinical *in vivo* data. The CNR estimated is around 60 from the phantom data and 20 from the clinical data. We added Gaussian noise to the phantom data and decreased its CNR to 20 to mimic the condition of the *in vivo* data. The generated *in vivo*-like images are shown in **Figure 4B**. We compared the localization error between the phantom data and the mimicked *in vivo* data in **Figure 4**. The overall localization error increased after adding more noise. The largest localization error before and after correction are 2.4 and 1.6 mm, respectively. The mean error after correction increased from 0.42 to 0.79 mm.

Comparison Between Different Templates

The 12 × 12 correlation matrix show pairwise correlation of all individual templates (**Figure 5**). All 12 templates were registered to each other, and correlation coefficients were calculated after registration. This similarity measurement provides us the explanation of the difference between mean template and near template. In image registration algorithm based on intensity, similarity can give us a hint on the potential registration behavior. In our condition, the localization error depends on registration accuracy, which can be reflected in template similarity. The individual template was used to mimic the widely used template matching method. However, the result is not as good as the individual template result. The best individual template registration result exceeds the result of the mean template registration. The mean template has lower correlation coefficient than the best correlated template (**Figure 6**).

DISCUSSION

Knowing the accurate location of the implanted DBS lead inside the target nucleus is important to understand the mechanisms and promote the therapy development. Direct localization from MR images is the handiest way but is hindered by electrode artifacts.

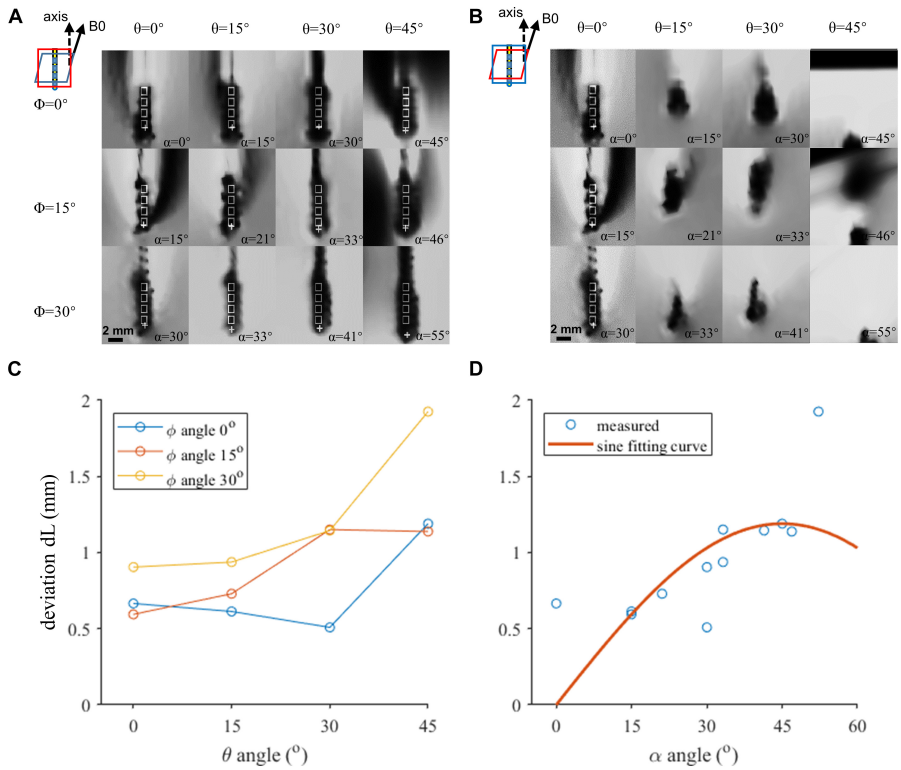

FIGURE 2 | The coronal view of the artifacts of four contacts in various orientations. **(A,B)** Artifact positions under different lead orientations. White rectangles indicate the outline of the contacts. Cross markers indicate the template-matched position of the proximal contact. **(A)** Image resliced parallel to the top surface of the rotatable fixture. **(B)** Image resliced parallel to the X–Z plane. **(C,D)** Localization deviation as a function of the axis direction. **(C)** Horizontal axis indicates the θ angle. Three curves represent different φ angles. Both θ and φ angles contribute to the deviation, and reduction of either of the angles can achieve a better accuracy. **(D)** Horizontal axis indicates α. The red plane in the zoomed-in figure shows the reconstruction plane we chose in each condition in **(A,B)**.

In this study, we designed phantom experiments with fiducial frames to guarantee direct localization accuracy of the DBS lead from MR images. Most previous studies focused on CT/MR image fusion localization error (Lee et al., 2010; Smith and Bakay, 2011), but our study intends to explore the possibility of localization with only MR images. Former studies used phantom experiments, which gives accurate reference for localization of lead but only in the parallel and perpendicular directions (Pollo et al., 2004, 2007). In our study, we took the typical lead direction range into consideration and analyzed the relationship between localization errors. Besides these analyses, we used simplified relationship to decrease the error to the level of 0.42 mm on average, which favors the feasibility of direct localization of the DBS lead from MR images. We also analyzed the localization error difference between the phantom study and *in vivo* condition by adding artificial noise to mimic the *in vivo* condition. The phantom experiment paradigm may also be used for further applications, such as generating artifact template for localization by registration method.

We conducted a systematic analysis on error propagation in the phantom experiment from two aspects: the accuracy of the phantom localization system and the reliability of the manually mimicking traditional localization method.

As for the phantom localization system, the propagation of error is from the phantom to fiducial points to the calculation of the contact center. The phantom and the lead fixture were machined with an accuracy of 0.1 mm, which is guaranteed by the machine tool. After upsampling the MR image to a resolution of 0.1 mm, the center of both the knob fixture and cover block have an accuracy of 0.1 mm in both u and v directions in **Figure 1E**. Thus, the uncertainty of lead position calculation in each direction can be derived by:

$$\sqrt{k^2\sigma^2 + (1-k)^2\sigma^2} = \sigma\sqrt{k^2 + (1-k)^2} < \sigma, 0 \le k \le 1 \quad (2)$$

in which k is the proportion of length l in the distance between the knob fixture center and cover block center, and σ is the standard deviation of both the knob fixture center and cover block center, which is 0.1 mm in our experiment. In addition, the magnetic field distortion is routinely corrected daily by the MRI scanner operator.

As for the manual localization results, we took the mean result from three experts to reduce random error. An influential factor for manual localization method is the magnetic susceptibility difference between brain tissue and the solution. The difference of the artifact shape lies in their difference in magnetic susceptibility. The magnetic susceptibility of Pt–Ir alloy is 231 ppm (C. Q. Jiang et al., 2013), while the brain tissue has a magnetic susceptibility in the range between −8.8 and −9.2 ppm, and our solution of −9 ppm (Duyn and Schenck, 2017). The influence of magnetic

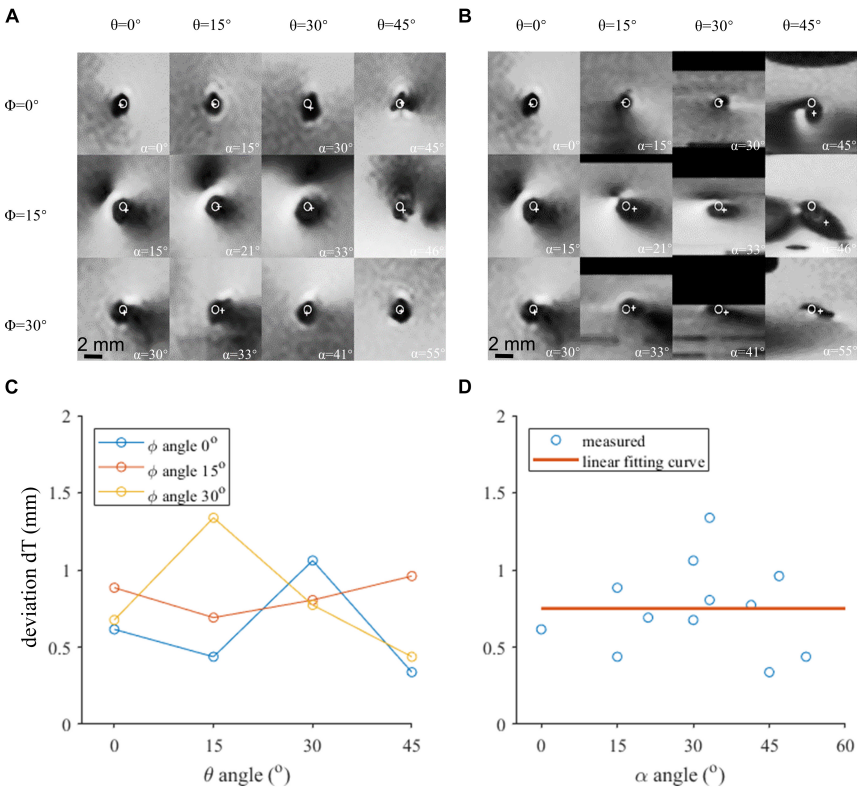

FIGURE 3 | The axial view of the contact 0 artifact in various orientations. **(A)** Image reconstructed perpendicular to the lead axis. **(B)** Image reconstructed perpendicular to the B0 field. **(C)** Localization deviation assessed in the axial view under different θ and φ angles. **(D)** The localization deviation of contact 0 with respect to α, reconstructed perpendicular to the B0 field.

susceptibility to magnetic field distortion can be described as a distortion factor (Ladd et al., 1996): $\frac{\mu_i - \mu_e}{\mu_i + \mu_e}$, where μ_i and μ_e stands for the magnetic susceptibility of the material inside and outside the lead. In the extreme case of brain magnetic susceptibility of –9.2 and –8.8 ppm, the distortion factor is 1.1077 and 1.1028, respectively, which has a difference of 0.2% in contrast to 1.1052 for water. We consider the difference of 0.2% to be of minor influence.

There are differences in noise level between phantom and *in vivo* condition. The noise in clinical condition is higher because of the complex background condition. Here we use the blank area, which contains no medium that generates signal to estimate the noise level in both the phantom and *in vivo* data. The localization error was increased after we added Gaussian noise. A possible explanation is that the artifact outlines have been changed after adding artificial noise. These images after treatment will bring more difficulty for us to distinguish the center of artifact hypointensity area, which deteriorates the localization accuracy. However, the localization accuracy is still acceptable after our correction method. After correction, localization error is no larger than 1.6 mm. The mean error increased from 0.42 to 0.79 mm, which does not change the conclusion that MR can be used as a localization approach.

This study also analyzed the difference between the individual template and mean artifact template, and showed the advantages in using the individual template. It was revealed that the individual artifact template can have better registration result than the mean template.

Previous studies generally treated the geometric center of the hypointensive artifact in MR images as the contact center (Pollo et al., 2004; Thani et al., 2011), which was only valid under special scenarios, namely, with the lead orientation parallel to the magnetic field, and with the reconstruction direction parallel or perpendicular to the lead axis. In fact, the artifact appearance was strongly dependent on lead orientation. On the other hand, black artifacts are mainly magnetic sensitive artifacts, as well as RF artifacts, which will not only cause local blackening, but also cause some areas to brighten, which makes the situation more complicated. Generally speaking, the geometric center of the artifact tends to deviate further from the electrode center as the angle increases. Even in parallel positions, there is a small difference. This error can be reduced by simple empirical formula fitting. The more accurate analysis can be used to model and calculate the artifacts and make more detailed correction. On the other hand, the hypointensity area mainly consists of the susceptibility artifact, while RF artifacts will not only cause local hypo-intensity but also cause local hyperintensity, which will make the situation more complicated. Generally speaking, as the main field angle increases, the geometric center of the artifact tends to deviate further from the contact center. Even in parallel

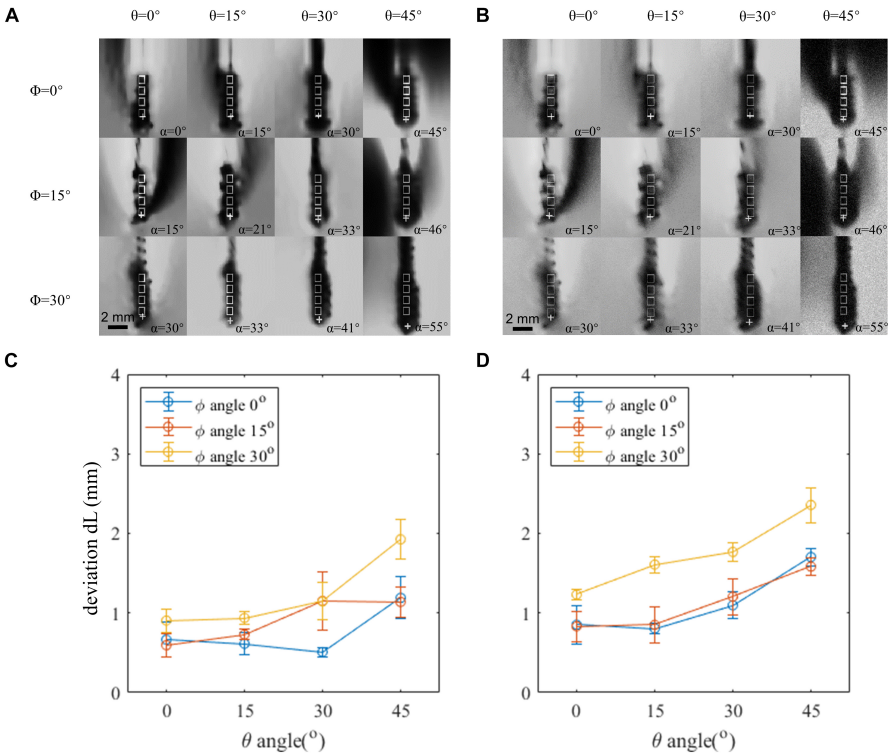

FIGURE 4 | Comparison between the phantom image and *in vivo* contrast-to-noise ratio (CNR)-mimicked image. **(A)** Artifact positions under different lead orientations in the phantom image. **(B)** Artifact positions under different lead orientations in the phantom image, which added an artificial noise to mimic the *in vivo* condition. **(C,D)** Localization error of the original phantom image and phantom image-added artificial noise. Horizontal axis indicates the θ angle. Three curves represent different φ angles. Both θ and φ angles contribute to the deviation, and reduction of either of the angles can achieve a better accuracy.

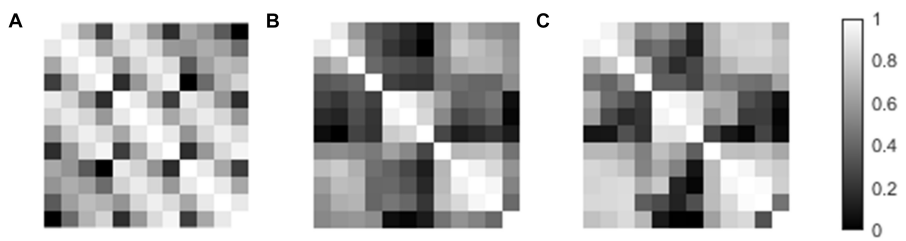

FIGURE 5 | The template paired correlation coefficient matrixes. **(A)** Paired matrix of the template direction vector. **(B)** Paired matrix of the template volume. **(C)** Paired matrix of template volume after registration.

positions, there is a small deviation. This error can be reduced by a simple regression formula. More accurate analysis can be achieved by modeling and calculating the artifacts.

The traditional method uses averaged lead template to register subject data. However, after averaging, the template loses some detailed information of the contact artifact feature. The averaged template is not as good as the closest direction template, but still have the potential to achieve an acceptable result. There are differences between individual templates. Their paired correlation coefficient matrixes show that the template pair with a smaller direction difference has a higher similarity score. This result indicates that choosing a template that has a small direction difference with the patient lead will have a better localization result. On the other hand, the mean template has a stable performance in registration.

The CT/MRI fusion method is widely used because of the low tissue resolution of MRI. However, this approach assumes that the brain remains the same before and after the surgery, while previous studies show that the brain keeps changing after the surgery (Tessitore et al., 2017; Gao, 2018). Specifically, patients with Parkinson's disease have cortical atrophy, and long-term DBS stimulation can lead to ventricular volume changes (Lewis et al., 2009), which will affect the accuracy of preoperative and postoperative registration. In addition, cerebrospinal fluid outflow can lead to brain drift (Elias et al., 2007; Matias et al., 2018), even up to 6.5 mm (Hamed

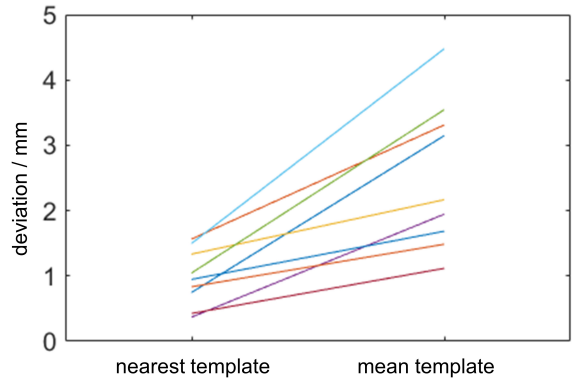

FIGURE 6 | Deviation of the center of proximal contact before and after registration.

et al., 2020). In addition, the accuracy of the CT/MR fusion has been changing for many years (Li et al., 2017). From 2000 to 2015, some operations were converted to frameless positioning, which improved the accuracy to a certain extent. However, more than 50% of the operations with frame positioning were still in use and were widely used, with the maximum deviation of 6 mm. Even the newly developed Leksell frameless system may achieve a positioning deviation of 2 mm (Li et al., 2017). The results of this paper, on the one hand, has an accuracy of 0.42 mm, and it is not necessary to conduct CT/MR fusion electrode positioning, and also can intuitively obtain the relative position relationship between the electrode and the nucleus from the postoperative data. Even if the electrode displacement or brain structure changes after operation, we will not be affected by the use of preoperative data. On the other hand, the traditional average template registration process is improved, and more accurate results are obtained with the individual template.

At present, for the relationship between the electrode implantation position and the activation area and even the curative effect, some studies have shown that the best implantation position for STN DBS in the treatment of Parkinson's disease motor symptoms is the dorsolateral STN (Hamani et al., 2004; Herzog et al., 2004); a deviation of 2 mm may lead to 60% difference in clinical effect (Horn et al., 2019). In order to compensate for the deviation from the target, it is necessary to increase the stimulation intensity, which leads to excessive stimulation in the surrounding area, whose volume can reach one to six times the volume of the STN nucleus (Kramme et al., 2020). Other studies have shown that there are complex functional connections in the basal ganglia (Greene et al., 2020). Small deviations can lead to stimulation in other areas of the cortex. There are similar differences within STN, which need to be treated with caution (Haynes and Haber, 2013). The accuracy of electrode position judgment will affect the mechanism analysis and curative effect prediction. Therefore, Andy Horn et al. (2019) proposed a probability method to infer sweet spot. A previous study has shown that the fiber bundles with different angles from the electrodes have different thresholds under fixed stimulation mode (Slopsema et al., 2019), and false stimulation of the nucleus can affect up to 60% of the postoperative outcomes. Both IC and HDP pathways are located near STN, which are related to the auditory system and motor symptoms, respectively, and are parallel to, and perpendicular to, the electrode direction.

MRI is more and more widely used, and has gradually become a physical examination tool. Through repeated scanning, it can track the changes in the brain for a long time and master the evolution of the disease (Elias et al., 2007; Matias et al., 2018; Hamed et al., 2020). For DBS-implanted patients, repeated scanning of radiation CT is not appropriate. In the past, due to safety considerations, repeated MRI scans were not acceptable. However, with the increasing understanding of DBS MRI safety, as well as new compatible devices (C. Jiang et al., 2014; Mo et al., 2016), this restriction is being removed. MRI study of long-term changes after DBS implantation will become a normal. This provides an opportunity to continuously track brain changes under long-term DBS stimulation.

There is agreement between our results and previous research in which the center of the artifact coincides with the contact center in special cases when the lead axis is parallel to the main field. The fiducial system achieved a relatively accurate localization result due to the small artifact induced by the PMMA material. Thus, the contact coordinate calculated by our fiducial system can be considered as the real position.

Our method implies that error can be corrected by reducing deviation from the artifact center. Notice that in a practical situation, surgeons need to image two leads at the same time, and neither the MF angles will reach 0 degrees. Then our correction formula can be used.

CONCLUSION

This study conducted the first assessment of MR-based lead localization deviation by measuring the deviation in coronal/transverse views, T1/T2 sequences, and different lead orientations and resliced directions. We also showed the advantage of the individual template compared with the mean template. These results indicate that the resliced direction and lead orientation are factors affecting the localization accuracy. More accurate localization results can be secured using carefully selected lead orientations and resliced directions, while taking the direction of the template into consideration when choosing a registration template.

DATA AVAILABILITY STATEMENT

The original contributions presented in the study are included in the article/supplementary material, further inquiries can be directed to the corresponding author/s.

AUTHOR CONTRIBUTIONS

CH conducted the study and prepared the manuscript with directions from CJ and LML. FZ provided important information

about the experiment technique. LZL, CJ, and LML reviewed the manuscript. All the authors approved the manuscript.

FUNDING

This work was supported by the National Natural Science Foundation of China (Nos. 51777115, 81527901, and 81830033), Shenzhen International Cooperative Research Project (No. GJHZ20180930110402104), Tsinghua University Initiative Scientific Research Program, and Major Achievements Transformation Project of Beijing's College.

ACKNOWLEDGMENTS

We thank the Center for Biomedical Imaging Research, Tsinghua University for help with the MRI imaging used in the study.

REFERENCES

Ashkan, K., Rogers, P., Bergman, H., and Ughratdar, I. (2017). Insights into the mechanisms of deep brain stimulation. *Nat. Rev. Neurol.* 13, 548–554. doi: 10.1038/nrneurol.2017.105

Benabid, A. L. (2003). Deep brain stimulation for Parkinson's disease. *Curr. Opin. Neurobiol.* 13, 696–706. doi: 10.1016/j.conb.2003.11.001

Butson, C. R., Cooper, S. E., Henderson, J. M., and McIntyre, C. C. (2007). Patient-specific analysis of the volume of tissue activated during deep brain stimulation. *Neuroimage* 34, 661–670. doi: 10.1016/j.neuroimage.2006.09.034

Chaturvedi, A., Butson, C. R., Lempka, S. F., Cooper, S. E., and McIntyre, C. C. (2010). Patient-specific models of deep brain stimulation: influence of field model complexity on neural activation predictions. *Brain Stimul.* 3, 65–77. doi: 10.1016/j.brs.2010.01.003

Duyn, J. H., and Schenck, J. (2017). Contributions to magnetic susceptibility of brain tissue. *NMR Biomed.* 30, 1–37. doi: 10.1002/nbm.3546

Elias, W. J., Fu, K. M., and Frysinger, R. C. (2007). Cortical and subcortical brain shift during stereotactic procedures. *J. Neurosurg.* 107, 983–988. doi: 10.3171/JNS-07/11/0983

Engelhardt, J., Guehl, D., Damon-Perrière, N., Branchard, O., Burbaud, P., and Cuny, E. (2019). Localization of deep brain stimulation electrode by image registration is software dependent: a comparative study between four widely used software programs. *Stereotact. Funct. Neurosurg.* 96, 364–369. doi: 10.1159/000494982

Gao, K. (2018). Neuroscience: automated brain mapping. *Nat. Methods* 15:101. doi: 10.1038/nmeth.4600

Greene, D. J., Marek, S., Gordon, E. M., Siegel, J. S., Gratton, C., Laumann, T. O., et al. (2020). Integrative and network-specific connectivity of the basal ganglia and thalamus defined in individuals. *Neuron* 105, 742.e–758.e. doi: 10.1016/j.neuron.2019.11.012

Hamani, C., Saint-Cyr, J. A., Fraser, J., Kaplitt, M., and Lozano, A. M. (2004). The subthalamic nucleus in the context of movement disorders. *Brain* 127, 4–20. doi: 10.1093/brain/awh029

Hamed, M. A., Ponce, F. A., Lambert, M., and Moguel-Cobos, G. (2020). Subcortical atrophy and motor outcomes in pallidal deep brain stimulation for Parkinson disease. *World Neurosurg.* 142, e89–e94. doi: 10.1016/j.wneu.2020.06.046

Haynes, W. I. A., and Haber, S. N. (2013). The organization of prefrontal-subthalamic inputs in primates provides an anatomical substrate for both functional specificity and integration: implications for basal ganglia models and deep brain stimulation. *J. Neurosci.* 33, 4804–4814. doi: 10.1523/JNEUROSCI.4674-12.2013

Herzog, J., Fietzek, U., Hamel, W., Morsnowski, A., Steigerwald, F., Schrader, B., et al. (2004). Most effective stimulation site in subthalamic deep brain stimulation for Parkinson's disease. *Mov. Disord.* 19, 1050–1054. doi: 10.1002/mds.20056

Horn, A., and Kühn, A. A. (2015). Lead-DBS: a toolbox for deep brain stimulation electrode localizations and visualizations. *Neuroimage* 107, 127–135. doi: 10.1016/j.neuroimage.2014.12.002

Horn, A., Wenzel, G., Irmen, F., Huebl, J., Li, N., Neumann, W. J., et al. (2019). Deep brain stimulation induced normalization of the human functional connectome in Parkinson's disease. *Brain* 142, 3129–3143. doi: 10.1093/brain/awz239

Huys, D., Bartsch, C., Koester, P., Lenartz, D., Maarouf, M., Daumann, J., et al. (2016). Motor improvement and emotional stabilization in patients with tourette syndrome after deep brain stimulation of the ventral anterior and ventrolateral motor part of the thalamus. *Biol. Psychiatry* 79, 392–401. doi: 10.1016/j.biopsych.2014.05.014

Jiang, C. Q., Hao, H. W., and Li, L. M. (2013). Artifact properties of carbon nanotube yarn electrode in magnetic resonance imaging. *J. Neural Eng.* 10:026013. doi: 10.1088/1741-2560/10/2/026013

Jiang, C., Mo, X., Ding, J., Dong, Y., Zhang, F., Hao, H., et al. (2014). Deep brain stimulation lead design to reduce radio-frequency heating in MRI. *Electron. Lett.* 50, 1898–1900. doi: 10.1049/el.2014.3482

Knight, E. J., Testini, P., Min, H. K., Gibson, W. S., Gorny, K. R., Favazza, C. P., et al. (2015). Motor and nonmotor circuitry activation induced by subthalamic nucleus deep brain stimulation in patients with Parkinson disease: intraoperative functional magnetic resonance imaging for deep brain stimulation. *Mayo Clin. Proc.* 90, 773–785. doi: 10.1016/j.mayocp.2015.03.022

Kramme, J., Dembek, T. A., Treuer, H., Dafsari, H. S., Barbe, M. T., Wirths, J., et al. (2020). Potentials and limitations of directional deep brain stimulation: a simulation approach. *Stereot. Funct. Neurosurg.* 99, 65–74. doi: 10.1159/000509781

Ladd, M. E., Erhart, P., Debatin, J. F., Romanowski, B. J., Boesiger, P., and Mckinnon, G. C. (1996). Biopsy needle susceptibility artifacts. *Magn. Reson. Med.* 32, 646–651.

Lee, J. Y., Kim, J. W., Lee, J. Y., Lim, Y. H., Kim, C., Kim, D. G., et al. (2010). Is MRI a reliable tool to locate the electrode after deep brain stimulation surgery? Comparison study of CT and MRI for the localization of electrodes after DBS. *Acta Neurochir.* 152, 2029–2036. doi: 10.1007/s00701-010-0779-2

Lewis, M. M., Smith, A. B., Styner, M., Gu, H., Poole, R., Zhu, H., et al. (2009). Asymmetrical lateral ventricular enlargement in Parkinson's disease. *Eur. J. Neurol.* 16, 475–481. doi: 10.1111/j.1468-1331.2008.02430.x

Li, Z., Zhang, J. G., Ye, Y., and Li, X. (2017). Review on factors affecting targeting accuracy of deep brain stimulation electrode implantation between 2001 and 2015. *Stereotact. Funct. Neurosurg.* 94, 351–362. doi: 10.1159/000449206

Liu, H., Hall, W. A., Martin, A. J., and Truwit, C. L. (2001). Biopsy needle tip artifact in MR-guided neurosurgery. *J. Magn. Reson. Imaging* 13, 16–22. doi: 10.1002/1522-2586(200101)13:1<16::AID-JMRI1003<3.0.CO;2-B

Lozano, C. S., Ranjan, M., Boutet, A., Xu, D. S., Kucharczyk, W., Fasano, A., et al. (2019). Imaging alone versus microelectrode recording–guided targeting of the STN in patients with Parkinson's disease. *J. Neurosurg.* 1306, 1847–1852. doi: 10.3171/2018.2.JNS172186

Matias, C. M., Frizon, L. A., Asfahan, F., Uribe, J. D., and Machado, A. G. (2018). Brain shift and pneumocephalus assessment during frame-based deep brain stimulation implantation with intraoperative magnetic resonance imaging. *Oper. Neurosurg.* 14, 668–674. doi: 10.1093/ons/opx170

Matsui, T., Koyano, K. W., Koyama, M., Nakahara, K., Takeda, M., Ohashi, Y., et al. (2007). MRI-based localization of electrophysiological recording sites within the cerebral cortex at single-voxel accuracy. *Nat. Methods* 4, 161–168. doi: 10.1038/nmeth987

Mo, X., Jiang, C., Ding, J., Zhang, F., and Li, L. (2016). Study of deep brain stimulation lead resonant length in 3.0 T MRI RF magnetic field. *Electron. Lett.* 52, 1098–1100. doi: 10.1049/el.2015.4191

National Electrical Manufacturers Association (2008). NEMA Standards Publication MS 1-2008, Determination of Signal-to-Noise Ratio (SNR) in Diagnostic Magnetic Resonance Imaging. 1–19. Available online at: http://www.nema.org/standards/pages/determination-of-signal-to-noise-ratio-in-diagnostic-magnetic-resonance-imaging.aspx?%5Cnpapers2://publication/uuid/CDE4FB6F-AC32-4A9E-B2F8-C0ADB3715C24 (accessed February 1, 2020).

Pollo, C., Villemure, J. G., Vingerhoets, F., Ghika, J., Maeder, P., Meuli, R., et al. (2004). Magnetic resonance artifact induced by the electrode Activa 3389: an *in vitro* and *in vivo* study. *Acta Neurochir.* 146, 161–164. doi: 10.1007/s00701-003-0181-4

Pollo, C., Vingerhoets, F., Pralong, E., Ghika, J., Maeder, P., Meuli, R., et al. (2007). Localization of electrodes in the subthalamic nucleus on magnetic resonance imaging. *J. Neurosurg.* 106, 36–44. doi: 10.3171/jns.2007.106.1.36

Schenck, J. F. (1996). The role of magnetic susceptibility in magnetic resonance imaging: MRI magnetic compatibility of the first and second kinds. *Med. Phys.* 23, 815–850. doi: 10.1118/1.597854

Schönecker, T., Gruber, D., Kivi, A., Müller, B., Lobsien, E., Schneider, G., et al. (2014). Postoperative MRI localisation of electrodes and clinical ef fi cacy of pallidal deep brain stimulation in cervical dystonia. *Mov. Disord.* 86, 833–839. doi: 10.1136/jnnp-2014-308159

Slopsema, J. P., Peña, E., Patriat, R., Lehto, L. J., Gröhn, O., Mangia, S., et al. (2019). Selective pathway activation. *J. Neural Eng.* 15, 1–27. doi: 10.1088/1741-2552/aad978.Clinical

Smith, A. P., and Bakay, R. A. E. (2011). Frameless deep brain stimulation using intraoperative O-arm technology: clinical article. *J. Neurosurg.* 115, 301–309. doi: 10.3171/2011.3.JNS101642

Starr, P. A., Martin, A. J., Ostrem, J. L., Talke, P., Levesque, N., and Larson, P. S. (2010). Subthalamic nucleus deep brain stimulator placement using high-field interventional magnetic resonance imaging and a skull-mounted aiming device: technique and application accuracy - clinical article. *J. Neurosurg.* 112, 479–490. doi: 10.3171/2009.6.JNS081161

Stefurak, T., Mikulis, D., Mayberg, H., Lang, A. E., Hevenor, S., Pahapill, P., et al. (2003). Deep brain stimulation for Parkinson's disease dissociates mood and motor circuits: a functional MRI case study. *Mov. Disord.* 18, 1508–1541. doi: 10.1002/mds.10593

Tessitore, A., Santangelo, G., De Micco, R., Giordano, A., Raimo, S., Amboni, M., et al. (2017). Resting-state brain networks in patients with Parkinson's disease and impulse control disorders. *Cortex* 94, 63–72. doi: 10.1016/j.cortex.2017.06.008

Thani, N. B., Bala, A., Swann, G. B., and Lind, C. R. P. (2011). Accuracy of postoperative computed tomography and magnetic resonance image fusion for assessing deep brain stimulation electrodes. *Neurosurgery* 69, 207–214. doi: 10.1227/NEU.0b013e318218c7ae

Zhao, S., Li, G., Tong, C., Chen, W., Wang, P., Dai, J., et al. (2020). Full activation pattern mapping by simultaneous deep brain stimulation and fMRI with graphene fiber electrodes. *Nat. Commun.* 11, 1–12. doi: 10.1038/s41467-020-15570-9

Conflict of Interest: The authors declare that the research was conducted in the absence of any commercial or financial relationships that could be construed as a potential conflict of interest.

Publisher's Note: All claims expressed in this article are solely those of the authors and do not necessarily represent those of their affiliated organizations, or those of the publisher, the editors and the reviewers. Any product that may be evaluated in this article, or claim that may be made by its manufacturer, is not guaranteed or endorsed by the publisher.

Advantages of publishing in Frontiers

OPEN ACCESS
Articles are free to read for greatest visibility and readership

FAST PUBLICATION
Around 90 days from submission to decision

HIGH QUALITY PEER-REVIEW
Rigorous, collaborative, and constructive peer-review

TRANSPARENT PEER-REVIEW
Editors and reviewers acknowledged by name on published articles

Frontiers
Avenue du Tribunal-Fédéral 34
1005 Lausanne | Switzerland

Visit us: www.frontiersin.org
Contact us: frontiersin.org/about/contact

REPRODUCIBILITY OF RESEARCH
Support open data and methods to enhance research reproducibility

DIGITAL PUBLISHING
Articles designed for optimal readership across devices

FOLLOW US
@frontiersin

IMPACT METRICS
Advanced article metrics track visibility across digital media

EXTENSIVE PROMOTION
Marketing and promotion of impactful research

LOOP RESEARCH NETWORK
Our network increases your article's readership